

Development of novel tools for purification and characterization of extracellular vesicles in aging and disease

Ph.D. thesis

Madhusudhan Reddy Bobbili

Vienna, November 2019

Supervisor

Assoc. Prof. Dipl.-Ing. Dr. Johannes Grillari

Arise, Awake and Stop not till the goal is reached...

- *Swami Vivekananda*

AFFIDAVIT

I hereby declare that I am the sole author of this work; no assistance other than that permitted has been used and all quotes and concepts taken from unpublished sources, published literature or the internet in wording or in basic content have been identified with precise source citations.

Ort, Datum

Name

I. Abstract

Extracellular vesicles are cell- derived lipid membrane nanoparticles that serve as messengers of intercellular communication, transferring bioactive molecules such as DNA, RNA, proteins and lipids to recipient cells. EVs have a natural therapeutic potential with high flexibility and biosafety for employing natural and synthetic biomolecules as therapeutic delivery vehicles. Considering the importance of EVs, their isolation methods are still a bottleneck. To get insights into the tissue-specific cargo *in vivo* for complete exploitation of EVs as therapeutic, biomarker and diagnostic tools, EV purification methods are critical. This thesis was brought about to develop an efficient EV purification method both *in vitro* and *in vivo* and to further investigate EVs as therapeutic targets in cellular senescence.

Firstly, to isolate tissue- specific EVs *in vivo* we developed recombinant EVs by genetically fusing snorkel-tag to the tetraspanin (CD81). The snorkel-tag enables on-column protease treatment for purifying EVs which does not rely on traditional immunoaffinity purification protocols using low pH or high salts solutions. We systematically evaluated the purification of EVs harboring snorkel-tag by employing different methodologies. Our findings suggest that EVs harboring snorkel-tag indeed can be purified at high purity without altering EV characteristics and uptake.

Secondly, we previously identified that senescent cells secrete relatively more EVs compared to their counterparts, quiescent cells. We further reported that senescent cell derived EVs are bona fide members of the SASP factors. Therefore, we explored if senescent cell- derived EVs might be a target for anti-senescence therapies. Considering the negative effects of senescent cell derived EVs on tissue microenvironment, we developed neutralizing antibodies for blocking the EV uptake into recipient cells. However, our results demonstrate an enhanced EV uptake when they are in complex with monoclonal antibodies against unknown antigens on EVs, contradicting our initial hypothesis. Henceforth, based on our results, we propose that binding of monoclonal antibodies to unknown antigens on EVs derived from fibroblasts, enhance their uptake into recipient cells. We are currently identifying the antigen to these monoclonal antibodies.

Finally, we are developing an *in vivo* model with recombinant CD81-snorkel-tag under p16^{ink4a} promoter. This will provide us detail insights into the EV cargo secreted from senescent derived cells, by purifying EVs harboring snorkel-tag under pathophysiological conditions, allowing us to develop biomarkers and therapeutic tools.

Summarized, we have here developed novel tools for studying content and function of EVs in the context of aging and disease. These tools will now pave the way for studying the molecular mechanisms underlying these EV functions *in vivo*.

II. Zusammenfassung

Extrazelluläre Vesikel (EVs) sind von Zellen sekretierte Lipidmembran-Nanopartikel, die als Boten der interzellulären Kommunikation dienen und bioaktive Moleküle wie DNA, RNA, Proteine und Lipide an Empfängerzellen übertragen. EVs haben ein natürliches therapeutisches Potenzial mit hoher Flexibilität und biologischer Sicherheit um natürliche und synthetische Biomoleküle spezifische Zielgewebe oder -Zellen zu steuern. Trotz der hohen Bedeutung von EVs, sind derzeit bestehende Isolierungsmethoden immer noch ein Engpass. Diese sind allerdings unabdingbar um Einblicke in die gewebespezifische Beladung für die vollständige Nutzung von EVs als Therapie-, Biomarker- oder Diagnostikum zu gewinnen. Diese Dissertation wurde erstellt, um eine effiziente Methode zur Reinigung von EVs *in vitro* und *in vivo* zu entwickeln und EVs als therapeutische Angriffspunkte in der zellulären Seneszenz weiter zu untersuchen.

Um gewebespezifische EVs *in vivo* zu isolieren, entwickelten wir rekombinante EVs durch genetische Fusion des Schnorchel-Tags mit dem Tetraspanin CD81, einem EV Membranprotein. Der Schnorchel-Tag ermöglicht eine Protease-Behandlung auf der Säule zur Reinigung von EVs, die nicht auf herkömmlichen Protokollen zur Reinigung der Immunaффinität unter Verwendung von Lösungen mit niedrigem pH-Wert oder hohem Salzgehalt beruht. Wir haben die Reinigung von EVs mit Schnorchel-Tag systematisch anhand verschiedener Methoden bewertet. Unsere Ergebnisse legen nahe, dass EVs mit Schnorchel-tag in der Tat mit hoher Reinheit hergestellt werden können, ohne die Eigenschaften oder Funktionalität zu beeinträchtigen.

Vorab konnten wir feststellen, dass seneszente Zellen mehr EVs als junge Zellen ausscheiden und dass diese EVs Mitglieder des ‚senescence associated secretory phenotypes‘ (SASP) sind. Daher untersuchten wir, ob von seneszenten Zellen abgeleitete EVs ein Ziel für Anti-Seneszenz-Therapien sein könnten. In Anbetracht der negativen Auswirkungen von EVs, die von seneszenten Zellen sezerniert werden auf die Gewebemikroumgebung, haben wir neutralisierende Antikörper entwickelt, um die EV-Aufnahme in Empfängerzellen zu blockieren. Unsere Ergebnisse zeigen jedoch eine verbesserte EV-Aufnahme, was unserer ursprünglichen Hypothese widerspricht.

Basierend auf diesen Ergebnissen schlagen wir nun vor, dass die Bindung von monoklonalen Antikörpern an derzeit noch unbekannte Antigenen von EVs, die von Fibroblasten stammen, deren Aufnahme in Empfängerzellen verbessert. Wir identifizieren derzeit die Antigene für diese monoklonalen Antikörper.

Schließlich entwickeln wir ein in-vivo-Modell mit rekombinatem CD81-Schnorchel-Tag unter p16ink4a-Promotor. Auf diese Weise erhalten wir detaillierte Einblicke in die EV Beladung, die aus alternden Zellen sekretiert wird, indem EVs mit Schnorchel-Tags unter pathophysiologischen Bedingungen gereinigt werden, um Biomarker und therapeutische Instrumente zu entwickeln.

Zusammenfassend haben wir hier neue Werkzeuge entwickelt, um den Inhalt und die Funktion von EVs im Kontext von Alterung und Krankheit zu untersuchen. Diese Werkzeuge werden nun den Weg für die Untersuchung der molekularen Mechanismen ebnet, die diesen EV-Funktionen *in vivo* zugrunde liegen.

CONTENTS

1. INTRODUCTION	7
1.1. Background and general overview	7
1.1.1. Cell-derived vesicles	7
1.1.2. History	8
1.2. Extracellular vesicles	9
1.2.1. EV classification and terminology	10
1.2.2. EV biogenesis and secretion	12
1.2.3. Molecular composition of EVs	19
1.2.4. Mechanisms of EV uptake	25
1.2.5. EV isolation methods	32
1.2.6. Characterization of EVs	39
1.2.7. Therapeutic potential of EVs	46
1.3. Aging and cellular senescence	55
1.3.1. Characteristics of cellular senescence	56
1.3.2. Clearance of senescent cells	57
1.3.3. Cellular senescence and EVs	58
2. AIMS	60
3. RESULTS	61
PART A	61
3.1. Establishment of Snorkel-Tag based Extracellular Vesicle Affinity Chromatography (StEVAC) method for recombinant EV purification	61
3.1.1. Design of recombinant tetraspanins for the production of recombinant EVs	61
3.1.2. Characterization of a CD81-snorkel-tag harboring EV producer cell line	65
3.1.3. Isolation of EVs using tangential flow filtration (TFF) and characterization	68
3.1.4. Confirmation of snorkel-tag presence on the recombinant EVs	76
3.1.5. Isolation of EVs by Snorkel-tag based EV Affinity Chromatography (StEVAC)	79
3.1.6. Characterization of EVs purified by StEVAC method	83
3.1.7. Confirming StEVAC as a method for purifying EVs from mixed cell sources of EVs	87
3.1.8. EV uptake studies for snorkel-tag carrying EVs	91
PART B	96
3.2. Evaluation of the neutralizing effect of monoclonal antibodies produced against human dermal fibroblast derived EVs	96
3.2.1. Extracellular vesicles are part of SASP	96
3.2.2. Evidence of extracellular vesicles in human skin	98
3.2.3. Characterization of EVs derived from human dermal fibroblasts for immunizing mice to produce monoclonal antibodies	101
3.2.4. Characterization of monoclonal antibodies	103
3.2.5. The effect of monoclonal antibodies on EV uptake	107
4. DISCUSSION	113
4.1. Establishment of the Snorkel-tag based Extracellular Vesicle Affinity Chromatography (StEVAC) method for recombinant EV purification	113

4.2.	<i>Evaluation of neutralizing effects of monoclonal antibodies produced against human dermal fibroblast EVs</i>	121
4.2.1.	EVs in skin are members of SASP in cellular senescence	121
4.2.2.	Therapeutic potential of senescent cell derived EVs	122
5.	<i>MATERIAL AND METHODS</i>	124
5.1.	<i>Material</i>	124
5.1.1.	Sequences:	124
5.1.2.	Primers	129
5.1.3.	Antibodies	130
5.2.	<i>Methods</i>	131
5.2.1.	Cell culture	131
5.2.2.	Stress induced premature senescence (SIPS)	132
5.2.3.	Generation of stable cell lines	132
5.2.4.	EV isolation procedures	133
5.2.5.	Nanoparticle Tracking Analysis (NTA)	135
5.2.6.	Snorkel-tag based Extracellular Vesicle Affinity Chromatography (StEVAC)	137
5.2.7.	Western blotting	137
5.2.8.	CLIP-tag labeling quantification by Flow cytometry	138
5.2.9.	Multiplex bead-based flow cytometry assay for EV surface protein profiling	139
5.2.10.	EV uptake assays using flow cytometry	140
5.2.11.	EV uptake study using confocal imaging	141
5.2.12.	Immunofluorescence staining of cells	142
5.2.13.	Transmission Electron Microscopy (TEM)	142
5.2.14.	Cre-loxP method for studying EV uptake	145
5.2.15.	Statistical analysis	145
6.	<i>SUPPLEMENTARY MATERIAL</i>	146
7.	<i>REFERENCES</i>	173
8.	<i>APPENDIX I</i>	216
8.1.	<i>List of figures</i>	216
8.2.	<i>List of tables</i>	218
8.3.	<i>Abbreviations</i>	218
9.	<i>APPENDIX II</i>	227
9.1.	<i>Publications</i>	227
10.	<i>APPENDIX III</i>	Error! Bookmark not defined.
10.1.	<i>Curriculum Vitae</i>	Error! Bookmark not defined.

1. INTRODUCTION

1.1. Background and general overview

1.1.1. Cell-derived vesicles

Intercellular communication is an important hallmark for cell-to-cell communication. Cells exchange information by direct interaction or by secretion of soluble proteins like growth hormones, cytokines, chemokines etc. In addition, cells release spherical particles enclosed by a phospholipid bilayer into the extracellular environment that can have impact on both neighboring and distinct cells. Body fluids such as blood, urine and saliva, but also conditioned cell culture media are enriched with these cell-derived vesicles. These cell-derived vesicles can be purified from almost all mammalian cells, namely for example primary cells, stem cells, immune cells, tumor cells. Following the current opinion, importance of cell-derived vesicles is not restricted to higher eukaryotes but also to lower eukaryotes and prokaryotes like bacteria and fungi. The diameter of these cell-derived vesicles ranges from 30 nm-1 μ m. Due to their heterogeneity and small size, their isolation, classification and detection is challenging. Although there are different types of cell-derived vesicles have been identified, “exosomes” and “microvesicles” are commonly used terminologies in the literature.

Recently, cell-derived vesicles have gained significant importance due to their innate ability to transfer cargo like DNA, RNA, proteins, lipids and metabolites from the donor cell to recipient cells within or between tissues either by paracrine or endocrine mode of communication. Since then, cell-derived vesicles have also been actively investigated under pathophysiological conditions. Recent developments have shown that these cell-derived vesicles secreted in the periphery can enter the central nervous system (CNS), pass the blood-brain barrier (BBB) and thus provide possible prospects for diagnostics and

treatment of neuroinflammatory/neurodegenerative diseases. Cell-derived vesicles, mainly exosomes and microvesicles are broadly considered as extracellular vesicles (EVs) which are intensively studied in normal biological processes as well as in diseased conditions to develop potential diagnostic markers and therapeutic interventions.

1.1.2. History

The first discovery of EVs dates back to 1940, describing the clotting factor isolation via high-speed centrifugation from plasma and modulation of clotting time (CHARGAFF and WEST 1946). Almost two decades later, in 1967 Wolf et. al., published the first evidence of cell-derived vesicles, originating from platelets and termed “platelet dust”(Wolf 1967). Electron microscopy images revealed that the size of these platelet dust particles was between 200 and 500 Å. In 1975, Dalton described that the fetal calf serum contains “extracellular microvesicles” with a diameter between 30-60 nm. Two years later, in 1981 Trams et al. proposed the term “exosomes” for the vesicles derived from plasma membrane (Trams et al. 1981). A couple of years later, studies on the transferrin receptor, a membrane protein, suggested that exosomes are formed in multivesicular bodies (MVBs) for segregating and that plasma membrane proteins are secreted via exosomes (Johnstone et al. 1987). Consequently, the term “exosomes” came into existence and has been widely accepted in the scientific community. Thereafter, EV research was largely neglected as cell-derived vesicles were considered being the “garbage bags” of cells until the functionality of EVs was shown. In 1996, Raposo et al. described that exosomes secreted from B lymphocytes carrying MHC class II are able to trigger T cell response, pointing towards a functional role of EVs in cell-to-cell communication (Raposo et al. 1996).

In the following years, important milestones in EV-research were the discoveries of horizontal transfer of genetic material like mRNA and microRNA between cells (Ratajczak et al. 2006), as well as EVs from periphery being able to cross blood-brain-barrier (EL Andaloussi et al. 2013). These discoveries paved the way for enormous and diverse EV-

research over several fields decoding the cargo carried by EVs in natural biological processes and pathophysiological conditions to exploit the underlying potential for therapeutic purposes.

1.2. *Extracellular vesicles*

Ever since the discovery of cell-derived vesicles, their reputation in the scientific field has changed from being the cells' garbage bags to being described as "extracellular vesicles", implying knowledge on their mode of secretion and most importantly their role as natural carriers of cargo. Hand in hand goes the constant urge for improved tools and methods for EV isolation and quantification. Investigations on extracellular vesicles have become a common object, literally in every field of biomedicine. EVs are ubiquitous, they are released from bacteria as well as from every single cell in multicellular organisms. EVs as a natural delivery vectors have the ability to transfer nucleic acids, proteins, lipids and metabolites to neighboring cells and are thus regulating the function of the recipient cells. In the pioneering text from *Gould and Hildreth*, they hypothesized about the similarities between retroviral and EV biogenesis; secretion and uptake, proposing "The Trojan exosome hypothesis" (Gould, Booth, and Hildreth 2003).

In recent years, explosion of new data on EVs paved the way for new fields of research. In spite of the guidelines set by the International Society for Extracellular Vesicles (ISEV) aiming at unifying nomenclature, isolation methods, characterization and information on EV profiles (subsumized under the term 'MISEV'), there is still a lack of standardization and consensus among researchers, as many aspects of EV research like their release mechanisms, terminologies and classification, cargo incorporation and delivery of bioactive molecules to recipient cells still remain a mystery. Here, I discuss the actual status quo on EV research with regard to their classification, terminologies, secretion mechanisms, isolation methods, mode of uptake and their therapeutic potential.

1.2.1. EV classification and terminology

Due to the heterogeneity in size and difficulties with the detection, all secreted membrane vesicles are generically termed EVs. Based on current knowledge about their size and biogenesis, EVs are classified into two categories, namely “exosomes” and “microvesicles”. Due to multidisciplinary research fields, sometimes the classification is also based on their specific function or the type of the cell or tissue they originate. For example, EVs derived from prostate are termed as “prostasomes” (Stegmayr and Ronquist 1982), the term “dexosomes” (Le Pecq 2005) is used for exosomes released from dendritic cells, “tolerosomes” (Karlsson et al. 2001) are exosomes which induce immunological tolerance to dietary antigens, “synaptic vesicles” are shedded by neurons (G. Fischer et al. 1990), the term “oncosomes” is used for vesicles that are derived from tumor cells (Li et al. 2012; Sedgwick et al. 2015), “apoptotic bodies” are formed by dying cells (Théry, Ostrowski, and Segura 2009; Mathivanan, Ji, and Simpson 2010), “migrasomes” are vesicles that transport cytoplasmic contents during cell migration (Ma et al. 2015).

As mentioned above, based on biogenesis, EVs are in general broadly classified into exosomes and microvesicles. Exosomes are intraluminal vesicles (ILVs) formed within multivesicular bodies (MVBs) via inward budding of their membrane and are released into extracellular space by fusion of MVBs to the plasma membrane. Typically, their size ranges between 30-120 nm in diameter. Microvesicles range in size from 100-1000 nm in diameter and are formed by budding of the plasma membrane into the extracellular environment. In case of oncosomes, they can have a size of up to 10 μ m. Apoptotic bodies, which are considered as one of the EV subgroups, originate from plasma membrane blebbing and carry contents from deriving from endoplasmic reticulum as well as nuclear fragments and their size ranges between 1000- 5000 nm.

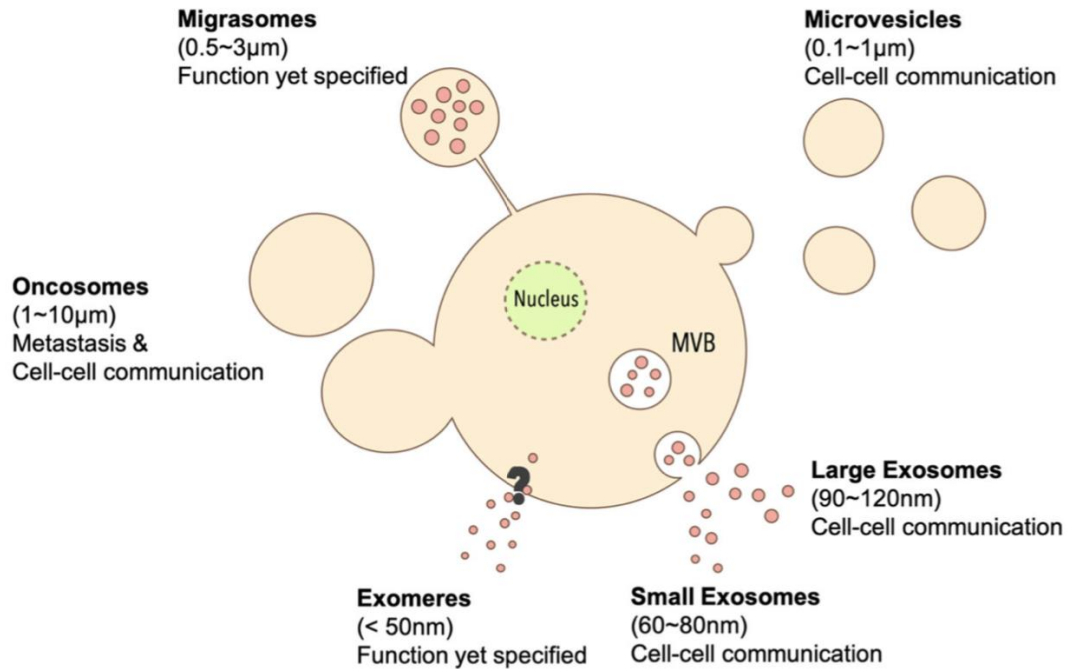


Figure 1: Schematic view of different EV subpopulations.

From Chuo et al. journal of Biomedical Science (2018) 21:91

Zhang et al. described the new subtypes of EVs such as small-exosomes (Exo-S), large-exosomes (Exo-L) and exomeres (H. Zhang and Lyden 2019). Using the state-of-the-art asymmetric flow field-flow fractionation (AF4) technology, they were able to separate two subpopulations of exosomes and discovered non-membranous nanoparticles termed as “exomeres” that exhibit distinct molecular and biophysical properties. The exomeres (~35 nm) showed different biophysical properties compared to Exo-S (60-80 nm) and Exo-L (90-120 nm) derived from endosomal sorting (H. Zhang et al. 2018). Results also demonstrate that single subtypes of EVs are enriched with specific cargo in terms of nucleic acids, lipids, proteins and their glycosylation patterns. These discoveries further opened new avenues in unraveling the role of different subtypes of EVs in cellular and organ function. Furthermore, the increasing number of reports on EV subtypes, nomenclature and characterization led to a good deal of confusion concerning nomenclature and data interpretation. In the light of these issues and to circumvent the confusion with nomenclature and data interpretation, ISEV established the so called Minimal Information

for Studies of Extracellular Vesicles (MISEV 2018) (Théry et al. 2018), a comprehensive guidelines provides a minimal set of biophysical, biochemical and functional standards that should be met to determine the subtype or specific biological cargo or function of EVs. At last, sophisticated nomenclature is required considering the EV subtype biogenesis and their functional implication on recipient cells. Here, I use the generic term EVs to refer to all the cell-derived membranous nanoparticles except for apoptotic bodies.

1.2.2. EV biogenesis and secretion

A major part of communication within the cells is achieved by the vesicles between different compartments of cells via intracellular-vesicle transport. Vesicular transport enables exchange of cargo between different cell compartments. Two major pathways involving vesicular transport are exocytic and endocytic pathways. In the exocytic pathway, proteins or metabolites which are synthesized within the cytoplasm or different organelles are carried by intracellular vesicles and released to the extracellular environment by fusion of the vesicles to the plasma membrane. This also enables the transport of plasma membrane proteins, which are synthesized in endoplasmic reticulum, to its destiny (Chieriegatti and Meldolesi 2005; Verhage and Sørensen 2008; Liang, Wei, and Chen 2017). On the other hand, in the endocytic pathway, proteins and membranes are internalized forming clathrin-coated vesicles. Later, these clathrin-coated vesicles proceed to form early and late endosomes (Elkin, Lakoduk, and Schmid 2016). The cargo from late endosomes is sorted to the plasma membrane, recycled, or transported to the lysosomes for degradation (Pryor and Luzio 2009). During the latter process, the late endosomes accumulate ILVs in their lumen. The ILVs that are formed by inward budding of late endosomal membranes, during this process the membrane proteins, lipids and cytosol components like nucleic acids, proteins are specifically sorted into these vesicles. These late endosomes containing a multitude of small vesicles are termed MVBs. The main fate of MVBs is to fuse to lysosomes where their contents get degraded due to the acidic nature of lysosomes (Piper and Katzmann 2010). However, some MVBs escape endosomal

degradation routes which ultimately leads to the release of exosomes into the extracellular milieu (Vidal & Stahl 1993). The discoveries of these degradation escape routes of the endosomal system revealed a number of different components involved in exosome biogenesis.

1.2.2.1. Exosome Biogenesis

The formation of exosomes in the MVBs is driven mainly by the endosomal sorting complex required for transport (ESCRT) or by tetraspanin CD63. However, reports show that inactivation of ESCRT also led to the formation of MVBs suggesting ESCRT-independent mechanism. Therefore, the exosome biogenesis is mainly driven by two intracellular pathways: ESCRT-dependent and -independent pathways.

ESCRT-dependent pathway: ESCRT-dependent exosome biogenesis is driven by approximately 30 proteins building four complexes (ESCRT-0, -I, -II, -III) which are further associated with proteins like AGL-2-interacting protein X (ALIX/PDCD6IP), syntenin, syndecan and VPS4. Recent studies reveal downregulation of syntenin, syndecan and ALIX impairs the exosome release and overexpression of syntenin induces an increase in ALIX-dependent exosome release. Furthermore, ESCRT-dependent exosomes release is depend on the function of ESCRT-I, -II, -III and VPS4 and their associated protein (syntenin, syndecan and ALIX). Possible mechanisms for ESCRT-driven MVB formation were well described in many studies (Hanson and Cashikar 2012) outlining the involvement of different components of ESCRT-0, -I, -II and-III complexes. The components of ESCRT-0, Hepatocyte growth factor–regulated tyrosine kinase substrate (HRS) (Tamai et al. 2010; Gross et al. 2012) and signal transducing adaptor molecule (STAM) (Colombo et al. 2013) are involved in the recognition and binding of ubiquitinated cargo protein on the endosomal outer membrane upon stimulation by phosphatidylinositol 3-phosphate (PIP3) (Shields et al. 2009; Katzmann, Babst, and Emr 2001; Fernandez-Borja et al. 1999). Tumor susceptibility gene 101 (TSG101), a component of ESCRT-I complex

is recruited by HRS (Bache et al. 2003), upon which MVB protein 4A (CHMP4A) components of the ESCRT-III, associates with TSG101 via ESCRT-II or ALIX (Baietti et al. 2012). Therefore, ESCRT-I and -II are considered as the initiators of the intraluminal membrane budding (Henne, Stenmark, and Emr 2013). Formation of ESCRT complex on the endosomal membrane recruits deubiquitinating enzymes, which removes the ubiquitin from the cargo proteins before sorting them into ILV. Finally, AAA-ATPase suppressor-of-potassium-transport-growth-defect-1 protein (SKD1) is involved in the recycling of the ESCRT machinery (Bishop and Woodman 2001; Liégeois et al. 2006).

The importance of the ESCRT machinery in MVB formation is well understood due to knockdown studies. Reports suggest that HRS-depletion in dendritic cells (Tamai et al. 2010) and HEK293 cells (Gross et al. 2012) showed reduced exosome secretion. A comprehensive study by Colombo et al. gives an overview of individual proteins involved in MVB formation (Colombo et al. 2013). The results show that silencing of the components of ESCRT-0/I (HRS, STAM and TSG101) in HeLa cells decreased exosome secretion and associated proteins (CD63, MHC II) but also these proteins might act differently during exosome biogenesis and secretion (Colombo et al. 2013). Depletion of HRS resulted in reduced secretion of exosomes with a diameter between 50-200 nm, whereas depletion of STAM1 decreased the secretion of particles with 30-100 nm diameter. These results suggest that individual components of ESCRT-0 are involved in the secretion of different population of exosomes. Silencing TSG101 on the other hand resulted in vesicles devoid of CD63 and MHC II in all size categories, suggesting that it is mainly involved in sorting the cargoes into ILVs. On contrary, depletion of VPS4B resulted in increased exosome secretion of all sizes without altering their composition, whereas depletion of ALIX led to an increase in MHC II levels in exosomes without affecting the levels of exosome secretion. Further, Baietti et al. showed that the depletion of ALIX decreases the exosome secretion and that overexpression of syntenin enhances the increase in exosome biogenesis and secretion in MCF7 cells (Baietti et al. 2012). Syndecan-syntenin-ALIX mediated exosome biogenesis is suggested to be an alternative ESCRT pathway (Baietti et al. 2012). Here the biogenesis of exosomes is dependent on heparinase

stimulation and ILV budding is controlled by ADP ribosylation factor 6 (ARF6) and phospholipase D2 (PLD2).

In summary, ESCRT-dependent exosome biogenesis involves multiple mechanism which as a result determines the type of exosomes and their composition. MVB associated proteins like syntenin, HRS, TSG101 and ALIX play a crucial role in exosome biogenesis and cargo sorting. This highlights the molecular and mechanistic heterogeneity of the different types of EVs secreted from different cell types.

ESCRT-independent pathway: Stuffers et al. reported that the inactivation of all four ESCRT complexes by combinatorial knockdown did not alter the MVB formation and exosome secretion, suggesting the existence of an ESCRT-independent exosome biogenesis(Stuffers et al. 2009). Similarly, Trajkovic et al. 2008 demonstrated that exosome biogenesis can occur independently of the ESCRT complex in oligodendroglial cells (Trajkovic et al. 2008). The knockdown of TSG101, ALIX or HRS neither had influence on inward budding of PLP nor on colocalization of proteolipid protein (PLP) and LAMP1. In experiments, where cells were treated with GW4869, a neutral sphingomyelinase (nSMase; enzyme required for ceramide synthesis) inhibitor, treated cells showed reduced exosomes release (Trajkovic et al. 2008). The hydrolysis of sphingomyelin to ceramide by nSMase leads to a negative curvature on the membranes and subsequently to generation of subdomains similar to lipid rafts initiating ILVs in MVBs.

Recent studies have also shown that CD63-dependent ILV formation is independent of ESCRT and ceramide pathways. CD63 is a tetraspanin protein mainly enriched in lipid microdomains that has the potential to recruit ESCRT-independent components for ILV formation. It was shown that CD63 is not only involved in sorting of PMEL protein (Theos et al. 2006) into ILVs but also in their formation.

To conclude, exosome biogenesis is certainly complex, influenced by different stimuli. Several mechanisms could act concomitantly or sequentially in the formation of MVBs and could be targeted by different sorting machineries. The complexity of the mechanisms of exosome biogenesis can help to explain the heterogeneity of EVs originating from a single cell or different cell type. However, it also highlights the need for better techniques to differentiate between those EVs derived by the various biogenesis pathways to then also have ultimately a clear nomenclature for these still heterogeneously appearing particles.

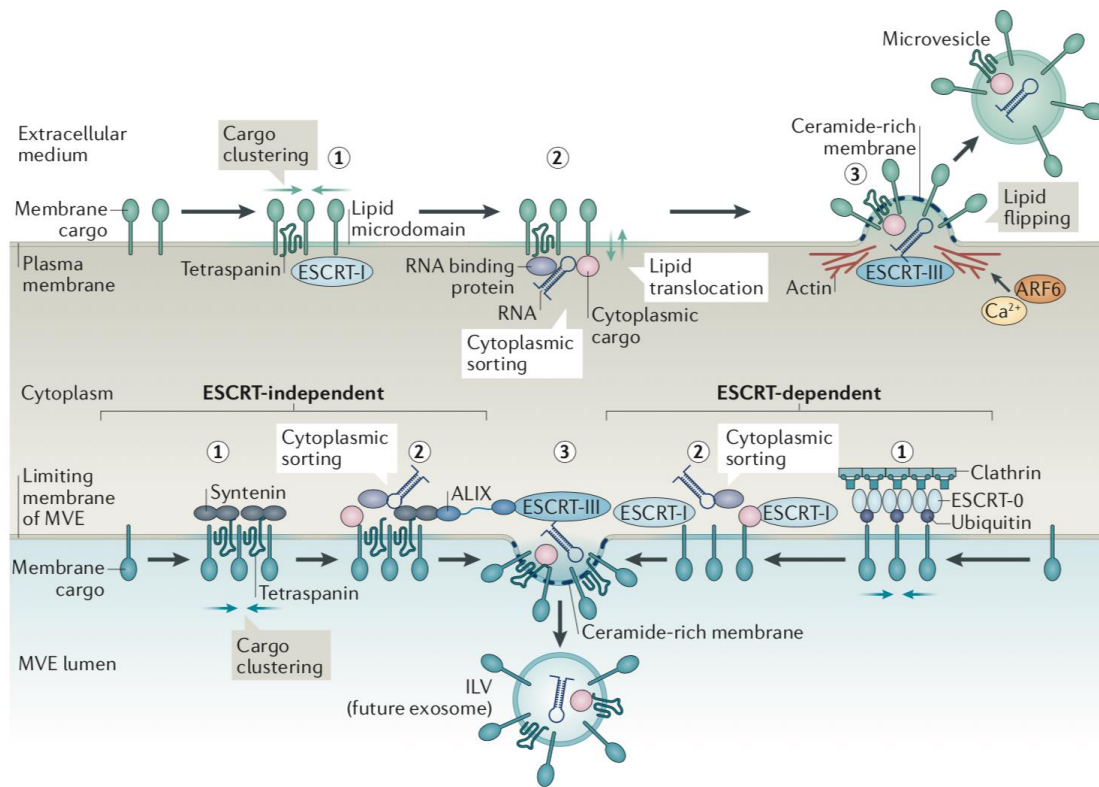


Figure 2: Biogenesis of extracellular vesicles.

Several sorting machineries are involved in the different steps required for generating exosomes and microvesicles. First, lipids and membrane-associated proteins are clustered in discrete membrane microdomains of the plasma membrane for microvesicles (top) and of the limiting membrane of the multivesicular endosome (MVE) for exosomes (bottom) (step 1). Such microdomains certainly also participate in the recruitment of soluble components, such as cytosolic

proteins and RNA species, that are fated for sorting in extracellular vesicles (step 2). Altogether, formation of these clustered microdomains together with additional machineries promotes membrane budding followed by a fission process either at the plasma membrane towards the extracellular medium or at the limiting membrane of the MVE towards the lumen of the MVE (step 3). Transmembrane proteins sorted on exosomes and microvesicles keep the same topology as at the plasma membrane. Mechanisms of exosome biogenesis are fairly well understood and importantly involve subunits of endosomal sorting complex required for transport (ESCRT), although to different degrees — ESCRT- III is required for the scission of the intraluminal vesicles (ILVs) into the MVE lumen, but cargo clustering and membrane budding can occur by either ESCRT- dependent or ESCRT- independent mechanisms. *From Niel et al. Nat Rev Mol Cell Biol. 2018 Apr;19(4):213-228.*

1.2.2.2. Microvesicle biogenesis

MV biogenesis is far less complex and less defined than that of exosomes. MVs or plasma membrane-derived vesicles are formed by outward budding and fission of the plasma membrane and the mechanisms involved in their secretion have recently started to emerge. The biogenesis of microvesicles involves a cascade of events such as phospholipid rearrangements, change of Ca^{2+} levels, Ca^{2+} dependent enzymatic processes and cytoskeletal remodeling (Akers et al. 2013). Membrane asymmetry is achieved by a combination of factors that induce the activation of aminophospholipid translocases (flippases and floppases) which drive the exposition of phosphatidylserine from inner leaflet to the outer leaflet of the plasma membrane. This causes physical bending and cytoskeletal remodeling underneath the plasma membrane (Hugel et al. 2005). In addition, ARF6 and myosin light chain kinase (MLCK) are involved in actin-myosin restructuring which triggers the release of MVs (Muralidharan-Chari et al. 2009). It has recently been shown that RAB22A promotes the release of MVs in tumor cells under hypoxia (T. Wang et al. 2014). Interestingly, a recent study provided evidence for the presence of TSG101, a component of the ESCRT-I complex in MVs, suggesting a possible role of TSG101 in MV secretion in addition to the one in exosome secretion. For this, interaction of TSG101

with arrestin domain–containing protein 1 (ARRDC1) at the plasma membrane promotes the outward budding of EVs (Nabhan et al. 2012). As for the cargo of MVs, the cytoplasmic components fated for secretion are anchored to the inner leaflet of the plasma membrane either by palmitoylation, prenylation or myristoylation. It is still unclear how nucleic acids are targeted to the plasma membrane and sorted into MVs. Figure 2 illustrates the biogenesis of exosomes and microvesicles.

1.2.2.3. Secretion of extracellular vesicles

The secretion mechanisms for microvesicles are generally fast and simple, once they are generated, they pinch off from the plasma membrane into the extracellular milieu, whereas secretion of exosomes is characterized by complex mechanisms involving additional regulatory checkpoints. Primarily, MVBs have been considered locations of lysosomal degradation, however, recent discoveries of lysosomal degradation escape routes sheds light on how balance is kept between targeting MVBs for degradation and secretion. Similar to exosome biogenesis, a variety of mechanisms are proposed for the secretion of exosomes. The secretion of exosomes requires tightly regulated steps of transport, docking and fusion of MVBs to the plasma membrane. Targeting MVBs to the plasma membrane occurs by anterograde transport via the microtubule network. The ubiquitylation status of RAB7 determines the fate of MVBs either to lysosomes or to plasma membrane. Interestingly, exosomes released by breast tumor cells via RAB7 are enriched for ALIX and syntaxin (Baietti et al. 2012). Although RAB27A and RAB27B are the main regulators for exosome secretion (Ostrowski et al. 2010), a number of Rab GTPases are recognized as key players, including RAB11 (Savina et al. 2005) and RAB35 (Hsu et al. 2010). RAB27B regulates the motility of MVBs to the plasma membrane and RAB27A promotes docking and fusion to the plasma membrane. The exosomes released via RAB27A and RAB27B are enriched with late endosomal proteins like ALIX, CD63 and TSG101 whereas, the exosome release facilitated by RAB11 and RAB35 are enriched for flotillin and cell-specific proteins like Wnt, PLP and Transferrin receptor (TfR) (Laulagnier et al. 2004).

Once the MVBs reach the vicinity of the plasma membrane, the final steps of the exosome release require docking and fusion to the plasma membrane. SNAREs [for soluble N-ethylmaleimide-sensitive fusion attachment protein (SNAP) receptors], are well studied in the synaptic vesicle exocytosis; secretion of neurotransmitters and peptides/neuromodulators at nerve terminals. In general, v-SNARE (a vesicle membrane protein) and t-SNARE (a target membrane protein) form complexes with SNAPs docking the vesicles to membrane. Following the trigger by Ca^{2+} influx the docked vesicles fuse to the plasma membrane. Accumulating evidence suggests that SNAP23 at the plasma membrane and VAMP7 on lysosomes promote Ca^{2+} -regulated MVB exocytosis in epithelial cells and neutrophils (Rao et al. 2004; Logan et al. 2006). The diversity involved in exosome secretion, depending on the cell type and MVB subtype, distinct SNAREs maybe involved in regulating exosome release. The role of SNAREs in exosome release so far is poorly studied and a better understanding certainly requires new techniques and tools to follow the docking and fusion mechanisms.

Thus, secretion of MVBs involves complex mechanisms regulated by different proteins and lipids. Additionally, different MVB subclasses add an extra layer of complexity to the process as these themselves can contain different population of ILVs.

1.2.3. Molecular composition of EVs

EVs, a heterogenous group of cell-derived vesicles, are important mediators for intercellular communication via transfer of functional biomolecules, including proteins, lipids and nucleic acids. The first breakthrough in the field of determining EVs as a natural carrier happened in 2007, when Valadi et al. demonstrated that mRNA and miRNA shuttled via exosomes regulate the recipient cells (Valadi et al. 2007). Since then, there is an increasing research in understanding the cargoes of EVs, which has resulted in the

assembly of three different databases (Exocarta (Mathivanan et al. 2012; Mathivanan and Simpson 2009; Keerthikumar et al. 2016; Simpson, Kalra, and Mathivanan 2012), Vesiclepedia (Kalra et al. 2012), and EVpedia (D. K. Kim et al. 2013)) collecting datasets from various EV studies. These databases include information on proteins, lipids and nucleic acid content in EVs alongside with their isolation and purification procedures used. However, the nature and abundance of EV cargos is determined by the mechanisms of EV biogenesis, cell-type or vesicle-specific per se and often influenced by the pathophysiological state of the donor cell. Hereafter, the EV cargo with respect to proteins, lipids and nucleic acids composition will be discussed in more detail. Molecular composition of exosomes and microvesicles are represented in brief in Figure: 3

1.2.3.1. Proteins

Proteins are the most abundant biomolecules in EVs and are often related to the cell-type and mode of biogenesis. Proteomic analysis techniques allowed large-scale identification of nonpredetermined in EV preparations. The abundance of proteins in EVs is often exploited for the characterization and for determining the purity of EVs after different preparations, because of their heterogeneity in types and varying composition from EVs derived from the same cell. Furthermore, different isolation and purification methods enriches different mixtures of EV subgroups. Nevertheless, it is often recommended to probe for a combination of surface and luminal markers for the characterization of isolated EVs.

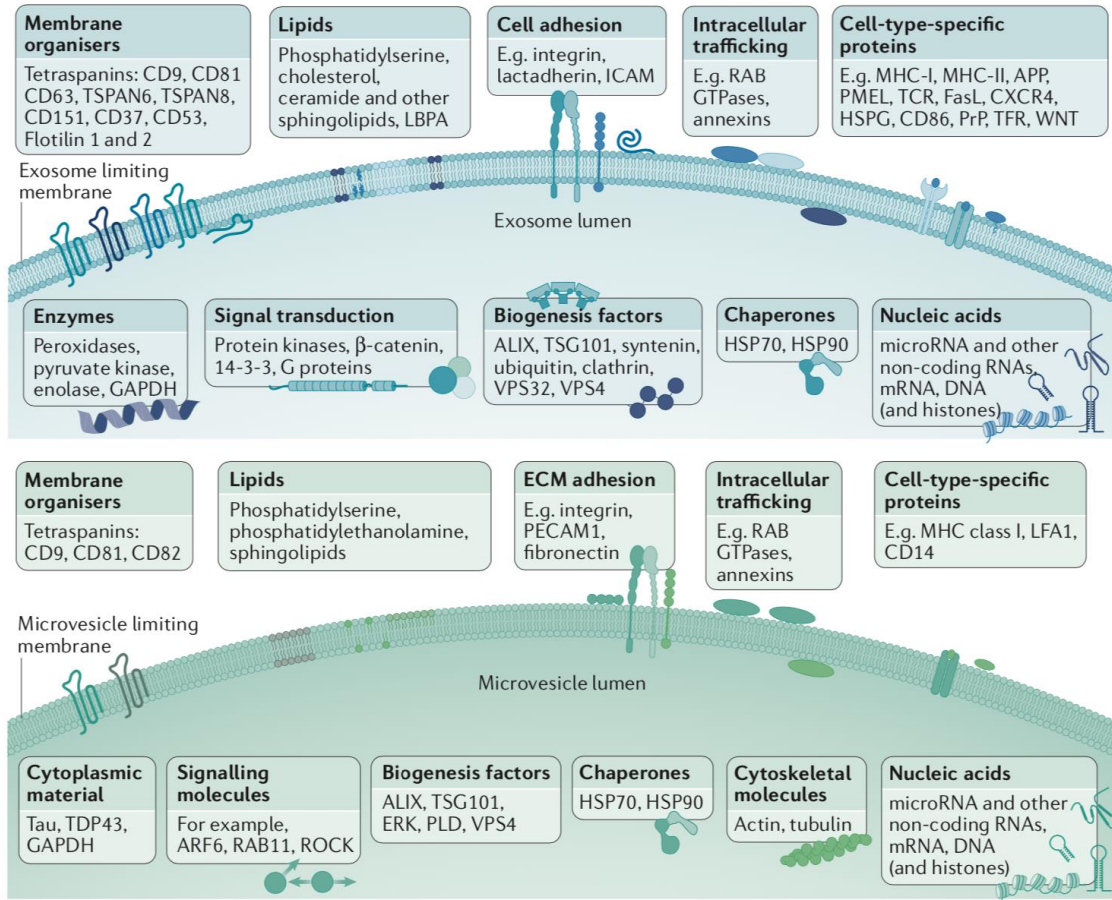


Figure 3: Main features of extracellular vesicles

General molecular composition of microvesicles (top) and exosomes (bottom). *From Niel et al. Nat Rev Mol Cell Biol. 2018 Apr;19(4):213-228.*

The protein content in EVs is determined by their mode of biogenesis. Almost all exosomes which are secreted via the endosomal pathway contain proteins related to MVB biogenesis (ALIX, TSG101, syntenin, CD9, CD63, CD81) and proteins involved in MVB transport and fission (Rab GTPases, flotillin, VAMP7). However, presence of CD9, CD63 and CD81 are regularly observed in plasma-membrane derived EVs (Reka A. Haraszti et al. 2016a). Proteomic studies showed that exosomes contain both, cellular proteins involved in their biogenesis and also proteins from endosomes, plasma membrane and cytosol. Proteins from other cellular compartments such as the endoplasmic reticulum, mitochondria and

nucleus are often absent in EVs. To determine the purity of EVs it is recommended to probe for the absence of markers from other cellular compartments; Calnexin and HSP90B1 for ER; GP130 for the golgi complex and cytochrome C for mitochondria (Théry, Ostrowski, and Segura 2009; Théry et al. 2001). Nevertheless, ER-derived chaperones (HSPs) and nuclear markers like histones are still frequently detected in EVs contributing to their physiological phenomenon. Exosomes secreted via ESCRT mechanisms are generally enriched with proteins associated to ESCRT complexes like ALIX, TSG101, CHMP4B, syntenin and syndecan. The protein composition of different EV subtypes shows a large overlap, however, some proteins are highly enriched in one subtype, suggesting the importance of the isolation techniques.

The sorting of the protein cargos into EVs is dependent on their post-translational modifications like ubiquitination, phosphorylation, sumoylation, glycosylation and ISGylation. Kowal J et al., performed comprehensive comparative proteomic analysis of different subtypes of EVs secreted from HeLa-CIITA and DC cells to define novel markers for EV subtypes (Kowal et al. 2016). EVs isolated via density gradient from a 100K pellet of ultracentrifugation showed two subtypes, namely s-EVs and l-EVs with syntenin- 1, TSG101, ADAM10, and EHD4 as markers for s-EVs; actinin-4 and mitofilin qualified as markers for the large- and medium-sized EVs. Immuno-isolation of EV subtypes using anti-tetraspanin antibodies (targeting CD9, CD63 and CD81) from 100K pellets of ultracentrifugation are significantly enriched with proteins involved in the endosomal pathway. These results emphasize that sEVs not bearing tetraspanins do not correspond to the original definition of exosomes (Kowal et al. 2016).

On the other hand, MVs carry proteins that are involved in their budding process such as AARDC1, ARF6 and cytoskeletal remodeling proteins. Using SILAC quantitative proteomics analysis, Palmisano et al., compared the proteome of exosomes and microvesicles (Palmisano et al. 2012). The study identified that MVs are highly enriched with proteins with post-translational modifications like glycosylation and phosphorylation. All the studies mentioned above show that vesicular protein compositions differ between

different subtypes and highlights the importance of standardizing isolation and quantification methods for identifying reliable EV protein components.

1.2.3.2. Lipids

Just like proteins, lipids play an important role in EV biogenesis and uptake mechanisms. A comparative lipidome analysis of exosomes and microvesicles identified 1961 lipid species and showed that lipid enrichment in EVs is cell type specific. In general, EVs are enriched with sphingomyelin, PS, cholesterol, ganglioside GM3, and ceramide or its derivatives. In addition, enrichment of lipid classes and species in EVs varies in different settings. Two independent studies (Brzozowski et al. 2018; Llorente et al. 2013) show that sphingomyelin, glycerophospholipids, cholesterol and phosphatidylserine are enriched in exosomes secreted from metastatic cells. These results demonstrate the presence of subdomains on EVs with features similar to PM lipid rafts, which is consistent with the presence of lipid raft-associated proteins, flotillins and GPI-anchored proteins (Wubbolts et al. 2003). Although the MV lipid composition is similar to the PM of the donor cell, recent observations have unraveled that the enrichment of phosphatidylserine in MVs is less compared to that of the exosomes. The differences in the lipid composition in different types of EVs reflect their biogenesis, cell type and pathophysiological conditions. Unlike the characterization of protein and nucleic acids in EVs, the EV lipidome is poorly studied so far and deeper understanding of EV lipid species such as lysopalmitoylphosphatidylcholine (Pils V et al. in preparation) may represent an unique biomarkers for different diseases.

1.2.3.3. Nucleic acids

Ever since the first report on functional EV cargo, transfer research in understanding the cargoes of EVs has been exploded. In 2007, Jan Lötvald and colleagues demonstrated that exosomes from MC/9 and HMC-1 (mouse and human mast cell lines, respectively) and primary bone marrow-derived mouse mast cells contain large amounts of mRNA, including miRNAs and small RNAs (Valadi et al. 2007). Microarray assessment revealed

the presence of ~1300 gene transcripts in exosomes, and out of which 270 mRNA transcripts were exclusively present in the exosomes and not in the cytoplasm of the donor cell. Importantly, the packaged mRNA was functional, as new mouse protein in human mast cells after the transfer of exosomes from mouse mast cells was observed. Henceforth, RNA packaged and shuttled to distinct cells via exosomes was termed as “exosomal shuttle RNA” (esRNA). These observations boosted the field and led to further explore on understanding the transfer of functional cargo via EVs. In general, EVs contain potentially active RNA species such as mRNA, miRNA, rRNA, mtRNA (mitochondrial RNA), coding and non-coding RNA, piwi-interacting RNA, tRNA, small nuclear and nucleolar RNA, VT-RNA (vault RNA) and Y-RNA, along with RNA binding proteins that are probably involved in RNA selection and sorting.

EV encapsulated RNA transfer has gained significant importance due to the profound impact on the regulation of the recipient cell, resulting in the novel protein production via mRNA or miRNA mediated regulation of gene expression (Valadi et al. 2007; Skog et al. 2008; Van Der Vos et al. 2016). RNA packing mechanisms into EVs are still poorly understood. After initially random packaging was the common understanding, later on, it was revealed that sorting of miRNA into vesicles is driven either by Ago2 protein or by ribonucleoproteins. Bioinformatic analysis identified specific RNA nucleotide motifs that are enriched in the RNAs sorted to exosomes (Van Der Vos et al. 2016) followed by identifying RNA binding proteins like e.g. NSUN2 [tRNA (Cytosine(34)-C(5))-Methyltransferase] and Y-B1 [Y-box binding protein] that bind to these motifs on exosomal mRNA and miRNA (Kossinova et al. 2017). miRNA packaging into EVs could also be driven by RNA-binding protein, as for instance in T-cells, where hnRBPA2B1 (heterogenous RNA-binding protein A2/B1) binds to GGAG motifs (EXOmotifs) on miRNA. Moreover, hnRBPA2B1 is sumoylated in exosomes and consequently, the interaction between sumoylated hnRBPA2B1 and EXOmotifs on miRNAs and its high affinity to ceramide-rich regions in the lipid rafts drives sorting of miRNAs into exosomes (Villarroya-Beltri et al. 2013). Santangelo et al. identified SYNCRIP (synaptotagmin-binding cytoplasmic RNA-interacting protein; also known as hnRNP-Q or NSAP1) with

binding affinity to miRNAs sharing GGUC as EXOmotif and influencing their exosomal compartmentalization. Mutations in the GGUC sequence impaired the binding of SYNCRIP to miRNAs and an insertion of the GGUC motif significantly increased exosome/cellular ratio (Santangelo et al. 2016). In addition, Terlecki-Zaniewicz et al. showed differentially loading of miRNAs into exosomes is not only cell type specific but also on cell condition (Terlecki-Zaniewicz et al. 2018). These results confirm that RNA packing into exosomes is well regulated mechanism and cell type specific. However, improved understanding of RNA composition and sorting mechanisms into EVs is crucial in order to develop RNAs, especially miRNAs as a potential biomarkers for diagnostic of different diseases (Weilner, Schraml, et al. 2016).

1.2.4. Mechanisms of EV uptake

Seeing EVs as natural carrier vehicle in the cell-to-cell communication implies that EVs secreted into extracellular space must interact with the recipient cell and/or deliver their contents to have an impact on recipient cell physiology. EV-mediated cell-to-cell communication requires docking at the plasma membrane, activation of surface molecules, followed by internalization or fusion to the plasma membrane of the recipient cell. So far, it has been proposed that the internalization of EVs is mediated via endocytosis or direct fusion of the vesicles to the plasma membrane and consequent release of their contents. Endocytosis of EVs can involve different mechanisms depending on the surface molecule interactions. Nevertheless, it has been proposed that endocytosis of EVs can be categorized into different types such as caveolin-, clathrin-, lipid raft-mediated endocytosis, phagocytosis and macropinocytosis (Figure 4). In some cases, the surface interaction of EVs with the target cell is sufficient to lead to the physiological changes. Understanding the mechanisms involved in EV uptake is gaining its importance alongside with insights into the cargo loading machinery in order to improve the development of EV therapeutics.

1.2.4.1. Docking or surface molecule interaction

The first step in EV uptake is the interaction of surface molecules from EVs and the plasma membrane. The fate of EVs is determined by their surface molecule composition and by the receptors on the target cell plasma membrane. A wide range of molecules such as intracellular adhesion molecules (ICAMs), integrins, extracellular matrix components, lipids, lectins, heparan sulfate proteoglycans and MHCs act as interaction mediators between EVs and the plasma membrane. For instance, interaction of ICAMs (ICAM-1) on EVs with the integrins (αv or $\beta 3$ integrins) on the plasma membrane of the recipient cell promotes the docking of EVs for internalization (Morelli et al. 2004). Integrins on the surface of the EVs can enhance the docking with the plasma membrane by interacting with extracellular matrix components (Sung et al. 2015; Purushothaman et al. 2016). In addition, specific exosomal integrins on EVs drive them to specific target organs *in vivo*. For example, presence of ITG $\alpha v\beta 5$ direct tumor exosomes to fibronectin-rich liver microenvironments, whereas tumor exosomal ITG $\alpha 6\beta 4$ and ITG $\alpha 6\beta 1$ promotes binding to laminin-rich lung microenvironments preparing a pre-metastatic niche (Hoshino et al. 2015). These findings suggest that integrins could dictate the organotropism of EVs and could serve as a potential biomarker.

Exosomal tetraspanins can promote docking and internalization of EVs either by interacting with integrins (Rana et al. 2012) or with other surface proteins (Nazarenko et al. 2010; Rana et al. 2011). Interaction between the leptin receptor Siglec (CD169) on macrophages captures the splenocyte EVs bearing $\alpha 2,3$ -sialic acid promoting the EV uptake *in vivo* (Saunderson et al. 2014). A proteoglycan, Glypican-1 (GPC1) on tumor derived EVs is involved in docking to the cell membranes, furthermore, GPC1 carrying EVs may serve as a screening and diagnostic tool to detect early pancreatic cancer (Melo et al. 2015). Galectin-5 on the EV surface binds to C-type lectin receptors on the macrophages promoting clathrin-mediated endocytosis (Barrès et al. 2010). On the other hand, lipid composition of EVs can also have an impact on targeting EVs. PS which recruits lipid binding proteins such as lactadherin that induce docking of EVs to the plasma

membrane is known to be enriched on the outer leaflet of EV membranes (Morelli et al. 2004).

Taken together, target specificity of EVs is determined by their surface molecule composition and specific interactions with the target cell membranes. Target specificity of EVs can also be achieved by engineering the EV surface proteins, thus exploiting their therapeutic potential. For example, engineered dendritic cell (DC) EVs bearing a neuro-specific RVG peptide on Lamp2b are specifically targeted to neurons, microglia and oligodendrocytes in the brain (Alvarez-Erviti et al. 2011).

1.2.4.2. EV Uptake or fate of EVs in recipient cells

The second step of the EV uptake is internalization into the recipient cell. The mechanism of EV internalization solely depends on the molecules localized on the membranes of EVs and acceptor cells such as integrins, proteoglycans, immunoglobulins, tetraspanins and lipid compositions which contribute to the EV target specificity and uptake. Although many studies report about the internalization of EVs, it is still unclear whether the uptake of EVs is through specific receptor mediated mechanisms, or through non-specific macropinocytosis. EV internalization and release of its contents into cells determines their functionality. The mode of entry can occur through clathrin-dependently in macrophages (Barrès et al. 2010), through PI3-kinase-, actin polymerization, TIM4-, dynamin2-dependent phagocytosis in macrophages (Barrès et al. 2010), lipid raft- and caveolae-dependent endocytosis in epithelial and endothelial cells respectively (Nanbo et al. 2013; Svensson et al. 2013). Recent evidences suggest that most of the EV internalization occurs via macropinocytosis to support engulfment of large aggregates of EVs. A study by Raghu Kalluri and colleagues demonstrated that engineered EVs carrying therapeutic cargo are internalized in pancreatic cells via macropinocytosis (Kamerkar et al. 2017).

The fate of the EVs is determined by the specific molecular composition on both, EV surface and the recipient' plasma membrane. For instance, when it comes to EV surface

composition, exosomes subtypes enriched with CD63 are targeted to neuronal and glial cells, while presence of APP (amyloid precursor protein) on exosomes targets them to neurons (Laulagnier et al. 2018), and presence of CD47 ('do not eat me' signal) on EVs increases their half-life in circulation preventing phagocytosis by monocytes and macrophages (Kamerkar et al. 2017). On the other hand, the molecular composition on the plasma membrane can play an important part in determining the fate of EVs. For example, a specific lipid composition such as presence of lipid rafts on the plasma membrane promotes the EV internalization, while depletion of its components such as cholesterol reduces the EV uptake (Escrevente et al. 2011).

Following the uptake of EVs by different mechanisms mentioned above, the EVs deliver their contents into the target cell. In case of plasma membrane derived EVs, studies suggest that they directly release cargo directly into the cytoplasm by fusing to the plasma membrane. For EVs internalized via clathrin-dependent or -independent mechanism, engulfed vesicles fuse to the lysosomes and inherently undergo degradation pathways. In order to deliver functional molecules, the EVs' cargo need to escape the endosomal degradation and enter cytosol, a process still poorly understood. However, a few studies reported target specific delivery of functional nucleic acids being achieved both, *in vitro* and *in vivo* (Loughmiller and Klintworth 2011; Kamerkar et al. 2017).

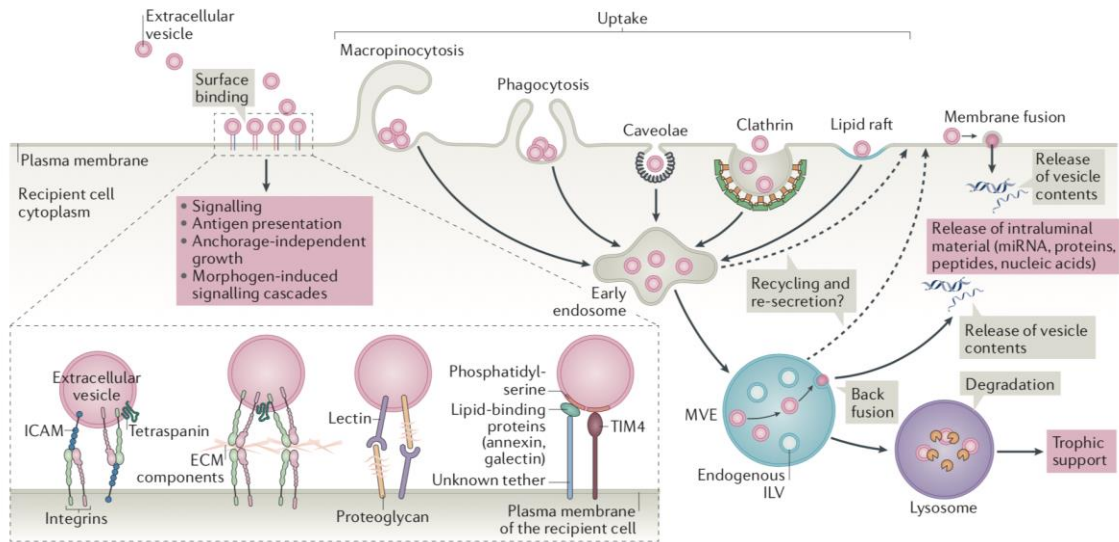


Figure 4: Fate of extracellular vesicles in recipient cells.

From Niel et al. *Nat Rev Mol Cell Biol.* 2018 Apr;19(4):213-228.

Cargo delivered via EVs leads to various responses in recipient cells, For example internalized epithelial EVs are processed in the endosomal compartments of dendritic cells for antigen presentation (Mallegol et al. 2007; Morelli et al. 2004). In some cases, internalized EVs are processed in endosomes and secreted into the extracellular space. A study revealed such findings showing that CD81+ EVs secreted by fibroblasts are internalized by breast cancer cells (BCCs), loaded with BCC-associated Wnt11 and recycled back into the extracellular milieu promoting BCC motility and metastasis (Luga et al. 2012). However, the main characteristic feature of EVs is to deliver functional molecules such as nucleic acids which can regulate the processes in target cell. Many reports demonstrated the transfer of RNA and DNA via EVs thus regulating the recipient cells. For example, the protective effect of MSC-EV on kidney disease is driven by transfer of mRNA and miRNA, which is well reviewed by Rani et al., (Rani et al. 2015). Sometimes, interactions of EV surface molecules with receptors on the plasma membrane is sufficient to trigger responses in the recipient cells, for instance exosomes derived from B cells and dendritic cells carry MHC-peptide complexes for antigen presentation to antigen-specific T cells (Segura et al. 2007); promoting anchorage-dependent growth of

non-transformed fibroblasts by fibronectin carrying tumor-derived microvesicles (Antonyak et al. 2011). To conclude, different cell types can internalize EVs using various mechanisms which is further depending on the surface molecular composition of EVs and cell membranes. Yet, the development of new imaging techniques and standard methods will help for better understanding the fate of cargo in recipient cells. Overview of uptake mechanisms is shown in Figure 4.

1.2.4.3. Methods to study EV uptake or cargo transfer in vitro and in vivo

Monitoring EV uptake generally relies on fluorescent or luminescent reporters *in vitro* and *in vivo*. Different fluorescent lipophilic dyes/lipid-anchored fluorophores (LAFs) such as PKH26, PKH67, DiR, DiI and rhodamine (Alvarez-Erviti et al. 2011)(Cao et al. 2019; Peinado et al. 2012a; Zhuang et al. 2011; Silva et al. 2013; Dabrowska et al. 2018) are used on purified EVs to track the EV fate in target cells or tissues. However, the use of lipophilic dyes is associated with several pitfalls. The half-life of these dyes can range from 5 to >100 days compared to the half-life of EVs ranging between 2 minutes to 24 hours. Dye-labelled EVs may be degraded or recycled *in vivo* but the dye itself remains intact in the cells or tissues, resulting in inaccurate outcomes in studying the fate of EVs *in vivo*. The second major issue with LAFs is that they don't selectively label EVs but also other aggregates and lipoproteins which are co-isolated with EVs, leading to false results (C. P. Lai et al. 2015). To circumvent these issues, the approach of genetically encoded fluorescent reporters such as CD63-eGFP or CD63-mCherry, CD81-eGFP which are enriched in EVs is widely common and enables to study the uptake dynamics of EVs at single particle level in target cells (Cossetti et al. 2014; Heusermann et al. 2016). However, the use of fluorescent reporters to study the fate of EVs is very much limited to cell cultures. Recent advances in imaging techniques made the tracking of the fluorescent labelled EVs *in vivo* possible. Using multiphoton intravital microscopy (MP-IVM), Lai et al. could show the EV trafficking in solid tumors stably expressing GFP or tdTomato with palmitoylation signal at the N-terminus (C. P. Lai et al. 2015).

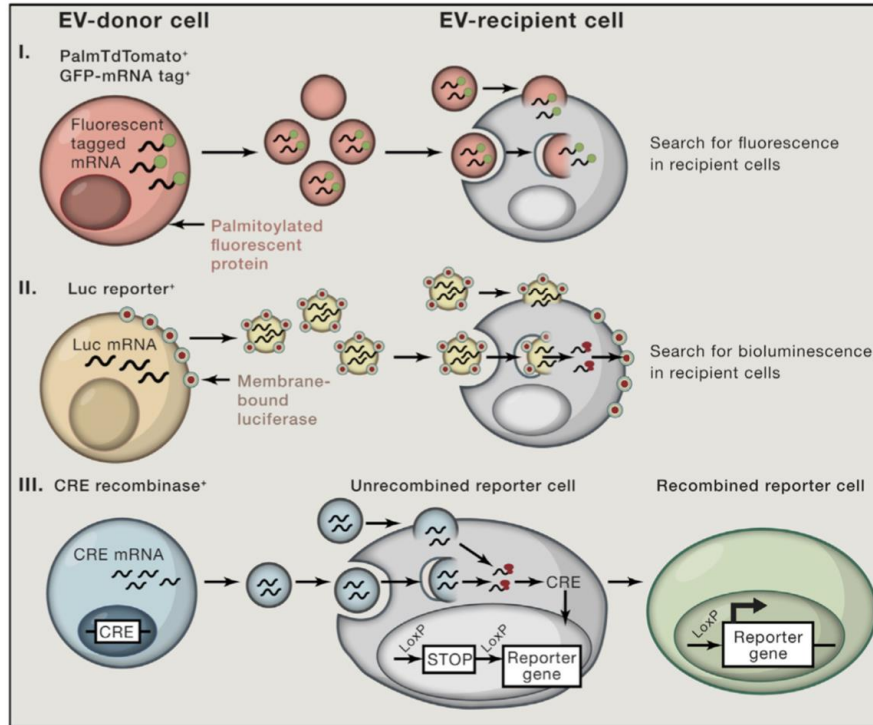


Figure 5: Approaches Used to Analyze EV- Mediated Transfer *in vivo*.

From Tkach M et al. *Cell*. 2016 Mar 10;164(6):1226-1232.

In an *in vivo* setting, lipophilic fluorescent dyes have widely been used to study the fate of EVs, accompanied by various pitfalls as mentioned above. To exploit the therapeutic potential of EVs, understanding the biodistribution of systemically injected EVs is, however, of utmost importance. Despite their drawbacks, the use of lipophilic fluorescent dyes gave some insights into the biodistribution of EVs. A comparative study evaluated how the routes of injections, cellular origin of EVs and different EV doses affect the biodistribution *in vivo* (Wiklander et al. 2015a). Besides, apart from fluorescent reporters and lipophilic fluorescent dyes, bioluminescent reporters such as Renilla luciferase (Rluc) and nano-luciferase (Nluc) tagged to tetraspanins have been used to study the fate of EVs *in vitro* and *in vivo*. Recent reports demonstrate that using bioluminescent reporter systems enables noninvasive imaging of EV biodistribution *in vivo* (Gangadaran, Li, et al. 2017; Hikita et al. 2018), paving a way for developing EV-based theranostic strategies.

In an *in vivo* setting, it is important to have a system which can discriminate between cells that have taken up the EVs with functional cargo and the ones that have not. Zomer et al., designed the Cre-loxP system to demonstrate the functionality of EVs upon their internalization. In brief, the color switch, from DsRed to eGFP in the reporter expressing cells that take up the EVs carrying Cre recombinase transcript from Cre expressing cells (Zomer et al. 2015). However, this approach demands the generation of donor- and recipient reporter systems and is a highly sensitive method demonstrating the functionality of EVs. Still, loading of Cre mRNA into EVs has unclear efficiency, especially if using stable Cre transfected cell lines.

1.2.5. EV isolation methods

The natural therapeutic potential of EVs has paved the way for explosive research in studying the mechanisms of their biogenesis and macromolecule loading, on EV uptake mechanisms and functional cargo delivery. In addition, increasing attention has been paid on developing methods for EV isolation. Considering EVs as being omnipresent, every cell has the ability to secrete EVs into the extracellular milieu. EVs are commonly isolated from conditional cell culture medium and from biological fluids such as blood, urine, cerebrospinal fluid, milk and saliva. Apart from EVs, these materials are highly complex, containing non-vesicular macromolecules such as lipoproteins, protein aggregates along with cell debris and apoptotic bodies. Considering the EVs' size and heterogeneity and the complexity of their surrounding environment, their isolation and method of choice is a challenging obstacle.

The starting material is of utmost importance for choosing the right method, since any starting material will have significant amounts of non-vesicular components that can be co-isolated with EVs. For instance, the presence of additional EVs in cell culture media originating from fetal bovine serum (FBS), apoptotic bodies or from other media supplements poses a high risk of misinterpreting the results. It is advised to remove cell

debris and apoptotic bodies by centrifugation at 300-700 x g and 2,000-3,000 x g respectively. A recent study demonstrates that EVs derived from FBS can induce phenotypic and behavioral changes in cell cultures (Shelke et al. 2014). The removal of EVs and other macromolecules via 18-hours centrifugation protocol leads to a depletion of 95% of EVs from serum. Of note, while using EV-depleted media or serum free media for culturing cells, one should consider the effect of EV-depleted media or serum free media on cell phenotype and behavior.

Conditioned cell culture medium is rather well defined, compared to the complex nature of biological fluids, which demands different approaches for the removal of contaminants to achieve pure EV preparations. Plasma, for example, contains high amounts of lipoproteins such as low- and high-density lipoproteins along with EVs, posing a high risk for incorrectly interpreting the results (Yuana Yuana et al. 2014; Sódar et al. 2016). For example, the majority of circulating RNAs is extravesicularly either bound to proteins like AGO or to lipoproteins and is co-purified with EVs, posing further challenges in understanding EV mediated effects. Thus, not only robust methods for isolation and purification are in great need, but also after isolation, carefully monitoring the analysis is needed to correctly interpret the results. A few EV isolation methods based on their physical and chemical properties, which are widely employed, are discussed below.

1.2.5.1. Isolation methods based on physical characteristics

1.2.5.1.1. Ultracentrifugation

The invention of the ultracentrifuge in the early 20th century led to the development of separation techniques including the application for EVs. To date, ultracentrifugation (UC) for EV isolation has been employed for all kinds of starting material (from conditioned cell culture media to biological fluids) and is widely considered as a golden standard method. The method involves sequential centrifugation steps from low- to high speed, where cell debris is removed by centrifugation at 300-700 x g for 5-10 min and apoptotic bodies at 2,000-3,000 x g. For the isolation of MVs, the supernatant is subjected to sterile 0.8 µm

filtration, followed by centrifugation at 10,000-20,000 X g. To enrich exosomes, the supernatant is sterile filtered with 0.22 μm and further processed with high-speed ultracentrifugation at 100,000-120,000 x g for 90-120 min. Schematic representation of ultracentrifugation based EV isolation Figure: 6

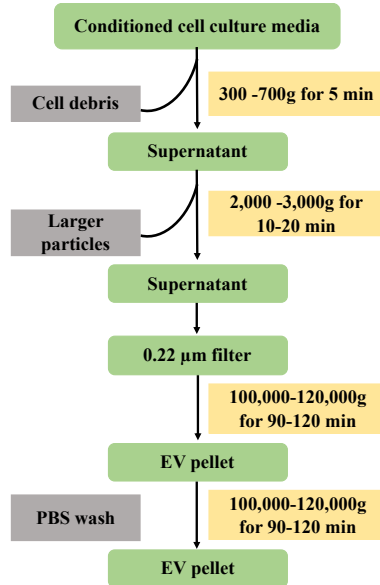


Figure 6: Schematic representation of differential ultracentrifugation procedure.

However, due to the heterogeneity of EVs concerning size and density, high speed ultracentrifugation cannot achieve absolute separation of particles. Smaller particles which are at a higher distance from the bottom of the tube may not sediment. Secondly, high speed centrifugation steps cause aggregation of particles in the pellet which can impact their biological function. Thirdly, protein aggregates, lipoproteins and other contaminants with similar sizes to EVs tend to co-sediment in the EV pellets. Hence, protein measurements of EV-containing pellets cannot determine the recovery of EVs. In order to remove impurities at least to some extent, EV pellets can be resuspended in sterile PBS and recentrifuged. Of note, repeating wash steps will lead to the loss of particles and it is absolutely difficult to get rid of all the impurities and to achieve pure EV preparations by this method alone.

1.2.5.1.2. Density-gradient separation

Due to the differences in biogenesis and cargo, different subtypes of EVs have different densities. To remove impurities/contaminants from EV pellets after UC, by applying density gradient centrifugation, one can efficiently separate different impurities such as protein-RNA aggregates from EVs (Raposo et al. 1996; Théry et al. 2006). Commonly used gradients are sucrose and iodixanol, allowing separations of particles between 1.1 and 1.19 g/ml according to their densities. However, this method is still not feasible to separate EV subclasses with the same densities. By employing density gradient centrifugation in combination with UC, one can achieve pure EV preparations.

1.2.5.1.3. Size-exclusion

Size exclusion-based techniques are widely used for the separation of biomolecules such as proteins, polysaccharides and proteoglycans and can also be employed for separating EVs from conditioned cell culture media or from biological fluids. A brief overview of EV isolation techniques which are employed in the study such as column-based size exclusion chromatography (SEC), ultrafiltration and tangential flow filtration (TFF) (commercially available crossflow filtration) are discussed hereafter.

Size exclusion chromatography/gel filtration:

The separation of EVs using SEC is recommended for biological fluids such as plasma or urine and for samples which are ultracentrifuged. Size exclusion chromatography allows for sequential elution of fractions based on their size. The principle relies in trapping the smaller particles in the porous beads and allowing large particles such as EVs to elute earlier. SEC is increasingly practiced in the EV community, due to the results that show improved purity, integrity and functionality of the isolated EVs. SEC has been used for isolating EVs from biological fluids such as serum and saliva. EVs isolated via SEC are relatively pure and mostly depleted for proteins and lipoproteins such as HDLs (Böing et

al. 2014). Recently, commercially packed columns such as qEV (IZON Science Ltd., United Kingdom) (An et al. 2018), Exo-Spin™ Midi Columns (CellGS; Cambridge, UK) (Welton et al. 2015) are gaining popularity considering the robustness, purity and reliability. Furthermore, SEC has more advantages compared to the widely applied UC. Having no risk of protein contamination or EV aggregation, SEC gained increasing popularity. Yet, the method is constrained in its scalability and applicable for smaller sample size only, restricting large-scale isolations for clinical applications. However, when combined with other high throughput methods, such as filtration, UC or TFF, one can achieve relatively pure, clinical grade EVs in large numbers.

Ultrafiltration:

Filter-based methods in particular serve as an alternative for UC or as an additional step to gel filtration. When isolating EVs by ultrafiltration, the pore size of the filters often matters for the separation of EVs. Commercially available ultrafiltration columns, such as Amicon® Ultra 15 ml/50 ml Centrifugal Filters (Merckmilipore) are widely in use (Merchant et al. 2010; Nordin et al. 2015), filter membranes with fixed molecular weight cut-off (MWCO) of 100 kDa can retain EVs with particle sizes below 200 nm, allowing other components such as proteins to pass through the membrane. However, these can only be employed for smaller sample volumes. Additionally it was shown that the composition of some exosome subpopulations may promote stable binding of EVs to the membranes, leading to a decline in recovery (Cheruvanky et al. 2007).

Tangential flow filtration (TFF):

Although gel filtration and ultrafiltration provide reasonably pure exosomes, scalability and obtained yield are major setbacks. Recently, a commercially available TFF system has gained popularity for isolating large-scale clinically grade EVs from conditioned cell culture supernatants. The TFF method is based on a crossflow filtration with modified Polyethersulfone (mPES) membrane filters which have fixed molecular weight cut-off

(MWCO) limits. Pores in the membrane allow the smaller particles to pass through, following concentrated EVs in the circulation (Figure 7). This method enables large scale isolation of EVs, which are intact and biologically active with minimal batch-to-batch variations (Corso et al. 2017). A few recent studies compared the clinical potency of TFF isolated EVs with EVs derived from ultracentrifugation. Results demonstrate that EVs isolated via TFF are highly potent in delivering therapeutic molecules to target cells (Reka Agnes Haraszti et al. 2018), implying the importance of TFF for clinical grade applications.

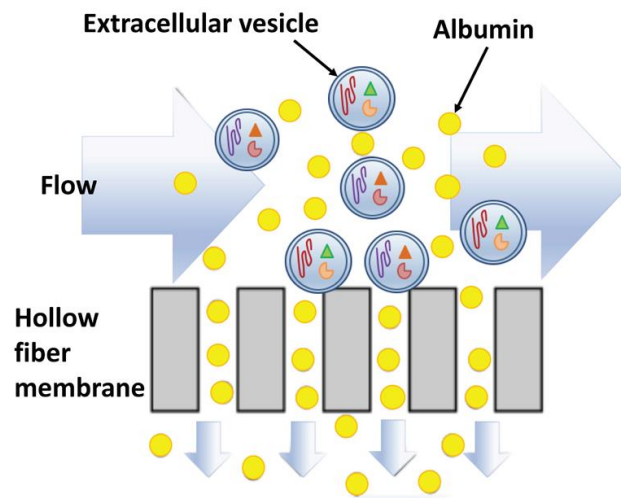


Figure 7: Schematic illustrating of TFF.

Adapted from Busatto et al. Cells 7(12).

1.2.5.2. Isolations methods based on biochemical characteristics

1.2.5.2.1. Immunoaffinity isolation

The presence of a characteristic surface molecule composition on different subtypes of EVs has been exploited for the immunoaffinity isolation of EVs. The antibodies against the EV

surface molecules are covalently bound to magnetic-, agarose-beads or to other matrices enabling enrichment/trapping of a specific population and facilitating separation through affinity interactions. So, the abundance of specific EV surface molecules such as CD9, CD63, CD81, EpCAM and PS is employed for the isolation of specific subtypes of EVs. One can isolate EVs secreted from a specific cell type depending on the availability and specificity of the antibodies. Commercially available pan-tetraspanin immunoaffinity isolation kits (from miltenyi Biotec) are widely used for both, qualitative and quantitative determination of EVs (Koliha et al. 2016). The major advantage of using immunoaffinity based techniques is that tissue specific EVs can be isolated. For instance, paramagnetic beads coated with HLA DP, DQ, DR antibodies can be used for isolation of exosomes secreted from B-cells (Clayton et al. 2001). In addition, several magnetic bead based isolations have been employed, for example the use of heparin coated beads for isolation of abundant populations of EVs (Balaj et al. 2015), binding affinity of Tim4 to PS has been exploited for isolating EVs (Miyaniishi et al. 2007; Nakai et al. 2016). In general, compared to gold-standard methods, affinity isolation of EVs reduces isolation time, elevates the purity of EVs isolated and can improve tissue specific EV isolations. However, this method also comes with its own pitfalls, is not applicable for large scale isolations and can be expensive.

1.2.5.3. Other isolation methods

Recent advances in EV research led to the development of new techniques based on physical and biochemical characteristics of EVs. For instance, hydrophobic polymers such as PEG (polyethylene glycol) have widely been used for precipitating EVs. Some of the commercially available reagents based on PEG precipitation are- ExoQuick (System Biosciences, United States), Total Exosome Isolation Reagent (Invitrogen, United States) and ExoPrep (HansaBioMed, Estonia). Others employ different microfluidic devices based on the immunoaffinity principle (Zhao et al. 2016) or with the use of microporous filtration systems (Davies et al. 2012).

Given the complexity and heterogeneity of EVs, a wide variety of approaches for their isolation has been developed. Cell culture derived EV preparations are mostly uniform compared to biological material due to the complex nature and limited sample volume. On the other hand, scalability is a major issue with cell culture material. Overall, it might not be possible to develop a universal method for isolating EVs but, one should carefully consider the starting material and downstream application of the isolated EVs for finding the method of choice.

1.2.6. Characterization of EVs

To access the results of EV isolation and to demonstrate the biological significance of EVs, their characterization via multiple techniques is important. Therefore, the ISEV provided guidelines by releasing a series of position papers (Lötvall et al. 2014; Théry et al. 2018; Witwer et al. 2017), providing the minimal experimental needs and clarifying the definition of cell- derived vesicles.

The assessment of the quality of EVs is defined by their size, density, morphology and molecular features such as the presence of EV-associated proteins. Important characterizations and techniques involved in evaluating the EV preparations are discussed hereafter.

1.2.6.1. *Physical analysis of EVs*

Determining the size, concentration and morphology of EVs is a main parameter for characterizing EV types (exosomes, microvesicles and apoptotic bodies). A few studies reported that circulating EV/plasma EV size and concentration vary from normal to pathological conditions, implying that the physical characteristics of EVs could potentially be useful as clinical diagnostic tools (Magdalena Derbis 2012; Baran et al. 2010). Most commonly used EV characterization techniques either directly by high-resolution imaging such as EM (electron microscopy) and AFM (atomic force microscopy) or indirectly using optics such as NTA (nanoparticle tracking analysis) and DLS (dynamic light scattering).

1.2.6.1.1. *Electron microscopy (EM)*

Due to the high resolution obtained by EM, it is a widely used technique to determine the size and morphology of EVs at single EV level. The most widely used EM technique for determining the size and morphology is TEM (transmission-EM)(Park et al. 2016; Linares et al. 2014; Böing et al. 2014) and in a few cases SEM (scanning-EM) (Sokolova et al. 2011; Nanou et al. 2018; Casado, Del Val Toledo Lobo, and Paíno 2017). Sample preparations for TEM involves heavy metals like uranyl acetate, osmium tetroxide or phosphotungstic acid increasing the contrast of the samples. However, the use of heavy metals and fixation agents like glutaraldehyde, leads to dehydration of the samples, resulting in deformation or shrinking of EVs and to a cup-shaped distinct morphology on grids, which was initially considered as a characteristic feature of EVs. Recently, the use of cryo-TEM techniques for characterizing EVs revealed that in fact, the cup-shaped morphology observed in TEM imaging is a mere artifact of sample preparation. Because the samples are snap-frozen in liquid nitrogen for cryo-TEM, and free from dehydration and fixation, EVs in cryo-TEM morphologically appear in their native state with their distinct lipid-bilayer (Yuana Yuana et al. 2013; Linares et al. 2014). Additionally, cryo-TEM offers the possibility to investigate the heterogeneity of EVs in biological fluids. For example, in a recent report, cryo-TEM imaging of blood plasma revealed the presence of

tubular and spherical structures of EVs, providing novel insights into the size, morphology and phenotype of EVs (N. Arraud et al. 2014). Furthermore, presence of specific surface molecules on different subsets of EVs enables their identification by using immunogold labeling. For instance, Brisson et al. combined immunogold labelling and cryo-TEM, providing the possibility of quantitative analysis to identify different subset of EVs (Brisson et al. 2017). Currently, cryo-TEM is regarded as the state-of-art method for characterization of EV size and morphology.

Although TEM and cryo-TEM provide vital information about the morphology and size of EVs, EM techniques are rather limited when used to estimate the concentration of EVs in a given sample. According to ISEV guidelines (Théry et al. 2018), it is suggested to obtain an overview image and close-up image to show the abundance and heterogeneity of EVs in the samples.

1.2.6.1.2. Atomic force microscopy

Atomic force microscopy (AFM) is a reliable surface-based imaging technique for characterizing EV size and their mechanical stiffness. The sharp tip at the end of the cantilever interacts with the surface of the sample leading to a deflection of the cantilever allowing to image the topology in nanometer resolution. The advantage of AFM is that it involves minimal sample preparation allowing to measure EVs in liquid suspension (Hardij et al. 2013) or even in fixed state (Biggs et al. 2016) where the mica coated with antibodies for specific EVs to be imaged (Sharma et al. 2010; Y. Yuana et al. 2010; Sebaihi et al. 2017). Additionally, the AFM technique is suitable to understand the mechanical properties of EVs, such as stiffness and elasticity (Vorselen, Marchetti, et al. 2018), providing insights into EVs differing between normal to physiological conditions, which consequently could help in the characterization and development of EV-based approaches in nanomedicine (Vorselen, van Dommelen, et al. 2018). Furthermore, Casado et al. recently applied AFM to study the dynamics of bulges on the plasma membrane of ASCs and the release of exosomes correlating to the size of the EVs produced by SEM (Casado, Del Val Toledo

Lobo, and Paíno 2017). However, the technique is of limited use due to the lack of expertise and equipment availability.

1.2.6.1.3. Dynamic light scattering

Dynamic light scattering (DLS), provides the average size of the particles by measuring the diffusion coefficient of scattering particles in a medium. Unlike EM and AFM that resolve the size of single EVs, DLS analyses the collective size of EVs by measuring the scattered laser light dispersed by EVs. The principle behind DLS is particle Brownian motion in the solution, resulting in time-dependent fluctuations in scattered light intensities which is directly converted to the diffusivity to determine the hydrodynamic diameter of particles by applying the Stokes- Einstein equation (Sitar et al. 2015). The simplicity and speed of measurements gives DLS an advantage over other methods. However, DLS measurements are used for quantitative analysis of EVs with relatively homogenous nature. DLS is used to determine the size of EVs in many studies involving high-throughput measurements (Palmieri et al. 2014; Baddela et al. 2016). The application of DLS is quite limited to biological samples as due to their complex nature the readouts can be misread. Although a few studies report using DLS for characterizing EVs from plasma (Lawrie et al. 2009), but by coupling DLS measurements for EVs isolated by SEC (Varga et al. 2014) or asymmetrical flow field flow fractionation (AF4) (Petersen et al. 2014) achieving pure and homogenous EV preparations.

1.2.6.1.4. Nanoparticle tracking analysis

Nanoparticle tracking analysis (NTA) is the most widely used technique to determine the hydrodynamic diameter and concentration of EVs. NTA allows tracking of EVs at individual level replacing DLS for characterizing EVs in recent times. The principle behind NTA analysis is the same as in DLS, which records Brownian motion of particles. Furthermore, the scattered light from particles is recorded by a camera which enables visualization of single particles in the solution. This enables individual particle size

calculation using a special algorithm. Currently, commercial instruments such as Malvern (Nanosight) and ParticleMetrix (ZetaView) are extensively used to determine the size and concentration of EVs. However, the presence of contaminants such as protein aggregates and lipoproteins in the sample can misrepresent the size and concentration distribution in the sample. Recent advancements in technology allows the use of EV specific antibodies or fluorescent dyes that can discriminate between EVs and contaminants. However, one should consider bleaching of the fluorescent dyes due to high laser beams and chose photo-stable fluorescent dyes (Lobb and Mo 2017; Dragovic et al. 2011). Nevertheless, NTA provides robust quantification of EV size and concentration. Although one should take care of using standards to ensure for reproducibility and correct data interpretation (Vestad et al. 2017; C. M. Maguire et al. 2017)

1.2.6.2. Biochemical analysis of EVs

Determination of protein concentrations in the EV preparations by micro-bicinchoninic acid (BCA) or by Bradford assay is a straightforward characterization of EVs. However, the protein contaminants in the preparations limit the accuracy of the measurements. EVs are heterogenous in physical and molecular characteristics which mainly depend on their origin and biogenesis. As mentioned before in the EV biogenesis section (1.2.2), different proteins and lipids are involved in EV biogenesis mechanisms and cargo sorting. With the current knowledge on biogenesis mechanisms, molecular profiles available for physiological or pathological status, certain biomarkers can serve as a component for molecular characterization of EVs. Probing for specific EV markers via immunoblotting or by flow cytometry is commonly used to evaluate the molecular composition. Here, I summarize the most commonly used biochemical characterization methods, namely immunoblotting and flow cytometry and recent advancements in the molecular characterization of EVs.

1.2.6.2.1. Immunoblotting

Immunoblotting is a most widely used analytical method for detection of EV specific/EV-associated protein enrichment in EV preparations. EVs purified by UC are subjected to lysis and released proteins are separated on SDS-PAGE and probed for specific EV associated proteins. One can use the total protein concentrations or particle concentrations as a loading constant. According to the guidelines set by ISEV in the recent position paper MISEV2018 (Théry et al. 2018), it is recommended to analyze the enrichment of at least one of the tetraspanins (CD9, CD63, CD81), transmembrane proteins associated to EVs (van Niel et al. 2011; Verweij et al. 2011) and one of the intravesicular proteins (ALIX, TSG101, Syntenin) in EV samples. Additionally, EVs are enriched with proteins involved in their biogenesis and secretion such as flotillin-1, ARF6, annexins, Rab GTPases, syndecans and cytoskeletal proteins (actin and tubulin), chaperones (HSP70, HSP90), metabolic enzymes (enolase, GAPDH, peroxidases) and ribosomal proteins (RPL12, RPS18) (Statello et al. 2018; Choi et al. 2015). Plasma membrane derived EVs are often enriched with proteins such as integrins, lectins, fibronectin (discussed in section 1.2.4), specific plasma membrane receptors such as EGFR (epidermal growth factor receptors) (Graner et al. 2009; Al-Nedawi et al. 2009) and cell adhesion molecules such as CD24, CD44 and EpCAM (epithelial cell adhesion molecule) (Tauro et al. 2013; Im et al. 2014), which can be used as EV biomarkers under normal and pathological conditions. However, to assess the purity of EVs isolated from biological fluids such as plasma, saliva and urine, it is highly recommended to quantify for contaminants (apoproteins, albumins) which are often co-purified with EVs. Furthermore, the presence of *not expected* EV proteins from ER (HSP90B1, calnexin), Golgi (GM130), mitochondria (cytochrome C) and nucleus (histones) should be checked for determining the purity of EV samples. Immunoblotting enables the simple detection of EV associated proteins. However, it requires bulk amounts of EVs which often limits its applicability for biological fluids. Moreover, immunoblotting doesn't provide complete information of heterogeneity within EVs and individual EV protein content.

1.2.6.2.2. Flow cytometry

For exploiting the surface molecular composition of EVs, flow cytometry (FC) is the most commonly used technique. However, most of the conventional flow cytometers can only detect particles above 500 nm in diameter due to the limitation concerning sensitivity. MVs with diameter ranging from 100 nm to 1000 nm, facilitates the use of FCs by many research groups (Chandler 2016; Nolan and Jones 2017). Additionally, the use of fluorescent labels or fluorescent antibodies enables discrimination of specific EV populations from contaminants or from EVs from other sources (Nicolas Arraud et al. 2016; Ayers et al. 2011; Fendl et al. 2016; Wisgrill et al. 2016). Importantly, the detection of small EVs is underestimated or if detected, they are collectively counted as a single event which is called swarm detection (Van Der Pol et al. 2012). By using immune capture of EVs on magnetic beads coated with tetraspanin specific antibodies enable highly sensitive detection of specific population of EVs (Campos-Silva et al. 2019). Recently, Koliha et al. developed a multiplex bead-based platform to detect up to 37 EV surface markers in one sample providing an EV protein surface signature (Koliha et al. 2016). Furthermore, Wiklander et al. systemically evaluated the multiplex bead-based flow cytometry assay to detect, quantify and compare EV protein surface signatures from different cell-types (Wiklander et al. 2018). The introduction of imaging flow cytometers (IFC) allowed to discriminate EVs from protein aggregates by combining flow cytometry with fluorescent imaging. However, until now, the use of IFC was limited only for characterizing larger EVs (Erdbrügger et al. 2014; Headland et al. 2014; Lannigan and Erdbruegger 2017). Lately, Görgens et al. demonstrated the usability of IFC for small EVs by comprehensive stepwise validation and optimization (Görgens et al. 2019). Recent advancements in the field of flow cytometry enabled the characterization of small EVs with 40 nm in diameter. Nano flow cytometer (NanoFCM) is the only flow cytometry device with a versatile platform enabling both, physical (size) and molecular characterization of EVs (Ye Tian et al. 2018).

The molecular composition of EVs mainly reflects the biogenesis mechanisms involved and the originating cell-type. Unlike proteins, lipids characterization of EVs is poorly studied. However, employing mass spectrometric analysis of the global EV proteome (Kreimer et al. 2015; Choi et al. 2015) and lipidome (Llorente et al. 2013; Reka A. Haraszti

et al. 2016b) shed light on functional activities of EV cargo, biogenesis and cargo sorting. Apart from proteins and lipids, EVs are highly enriched with nucleic acids. The presence of RNA and DNA in EVs can be detected by using fluorescent dyes such as SYTO 13 (Ullal, Pisetsky, and Reich 2010). Several studies have reported specific and non-specific loading of RNA into EVs (Bæk et al. 2016; Crescitelli et al. 2013; Nolte, T. Hoen et al. 2012; Villarroya-Beltri et al. 2013; Vojtech et al. 2014). In some instances, extracellular RNA (Deregibus et al. 2007) or DNA (Németh et al. 2017; Thakur et al. 2014) bound to the outer surface of the EV membrane can induce functional responses in recipient cells leading to misinterpretation. Hence, for EV RNA and DNA analysis (quantitative reverse transcription PCR (RT-PCR), microarrays, next-generation sequencing) it is recommended to include RNase and DNase combined with protease treatment to specifically define the EV nucleic acid composition (Théry et al. 2018; Hill et al. 2013).

The availability of databases greatly expanded our understanding of the molecular composition and characterization of EVs (Mathivanan et al. 2012; Kalra et al. 2012; D. K. Kim et al. 2013; Simpson, Kalra, and Mathivanan 2012; Keerthikumar et al. 2016; Mathivanan and Simpson 2009). However, the small size, heterogeneity and our poor knowledge on EV biology made a real challenge for EV characterization.

1.2.7. Therapeutic potential of EVs

EVs have an innate ability to transfer cargo either by paracrine or endocrine manner, enabling EVs to potentially outperform their counterparts (liposomes and synthetic nanovesicles) as therapeutic carrier vehicles. EVs have a natural therapeutic potential. For instance, in tissue regeneration, EVs from stem cells have the potential to stimulate cell proliferation (Gatti et al. 2011) and angiogenesis (Deregibus et al. 2007) in quiescent endothelial cells and cell reprogramming by horizontal transfer of bioactive molecules (Ratajczak et al. 2006). The therapeutic potential of stem cells has been widely exploited for many clinical studies so far. The discovery of reprogramming mouse fibroblasts to

pluripotent cells was the turning point in stem cell-therapy (K. Takahashi and Yamanaka 2006). From then on, stem cell-therapy has been carried out in many pre-clinical and early stage clinical studies for treating different diseases. MSCs (mesenchymal stem cells), used as a potential cellular therapy have been widely employed in many clinical studies in regenerative medicine (Le Blanc et al. 2008; Trounson and McDonald 2015; Tompkins et al. 2017). However, there have also been reports about MSC cell therapy with negative implications on many diseases (Trounson and McDonald 2015). Some of the reasons for the failure of MSC clinical trials are the loss of the therapeutic potential (N. Kim and Cho 2015), the induction of immunogenicity (N. Kim and Cho 2015), limited direct access to disease sites (U. M. Fischer et al. 2009) and lack of validation for individual diseases. Recent studies have shown promising application for MSC derived EVs as potential therapeutic agents because of their apparent natural ability to deliver active biomolecules by crossing the physiological barriers such as the blood-brain barrier (EL Andaloussi et al. 2013). The discovery of cardioprotective effects of MSC-derived EVs led to great interest in their therapeutic potential. From then on, increasing studies have demonstrated the therapeutic potential of MSC-derived EVs in different pathological conditions. From here on, I discuss in brief the therapeutic application of EVs in different diseases, EVs as natural vehicles for drug delivery and engineered EVs for potential targeting.

1.2.7.1. EVs as therapeutic agents

The potential use of EVs as therapeutic agents has been exploited widely after the discovery that dendritic cell-derived exosomes carrying antigen presenting MHC I and II molecules could suppress tumor growth by activating T-cells (Zitvogel et al. 1998). This was soon followed by the production of clinical grade DC-derived exosomes (Dex) (Lamparski et al. 2002) and their administration in phase I clinical trials to patients with metastatic melanoma or non-small cell lung carcinoma, showing low toxicity and feasibility of exosome vaccination (Morse et al. 2005; Escudier et al. 2005). The potential of DC-derived exosomes in phase II trial failed to reach the primary end point in 50% of the patients (Besse et al. 2016). However, these studies triggered scientific interest towards

the therapeutic potential of EVs. The advantages of EVs over cell-based therapies is that they possess less immunogenicity than cells when administered as they harbor only a few of MHC molecules (Ong and Wu 2015) and have a longer shelf life compared to parent cell.

The therapeutic application of MSC-derived EVs in many pre-clinical studies for the treatment of diseases and pathological conditions has been reported. However, further progress has to be made with regard to their isolation, characterization, production and routes of administration. Nevertheless, the therapeutic application of MSC-derived EVs attracts lots of interest simply because EVs can be produced from MSCs isolated from patients' bone marrow and their ability to circumvent the immune responses in regenerative medicine. On contrary, EVs can also modulate immune responses which is beneficial for cancer immunotherapy (Zitvogel et al. 1998). In regenerative medicine, the therapeutic effects of MSC-derived EVs in circumventing the adverse effects of diseases rely on their cargo, activation of vital signaling pathways by their interactions with membrane receptors, suppression or promotion of immune responses or by promoting angiogenesis (R. C. Lai et al. 2010; Zitvogel et al. 1998; Cosenza et al. 2018; Liu et al. 2017; Gangadaran, Rajendran, et al. 2017; J. Zhang et al. 2015). The treatment of graft-versus-host disease (GvHD) using bone marrow derived MSC EVs has shown improvements in clinical GvHD symptoms within a week of EV therapy and patients remained stable for the next four months (Kordelas et al. 2014). A few studies have investigated the clinical safety and efficacy of MSC EVs. An application of human cord blood derived EVs to ameliorate the progression of grade III and IV CKD (chronic kidney disease) in a randomized, placebo-controlled, phase II/III pilot study showed that human cord blood derived EVs are safe, have immunomodulatory functions and can improve kidney function in phase III and IV CKD patients (Nassar et al. 2016). The same group conducted a phase I clinical trial to evaluate the modulation of inflammation and pancreatic β -cell mass modulation along with glucose control in T1DM (type 1 diabetes mellitus) patients by human umbilical cord blood-derived MSC-EVs (ClinicalTrials.gov; identifier NCT02138331). However, until now no further information on this trial is available. Furthermore, another ongoing phase I

clinical trial is assessing the safety and efficacy of MSCs and MSC-derived exosomes for the healing of large and refractory macular holes (MHs) (NCT03437759).

Apart from MSC EVs, EVs derived from other cell types with stem cell-like properties, or from other regenerative and immunomodulatory cell sources have been harnessed for therapeutic applications. So far there are no direct comparisons of parent cell therapy with EVs to evaluate the therapeutic potential of EV based therapies. However, a few reports have shown minimal potency of EV therapy compared to parent cell therapy (Xie et al. 2017). Ultimately, EVs for therapeutic applications also depend on several factors such as their parent cell culture conditions which can alter the EV properties (Eguchi et al. 2018).

1.2.7.2. EVs as therapeutic targets

Given the importance of the therapeutic potential of EVs to ameliorate the disease progression, EVs also play a crucial role in promoting disease pathogenesis. For instance, concerning the role of EVs in tumor biology, various studies have implicated the role of EVs in driving the pre-metastatic niche formation by stimulating cell proliferation, angiogenesis, matrix remodeling, modulating T-cell activation and inducing metastasis (Rak and Guha 2012; Peinado et al. 2012b; Sidhu et al. 2004; Jeong et al. 2005; Al-Nedawi et al. 2008; Skog et al. 2008; Al-Nedawi et al. 2009). The role of EVs in tumor progression was elegantly demonstrated by Al-Nedawi et al. by showing EV mediated horizontal transfer of epidermal growth factor receptor (EGFRvII) from glioma cells to adjacent tumor cells including blood, promoting angiogenesis by stimulating expression of vascular endothelial growth factor (VEGF) (Al-Nedawi et al. 2008). Furthermore, the blocking of oncogenic EGFR harboring EVs by annexin V derivatives (e.g: diannexin) leads to antitumor growth and antiangiogenic effects (Al-Nedawi et al. 2009). These studies collectively represent oncogene harboring EVs as a therapeutic target in cancer. Beyond cancer, EVs play an important role in neurodegenerative diseases (Lee and Kim 2017) and in the spread of pathogens (Rodrigues et al. 2018). In the context of aging, we have observed negative effects of EVs from senescent cells on cell differentiation in bone and

skin (Weilner, Schraml, et al. 2016; Terlecki-Zaniewicz et al. 2018, 2019; Weilner, Keider, et al. 2016). However, four strategies could be applied to target EV-driven pathologies. Considering the EV biology, composition and mode of action; EVs can be targeted either by inhibiting their biogenesis, release, uptake or a specific component of the EVs that could contribute to disease progression.

EV/exosome biogenesis is driven by ESCRT-dependent or -independent, CD63- and ceramide dependent pathways. The molecules involved in EV biogenesis and cargo sorting define the molecular nature. Inhibition of one of the components involved in biogenesis results in reduced EV secretion. For instance, silencing of ESCRT-0/1 complex components such as hepatocyte growth factor regulated tyrosine kinase substrate (HRS), signal-transducing adaptor molecule 1 (STAM1), and TSG101 in HeLa cells reduces the EV secretion (Colombo et al. 2013). In another instance, the inhibition of neutral sphingomyelinase 2 (sMase2), an enzyme that regulates the biogenesis of ceramide by a small molecule GW4869, decreased the exosome secretion both *in vitro* (Trajkovic et al. 2008; Kosaka et al. 2010) and *in vivo* (Fabbri et al. 2012). Similarly, inhibition of endocytic vesicle recycling by dimethyl amiloride decreased membrane-associated heat shock protein 72 (HSP72) harboring tumor-derived exosome secretion and their immunosuppressive effects in both mice and humans (Chalmin et al. 2010). RNA-mediated interference (RNAi) of syntenin, syndecan or ALIX reduced the secretion of exosomes suggesting a possible strategy for therapeutic targeting of EVs (Baietti et al. 2012). On the other hand, many proteins such as Rab GTPases and Arf6 are involved in the release of exosomes and can provide an opportunity for targeting EV release. One such example is reduced exosome secretion (Ostrowski et al. 2010) after RNAi knockdown of RAB27A. RAB27A blockade resulted in decreased tumor growth and metastasis *in vivo* (Bobrie et al. 2012). Apart from RAB27A and RAB27B, other Rab GTPases such as RAB11 and RAB35 have been involved in docking of MVBs to the plasma membrane. The inhibition of RAB11 or RAB35 leads to an accumulation of MVBs in cells, thus impairing exosome secretion (Hsu et al. 2010; Savina et al. 2005).

Several mechanisms have been proposed for the uptake of EVs into recipient or target cells. However, detailed knowledge on uptake mechanisms for specific subtypes of EVs is still lacking. Nevertheless, with the current knowledge, one could block the uptake of EVs by targeting the EV surface molecules or the receptors on the recipient cells. For instance, blockade of phosphatidylserine on EVs with diannexin leads to antitumor and antiangiogenic effects (Al-Nedawi et al. 2009). Blocking specific signaling molecules on EVs is sometimes sufficient to inhibit the disease progression. For example, antibodies targeting FASL1 to reduce tumor growth (Cai et al. 2012) or knockdown of MET by RNAi can help to diminish the metastatic effect of melanoma derived exosomes (Peinado et al. 2012b). Importantly, inhibition of components of EV biogenesis or release can have beneficial effects in cancer therapy. However, this can affect normal cell function. Moreover, developing targeted approaches for the clearance of tumor-derived EVs or neutralizing their uptake can be promising and needs further deep understanding of EV cell-to-cell communication and their uptake mechanisms.

1.2.7.3. EVs as a novel drug delivery vehicles

The innate ability of EVs to transport cargo across biological barriers is an intriguing feature which can be exploited for drug delivery. The fact that almost all cells secrete EVs which are loaded with biomolecules such as RNA, DNA, lipids and protein and are transferred to the recipient cells and protect their cargo from extracellular environment, makes them especially interesting for this application. Employing EVs as drug delivery vectors has advantages over the conventional drug delivery vectors such as liposomes. In contrast to liposomes, EVs are natural transporters with less immunogenicity and their ability to cross natural barriers such as the BBB, engineer or modify the EV surface for targeted delivery. Loading EVs with therapeutic biomolecules can be achieved in two ways; exogenously or endogenously. Exogenous loading of small molecules/RNAs is achieved either by electroporation (Mendt et al. 2018; Alvarez-Erviti et al. 2011), freeze-thaw cycles (Akuma, Okagu, and Udenigwe 2019) or by sonication (Lamichhane et al. 2016). These techniques were employed for loading EVs with small molecules such as

curcumin (Akuma, Okagu, and Udenigwe 2019) and doxorubicin (Yanhua Tian et al. 2014). Alternatively, the parent cell can be engineered to produce therapeutically potential bioactive molecules which can be naturally incorporated into EVs.

One of the first reports to demonstrate targeted drug delivery via EVs was an *in vivo* study by Alvarez-Erviti et al. In this study, engineered DC-derived EVs were loaded with siRNA by electroporation. Intravenously injected EVs carrying siRNA could then knockdown the BACE1 gene in the brain, responsible for Alzheimer's disease pathogenesis (Alvarez-Erviti et al. 2011). Subsequently, a similar *in vivo* study performed by Raghu Kalluri and colleagues could target exosomes carrying drugs to pancreatic cancer. Here, exosomes derived from fibroblast-like mesenchymal cells were loaded with siRNA/shRNA specific to oncogenic Kras^{G12D}, a mutation commonly seen in pancreatic cancers (Kamerkar et al. 2017). Partly, the efficacy of iExosomes is due to the presence of the CD47 molecule ('don't eat me' signal) on exosomes which helps exosomes to escape from being phagocytosed by immune cells (Kamerkar et al. 2017). Eventually, they were able to produce clinical grade exosome for targeting specifically oncogene Kras (known as iExosomes) in pancreatic cancer (Mendt et al. 2018) and recently registered a clinical trial to target pancreatic cancer by using iExosomes (NCT03608631). Loading efficiency of siRNA into exosomes by electroporation still remains controversial. Studies report that electroporation of siRNA into exosomes leads to the formation of siRNA/exosome/metal-ion precipitates which decrease the efficacy of therapeutic exosomes (Kooijmans, Vader, and Schiffelers 2017; Kooijmans et al. 2013). There is an urgent need for the improvement of using electroporation techniques for drug loading; in-depth characterization of the composition; reproducibility and potency of the resulting therapeutically active EVs.

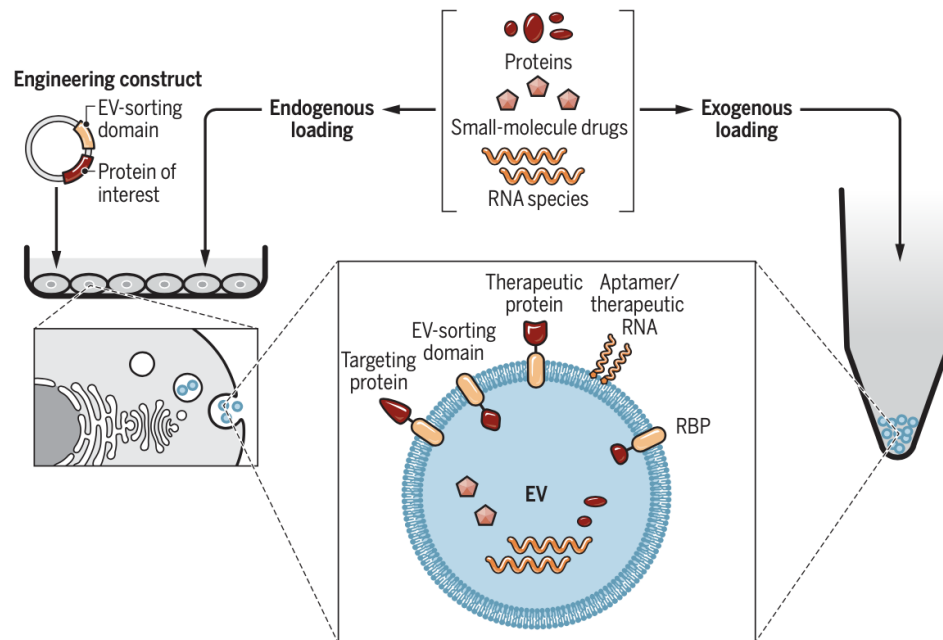


Figure 8: EV engineering and loading strategies.

From Wiklander et al., *Sci. Transl. Med.* 11, eaav8521 (2019)

1.2.7.4. Engineered EVs

Exogenous loading of EVs using electroporation, sonication and freeze thaw cycles has many pitfalls which can decrease the efficacy of the resulting EVs. However, endogenous loading or engineering the parent cell to produce therapeutically active EVs can be more efficient and maintains the integrity and target specificity of EVs. In the pioneering work by Alvarez-Erviti et al., they demonstrated the engineering of parent cells (dendritic cells) to produce EVs with targeting peptide RVG (rabies viral glycoprotein) by fusing RVG to lysosomal-associated membrane protein 2 (LAMP2b; also known as CD107b). Henceforth, the RVG peptide is displayed on the surface of the EVs (RVG-exosomes). Furthermore, loading of RVG-exosomes with a gene drug (siRNA) by electroporation and subsequent intravenous injection into mice resulted in specific gene knockdown in the target site (brain) (Alvarez-Erviti et al. 2011). RVG-exosomes loaded with miRNA-124

are used for protecting from ischemia injury by systemic administration (Yang et al. 2017). Based on this, a phase I/II clinical trial to treat acute ischemic strokes has been registered (NCT03384433). Other strategies such as, tumor-homing peptide, iRGD (CRGDK/RGPD/EC) specific to αv integrin (Sugahara et al. 2009), fused to LAMP2b targets the EVs loaded with doxorubicin to tumors resulting in tumor growth reduction (Yanhua Tian et al. 2014); parent cell expressing GE11 peptide (YHWYGYTPQNVI) fused to transmembrane domain of platelet-derived growth factor (PDGF) receptor secretes EVs harboring GE11 peptide fusion protein can specifically target EGFR expressing tumor cells (Ohno et al. 2013); ARRDC-1 mediated microvesicles (ARRMs), can efficiently package and deliver functional molecules such as suppressor p53, RNA molecules, CRISPR-Cas9/gRNA complexes which can carry out specific biological functions in recipient cells (Q. Wang et al. 2018). Figure 8 illustrates the general engineering of EVs and loading strategies.

Additionally, expressing suicide gene mRNA and protein–cytosine deaminase (CD) fused to uracil phosphoribosyltransferase (UPRT) in MV donor cells, leads to the production of MVs with CD-UPRT mRNA/protein which can serve as a novel tool for the treatment of diseases (Mizrak et al. 2013). Alternatively, there are EXOtic devices (engineered exosome producer cells) applied for boosting EV secretion, customized specific mRNA packaging and targeted delivery (Kojima et al. 2018). Furthermore, engineered EVs are employed in understanding the biodistribution of EVs *in vivo*. For instance, engineered EVs carrying the *Gaussia* luciferase reporter system are used for evaluating the biodistribution and clearance of intravenously administered EVs (C. P. Lai et al. 2014). Another prominent strategy in gene therapy is the use of AAVs (Adeno-associated vectors) as a tool to target a variety of diseases. However, the use of AAVs has its limitations, as high doses of AAVs trigger immune responses and often lead to the production of neutralizing antibodies. EVs carrying AAVs termed as vexosomes (vector-exosomes) (C. A. Maguire et al. 2012), EV-AAV (EV-associated AAV) (György et al. 2014) or exo-AAV (exosome-associated AAV) (Meliani et al. 2017) can potentially be employed to deliver a transgene to a specific target by evading immune responses.

In summary, the natural therapeutic potential of EVs has paved a way for modifying EVs which triggers huge interest in EVs as biomarker, diagnostic tools, gene expression regulators and biomolecule drug delivery vehicles. Due to the lack of standardization in their isolation, characterization methods and the lack of knowledge in EV biodistribution and clearance *in vivo* after administration, poor understanding of therapeutic EV efficacy hampered the development of EV therapeutics.

1.3. Aging and cellular senescence

Aging can be seen as the progressive loss of cellular function, eventually at organismal level, leading to many age-associated diseases such as cancer, cardiac diseases and diabetes (Flatt 2012). In 1961, Hayflick and Moorhead first demonstrated replicative senescence, meaning that somatic mammalian cells have a finite cell division capacity and proposed the so called ‘Hayflick limit’ for the ‘passage potential’ of mammalian diploid cells (Hayflick and Moorhead 1961). Given the complexity of the factors influencing aging processes, nine candidate hallmarks have been proposed contributing to aging process, cellular senescence being one of them (Figure 9) (López-otín et al. 2013). Cellular senescence is characterized by an irreversible growth arrest, resistance to cell death and secretion of many factors which promote tissue failure and inflammation (Campisi and D’Adda Di Fagagna 2007; Kuilman et al. 2010; He and Sharpless 2017). The factors secreted by senescent cells are collectively called the ‘senescent associated secretory phenotype’ (SASP) (J. P. Coppé et al. 2008). Multiple factors trigger cellular senescence, either by naturally occurring telomere shortening or by external stimuli such as oncogene activation, epigenetic changes, oxidative stress, mitochondrial dysfunction and accumulation of DNA damage.

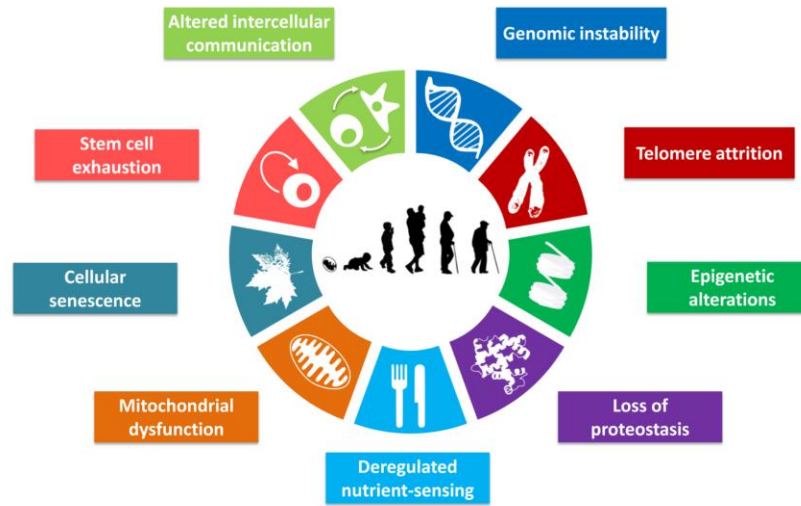


Figure 9: The Hallmarks of Aging.

From López-Otín et al. Cell. 2013 June 6; 153(6): 1194–1217.

1.3.1.Characteristics of cellular senescence

Cellular senescence, an irreversible growth arrest of metabolically active cells, is triggered by persistent DNA damage response (DDR) mechanisms, by constitutive activation of p16^{ink4a}-retinoblastoma (RB) and/or p19^{ARF}-p53 signaling pathways (Serrano et al. 1997). Progressive telomere erosion triggering activation of the ATM-p53-p21 axis, preventing permanent cell cycle arrest (Alcorta et al. 1996; Beauséjour et al. 2003). Apart from DDR, other factors such as oncogenic Ras overexpression (Di Micco et al. 2006), UV or gamma radiation (Webley et al. 2000) and chemotherapeutics (e.g: Doxorubicin) (Maejima et al. 2008) can lead to an activation of the ATM-p53-p21 axis. On the other hand, p16^{ink4a}-mediated growth arrest is mediated by CDK4 and CDK6 via inactivating RB. p16^{ink4a} can act independently or in combination with p21-p53 pathways (Van Deursen 2014). The elevated levels of p16^{ink4a}, p19^{ARF}, p53 and p21 are often seen in senescent cells or aging tissues compared to quiescent or normal tissues (Krishnamurthy et al. 2004).

Other than cell-cycle regulators, senescent cells exhibit elevated activity of lysosomal β -galactosidase which facilitates the identification of senescent cells in culture and tissue samples (Dimri et al. 1995). Henceforth, this senescence marker is termed as senescence-associated β -galactosidase (SA- β -gal) activity. Senescence-associated changes in gene expression are often related to cell-cycle and metabolism related genes along with changes in secretory proteins which constitute the SASP. SASP factors majorly constitute of signaling molecules (cytokines, chemokines and growth factors), extracellular matrix remodeling proteins (matrix metalloproteinases (MMPs), serine proteases) and extracellular insoluble proteins (fibronectin, laminins, collagens) (J.-P. Coppé et al. 2010; Lämmermann et al. 2018). SASP factors are known to alter the tissue microenvironment by stimulating cell invasion, proliferation, migration and modulating immune response, therefore impacting aging itself and age-associated diseases. As aforementioned, considering the nature of the SASP factors, their ability to alter intercellular communication is considered as being one of the candidate hallmarks of aging.

1.3.2. Clearance of senescent cells

It is known that senescent cells accumulate in tissues and organs with age and that their secretome influences age-associated pathologies. However, many studies reported that the clearance of senescent cells from the system can improve the healthy life span of an organism. One such study from Baker et al. elegantly demonstrated that the genetic inactivation of p16^{ink4a} and p19^{ARF} in BubR1 progeroid mice increases the life span in mice by removal of p16^{ink4a} positive senescent cells (Baker et al. 2008). For the proof-of-principle, a drug inducible transgene INK-ATTAC (apoptosis through targeted activation of caspase) was expressed under 2, 617 bp fragment of the p16^{ink4a} gene promoter (W. Wang et al. 2001). A synthetic drug, AP20187 can then induce dimerization of a membrane-bound myristoylated FK506-binding-protein–caspase 8 (FKBP–Casp8) and eliminates p16^{ink4a} positive senescent cells by inducing apoptosis. Removal of senescent

cells from BubR1 mice increased their life span and delayed the onset of age-related diseases (Baker et al. 2011, 2016). Since senescent cells accumulate with aging and are considered as a primary factor influencing aging. However, the primary role of senescent cells in the system is to get rid of damaged tissue or oncogenic cells or the suppression of atherosclerosis.

1.3.3. Cellular senescence and EVs

The senescent cell secretome (SASP factors) constitutes of growth factors, chemokines, cytokines, matrix metalloproteinases (MMPs) and extracellular matrix components (fibronectins, laminins and collagens). In addition, EV secretion is influenced by various stress stimuli and the pathological status of cells/tissues. SASP factors are known to induce senescence in neighboring cells and alter tissue microenvironment. It's still unclear how SASP factors regulate senescence. Until now, only a handful of studies report about enhanced EV secretion in senescent cells compared to non-senescent counterparts (Lehmann et al. 2008; Effenberger et al. 2014; Terlecki-Zaniewicz et al. 2018; Jeon et al. 2019; A. Takahashi et al. 2017). However, EVs as SASP mediators are still poorly studied. Very recent studies report that EVs secreted from senescent cells harboring biomolecules such as nucleic acids and proteins which can influence the initiation of senescence in neighboring cells in a paracrine fashion (Terlecki-Zaniewicz et al. 2018; Borghesan et al. 2019). Senescent cells selectively sort the cargo such as miRNAs with anti-apoptotic and senescence inducing properties into EVs (Terlecki-Zaniewicz et al. 2018, 2019). Furthermore, activation of DDR pathways in senescent cells results in the accumulation of harmful nuclear DNA in the cytoplasm which is further sorted and secreted via exosomes. Additionally, it has been shown that senescent cell secreted exosomes have the potential to activate DDR pathways in recipient non-/pre-senescent cells (A. Takahashi et al. 2017). Taken together, EVs secreted from senescent cells are part of the SASP factors and possess therapeutic potential. Blocking or clearance of the senescent cell secreted EVs can

minimize the spreading of senescence in aging tissues. However, for all this work, better isolation strategies and *in vivo* tracing methods are necessary.

2. AIMS

Although there has been accelerating increase in studies of EV biogenesis, molecular composition and therapeutic applications, the fundamental problem still remains to be solved regarding isolation of tissue or cell-specific EVs from biological fluids, their purity and the efficiency of the purification method. The main aim of this study is therefore to develop and evaluate a novel affinity based EV purification method using snorkel-tag (Brown et al. 2013); Snorkel-tag based Extracellular Vesicle Affinity Chromatography (StEVAC). Snorkel-tag was especially designed to study membrane proteins where N- and C-termini of the proteins are inside the lumen. We genetically fused the snorkel-tag to the C-terminus of CD81, which enables tags to be displayed on the surface of the EVs. Finally, using affinity based chromatography, EVs are purified by on-column proteolytic cleavage. In addition, we systematically evaluated the StEVAC method by using multiple EV characterization techniques (Part A).

Striking evidences have been reported on clearance of senescence cells in improving healthy life span in mice. EVs being the members of SASP are great potential targets for therapeutic intervention. For this purpose, (Part B) we wanted to evaluate monoclonal antibodies produced against human dermal fibroblast derived EVs for their neutralizing effects. In the next step we planned to identify the epitope of novel monoclonal antibody and its role in EV internalization (Part B).

Finally, we planned to generate an *in vivo* model with CD81-snorkel-tag expressed under p16^{ink4a} promoter to get insights in the EV cargo under pathophysiological conditions.

3. RESULTS

PART A

3.1. Establishment of Snorkel-Tag based Extracellular Vesicle Affinity Chromatography (StEVAC) method for recombinant EV purification

3.1.1. Design of recombinant tetraspanins for the production of recombinant EVs

To isolate cell- or tissue-specific EVs, we fused tetraspanins (CD81) with a snorkel-tag, enabling mild isolation and tracking of EVs harboring these recombinant tetraspanins. For this, we designed different constructs with the snorkel-tag fused to either the C- or N-termini of CD81. Additionally, components of the snorkel-tag are fused either to the small extracellular loop or to the large extracellular loop to a truncated CD81 (TMD1 or TMD4 truncations). Schematic representation of the different snorkel-tag constructs is depicted in Figure 10A. Accordingly, snorkel-tags were fused to either C- or N- terminus of CD81 represented in Figure 10B. Complete structural representation of the different CD81 constructs are shown in supplementary figure 1

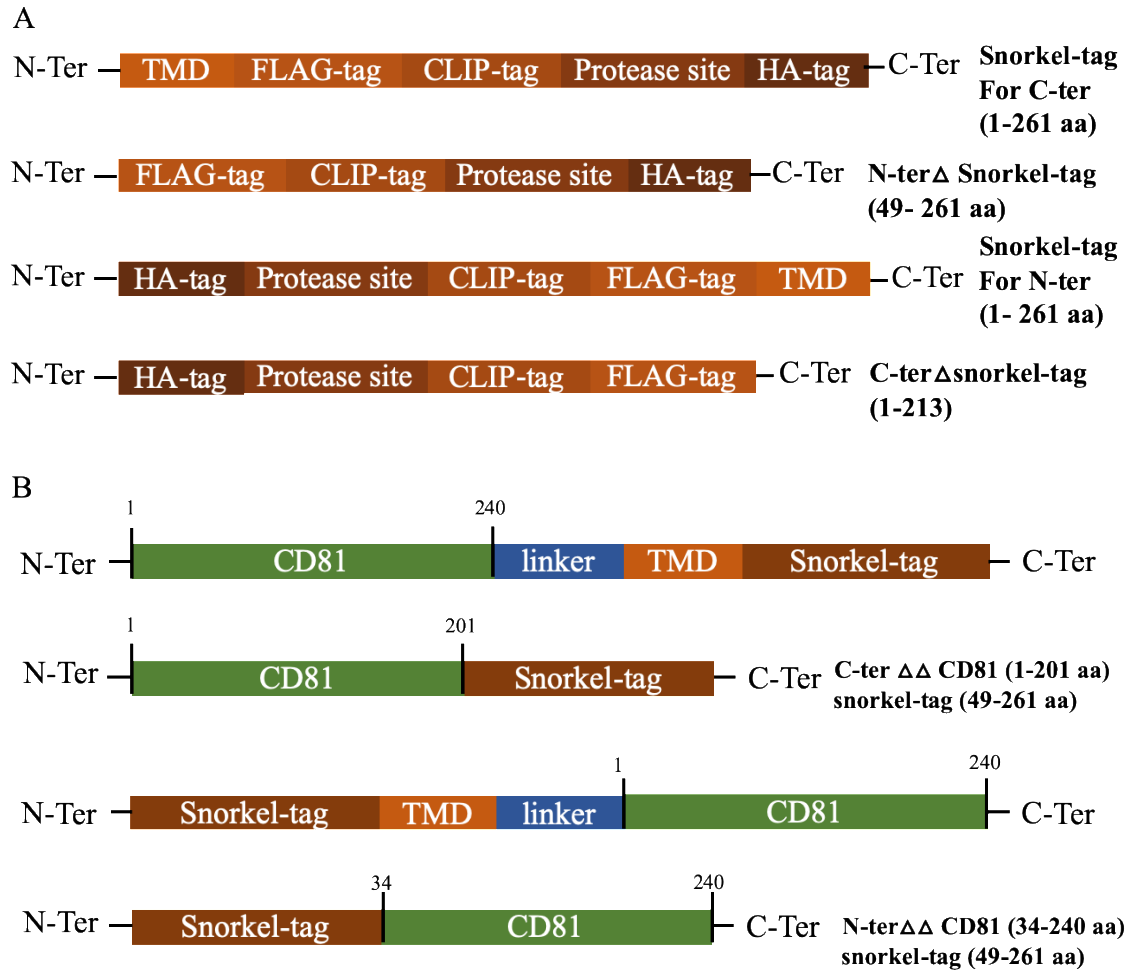


Figure 10: Schematic representation of different snorkel-tags (A), and snorkel-tags fused to CD81 full length or truncated versions (B).

All four different constructs were cloned into pcDNA 3.1 plasmid and stably expressed in HeLa cells. HeLa whole cell extracts were analyzed for components of the fusion proteins with snorkel-tag by immunoblotting. We observed all the versions of CD81-snorkel-tag detected at the desired size except for N-terminal truncation version (Figure 11). Next, we confirmed the localization of CD81-snorkel-tag versions by immunofluorescence. We found that the membrane localization is impaired when snorkel-tag was fused to N-terminus of CD81 (data not shown). Therefore, we decided to select CD81-C-terminal snorkel tag for all further experiments.

To evaluate if the PreScission protease cleavage site is accessible when CD81-snorkel-tag is bound to anti-HA affinity matrix, we incubated the total cell lysate of HeLa cells expressing CD81-C-terminal snorkel-tag overnight at 4°C and applied PreScission protease of 5 μ l (10 units) for overnight digestion. Post incubation, the beads were separated, and lysate was loaded onto SDS-PAGE for immunoblotting. Immunoblot results revealed PreScission protease site was not accessible when bound to anti-HA matrix (Figure 12).

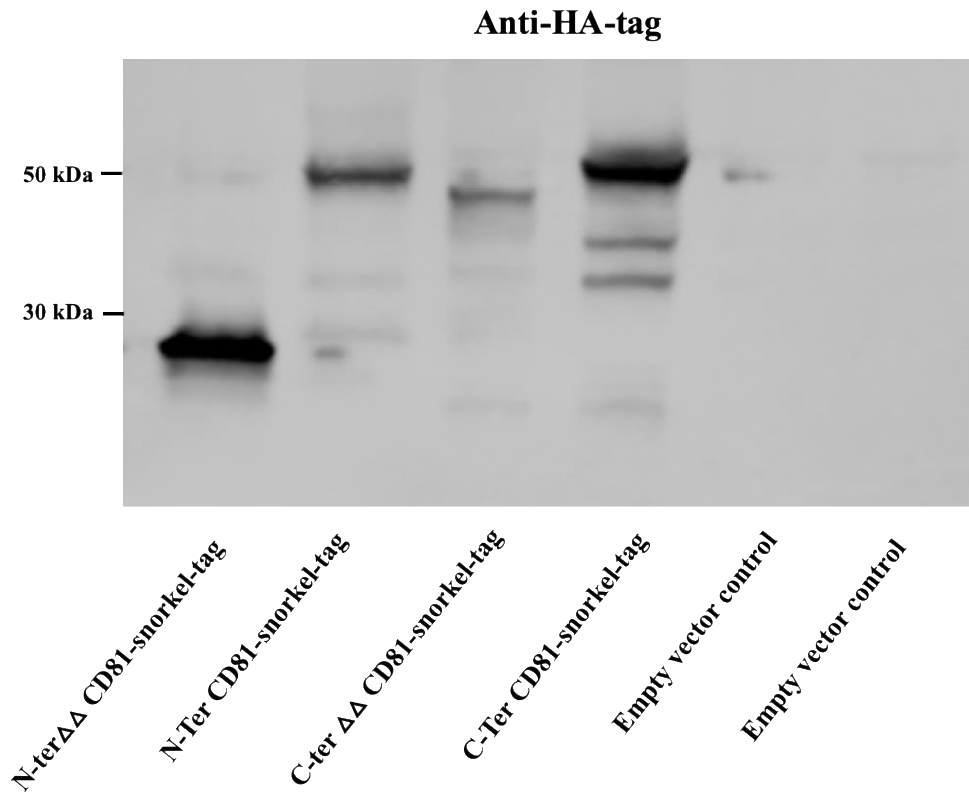


Figure 11: Western blot for snorkel-tag epitope (HA-tag) from HeLa cell lysates expressing all variants of CD81-snorkel-tag.

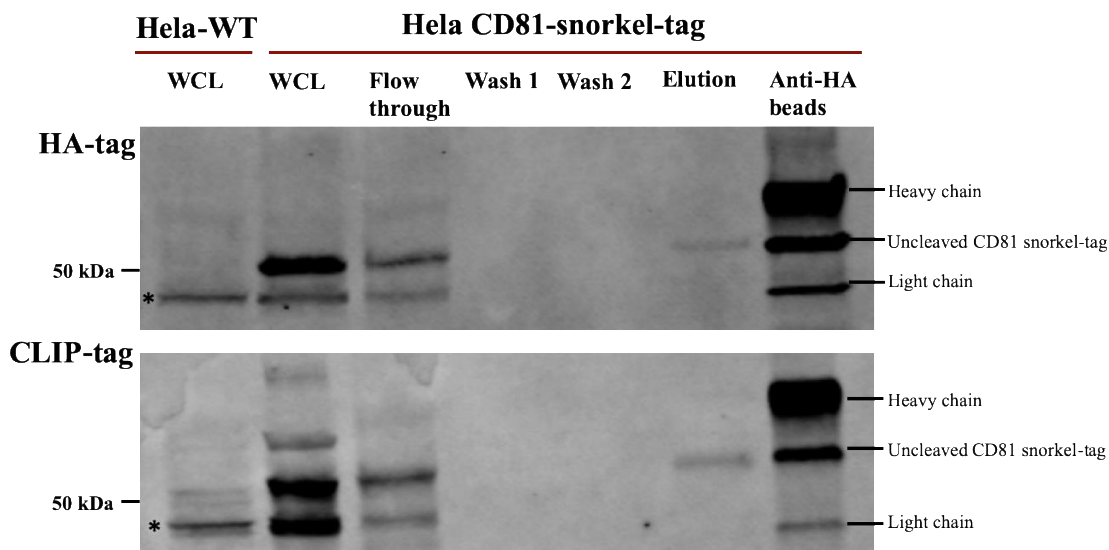


Figure 12: Confirmation of PreScission protease cleavage site accessibility on snorkel-tag bound to anti-HA affinity matrix.

100 μ g of HeLa cell lysates expressing CD81-snorkel-tag was incubated with anti-HA affinity magnetic beads overnight. Flow through was collected and beads were washed twice with PBS. Beads were incubated with PreScission protease overnight. Elutes were collected by separating magnetic beads. All the samples including anti-HA magnetic beads were processed and loaded on to SDS-PAGE for immunoblotting. Western blot for HA-tag and CLIP-tag is shown. WCL: whole cell lysate; '*' represents unspecific band.

Hence, we decided to introduce flexible G4S linkers on either side of PreScission protease site and a rigid linker between the transmembrane domain and FLAG-tag. The schematic representation of C-terminal snorkel tag and CD81-snorkel-tag with linkers is depicted in Figure 13. We used the new version of snorkel-tag with linkers for developing the StEVAC method.





Figure 13: schematic representation of snorkel-tag with G4S linker on either side of PreScission protease and rigid linker between transmembrane domain (TMD) and FLAG-tag (A), and snorkel-tag fused to C-terminal of CD81 full length (B).

3.1.2. Characterization of a CD81-snorkel-tag harboring EV producer cell line

To produce recombinant EVs harboring the snorkel-tag on their surface, we stably expressed the selected construct of snorkel-tag fused to the C-terminus of CD81 in HeLa cells. Therefore, it was cloned into pBMN plasmid which allows for retroviral packaging, produced in phoenix cells, and retroviral non-replication competent virus was used to transduce HeLa cells for stable expression. Whole cell extracts were analyzed for the recombinant protein containing the snorkel-tag by immunoblotting using an anti-HA antibody to detect the HA epitope, an anti-CLIP antibody to detect the CLIP epitope and an anti-FLAG antibody to detect the FLAG epitope. Furthermore, an anti-CD81 antibody could detect wild type (WT) and recombinant CD81 (CD81-snorkel-tag). A prominent band at ~50 kDa was detected for all the components carrying the snorkel-tag, whereas for CD81 two prominent bands, one for WT (~24 kDa) and the other for recombinant CD81 (~50 kDa) were detected (Figure 14A).

Furthermore, flow cytometry analysis was performed on HeLa cells expressing CD81-snorkel-tag with a membrane impermeable CLIP substrate (CLIP-SurfaceTM 647) to validate the functionality of the CLIP-tag. Indeed, we observed covalently labelled CLIP substrates in the flow cytometry analysis (Figure 14B) proofing that the snorkel-tag fused tags are displayed on the surface of the cell. For localization of CD81 and the snorkel-tag, we performed confocal imaging on membrane permeabilized and non-permeabilized cells.

We observed localization of the snorkel-tag on the plasma membrane in non-permeabilized cells and intracellular localization in permeabilized cells. These results indicate that fusion of the snorkel-tag to CD81 enables tags to be displayed on the surface of the cell membrane (Figure 15) and therefore correct localization of the fusion protein.

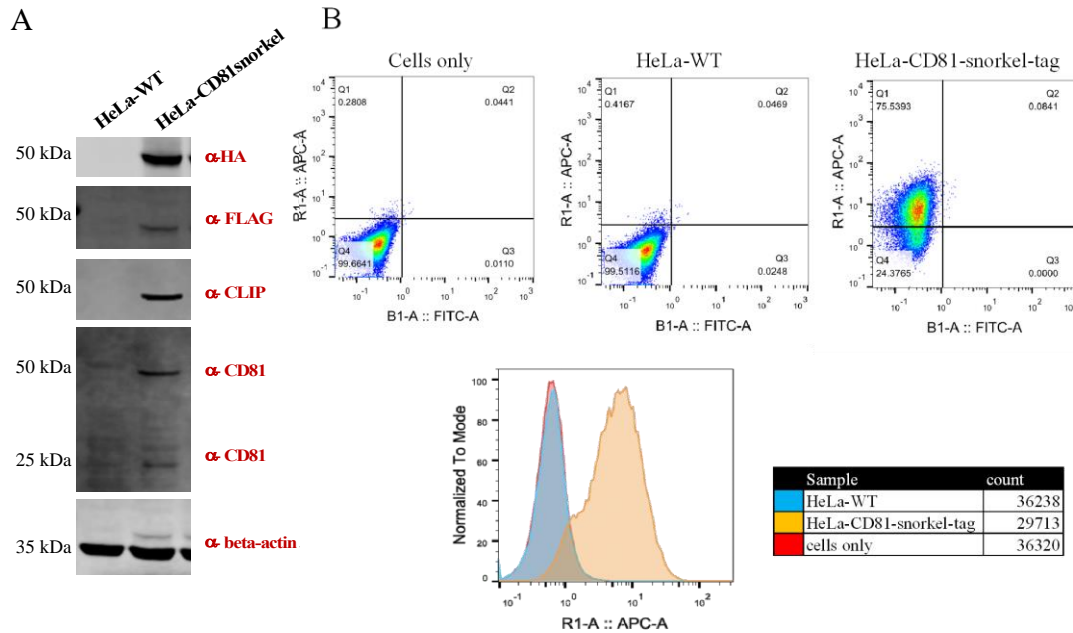


Figure 14: Evaluation of CD81-snorkel-tag in stably expressing HeLa cell.

(A) Western blot for snorkel epitopes (HA, CLIP, FLAG), CD81 proteins of HeLa-WT and HeLa-CD81-snorkel-tag lysates. (B) Flow cytometry analysis for CLIP-tag functionality by covalent labeling of CLIP-Surface™ 647.

Aforementioned, PreScission protease cleavage site was introduced to the snorkel-tag between CLIP-tag and HA-tag. PreScission protease enables specific, simple and on-column elution by cleavage during affinity purification at low temperatures. PreScission protease specifically cleaves between the Gln and Gly residues of the recognition sequence LeuGluValLeuPheGln/GlyPro (Kinloch et al. 2008; Todi et al. 2010). To check the specificity of PreScission protease, we treated 100 µg of whole cell lysate from HeLa-CD81-snorkel-tag at different time points at 4° C. We observed that overnight treatment of

PreScission protease cleaves off >95% of the HA-tag (Figure 16). This confirmed that proteins or EVs carrying snorkel-tag can be cleaved and thus might indeed allow on-column cleavage using PreScission protease.

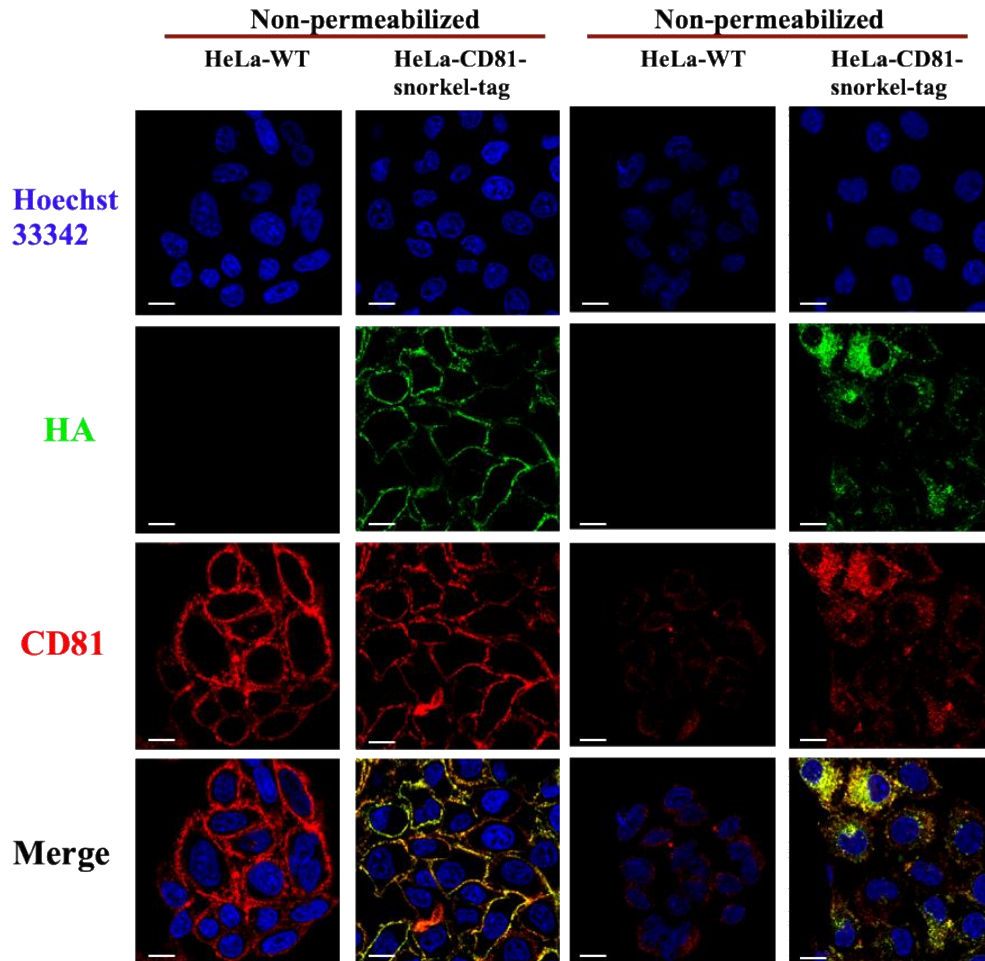


Figure 15: CD81-snorkel-tag expressing HeLa cells display snorkel-tag on the surface of the cell membrane.

Right two panels: Immunofluorescence (IF) for CD81 and HA-tag in non-permeabilized HeLa cells, Left two panels: IF for CD81 and HA-tag in permeabilized HeLa cells. Counterstaining with Hoechst 33342 for DNA.

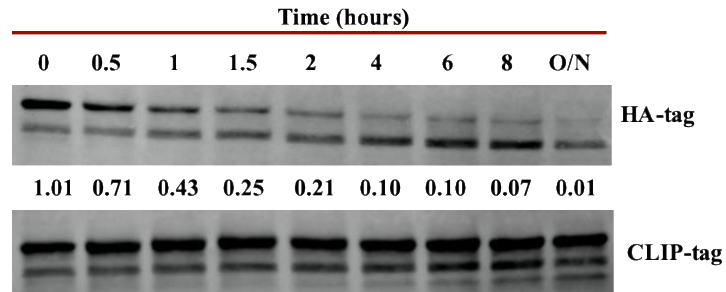


Figure 16: Specificity of PreScission protease activity.

Western Blot of HeLa cells expressing CD81-snorkel-tag treated with PreScission protease for indicated time periods mentioned above. The blots were probed with antibodies against HA-tag and CLIP-tag. The mean intensity of the bands was quantified and the ratio of the HA-tag vs. CLIP-tag is shown.

3.1.3. Isolation of EVs using tangential flow filtration (TFF) and characterization

Differential ultracentrifugation (UC) is the most commonly used technique for purifying EVs. However, some of the pitfalls using UC for purifying EVs are that it is time consuming, not feasible for large-scale isolations, leads to co-isolation of contaminants and formation of EV aggregates. Tangential flow filtration can be used for large-scale EV isolations in less time and can avoid aggregation of EVs. For this, we collected the conditioned media (CM) from HeLa-WT and HeLa-CD81-snorkel-tag expressing cells after 48 hours of cultivation. CM was subjected to differential centrifugation to remove cell debris at 700 x g and larger vesicles at 2000 x g, filtered through 0.22 μ filter followed by a step for concentration, using TFF with a 300 kDa MWCO hollow fiber. Schematic representation of the workflow for TFF based EV isolation is depicted in Figure 17A. Concentrated EVs were characterized for size and concentration via nanoparticle tracking analysis (Figure 17: B, C). We observed there is no significant difference in the size WT and CD81-snorkel-tag carrying EVs (Figure 17D).

A

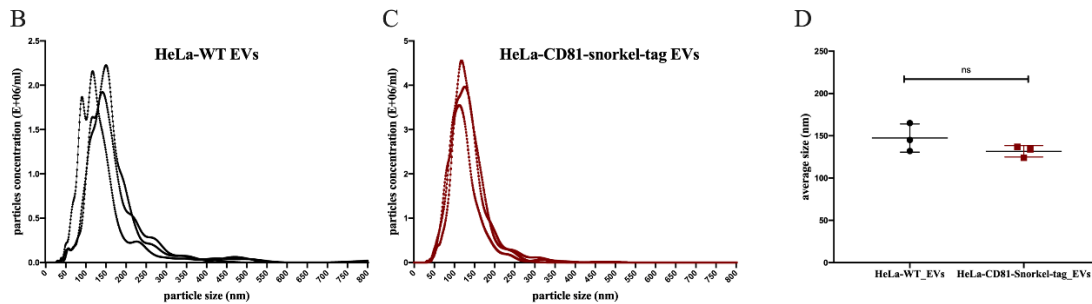
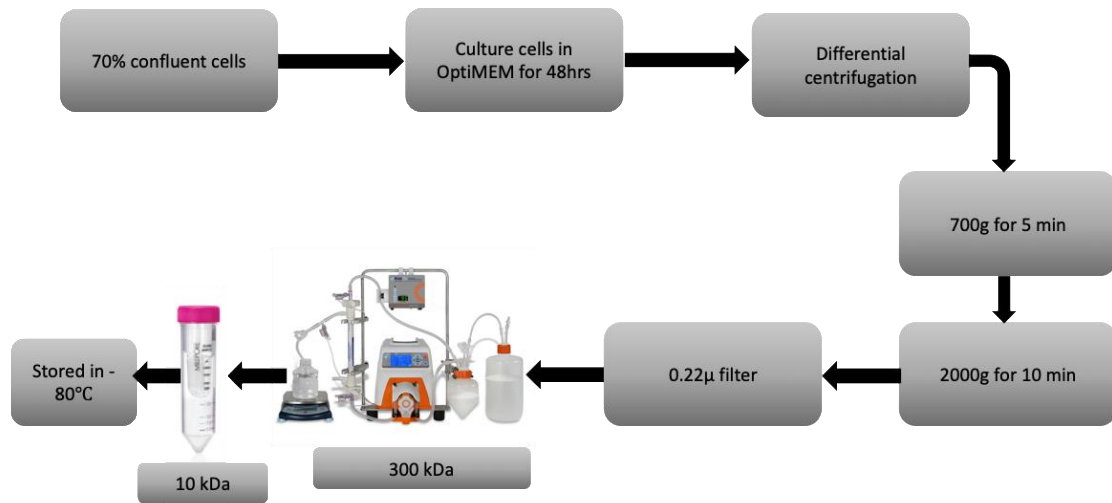


Figure 17: Isolation of EVs using TFF and characterization.

(A) Schematic overview of workflow. Processed conditioned media (CM) were concentrated by TFF with 300 kDa hollow fiber system to 10th of initial volume and further to 1 ml by ultrafiltration using 100 kDa amicon centrifuge tubes. (B, C) Representative particle size distribution and concentration for HeLa-WT and HeLa-CD81-snorkel-tag cell line derived EVs analyzed using nanoparticle tracking analysis (NTA) (n=3). (D) Mean size of the particles was assessed to check the reproducibility. Unpaired t-test was applied on raw values; ^{ns}P > 0.05.

To assess the purity of the EVs isolated by TFF and check the enrichment of EV-associated proteins in the EV preparations, we performed immunoblotting. All EV-associated proteins such as TSG101, ALIX and syntenin were detected (Figure 18A). Furthermore, to test for

cytoplasmic contaminations, blots were analyzed for calnexin (ER protein) presence, a protein known to be excluded from EVs (REF). Indeed, calnexin was detected only in cell lysates and not in the EV preparations (Figure 18A). To assess the size and morphology of the EVs, transmission electron microscopy (TEM) was performed. TEM showed intact cup-shaped EVs on electron micrograph with similar sizes quantified by NTA (Figure 15B, C). Also, no size difference between HeLa-WT EVs (Figure 18B) and HeLa-CD81-snorkel-tag EVs were observed, indicating that the recombinant CD81 does not change principle morphology of the EVs. In order not to be biased and as recommended by the MISEV guidelines, an overview image to show the abundance of EVs with a 1 μm scale-bar is presented for HeLa-CD81-snorkel-tag EVs (Figure 18C, left image).

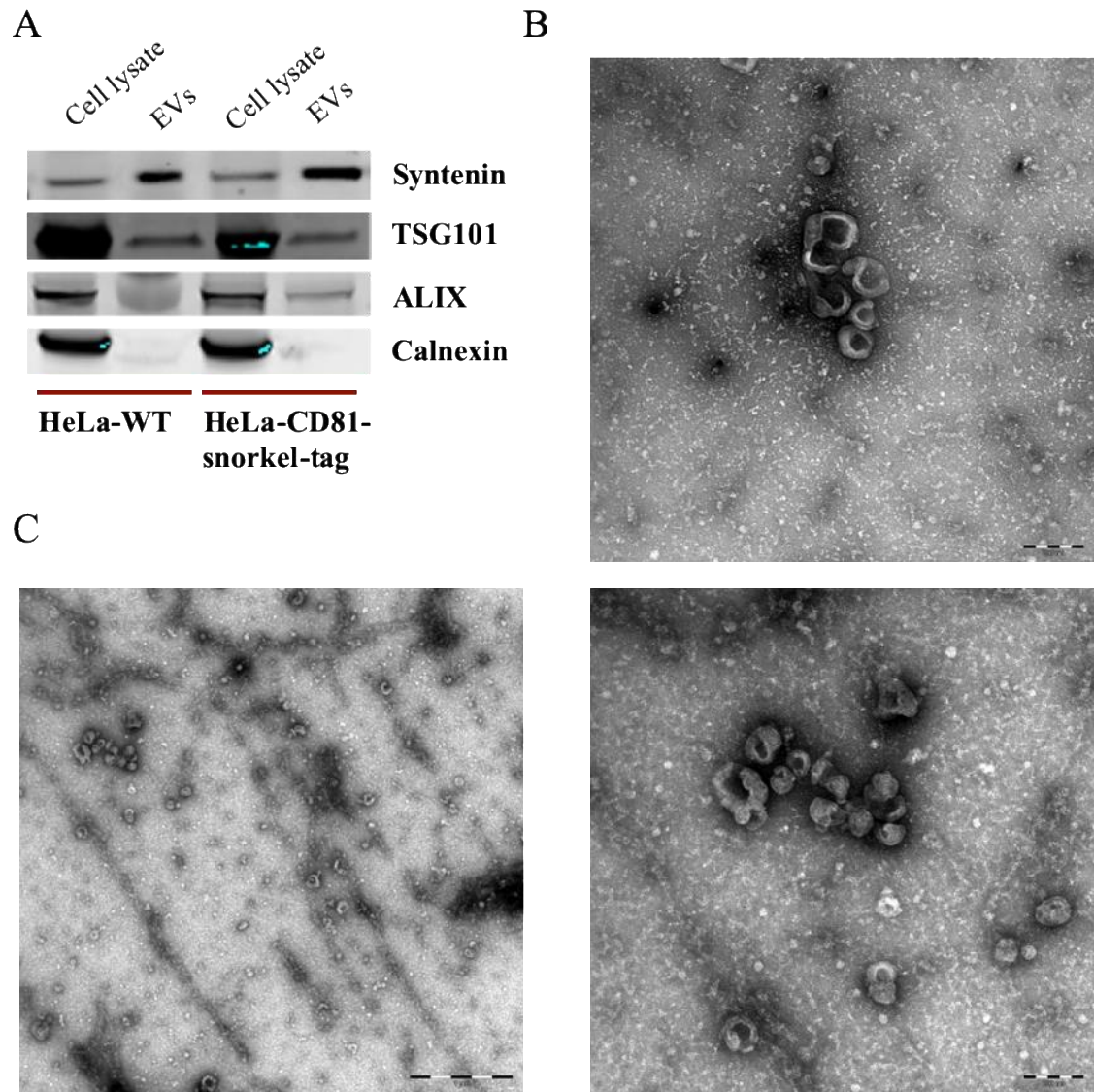


Figure 18: Characterization of EVs for purity, size and morphology.

(A) Western blot of HeLa-WT and HeLa-CD81-snorkel-tag cell lysates and EV lysates for EV-associated proteins such as syntenin, TSG101 and ALIX and non-EV associated protein calnexin. (B) Transmission electron microscopy (TEM) images for HeLa-WT EVs. EVs are within the range of 50-100 nm in diameter. (C) TEM images for HeLa-CD81-snorkel-tag carrying EVs. Overview image (Left, scale bar 1 μ m) shows the abundance of EVs in the preparation and image showing (right, scale bar 200 nm) the size of the EVs ranging between 50-200 nm.

In addition, we performed multiplex bead-based flow cytometry to evaluate if the surface protein composition of EVs might be changed by snorkel-tag CD81 overexpression. The multiplex bead-based flow cytometry provides a robust and semi-quantitative analysis of 37 different potential EV surface proteins to investigate the heterogeneity of EV subtypes. Our results demonstrate that TFF isolated EVs from HeLa-WT and HeLa-CD81-snorkel-tag conditioned media (CM) possess a similar EV protein surface signature when detected by pan-tetraspanin detection antibodies. Both EV preparations showed enrichment for all tetraspanins (CD9, CD63 and CD81). Besides tetraspanins, other HeLa-cell specific markers such as CD24, CD44, CD146 and MCSP showed strong signals in our preparations. Other marker proteins like CD29, CD105 and HLA-ABC showed intermediate- or low-level signals for both HeLa-WT and HeLa-CD81-snorkel-tag EVs (Figure 19). However, we observed a slight signal with CD56 in samples with CD81-snorkel-tag EVs which is below detection level in WT EVs. This could be because of its unspecific nature of CD56 capture beads which we repeatedly observed in consecutive experiments. Taken together, our results indicate that with the methods used so far, we do not observe differences in the EV surface composition induced by snorkel tag CD81.

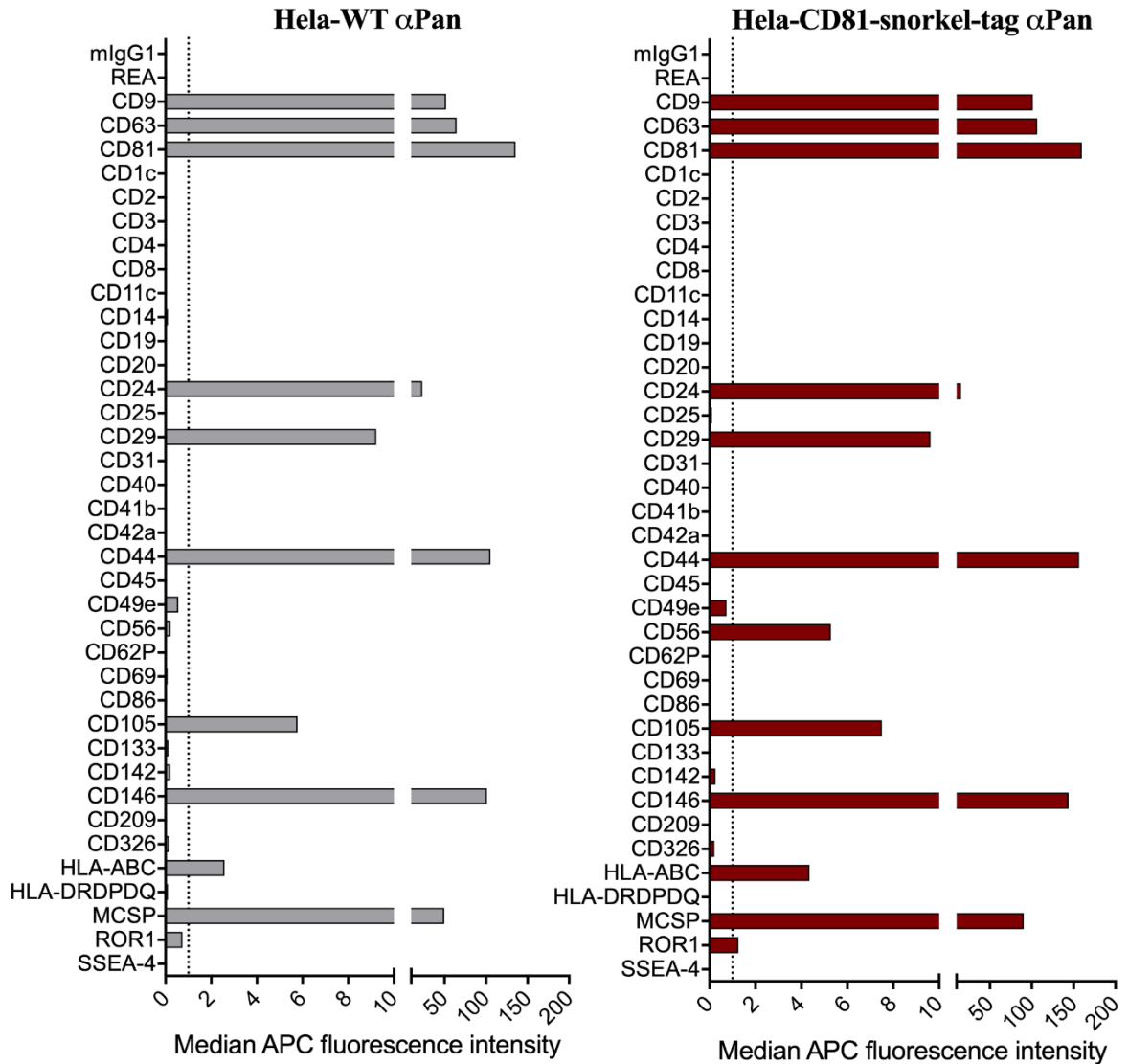


Figure 19: Multiplex bead-based flow cytometry assay for detection of EV surface protein signature.

Representative quantification of media APC fluorescent intensity for all the bead populations after background correction with PBS control. HeLa-WT EVs (Left panel) and HeLa-CD81-snorkel-tag carrying EVs (right) show no difference in their surface protein signature. For results after analyzing HeLa-WT and HeLa-CD81-snorkel-tag EVs compared to PBS control.

To explore further insights into the EV protein surface signature, we evaluated it for EVs isolated from different primary cell lines such as HUVEC, ASCs and HDFs. EVs from different cell sources are enriched for EV/exosome markers like CD9, CD63 and CD81 followed by other markers which are cell-specific. Analysis of the EV surface protein signature by multiplex bead-based flow cytometry revealed that EVs from different cell sources carry different surface protein signatures (Figure 20).

Furthermore, to check for donor variability, we compared HDF76 and HDF164-hTert overexpressing cell line derived EVs for EV markers. Our results demonstrate that there is no change in the EV surface marker detection between two different donors. In addition, the EV purification technique can have an influence on the subtype of EVs isolated. To check for this, we analyzed HDF76 EVs isolated by TFF and ultrafiltration by multiplex bead-based flow cytometry (Supplementary Figure 2). Our results confirm that there is no variability in the EVs isolated by TFF and ultrafiltration. These results demonstrate the sensitivity and reproducibility of the assay for the quantification of EVs.

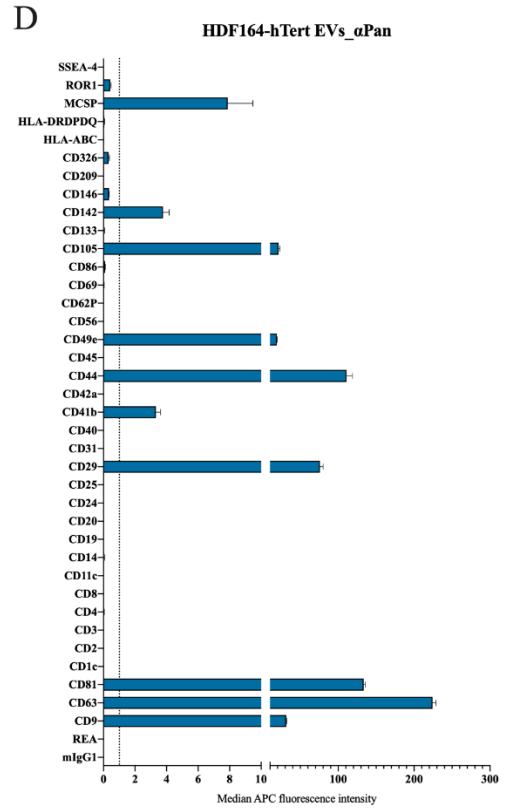
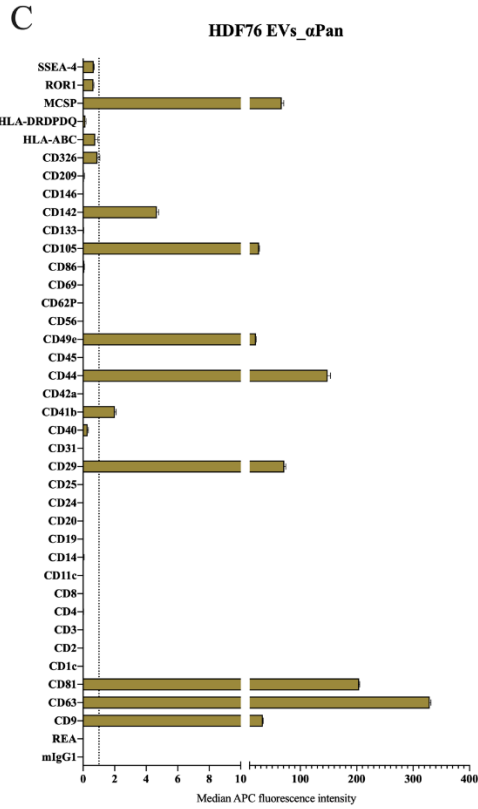
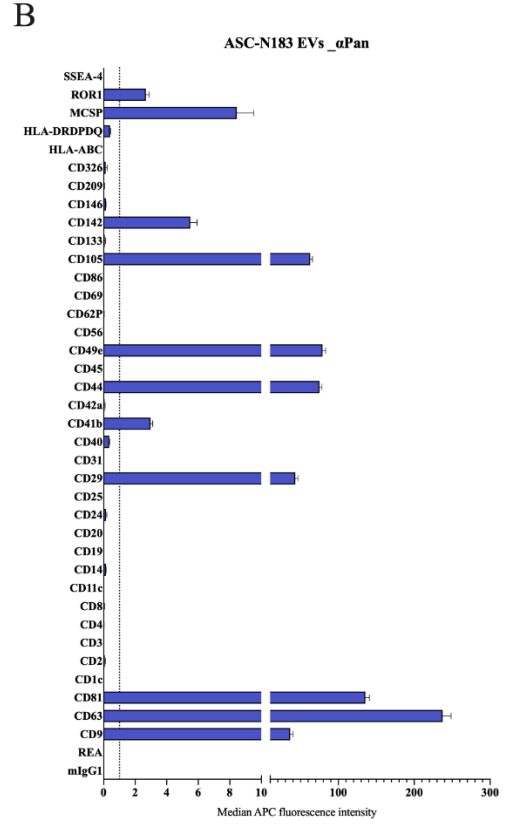
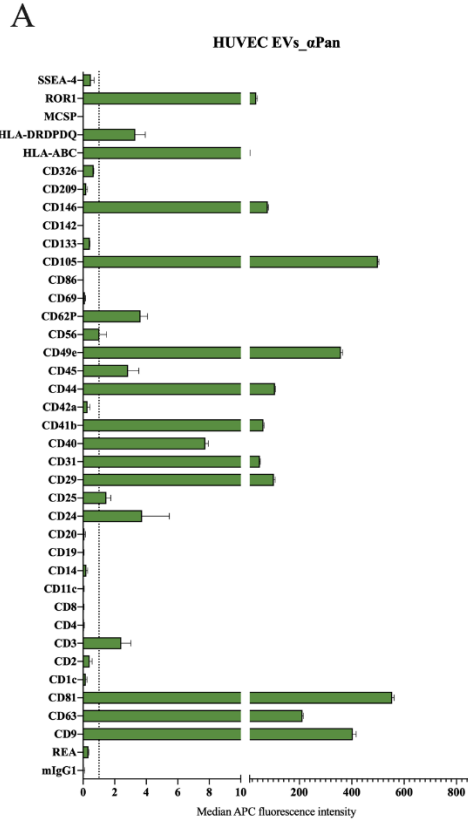


Figure 20: Multiplex bead-based flow cytometry assay for detection of EV surface protein signature for EVs derived from different cell lines.

(A) HUVEC derived EVs. (B) ASC derived EVs. (C) HDF76 derived EVs. (D) HDF164-hTert overexpressing cell derived EVs.

3.1.4. Confirmation of snorkel-tag presence on the recombinant EVs

In order to confirm the presence of the snorkel-tag on EVs derived from CD81-snorkel-tag overexpressing cells, we performed several experiments. Firstly, immunoblot analysis of EVs derived from HeLa-WT and HeLa-CD81-snorkel-tag overexpressing cells were used to reveal the presence of snorkel-tag components in EV lysates from HeLa-CD81-snorkel-tag overexpressing cells only, whereas syntenin, an EV-associated protein used as positive control for EV isolation was detected in control and snorkel-tag carrying EV lysates (Figure 21A). In addition, TEM with immunogold labeling against CD81 and the HA-tag contained in the snorkel-tag using differently sized gold particles to differentiate between these two was performed. Indeed, we observed clear labeling for both snorkel-tag and CD81 on the EVs derived from HeLa-CD81-snorkel-tag (Figure 21C), whereas for wildtype EVs we only detected CD81 (Figure 21B). These results confirm the presence of the snorkel-tag on the surface of EVs.

Furthermore, multiplex bead-based flow cytometry was performed – now using an HA tag detection antibody instead of the directly labeled pan-tetraspanin one. In brief, after capturing the EVs on capture beads coupled to all the single surface marker antibodies, anti-HA antibody (rabbit) followed by an anti-rabbit detection antibody (Dylight-649) was used for counterstaining. These results confirm the presence of the snorkel-tag on the surface of our recombinant EVs only, and further clearly show that the surface protein signature is still similar to the pan-detection shown above (fig. 19). However, in spite of using the same number of EVs (1×10^9 EVs) for both assays (Figure 22), the median

fluorescence intensities in the indirect labelling are lower compared to the pan-detection. This might be due to either the extra labeling step involved which might have led to the loss of EVs or the probability that not all EVs carry the snorkel tagged CD81 resulting in lower EV numbers bound to the beads.

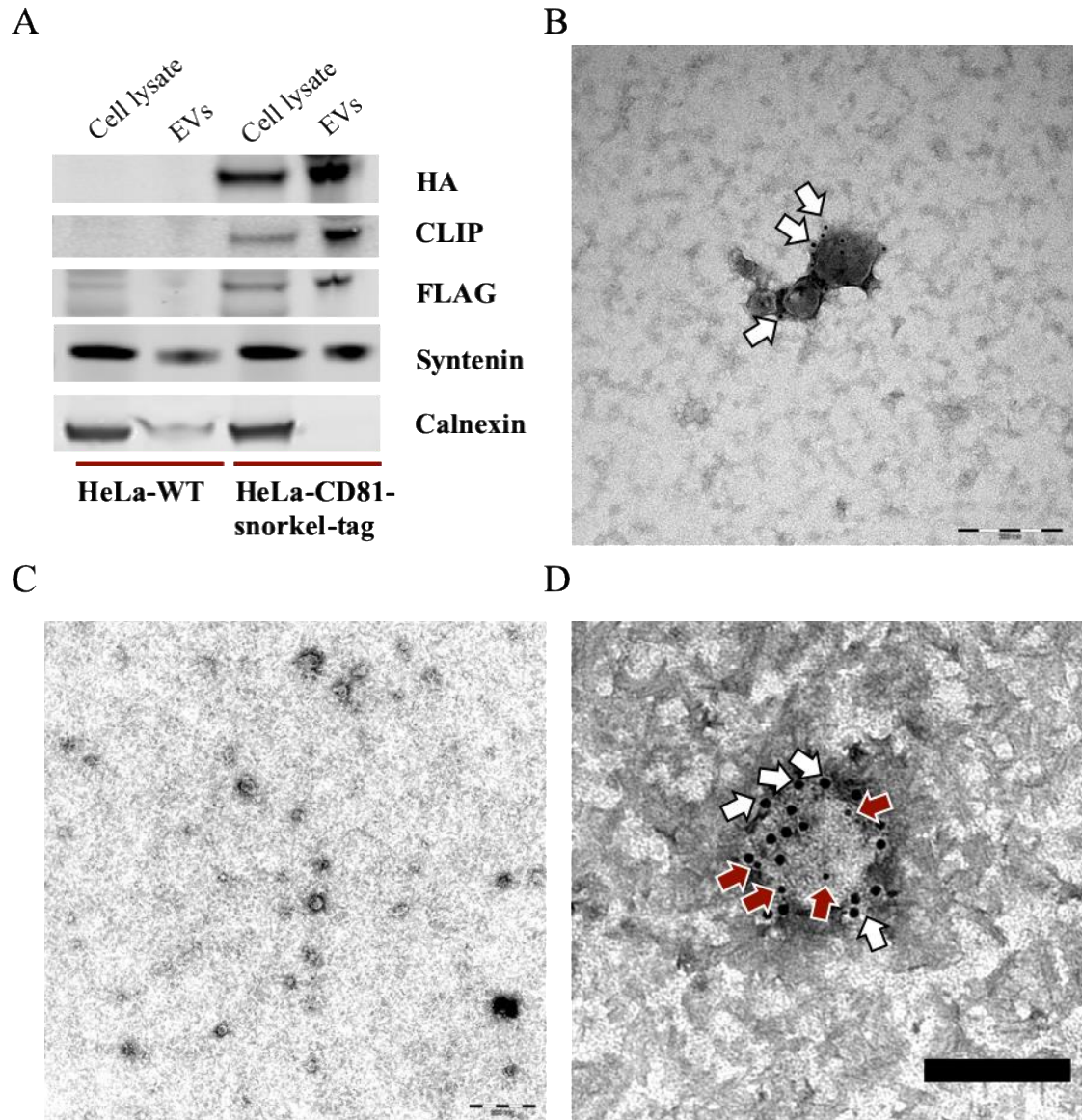


Figure 21: Characterization of EVs carrying snorkel-tag.

(A) Western blotting analysis of TFF purified EVs derived from HeLa-WT and HeLa-CD81snorkel (5×10^9 particles loaded per well) for the snorkel tag components. (B, C, D) TEM images showing immunogold labeling against CD81 and snorkel tag for EVs secreted from HeLa-WT and HeLa-

CD81-snorkel-tag cells. (B) HeLa-WT EVs detected only for CD81 (scale bar: 200 nm), (C) HeLa-CD81-snorkel EVs showing a wide field (scale bar: 1 μ m) (D) a close-up/zoomed-in picture of (C) HeLa-CD81-snorkel-tag EVs detected for both CD81 and snorkel-tag (probed for HA-tag). White arrows label CD81 and red arrows label snorkel tag (scale bar: 100 nm).

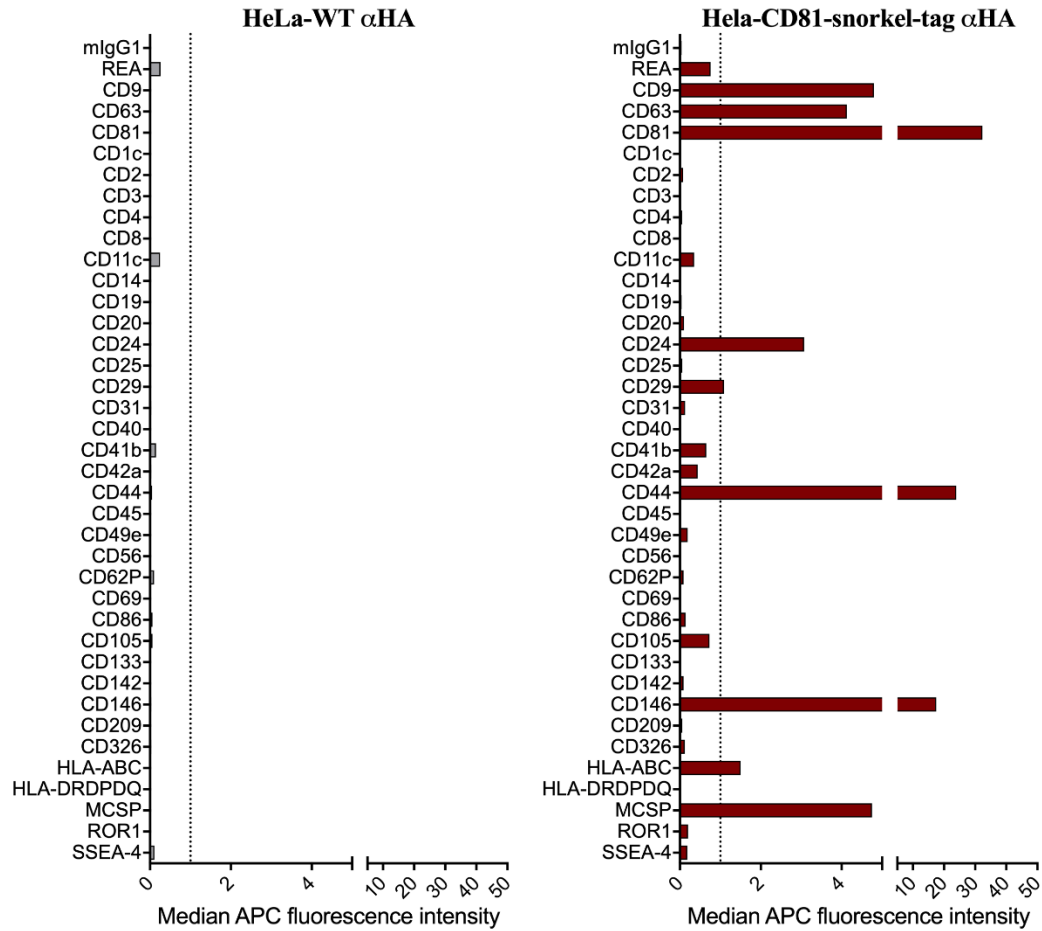


Figure 22: Multiplex bead-based flow cytometry by indirect labeling.

EVs captured on antibody coated beads were labeled with anti-HA antibody (rabbit) followed by Dylight-649 conjugated anti-rabbit IgG antibody. Snorkel-tag carrying EVs show characteristic HeLa EV surface protein signature. As controls for the experiment we included pan-detection labeling for both HeLa-WT and HeLa-CD81-snorkel-tag EVs (Supplementary figure 3).

To summarize, we here show the presence of the snorkel-tag on the surface of EVs and successfully prove that EVs carrying the snorkel tag do maintain the surface protein signature as detectable by MACSplex using pan tetraspanin and HA-tag detection antibodies.

3.1.5. Isolation of EVs by Snorkel-tag based EV Affinity Chromatography (StEVAC)

EVs are commonly isolated using different techniques such as ultracentrifugation, TFF and size-exclusion. However, the use of these techniques results in an isolation of the total EV population. For isolating EVs from specific cell types one can choose immunoaffinity based isolation techniques. For this, knowledge of the EV surface composition is required to isolate cell- or tissue-specific EVs. The main disadvantage of using immunoaffinity based methods is that these EVs can then only be used for quantitative purposes and not for functional studies as elution methods available so far rely on EV destroying low pH or high salt methods. To overcome these issues, we wanted to confirm that our snorkel-tag based EV affinity chromatography which involves on-column protease treatment for isolating EVs does result in functional EVs. For this, conditioned media was pre-cleaned and filtered through 0.22 μm filter and concentrated to 1 ml using the ultrafiltration technique. Isolated EVs were quantified for their size and concentration using NTA (Figure 23).

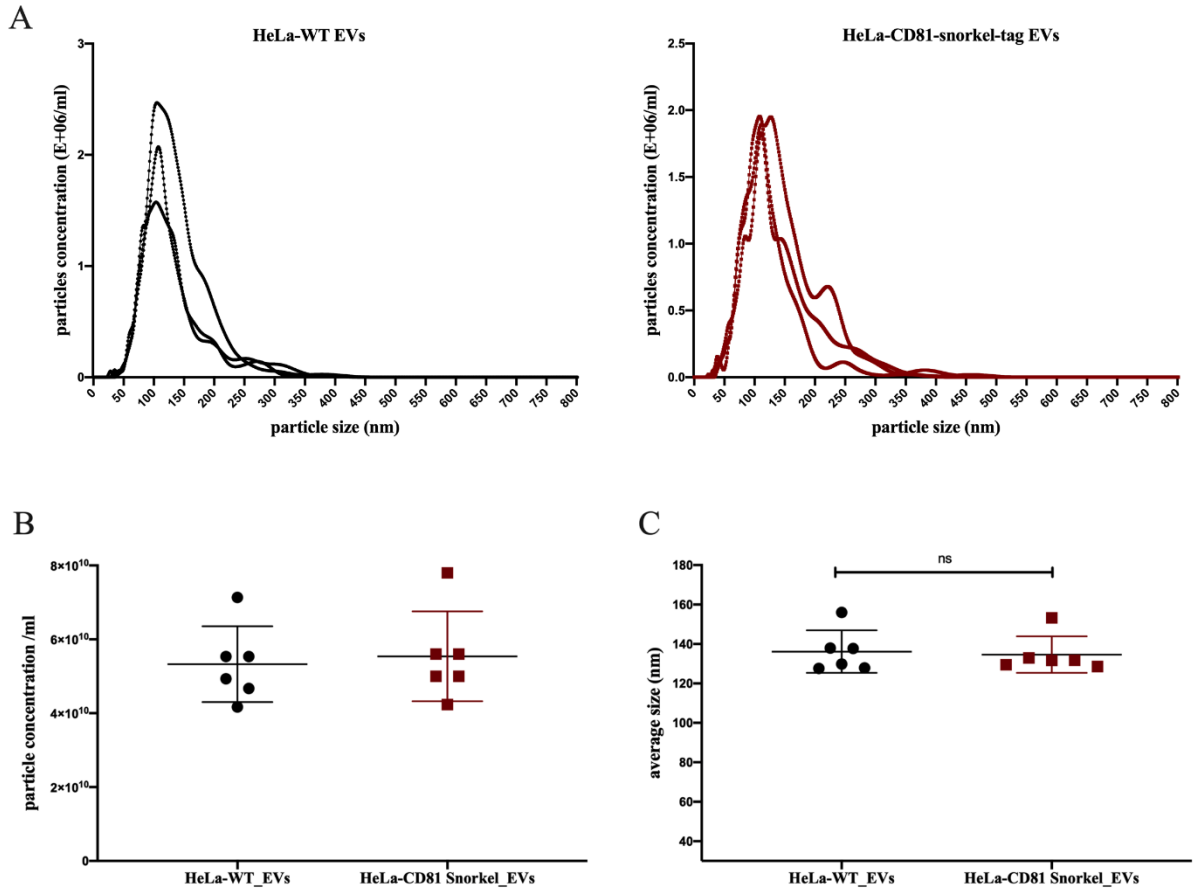
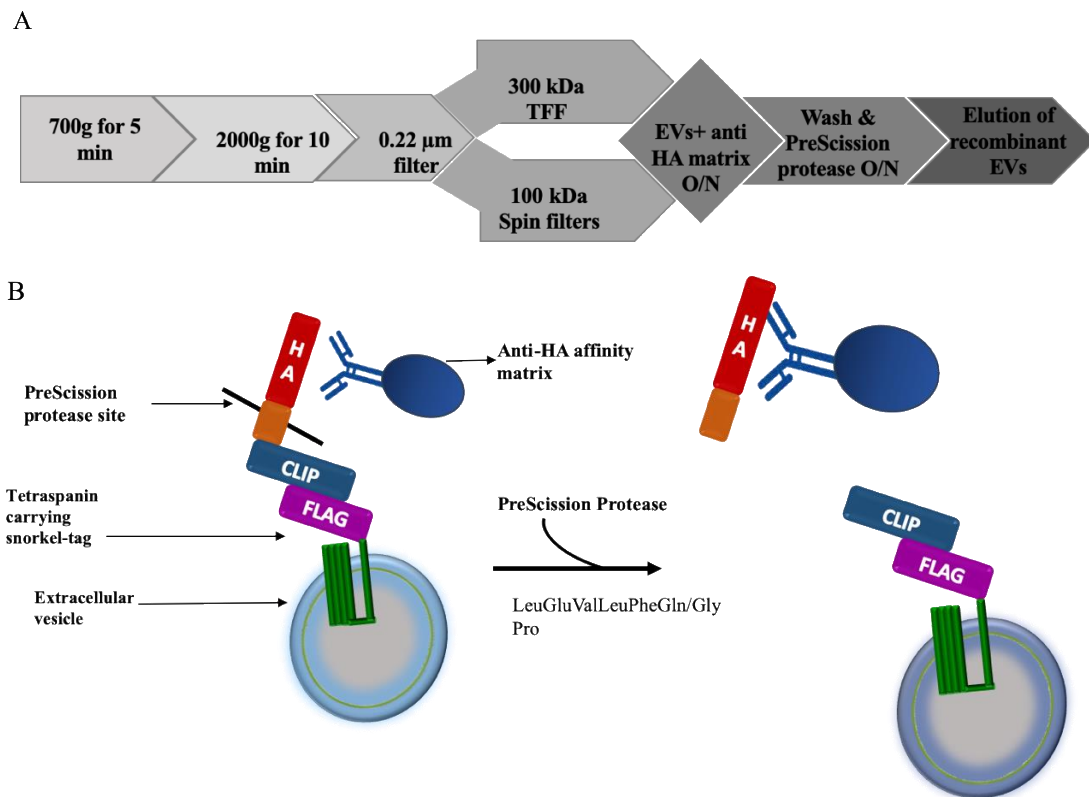


Figure 23: Quantification of EVs isolated by ultrafiltration.

(A) Representative particle size and concentration for EVs derived from HeLa-WT and HeLa-CD81-snorkel-tag cell lines (n=3). (B) Particle concentrations isolated from 75 ml conditioned media from 6 individual experiments. (C) Average particle average size was assessed for reproducibility. Unpaired t-test was applied on raw values; ^{ns}P > 0.05.

EVs isolated using ultrafiltration were then captured by allowing them to bind to beads coated with an anti-HA antibody. After overnight incubation at 4°C, the magnetic beads were collected by placing the tubes on magnetic rack followed by a washing step with 1x PBS. Magnetic beads were suspended in 1 ml of PBS and 5 µl (10 units) of PreScission protease were added to the bead solution and gently mixed. The mixture was placed on shaking rack overnight at 4°C for on-column cleavage of PreScission protease site allowing

mild and precise elution of snorkel-tag carrying EVs. To check for reproducibility, we kept the input concentration of particles ($\sim 2.5 \times 10^{10}$ / ml) constant along with the capture bead solution (250 μ l). At every step of the process, the particle concentrations and sizes were quantified by nanoparticle tracking analysis (NTA). The workflow of snorkel-tag EV affinity chromatography (StEVAC) is shown in Figure: 24A. Schematic representation of on-column elution of EVs is shown in Figure 24B. Our results demonstrate that indeed we could specifically enrich EVs carrying the snorkel-tag (Figure 24B). Furthermore, the comparison of size profiles of the particles eluted and unbound particles showed no significant differences (Figure 24C).



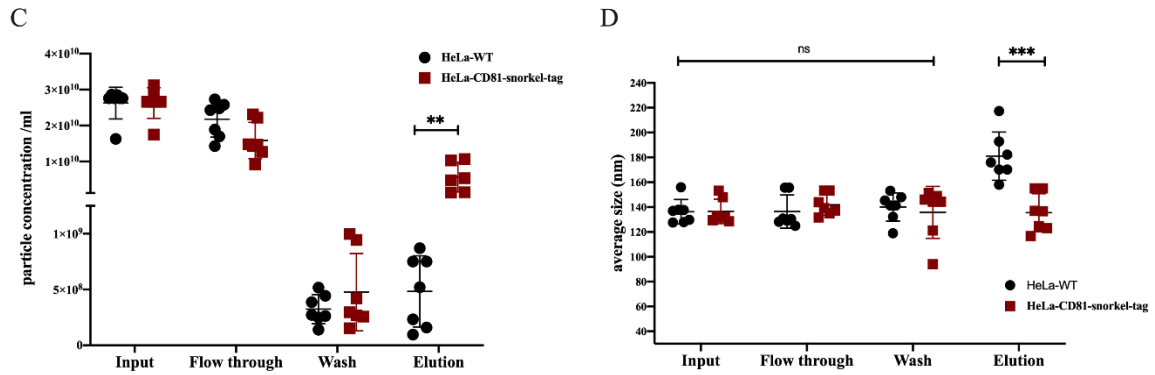


Figure 24: Isolation of EVs using Snorkel-Tag based EV Affinity Chromatography (StEVAC).

(A) Overview of workflow. (B) Schematic representation of StEVAC principle for EV isolation. (C) Nanoparticle tracking analysis (NTA) counts of purified EVs eluted after incubation with PreScission protease treatment overnight and a following wash step (n=7). (D) Particle size quantification revealed no significant size difference appeared during the isolation process (n=7). Unpaired t-test was applied on raw values; ^{ns}P > 0.05, **P < 0.01, ***P < 0.001.

However, we observed a significant difference in the size of the particles eluted from HeLa-WT and HeLa-CD81-snorkel-tag conditioned media. The reason for the bigger size of the particles in HeLa-WT eluted EVs is background due to no particles detected or 1 to 2 particles per frame in NTA. In addition, to determine whether the binding of EVs to anti-HA capture beads is specific, we preincubated the capture beads (anti-HA antibody coated) with HA-peptides for 2 hours, followed by washes to remove unbound HA-peptides. HA-peptide bound capture beads were mixed with concentrated conditioned media and incubated overnight at 4°C on rotospin test tube rotor. After overnight incubation, magnetic beads were collected on a magnetic rack and unbound particles were collected. The magnetic beads were further washed with 1X PBS and incubated with 5µl (10 units) of PreScission protease overnight at 4°C on a rotospin test tube rotor for on-column elution of EVs. NTA particle count demonstrates that the preincubation of capture beads with HA-peptide leads to more unbound EVs as all the epitopes on the capture antibody are preoccupied by HA-peptides (Supplementary Figure 4). Blocking of the epitope on the capture antibody demonstrates the specificity of the method.

3.1.6. Characterization of EVs purified by StEVAC method

To evaluate the purity of snorkel-tag carrying EVs isolated by StEVAC, we performed a wide range of characterization techniques to demonstrate the enrichment of EVs in the elution. Detection of the EV-associated protein, syntenin on EVs eluted by the StEVAC method by immunoblotting revealed enrichment for EVs, while calnexin was not detected in the eluted samples (Figure 25A). To directly examine the size and morphology of the EVs purified by StEVAC, we performed TEM. EVs isolated via StEVAC showed an intact, cup shaped morphology, that had a size distribution of ~50-200 nm and has the typical size and morphology similar to that of the input samples isolated by ultrafiltration (Figure 25B) (Supplementary Figure 5). However, EV profiles of input and flow through samples appeared to electron-dense structures on the micrographs which could be protein aggregates or other contaminants. EVs eluted using the StEVAC method are devoid of these electron-dense structures (Supplementary Figure 6).

In order to demonstrate that EVs purified by StEVAC still retain their surface protein signature, we performed multiplex bead-based flow cytometry on eluted EVs versus input EVs or unbound EVs from flow-through. The signal intensities detected by APC-conjugated detection antibodies mainly relies on the number of EVs added to the assay. Hence the amount of EVs used in the assay is important to compare the signals detected between different samples. Therefore, we used 1×10^9 EVs from input and from flow-through, while for affinity purified EVs we used $\sim 8 \times 10^7 - 6 \times 10^8$ particles in 60 μ l assay reaction as quantified by NTA. Of note, particle concentrations in HeLa-WT elution were below the detection level in NTA, here we took 60 μ l of elute for the assay. As expected, all the tetraspanins (CD9, CD63, CD81) and other HeLa specific protein markers like CD24, CD44, CD146 and MCSP were strongly detected in all the samples except for the HeLa-WT elution (Figure: 26A), corroborating the sensitivity and specificity of our

StEVAC method. Other HeLa specific protein markers like CD29, CD105, CD56 and HLA-ABC were detected at intermediate-positive APC fluorescence intensity levels (Figure 26B). However, in the elutions from snorkel-tag carrying EVs, other protein markers such as CD3, CD25, CD49e and HLA-DRDPDQ were detected at intermediate-to low fluorescence intensities as compared to input and flow through samples, where their detection levels remained low. We hypothesise that this is an indication of higher purity and/or enrichment of a subpopulation (or subpopulations) of EVs that carry snorkel tagged CD81 after StEVAC – in the latter case, the result might mean that CD81 is preferably co-present on CD3, CD25, CD49e and / or HLA-DRDPDQ positive EVs. Another interpretation, as CD3 as the T cell co-receptor should be absent in HeLa cells, is that due to more CD81 present on EVs, more CD3 present in the media binds to it (Rocha-Perugini et al. 2013). Similarly, CD25 being a T cell antigen, overexpression of CD81 might slightly enrich these CDs. However, it is clear that further experiments are necessary to discriminate this.

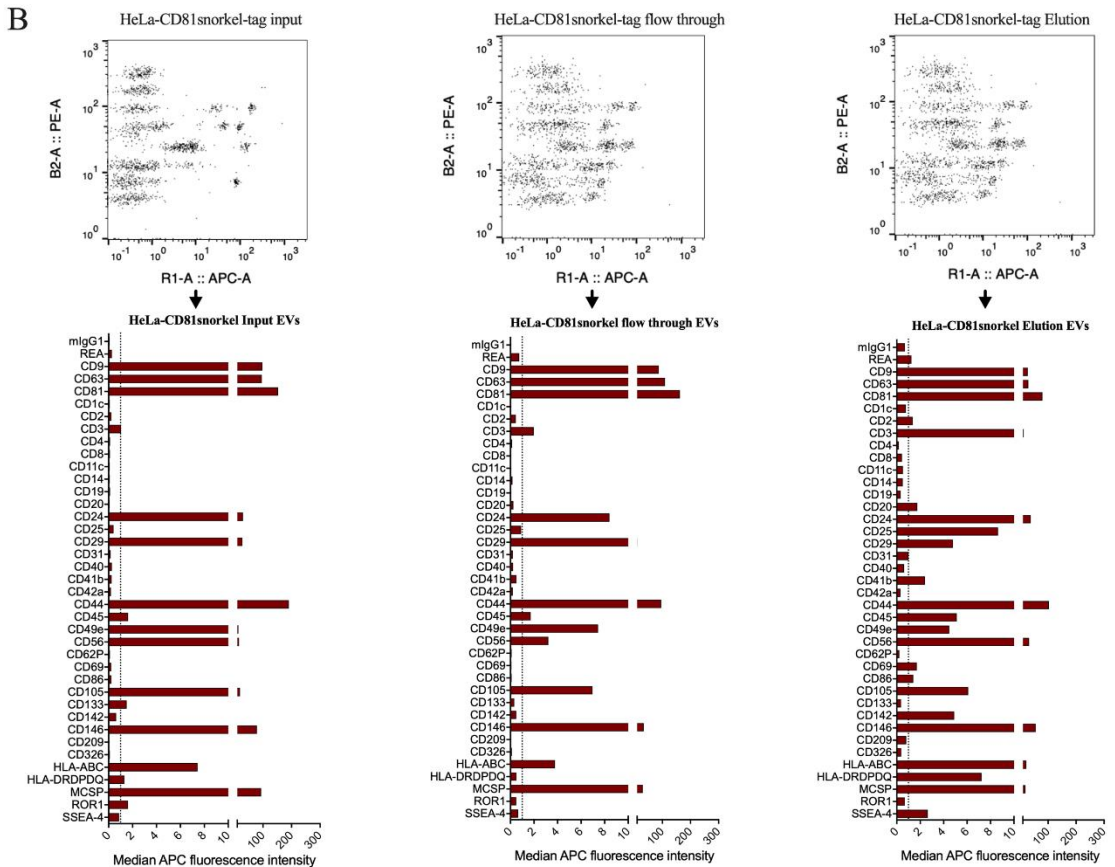
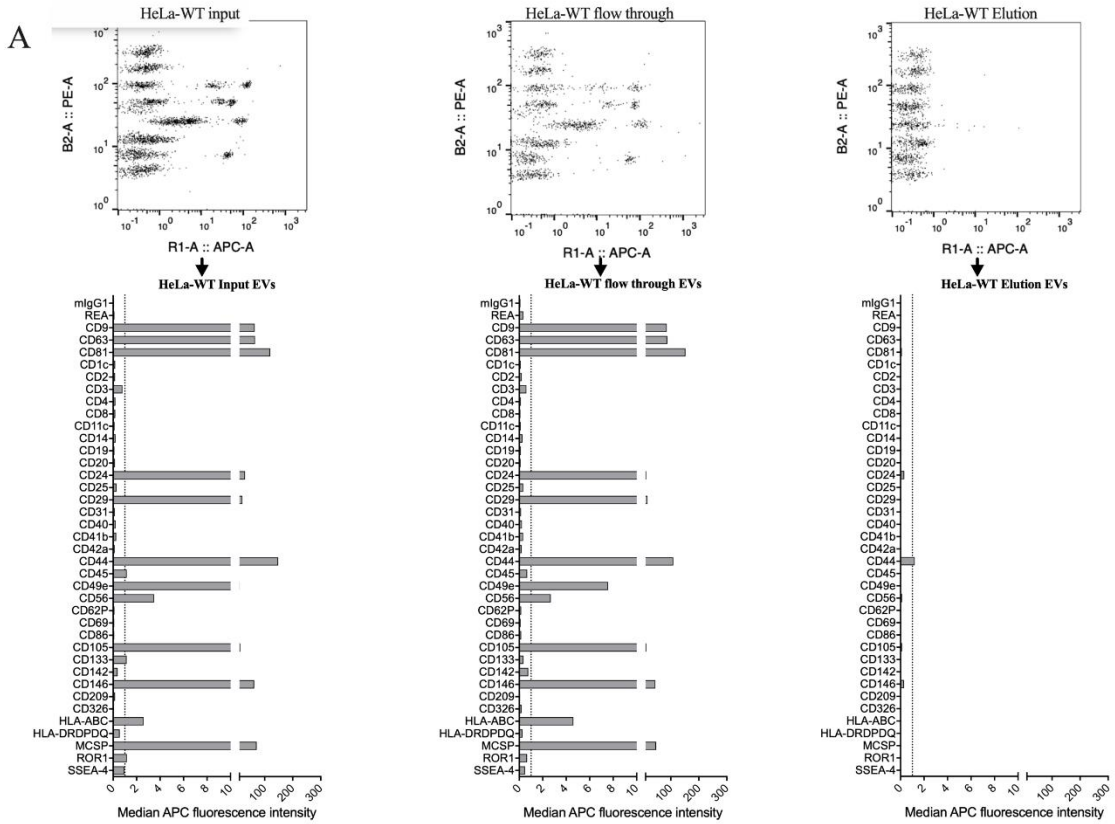


Figure 26: Multiplex bead-based flow cytometry assay to evaluate the StEVAC method.

(A) Assay results for HeLa-WT; input, flow through (unbound EVs) and elution. (B) Assay results for HeLa-CD81-snorkel-tag; input, flow through (unbound EVs) and elution.

3.1.7. Confirming StEVAC as a method for purifying EVs from mixed cell sources of EVs

To further investigate the sensitivity of StEVAC purification, we mixed EVs from two different cell types; HeLa-CD81-snorkel-tag overexpressing cells and HDF76 primary cells in order to purify EVs only carrying only the snorkel-tag. In brief, $\sim 2.5 \times 10^9$ HeLa-CD81-snorkel-tag EVs were mixed with $\sim 1-2 \times 10^9$ EVs derived from HDF76 cell line. The EV mixture was incubated with 250 μ l of capture bead solution overnight at 4°C on a rotospin test tube rotor. After overnight incubation, magnetic capture beads were separated on a magnetic rack and washed with 1X PBS to remove unbound EVs. Magnetic beads were suspended in 1X PBS with 5 μ l (10 units) of PreScission protease overnight at 4°C on a rotospin test tube rotor for on-column protease site cleavage. After overnight protease treatment, the elute was collected by placing the solution on a magnetic rack. All the samples were quantified for particle concentration and size distribution by nanoparticle tracking analysis (NTA). As a control we processed HeLa-CD81-snorkel-tag EVs (positive) and HDF76 EVs (negative) with the similar concentrations used in mixed population. NTA measurements demonstrate that we specifically purified EVs carrying the snorkel-tag from a mixed EV population (Figure 27A). Mean size of the particles in all mixtures and elutes was assessed and did not show differences (Figure 27B).

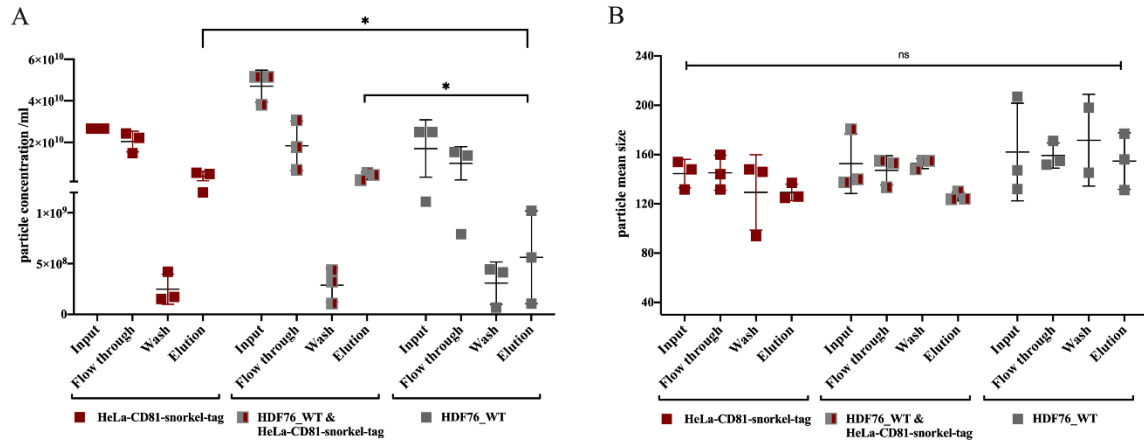


Figure 27: Confirming StEVAC to purify EVs carrying snorkel-tag from mixed population of EVs.

~2.5 × 10⁹ EVs derived from HeLa-CD81-snorkel-tag cell line are mixed with ~1-2 × 10⁹ EVs derived from primary HDF76 cells and the StEVAC method was applied to purify snorkel-tag carrying EVs. (A) NTA measurements for eluted EVs from mixed sample shows similar counts compared to that of the positive experimental control (HeLa-CD81-snorkel-tag) (n=3). (B) to check for reproducibility, average mean size of EVs was assessed. No significant difference was observed in the EV sizes. Eluted EVs fall within the range of 120- 150 nm in diameter (n=3). Unpaired t-test was applied on raw values; ^{ns}P > 0.05, *P < 0.05.

Considering the sensitivity of the multiplex bead-based flow cytometry assay, we compared the EV surface protein signature of HeLa-CD81-snorkel-tag cell derived EVs and HDF76 cell derived EVs. In both of the EV types CD9, CD63, CD81 and CD44 were detected abundantly; in contrast, CD24, CD146 and HLA-ABC were specific to HeLa-derived EVs and CD41b was specific to HDF76 derived EVs. Hence, we evaluated the EV elutes from the mixed population (Figure 28C) along with HeLa-CD81-snorkel-tag input EVs (Figure 28A) and HDF76 input EVs as positive and negative controls respectively (Figure 28C). For respective EVs analysis for flow through, elution and input samples are described in supplementary figure 7. Indeed, our results demonstrate that we specifically purified EVs carrying the snorkel-tag from mixed populations (Figure 28D). However, CD41b is detected at very low level in the elute which is very close to being negligible. This was also seen in the control elutes where HDF76 EVs are absent. In the end, as the

multiplex bead-based flowcytometry assay is semi-quantitative, we considered this slight detection of CD41b as being a mere background.

In summary, using snorkel-tag based EV affinity chromatography we could specifically pull-down EVs carrying the snorkel-tag from a mixture of EVs derived from different cell sources.

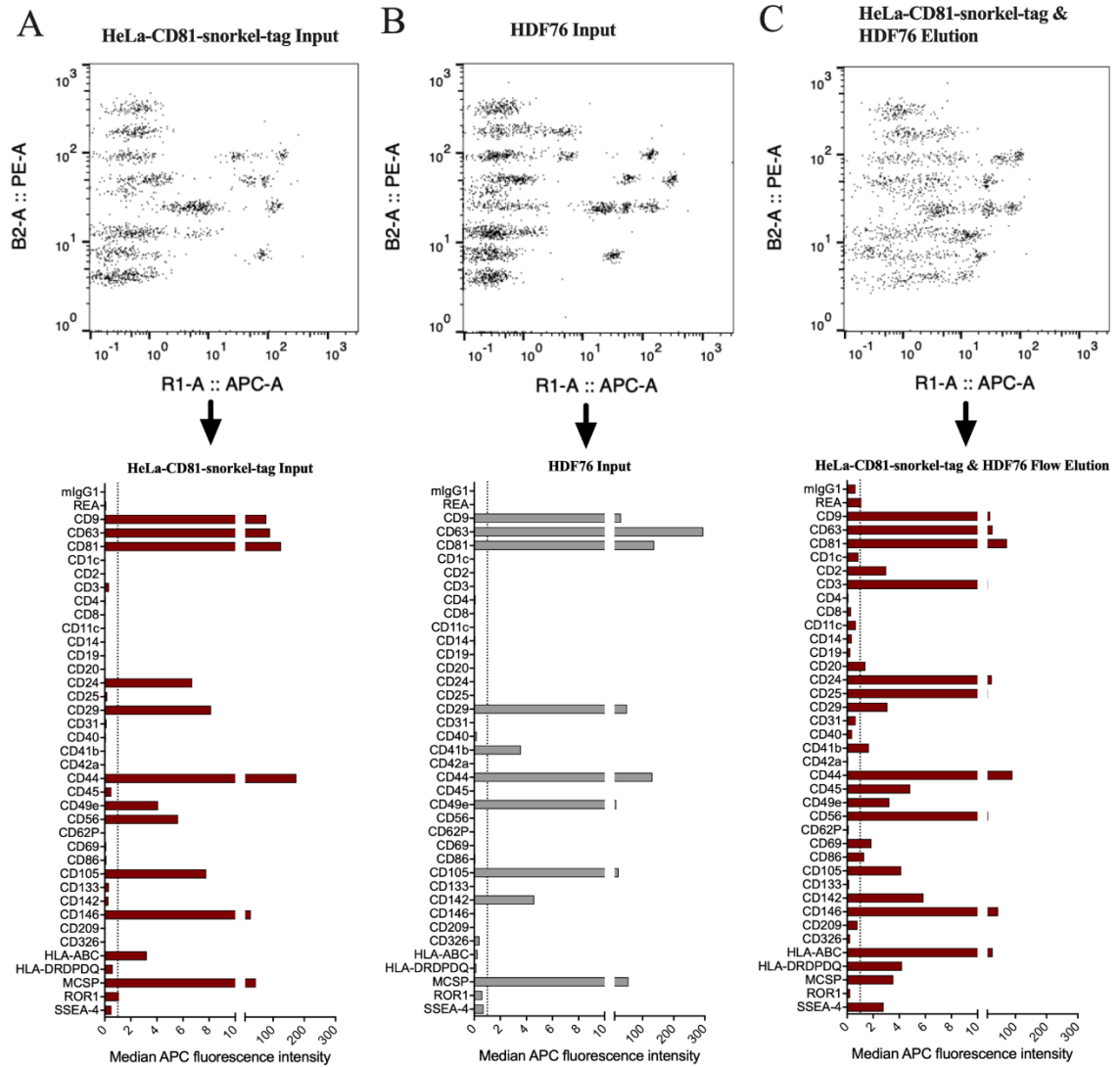


Figure 28 | continued

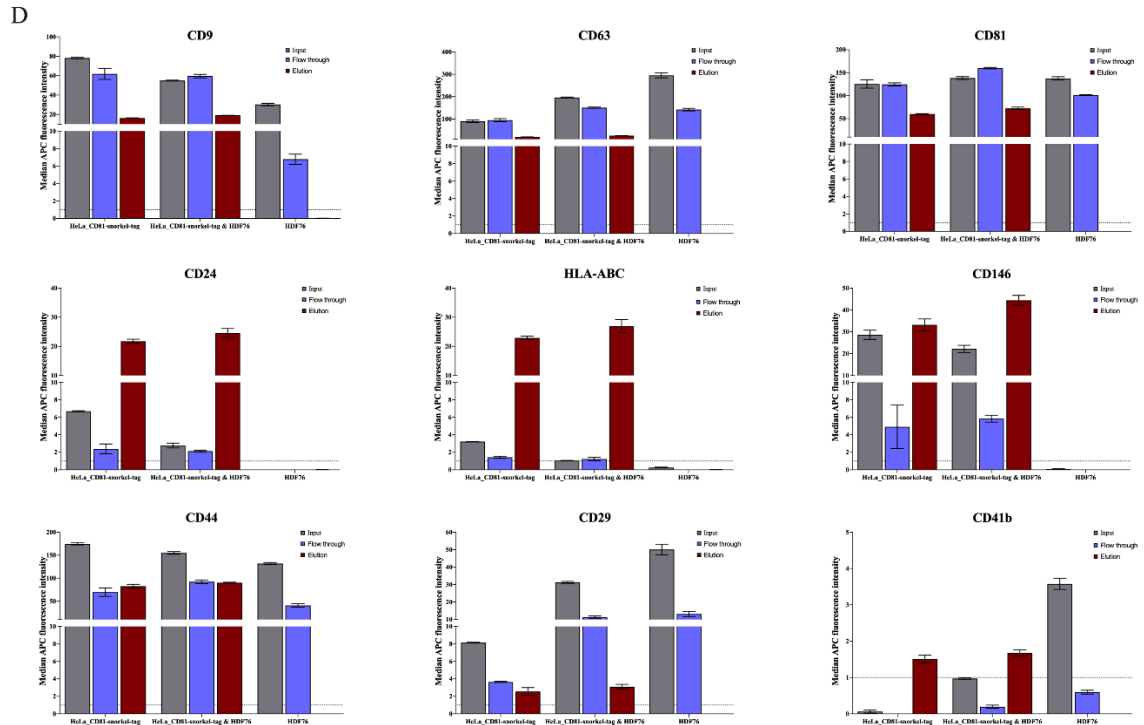


Figure 28: Confirming purity of EVs from mixed populations after StEVAC using the multiplex bead-based flow cytometry assay.

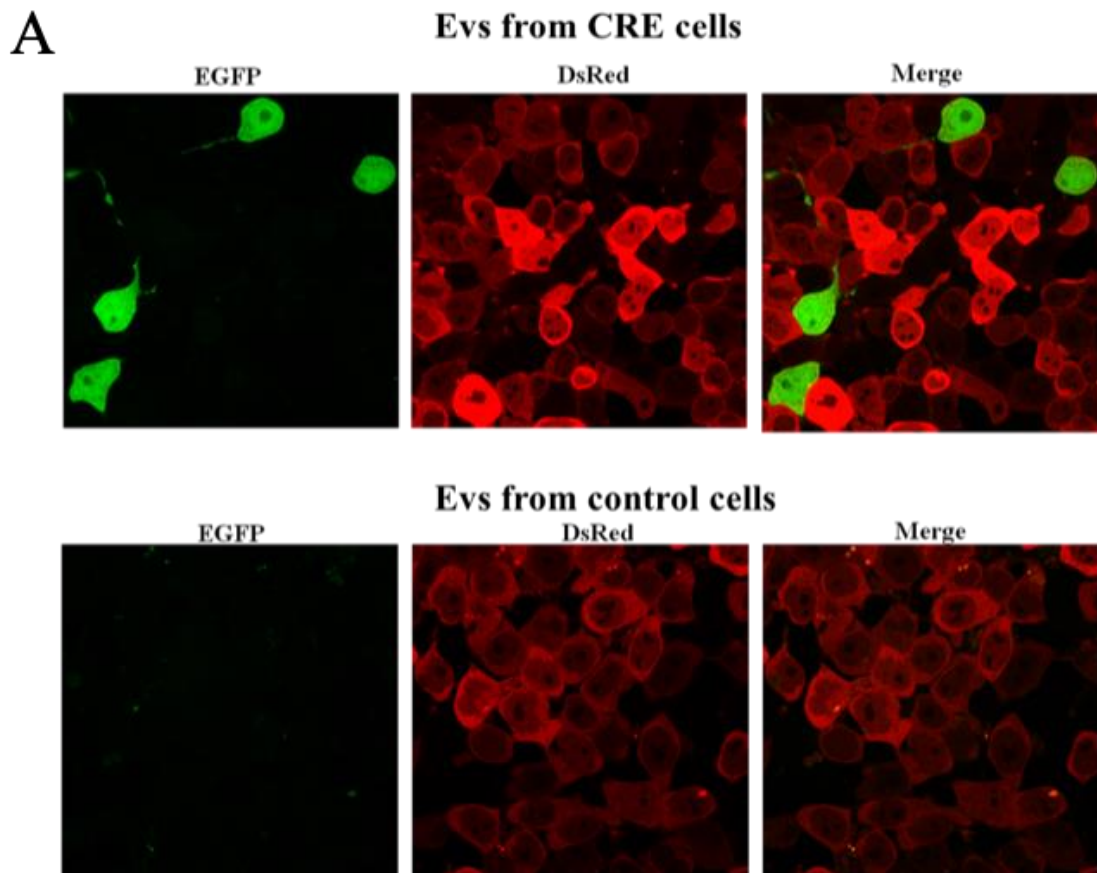
Comparison of EV surface protein markers eluted from mixed population for specificity of the EVs pulled down alongside with input and flow through samples. (A) HeLa-CD81-snorkel-tag cell derived EVs subjected to the StEVAC method of purification (positive control). (B) Assay results for the elutes from the mixture of HeLa-CD81-snorkel-tag EVs and HDF76 EVs. (C) Assay results for the elutes from HDF76 EVs. (D) Same experimental datasets shown in (A, B, C) sorted for individual marker.

3.1.8. EV uptake studies for snorkel-tag carrying EVs

The CD81-snorkel-tag is designed to purify and track EVs when expressed under a tissue-specific promoter in *in vivo* models. However, it is crucial to confirm the functionality of

EVs carrying the snorkel-tag. For this purpose, we used the Cre-loxP method to study the functional transfer of EVs which was established by Zomer et al (Zomer et al. 2016).

To study the functionality of EVs carrying the snorkel-tag, we stably overexpressed Cre recombinase along with the fluorescent marker CFP in HeLa cells expressing the CD81-snorkel-tag (HeLa-Cre⁺ cells). To study functional EV transfer, a reporter HEK293 cell line (color switch from red to green) was created using plasmid carrying a floxed DsRed-Stop sequence followed by an eGFP gene. As reported, overexpression of Cre recombinase in HeLa Cre⁺ cells allows sorting of Cre mRNA into EVs. Upon the Cre mRNA carrying EV uptake into the recipient reporter cell, this results in the color-switch of the reporter cell by active Cre recombinase. To confirm, if HeLa-Cre⁺ cell derived EVs carry Cre mRNA, we isolated EVs from conditioned media of HeLa-Cre⁺ cells by ultracentrifugation. RT-PCR from RNA isolated from EV pellets confirmed the presence of Cre mRNA in the EVs secreted from HeLa-Cre⁺ cells (Supplementary Figure 8).



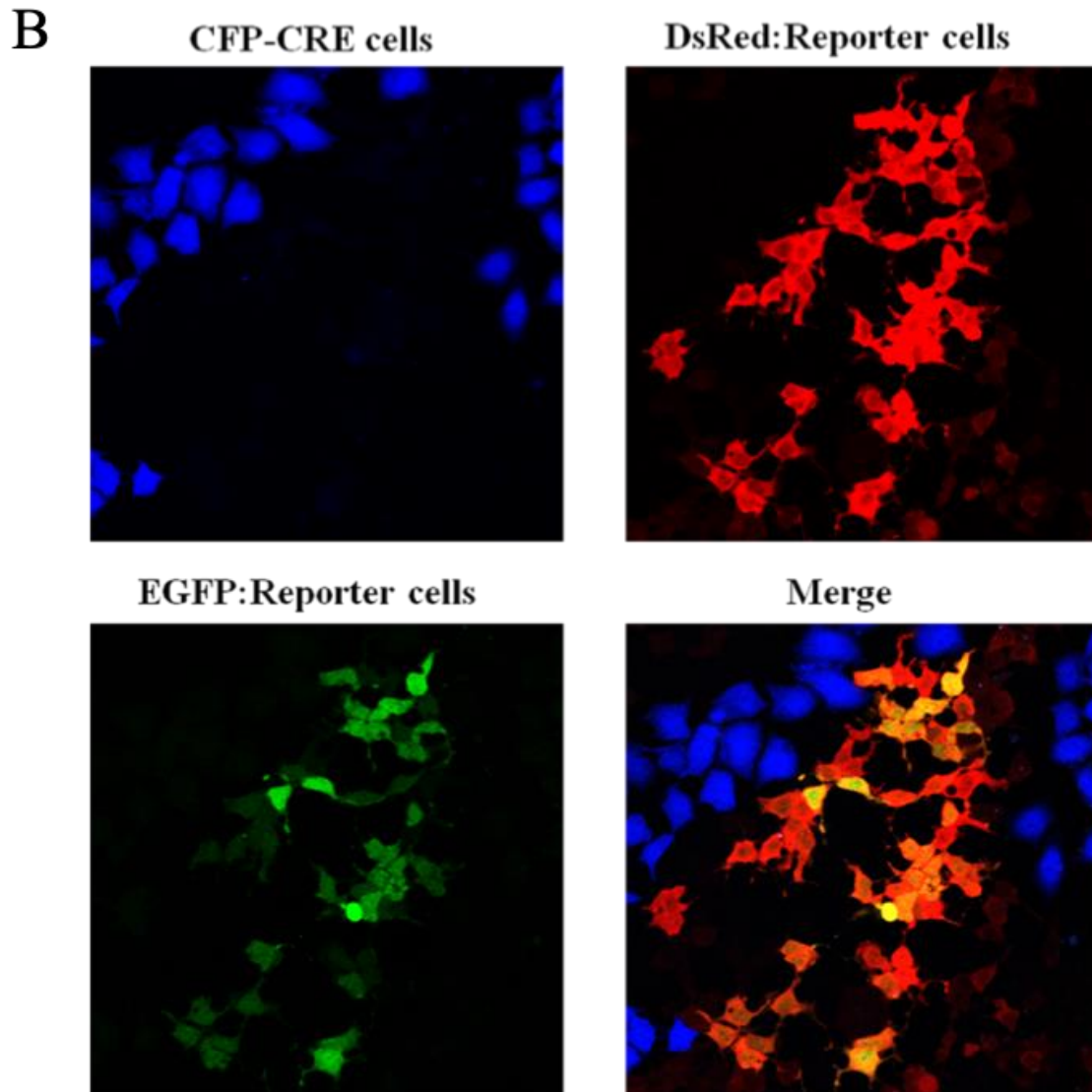


Figure 29: Cre-loxP method to study the functional transfer of EVs.

(A) Confocal images of HEK293 reporter cells that have taken up EVs. (B) Co-culture experiment: Confocal images of Cre⁺ expressing cells co-expressing CFP (Cyan), reporter⁺ cells (Red), eGFP⁺ reporter cells (green with Cre activity).

Next, in order to determine whether Cre from HeLa-Cre⁺ cells can be functionally transferred to reporter cells and to induce the color-switch, we isolated EVs from HeLa-Cre⁺ cells and performed uptake studies on the HEK293-reporter cell line. HEK293-

reporter cells were supplied with fresh EVs every 72 hours for ~10 days. We observed the color-switch in a few HEK293-reporter cells, demonstrating the functionality of the EVs (Figure: 29A) at a very low efficiency of estimated less than 1 %. In parallel, we co-cultured HeLa-Cre⁺ cells with HEK293 reporter cells in a ratio of 1 to 100 for ~2 weeks to confirm the functional transfer of EVs. Confocal images reveal functional transfer of EVs from HeLa-Cre⁺ cells to HEK293 reporter cells (Figure 29B). However, the percentage of eGFP⁺ reporter cells were very low as reported previously (Zomer et al. 2015).

To evaluate whether EVs isolated by the StEVAC are taken up by recipient cells, we covalently labelled EVs with a membrane impermeable CLIP substrate (CLIP-SurfaceTM 647) and performed uptake studies on Huh7 cells. Confocal images show that the EVs labelled with the CLIP substrate are taken up in recipient Huh7 cells after 2 hours (Figure 30). We observe CLIP labelled EVs inside of Huh-7 cells when comparing EVs purified by ultrafiltration to StEVAC purified EVs as estimated from inspection of random visual fields.

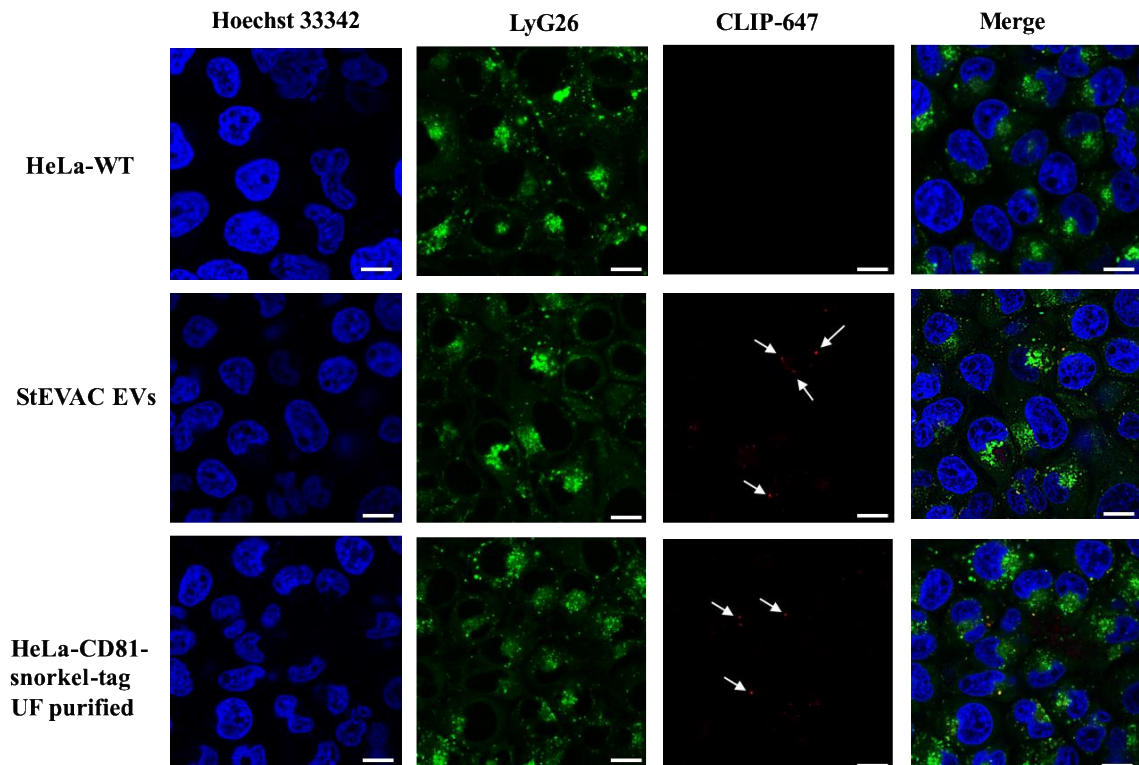


Figure 30: StEVAC purified EV uptake in Huh7 cells.

StEVAC purified EVs versus ultrafiltration purified EVs derived from HeLa-WT (negative control) and HeLa-CD81-snorkel-tag overexpressing cells (positive control) were labeled with CLIP substrate (CLIP-Surface™ 647) for 1 hr and incubated on Huh7 cells for uptake. Live-cell imaging show the co-localization of snorkel-tag carrying EVs with lysosomes (lysotracker: LyG26). Counterstaining with Hoechst 33342 for DNA.

To sum up, StEVAC purification results in pure snorkel-tag positive EVs that differ only minimally in morphology, surface marker profiles, and uptake behavior.

PART B

3.2. Evaluation of the neutralizing effect of monoclonal antibodies produced against human dermal fibroblast derived EVs

3.2.1. Extracellular vesicles are part of SASP

The senescence-associated secretory phenotype (SASP) is known to be a main driver of aging and age-associated diseases and hence an attractive therapeutic target to age-related dysfunctions and to promote healthy aging as outlined above in the introduction. In order to investigate whether EVs are part of the SASP, we induced premature senescence in primary human dermal fibroblasts (HDFs) from three different donors by exposing to H₂O₂ repeatedly for 2 weeks. Onset of senescence was confirmed by senescence-associated β -gal staining and expression of senescent markers such as p21 (data not shown). To compare whether senescent cells secrete more EVs compared to their counterparts quiescent cells, we isolated EVs from stress-induced premature senescent cells (SIPS) and quiescent cell (Q) supernatants at 7 days and 21 days of inducing senescence. Isolated EVs were characterized for their size and number by nanoparticle tracking analysis (NTA). The particle size analysis revealed that the size of the particles falls within the range of 15- 135 nm (Figure 31A) and median size of the particles is between 65- 80 nm for both SIPS- and Q- derived EVs. In addition, we did not observe significant difference in median size of the particles between SIPS- and Q- derived EVs at 7 day and 21-day time points (Figure 31B). Furthermore, we confirmed the morphology and size of EVs by transmission electron microscopy (TEM) (Figure 31C). Immunoblotting results showed the enrichment of EV-associated protein TSG101 in the EV pellets of SIPS and Q (Figure 31D).

Finally, we compared the relative number of EVs secreted per cell from SIPS and Q of all the three donors. We observed SIPS cells secrete 4-fold more EVs compared to quiescent cells (Figure 31E). Henceforth, considering the phenomenon of increased EV secretion from SIPS cells alongside of SASP factors, we proposed EVs as part of SASP factors which influence the tissue microenvironment by transporting its cargo (e.g.: miRNA) in a recent publication (Terlecki-Zaniewicz et al. 2018).

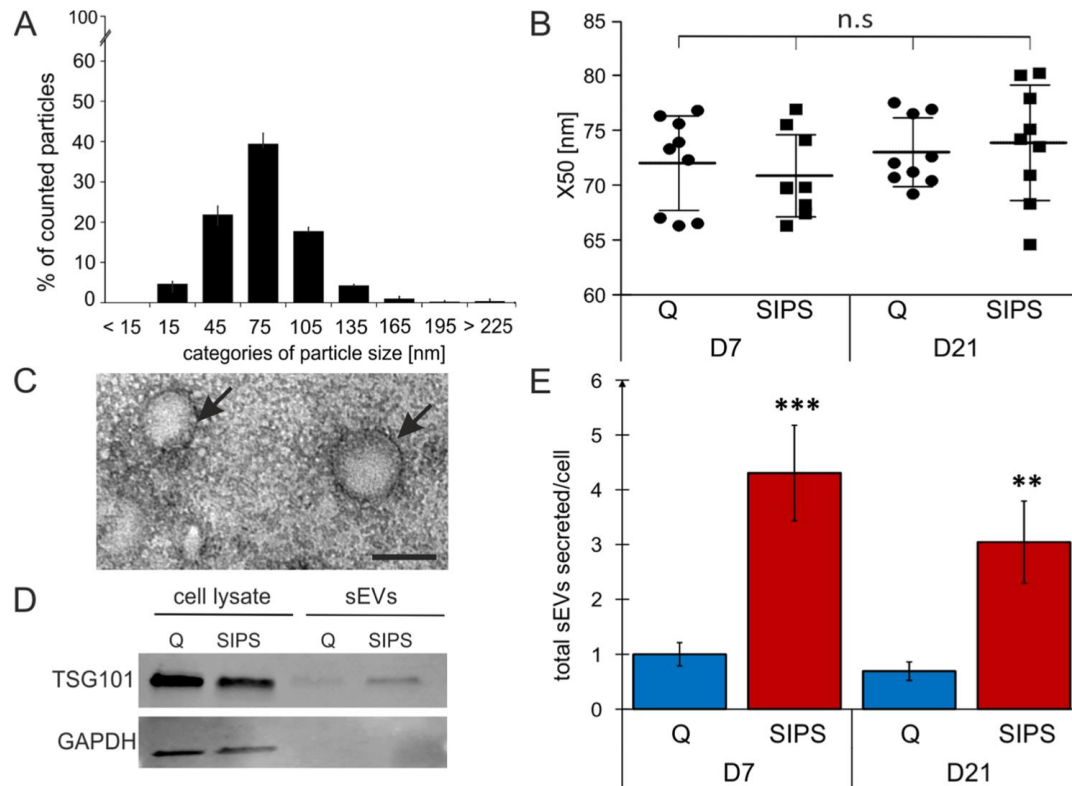


Figure 31: EVs are part of the senescent-associated secretory phenotype (SASP).

(A) NTA reveals a vesicle population below 220 nm. Size distribution of vesicles determined by NTA shows percentage (%) of total counted particles against size presented in categories. (B) Median size (X50) of the EVs range from 65 to 80 nm. X50 values from peak analysis of NTA are indicated +/- SEM. circle: Q, squares: SIPS. Statistical analysis using one-way ANOVA was performed: not significant (n.s) $p > 0.05$. (C) Transmission electron microscopy image of EVs isolated from HDF85 at D7 after induction of senescence is shown. (D) Western blot analysis for HDF85 donor SIPS and Q cell lysates and EV lysates for EV-associated protein TSG101 (top) and GAPDH (below). 20 μ g of total protein content from cell lysates and EV lysates was loaded for

analysis. (E) Total number of particles tracked was normalized to the total cell number. Particle fold change secreted per cell, relative to Q control cells from D7, +/- relative SEM, are shown. Statistical analysis was performed using 2-way RM ANOVA tested for condition ($p < 0.0001$) and day ($p = 0.28$) following Bonferroni posttest. $**p < 0.01$; $***p < 0.01$. (A-B and E) Averages from three biological triplicates ($n = 3$) and two different time points each SIPS and Q, were measured in technical triplicates ($n = 18$) +/- relative SEM.

3.2.2. Evidence of extracellular vesicles in human skin

Knowing that the senescent cell-derived EVs are members of SASP factors, we further provided evidence of EV cross-talk between dermal fibroblasts and keratinocytes *in vitro* in both 2D cultures and 3D skin equivalents (Terlecki-Zaniewicz et al. 2019). Here, we wanted to provide evidence of EVs in human skin *ex vivo*. For this, we performed transmission electron microscopy on human skin sections and TEM images revealed the presence of EV-like structures intracellularly within the MVBs (Figure 32A). To confirm if these EV-like structures are positive for EV-associated proteins, we performed immunogold labeling for CD63 on cryosections of skin. Indeed, we found positive staining for CD63 for these EV-like structures which confirms the presence of EVs in human skin (Figure 32B).

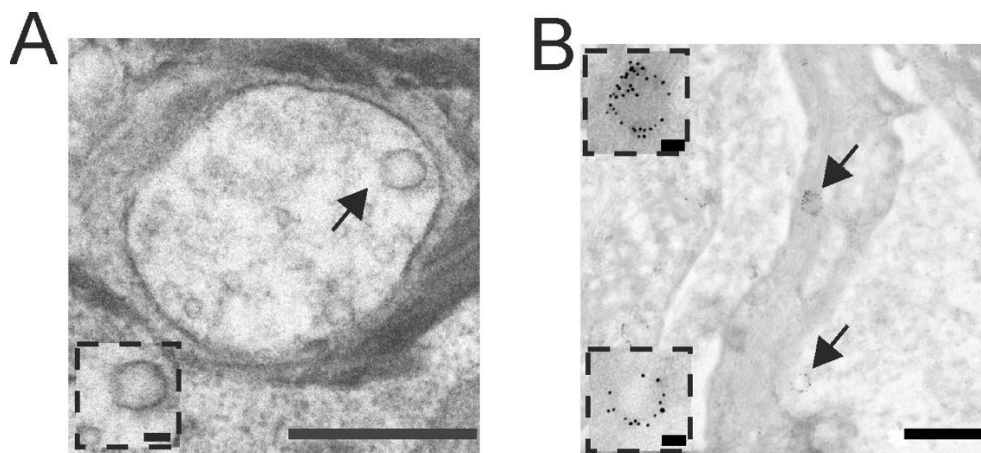


Figure 32: Evidence of EV-like structures in skin sections.

(A) MVBs with ILVs in the basal layer of epithelial cells. (B) Immunogold labeling of skin cryosections detected positive for CD63 enriched EVs (arrows).

Additionally, in order to isolate and characterize EVs from skin, we disintegrated the tissue biopsies from two independent donors using diapase and EVs contained in accessible material (crude extract) was pre-cleaned by differential centrifugation and sterile filtered with 0.22 μ M filter. The filtrate was further subjected to TFF with 300 kDa cut-off hollow fiber membrane. NTA analysis of the concentrated material revealed the media size of the particles is \sim 110 nm (Figure 33A). Furthermore, immunoblotting of TFF concentrated material showed positive for EV- associated proteins such as syntenin and TSG101 (Figure 33B). However, the samples were also positive for calnexin, *not expected* EV protein. Therefore, using qEV columns we performed size exclusion chromatography (SEC) on TFF concentrated material and SEC fractions were pooled into two parts; fractions 1- 3 (SEC 1- 3) and fractions 4- 6 (SEC 4- 6) for further EV characterization. Particle concentration and size in both fractions were quantified by using NTA (Figure 33C). NTA showed particles were highly enriched in SEC 1-3 fractions compared to SEC 4-6 fractions, however, median size of the particles did not differ (Figure 33D). Immunoblotting for Syntenin and calnexin revealed strong enrichment of syntenin and not for calnexin (Figure 33E).

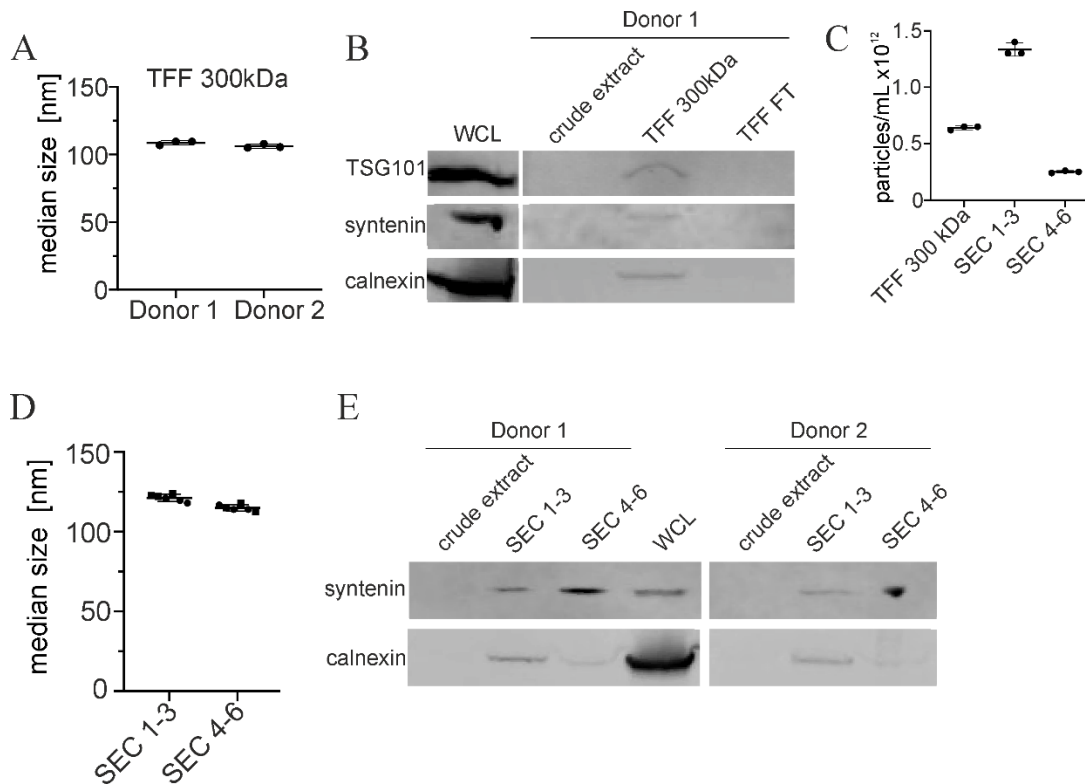


Figure 33: Characterization of EVs purified from tissue biopsies.

(A) NTA measurements of EVs from human skin sections of two donors in triplicates. The size of the EVs enriched using TFF with a cut-off of 300 kDa show a median size of ~110 nm. (B) Western blot analysis for TFF purified EVs show enrichment for EV-associated proteins such as syntenin and TSG101 and also calnexin (non-EV protein). Fibroblast whole cell lysate (WCL) as a positive control and TFF flow through (FT) as a negative control. (C) Enriched EVs from (A) were further purified by SEC with eluted fractions 1- 3 (SEC 1- 3) and fractions 4- 6 (SEC 4- 6) were pooled. Particle concentration was measured by NTA. (D) The median size of the particles in SEC 1- 3 is ~121 nm and for SEC 4- 6 is ~114. Each donor (•, ▪) was measured in triplicates. (E) Immunoblotting on SEC purified EVs confirmed the enrichment of EV-associated protein syntenin and not for calnexin. Fibroblast whole cell lysate (WCL) served as a positive control.

These results strongly suggest the presence of EVs in human skin, which we were able to enrich using different isolation methods. These data also were included in the publication Terlecki-Zaniewicz, JID 2019, to which I am a co-author.

3.2.3. Characterization of EVs derived from human dermal fibroblasts for immunizing mice to produce monoclonal antibodies

After giving evidence of EVs in human skin (Terlecki-Zaniewicz et al. 2019) and increased secretion of EVs from senescent cell modulating the surrounding tissue microenvironment (Terlecki-Zaniewicz et al. 2018), we proposed EVs to be members of the SASP. Previous reports suggest clearance of senescent cells can delay onset of age-associated disease and improves healthy life span in mice (Baker et al. 2011, 2016) and we showed recently that EVs from senescent cells have anti-apoptotic activity probably by their miRNA cargo (Terlecki-Zaniewicz et al. 2018). Hence, senescent cell-derived EVs can be a potential therapeutic target and their clearance could be beneficial. In order to neutralize the effect of senescent cell derived EVs, we aimed to produce monoclonal antibodies against primary human dermal fibroblast (HDF) derived EVs. For this, we isolated EVs from HDF5 conditioned media using differential ultracentrifugation and characterized for particle concentration and size using NTA (Figure 34A). Transmission electron microscopy images confirmed the size of the EVs are ~100 nm in diameter (Figure 34B). Total EV protein concentration was quantified by using BCA method. Production of monoclonal antibodies against EVs was performed by our cooperation partner within the FP7 EU consortium 'SYBIL', PRIMM, specialized in generating monoclonal antibodies against desired antigens. Finally, we received 17 monoclonal antibodies from PRIMM which were produced against HDF derived EVs (table 1). From hereafter, we characterized all the monoclonal antibodies for potential neutralizing effects on EV uptake.

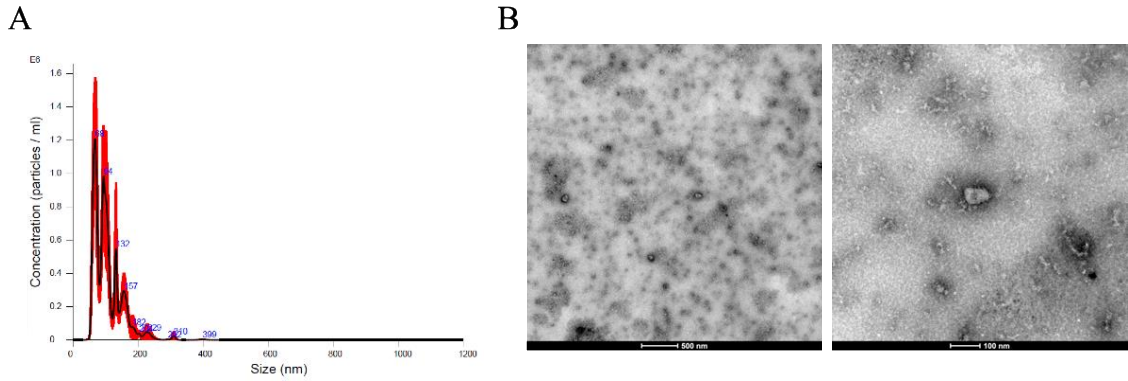


Figure 34: Characterizations of EVs derived from HDF5 cells.

(A) NTA measurements showed the particle size is ~120 nm in diameter. (B) TEM images reveal the size and morphology of the EVs (left overview image; scale bar 500 nm, Right zoom in image; scale bar 100 nm).

Clones	Concentrations (mg/ml)
53E6-C7	0.33
53E6-D8	0.32
53E6-E9	0.33
53E6-G7	0.38
52F8-G4	0.3
52F8-G6	0.27
51B3-D10	0.32
51B3-D12	0.33
51B3-G11	0.21
51B3-H10	0.27
53F2-A1	0.39
53F2-C1	0.3
53F2-D6	0.3
53F2-E1	0.42
53F2-F2	0.31
52F8-A7	0.29
52F8-D7	0.36

Table 1: monoclonal antibody clones with respective concentrations.

3.2.4. Characterization of monoclonal antibodies

To evaluate whether all the monoclonal antibody clones produced against human dermal fibroblast (HDF) derived EVs can detect antigens in HDF cell lysate, we performed immunoblot analysis for all the monoclonal antibody clones from HDFs as well as from HeLa cell lysates to see specificity against human fibroblasts. We observed that indeed some of the clones detect antigens in HDF cell lysates only at ~30 kDa (Figure 35). Based on the immunoblotting results we selected a few monoclonal antibodies for further analysis.

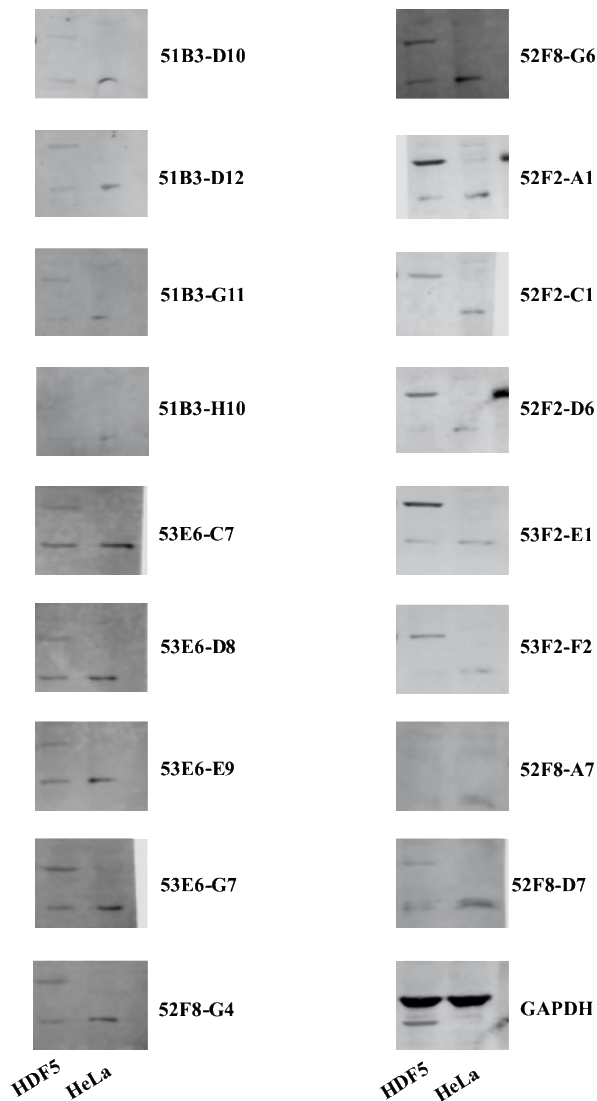


Figure 35: Western blot analysis of 17 monoclonal antibodies against HDF and HeLa cell lysates.

In addition, to identify if the monoclonal antibodies bind to HDF specific antigens or common EV-associated biomolecule, we performed flow cytometry analysis for all the selected monoclonal antibodies using different cell types (HDF164-hTert, HeLa, HEK293). To identify if the particular antigen is located on the cell surface or endogenously, we used permeabilized and non-permeabilized cells for labeling. The results from flow cytometry further substantiate the western blot results. The antigen for all the antibodies is specific to human dermal fibroblasts (HDFs) and not present or below

detection levels in HeLa and HEK293 cell lines (Fig 36 A-C). Interestingly, our flow cytometry results further demonstrate that the antigen detection was observed only in permeabilized cells, shedding light on the localization of antigen. However, colocalization experiments with MVB and lysosomal markers yet to be performed to understand the cellular localization of unknown antigen.

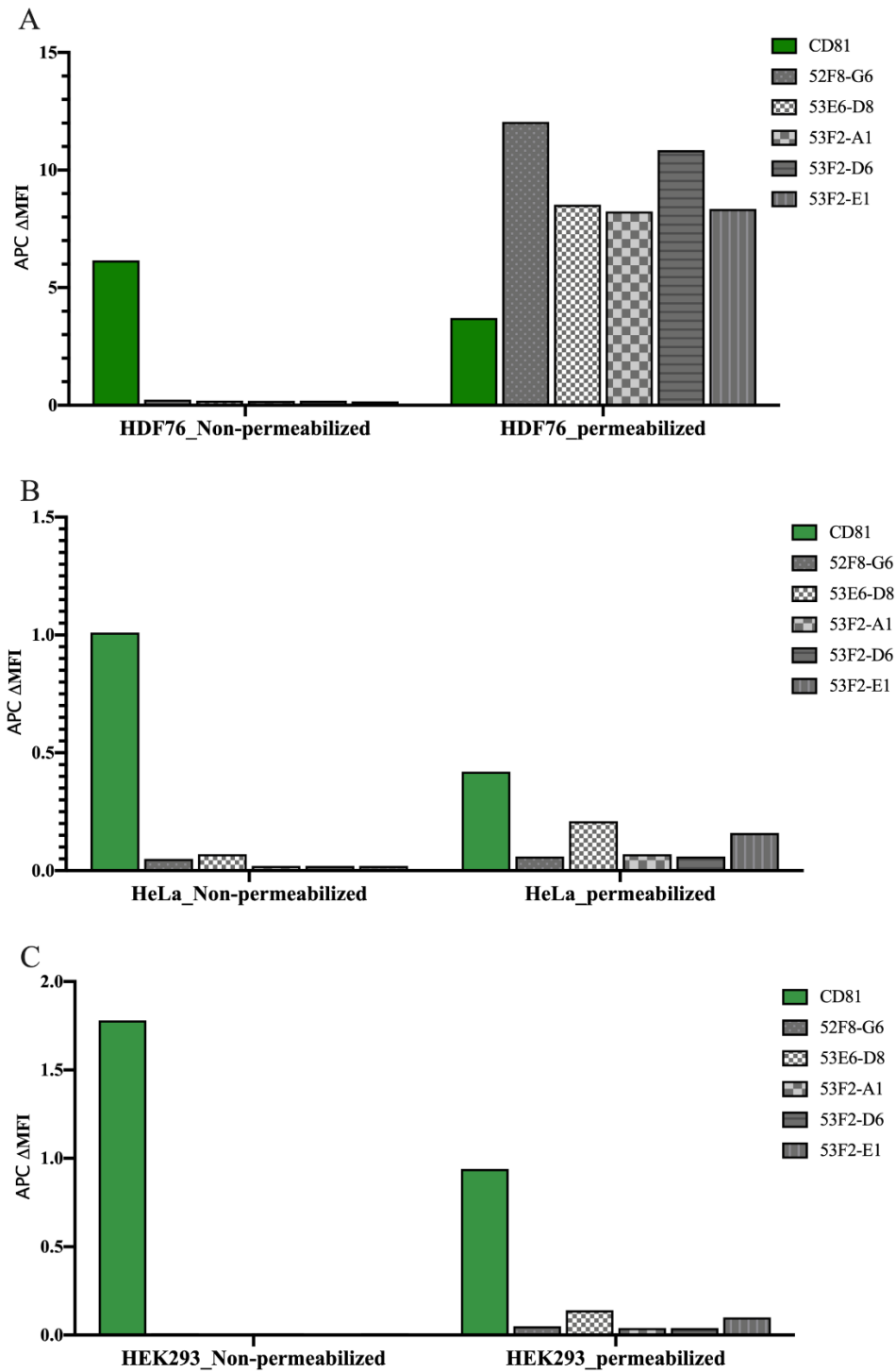


Figure 36: Flow cytometry analysis for monoclonal antibodies using different cell lines.

Here, HDF164-hTert (A), HeLa (B), HEK293 (C) were either permeabilized or non-permeabilized before labeling with specific antibody. Anti-mouse Cy3 was used as a detection antibody. Median

PE fluorescence intensity values for all the samples after background correction (detection antibody values were subtracted from corresponding measurements). For non-permeabilized cells, dead cells were excluded by DAPI staining and doublets were excluded by forward scatter height versus area. Data represents one experiment. Supplementary Figure 9 A, B, C for details of the measurements and Supplementary table 1 A, B, C for sample ID's.

3.2.5. The effect of monoclonal antibodies on EV uptake

Next, we evaluated if the monoclonal antibodies produced against HDF derived EVs have an effect on their uptake in recipient cells. For this, we stably expressed CD63-GFP fusion protein in HDF164-hTert overexpressing cells. We used tangential flow filtration (TFF) for isolation of EVs from conditioned media of HDF164-hTert cells stably expressing CD63-GFP fusion protein. Purified EVs were characterized for concentration and size in both scatter mode and fluorescence mode using NTA (Figure 37). No significant difference was observed with average size of the particles in scatter mode (~140 nm) and in fluorescent mode (~150 nm). However, concentration of the particles in fluorescent mode is 5 times lower to that of the scatter mode. This could be the result of fast quenching of GFP in fluorescent mode. For all the experiments performed using CD63-GFP EVs we considered EV numbers based on scatter mode.

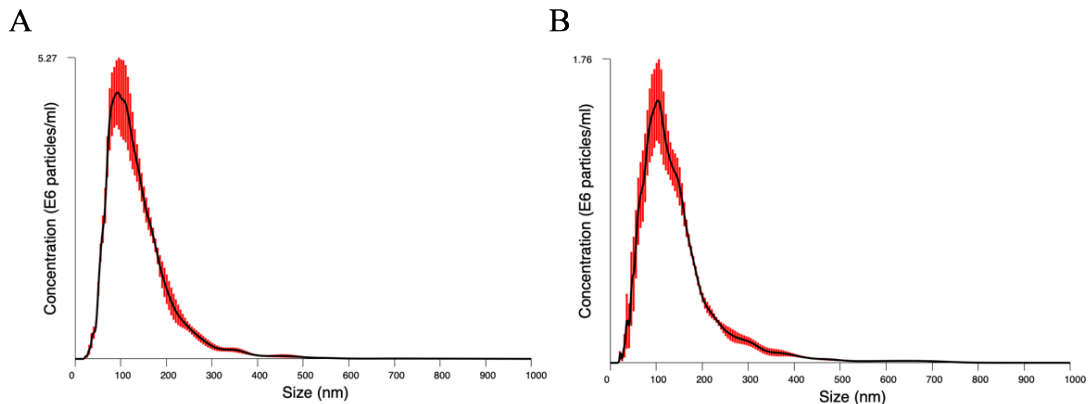


Figure 37: NTA measurements for EVs derived from HDF164-hTert cells expressing CD63-GFP.

(A) average size of particles against concentration in scatter mode. (B) average size of particles against concentration in fluorescent mode.

To determine the amount of EVs and antibody concentrations to be used for uptake studies, we titrated the different EV concentrations (1×10^9 , 5×10^9 and 1×10^{10}) with increasing different concentrations of 53F2-D6 clone (200 ng, 1 μ g, 2 μ g and 4 μ g) for EV uptake into the Huh7 cell line. In brief, specific amount of EVs were mixed with the above mentioned concentrations of the monoclonal antibody and incubated for 1 hour to allow the antibody- EV complex formation. Post incubation, the antibody-EV complexes were added to Huh-7 cells that had been seeded one day before with a density of 2,000 cells per well in a 96-well plate. Cells were incubated for 2 hours at 37°C. Internalization of CD63-GFP EVs in Huh-7 cells was evaluated using flow cytometry by analyzing the median fluorescence intensity normalized over the control (CD63-GFP EVs without antibody) (Δ MFI). EVs were taken up in a dose-dependent manner for antibody concentrations regardless of the EV concentrations of EVs used. However, the higher percentage of EVs were internalized when higher concentrations of the antibody were used (Figure 38 A-C). Based on these results, we used 2.5×10^9 EVs for further follow up EV uptake studies.

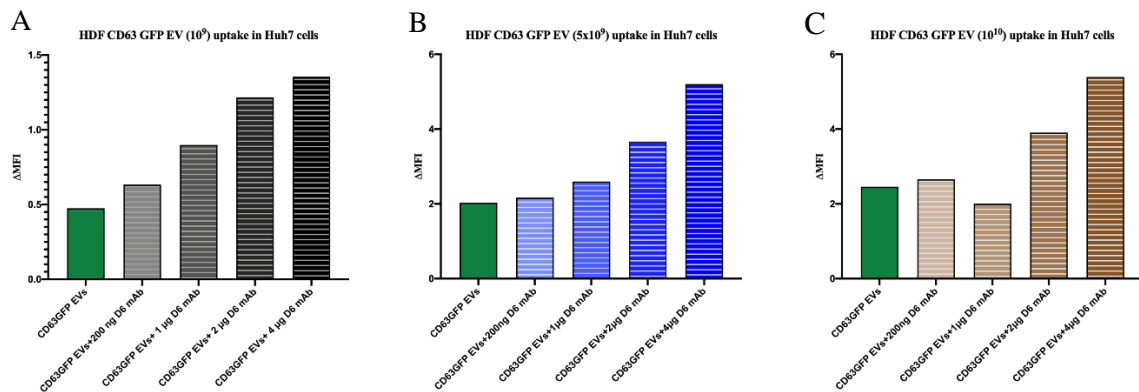


Figure 38: Titration of EV and 53F2-D6 clone antibody concentrations for EV uptake analysis by flow cytometry.

Median fluorescence intensity normalized over the control (Δ MFI) (n = 1). (A) 1×10^9 CD63-GFP EV uptake in Huh-7 cells. (B) 5×10^9 CD63-GFP EV uptake into Huh-7 cells. (C) 1×10^{10} CD63-GFP EV uptake into Huh-7 cells. Data represents one experiment. Details of scatter plots

correlating EV uptake (CD6-GFP Internalized EVs) with APC autofluorescence in Supplementary Figure 10 and Supplementary table 2 for sample ID's.

Next, we evaluated the effect of the selected monoclonal antibodies (52F8-G6, 53E6-D8, 53F2-A1, 53F2-D6 and 53F2-E1) on the HDF derived CD63-GFP EV uptake in Huh-7 cells. An anti-CD63 antibody and an anti-ALIX antibody were included as isotype controls. CD63-GFP EVs were incubated with antibodies at varying concentrations (200 ng, 1 μ g, 2 μ g and 4 μ g) for 1 hours and added to Huh-7 cells and incubated for 2 hours. Huh-7 cells were evaluated for internalized CD63-GFP EVs by flow cytometry. Interestingly, we observed dose-dependent increase in the uptake for all the different monoclonal antibodies while anti-CD63 antibody did not increase EV uptake (Figure: 39 A-E).

Considering the amount of EVs and antibody concentrations, we wanted to confirm the antibody effect on the EV uptake using 2.5×10^9 CD63-GFP EVs and 4 μ g of monoclonal antibody. In addition, 2 μ g of anti-CD63 antibody were used as an isotype control. As in the titration experiments, we observed a significant increase in CD63-GFP EV uptake when 52F8-G6 and 53F2-D6 monoclonal antibodies were used (Figure 40). Unlike our monoclonals, anti-CD63 antibody blocked the uptake of EVs into Huh-7 cells.

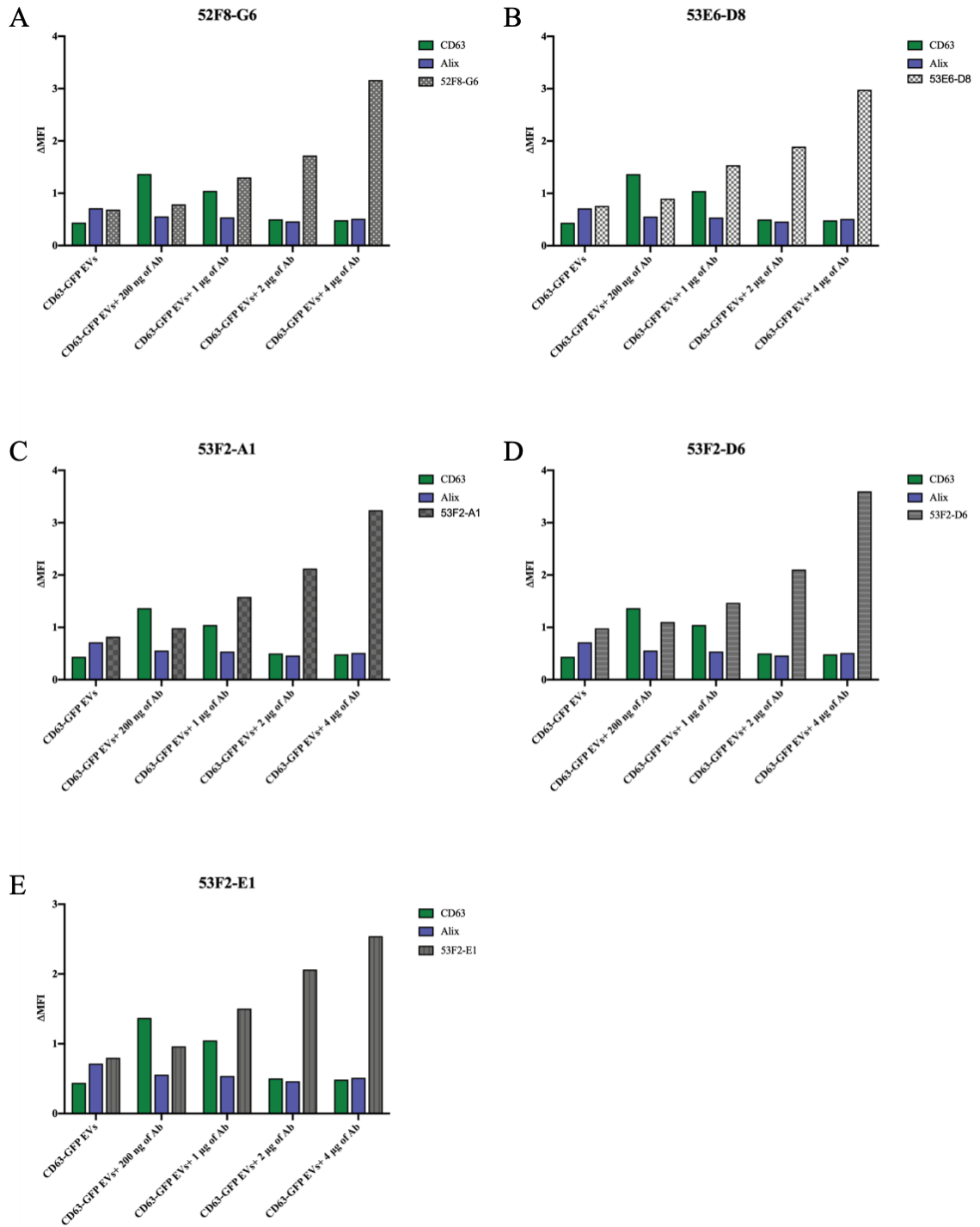


Figure 39: Titration of monoclonal antibody concentrations for EV uptake analysis by flow cytometry.

2.5 X 10⁹ CD63-GFP EVs were used, combined with different concentrations of monoclonal antibodies. Median fluorescence intensity normalized to the control (Δ MFI) (A-E). Data represents one experiment. Details of scatter plots correlating EV uptake (CD63-GFP Internalized EVs) with APC autofluorescence in Supplementary Figure 11 and Supplementary table 3 for sample ID's.

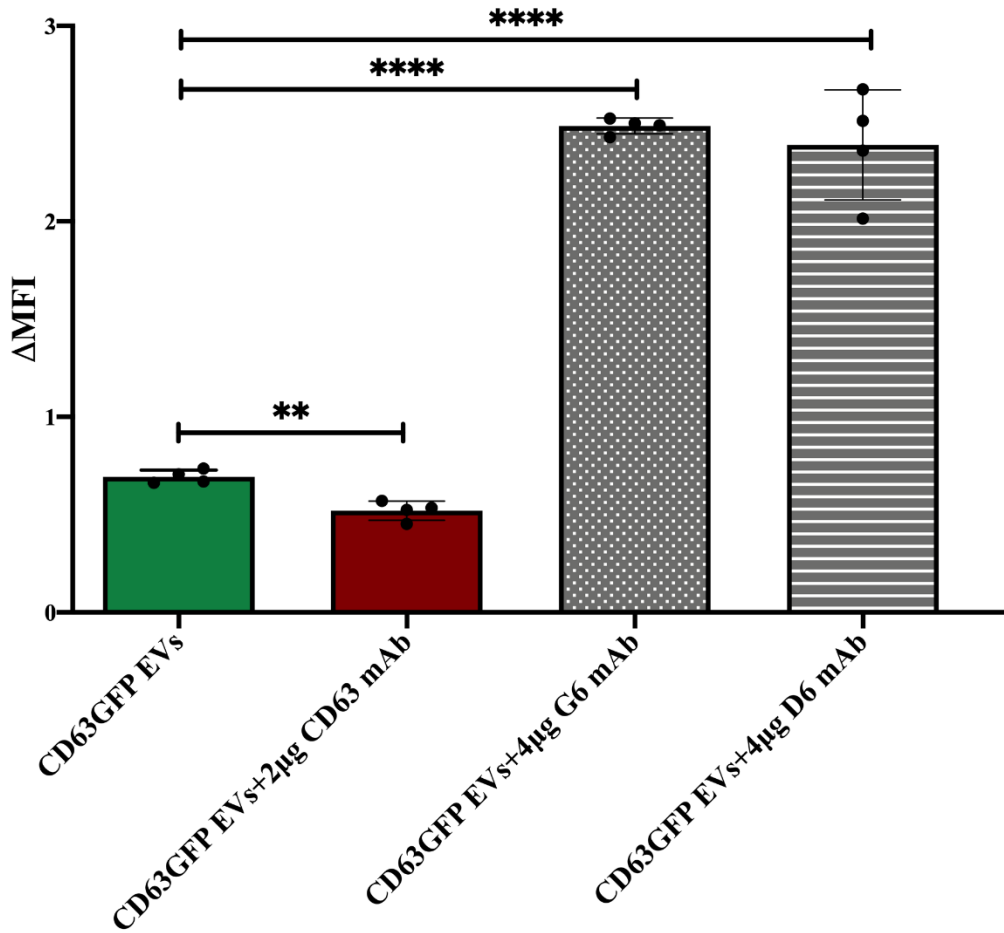


Figure 40: 52F8-G6 and 53F2-D6 monoclonal antibodies for EV uptake analysis by flow cytometry.

2.5 X 10⁹ CD63-GFP EVs were used, combined with a 4 μ g concentration monoclonal antibodies. Median fluorescence intensity normalized over to the control (Δ MFI) (n = 4). Unpaired t-test was applied on raw values; **P < 0.01, ****P < 0.0001. Details of scatter plots correlating EV uptake (CD63-GFP Internalized EVs) with APC autofluorescence in Supplementary Figure 12 and Supplementary Table 4 for sample ID's.

These results indicate that monoclonal antibodies produced against HDF EVs enhance the uptake of HDF-derived EVs into Huh-7 cells, which was contradictory to our initial hypothesis. However, based on these results, we postulate a new hypothesis, which is still out for testing, that binding of mAbs against the unknown antigen on fibroblast derived EVs does mediate enhanced uptake. As a next step in the near future, identification of such antigens using mass spectrometry after affinity purification of the antigen using our mAbs is currently executed.

4. DISCUSSION

4.1. Establishment of the Snorkel-tag based Extracellular Vesicle Affinity Chromatography (StEVAC) method for recombinant EV purification

Cell-derived vesicles or extracellular vesicles are small membrane vesicles derived either from the endocytic pathway or from budding from plasma membrane. These vesicles carry biomolecules from donor cell to recipient cell which can then affect the physiological state of the cell upon their delivery. Widely adapted nomenclature of EVs divides them into three groups based on their size and biogenesis: Exosomes, microvesicles and apoptotic bodies. Exosomes are small EVs derived from endocytic origin with the size ranging from 30- 150 nm in diameter. Microvesicles are derived from budding of the plasma membrane with size the ranging from 100- 1000 nm. However, recent reports showed the presence of subtypes of exosomes with varying size and composition. For instance, density gradient separation of ultracentrifuged EV pellets results in two distinct subtypes, LD-Exo (low density- exosomes) with mode size of 117 nm and HD-Exo (high density- exosomes) with mode size of 66 nm with unique molecular composition (Willms et al. 2016). In another recent study, in which AF4 was used for exosome isolation, two subpopulation of exosomes were revealed: Exo-S (60- 80 nm) and Exo-L (90- 120 nm) along with new subtype EVs called ‘exomeres’ (~35 nm) (H. Zhang et al. 2018). Considering the size of microvesicles (100- 1000 nm) and the method used for isolating EVs, there might also be a slight microvesicle contamination in the EV preparations (Patel et al. 2019). The size of the EVs/exosomes majorly depends on the method of isolation applied. In our study, we majorly used tangential flow filtration and ultrafiltration using spin columns with pre-cleaning at low centrifugation steps for EV purification. Due to the ambiguity concerning the nature of EVs purified we used the generic term ‘extracellular vesicles (EVs)’ rather than ‘exosomes’.

Tetraspanins are the largest members of transmembrane proteins and are believed to play a pivotal role in cell-cell interactions and in the physiology of mammals. For instance, knockout of or mutations in tetraspanins can have a major impact on the physiology of organisms (Schroder et al. 2009; Crew et al. 2004; Claude Boucheix 2000). The tetraspanins family of proteins comprises of CD9, CD37, CD63, CD81, CD82 and CD151 (C. Boucheix and Rubinstein 2001). CD81 is the most characterized among all of them because of its role in B cell function and in sorting CD19 to cell surface which is important for B cell receptor stimulation (Mattila et al. 2013; Van Zelm et al. 2010). Tetraspanins are predicted to contain 4 transmembrane domains (TMD) with the N- and C- termini located inside the lumen and two extracellular loops; EC1 between TMD1 and TMD2, EC2 between TMD3 and TMD4 and a short intracellular loop between TMD3 and TMD4. All the tetraspanins are palmitoylated on intracellular cysteine residues. This modification is required for the interactions with other proteins and formation of tetraspanin-enriched microdomains (TERMs) on the plasma membrane (Yáñez-Mó et al. 2009). The structural characterization of the large EC2 of CD81 revealed the importance of the EC2 domain for protein-protein interactions of tetraspanins (Rajesh et al. 2012). The first crystal structure of full length CD81 sheds light on its interaction with cholesterol and its importance in maintenance and functionality of CD81 (Zimmerman et al. 2016). This further confirms that CD81 is highly enriched in detergent-resistant microdomains. In addition, CD81 is enriched in almost all cell-derived EVs such as exosomes and microvesicles. It is majorly used and recommended as an EV-specific marker for characterizing EVs (Théry et al. 2018).

Considering the importance of CD81 in physiology, we engineered CD81 without hampering the main structural domains of the protein. We specially designed the snorkel-tag, designed to study membrane proteins such as GPCRs (G-protein coupled receptors) and ion channels where N and C termini of the proteins are inside the lumen of the cell. The linker between the CD81 and TMD of the snorkel-tag enables the tags to be displayed away from the CD81 EC2 domain, assuming the functionality of CD81 not to be

compromised. In addition, we also produced different constructs by fusing the tags to truncated versions of CD81 (Figure 10 and supplementary figure 1). However, truncated CD81 versions and the N-terminal snorkel tag could either not be expressed in full length (Figure 11) or were hampered in their cellular localization. The removal of one of the transmembrane domains of the CD81 might severely disturb the interaction of CD81 with lipids such as cholesterol and other interacting partners (Zimmerman et al. 2016; Rajesh et al. 2012), further hampering their enrichment in EVs and their biogenesis. Henceforth, we decided to fuse the snorkel-tag to the C-terminal region of CD81. However, we observed no activity of the PreScission protease when the snorkel-tag was bound to an anti-HA affinity matrix (Figure 12). This might be due the steric hinderance or impaired accessibility of the PreScission protease cleavage site when bound to HA antibody. Therefore, we re-engineered our C-terminal snorkel by introducing flexible linkers (G4S)₃ on either side of the PreScission protease site to allow a certain degree of movements to ensure that it is easily accessible for the protease when bound to an affinity matrix without changing the performance of the protein (Argos 1990; Waldo et al. 1999). In addition, we introduced a rigid linker (EA3K)₂ between the transmembrane domain and FLAG-tag of the snorkel-tag in order to avoid non-specific interactions between the snorkel-tag and the plasma membrane or other membrane proteins displayed on the surface of the plasma membrane or EVs (Arai et al. 2001).

Extracellular vesicles, being nanoparticles are very heterogenous in size and composition. The isolation of EVs is the very first and important step which determines their efficacy in therapeutic application. Ultracentrifugation is the most widely used method for purification of EVs (Gardiner et al. 2016). However, it comes with certain limitations such as vesicle aggregation, disruption and coprecipitation of non-EV components when employed on biological fluids (Linares et al. 2015; Lener et al. 2015). In addition, the large-scale production and isolation of EVs is another limiting factor for UC based EV isolations. In our study, we employed TFF with 100 kDa MWCO hollow fiber system for isolation of EVs (Nordin et al. 2015). The application of TFF for large-scale isolation of EVs is an efficient method over UC with regard to the yields, high purity of EVs and batch-to-batch

consistency (Busatto et al. 2018). In addition, TFF can be further coupled with size exclusion systems in order to obtain relatively pure EVs for clinical applications (McNamara et al. 2018; Corso et al. 2017). EVs isolated by applying TFF on conditioned media from HeLa-WT and HeLa-CD81-snorkel-tag demonstrate that isolated EVs are relatively pure with typical EV morphology and size which was judged by TEM and NTA. The presence of EV-associated proteins ALIX, syntenin and TSG101 was detected by western blotting. Furthermore, typical EV marker proteins such as CD9, CD63, CD81 and HeLa EV- specific markers were detected by a multiplex bead-based flow cytometry assay. Additionally, snorkel-tag epitopes were probed in the EVs derived from HeLa-CD81-snorkel-tag cells by western blotting, TEM and by indirect labelling of the snorkel-tag in a multiplex bead-based flow cytometry assay. Aforementioned, along with TFF one can employ ultrafiltration by using 100 kDa spin columns for concentrating EVs from conditioned media which yields higher concentrations of EVs compared to UC with improved purity (Nordin et al. 2015; Guerreiro et al. 2018).

Taken together, these EV characterizations demonstrate that there is no significant difference in the amount of EVs secreted, in their size and EV protein surface composition when comparing EVs harboring the snorkel-tag with WT EVs. Hence, with these observations we conclude that the presence of the snorkel-tag on the surface of the EVs won't alter the nature of EVs. However, further studies need to be done to precisely address the effects of the snorkel-tag on plasma membrane compositions, biogenesis of EVs and on their cargo sorting.

A wide variety of affinity based EV isolation techniques have been developed for exploiting the surface molecular composition of EVs. Affinity immunoprecipitation of EVs using CD9, CD63, CD81 and heat shock protein-binding peptides are widely used for isolating EVs (Ghosh et al. 2014). However, these methods can only be employed for quantitative analysis of EVs and for smaller starting material. EVs isolated by immunoprecipitation methods cannot be used for functional analysis as it is hard to detach specific antibodies bound to EVs without harming the EV membrane. Other affinity based

EV isolation methods were developed to isolate a total population of EVs. For instance, heparin-based affinity purification of EVs showed better quality of EVs compared to UC based isolation (Balaj et al. 2015). In another instance, a Tim4 based affinity purification method was developed which uses Ca^{2+} dependent affinity interaction of Tim4 to phosphatidylserine (PS) (Miyanishi et al. 2007; Nakai et al. 2016). However, all these methods require high salt concentrations such as NaCl or chelating agents for the elution of EVs.

In our study, we developed a snorkel-tag based extracellular vesicle affinity chromatography (StEVAC) which allows on-column mild elution of EVs by proteolytic cleavage of the snorkel-tag bound to the affinity matrix by PreScission protease. Characterization studies on StEVAC purified EVs confirmed the enrichment of EV-associated proteins such as syntenin by western blot and enrichment of all the EV specific markers such as CD9, CD63, CD81 by using the MACSPlex assay system (Figure 24 and 25). TEM images further revealed that EVs purified after the StEVAC method were relatively pure in retaining their EV shaped morphology and devoid of protein aggregates or protein complexes which were very evident after ultrafiltration or TFF (Figure 24B and S7, S8). Additionally, a multiplex bead-based flow cytometry assay confirmed the specificity of the StEVAC method for purifying EVs harboring the snorkel-tag. In order to demonstrate the specificity of our method we purified EVs harboring the snorkel-tag from a mixture of EVs derived from different cell sources. Considering the sensitivity of the MACSPlex assay system we compared the elutes from mixed population to the elutes obtained from homogenous EVs harboring the snorkel-tag. Our results demonstrate, using the StEVAC method of EV purification on engineered EVs we could enrich EVs carrying the snorkel-tag. However, we did not perform additional characterization studies on elutes obtained from mixed sources due to relatively low amounts of EVs used in the study.

In our experimental setup, by keeping the input concentration of EVs and anti-HA affinity matrix constant for the StEVAC purification of EVs, we could enrich ~35% of EVs based on NTA quantification. However, in the flow through we did not observe the same

reduction of 35%. Considering that the NTA quantification is not absolute quantitative and cannot differentiate between EVs and other contaminants such as protein aggregates (Van Der Pol et al. 2010; Bulte and Modo, n.d.; Varga et al. 2014), we consider two possible explanations. One possible explanation is based on our results, namely that the EVs isolated by employing the StEVAC method show higher purity eliminating other contaminants. Considering the ability of a cell to secrete different subtypes of EVs, the other possibility is that some of the EVs secreted from CD81-snorkel-tag overexpressing cells may not be harboring the snorkel-tag. However, due to the limitations in the characterization techniques we could not rule-out the possibility of EVs devoid of the snorkel-tag. A recently developed nanoFCM can be the solution to address the heterogeneity of EVs. In addition, it would be of great interest to characterize how many recombinant CD81 molecules are harbored on a single EV for better development of isolation techniques.

Aforementioned, scalability is the major limiting factor for the production of EVs for therapeutic applications. Combining TFF with other isolations methods such as BE-SEC (bind-elute size exclusion chromatography) (Corso et al. 2017) or Tim4 affinity based methods (Nakai et al. 2016) yields relatively pure EVs. The StEVAC method falls in line with the mentioned affinity-based methods. The additional advantage of the StEVAC method for the purification is that EVs are not subjected to harsh conditions for elution. The PreScission protease is specially designed to perform on-column protease treatments at relatively low temperatures such as 4°C and can employ simple buffer conditions such as PBS allowing EVs to retain their intactness and functionality.

Labeling of EVs for functional studies is another bottleneck in studying functionality of the EVs. Use of lipid dyes or fluorescent and luminescent reporters are generally employed to study EV uptake and functionality. Previous studies used lipophilic dyes such as DiR, DiD, PKH67 and PKH26 for labeling EVs to study EV biodistribution and their properties *in vivo* (Wiklander et al. 2015b; Grange et al. 2014; Tamura, Uemoto, and Tabata 2016; Deddens et al. 2016). However, the half-life of lipophilic dyes lasts longer *in vivo* compared to half-life of EVs which can be maximum of 24 hours results in wrong assumptions on

EV fate *in vivo* (Teare et al. 1991; Skardelly et al. 2011; Kuffler 1990). Fluorescent reporter such as GFP (Mittelbrunn et al. 2011) fused to tetraspanins or fusion of palmitoylation signal GFP (PalmGFP) and tandem dimer Tomato (PalmtmTomato) have been employed to study dynamics of EV uptakes (C. P. Lai et al. 2015). Although fluorescent and luminescent reporters serve as a versatile tool for labeling EVs to study the fate of EVs may compromise the cargo content within the EVs. Snorkel-tag not only enables simple and mild purification of EVs by StEVAC method, it also provides space for efficient labeling of purified EVs for functional studies. CLIP-tag as a component of snorkel-tag still will be displayed on the surface of the EVs after purification. CLIP-tag substrates consist of a fluorophore conjugated to cytosine. The labeling reaction enables transfer of fluorophore from CLIP-substrates onto CLIP-tag covalently (Gautier et al. 2009, 2008; Schultz and Köhn 2008). In addition, one can choose CLIP-substrates which are cell-permeable and impermeable, enabling to study EV uptake dynamics alongside labeling. However, expression of fluorescent proteins or snorkel-tag fused to tetraspanins may affect the membrane dynamics along with cargo sorting or its content in EVs which require further detailed investigations.

These findings provide evidence for uptake of EVs after the StEVAC purification. However, we want to be sure if snorkel-tag harboring EVs are functional in the first place. Therefore, we adapted Cre-loxP method for studying functionality of EVs (Zomer et al. 2016, 2015; Steenbeek et al. 2018; Ridder et al. 2015). Snorkel-tag harboring cells were allowed to overexpress Cre recombinase and color-switch loxP system was established in reporter cell line. We observed color-switch in reporter cells upon internalization of EVs derived from Cre recombinase overexpressing cells. However, the percentage of color-switch cells were relatively low which was previously addressed by Zomer et al.

To sum up, we systematically evaluated the StEVAC method for purifying EVs harboring snorkel-tag. Now we are excited to extend our studies to *in vivo* models by expressing CD81-snorkel-tag under tissue-specific promoter and understand the insights of cargo under pathophysiological conditions.

4.2. Evaluation of neutralizing effects of monoclonal antibodies produced against human dermal fibroblast EVs

Aging is a progressive cellular functional decline leading to age-associated diseases. Aging is a major risk factor for many pathologies such as cancer, diabetes, cardiovascular diseases and neurodegenerative diseases. Senescent cells often accumulate in aging tissue and generate pro-inflammatory and pro-tumorigenic factors influencing the microenvironment of the tissue (Krtolica et al. 2001; Zhu et al. 2014). These factors secreted by senescent cells are collectively called SASP factors which have negative effects on the surrounding environment. Selective elimination of accumulated senescent cells increases the healthy life span and delays the on-set of age-associated diseases (Baker et al. 2016, 2011; van Deursen 2019).

4.2.1. EVs in skin are members of SASP in cellular senescence

SASP factors majorly comprise of cytokines, chemokines, growth factors and matrix metalloproteinases (MMPs) secreted by senescent cells mediate the ECM remodeling, induction of pro-inflammatory and pro-tumorigenic environment in the surrounding tissues (J.-P. Coppé et al. 2010). Various external factors such as irradiation (Arscott et al. 2013), hypoxia (Svensson et al. 2011; HW, MZ, and JM 2012; Kucharzewska et al. 2013), Ca²⁺ ionophores (Savina et al. 2003) and oxidative stress (Eldh et al. 2010) has been shown to trigger secretion of EVs. We observed 4-fold increase in EV secretion in senescent cells compared to quiescent cells, which is in line with other recent reports (Lehmann et al. 2008; Effenberger et al. 2014; Jeon et al. 2019; A. Takahashi et al. 2017). Many recent reports provide strong evidence on EV-mediated cross-talk *in vitro* between skin cells such as HDFs, keratinocytes and melanocytes modulating several physiological processes (Huang

et al. 2015; Cicero et al. 2015; Wäster et al. 2016). Knowing EVs are members of SASP (Terlecki-Zaniewicz et al. 2018) and able to cross biological barriers, the question raised, if EVs can pass through the dense extracellular matrix in skin to communicate with other cell types? In order to validate this, we used two different strategies to isolate EVs from skin interstitium, one using skin biopsies and disintegrating dermis and epidermis by dispase and isolating EVs from accessible material and the other by performing open flow perfusion (OFM) to collect dermal interstitial fluid (dISF) for isolating EVs. Intriguingly, our EV characterization studies suggest that using different enrichment strategies we can isolate EVs from human skin. Additionally, transmission electron microscopy on skin cryosections stained positive for EV- specific marker CD63 further substantiate our characterization results on EVs isolated from skin.

4.2.2. Therapeutic potential of senescent cell derived EVs

Considering growing evidence on negative effects of senescent cell secretome on tissue microenvironment, it is of high interest for developing senolytic drugs which can attenuate the effects of senescent cell secretome by eliminating senescent cells. Given that senescent cells do not proliferate and resistant to apoptosis, targeting anti-apoptotic proteins such as BCL-2, BCL-XL and BCL-W could potentially eliminate senescent cells. Two such targeted drugs ABT-263 (Chang et al. 2016) and ABT-737 (Yosef et al. 2016) serves as a senolytics by selectively eliminating senescent cells mice. In addition to employing cancer drugs as senolytics various other approaches have been used to eliminate senescent cells. For instance, peptide drug which induces apoptosis by interfering with the interaction between FOXO4 and p53 (Baar et al. 2017), use of nanoparticles specialized to identify senescent cells and deliver cytotoxic drugs (Muñoz- Espín et al. 2018) or use of quercetin, fisetin, and dasatinib as senolytics. However, use of these drugs can have toxic side effects on other normal cell populations in addition to drug resistance. Hence, new strategies are underway to develop “next generation” senolytics that are safe and selectively eliminate the senescent cells.

Aforementioned, increased secretion of EVs in senescent cells are attributable for anti-apoptotic (Terlecki-Zaniewicz et al. 2018) and pro-tumorigenic activity (Takasugi et al. 2017). Inhibition of EV biogenesis or secretion pathway can be deleterious to the normal cell populations. Hence, other possible best strategy is to inhibit EV uptake by blocking or clearing the EVs using neutralizing agents. Combining all the observations and reports mentioned, we came up with a strategy for neutralizing effects of senescent derived EVs. In order to pursue our idea, we produced monoclonal antibodies against human dermal fibroblast derived EVs and could confirm the epitope for these antibodies are specifically expressed in HDFs (Figure: 35). Interestingly, in our EV uptake assays we found out that HDF- derived EVs when incubated with these monoclonal antibodies showed dose-dependent EV internalization in Huh-7 cells. However, this was not true when anti-CD63 antibody was used. Here, we saw significant inhibition in EV uptake when blocked with anti-CD63 antibody. These results further confirm the role of tetraspanins in target selection by interaction with receptors on the recipient cell surface (Yáñez-Mó et al. 2009).

Considering the diversity involved in EV uptake mechanisms, we believe that uptake of EV-antibody complex could be the result of macropinocytosis, a nonselective uptake mechanism. However, we are yet to determine the epitope for monoclonal antibodies synthesized against HDF- derived EVs. The information on antigen can shed light on their role in enhancing EV uptake.

Taken all together, we further plan to extend our investigation on the senescent cell derived EV cargo *in vivo* model. For this we want employ CD81-snorkel-tag expressed under p16^{ink4a} promoter. This will enable us to specifically purify EVs derived from senescent cells using StEVAC method. Finally, allowing us to understand the insights of senescent cell- derived EV cargo which can have huge diagnostic and therapeutic potential.

5. MATERIAL AND METHODS

5.1. Material

5.1.1. Sequences:

Different versions of snorkel-tag sequences and CD81 full length and truncation sequences mentioned below:

Snorkel-tag for C-terminal:

```
GGGGCGAGCAGCGGGAGCAGCCCCGGGAGCGGTTCTCAAAGAAGCCTCGG
TACGAAATCAGGTGGAAAGTCGTTGTGATCAGCGCCATCCTGGCACTCGTGG
TCCTGACCGTGATTTCCCTGATTATCCTGATTATGCTGTGGGGCTCTGACTAT
AAAGACGATGACGATAAAGGCATGCCATGGACAAAGACTGCGAAATGAAG
CGCACCACCCTGGATAGCCCTCTGGGCAAGCTGGAAGTGTCTGGGTGCGAAC
AGGGCCTGCACCGTATCATCTTCCTGGGCAAAGGAACATCTGCCGCCGACGC
CGTGGAAGTGCCTGCCCCAGCCGCCGTGCTGGGCGGACCAGAGCCACTGATC
CAGGCCACCGCCTGGCTCAACGCCTACTTTCACCAGCCTGAGGCCATCGAGG
AGTTCCTGTGCCAGCCCTGCACCACCCAGTGTTCAGCAGGAGAGCTTTACC
CGCCAGGTGCTGTGGAAACTGCTGAAAGTGGTGAAGTTCGGAGAGGTCATCA
GCGAGAGCCACCTGGCCGCCCTGGTGGGCAATCCCGCCGCCACCGCCGCCGT
GAACACCGCCCTGGACGGAAATCCCGTGCCATTCTGATCCCCTGCCACCGG
GTGGTGCAGGGCGACAGCGACGTGGGGCCCTACCTGGGCGGGCTCGCCGTGA
AAGAGTGGCTGCTGGCCCACGAGGGCCACAGACTGGGCAAGCCTGGGCTGG
GTCTGGAAGTTCTGTTCCAGGGGCCCTACCCATATGACGTTCTGATTACGCT
TGA
```

N-Ter — **TMD** **FLAG-tag** **CLIP-tag** **Protease site** **HA-tag** —C-Ter **Snorkel-tag
For C-ter
(1-261 aa)**

Snorkel-tag (without TMD) for C-terminal truncated CD81:

GGCTCTGACTATAAAGACGATGACGATAAAGGCATGCCCATGGACAAAGACT
GCGAAATGAAGCGCACCACCCTGGATAGCCCTCTGGGCAAGCTGGAAGCTGTC
TGGGTGCGAACAGGGCCTGCACCGTATCATCTTCCTGGGCAAAGGAACATCT
GCCGCCGACGCCGTGGAAGTGCCTGCCCCAGCCGCCGTGCTGGGCGGACCAG
AGCCACTGATCCAGGCCACCGCCTGGCTCAACGCCTACTTTCACCAGCCTGA
GGCCATCGAGGAGTTCCTGTGCCAGCCCTGCACCACCCAGTGTTCCAGCAG
GAGAGCTTTACCCGCCAGGTGCTGTGGAAACTGCTGAAAGTGGTGAAGTTCG
GAGAGGTCATCAGCGAGAGCCACCTGGCCGCCCTGGTGGGCAATCCCGCCGC
CACCGCCGCCGTGAACACCGCCCTGGACGGAAATCCCGTGCCCATCTGATC
CCCTGCCACCGGGTGGTGCAGGGCGACAGCGACGTGGGGCCCTACCTGGGCG
GGCTCGCCGTGAAAGAGTGGCTGCTGGCCACGAGGGCCACAGACTGGGCA
AGCCTGGGCTGGGTCTGGAAGTTCTGTTCCAGGGGCCCTACCCATATGACGTT
CCTGATTACGCTTGA

N-Ter — **FLAG-tag** **CLIP-tag** **Protease site** **HA-tag** —C-Ter **N-ter Δ Snorkel-tag
(49- 261 aa)**

Snorkel-tag for N-terminal:

ATGTACCCATATGACGTTCTGATTACGCTCTGGAAGTTCTGTTCCAGGGGCC
CATGGACAAAGACTGCGAAATGAAGCGCACCACCCTGGATAGCCCTCTGGGC
AAGCTGGAAGTGTCTGGGTGCGAACAGGGCCTGCACCGTATCATCTTCCTGG
GCAAAGGAACATCTGCCGCCGACGCCGTGGAAGTGCCTGCCCCAGCCGCCGT
GCTGGGCGGACCAGAGCCACTGATCCAGGCCACCGCCTGGCTCAACGCCTAC
TTTCACCAGCCTGAGGCCATCGAGGAGTTCCTGTGCCAGCCCTGCACCACCC
AGTGTTCCAGCAGGAGAGCTTTACCCGCCAGGTGCTGTGGAAACTGCTGAAA
GTGGTGAAGTTCGGAGAGGTCATCAGCGAGAGCCACCTGGCCGCCCTGGTGG

GCAATCCCGCCGCCACCGCCGCCGTGAACACCGCCCTGGACGGAAATCCCGT
 GCCCATTCTGATCCCCTGCCACCGGGTGGTGCAGGGCGACAGCGACGTGGGG
 CCCTACCTGGGCGGGCTCGCCGTGAAAGAGTGGCTGCTGGCCCACGAGGGCC
 ACAGACTGGGCAAGCCTGGGCTGGGTGGCTCTGACTATAAAGACGATGACGA
 TAAAGGCATGCCCGTCGTTGTGATCAGCGCCATCCTGGCACTCGTGGTCCTGA
 CCGTGATTTCCCTGATTATCCTGATTATGCTGTGGGGGGCGAGCAGCGGGAG
 CAGCCCCGGGAGCGGTTCTCAAAGAAGCCTCGGTACGAAATCAGGTGGAA
 A

N-Ter — HA-tag Protease site CLIP-tag FLAG-tag TMD — C-Ter **Snorkel-tag
 For N-ter
 (1- 261 aa)**

Snorkel-tag (without TMD) for N-terminal truncated CD81:

TGTACCCATATGACGTTCTGATTACGCTCTGGAAGTTCTGTTCCAGGGGGCCC
 ATGGACAAAGACTGCGAAATGAAGCGCACCACCCTGGATAGCCCTCTGGGCA
 AGCTGGAACTGTCTGGGTGCGAACAGGGCCTGCACCGTATCATCTTCCTGGG
 CAAAGGAACATCTGCCGCCGACGCCGTGGAAGTGCCTGCCCCAGCCGCCGTG
 CTGGGCGGACCAGAGCCACTGATCCAGGCCACCGCCTGGCTCAACGCCTACT
 TTCACCAGCCTGAGGCCATCGAGGAGTTCCCTGTGCCAGCCCTGCACCACCC
 AGTGTTCAGCAGGAGAGCTTTACCCGCCAGGTGCTGTGGAACTGCTGAAA
 GTGGTGAAGTTCGGAGAGGTCATCAGCGAGAGCCACCTGGCCGCCCTGGTGG
 GCAATCCCGCCGCCACCGCCGCCGTGAACACCGCCCTGGACGGAAATCCCGT
 GCCCATTCTGATCCCCTGCCACCGGGTGGTGCAGGGCGACAGCGACGTGGGG
 CCCTACCTGGGCGGGCTCGCCGTGAAAGAGTGGCTGCTGGCCCACGAGGGCC
 ACAGACTGGGCAAGCCTGGGCTGGGTGCATGCGGCTCTGACTATAAAGACGA
 TGACGATAAAG

N-Ter — HA-tag Protease site CLIP-tag FLAG-tag — C-Ter **C-ter Δ snorkel-tag
 (1-213)**

CD81 full length:

ATGGCGGTGGAAGGAGGAATGAAATGTGTGAAGTTCTTGCTCTACGTCCTCC
TGCTGGCCTTTTGCGCCTGTGCAGTGGGACTGATTGCCGTGGGTGTCGGGGCA
CAGCTTGTCTGAGTCAGACCATAATCCAGGGGGCTACCCCTGGCTCTCTGTT
GCCAGTGGTCATCATCGCAGTGGGTGTCTTCCTCTTCCTGGTGGCTTTTGTGG
GCTGCTGCGGGGCCTGCAAGGAGAACTATTGTCTTATGATCACGTTTGCCATC
TTTCTGTCTCTTATCATGTTGGTGGAGGTGGCCGCAGCCATTGCTGGCTATGT
GTTTAGAGATAAGGTGATGTCAGAGTTTAATAACAACCTCCGGCAGCAGATG
GAGAATTACCCGAAAAACAACCACACTGCTTCGATCCTGGACAGGATGCAGG
CAGATTTTAAGTGCTGTGGGGCTGCTAACTACACAGATTGGGAGAAAATCCC
TTCCATGTCGAAGAACCGAGTCCCCGACTCCTGCTGCATTAATGTTACTGTGG
GCTGTGGGATTAATTTCAACGAGAAGGCGATCCATAAGGAGGGCTGTGTGGA
GAAGATTGGGGGCTGGCTGAGGAAAAATGTGCTGGTGGTAGCTGCAGCAGCC
CTTGAATTGCTTTTGTGCGAGGTTTGGGAATTGTCTTTGCCTGCTGCCTCGTG
AAGAGTATCAGAAGTGGCTACGAGGTGATGA

C-terminal truncated CD81 (without TMD4):

ATGGGAGTGGAGGGCTGCACCAAGTGCATCAAGTACCTGCTCTTCGTCTTCA
ATTTTCGTCTTCTGGCTGGCTGGAGGCGTGATCCTGGGTGTGGCCCTGTGGCTC
CGCCATGACCCGCAGACCACCAACCTCCTGTATCTGGAGCTGGGAGACAAGC
CCGCGCCCAACACCTTCTATGTAGGCATCTACATCCTCATCGCTGTGGGCGCT
GTCATGATGTTTCGTTGGCTTCCTGGGCTGCTACGGGGCCATCCAGGAATCCCA
GTGCCTGCTGGGGACGTTCTTCACCTGCCTGGTCATCCTGTTTGCCTGTGAGG
TGGCCGCCGGCATCTGGGGCTTTGTCAACAAGGACCAGATCGCCAAGGATGT
GAAGCAGTTCTATGACCAGGCCCTACAGCAGGCCGTGGTGGATGATGACGCC
AACAACGCCAAGGCTGTGGTGAAGACCTTCCACGAGACGCTTGACTGCTGTG
GCTCCAGCACACTGACTGCTTTGACCACCTCAGTGCTCAAGAACAATTTGTGT

CCCTCGGGCAGCAACATCATCAGCAACCTCTTCAAGGAGGACTGCCACCAGA
AGATCGATGACCTCTTCTCCGGGAAG

N-terminal truncated CD81 (without TMD1):

CTCCGCCATGACCCGCAGACCACCAACCTCCTGTATCTGGAGCTGGGAGACA
AGCCCGCGCCCAACACCTTCTATGTAGGCATCTACATCCTCATCGCTGTGGGC
GCTGTCATGATGTTTCGTTGGCTTCCTGGGCTGCTACGGGGCCATCCAGGAATC
CCAGTGCCTGCTGGGGACGTTCTTCACCTGCCTGGTCATCCTGTTTGCCTGTG
AGGTGGCCGCCGGCATCTGGGGCTTTGTCAACAAGGACCAGATCGCCAAGGA
TGTGAAGCAGTTCTATGACCAGGCCCTACAGCAGGCCGTGGTGGATGATGAC
GCCAACAACGCCAAGGCTGTGGTGAAGACCTTCCACGAGACGCTTGACTGCT
GTGGCTCCAGCACACTGACTGCTTTGACCACCTCAGTGCTCAAGAACAATTTG
TGTCCTCGGGCAGCAACATCATCAGCAACCTCTTCAAGGAGGACTGCCACC
AGAAGATCGATGACCTCTTCTCCGGGAAGCTGTACCTCATCGGCATTGCTGCC
ATCGTGGTCGCTGTGATCATGATCTTCGAGATGATCCTGAGCATGGTGTGTG
CTGTGGCATCCGGAACAGCTCCGTGTACTGA

C-terminal snorkel-tag with linkers:

GGGGCGAGCAGCGGGAGCAGCCCCGGGAGCGGTTCTCAAAGAAGCCTCGG
TACGAAATCAGGTGGAAAGTCGTTGTGATCAGCGCCATCCTGGCACTCGTGG
TCCTGACCGTGATTTCCCTGATTATCCTGATTATGCTGTGGGAAGCAGCGGCT
AAAGAAGCGGCTGCTAAAGGCTCTGACTATAAAGACGATGACGATAAAGGC
ATGCCCATGGACAAAGACTGCGAAATGAAGCGCACCCACCCTGGATAGCCCTC
TGGGCAAGCTGGAAGTGTCTGGGTGCGAACAGGGCCTGCACCGTATCATCTT
CCTGGGCAAAGGAACATCTGCCGCCGACGCCGTGGAAGTGCCTGCCCCAGCC
GCCGTGCTGGGCGGACCAGAGCCACTGATCCAGGCCACCGCCTGGCTCAACG
CCTACTTTCACCAGCCTGAGGCCATCGAGGAGTTCCCTGTGCCAGCCCTGCAC
CACCCAGTGTTCCAGCAGGAGAGCTTTACCCGCCAGGTGCTGTGGAAACTGC

TGAAAGTGGTGAAGTTCGGAGAGGTCATCAGCGAGAGCCACCTGGCCGCCCT
 GGTGGGCAATCCCGCCGCCACCGCCGCGGTGAACACCGCCCTGGACGGAAAT
 CCCGTGCCATTCTGATCCCCTGCCACCGGGTGGTGCAGGGCGACAGCGACG
 TGGGGCCCTACCTGGGCGGGCTCGCCGTGAAAGAGTGGCTGCTGGCCCACGA
 GGGCCACAGACTGGGCAAGCCTGGGCTGGGTGGGGGAGGAGGGTCAGGTGG
 TGGGGGTAGTGGAGGTGGAGGTAGTCTGGAAGTTCTGTTCCAGGGGCCCGGG
 GGAGGAGGGTCAGGTGGTGGGGGTAGTGGAGGTGGAGGTAGTTACCCATAT
 GACGTTCTGATTACGCTTGA



5.1.2. Primers

Name	sense	antisense
CD81- Full length for C-terminal snorkel	ATCCGAATTCATGGGAGTGG AGGGCTGCAC	ATCTGCGGCCGCTC AGTACACGGAGCTG TTCCGGATGCCAC
CD81- C-Terminal truncation	ATCCGAATTCATGGGAGTGG AGGGCTGCAC	ATCTACCGGTCTTC CCGGAGAAGAGGT CATCG
CD81- N-Terminal truncation	ATTCACCGGTCTCCGCCATG ACCCGCAGACCAC	ATCTGCGGCCGCTC AGTACACGGAGCTG TTCCGGATGCCAC
C-Terminal snorkel-tag	ATAATATTACCGGTGGGGCG AGCAGCGGGAGCAG	ATCTGCGGCCGCTC AAGCGTAATC
Snorkel-tag for C-terminal truncated CD81	ATCCACCGGTGGCTCTGACT ATAAAGACGATGACGATAA AGG	ATCTGCGGCCGCTC AAGCGTAATC

Snorkel-tag for N-terminal truncated CD81	GCAGGAATTCATGTACCCAT ATGACG	ACTGACCGGTCTTT ATCGTCATCGTCTT TATAGTCAGAGG
C-terminal Snorkel-tag with linkers	ATAATATTACCGGTGGGGCG AGCAGCGGGAGCAG	ACTGACCGGTCTTT ATCGTCATCGTCTT TATAGTCAGAGG

5.1.3. Antibodies

Antibodies and their respective dilution for Western Blots (WB), Immunofluorescence (IF), Flow cytometry (FC) and Transmission Electron Microscopy (TEM) are show below.

target	manufacturer	catalog #	host	conjugate	WB	IF	FC	TEM
HA-tag	Cell signaling	3724	rabbit	-	1:1,000	1:800	1:1,000	1:50
SNAP/CLIP-tag	NEB	P9310S	rabbit	-	1:1,000	-	-	-
FLAG-tag	Sigma	F3165	mouse	-	1:5,000	-	-	-
CD81	Santa Cruz	sc-166029	mouse	-	1:200	-	-	-
CD81	TheroFisher Scientific	11525542	mouse	-	-	1:500	-	1:50
TSG101	abcam	ab125011	rabbit	-	1:1,000	-	-	-
Alix	abcam	ab117600	mouse	-	1:2,000	-	-	-
Syntenin	origene	TA50479 6	mouse	-	1:1,000	-	-	-
Calnexin	abcam	ab22595	rabbit	-	1:1,000	-	-	-
CD63	Invitrogen	10628D	mouse	-	2 µg/ml	-	-	-
CD63	abcam	ab8219	mouse	-	-	-	-	1:1,000
Mouse IgG	LI-COR	926- 68072	donkey	IRDye 680RD	1:10,000	-	-	-
Rabbit IgG	LI-OR	925- 32213	donkey	IRDye 800CW	1:10,000	-	-	-
Rabbit IgG	abcam	ab96902	goat	DyLight649	-	-	1:1,000	-

Rabbit IgG	Jackson immunoresearch	711-545-152	donkey	Alexa fluor 488	-	1:200	-	-
Mouse IgG	Jackson immunoresearch	715-605-150	donkey	Alexa fluor 647	-	1:200	-	-
Mouse IgG	-	-	sheep	10 nm gold particle	-	-	-	1:50
Rabbit IgG	-	-	sheep	10 nm gold particle	-	-	-	1:50
Mouse IgG	-	-	-	Cy3	-	-	1:1000	-

5.2. Methods

5.2.1. Cell culture

Cell culture experiments were performed under sterile and antibiotic free conditions. Human dermal fibroblasts (HDFs) from adult skin three healthy donors (HDF76, HDF85, HDF161), HDF164-hTert and phoenix were provided by Evercyte GmbH. Cells were grown in DMEM/Ham's F-12 (1:1 mixture) (BIOCHROME, Germany) supplemented with 10 % fetal calf serum (FCS) and 4 mM L-Glutamine (Sigma Aldrich GmbH St Louis, MO, USA) at 7% CO₂ and 37°C. HEK293 cells were cultivated in DMEM with Na-pyruvate (BIOCHROME, Germany) supplemented with 10 % fetal calf serum (FCS) and 4 mM L-Glutamine (Sigma Aldrich GmbH St Louis, MO, USA) at 7% CO₂ and 37°C. Huh-7 cells were provided by Samir EL Andaloussi's lab at Department of laboratory medicine, Karolinska Institutet, Stockholm, Sweden. Huh-7 cells were cultivated in DMEM (ThermoFisher Scientific) supplemented with 10% fetal calf serum (FCS) (Sigma Aldrich GmbH St Louis, MO, USA) and 1 X GlutaMAX (ThermoFisher Scientific) at 5% CO₂ and 37°C. Primary HUVECs and ASCs were provided by Wolfgang Holnthoner at Ludwig Boltzmann Institute for Experimental and Clinical Traumatology, Vienna. HUVECs and ASCs were cultivated in EBM-2 media supplemented with EGM-2 (Lonza) and 5% FCS (Sigma Aldrich GmbH St Louis, MO, USA) at 7% CO₂ and 37°C. HeLa cells were grown

in RPMI 1640 (ThermoFisher Scientific) supplemented with 10% fetal calf serum (FCS) (Sigma Aldrich GmbH St Louis, MO, USA) and 1 x GlutaMAX (ThermoFisher Scientific) at 5% CO₂ and 37°C.

5.2.2. Stress induced premature senescence (SIPS)

For induction of SIPS, HDFs (HDF161, HDF85 and HDF76) were seeded with 3500 cells/cm² one day (d) prior stress treatment using 9 (4 d stress – 2 d recovery – 5 d stress) with 100 µM H₂O₂ for one hour per day followed by a media change. Non-stressed control cells reached quiescence (Q) by contact inhibition. Induction of SIPS was confirmed by bromodeoxyuridine (BrdU) incorporation, senescence-associated (SA)-β-Gal staining, CDKN1A (p21) expression and Annexin-V-PI staining after 7 (D7) and 21 days (D21) post stress treatment (Terlecki-Zaniewicz et al. 2018).

5.2.3. Generation of stable cell lines

For all the variants of CD81-snorkel-tag stable cell line generation, we cloned CD81-snorkel-tag in pCI-neo vector. HeLa cells were transfected with respective plasmids carrying variants of CD81-snorkel-tag were transfected using JetPrime (Polyplus) according to manufacturer's instruction. 3 days after transfection, 600 µg/ml G418 were applied as selection pressure. After two weeks single colonies were isolated and screened for expression (data not shown)

For CD81-snorkel-tag with linkers, insert was cloned into pBMN vector. Phoenix cells were transfected with pBMN:CD81-snorkel-tag plasmid using JetPrime (Polyplus) in serum free conditions. 24 hours post transfection, media was removed, and fresh growth media was added. After 24 hours, media from phoenix cells were filtered with 0.45 µm

sterile filter and mixed with polybrene (8 µg/ml), added on top of HeLa cells seed in 6-well plate a day before and spun at 800 x g for 1 hour at room temperature. Then, virus supernatant was discarded, and fresh growth media was added and cells were incubated 7% CO₂ and 37°C. These steps were repeated for 4-5 days for stable expression of CD81-snorkel-tag.

For generating HDF164-hTert: CD63-neonGFP cells were transduced with pLEX-CD63-neonGFP carrying viral particles. Cells were incubated at 5% CO₂ and 37°C overnight and viral particle containing media was removed and fresh growth media was added. After propagation cells were checked for neonGFP expression using MACSQuant Analyzer 10 flow cytometer (Miltenyi Biotec).

Generation of Cre recombinase expression cells: HeLa-CD81-snorkel-tag carrying cells were transfected with pcDNA 3.1 Cre plasmid using JetPrime (Polyplus). 3 days after transfection, 50 µg/ml zeocin was applied as selection pressure. After two weeks cells were collected, expanded for EV isolations.

Generation of loxP reporter HEK293 cells: loxP color-switch system was cloned into pBMN vector. For stable expression we used same procedure used for generating CD81-snorkel-tag (with linkers) cell line.

5.2.4. EV isolation procedures

We employed different EV isolation protocols depending on the downstream application. Stated briefly in results section which of the following method was applied for isolating EVs.

5.2.4.1. EV isolation using differential ultracentrifugation (UC)

EV Isolation using differential ultracentrifugation was performed according to guidelines recommended by international society for extracellular vesicles (ISEV)(Théry et al. 2018). EVs from FCS were depleted from growth media (DMEM/Ham'S F-12 + FCS) by ultracentrifugation at 100,000 x g overnight and sterile filtered using 0.22 µm filter cups (MILLIPORE, Germany). Conditioned media (after 48 hours secretion) was centrifuged for 15 min at 500 x g (Eppendorf, 5804R) at 4° C to remove cellular debris and 14,000 x g (Beckmann, Coulter, Brea, CA, USA, Avanti JXN-26) at 4°C for 15 mi to remove larger EVs followed by sterile filtration using 0.22 µm filter cups to remove EVs above 220 nm in size. Conditioned media from SIPS and from Q cells were filled into Quick-Seal, Polyallomer, 39 ml, 25x89 mm tubes (BECKMANN, Brea, CA, USA). Sealed tubes were subjected to ultracentrifugation using a 70Ti Rotor Beckman coulter at 100,000 x g for 90 min (BECKMANN, Brea, CA, USA) and EV pellets in different tubes but from the same samples were pooled. EV pellet was resuspended in sterile filtered 1 x PBS and quantified for size and concentration by nanoparticle tracking analysis (NTA).

5.2.4.2. Large batch EV isolation using tangential flow filtration (TFF)

Conditioned media from HeLa-WT and HeLa-CD81-snorkel-tag overexpressing cells was collected and subjected to a low speed spin at 700 × g for 5 minutes at 4° C to remove cellular debris, followed by 2000 × g spin for 10 minutes at 4°C to remove larger particles and cell debris. The supernatant was then sterile filtered with a 0.22 µm filter cups. Conditioned media was diafiltrated using 2 volumes of initial volume to ~ 35 ml using KR2i TFF system (SpectrumLabs) with 300 kDa cut-off hollow fibre filters (MidiKros, 370 cm² surface area, SpectrumLabs) at a flow rate of 100 ml/min (transmembrane pressure at 3.0 psi and shear rate at 3700 sec⁻¹) (Corso et al. 2017; Wiklander et al. 2018). Diafiltrated was further concentrated to ~1 ml using Amicon ultra-15 centrifugal filter unit (Catalog # UFC910024) at 4°C with 3500 x g. Concentrated EV solution was quantified

for size and concentration and 100 μ l aliquotes were stored in -80°C for subsequent characterization studies.

Unless indicated otherwise, above mentioned TFF protocol was implied on conditioned media from HDF164-hTert, HDF164-hTert cells expressing CD63-neonGFP, HUVEC and ASC cells for EV isolations.

5.2.4.3. EV isolation using ultrafiltration (UF)

Pre-cleaned conditioned media (700 x g for 5 min and 2000 x g for 10 min) from HeLa-WT and HeLa-CD81-snorkel-tag overexpressing cells was sterile filtered using syringe (VWR) with cellulose acetate membrane filters (0.22 μm pore size) to remove any larger particles. The filtered conditioned media was ultrafiltered using 100 kDa MWCO Amicon ultra-15 centrifugal filter unit (Catalog # UFC910024) at 4°C with 3500 x g (Balaj et al. 2015). The concentrate was diafiltrated with 2 volumn of 1 x PBS and concentrated to final volume of ~ 1 ml. Final volume was quantified by NTA for size and concentration of EVs. After quantification EV sample were freshly used for further purification by StEVAC method.

5.2.5. Nanoparticle Tracking Analysis (NTA)

Nanoparticle tracking analysis was applied to determine particle size and concentration of all samples. All samples concentrated by TFF and UF were characterized by NTA with a NanoSight NS500 instrument equipped with NTA 2.3 analytical software and an additional 488 nm laser. Samples were diluted to 1:1000 in sterile filtered PBS (0.22 μm filter). Diluted samples were loaded in the sample chamber with camera level 13. Four to five 30 sec videos were recorded per sample in light scatter mode with 5 sec delay between each

recording. Screen gain 10, detection threshold 7 were kept constant for all the recordings. Using batch process facility all the measurements were analyzed automatically.

For quantification of EVs isolated by UC from Q and SIPS cells we used the Zetaview system (Particle Metrix, Meerbusch, Germany) (Terlecki-Zaniewicz et al. 2019, 2018). Calibration of the system was conducted with 110 nm polystyrene standard beads (Particle Metrix, Meerbusch, Germany). Vesicles were diluted in filtered 1 x PBS and each sample was measured in technical triplicates. For optimized performance, camera sensitivity was adjusted to fit the highest and lowest concentrated sample into the dynamic range and all samples were measured with the same dilution and settings. Settings: Gain 904, 98; Offset 0. Measurements were taken at two different camera positions. EVs secreted per cell were calculated using the cell number measured with Vi-CELL XR (Beckman Coulter, Brea, CA, USA).

5.2.6. Snorkel-tag based Extracellular Vesicle Affinity Chromatography (StEVAC)

Conditioned media from HeLa-WT and HeLa-CD81-snorkel-tag overexpressing cells were processed using ultrafiltration based EV isolation. Isolated EVs were quantified using NTA and $\sim 2.5 \times 10^{10}/\text{ml}$ were incubated with 250 μl of anti-HA magnetic beads (Catalog # 88836, ThermoFisher Scientific; bead concentration 10 mg/ml) overnight at 4° C on a rotospin test tube rotator. Post incubation, beads were separated on magnetic rack and unbound EV solution was collected and beads were washed with 0.22 μm filtered PBS. After washing step, beads were suspended in 0.22 μm filtered PBS with 5 μl (10 units) of PreScission protease (catalog # 27084301; GE healthcare Life Sciences) and incubated overnight at 4°C on a rotospin test tube rotator for on-column PreScission protease cleavage. After overnight incubation, tubes were placed on magnetic rack for separating beads and elutes were collected. Collected elutes along with flow through and wash samples were quantified for size and concentration using NTA. For characterization studies samples were freshly used.

5.2.7. Western blotting

HeLa-WT cells and HeLa-CD81-snorkel-tag expressing cells were collected and the cell pellet was lysed with 100 μL of RIPA buffer, kept on ice, and vortexed five times every 5 min. The cell lysate was then spun at $12,000 \times g$ for 10 min at 4°C and the supernatant was transferred to a new tube and kept on ice. Protein concentrations for the supernatants were quantified by BCA assay (ThermoFisher Scientific) according to manufacturer's instructions. 50 μg of cell lysates and 1×10^9 to 5×10^9 particles were mixed with buffer containing 0.5 M dithiothreitol, 0.4 M sodium carbonate (Na_2CO_3), 8% SDS, and 10% glycerol, and heated at 95°C for 10 min. The samples were loaded onto a NuPAGE Novex 4–12% Bis-Tris Protein Gel (Invitrogen, Thermo Fisher Scientific) and run at 120 V in

NuPAGE MES SDS running buffer (Invitrogen, Thermo Fisher Scientific) for 2 h. The proteins on the gel were transferred to an iBlot nitrocellulose membrane (Invitrogen, Thermo Fisher Scientific) for 7 min using the iBlot system. The membrane was blocked with Odyssey blocking buffer (LI-COR) for 1 hour at room temperature with gentle shaking. After blocking, the membrane was incubated overnight at 4°C or 1 hour at room temperature with primary antibody solution. The membrane was washed with PBS supplemented with 0.1% Tween-20 (PBS-T, Sigma) three times for every 5 min and incubated with the corresponding secondary antibody (LI-COR) for 1 hour at room temperature. Finally, the membrane was washed with PBS-T for three times with 5 min interval, twice with PBS and visualized on the Odyssey infrared imaging system (LI-COR) at 700 and 800 nm.

5.2.8. CLIP-tag labeling quantification by Flow cytometry

HeLa-WT cells and HeLa-CD81-snorkel-tag overexpressing cells were collected and suspended in 1 ml of growth media (RPMI 1640 + 10% FCS + 1 X GlutaMAX). To this, non-cell-permeable CLIP-substrate (CLIP-SurfaceTM 647; Catalog #S9234, NEB) with final dilution of 1:100,000 was added and incubated at for 1 hour at 95% humidity, 5% CO₂ and 37°C. Post incubation, cells were spun at 300 x g for 5 min to remove the unlabeled dye and washed twice with PBS and pelleted at 300 x g for 5 min and resuspended in 100 µl of PBS. Dead cells were excluded by 4',6-diamidino-2-phenylindole (DAPI) staining and doublets were excluded by forward/side scatter area versus height gating. Samples were kept on ice and measured with MACSQuant Analyzer 10 flow cytometer (Miltenyi Biotec). GraphPadPrism 8.2.1 (GraphPadPrism Software, La Jolla, CA, USA) was used to analyze data and assemble figures.

5.2.9. Multiplex bead-based flow cytometry assay for EV surface protein profiling

Different sample types were subjected to bead-based multiplex EV analysis by flow cytometry (MACSPlex Exosome Kit, human, Miltenyi Biotec). Unless indicated otherwise, EV-containing samples were processed as follows: Samples were diluted with MACSPlex buffer (MPB) to, or used undiluted at, a final volume of 60 μ L and loaded onto wells of a pre-wet and drained MACSPlex 96-well 0.22 μ m filter plate before 3 μ l of MACSPlex Exosome Capture Beads (containing 39 different antibody-coated bead subsets) were added to each well. Generally, particle counts quantified by NTA, and not protein amount, were used to estimate input EV amounts. We used 1×10^9 particles as input EV amounts. Filter plates were then incubated on an orbital shaker overnight (14–16 hours) at 450 rpm at room temperature protected from light. To wash the beads, 200 μ l of MPB was added to each well and the filter plate was put on a vacuum manifold with vacuum applied (Sigma-Aldrich, Supelco PlatePrep; -100 mBar) until all wells were drained. For counterstaining of EVs bound by capture beads with detection antibodies, 135 μ l of MPB and 5 μ l of each APC-conjugated detection antibody cocktail (anti-CD9, anti-CD63, and anti-CD81) were added to each wells and plates were incubated on an orbital shaker at 450 rpm protected from light for 1 h at room temperature. Next, plates were washed by adding 200 μ L MPB to each well followed by draining on a vacuum manifold. This was followed by another washing step with 200 μ l of MPB, incubation on an orbital shaker at 450 rpm protected from light for 15 min at room temperature and draining all wells again on a vacuum manifold. Subsequently, 150 μ l of MPB was added to each well, beads were resuspended by pipetting and transferred to V-bottom 96-well microtiter plate (Thermo Scientific). Flow cytometric analysis was performed using MACSQuant Analyzer 10 flow cytometer (Miltenyi Biotec). All samples were automatically mixed immediately before 70–100 μ l were loaded to and acquired by the instrument, resulting in approximately 3,000–5,000 single bead events being recorded per well. FlowJo software (v10, FlowJo LLC) was used to analyze flow cytometric data. Median fluorescence intensity (MFI) for

all 39 capture bead subsets were background corrected by subtracting respective MFI values from matched non-EV buffer (PBS) that were treated exactly like EV-containing samples (buffer/medium + capture beads + antibodies). GraphPadPrism 8.2.1 (GraphPadPrism Software, La Jolla, CA, USA) was used to analyze data and assemble figures (Wiklander et al. 2018; Johnston et al. 2016).

For indirect labeling of snorkel-tag, samples were incubated with capture beads overnight (14-16 hours) at 450 rpm at room temperature protected from light. The beads were washed with 200 μ l MPB and 135 μ l MPB added to each well and 15 μ l of anti-HA-tag antibody (1:1000 final dilution) was added and incubated for 1 hour at room temperature on an orbital shaker at 450 rpm protected from light. After incubation, the MPB in the wells was drained and wash steps were repeated. For counterstaining of anti-HA-tag antibody labeled on EVs bound capture beads, 135 μ l of MPB and 15 μ l of Dylight-649 conjugated to anti-rabbit detection antibody (1:1000 final dilution) was added and plates were incubated on an orbital shaker at 450 rpm protected from light for 1 hour at room temperature. After incubation, MPB was drained, washed and flow cytometry analysis was performed using MACSQuant Analyzer 10 flow cytometer (Miltenyi Biotec) as mentioned above. MFI for all 39 capture bead subsets were background corrected by subtracting respective MFI values from matched non-EV buffer (PBS) that were treated exactly like EV-containing samples (buffer + capture beads + Dylight 649 detection antibody).

5.2.10. EV uptake assays using flow cytometry

HDF164-hTert:CD63-neonGFP derived EVs were isolated using TFF as previously described. Particle concentration and size were analysed with NTA both in scatter and fluorescence mode. A fixed number of particles (particles based on NTA scatter mode) were mixed with different concentrations of monoclonal antibodies (details in the result section) and incubated at 37°C in dark for 1 hour to allow formation of EV-antibody complex. Then the complex with predetermined number were added to human

hepatocellular carcinoma cells (Huh-7) seeded the day before at a density of 2,000 cells per well in a 96-well plate. Cells were incubated for 2 h at 37°C, 5% CO₂ atmosphere. After incubation, the cells were washed thrice with ice-cold PBS, collected, spun down at 300 × g for 5 minutes and resuspended in 100 µl of PBS. Dead cells were excluded from DAPI staining and doublets were excluded by forward/side scatter area versus height gating. Samples were kept on ice and measured with the. Data was analyzed with MACSQuant Analyzer 10 flow cytometer (Miltenyi Biotec). the FlowJo software (version 10.0.7). Median fluorescence intensity was normalized over the control/untreated cell sample (Δ MFI). GraphPadPrism 8.2.1 (GraphPadPrism Software, La Jolla, CA, USA) was used to analyze data and assemble figures. One unpaired student t-test was performed and a P-value < 0.05 was considered statistically significant.

5.2.11. EV uptake study using confocal imaging

For comparison, HeLa-WT, HeLa derived snorkel-tag carrying EVs were purified with StEVAC method and ultrafiltration as previously described. After particle quantification by NTA ~1 x 10⁹ particles were labeled with CLIP substrate (CLIP-Surface™ 647; Catalog #S9234, NEB) with 1:100,000 dilution and incubated at 37° C for 1 hour. After incubation, excess substrate was removed by using Amicon ultra-0.5 centrifugal filter (Catalog #UFC501096; MerckMilipore) with 100 kDa MWCO and further diafiltrated using 0.22 µm filtered PBS. The concentrated labelled EV solution was added onto Huh-7 cells which were seeded onto coverslips or µ-slides (ibidi GmbH, Martinsried, Germany) a day before. Cells were incubated for 2 hours at 37 °C, 5% CO₂ atmosphere. After incubation, cells were washed thrice with PBS and lysotracker LyG26 (Catalog #8783S; Cell signaling technology) was used according to manufacturer's instruction. In the last but one wash, Hoechst 33342 was included for counterstaining DNA.

5.2.12. Immunofluorescence staining of cells

For primary and secondary antibody concentrations, see above.

HeLa-WT and HeLa-CD81-snorkel-tag overexpressing cells were seeded onto coverslips or μ -slides (ibidi GmbH, Martinsried, Germany) and incubated over night at 37°C. Following day, cells were fixed with 4% paraformaldehyde for 15 min, washed two times with PBS, and permeabilized for 10 min in 0.3% Triton X-100 followed by two PBS-washes. Cells were blocked with 2% BSA for 30-60 min. After blocking, slides were incubated in primary and secondary antibody solutions prepared in 2% BSA solution for 60 and 30 min respectively in a humidified chamber at room temperature, each followed by 3 washes in PBS. Hoechst 33342 was included for counterstaining of DNA right before the last wash step.

For staining non-permeabilized cells, no fixation and permeabilization steps were involved. Cells were blocked in 2% BSA for 60 min and were directly incubated with primary and secondary antibodies as mentioned above.

5.2.13. Transmission Electron Microscopy (TEM)

For primary and secondary antibody concentration, see above.

For TEM analysis we used 4 different protocols based on the sample and application.

All the solutions used for the staining procedure were pre-filtered using 0.22 μ m filter units (Milipore/VWR).

For Figure 33B: Freshly prepared EVs were adhered on Athene Old 300 mesh copper grids (Agar Scientific, Stansted, Essex, UK) and fixed with 1% glutaraldehyde. Grids were washed three times with nuclease free water (NFW) and stained for 5 min with 2%

phosphotungstic acid hydrate (Carl Roth, Karlsruhe, Germany). The grids were left to dry and the specimens were visualized using TEM (FEI Tecnai T20, FEI Eindhoven, Netherlands) operated at 160 kV.

For all other TEM images, 5 μ l of sample were added onto glow-discharged formvar-carbon type B coated electron microscopy grids for 3 min. Samples were removed by using wet whatmann filter paper. Grids were either prepared for immunogold labeling (see below) or carefully washed twice with filtered PBS. After washes, 5 μ L of filtered 2% uranyl acetate were added for 10-30 sec, uranyl acetate was removed using wet whatman filter paper, grids were air dried and using visualized using a transmission electron microscope (Tencai 10).

For immunogold labeling, grids were blocked after the initial binding step of the sample using filtered 2% BSA (in PBS) for 10 min. Primary and secondary antibodies were diluted in 0.2% BSA solution. After blocking, grids were placed on 15 μ L primary antibody solution (anti-CD81, 1:50; anti-HA-tag, 1:50) for 60 min. Post incubation, grids were washed with 0.2% BSA 6 times and incubated with secondary antibody (goat anti-mouse secondary antibody conjugated with 10 nm gold particles & goat anti-rabbit secondary antibody conjugated with 4 nm gold particle) with dilution of 1:50 for 60 min. After incubation, grids were washed 6 times with PBS followed by 6 washing steps with ddH₂O. Finally, grids were stained with 0.2% uranyl acetate for 10 to 30 sec. Excess uranyl acetate was removed using a wet whatman filter paper, grids air dried and visualized using a transmission electron micro- scope (Tencai 10).

TEM of resin embedded skin sections (Figure 32A): All specimens were fixed in a buffered 3% glutaraldehyde solution, postfixed in osmium tetroxide (3%) for 2 h, dehydrated through a graded acetone series, and embedded in Araldite (Fluka, Buchs, Switzerland). Ultrathin sections (60-90 nm thickness) were prepared using a diamond knife, collected on copper grids (G 300 Cu), and examined with a Jeol JEM-1400 Plus electron microscope.

Immunolabeling of resin-free ultra-thin cryo-cut sections (Figure 32B): Human skin biopsies were fixed in 2% paraformaldehyde and 0.2 % glutaraldehyde (both from EMS, Hatfield, USA) in 0.1 M PHEM buffer pH 6.9 for 2 h at RT, then over night at 4 °C. Samples were cut into 1 mm³ blocks which were immersed in 2.3 M Sucrose for one week at 4 °C. These blocks were mounted onto Leica specimen carrier (Leica Microsystems, Vienna, Austria) and frozen in liquid nitrogen. With a Leica UCT/FCS cryo-ultramicrotome (Leica Microsystems, Vienna, Austria) the frozen blocks were cut into ultra-thin sections at a nominal thickness of 60 nm at -120°C. A mixture of 2% methylcellulose and 2.3 M sucrose in a ratio of 1:1 was used as a pick-up solution. Sections were picked up onto 200 mesh Ni grids (Gilder Grids, Lincolnshire, UK) with a carbon coated Formvar film. [Fixation, embedding and cryo-sectioning as described previously] (Tokuyasu 1973).

Prior to immunolabeling, grids were placed on plates with solidified 2% gelatine and warmed up to 37 °C for 20 min to remove the pick-up solution. After quenching of free aldehyde-groups with glycine (0.1 % for 15 min), a blocking step with 1% BSA (fraction V) in 0.1M Sörensen phosphate buffer pH 7.4 was performed for 30 min. The grids were incubated in primary antibody, Abcam ab8219 mouse anti-CD63 (Abcam, Cambridge, UK), diluted 1:1000 in 0.1 M Sörensen phosphate buffer containing 0.1 % BSA (Fraction V) over night at 4 °C, followed by a 2 h incubation in the secondary antibody, a goat-anti-mouse antibody coupled with 6 nm gold (GAR 6 nm, Aurion, Wageningen, The Netherlands), diluted 1:20 in 0.1 M Sörensen phosphate buffer containing 0.1% BSA (Fraction V), performed at RT. The sections were stained with 4 % uranyl acetate (Merck, Darmstadt, Germany) and 2 % methylcellulose in a ratio of 1:9 (on ice). All labeling steps were done in a wet chamber. The sections were inspected in a FEI Morgagni 268D TEM (FEI, Eindhoven, The Netherlands) operated at 80 kV. Electron micrographs were acquired using an 11-megapixel Morada CCD camera from Olympus-SIS (Münster, Germany).

5.2.14. Cre-loxP method for studying EV uptake

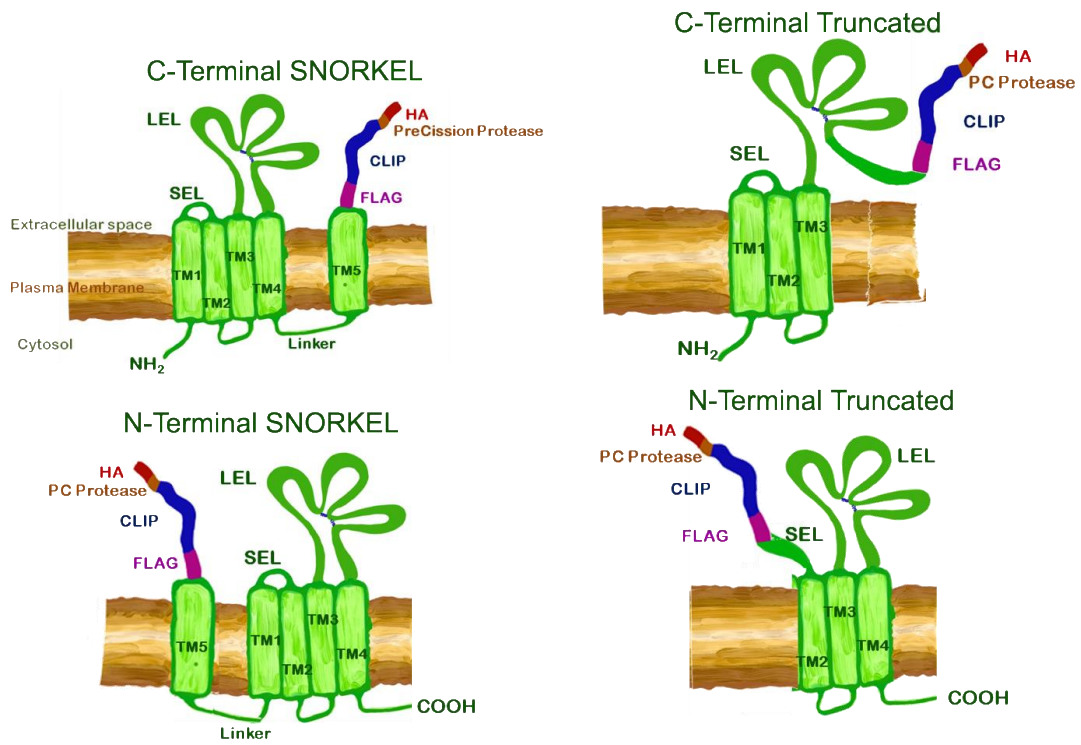
HEK293 cells expressing loxP color-switch reporter system were seeded onto coverslips or μ -slides (ibidi GmbH, Martinsried, Germany) and incubated over night at 37°C. EVs isolated from conditioned media of HeLa-CD81-snorkel-tag cells overexpressing Cre recombinase were isolated by ultracentrifugation. Isolated EVs were added to HEK293 reporter cells and incubated for 72 hours. This sequential addition of EVs was done for ~10 days. After final round of EV treatment, cells were washed 3 times with PBS and visualized under confocal microscopy.

For co-culture experiments: HeLa-CD81-snorkel-tag cells overexpressing Cre recombinase were co-cultured with HEK293 reporter cells in a ratio of 1:100. ~2 weeks after cultivation cells were visualized under confocal microscopy.

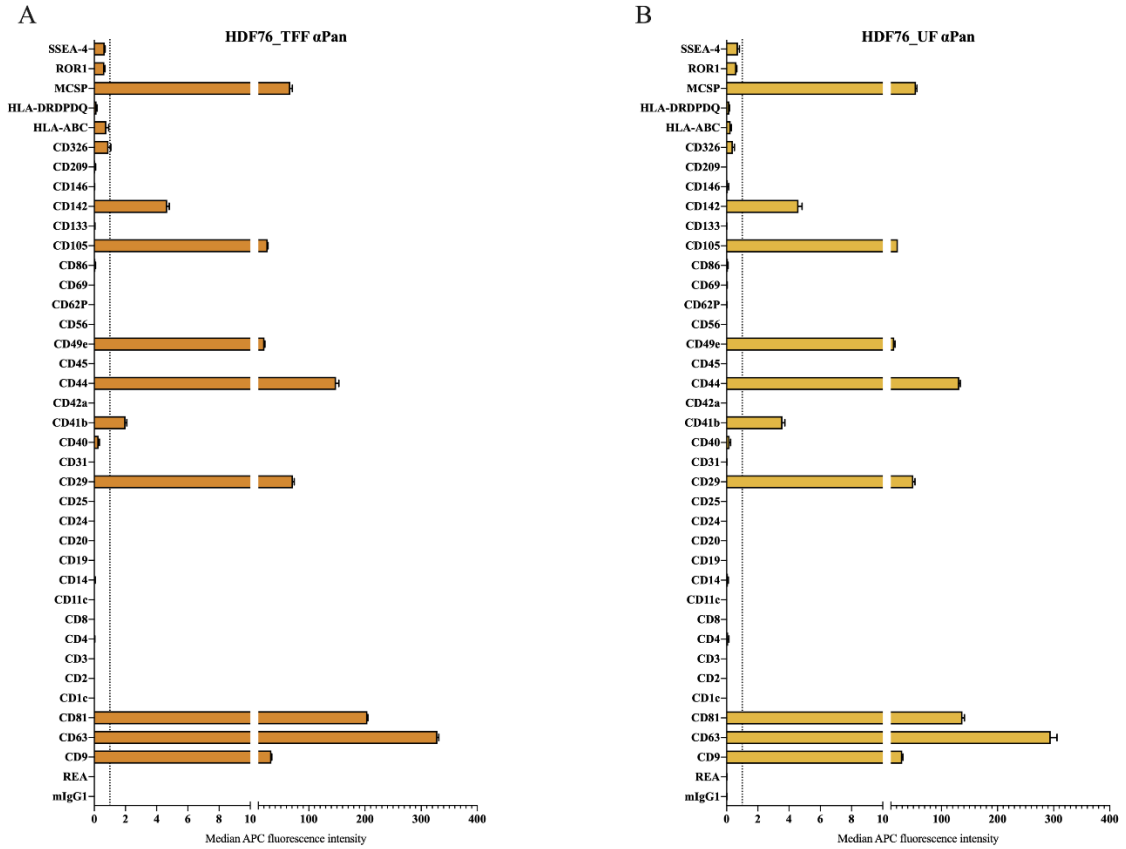
5.2.15. Statistical analysis

Statistics were either calculated with Excel or Graph Pad Prism, and respective tests are indicated below figures in result sections. \pm Standard deviations were derived from at least 3 independent experiments. Two tailed tests were performed using an error probability of 0.05. If not indicated, the experiments were performed less than three times.

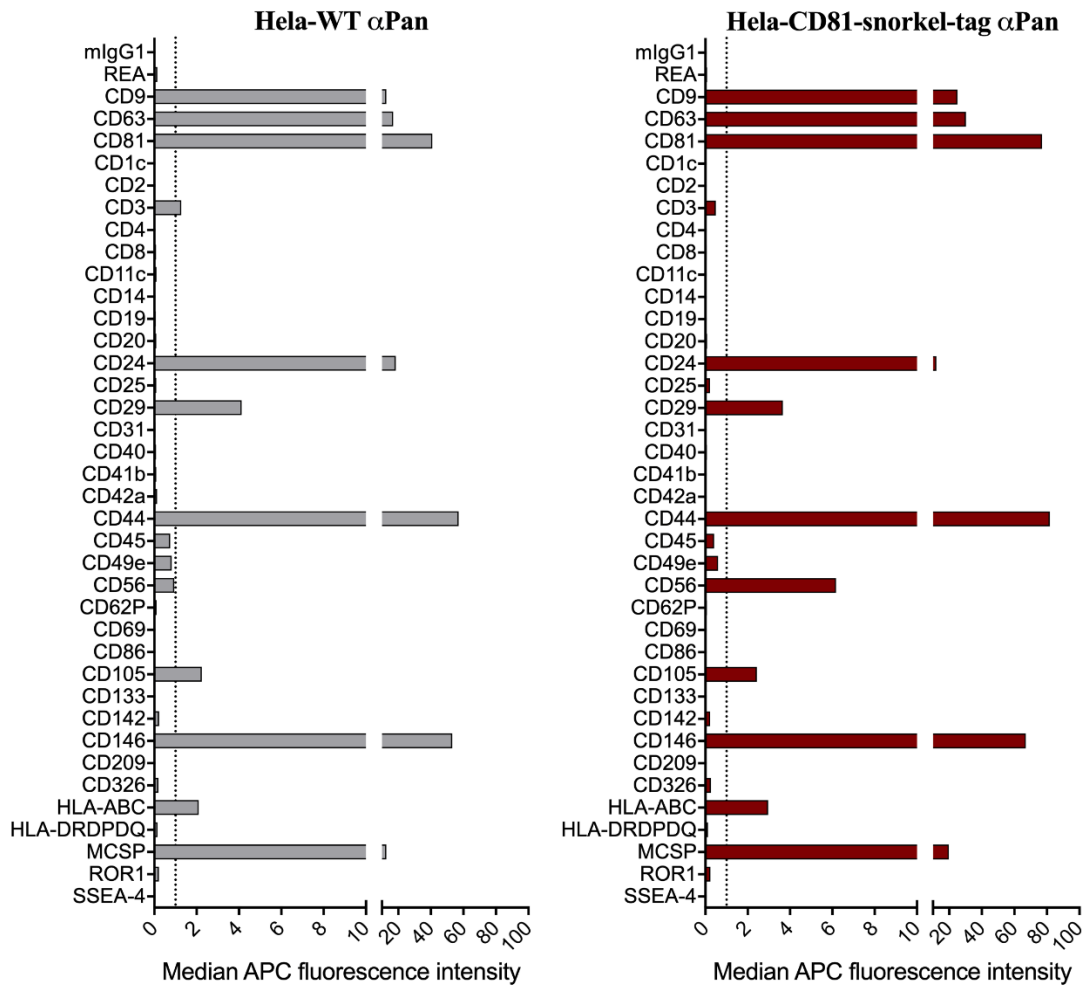
6. SUPPLEMENTARY MATERIAL



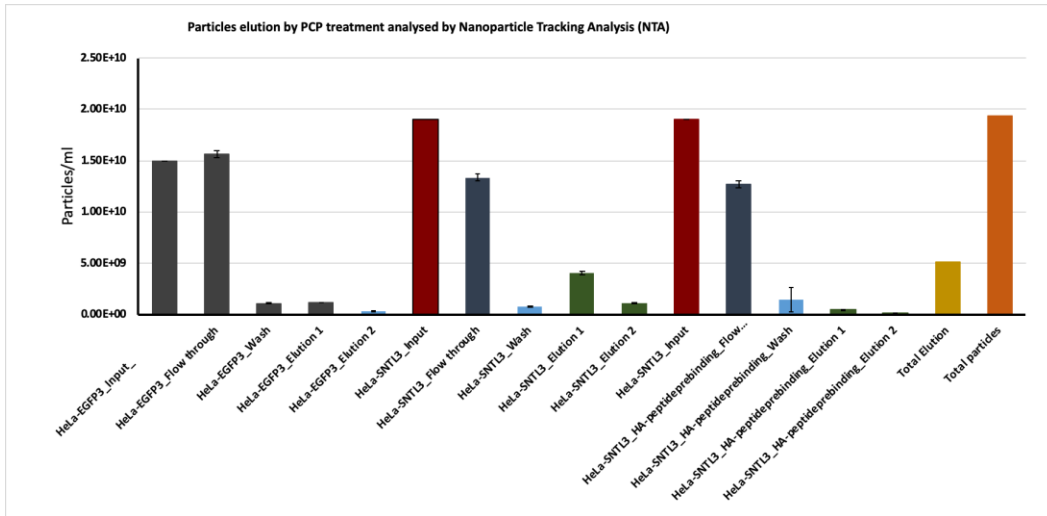
Supplementary Figure 1: Pictorial representation of CD81-snorkel-tag variants



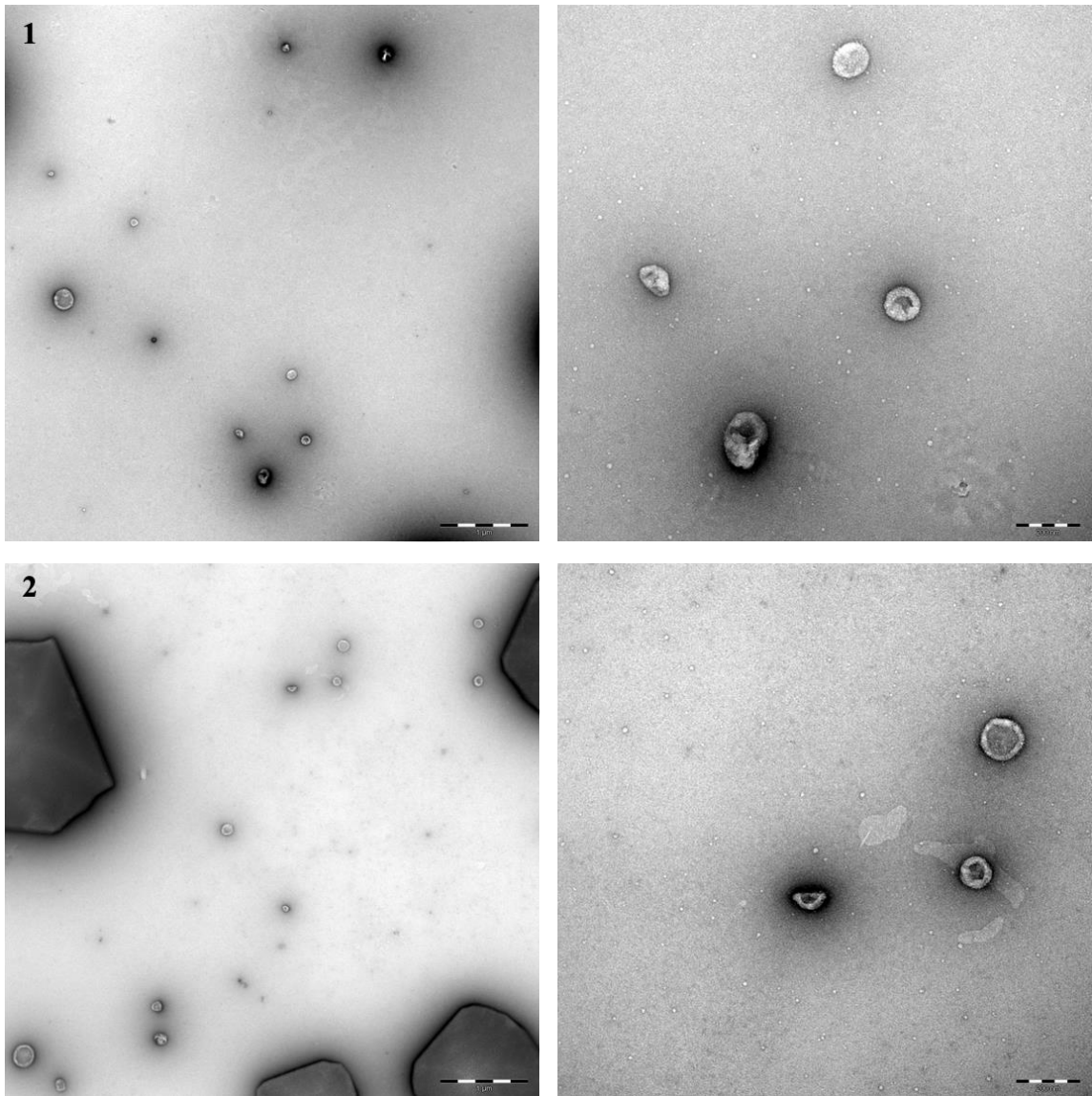
Supplementary Figure 2: Multiplex bead-based flow cytometry assay for detection of EV surface protein signature for EVs derived from HDF76 cell line. (A) HDF76 EVs isolated by using TFF technique. (B) HDF76 EVs isolated by using ultrafiltration technique.



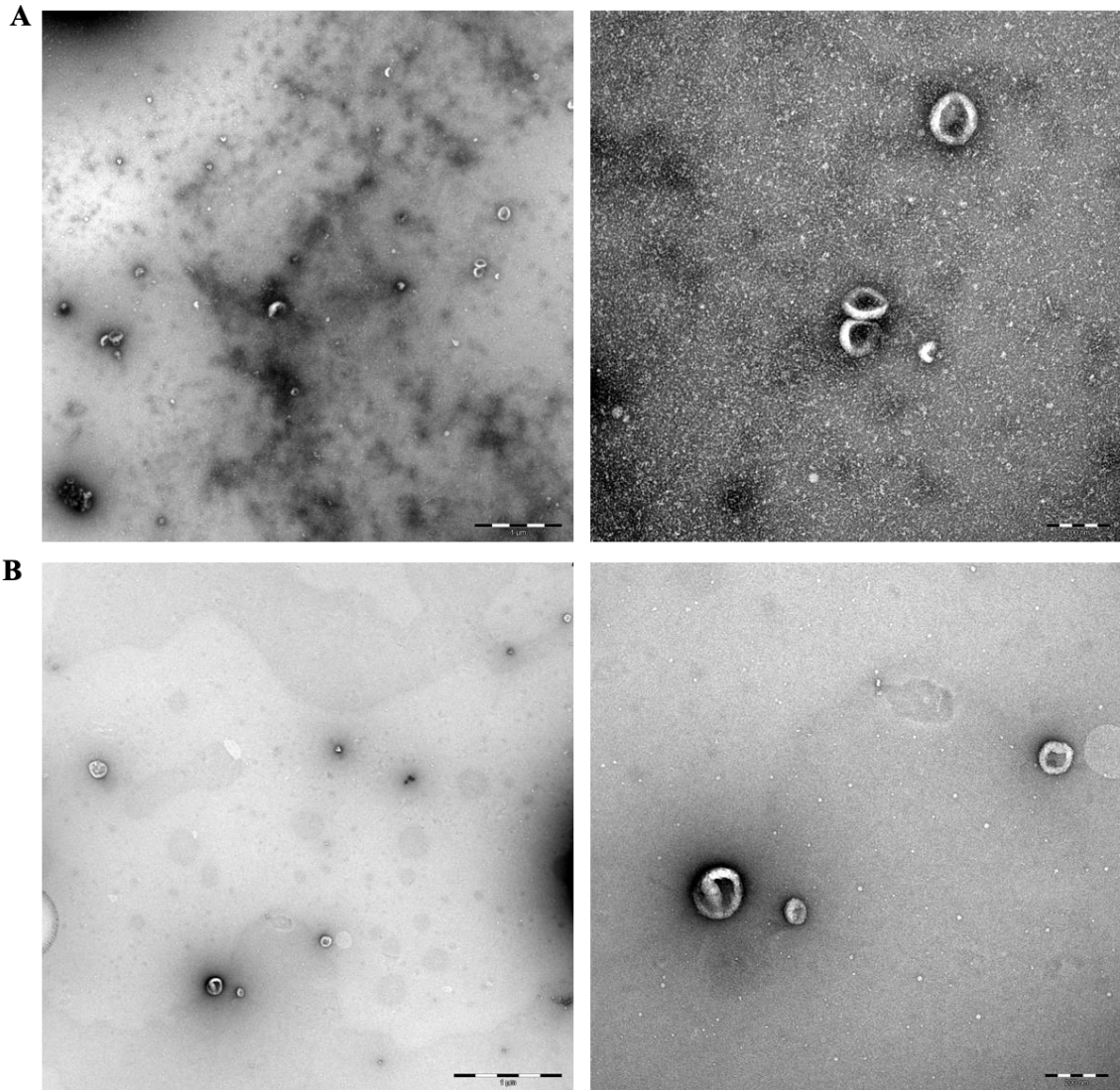
Supplementary Figure 3: Multiplex bead-based flow cytometry assay for detection of surface protein signature for EVs derived from HeLa-WT and HeLa-CD81-snorkel-tag cell lines.



Supplementary Figure 4: Pre blocking of anti-HA matrix before StEVAC method.

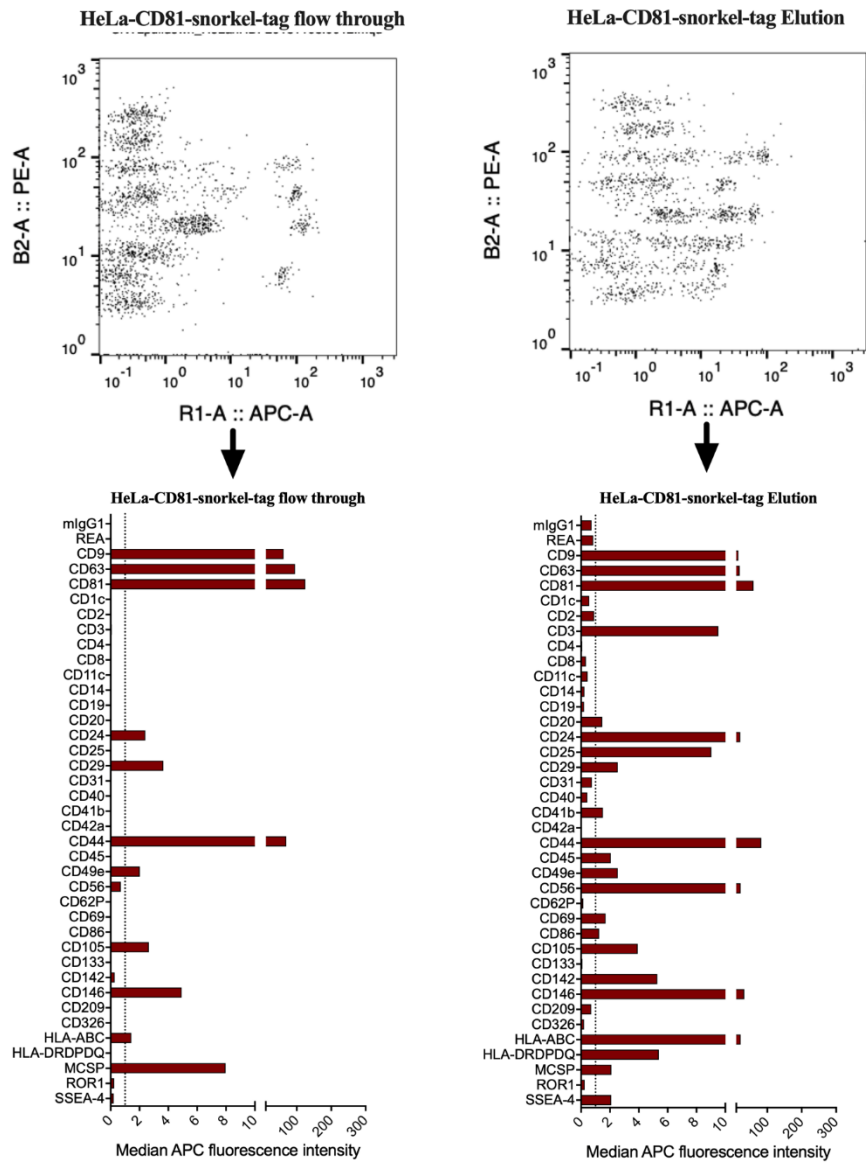


Supplementary Figure 5: Transmission electron microscopy images for EVs purified by StEVAC method. TEM images showing wide-field (Left panel, 1 μm scale bar) and close-up/zoom-in images (Right panel, scale bar 200 nm).

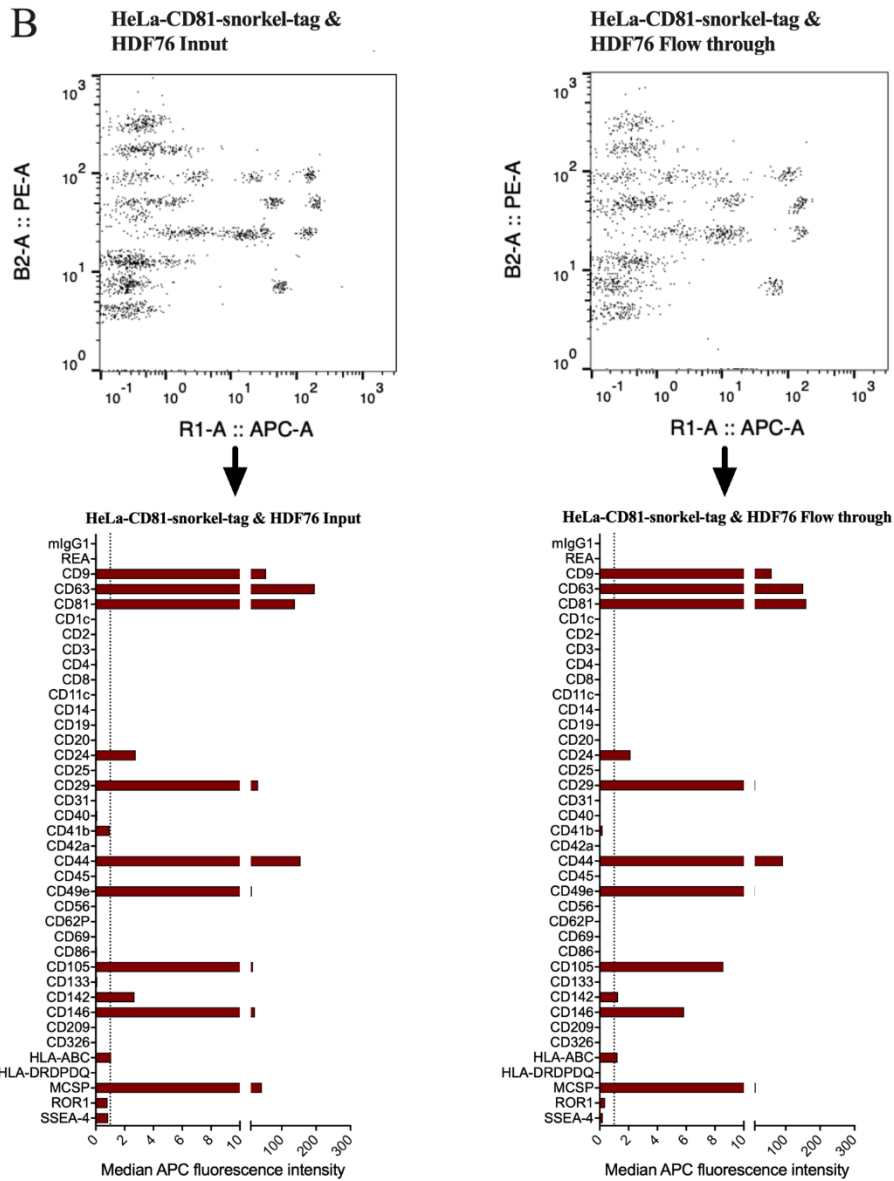


Supplementary Figure 6: Transmission electron microscopy comparison of EVs isolated by ultrafiltration and followed by StEVAC method. (A) EVs isolated from HeLa-CD81-snorkel-tag cell line conditioned media by ultrafiltration; an overview image in right panel (scale bar: 1 μm) and zoom-in image in left panel (scale bar: 200 nm). (B) EVs isolated from HeLa-CD81-snorkel-tag cell line conditioned media by ultrafiltration and further purified by StEVAC method; an overview image in right panel (scale bar: 1 μm) and zoom-in image in left panel (scale bar: 200 nm).

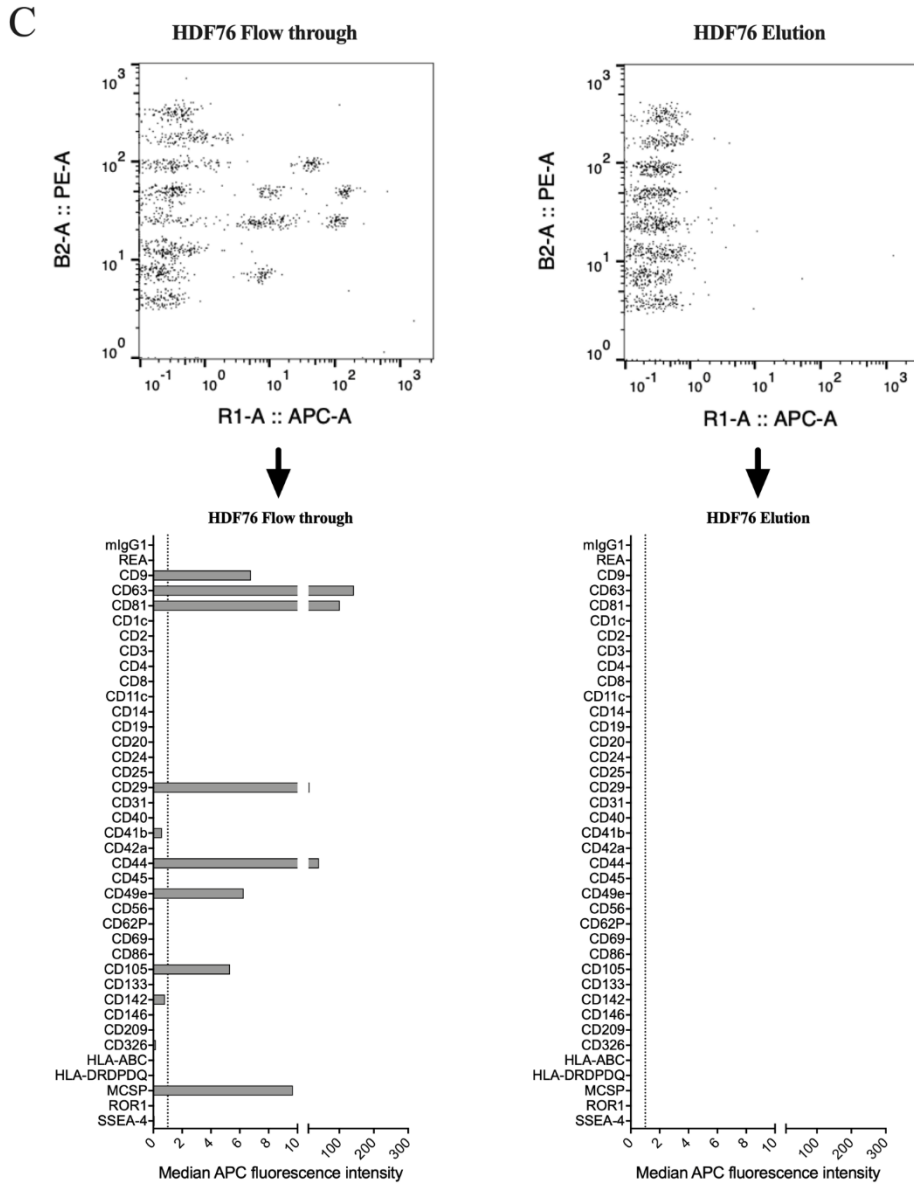
A



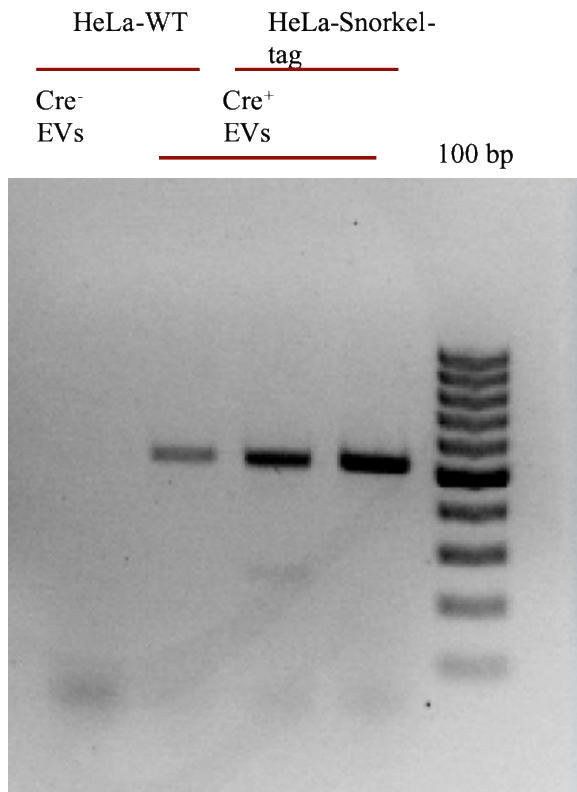
Supplementary Figure 7 | continued



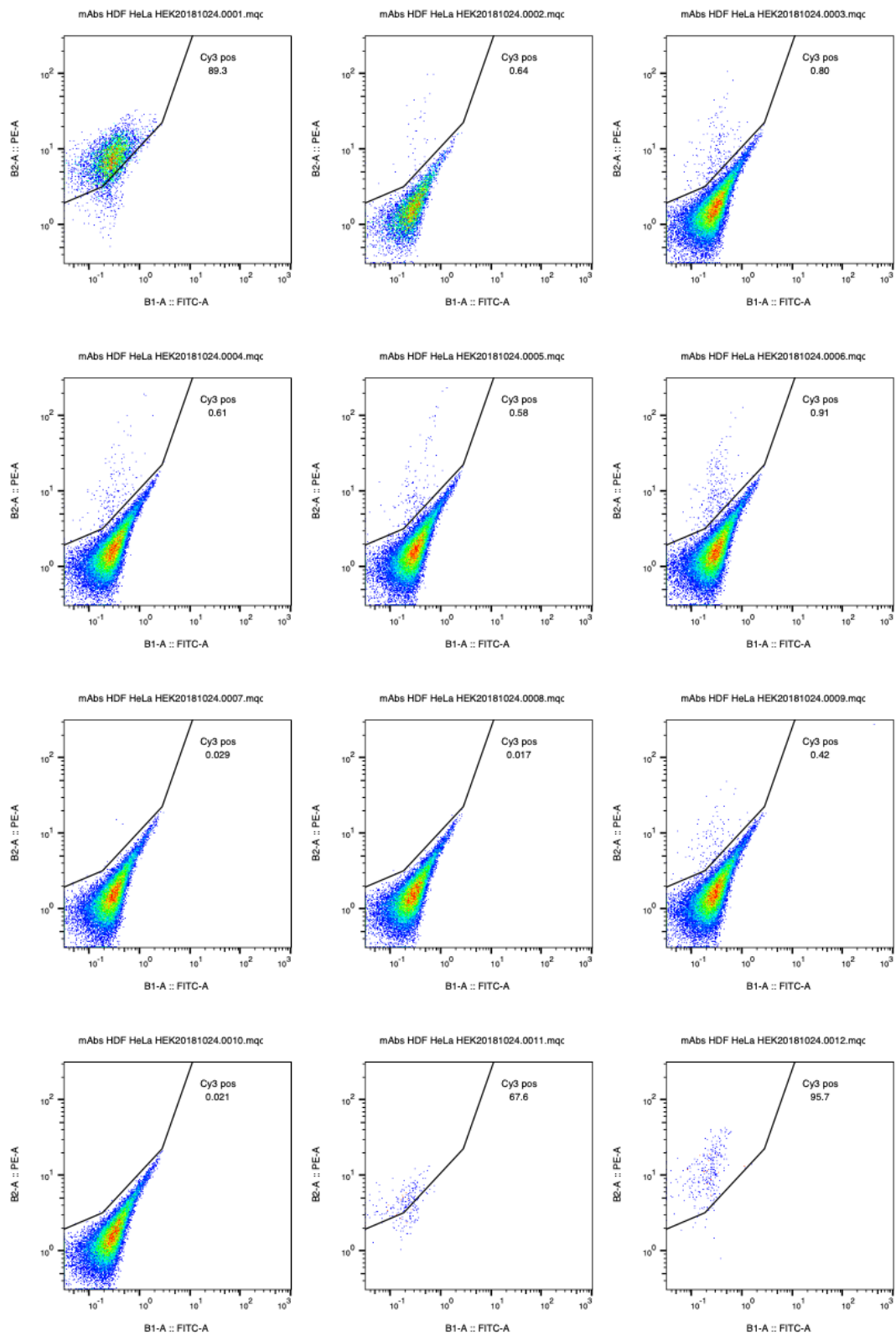
Supplementary Figure 7 | continued

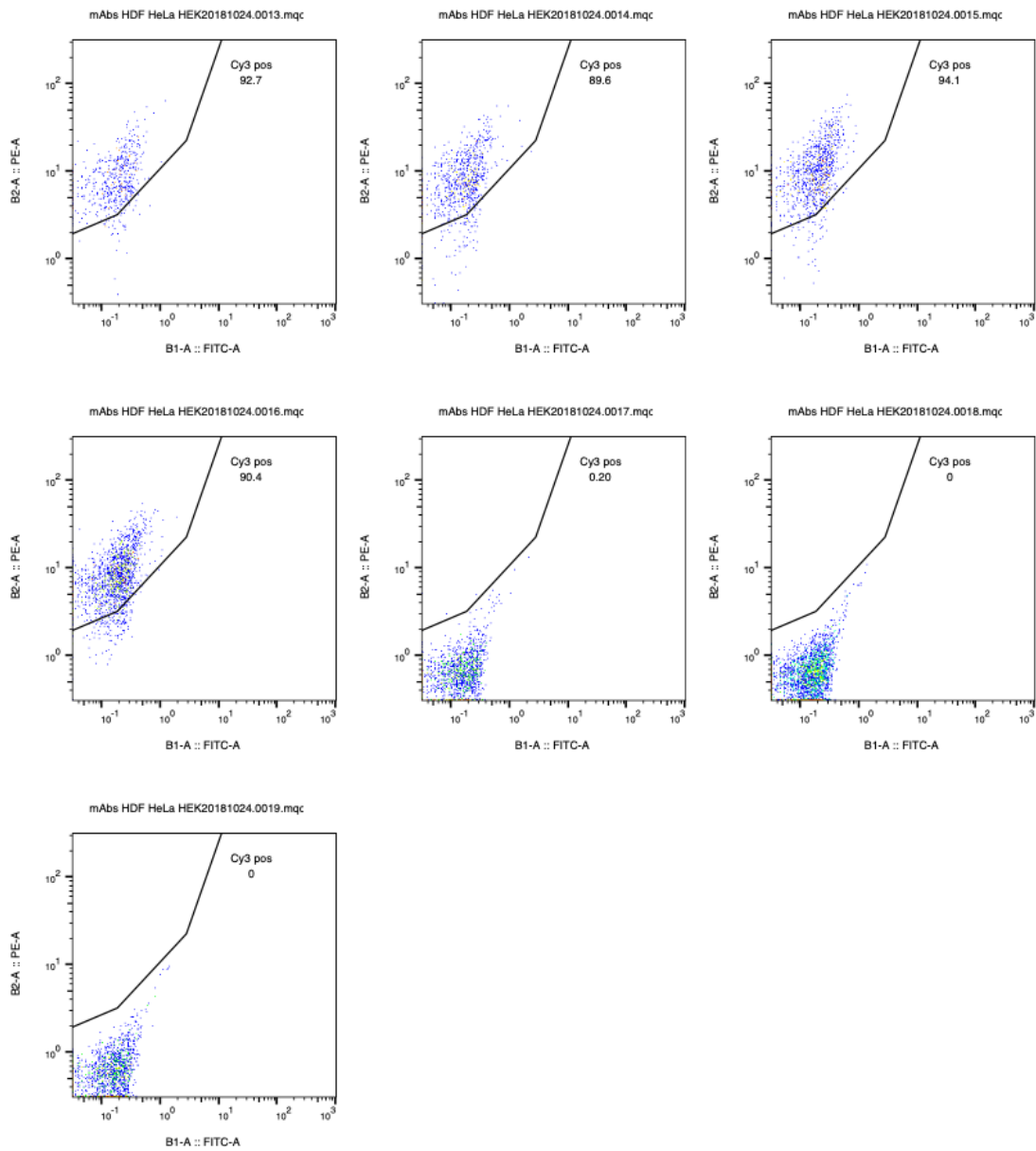


Supplementary figure 7: Comparison of EV surface protein markers eluted from mixed population for specificity of the EVs pulled down alongside with input and flow through samples. (A) HeLa-CD81-snorkel-tag cell derived EVs from flow through and elution after StEVAC method of purification. (B) Assay results for input and flow through from the mixture of HeLa-CD81-snorkel-tag EVs and HDF76 EVs. (C) Assay results for the flow through and elutes from HDF76 EVs.



Supplementary Figure 8: EVs were isolated from Cre⁺ and Cre⁻ cells. Shown is the RT-PCR of respective sample.

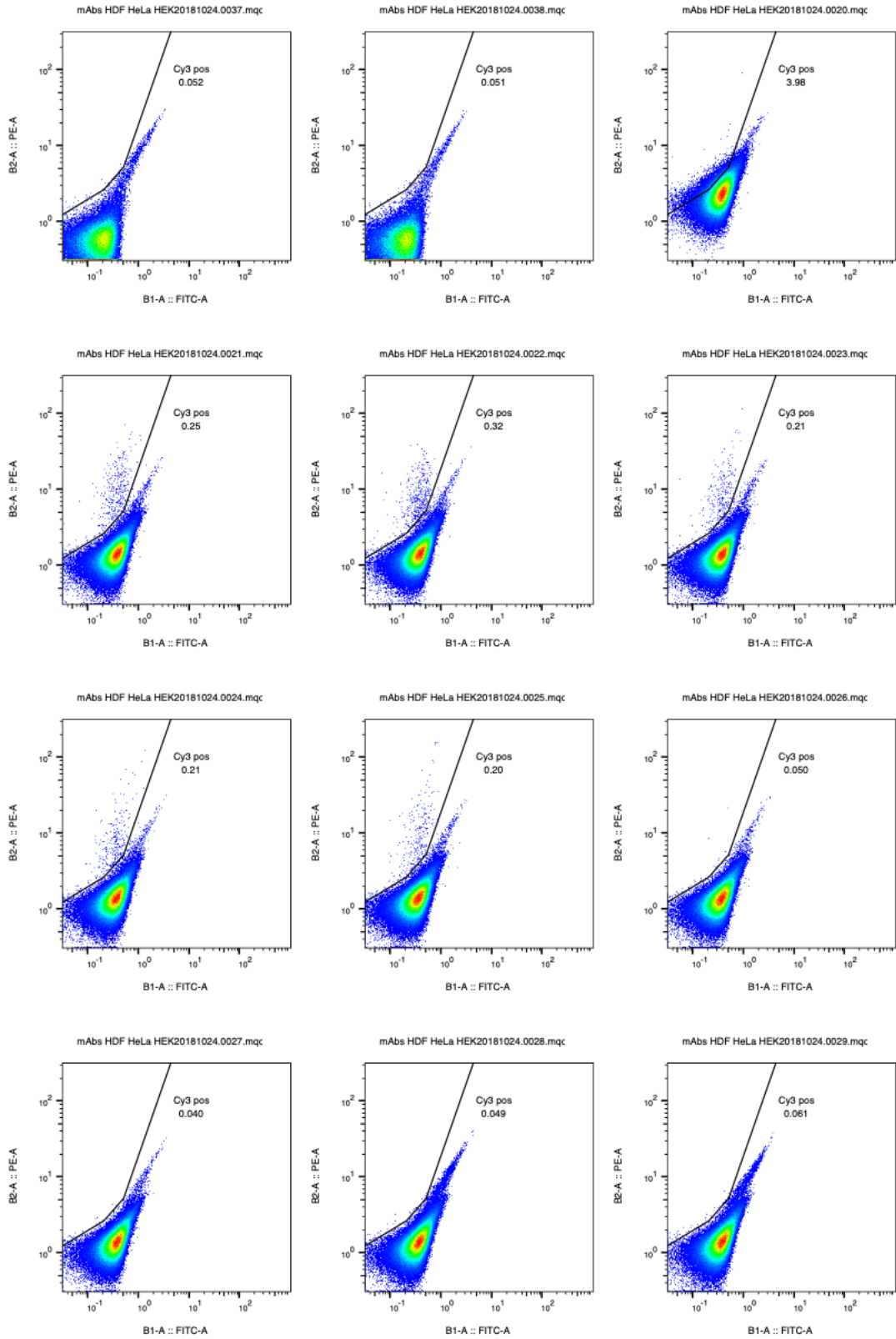


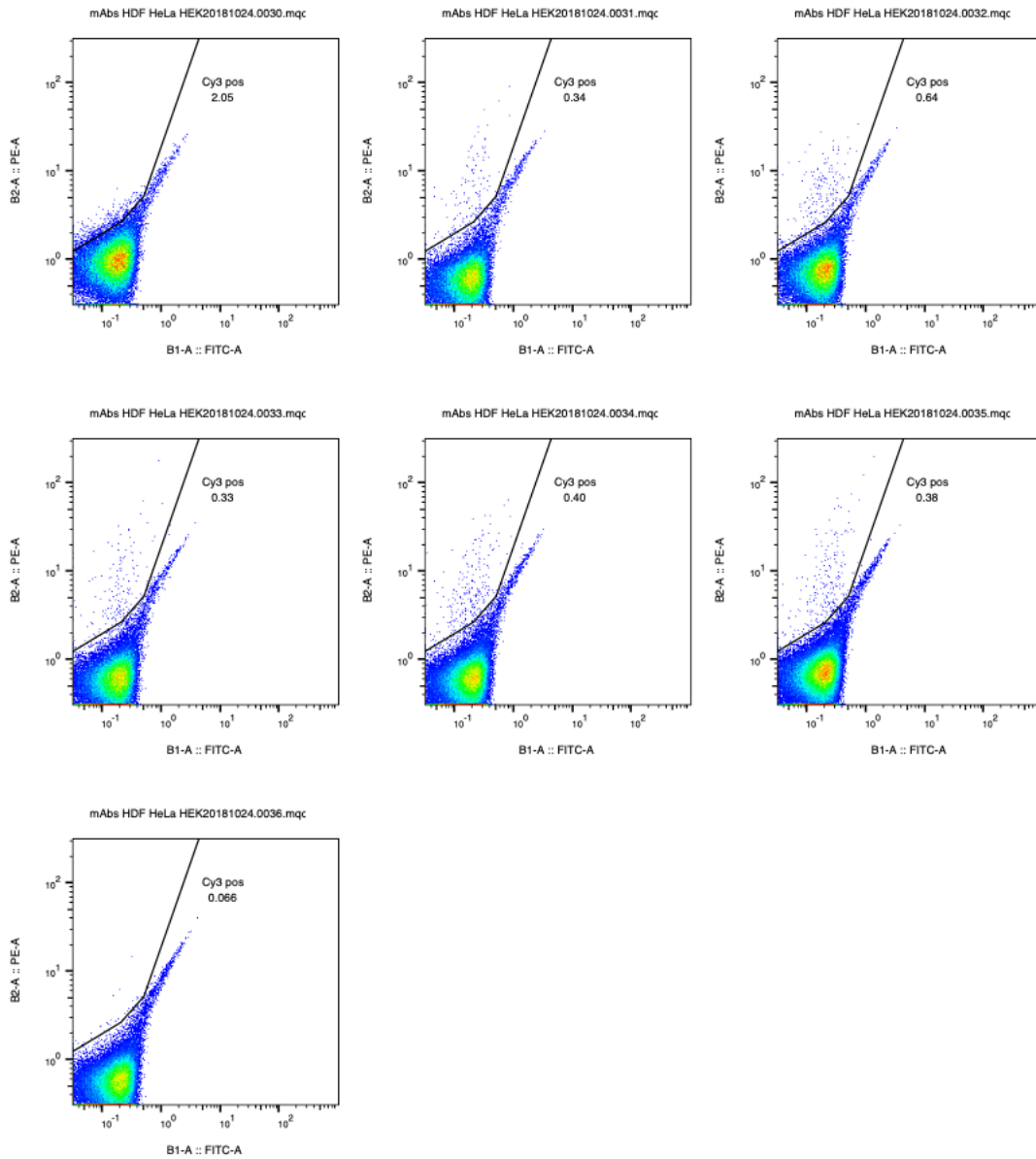


Supplementary Figure 9A: scatter plots correlating antigen detection on HDF164-hTert cells (permeabilized and non-permeabilized) with FITC autofluorescence.

mAbs HDF HeLa HEK20181024.0001.mqd	HDF164-hTert_Non-permeabilized	CD81
mAbs HDF HeLa HEK20181024.0002.mqd		52F8-G6
mAbs HDF HeLa HEK20181024.0003.mqd		53E6-D8
mAbs HDF HeLa HEK20181024.0004.mqd		53F2-A1
mAbs HDF HeLa HEK20181024.0005.mqd		53F2-D6
mAbs HDF HeLa HEK20181024.0006.mqd		53F2-E1
mAbs HDF HeLa HEK20181024.0007.mqd		anti-mouse Cy3 antibody
mAbs HDF HeLa HEK20181024.0008.mqd		DAPI
mAbs HDF HeLa HEK20181024.0009.mqd		cells only
mAbs HDF HeLa HEK20181024.0010.mqd		cells only
mAbs HDF HeLa HEK20181024.0011.mqd	HDF164-hTert_permeabilized	CD81
mAbs HDF HeLa HEK20181024.0012.mqd		52F8-G6
mAbs HDF HeLa HEK20181024.0013.mqd		53E6-D8
mAbs HDF HeLa HEK20181024.0014.mqd		53F2-A1
mAbs HDF HeLa HEK20181024.0015.mqd		53F2-D6
mAbs HDF HeLa HEK20181024.0016.mqd		53F2-E1
mAbs HDF HeLa HEK20181024.0017.mqd		anti-mouse Cy3 antibody
mAbs HDF HeLa HEK20181024.0018.mqd		cells only
mAbs HDF HeLa HEK20181024.0019.mqd		cells only

Supplementary Table 1A: Sample ID's and antibodies used for labeling for HDF164-hTert cells (permeabilized and non-permeabilized cells)

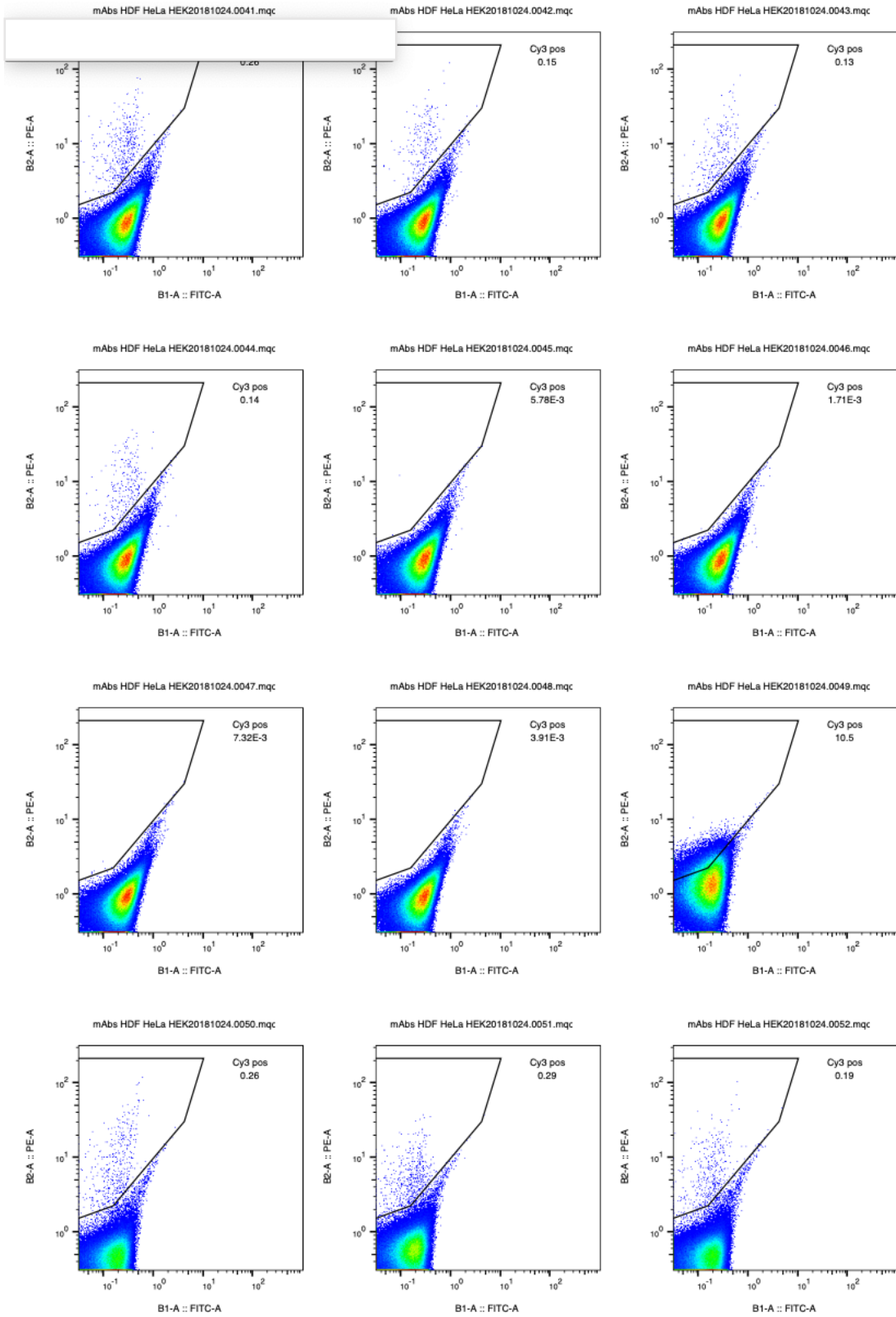


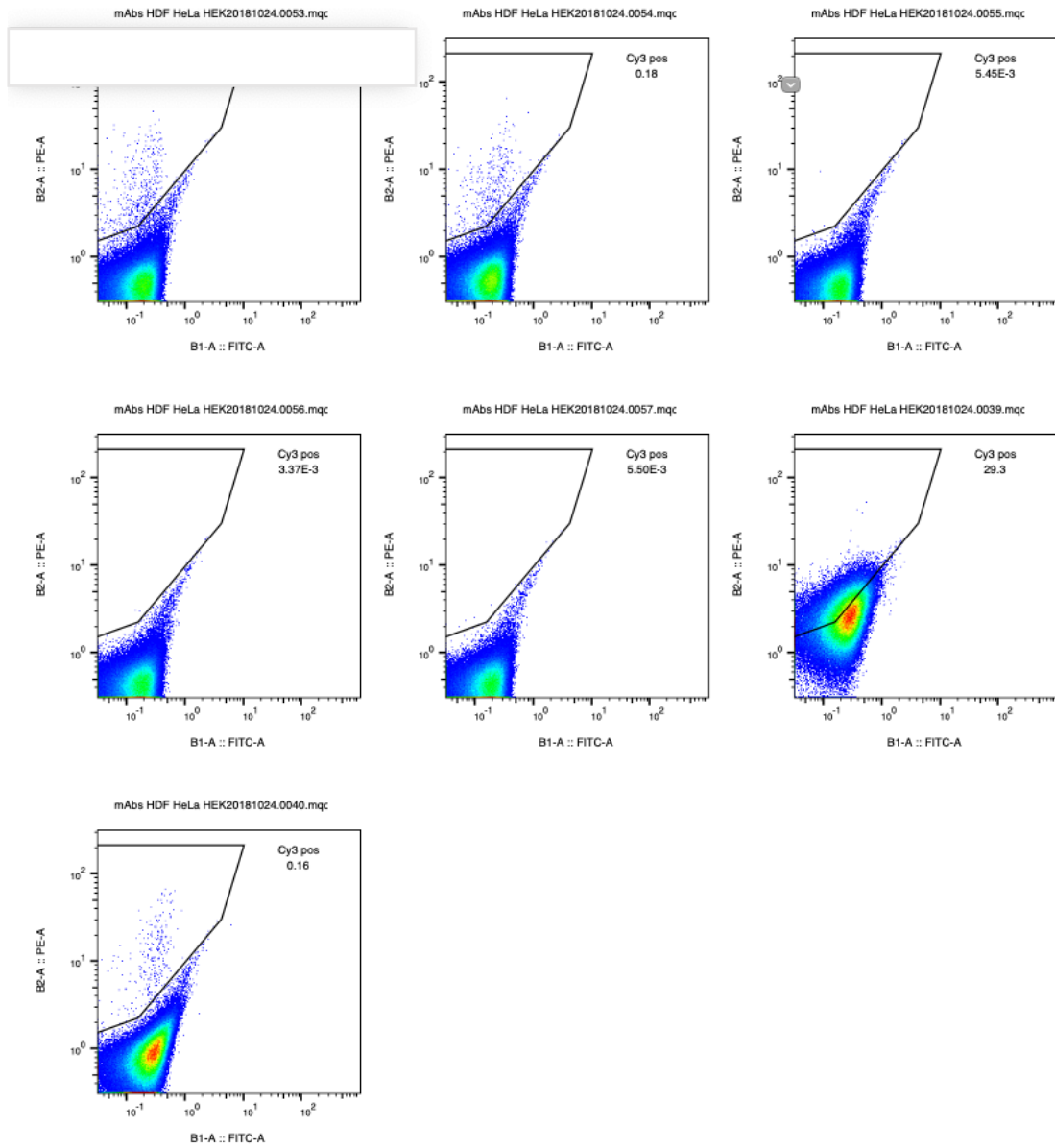


Supplementary Figure 9B: scatter plots correlating antigen detection on HeLa cells (permeabilized and non-permeabilized) with FITC autofluorescence.

mAbs HDF HeLa HEK20181024.0020.mqd	HeLa_Non-permeabilized	CD81
mAbs HDF HeLa HEK20181024.0021.mqd		52F8-G6
mAbs HDF HeLa HEK20181024.0022.mqd		53E6-D8
mAbs HDF HeLa HEK20181024.0023.mqd		53F2-A1
mAbs HDF HeLa HEK20181024.0024.mqd		53F2-D6
mAbs HDF HeLa HEK20181024.0025.mqd		53F2-E1
mAbs HDF HeLa HEK20181024.0026.mqd		anti-mouse Cy3 antibody
mAbs HDF HeLa HEK20181024.0027.mqd		DAPI
mAbs HDF HeLa HEK20181024.0028.mqd		cells only
mAbs HDF HeLa HEK20181024.0029.mqd		cells only
mAbs HDF HeLa HEK20181024.0030.mqd	HeLa_permeabilized	CD81
mAbs HDF HeLa HEK20181024.0031.mqd		52F8-G6
mAbs HDF HeLa HEK20181024.0032.mqd		53E6-D8
mAbs HDF HeLa HEK20181024.0033.mqd		53F2-A1
mAbs HDF HeLa HEK20181024.0034.mqd		53F2-D6
mAbs HDF HeLa HEK20181024.0035.mqd		53F2-E1
mAbs HDF HeLa HEK20181024.0036.mqd		anti-mouse Cy3 antibody
mAbs HDF HeLa HEK20181024.0037.mqd		cells only
mAbs HDF HeLa HEK20181024.0038.mqd	cells only	

Supplementary Table 1B: Sample ID's and antibodies used for labeling for HeLa cells (permeabilized and non-permeabilized cells)

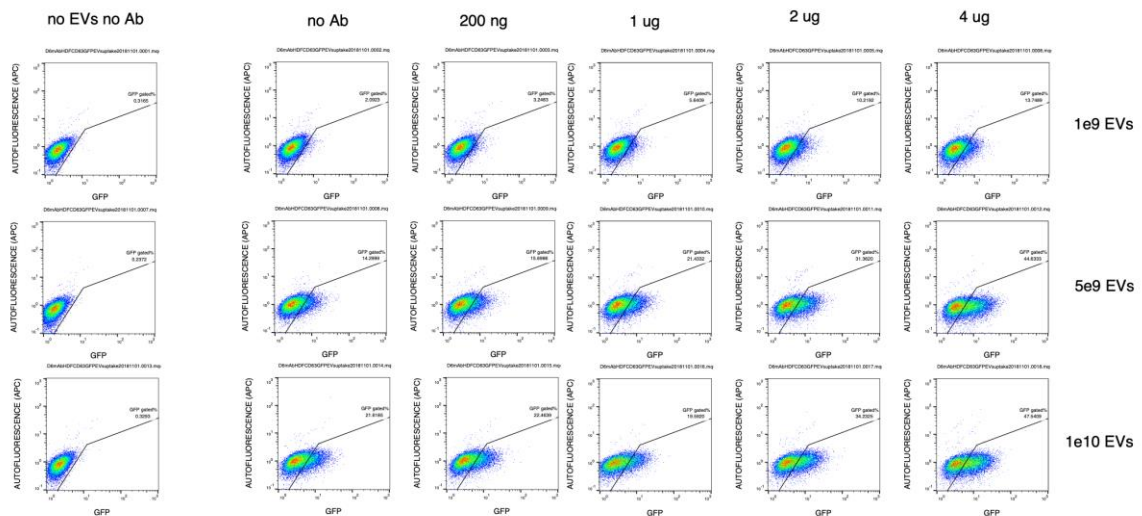




Supplementary Figure 9C: scatter plots correlating antigen detection on HEK293 cells (permeabilized and non-permeabilized) with FITC autofluorescence.

mAbs HDF HeLa HEK20181024.0039.mqd	HEK293_Non-permeabilized	CD81
mAbs HDF HeLa HEK20181024.0040.mqd		52F8-G6
mAbs HDF HeLa HEK20181024.0041.mqd		53E6-D8
mAbs HDF HeLa HEK20181024.0042.mqd		53F2-A1
mAbs HDF HeLa HEK20181024.0043.mqd		53F2-D6
mAbs HDF HeLa HEK20181024.0044.mqd		53F2-E1
mAbs HDF HeLa HEK20181024.0045.mqd		anti-mouse Cy3 antibody
mAbs HDF HeLa HEK20181024.0046.mqd		DAPI
mAbs HDF HeLa HEK20181024.0047.mqd		cells only
mAbs HDF HeLa HEK20181024.0048.mqd		cells only
mAbs HDF HeLa HEK20181024.0049.mqd	HEK293_permeabilized	CD81
mAbs HDF HeLa HEK20181024.0050.mqd		52F8-G6
mAbs HDF HeLa HEK20181024.0051.mqd		53E6-D8
mAbs HDF HeLa HEK20181024.0052.mqd		53F2-A1
mAbs HDF HeLa HEK20181024.0053.mqd		53F2-D6
mAbs HDF HeLa HEK20181024.0054.mqd		53F2-E1
mAbs HDF HeLa HEK20181024.0055.mqd		anti-mouse Cy3 antibody
mAbs HDF HeLa HEK20181024.0056.mqd		cells only
mAbs HDF HeLa HEK20181024.0057.mqd	cells only	

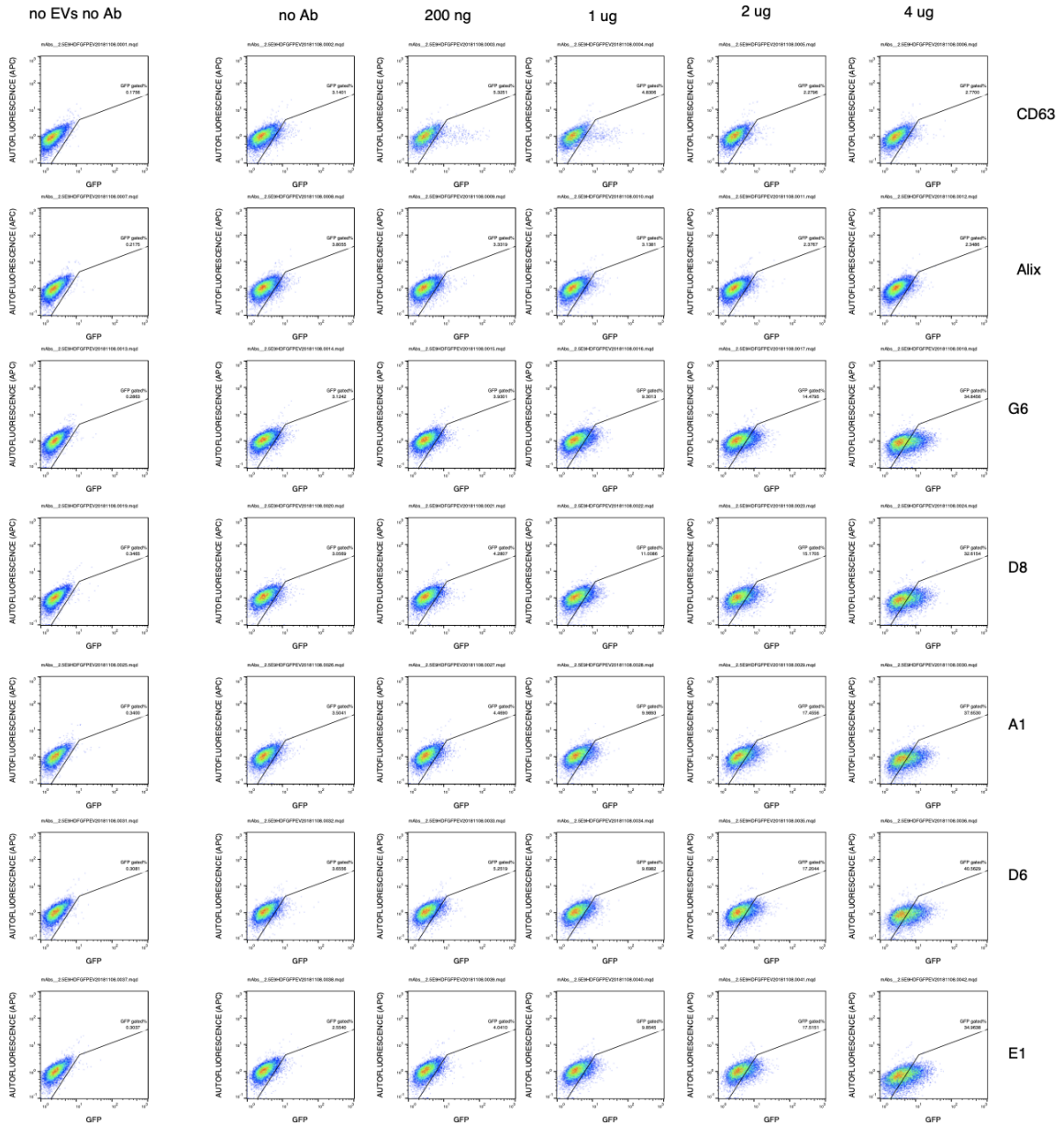
Supplementary Table 1C: Sample ID's and antibodies used for labeling for HEK293 cells (permeabilized and non-permeabilized cells)



Supplementary Figure 10: scatter plots correlating EV uptake (CD63-GFP Internalized EVs) with APC autofluorescence. Titration of CD63-GFP EVs and 53F2-D6 mAb concentrations (mentioned in ST: 2)

D6mAbHDFCD63GFPEVsuptake20181101.0001.mqd	1E9 EVs	Cells only
D6mAbHDFCD63GFPEVsuptake20181101.0002.mqd		CD63-GFP EVs
D6mAbHDFCD63GFPEVsuptake20181101.0003.mqd		CD63-GFP EVs+ 200 ng of 53F2-D6
D6mAbHDFCD63GFPEVsuptake20181101.0004.mqd		CD63-GFP EVs+1 µg of 53F2-D6
D6mAbHDFCD63GFPEVsuptake20181101.0005.mqd		CD63-GFP EVs+2 µg of 53F2-D6
D6mAbHDFCD63GFPEVsuptake20181101.0006.mqd		CD63-GFP EVs+4 µg of 53F2-D6
D6mAbHDFCD63GFPEVsuptake20181101.0007.mqd	5E9 EVs	Cells only
D6mAbHDFCD63GFPEVsuptake20181101.0008.mqd		CD63-GFP EVs
D6mAbHDFCD63GFPEVsuptake20181101.0009.mqd		CD63-GFP EVs+ 200 ng of 53F2-D6
D6mAbHDFCD63GFPEVsuptake20181101.0010.mqd		CD63-GFP EVs+1 µg of 53F2-D6
D6mAbHDFCD63GFPEVsuptake20181101.0011.mqd		CD63-GFP EVs+2 µg of 53F2-D6
D6mAbHDFCD63GFPEVsuptake20181101.0012.mqd		CD63-GFP EVs+4 µg of 53F2-D6
D6mAbHDFCD63GFPEVsuptake20181101.0013.mqd	1E10 EVs	Cells only
D6mAbHDFCD63GFPEVsuptake20181101.0014.mqd		CD63-GFP EVs
D6mAbHDFCD63GFPEVsuptake20181101.0015.mqd		CD63-GFP EVs+ 200 ng of 53F2-D6
D6mAbHDFCD63GFPEVsuptake20181101.0016.mqd		CD63-GFP EVs+1 µg of 53F2-D6
D6mAbHDFCD63GFPEVsuptake20181101.0017.mqd		CD63-GFP EVs+2 µg of 53F2-D6
D6mAbHDFCD63GFPEVsuptake20181101.0018.mqd		CD63-GFP EVs+4 µg of 53F2-D6

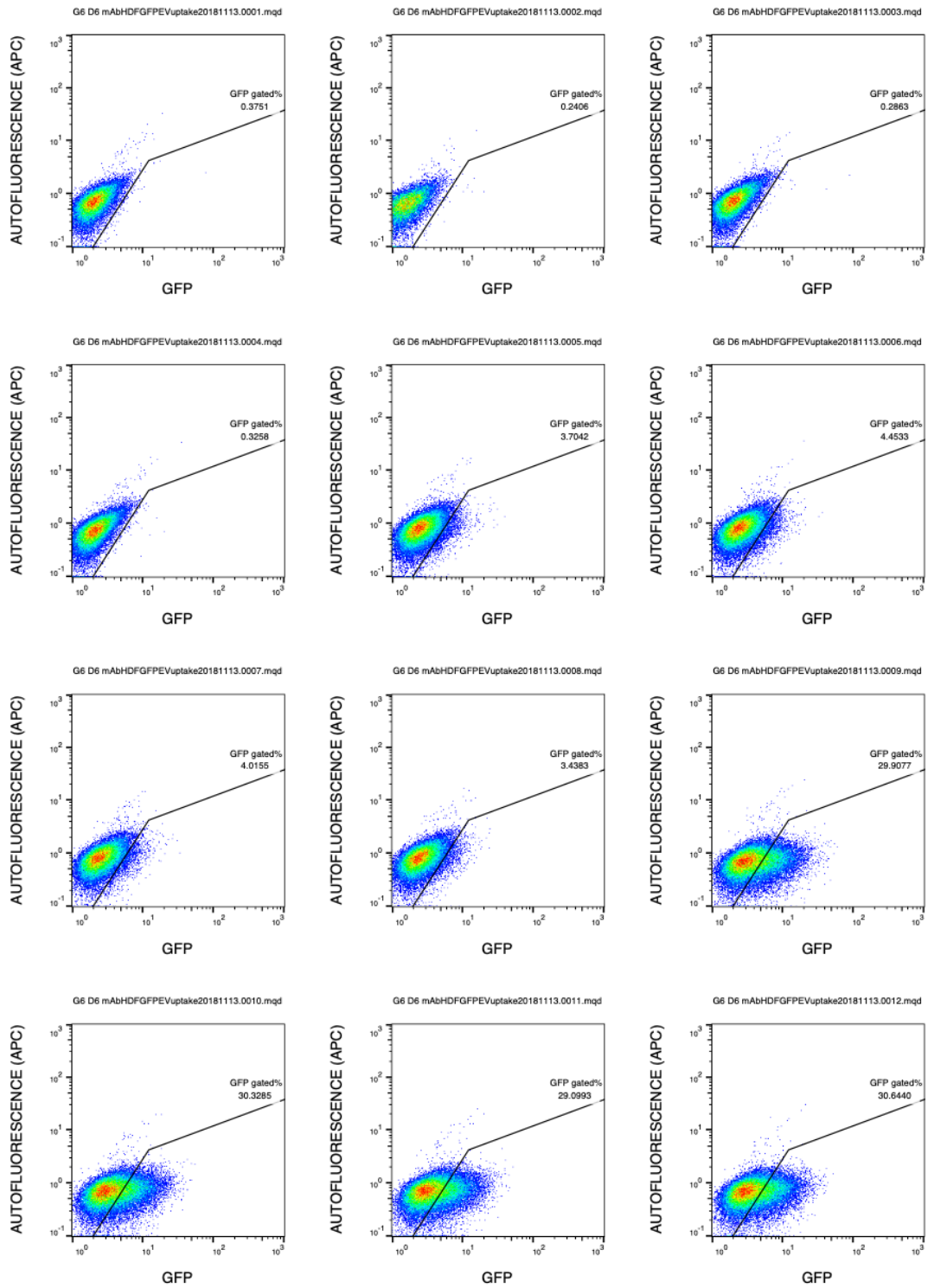
Supplementary Table 2: Sample ID's and antibody concentration and amount of EVs used for EV uptake assay in Huh-7 cells.

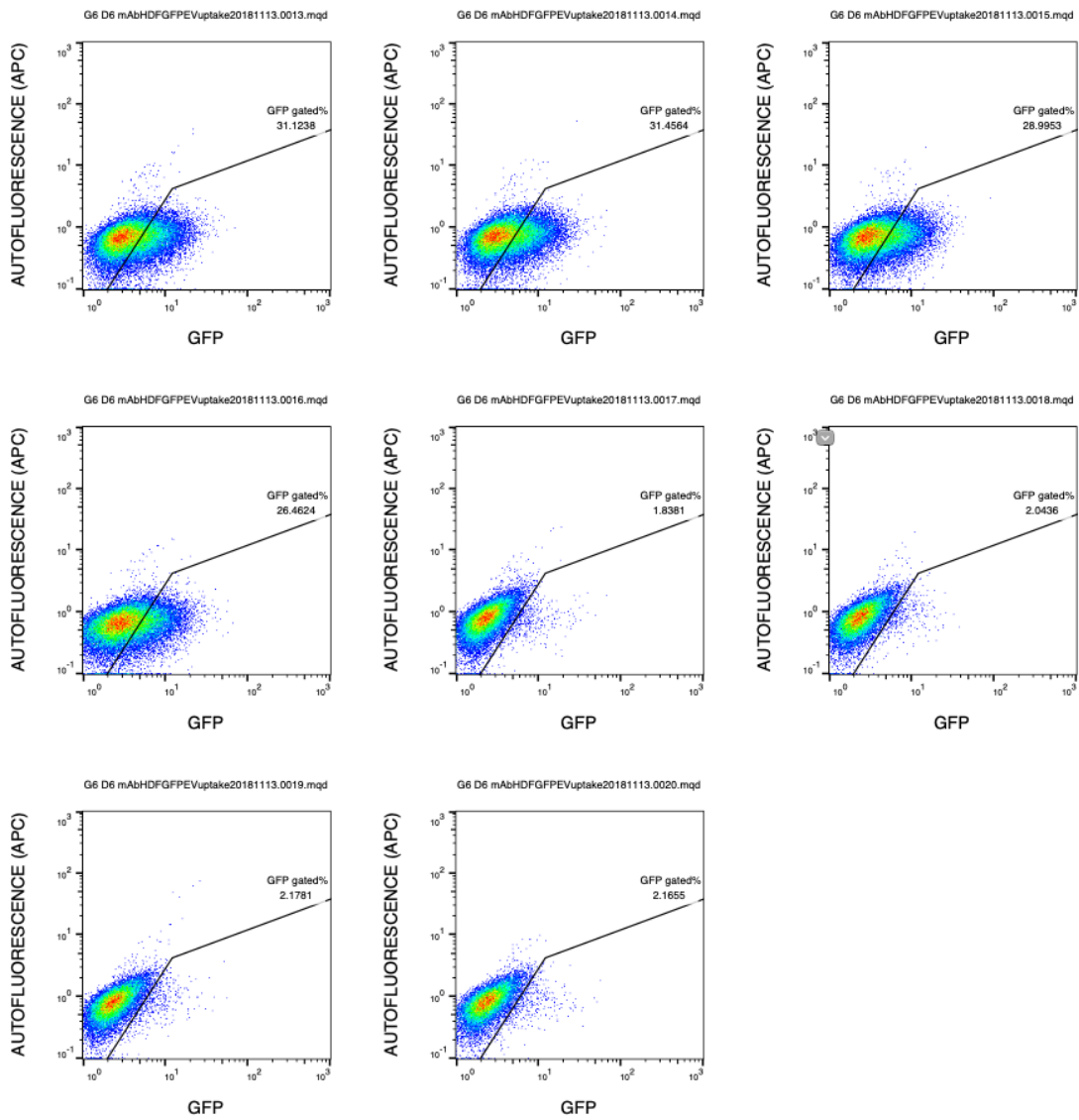


Supplementary Figure 11: scatter plots correlating EV uptake (CD63GFP Internalized EVs) with APC autofluorescence. 2.5×10^9 EVs used with different concentrations of mAb's (mentioned in ST: 3) in the EV uptake assay.

mAbs_2.5E9HDFGFPEV20181108.0001.mqd	CD63	Cells only
mAbs_2.5E9HDFGFPEV20181108.0002.mqd		CD63-GFP EVs
mAbs_2.5E9HDFGFPEV20181108.0003.mqd		CD63-GFP EVs+ 200 ng of mAb
mAbs_2.5E9HDFGFPEV20181108.0004.mqd		CD63-GFP EVs+ 1 µg of mAb
mAbs_2.5E9HDFGFPEV20181108.0005.mqd		CD63-GFP EVs+ 2 µg of mAb
mAbs_2.5E9HDFGFPEV20181108.0006.mqd		CD63-GFP EVs+ 4 µg of mAb
mAbs_2.5E9HDFGFPEV20181108.0007.mqd	ALIX	Cells only
mAbs_2.5E9HDFGFPEV20181108.0008.mqd		CD63-GFP EVs
mAbs_2.5E9HDFGFPEV20181108.0009.mqd		CD63-GFP EVs+ 200 ng of mAb
mAbs_2.5E9HDFGFPEV20181108.0010.mqd		CD63-GFP EVs+ 1 µg of mAb
mAbs_2.5E9HDFGFPEV20181108.0011.mqd		CD63-GFP EVs+ 2 µg of mAb
mAbs_2.5E9HDFGFPEV20181108.0012.mqd		CD63-GFP EVs+ 4 µg of mAb
mAbs_2.5E9HDFGFPEV20181108.0013.mqd	52F8-G6	Cells only
mAbs_2.5E9HDFGFPEV20181108.0014.mqd		CD63-GFP EVs
mAbs_2.5E9HDFGFPEV20181108.0015.mqd		CD63-GFP EVs+ 200 ng of mAb
mAbs_2.5E9HDFGFPEV20181108.0016.mqd		CD63-GFP EVs+ 1 µg of mAb
mAbs_2.5E9HDFGFPEV20181108.0017.mqd		CD63-GFP EVs+ 2 µg of mAb
mAbs_2.5E9HDFGFPEV20181108.0018.mqd		CD63-GFP EVs+ 4 µg of mAb
mAbs_2.5E9HDFGFPEV20181108.0019.mqd	53E6-D8	Cells only
mAbs_2.5E9HDFGFPEV20181108.0020.mqd		CD63-GFP EVs
mAbs_2.5E9HDFGFPEV20181108.0021.mqd		CD63-GFP EVs+ 200 ng of mAb
mAbs_2.5E9HDFGFPEV20181108.0022.mqd		CD63-GFP EVs+ 1 µg of mAb
mAbs_2.5E9HDFGFPEV20181108.0023.mqd		CD63-GFP EVs+ 2 µg of mAb
mAbs_2.5E9HDFGFPEV20181108.0024.mqd		CD63-GFP EVs+ 4 µg of mAb
mAbs_2.5E9HDFGFPEV20181108.0025.mqd	53F2-A1	Cells only
mAbs_2.5E9HDFGFPEV20181108.0026.mqd		CD63-GFP EVs
mAbs_2.5E9HDFGFPEV20181108.0027.mqd		CD63-GFP EVs+ 200 ng of mAb
mAbs_2.5E9HDFGFPEV20181108.0028.mqd		CD63-GFP EVs+ 1 µg of mAb
mAbs_2.5E9HDFGFPEV20181108.0029.mqd		CD63-GFP EVs+ 2 µg of mAb
mAbs_2.5E9HDFGFPEV20181108.0030.mqd		CD63-GFP EVs+ 4 µg of mAb
mAbs_2.5E9HDFGFPEV20181108.0031.mqd	53F2-D6	Cells only
mAbs_2.5E9HDFGFPEV20181108.0032.mqd		CD63-GFP EVs
mAbs_2.5E9HDFGFPEV20181108.0033.mqd		CD63-GFP EVs+ 200 ng of mAb
mAbs_2.5E9HDFGFPEV20181108.0034.mqd		CD63-GFP EVs+ 1 µg of mAb
mAbs_2.5E9HDFGFPEV20181108.0035.mqd		CD63-GFP EVs+ 2 µg of mAb
mAbs_2.5E9HDFGFPEV20181108.0036.mqd		CD63-GFP EVs+ 4 µg of mAb
mAbs_2.5E9HDFGFPEV20181108.0037.mqd	53F2-E1	Cells only
mAbs_2.5E9HDFGFPEV20181108.0038.mqd		CD63-GFP EVs
mAbs_2.5E9HDFGFPEV20181108.0039.mqd		CD63-GFP EVs+ 200 ng of mAb
mAbs_2.5E9HDFGFPEV20181108.0040.mqd		CD63-GFP EVs+ 1 µg of mAb
mAbs_2.5E9HDFGFPEV20181108.0041.mqd		CD63-GFP EVs+ 2 µg of mAb
mAbs_2.5E9HDFGFPEV20181108.0042.mqd		CD63-GFP EVs+ 4 µg of mAb

Supplementary Table 3: Sample ID's and antibody concentration used for EV uptake assay in Huh-7 cells.





Supplementary Figure 12: scatter plots correlating EV uptake (CD63-GFP Internalized EVs) with APC autofluorescence. 2.5×10^9 CD63-GFP EVs with 52F8-G6, 53F2-D6 of 4 μ g and CD63 mAb of 2 μ g of CD63-GFP EVs (mentioned in ST: 4)

G6 D6 mAbHDFGFPEVuptake20181113.0001.mqd	cells only
G6 D6 mAbHDFGFPEVuptake20181113.0002.mqd	
G6 D6 mAbHDFGFPEVuptake20181113.0003.mqd	
G6 D6 mAbHDFGFPEVuptake20181113.0004.mqd	
G6 D6 mAbHDFGFPEVuptake20181113.0005.mqd	CD63- GFP EVs
G6 D6 mAbHDFGFPEVuptake20181113.0006.mqd	
G6 D6 mAbHDFGFPEVuptake20181113.0007.mqd	
G6 D6 mAbHDFGFPEVuptake20181113.0008.mqd	CD63- GFP EVs + 52F8- G6 mAb
G6 D6 mAbHDFGFPEVuptake20181113.0009.mqd	
G6 D6 mAbHDFGFPEVuptake20181113.0010.mqd	
G6 D6 mAbHDFGFPEVuptake20181113.0011.mqd	
G6 D6 mAbHDFGFPEVuptake20181113.0012.mqd	CD63- GFP EVs + 53F2- D6 mAb
G6 D6 mAbHDFGFPEVuptake20181113.0013.mqd	
G6 D6 mAbHDFGFPEVuptake20181113.0014.mqd	
G6 D6 mAbHDFGFPEVuptake20181113.0015.mqd	CD63- GFP EVs + CD63 mAb
G6 D6 mAbHDFGFPEVuptake20181113.0016.mqd	
G6 D6 mAbHDFGFPEVuptake20181113.0017.mqd	
G6 D6 mAbHDFGFPEVuptake20181113.0018.mqd	
G6 D6 mAbHDFGFPEVuptake20181113.0019.mqd	
G6 D6 mAbHDFGFPEVuptake20181113.0020.mqd	

Supplementary Table 4: Sample ID's and mABs concentration used for EV uptake assay in Huh-7 cells. 2.5×10^9 CD63-GFP EVs with 52F8-G6, 53F2-D6 of 4 μ g and CD63 mAb of 2 μ g used for EV uptake assay

7. REFERENCES

- Akers, Johnny C., David Gonda, Ryan Kim, Bob S. Carter, and Clark C. Chen. 2013. “Biogenesis of Extracellular Vesicles (EV): Exosomes, Microvesicles, Retrovirus-like Vesicles, and Apoptotic Bodies.” *Journal of Neuro-Oncology* 113 (1): 1–11. <https://doi.org/10.1007/s11060-013-1084-8>.
- Akuma, Precious, Ogadimma D. Okagu, and Chibuike C. Udenigwe. 2019. “Naturally Occurring Exosome Vesicles as Potential Delivery Vehicle for Bioactive Compounds.” *Frontiers in Sustainable Food Systems* 3 (April): 1–8. <https://doi.org/10.3389/fsufs.2019.00023>.
- Al-Nedawi, Khalid, Brian Meehan, Robert S. Kerbel, Anthony C. Allison, and Anusz Rak. 2009. “Endothelial Expression of Autocrine VEGF upon the Uptake of Tumor-Derived Microvesicles Containing Oncogenic EGFR.” *Proceedings of the National Academy of Sciences of the United States of America* 106 (10): 3794–99. <https://doi.org/10.1073/pnas.0804543106>.
- Al-Nedawi, Khalid, Brian Meehan, Johann Micallef, Vladimir Lhotak, Linda May, Abhijit Guha, and Janusz Rak. 2008. “Intercellular Transfer of the Oncogenic Receptor EGFRvIII by Microvesicles Derived from Tumour Cells.” *Nature Cell Biology* 10 (5): 619–24. <https://doi.org/10.1038/ncb1725>.
- Alcorta, David A., Yue Xiong, Dawn Phelps, Greg Hannon, David Beach, and J. Carl Barrett. 1996. “Involvement of the Cyclin-Dependent Kinase Inhibitor P16 (INK4a) in Replicative Senescence of Normal Human Fibroblasts.” *Proceedings of the National Academy of Sciences of the United States of America* 93 (24): 13742–47. <https://doi.org/10.1073/pnas.93.24.13742>.
- Alvarez-Erviti, Lydia, Yiqi Seow, HaiFang Yin, Corinne Betts, Samira Lakhali, and Matthew J A Wood. 2011. “Delivery of siRNA to the Mouse Brain by Systemic Injection of Targeted Exosomes.” *Nature Biotechnology* 29 (4): 341–45. <https://doi.org/10.1038/nbt.1807>.
- An, Mingrui, Jing Wu, Jianhui Zhu, and David M. Lubman. 2018. “Comparison of an Optimized Ultracentrifugation Method versus Size-Exclusion Chromatography for Isolation of Exosomes from Human Serum.” Brief-report. *Journal of Proteome Research* 17 (10):

- 3599–3605. <https://doi.org/10.1021/acs.jproteome.8b00479>.
- Andaloussi, Samir EL, Samira Lakhal, Imre Mäger, and Matthew J.A. Wood. 2013. “Exosomes for Targeted SiRNA Delivery across Biological Barriers.” *Advanced Drug Delivery Reviews* 65 (3): 391–97. <https://doi.org/10.1016/j.addr.2012.08.008>.
- Antonyak, Marc A., Bo Li, Lindsey K. Boroughs, Jared L. Johnson, Joseph E. Druso, Kirsten L. Bryant, David A. Holowka, and Richard A. Cerione. 2011. “Erratum: Cancer Cell-Derived Microvesicles Induce Transformation by Transferring Tissue Transglutaminase and Fibronectin to Recipient Cells (Proceedings of the National Academy of Sciences of the United States of America (2011) 108, 12, (4852-4857) DOI: 1.” *Proceedings of the National Academy of Sciences of the United States of America* 108 (42): 17569. <https://doi.org/10.1073/pnas.1114824108>.
- Arai, R., H. Ueda, A. Kitayama, N. Kamiya, and T. Nagamune. 2001. “Design of the Linkers Which Effectively Separate Domains of a Bifunctional Fusion Protein.” *Protein Engineering* 14 (8): 529–32. <https://doi.org/10.1093/protein/14.8.529>.
- Argos, Patrick. 1990. “An Investigation of Oligopeptides Linking Domains in Protein Tertiary Structures and Possible Candidates for General Gene Fusion.” *Journal of Molecular Biology* 211 (4): 943–58. [https://doi.org/10.1016/0022-2836\(90\)90085-Z](https://doi.org/10.1016/0022-2836(90)90085-Z).
- Arraud, N., R. Linares, S. Tan, C. Gounou, J. M. Pasquet, S. Mornet, and A. R. Brisson. 2014. “Extracellular Vesicles from Blood Plasma: Determination of Their Morphology, Size, Phenotype and Concentration.” *Journal of Thrombosis and Haemostasis* 12 (5): 614–27. <https://doi.org/10.1111/jth.12554>.
- Arraud, Nicolas, Céline Gounou, Delphine Turpin, and Alain R. Brisson. 2016. “Fluorescence Triggering: A General Strategy for Enumerating and Phenotyping Extracellular Vesicles by Flow Cytometry.” *Cytometry Part A* 89 (2): 184–95. <https://doi.org/10.1002/cyto.a.22669>.
- Arscott, W. Tris, Anita T. Tandle, Shuping Zhao, Jacob E. Shabason, Ira K. Gordon, Cody D. Schlaff, Guofeng Zhang, Philip J. Tofilon, and Kevin A. Camphausen. 2013. “Ionizing Radiation and Glioblastoma Exosomes: Implications in Tumor Biology and Cell Migration.” *Translational Oncology* 6 (6): 638–48. <https://doi.org/10.1593/tlo.13640>.
- Ayers, Lisa, Malcolm Kohler, Paul Harrison, Ian Sargent, Rebecca Dragovic, Marianne Schaap, Rienk Nieuwland, Susan A. Brooks, and Berne Ferry. 2011. “Measurement of Circulating

- Cell-Derived Microparticles by Flow Cytometry: Sources of Variability within the Assay.” *Thrombosis Research* 127 (4): 370–77. <https://doi.org/10.1016/j.thromres.2010.12.014>.
- “B Lymphocytes Secrete Antigen-Presenting Vesicles.” 1996 183 (March).
- Baar, Marjolein P., Renata M.C. Brandt, Diana A. Putavet, Julian D.D. Klein, Kasper W.J. Derks, Benjamin R.M. Bourgeois, Sarah Stryeck, et al. 2017. “Targeted Apoptosis of Senescent Cells Restores Tissue Homeostasis in Response to Chemotoxicity and Aging.” *Cell* 169 (1): 132–147.e16. <https://doi.org/10.1016/j.cell.2017.02.031>.
- Bache, Kristi G., Andreas Brech, Anja Mehlum, and Harald Stenmark. 2003. “Hrs Regulates Multivesicular Body Formation via ESCRT Recruitment to Endosomes.” *Journal of Cell Biology* 162 (3): 435–42. <https://doi.org/10.1083/jcb.200302131>.
- Baddela, Vijay Simha, Varij Nayan, Payal Rani, Suneel Kumar Onteru, and Dheer Singh. 2016. “Physicochemical Biomolecular Insights into Buffalo Milk-Derived Nanovesicles.” *Applied Biochemistry and Biotechnology* 178 (3): 544–57. <https://doi.org/10.1007/s12010-015-1893-7>.
- Bæk, Rikke, Evo K.L. Søndergaard, Kim Varming, and Malene M. Jørgensen. 2016. “The Impact of Various Preanalytical Treatments on the Phenotype of Small Extracellular Vesicles in Blood Analyzed by Protein Microarray.” *Journal of Immunological Methods* 438: 11–20. <https://doi.org/10.1016/j.jim.2016.08.007>.
- Baietti, Maria Francesca, Zhe Zhang, Eva Mortier, Aurélie Melchior, Gisèle Degeest, Annelies Geeraerts, Ylva Ivarsson, et al. 2012. “Syndecan-Syntenin-ALIX Regulates the Biogenesis of Exosomes.” *Nature Cell Biology* 14 (7): 677–85. <https://doi.org/10.1038/ncb2502>.
- Baker, Darren J., Bennett G. Childs, Matej Durik, Melinde E. Wijers, Cynthia J. Sieben, Jian Zhong, Rachel A. Saltness, et al. 2016. “Naturally Occurring P16 Ink4a-Positive Cells Shorten Healthy Lifespan.” *Nature* 530 (7589): 184–89. <https://doi.org/10.1038/nature16932>.
- Baker, Darren J., Carmen Perez-Terzic, Fang Jin, Kevin Pitel, Nicolas J. Niederländer, Karthik Jeganathan, Satsuki Yamada, et al. 2008. “Opposing Roles for P16Ink4a and P19Arf in Senescence and Ageing Caused by BubR1 Insufficiency.” *Nature Cell Biology* 10 (7): 825–36. <https://doi.org/10.1038/ncb1744>.
- Baker, Darren J., Tobias Wijshake, Tamar Tchkonina, Nathan K. Lebrasseur, Bennett G. Childs,

- Bart Van De Sluis, James L. Kirkland, and Jan M. Van Deursen. 2011. "Clearance of P16 Ink4a-Positive Senescent Cells Delays Ageing-Associated Disorders." *Nature* 479 (7372): 232–36. <https://doi.org/10.1038/nature10600>.
- Balaj, Leonora, Nadia A. Atai, Weilin Chen, Dakai Mu, Bakhos A. Tannous, Xandra O. Breakefield, Johan Skog, and Casey A. Maguire. 2015. "Heparin Affinity Purification of Extracellular Vesicles." *Scientific Reports* 5: 1–15. <https://doi.org/10.1038/srep10266>.
- Baran, Jaroslaw, Monika Baj-Krzyworzeka, Kazimierz Weglarczyk, Rafal Szatanek, Maria Zembela, Jakub Barbasz, Antoni Czupryna, Antoni Szczepanik, and Marek Zembala. 2010. "Circulating Tumour-Derived Microvesicles in Plasma of Gastric Cancer Patients." *Cancer Immunology, Immunotherapy* 59 (6): 841–50. <https://doi.org/10.1007/s00262-009-0808-2>.
- Barrès, Céline, Lionel Blanc, Pascale Bette-Bobillo, Sabine André, Robert Mamoun, Hans Joachim Gubius, and Michel Vidal. 2010. "Galectin-5 Is Bound onto the Surface of Rat Reticulocyte Exosomes and Modulates Vesicle Uptake by Macrophages." *Blood* 115 (3): 696–705. <https://doi.org/10.1182/blood-2009-07-231449>.
- Beauséjour, Christian M., Ana Krtolica, Francesco Galimi, Masashi Narita, Scott W. Lowe, Paul Yaswen, and Judith Campisi. 2003. "Reversal of Human Cellular Senescence: Roles of the P53 and P16 Pathways." *EMBO Journal* 22 (16): 4212–22. <https://doi.org/10.1093/emboj/cdg417>.
- Besse, Benjamin, Mélinda Charrier, Valérie Lapierre, Eric Dansin, Olivier Lantz, David Planchard, Thierry Le Chevalier, et al. 2016. "Dendritic Cell-Derived Exosomes as Maintenance Immunotherapy after First Line Chemotherapy in NSCLC." *OncoImmunology* 5 (4): 1–13. <https://doi.org/10.1080/2162402X.2015.1071008>.
- Biggs, Colleen N., Khurram M. Siddiqui, Ali A. Al-Zahrani, Siddika Pardhan, Sabine I. Brett, Qiu Q. Guo, Jun Yang, et al. 2016. "Prostate Extracellular Vesicles in Patient Plasma as a Liquid Biopsy Platform for Prostate Cancer Using Nanoscale Flow Cytometry." *Oncotarget* 7 (8): 8839–49. <https://doi.org/10.18632/oncotarget.6983>.
- Bishop, Naomi, and Philip Woodman. 2001. "TSG101/Mammalian VPS23 and Mammalian VPS28 Interact Directly and Are Recruited to VPS4-Induced Endosomes." *Journal of Biological Chemistry* 276 (15): 11735–42. <https://doi.org/10.1074/jbc.M009863200>.
- Blanc, Katarina Le, Francesco Frassoni, Lynne Ball, Franco Locatelli, Helene Roelofs, Ian

- Lewis, Edoardo Lanino, et al. 2008. “Mesenchymal Stem Cells for Treatment of Steroid-Resistant, Severe, Acute Graft-versus-Host Disease: A Phase II Study.” *The Lancet* 371 (9624): 1579–86. [https://doi.org/10.1016/S0140-6736\(08\)60690-X](https://doi.org/10.1016/S0140-6736(08)60690-X).
- Bobrie, Angélique, Sophie Krumeich, Fabien Rey, Chiara Recchi, Luis F. Moita, Miguel C. Seabra, Matias Ostrowski, and Clotilde Théry. 2012. “Rab27a Supports Exosome-Dependent and -Independent Mechanisms That Modify the Tumor Microenvironment and Can Promote Tumor Progression.” *Cancer Research* 72 (19): 4920–30. <https://doi.org/10.1158/0008-5472.CAN-12-0925>.
- Böing, Anita N., Edwin van der Pol, Anita E. Grootemaat, Frank A.W. Coumans, Auguste Sturk, and Rienk Nieuwland. 2014. “Single-Step Isolation of Extracellular Vesicles by Size-Exclusion Chromatography.” *Journal of Extracellular Vesicles* 3 (1): 1–11. <https://doi.org/10.3402/jev.v3.23430>.
- Borghesan, Michela, Juan Fafián-Labora, Olga Eleftheriadou, Paula Carpintero-Fernández, Marta Paez-Ribes, Gema Vizcay-Barrena, Avital Swisa, et al. 2019. “Small Extracellular Vesicles Are Key Regulators of Non-Cell Autonomous Intercellular Communication in Senescence via the Interferon Protein IFITM3.” *Cell Reports* 27 (13): 3956-3971.e6. <https://doi.org/10.1016/j.celrep.2019.05.095>.
- Boucheix, C., and E. Rubinstein. 2001. “Tetraspanins.” *Cellular and Molecular Life Sciences* 58 (9): 1189–1205. <https://doi.org/10.1007/PL00000933>.
- Boucheix, Claude. 2000. “Severely Reduced Female Fertility in CD9-Deficient Mice.” *Science* 287 (5451): 319–21. <https://doi.org/10.1126/science.287.5451.319>.
- Brisson, Alain R., Sisareuth Tan, Romain Linares, Céline Gounou, and Nicolas Arraud. 2017. “Extracellular Vesicles from Activated Platelets: A Semiquantitative Cryo-Electron Microscopy and Immuno-Gold Labeling Study.” *Platelets* 28 (3): 263–71. <https://doi.org/10.1080/09537104.2016.1268255>.
- Brown, Michael, Lewis J. Stafford, Dale Onisk, Tony Joaquim, Alhagie Tobb, Larissa Goldman, David Fancy, James Stave, and Ross Chambers. 2013. “Snorkel: An Epitope Tagging System for Measuring the Surface Expression of Membrane Proteins.” *PloS One* 8 (9): 1–10. <https://doi.org/10.1371/journal.pone.0073255>.
- Brzozowski, Joshua S., Helen Jankowski, Danielle R. Bond, Siobhan B. McCague, Benjamin R.

- Munro, Melanie J. Predebon, Christopher J. Scarlett, Kathryn A. Skelding, and Judith Weidenhofer. 2018. "Lipidomic Profiling of Extracellular Vesicles Derived from Prostate and Prostate Cancer Cell Lines." *Lipids in Health and Disease* 17 (1): 1–12.
<https://doi.org/10.1186/s12944-018-0854-x>.
- Bulte, Je W M, and Michel M J Modo. n.d. <Jeff W.M. Bulte, Michel M.J. Modo (Eds.) - Design and Applications of Nanoparticles in Biomedical Imaging-Springer International Publishing (2017).Pdf>.
- Busatto, Sara, George Vilanilam, Taylor Ticer, Wen-Lang Lin, Dennis Dickson, Shane Shapiro, Paolo Bergese, and Joy Wolfram. 2018. "Tangential Flow Filtration for Highly Efficient Concentration of Extracellular Vesicles from Large Volumes of Fluid." *Cells* 7 (12): 273.
<https://doi.org/10.3390/cells7120273>.
- Cai, Zhijian, Fei Yang, Lei Yu, Zhou Yu, Lingling Jiang, Qingqing Wang, Yunshan Yang, Lie Wang, Xuetao Cao, and Jianli Wang. 2012. "Activated T Cell Exosomes Promote Tumor Invasion via Fas Signaling Pathway." *The Journal of Immunology* 188 (12): 5954–61.
<https://doi.org/10.4049/jimmunol.1103466>.
- Campisi, Judith, and Fabrizio D'Adda Di Fagagna. 2007. "Cellular Senescence: When Bad Things Happen to Good Cells." *Nature Reviews Molecular Cell Biology* 8 (9): 729–40.
<https://doi.org/10.1038/nrm2233>.
- Campos-Silva, Carmen, Henar Suárez, Ricardo Jara-Acevedo, Estefanía Linares-Espinós, Luis Martínez-Piñeiro, María Yáñez-Mó, and Mar Valés-Gómez. 2019. "High Sensitivity Detection of Extracellular Vesicles Immune-Captured from Urine by Conventional Flow Cytometry." *Scientific Reports* 9 (1): 1–12. <https://doi.org/10.1038/s41598-019-38516-8>.
- Cao, Hongmei, Zhiwei Yue, Heqi Gao, Chao Chen, Kaige Cui, Kaiyue Zhang, Yuanqiu Cheng, et al. 2019. "In vivo Real-Time Imaging of Extracellular Vesicles in Liver Regeneration via Aggregation-Induced Emission Luminogens." Research-article. *ACS Nano* 13 (3): 3522–33.
<https://doi.org/10.1021/acsnano.8b09776>.
- Casado, Santiago, Maria Del Val Toledo Lobo, and Carlos Luis Paíno. 2017. "Dynamics of Plasma Membrane Surface Related to the Release of Extracellular Vesicles by Mesenchymal Stem Cells in Culture." *Scientific Reports* 7 (1): 1–9.
<https://doi.org/10.1038/s41598-017-07265-x>.

- Chalmin, Fanny, Sylvain Ladoire, Grégoire Mignot, Julie Vincent, Mélanie Bruchard, Jean Paul Remy-Martin, Wilfrid Boireau, et al. 2010. "Membrane-Associated Hsp72 from Tumor-Derived Exosomes Mediates STAT3-Dependent Immunosuppressive Function of Mouse and Human Myeloid-Derived Suppressor Cells." *Journal of Clinical Investigation* 120 (2): 457–71. <https://doi.org/10.1172/JCI40483>.
- Chandler, Wayne L. 2016. "Measurement of Microvesicle Levels in Human Blood Using Flow Cytometry." *Cytometry. Part B, Clinical Cytometry* 90 (4): 326–36. <https://doi.org/10.1002/cyto.b.21343>.
- Chang, Jianhui, Yingying Wang, Lijian Shao, Remi Martin Laberge, Marco Demaria, Judith Campisi, Krishnamurthy Janakiraman, et al. 2016. "Clearance of Senescent Cells by ABT263 Rejuvenates Aged Hematopoietic Stem Cells in Mice." *Nature Medicine* 22 (1): 78–83. <https://doi.org/10.1038/nm.4010>.
- CHARGAFF, E, and R WEST. 1946. "The Biological Significance of the Thromboplastic Protein of Blood." *The Journal of Biological Chemistry* 166 (1): 189–97. <http://www.ncbi.nlm.nih.gov/pubmed/20273687>.
- Cheruvanky, Anita, Hua Zhou, Trairak Pisitkun, Jeffrey B. Kopp, Mark A. Knepper, Peter S.T. Yuen, and Robert A. Star. 2007. "Rapid Isolation of Urinary Exosomal Biomarkers Using a Nanomembrane Ultrafiltration Concentrator." *American Journal of Physiology - Renal Physiology* 292 (5): 1657–61. <https://doi.org/10.1152/ajprenal.00434.2006>.
- Chieriegatti, Evelina, and Jacopo Meldolesi. 2005. "Regulated Exocytosis: New Organelles for Non-Secretory Purposes." *Nature Reviews Molecular Cell Biology* 6 (2): 181–87. <https://doi.org/10.1038/nrm1572>.
- Choi, Dong-Sic, Dae-Kyum Kim, Yoon-Keun Kim, and Yong Song Gho. 2015. "Proteomics of Extracellular Vesicles: Exosomes and Ectosomes." *Mass Spectrometry Reviews* 34 (4): 474–90. <https://doi.org/10.1002/mas.21420>.
- Cicero, Alessandra Lo, Cédric Delevoeye, Floriane Gilles-Marsens, Damarys Loew, Florent Dingli, Christelle Guéré, Nathalie André, Katell Vié, Guillaume Van Niel, and Graça Raposo. 2015. "Exosomes Released by Keratinocytes Modulate Melanocyte Pigmentation." *Nature Communications* 6 (May). <https://doi.org/10.1038/ncomms8506>.
- Clayton, Aled, Jacquelyn Court, Hossein Navabi, Malcolm Adams, Malcolm D. Mason, Jan A.

- Hobot, Geoff R. Newman, and Bharat Jasani. 2001. "Analysis of Antigen Presenting Cell Derived Exosomes, Based on Immuno-Magnetic Isolation and Flow Cytometry." *Journal of Immunological Methods* 247 (1–2): 163–74. [https://doi.org/10.1016/S0022-1759\(00\)00321-5](https://doi.org/10.1016/S0022-1759(00)00321-5).
- Colombo, Marina, Catarina Moita, Guillaume Van Niel, Joanna Kowal, James Vigneron, Philippe Benaroch, Nicolas Manel, Luis F. Moita, Clotilde Théry, and Graça Raposo. 2013. "Analysis of ESCRT Functions in Exosome Biogenesis, Composition and Secretion Highlights the Heterogeneity of Extracellular Vesicles." *Journal of Cell Science* 126 (24): 5553–65. <https://doi.org/10.1242/jcs.128868>.
- Coppé, Jean-Philippe, Pierre-Yves Desprez, Ana Krtolica, and Judith Campisi. 2010. "The Senescence-Associated Secretory Phenotype: The Dark Side of Tumor Suppression." *Annual Review of Pathology: Mechanisms of Disease* 5 (1): 99–118. <https://doi.org/10.1146/annurev-pathol-121808-102144>.
- Coppé, Jean Philippe, Christopher K. Patil, Francis Rodier, Y. Sun, Denise P. Muñoz, Joshua Goldstein, Peter S. Nelson, Pierre Yves Desprez, and Judith Campisi. 2008. "Senescence-Associated Secretory Phenotypes Reveal Cell-Nonautonomous Functions of Oncogenic RAS and the P53 Tumor Suppressor." *PLoS Biology* 6 (12). <https://doi.org/10.1371/journal.pbio.0060301>.
- Corso, Giulia, Imre Mäger, Yi Lee, André Görgens, Jarred Bultema, Bernd Giebel, Matthew J.A. Wood, Joel Z. Nordin, and Samir El Andaloussi. 2017. "Reproducible and Scalable Purification of Extracellular Vesicles Using Combined Bind-Elute and Size Exclusion Chromatography." *Scientific Reports* 7 (1): 1–10. <https://doi.org/10.1038/s41598-017-10646-x>.
- Cosenza, Stella, Karine Toupet, Marie Maumus, Patricia Luz-Crawford, Olivier Blanc-Brude, Christian Jorgensen, and Danièle Noël. 2018. "Mesenchymal Stem Cells-Derived Exosomes Are More Immunosuppressive than Microparticles in Inflammatory Arthritis." *Theranostics* 8 (5): 1399–1410. <https://doi.org/10.7150/thno.21072>.
- Cossetti, Chiara, Nunzio Iraci, Tim R. Mercer, Tommaso Leonardi, Emanuele Alpi, Denise Drago, Clara Alfaro-Cervello, et al. 2014. "Extracellular Vesicles from Neural Stem Cells Transfer IFN- γ via Ifngr1 to Activate Stat1 Signaling in Target Cells." *Molecular Cell* 56

- (2): 193–204. <https://doi.org/10.1016/j.molcel.2014.08.020>.
- Crescitelli, Rossella, Cecilia Lässer, Tamas G. Szabó, Agnes Kittel, Maria Eldh, Irma Dianzani, Edit I. Buzás, and Jan Lötvall. 2013. “Distinct RNA Profiles in Subpopulations of Extracellular Vesicles: Apoptotic Bodies, Microvesicles and Exosomes.” *Journal of Extracellular Vesicles* 2 (1). <https://doi.org/10.3402/jev.v2i0.20677>.
- Crew, Vanja Karamatic, Nicholas Burton, Alexander Kagan, Carole A. Green, Cyril Levene, Frances Flinter, R. Leo Brady, Geoff Daniels, and David J. Anstee. 2004. “CD151, the First Member of the Tetraspanin (TM4) Superfamily Detected on Erythrocytes, Is Essential for the Correct Assembly of Human Basement Membranes in Kidney and Skin.” *Blood* 104 (8): 2217–23. <https://doi.org/10.1182/blood-2004-04-1512>.
- Dabrowska, Sylwia, Andrea Del Fattore, Elzbieta Karnas, Malgorzata Frontczak-Baniewicz, Hanna Kozłowska, Maurizio Muraca, Mirosław Janowski, and Barbara Lukomska. 2018. “Imaging of Extracellular Vesicles Derived from Human Bone Marrow Mesenchymal Stem Cells Using Fluorescent and Magnetic Labels.” *International Journal of Nanomedicine* 13: 1653–64. <https://doi.org/10.2147/IJN.S159404>.
- Davies, Ryan T., Junho Kim, Su Chul Jang, Eun Jeong Choi, Yong Song Gho, and Jaesung Park. 2012. “Microfluidic Filtration System to Isolate Extracellular Vesicles from Blood.” *Lab on a Chip* 12 (24): 5202–10. <https://doi.org/10.1039/c2lc41006k>.
- Deddens, Janine C., Krijn R. Vrijnsen, Johanna M. Colijn, Martinus I. Oerlemans, Corina H.G. Metz, Els J. van der Vlist, Esther N.M. Nolte-’t Hoen, et al. 2016. “Circulating Extracellular Vesicles Contain miRNAs and Are Released as Early Biomarkers for Cardiac Injury.” *Journal of Cardiovascular Translational Research* 9 (4): 291–301. <https://doi.org/10.1007/s12265-016-9705-1>.
- Deregibus, Maria Chiara, Vincenzo Cantaluppi, Raffaele Calogero, Marco Lo Iacono, Ciro Tetta, Luigi Biancone, Stefania Bruno, Benedetta Bussolati, and Giovanni Camussi. 2007. “Endothelial Progenitor Cell - Derived Microvesicles Activate an Angiogenic Program in Endothelial Cells by a Horizontal Transfer of mRNA.” *Blood* 110 (7): 2440–48. <https://doi.org/10.1182/blood-2007-03-078709>.
- Deursen, Jan M. van. 2019. “Senolytic Therapies for Healthy Longevity.” *Science* 364 (6441): 636–37. <https://doi.org/10.1126/science.aaw1299>.

- Deursen, Jan M. Van. 2014. "The Role of Senescent Cells in Ageing." *Nature* 509 (7501): 439–46. <https://doi.org/10.1038/nature13193>.
- Dimri, Goberdhan P., Xinhua Lee, George Basile, Meileen Acosta, Glynis Scott, Calvin Roskelley, Estela E. Medrano, et al. 1995. "A Biomarker That Identifies Senescent Human Cells in Culture and in Aging Skin *in vivo*." *Proceedings of the National Academy of Sciences of the United States of America* 92 (20): 9363–67. <https://doi.org/10.1073/pnas.92.20.9363>.
- Dragovic, Rebecca A., Christopher Gardiner, Alexandra S. Brooks, Dionne S. Tannetta, David J.P. Ferguson, Patrick Hole, Bob Carr, et al. 2011. "Sizing and Phenotyping of Cellular Vesicles Using Nanoparticle Tracking Analysis." *Nanomedicine: Nanotechnology, Biology, and Medicine* 7 (6): 780–88. <https://doi.org/10.1016/j.nano.2011.04.003>.
- Effenberger, Timo, Jan Von Der Heyde, Kareen Bartsch, Christoph Garbers, Klaus Schulze-Osthoff, Athena Chalaris, Gillian Murphy, Stefan Rose-John, and Björn Rabe. 2014. "Senescence-Associated Release of Transmembrane Proteins Involves Proteolytic Processing by ADAM17 and Microvesicle Shedding." *FASEB Journal* 28 (11): 4847–56. <https://doi.org/10.1096/fj.14-254565>.
- Eguchi, Takanori, Chiharu Sogawa, Yuka Okusha, Kenta Uchibe, Ryosuke Iinuma, Kisho Ono, Keisuke Nakano, et al. 2018. *Organoids with Cancer Stem Cell-like Properties Secrete Exosomes and HSP90 in a 3D Nanoenvironment*. *PLoS ONE*. Vol. 13. <https://doi.org/10.1371/journal.pone.0191109>.
- Eldh, Maria, Karin Ekström, Hadi Valadi, Margareta Sjöstrand, Bob Olsson, Margareta Jernås, and Jan Lötvall. 2010. "Exosomes Communicate Protective Messages during Oxidative Stress; Possible Role of Exosomal Shuttle RNA." *PLoS ONE* 5 (12): 1–8. <https://doi.org/10.1371/journal.pone.0015353>.
- Elkin, Sarah R., Ashley M. Lakoduk, and Sandra L. Schmid. 2016. "Endocytic Pathways and Endosomal Trafficking: A Primer." *Wiener Medizinische Wochenschrift* 166 (7–8): 196–204. <https://doi.org/10.1007/s10354-016-0432-7>.
- Erdbrügger, Uta, Christine K. Rudy, Mark E. Etter, Kelly A. Dryden, Mark Yeager, Alexander L. Klibanov, and Joanne Lannigan. 2014. "Imaging Flow Cytometry Elucidates Limitations of Microparticle Analysis by Conventional Flow Cytometry." *Cytometry Part A* 85 (9):

- 756–70. <https://doi.org/10.1002/cyto.a.22494>.
- Escrevente, Cristina, Sascha Keller, Peter Altevogt, and Júlia Costa. 2011. “Interaction and Uptake of Exosomes by Ovarian Cancer Cells.” *BMC Cancer* 11 (1): 108. <https://doi.org/10.1186/1471-2407-11-108>.
- Escudier, Bernard, Thierry Dorval, Nathalie Chaput, Fabrice André, Marie Pierre Caby, Sophie Novault, Caroline Flament, et al. 2005. “Vaccination of Metastatic Melanoma Patients with Autologous Dendritic Cell (DC) Derived-Exosomes: Results of the First Phase 1 Clinical Trial.” *Journal of Translational Medicine* 3: 1–13. <https://doi.org/10.1186/1479-5876-3-10>.
- Fabbri, Muller, Alessio Paone, Federica Calore, Roberta Galli, Eugenio Gaudio, Ramasamy Santhanam, Francesca Lovat, et al. 2012. “MicroRNAs Bind to Toll-like Receptors to Induce Prometastatic Inflammatory Response.” *Proceedings of the National Academy of Sciences of the United States of America* 109 (31). <https://doi.org/10.1073/pnas.1209414109>.
- Fendl, Birgit, René Weiss, Michael B. Fischer, Andreas Spittler, and Viktoria Weber. 2016. “Characterization of Extracellular Vesicles in Whole Blood: Influence of Pre-Analytical Parameters and Visualization of Vesicle-Cell Interactions Using Imaging Flow Cytometry.” *Biochemical and Biophysical Research Communications* 478 (1): 168–73. <https://doi.org/10.1016/j.bbrc.2016.07.073>.
- Fernandez-Borja, Mar, Richard Wubbolts, Jero Calafat, Hans Janssen, Nullin Divecha, Simone Dusseljee, and Jacques Neefjes. 1999. “Multivesicular Body Morphogenesis Requires Phosphatidylinositol 3-Kinase Activity.” *Current Biology* 9 (1): 55–58. [https://doi.org/10.1016/S0960-9822\(99\)80048-7](https://doi.org/10.1016/S0960-9822(99)80048-7).
- Fischer, G., G. A. Mignery, M. Baumert, M. S. Perin, T. J. Hanson, P. M. Burger, R. Jahn, and T. C. Sudhof. 1990. “Rab3 Is a Small GTP-Binding Protein Exclusively Localized to Synaptic Vesicles.” *Proceedings of the National Academy of Sciences of the United States of America* 87 (5): 1988–92. <https://doi.org/10.1073/pnas.87.5.1988>.
- Fischer, Uwe M., Matthew T. Harting, Fernando Jimenez, Werner O. Monzon-Posadas, Hasen Xue, Sean I. Savitz, Glen A. Laine, and Charles S. Cox. 2009. “Pulmonary Passage Is a Major Obstacle for Intravenous Stem Cell Delivery: The Pulmonary First-Pass Effect.” *Stem Cells and Development* 18 (5): 683–91. <https://doi.org/10.1089/scd.2008.0253>.

- Flatt, Thomas. 2012. "A New Definition of Aging?" *Frontiers in Genetics* 3 (AUG): 1–2.
<https://doi.org/10.3389/fgene.2012.00148>.
- Gangadaran, Prakash, Xiu Juan Li, Ho Won Lee, Ji Min Oh, Senthilkumar Kalimuthu, Ramya Lakshmi Rajendran, Seung Hyun Son, et al. 2017. "A New Bioluminescent Reporter System to Study the Biodistribution of Systematically Injected Tumor-Derived Bioluminescent Extracellular Vesicles in Mice." *Oncotarget* 8 (66): 109894–914.
<https://doi.org/10.18632/oncotarget.22493>.
- Gangadaran, Prakash, Ramya Lakshmi Rajendran, Ho Won Lee, Senthilkumar Kalimuthu, Chae Moon Hong, Shin Young Jeong, Sang Woo Lee, Jaetae Lee, and Byeong Cheol Ahn. 2017. "Extracellular Vesicles from Mesenchymal Stem Cells Activates VEGF Receptors and Accelerates Recovery of Hindlimb Ischemia." *Journal of Controlled Release* 264: 112–26.
<https://doi.org/10.1016/j.jconrel.2017.08.022>.
- Gardiner, Chris, Dolores Di Vizio, Susmita Sahoo, Clotilde Théry, Kenneth W. Witwer, Marca Wauben, and Andrew F. Hill. 2016. "Techniques Used for the Isolation and Characterization of Extracellular Vesicles: Results of a Worldwide Survey." *Journal of Extracellular Vesicles* 5 (1). <https://doi.org/10.3402/jev.v5.32945>.
- Gatti, Stefano, Stefania Bruno, Maria Chiara Deregibus, Andrea Sordi, Vincenzo Cantaluppi, Ciro Tetta, and Giovanni Camussi. 2011. "Microvesicles Derived from Human Adult Mesenchymal Stem Cells Protect against Ischaemia-Reperfusion-Induced Acute and Chronic Kidney Injury." *Nephrology Dialysis Transplantation* 26 (5): 1474–83.
<https://doi.org/10.1093/ndt/gfr015>.
- Gautier, Arnaud, Alexandre Juillerat, Christian Heinis, Ivan Reis Corrêa, Maik Kindermann, Florent Beaufils, and Kai Johnsson. 2008. "An Engineered Protein Tag for Multiprotein Labeling in Living Cells." *Chemistry and Biology* 15 (2): 128–36.
<https://doi.org/10.1016/j.chembiol.2008.01.007>.
- Gautier, Arnaud, Eiji Nakata, Gražvydas Lukinavičius, Kui Thong Tan, and Kai Johnsson. 2009. "Selective Cross-Linking of Interacting Proteins Using Self-Labeling Tags." *Journal of the American Chemical Society* 131 (49): 17954–62. <https://doi.org/10.1021/ja907818q>.
- Ghosh, Anirban, Michelle Davey, Ian C. Chute, Steven G. Griffiths, Scott Lewis, Simi Chacko, David Barnett, et al. 2014. "Rapid Isolation of Extracellular Vesicles from Cell Culture and

- Biological Fluids Using a Synthetic Peptide with Specific Affinity for Heat Shock Proteins.” *PLoS ONE* 9 (10). <https://doi.org/10.1371/journal.pone.0110443>.
- Görgens, André, Michel Bremer, Rita Ferrer-Tur, Florian Murke, Tobias Tertel, Peter A. Horn, Sebastian Thalmann, et al. 2019. “Optimisation of Imaging Flow Cytometry for the Analysis of Single Extracellular Vesicles by Using Fluorescence-Tagged Vesicles as Biological Reference Material.” *Journal of Extracellular Vesicles* 8 (1). <https://doi.org/10.1080/20013078.2019.1587567>.
- Gould, Stephen J., Amy M. Booth, and James E.K. Hildreth. 2003. “The Trojan Exosome Hypothesis.” *Proceedings of the National Academy of Sciences of the United States of America* 100 (19): 10592–97. <https://doi.org/10.1073/pnas.1831413100>.
- Graner, Michael W., Oscar Alzate, Angelika M. Dechkovskaia, Jack D. Keene, John H. Sampson, Duane A. Mitchell, and Darell D. Bigner. 2009. “Proteomic and Immunologic Analyses of Brain Tumor Exosomes.” *FASEB Journal* 23 (5): 1541–57. <https://doi.org/10.1096/fj.08-122184>.
- Grange, Cristina, Marta Tapparo, Stefania Bruno, Devasis Chatterjee, Peter J. Quesenberry, Ciro Tetta, and Giovanni Camussi. 2014. “Biodistribution of Mesenchymal Stem Cell-Derived Extracellular Vesicles in a Model of Acute Kidney Injury Monitored by Optical Imaging.” *International Journal of Molecular Medicine* 33 (5): 1055–63. <https://doi.org/10.3892/ijmm.2014.1663>.
- Gross, Julia Christina, Varun Chaudhary, Kerstin Bartscherer, and Michael Boutros. 2012. “Active Wnt Proteins Are Secreted on Exosomes.” *Nature Cell Biology* 14 (10): 1036–45. <https://doi.org/10.1038/ncb2574>.
- Guerreiro, Eduarda M., Beate Vestad, Lilly Alice Steffensen, Hans Christian D. Aass, Muhammad Saeed, Reidun Øvstebø, Daniela Elena Costea, Hilde Kanli Galtung, and Tine M. Søland. 2018. “Efficient Extracellular Vesicle Isolation by Combining Cell Media Modifications, Ultrafiltration, and Size-Exclusion Chromatography.” *PLoS ONE* 13 (9): 1–17. <https://doi.org/10.1371/journal.pone.0204276>.
- György, Bence, Zachary Fitzpatrick, Matheus H.W. Crommentuijn, Dakai Mu, and Casey A. Maguire. 2014. “Naturally Enveloped AAV Vectors for Shielding Neutralizing Antibodies and Robust Gene Delivery In Vivo.” *Biomaterials* 35 (26): 7598–7609.

- <https://doi.org/10.1016/j.biomaterials.2014.05.032>.
- Hanson, Phyllis I., and Anil Cashikar. 2012. "Multivesicular Body Morphogenesis." *Annual Review of Cell and Developmental Biology* 28 (1): 337–62. <https://doi.org/10.1146/annurev-cellbio-092910-154152>.
- Haraszti, Reka A., Marie Cecile Didiot, Ellen Sapp, John Leszyk, Scott A. Shaffer, Hannah E. Rockwell, Fei Gao, et al. 2016a. "High-Resolution Proteomic and Lipidomic Analysis of Exosomes and Microvesicles from Different Cell Sources." *Journal of Extracellular Vesicles* 5 (1). <https://doi.org/10.3402/jev.v5.32570>.
- . 2016b. "High-Resolution Proteomic and Lipidomic Analysis of Exosomes and Microvesicles from Different Cell Sources." *Journal of Extracellular Vesicles* 5 (1): 1–14. <https://doi.org/10.3402/jev.v5.32570>.
- Haraszti, Reka Agnes, Rachael Miller, Matteo Stoppato, Yves Y. Sere, Andrew Coles, Marie Cecile Didiot, Rachel Wollacott, et al. 2018. "Exosomes Produced from 3D Cultures of MSCs by Tangential Flow Filtration Show Higher Yield and Improved Activity." *Molecular Therapy* 26 (12): 2838–47. <https://doi.org/10.1016/j.ymthe.2018.09.015>.
- Hardij, Julie, Francesca Cecchet, Alexandre Berquand, Damien Gheldof, Christian Chatelain, François Mullier, Bernard Chatelain, and Jean Michel Dogné. 2013. "Characterisation of Tissue Factor-Bearing Extracellular Vesicles with AFM: Comparison of Air-Tapping-Mode AFM and Liquid Peak Force AFM." *Journal of Extracellular Vesicles* 2 (1). <https://doi.org/10.3402/jev.v2i0.21045>.
- Hayflick, L., and P. S. Moorhead. 1961. "The Serial Cultivation of Human Diploid Cell Strains." *Experimental Cell Research* 25 (3): 585–621. [https://doi.org/10.1016/0014-4827\(61\)90192-6](https://doi.org/10.1016/0014-4827(61)90192-6).
- He, Shenghui, and Norman E. Sharpless. 2017. "Senescence in Health and Disease." *Cell* 169 (6): 1000–1011. <https://doi.org/10.1016/j.cell.2017.05.015>.
- Headland, Sarah E., Hefin R. Jones, Adelina S.V. D'Sa, Mauro Perretti, and Lucy V. Norling. 2014. "Cutting-Edge Analysis of Extracellular Microparticles Using Imagestreamx Imaging Flow Cytometry." *Scientific Reports* 4: 1–10. <https://doi.org/10.1038/srep05237>.
- Henne, William Mike, Harald Stenmark, and Scott D Emr. 2013. "Sculpting ESCRT Pathway." *Cold Spring Harbour Perspectives in Biology* 5: a016766.

<https://doi.org/10.1101/cshperspect.a016766>.

- Heusermann, Wolf, Justin Hean, Dominic Trojer, Emmanuelle Steib, Stefan von Bueren, Alexandra Graff-Meyer, Christel Genoud, et al. 2016. “Exosomes Surf on Filopodia to Enter Cells at Endocytic Hot Spots, Traffic within Endosomes, and Are Targeted to the ER.” *Journal of Cell Biology* 213 (2): 173–84. <https://doi.org/10.1083/jcb.201506084>.
- Hikita, Tomoya, Mamiko Miyata, Risayo Watanabe, and Chitose Oneyama. 2018. “Sensitive and Rapid Quantification of Exosomes by Fusing Luciferase to Exosome Marker Proteins.” *Scientific Reports* 8 (1): 1–14. <https://doi.org/10.1038/s41598-018-32535-7>.
- Hill, Andrew F., D. Michiel Pegtel, Ulrike Lambertz, Tommaso Leonardi, Lorraine O’Driscoll, Stefano Pluchino, Dmitry Ter-Ovanesyan, and Esther N.M. Nolte-‘t Hoen. 2013. “ISEV Position Paper: Extracellular Vesicle RNA Analysis and Bioinformatics.” *Journal of Extracellular Vesicles* 2 (1): 22859. <https://doi.org/10.3402/jev.v2i0.22859>.
- Hoshino, Ayuko, Bruno Costa-Silva, Tang-Long Shen, Goncalo Rodrigues, Ayako Hashimoto, Milica Tesic Mark, Henrik Molina, et al. 2015. “Tumour Exosome Integrins Determine Organotropic Metastasis.” *Nature* 527 (7578): 329–35. <https://doi.org/10.1038/nature15756>.
- Hsu, Chieh, Yuichi Morohashi, Shin Ichiro Yoshimura, Natalia Manrique-Hoyos, Sang Yong Jung, Marcel A. Lauterbach, Mostafa Bakhti, et al. 2010. “Regulation of Exosome Secretion by Rab35 and Its GTPase-Activating Proteins TBC1D10A-C.” *Journal of Cell Biology* 189 (2): 223–32. <https://doi.org/10.1083/jcb.200911018>.
- Huang, Ping, Jiarui Bi, Gethin R. Owen, Weimin Chen, Anne Rokka, Leeni Koivisto, Jyrki Heino, Lari Häkkinen, and Hannu Larjava. 2015. “Keratinocyte Microvesicles Regulate the Expression of Multiple Genes in Dermal Fibroblasts.” *Journal of Investigative Dermatology* 135 (12): 3051–59. <https://doi.org/10.1038/jid.2015.320>.
- Hugel, Bénédicte, M. Carmen Martínez, Corinne Kunzelmann, and Jean Marie Freyssinet. 2005. “Membrane Microparticles: Two Sides of the Coin.” *Physiology* 20 (1): 22–27. <https://doi.org/10.1152/physiol.00029.2004>.
- HW, King, Michael MZ, and Gleadle JM. 2012. “Hypoxic Enhancement of Exosome Release by Breast Cancer Cells.” *BMC Cancer* 12: 421. <http://dx.doi.org/10.1186/1471-2407-12-421>.
- Im, Hyungsoon, Huilin Shao, Yong Il Park, Vanessa M. Peterson, Cesar M. Castro, Ralph Weissleder, and Hakho Lee. 2014. “Label-Free Detection and Molecular Profiling of

- Exosomes with a Nano-Plasmonic Sensor.” *Nature Biotechnology* 32 (5): 490–95.
<https://doi.org/10.1038/nbt.2886>.
- Jeon, Ok Hee, David R. Wilson, Cristina C. Clement, Sona Rathod, Christopher Cherry, Bonita Powell, Zhenghong Lee, et al. 2019. “Senescence Cell–Associated Extracellular Vesicles Serve as Osteoarthritis Disease and Therapeutic Markers.” *JCI Insight* 4 (7).
<https://doi.org/10.1172/jci.insight.125019>.
- Jeong, Whun Kim, Eva Wieckowski, Douglas D. Taylor, Torsten E. Reichert, Simon Watkins, and Theresa L. Whiteside. 2005. “Fas Ligand-Positive Membranous Vesicles Isolated from Sera of Patients with Oral Cancer Induce Apoptosis of Activated T Lymphocytes.” *Clinical Cancer Research* 11 (3): 1010–20.
- Johnston, Ian C D, Andreas Bosio, Nikolay Kladt, Susanne Krautha, Astrid Schauss, and Stefan Wild. 2016. “A Novel Multiplex Bead-Based Platform Highlights the Diversity of Extracellular Vesicles” 1 (17): 1–15.
- Johnstone, R. M., M. Adam, J. R. Hammond, L. Orr, and C. Turbide. 1987. “Vesicle Formation during Reticulocyte Maturation. Association of Plasma Membrane Activities with Released Vesicles (Exosomes).” *Journal of Biological Chemistry* 262 (19): 9412–20.
- Kalra, Hina, Richard J. Simpson, Hong Ji, Elena Aikawa, Peter Altevogt, Philip Askenase, Vincent C. Bond, et al. 2012. “Vesiclepedia: A Compendium for Extracellular Vesicles with Continuous Community Annotation.” *PLoS Biology* 10 (12): 8–12.
<https://doi.org/10.1371/journal.pbio.1001450>.
- Kamerkar, Sushrut, Valerie S. Lebleu, Hikaru Sugimoto, Sujuan Yang, Carolina F. Ruivo, Sonia A. Melo, J. Jack Lee, and Raghu Kalluri. 2017. “Exosomes Facilitate Therapeutic Targeting of Oncogenic KRAS in Pancreatic Cancer.” *Nature* 546 (7659): 498–503.
<https://doi.org/10.1038/nature22341>.
- Karlsson, Malin, Samuel Lundin, Ulf Dahlgren, Helena Kahu, Inger Pettersson, and Esbjörn Telemo. 2001. “‘Tolerosomes’ Are Produced by Intestinal Epithelial Cells.” *European Journal of Immunology* 31 (10): 2892–2900. [https://doi.org/10.1002/1521-4141\(2001010\)31:10<2892::AID-IMMU2892>3.0.CO;2-I](https://doi.org/10.1002/1521-4141(2001010)31:10<2892::AID-IMMU2892>3.0.CO;2-I).
- Katzmann, David J., Markus Babst, and Scott D. Emr. 2001. “Ubiquitin-Dependent Sorting into the Multivesicular Body Pathway Requires the Function of a Conserved Endosomal Protein

- Sorting Complex, ESCRT-I.” *Cell* 106 (2): 145–55. [https://doi.org/10.1016/S0092-8674\(01\)00434-2](https://doi.org/10.1016/S0092-8674(01)00434-2).
- Keerthikumar, Shivakumar, David Chisanga, Dinuka Ariyaratne, Haidar Al Saffar, Sushma Anand, Kening Zhao, Monisha Samuel, et al. 2016. “ExoCarta: A Web-Based Compendium of Exosomal Cargo.” *Journal of Molecular Biology* 428 (4): 688–92. <https://doi.org/10.1016/j.jmb.2015.09.019>.
- Kim, Dae Kyum, Byeongsoo Kang, Oh Youn Kim, Dong Sic Choi, Jaewook Lee, Sae Rom Kim, Gyeongyun Go, et al. 2013. “EVpedia: An Integrated Database of High-Throughput Data for Systemic Analyses of Extracellular Vesicles.” *Journal of Extracellular Vesicles* 2 (1). <https://doi.org/10.3402/jev.v2i0.20384>.
- Kim, Nayoun, and Seok Goo Cho. 2015. “New Strategies for Overcoming Limitations of Mesenchymal Stem Cell-Based Immune Modulation.” *International Journal of Stem Cells* 8 (1): 54–68. <https://doi.org/10.15283/ijsc.2015.8.1.54>.
- Kinloch, Andrew, Karin Lundberg, Robin Wait, Natalia Wegner, Han Lim Ngee, Albert J.W. Zendman, Tore Saxne, Vivianne Malmström, and Patrick J. Venables. 2008. “Synovial Fluid Is a Site of Citrullination of Autoantigens in Inflammatory Arthritis.” *Arthritis and Rheumatism* 58 (8): 2287–95. <https://doi.org/10.1002/art.23618>.
- Kojima, Ryosuke, Daniel Bojar, Giorgio Rizzi, Ghislaine Charpin El Hamri, Marie Daoud El-Baba, Pratik Saxena, Simon Ausländer, Kelly R. Tan, and Martin Fussenegger. 2018. “Designer Exosomes Produced by Implanted Cells Intracerebrally Deliver Therapeutic Cargo for Parkinson’s Disease Treatment.” *Nature Communications* 9 (1). <https://doi.org/10.1038/s41467-018-03733-8>.
- Koliha, Nina, Yvonne Wiencek, Ute Heider, Christian Jüngst, Nikolay Kladt, Susanne Krauthäuser, Ian C.D. Johnston, Andreas Bosio, Astrid Schauss, and Stefan Wild. 2016. “A Novel Multiplex Bead-Based Platform Highlights the Diversity of Extracellular Vesicles.” *Journal of Extracellular Vesicles* 5 (1). <https://doi.org/10.3402/jev.v5.29975>.
- Kooijmans, Sander A.A., Stephan Stremersch, Kevin Braeckmans, Stefaan C. De Smedt, An Hendrix, Matthew J.A. Wood, Raymond M. Schiffelers, Koen Raemdonck, and Pieter Vader. 2013. “Electroporation-Induced SiRNA Precipitation Obscures the Efficiency of SiRNA Loading into Extracellular Vesicles.” *Journal of Controlled Release* 172 (1): 229–

38. <https://doi.org/10.1016/j.jconrel.2013.08.014>.
- Kooijmans, Sander A.A., Pieter Vader, and Raymond M. Schiffelers. 2017. "Tumour-Bound RNA-Laden Exosomes." *Nature Biomedical Engineering* 1 (8): 634–36.
<https://doi.org/10.1038/s41551-017-0119-4>.
- Kordelas, L., V. Rebmann, A. K. Ludwig, S. Radtke, J. Ruesing, T. R. Doepfner, M. Epple, P. A. Horn, D. W. Beelen, and B. Giebel. 2014. "MSC-Derived Exosomes: A Novel Tool to Treat Therapy-Refractory Graft-versus-Host Disease." *Leukemia* 28 (4): 970–73.
<https://doi.org/10.1038/leu.2014.41>.
- Kosaka, Nobuyoshi, Haruhisa Iguchi, Yusuke Yoshioka, Fumitaka Takeshita, Yasushi Matsuki, and Takahiro Ochiya. 2010. "Secretory Mechanisms and Intercellular Transfer of MicroRNAs in Living Cells." *Journal of Biological Chemistry* 285 (23): 17442–52.
<https://doi.org/10.1074/jbc.M110.107821>.
- Kossinova, Olga A., Alexander V. Gopanenko, Svetlana N. Tamkovich, Olga A. Krasheninina, Alexey E. Tupikin, Elena Kiseleva, Darya D. Yanshina, et al. 2017. "Cytosolic YB-1 and NSUN2 Are the Only Proteins Recognizing Specific Motifs Present in MRNAs Enriched in Exosomes." *Biochimica et Biophysica Acta - Proteins and Proteomics* 1865 (6): 664–73.
<https://doi.org/10.1016/j.bbapap.2017.03.010>.
- Kowal, Joanna, Guillaume Arras, Marina Colombo, Mabel Jouve, Jakob Paul Morath, Bjarke Primdal-Bengtson, Florent Dingli, Damarys Loew, Mercedes Tkach, and Clotilde Théry. 2016. "Proteomic Comparison Defines Novel Markers to Characterize Heterogeneous Populations of Extracellular Vesicle Subtypes." *Proceedings of the National Academy of Sciences of the United States of America* 113 (8): E968–77.
<https://doi.org/10.1073/pnas.1521230113>.
- Kreimer, Simion, Arseniy M. Belov, Ionita Ghiran, Shashi K. Murthy, David A. Frank, and Alexander R. Ivanov. 2015. "Mass-Spectrometry-Based Molecular Characterization of Extracellular Vesicles: Lipidomics and Proteomics." *Journal of Proteome Research* 14 (6): 2367–84. <https://doi.org/10.1021/pr501279t>.
- Krishnamurthy, Janakiraman, Lishan Su, Norman E Sharpless, Chad Torrice, Matthew R Ramsey, Grigoriy I Kovalev, and Khalid Al-Regaiey. 2004. "Ink4a/Arf Expression Is a Biomarker of Aging Find the Latest Version." *The Journal of Clinical Investigation* 114 (9):

- 1299–1307. <https://doi.org/10.1172/JCI22475>.
- Krtolica, Ana, Simona Parrinello, Stephen Lockett, Pierre Yves Desprez, and Judith Campisi. 2001. “Senescent Fibroblasts Promote Epithelial Cell Growth and Tumorigenesis: A Link between Cancer and Aging.” *Proceedings of the National Academy of Sciences of the United States of America* 98 (21): 12072–77. <https://doi.org/10.1073/pnas.211053698>.
- Kucharzewska, Paulina, Helena C. Christianson, Johanna E. Welch, Katrin J. Svensson, Erik Fredlund, Markus Ringnér, Matthias Mörgelin, Erika Bourseau-Guilmain, Johan Bengzon, and Mattias Belting. 2013. “Exosomes Reflect the Hypoxic Status of Glioma Cells and Mediate Hypoxia-Dependent Activation of Vascular Cells during Tumor Development.” *Proceedings of the National Academy of Sciences of the United States of America* 110 (18): 7312–17. <https://doi.org/10.1073/pnas.1220998110>.
- Kuffler, Damien P. 1990. “Long- term Survival and Sprouting in Culture by Motoneurons Isolated from the Spinal Cord of Adult Frogs.” *Journal of Comparative Neurology* 302 (4): 729–38. <https://doi.org/10.1002/cne.903020405>.
- Kuilman, Thomas, Chrysiis Michaloglou, Wolter J. Mooi, and Daniel S. Peeper. 2010. “The Essence of Senescence.” *Genes and Development* 24 (22): 2463–79. <https://doi.org/10.1101/gad.1971610>.
- Lai, Charles P., Osama Mardini, Maria Ericsson, Shilpa Prabhakar, Casey A. Maguire, John W. Chen, Bakhos A. Tannous, and Xandra O. Breakefield. 2014. “Dynamic Biodistribution of Extracellular Vesicles *in vivo* Using a Multimodal Imaging Reporter.” *ACS Nano* 8 (1): 483–94. <https://doi.org/10.1021/nn404945r>.
- Lai, Charles P, Edward Y Kim, Christian E Badr, Ralph Weissleder, Thorsten R Mempel, Bakhos A Tannous, and Xandra O Breakefield. 2015. “Multiplexed Reporters.” *Nature Communications* 6 (May): 1–12. <https://doi.org/10.1038/ncomms8029>.
- Lai, Ruenn Chai, Fatih Arslan, May May Lee, Newman Siu Kwan Sze, Andre Choo, Tian Sheng Chen, Manuel Salto-Tellez, et al. 2010. “Exosome Secreted by MSC Reduces Myocardial Ischemia/Reperfusion Injury.” *Stem Cell Research* 4 (3): 214–22. <https://doi.org/10.1016/j.scr.2009.12.003>.
- Lamichhane, Tek N., Anjana Jeyaram, Divya B. Patel, Babita Parajuli, Natalie K. Livingston, Navein Arumugasaamy, John S. Schardt, and Steven M. Jay. 2016. “Oncogene Knockdown

- via Active Loading of Small RNAs into Extracellular Vesicles by Sonication.” *Cellular and Molecular Bioengineering* 9 (3): 315–24. <https://doi.org/10.1007/s12195-016-0457-4>.
- Lämmermann, Ingo, Lucia Terlecki-Zaniewicz, Regina Weinmüllner, Markus Schosserer, Hanna Dellago, André Dargen de Matos Branco, Dominik Autheried, et al. 2018. “Blocking Negative Effects of Senescence in Human Skin Fibroblasts with a Plant Extract.” *Npj Aging and Mechanisms of Disease* 4 (1). <https://doi.org/10.1038/s41514-018-0023-5>.
- Lamparski, Henry G., Anita Metha-Damani, Jenq Yuan Yao, Sanjay Patel, Di Hwei Hsu, Curtis Ruegg, and Jean Bernard Le Pecq. 2002. “Production and Characterization of Clinical Grade Exosomes Derived from Dendritic Cells.” *Journal of Immunological Methods* 270 (2): 211–26. [https://doi.org/10.1016/S0022-1759\(02\)00330-7](https://doi.org/10.1016/S0022-1759(02)00330-7).
- Lannigan, Joanne, and Uta Erdbruegger. 2017. “Imaging Flow Cytometry for the Characterization of Extracellular Vesicles.” *Methods* 112: 55–67. <https://doi.org/10.1016/j.ymeth.2016.09.018>.
- Laulagnier, Karine, David Grand, Arnaud Dujardin, Safouane Hamdi, H  l  ne Vincent-Schneider, Danielle Lankar, Jean Pierre Salles, Christian Bonnerot, Bertrand Perret, and Michel Record. 2004. “PLD2 Is Enriched on Exosomes and Its Activity Is Correlated to the Release of Exosomes.” *FEBS Letters* 572 (1–3): 11–14. <https://doi.org/10.1016/j.febslet.2004.06.082>.
- Laulagnier, Karine, Charlotte Javalet, Fiona J. Hemming, Mathilde Chivet, Ga  lle Lachenal, B  atrice Blot, Christine Chatellard, and R  my Sadoul. 2018. “Amyloid Precursor Protein Products Concentrate in a Subset of Exosomes Specifically Endocytosed by Neurons.” *Cellular and Molecular Life Sciences* 75 (4): 757–73. <https://doi.org/10.1007/s00018-017-2664-0>.
- Lawrie, A. S., A. Albanyan, R. A. Cardigan, I. J. MacKie, and P. Harrison. 2009. “Microparticle Sizing by Dynamic Light Scattering in Fresh-Frozen Plasma.” *Vox Sanguinis* 96 (3): 206–12. <https://doi.org/10.1111/j.1423-0410.2008.01151.x>.
- Lee, Ji Yong, and Han Soo Kim. 2017. “Extracellular Vesicles in Neurodegenerative Diseases: A Double-Edged Sword.” *Tissue Engineering and Regenerative Medicine* 14 (6): 667–78. <https://doi.org/10.1007/s13770-017-0090-x>.
- Lehmann, Brian D., Matthew S. Paine, Adam M. Brooks, James A. McCubrey, Randall H.

- Renegar, Rong Wang, and David M. Terrian. 2008. "Senescence-Associated Exosome Release from Human Prostate Cancer Cells." *Cancer Research* 68 (19): 7864–71. <https://doi.org/10.1158/0008-5472.CAN-07-6538>.
- Lener, Thomas, Mario Gimona, Ludwig Aigner, Verena Börger, Edit Buzas, Giovanni Camussi, Nathalie Chaput, et al. 2015. "Applying Extracellular Vesicles Based Therapeutics in Clinical Trials - An ISEV Position Paper." *Journal of Extracellular Vesicles* 4 (1). <https://doi.org/10.3402/jev.v4.30087>.
- Li, B., M. A. Antonyak, J. Zhang, and R. A. Cerione. 2012. "RhoA Triggers a Specific Signaling Pathway That Generates Transforming Microvesicles in Cancer Cells." *Oncogene* 31 (45): 4740–49. <https://doi.org/10.1038/onc.2011.636>.
- Liang, Kuo, Lisi Wei, and Liangyi Chen. 2017. "Exocytosis, Endocytosis, and Their Coupling in Excitable Cells." *Frontiers in Molecular Neuroscience* 10 (April): 1–10. <https://doi.org/10.3389/fnmol.2017.00109>.
- Liégeois, Samuel, Alexandre Benedetto, Jean Marie Garnier, Yannick Schwab, and Michel Labouesse. 2006. "The V0-ATPase Mediates Apical Secretion of Exosomes Containing Hedgehog-Related Proteins in *Caenorhabditis Elegans*." *Journal of Cell Biology* 173 (6): 949–61. <https://doi.org/10.1083/jcb.200511072>.
- Linares, Romain, Sisareuth Tan, Céline Gounou, Nicolas Arraud, and Alain R. Brisson. 2015. "High-Speed Centrifugation Induces Aggregation of Extracellular Vesicles." *Journal of Extracellular Vesicles* 4 (1): 1–7. <https://doi.org/10.3402/jev.v4.29509>.
- Linares, Romain, Sisareuth Tan, Céline Gounou, and Alain R Brisson. 2014. "Exosomes and Microvesicles: Methods and Protocols" 1545: 139–76. <https://doi.org/10.1007/978-1-4939-6728-5>.
- Liu, Liang, Xian Jin, Cui Fen Hu, Rong Li, Zhong'e Zhou, and Cheng Xing Shen. 2017. "Exosomes Derived from Mesenchymal Stem Cells Rescue Myocardial Ischaemia/Reperfusion Injury by Inducing Cardiomyocyte Autophagy Via AMPK and Akt Pathways." *Cellular Physiology and Biochemistry* 43 (1): 52–68. <https://doi.org/10.1159/000480317>.
- Llorente, Alicia, Tore Skotland, Tuulia Sylvänne, Dimple Kauhanen, Tomasz Róg, Adam Orłowski, Ilpo Vattulainen, Kim Ekroos, and Kirsten Sandvig. 2013. "Molecular

- Lipidomics of Exosomes Released by PC-3 Prostate Cancer Cells.” *Biochimica et Biophysica Acta - Molecular and Cell Biology of Lipids* 1831 (7): 1302–9.
<https://doi.org/10.1016/j.bbalip.2013.04.011>.
- Lobb, Richard, and Andreas Mo. 2017. “Extracellular Vesicles: Methods and Protocols, Methods in Molecular Biology” 1660: 105–10. <https://doi.org/10.1007/978-1-4939-7253-1>.
- Logan, M. R., P. Lacy, S. O. Odemuyiwa, M. Steward, F. Davoine, H. Kita, and R. Moqbel. 2006. “A Critical Role for Vesicle-Associated Membrane Protein-7 in Exocytosis from Human Eosinophils and Neutrophils.” *Allergy: European Journal of Allergy and Clinical Immunology* 61 (6): 777–84. <https://doi.org/10.1111/j.1398-9995.2006.01089.x>.
- López-otín, Carlos, Maria A Blasco, Linda Partridge, Manuel Serrano, and Guido Kroemer. 2013. “The Hallmarks of Aging Longevity.” *Cell* 153 (6): 1194–1217.
<https://doi.org/10.1016/j.cell.2013.05.039>.The.
- Lötvall, Jan, Andrew F. Hill, Fred Hochberg, Edit I. Buzás, Dolores Di Vizio, Christopher Gardiner, Yong Song Gho, et al. 2014. “Minimal Experimental Requirements for Definition of Extracellular Vesicles and Their Functions: A Position Statement from the International Society for Extracellular Vesicles.” *Journal of Extracellular Vesicles* 3 (1): 1–6.
<https://doi.org/10.3402/jev.v3.26913>.
- Loughmiller, Jim, and Gary Klintworth. 2011. “For the Records.” *Nature Biotechnology* 29 (4): 306–9. <https://doi.org/10.1038/nbt.1807>.
- Luga, Valbona, Liang Zhang, Alicia M. Vilorio-Petit, Abiodun A. Ogunjimi, Mohammad R. Inanlou, Elaine Chiu, Marguerite Buchanan, Abdel Nasser Hosein, Mark Basik, and Jeffrey L. Wrana. 2012. “Exosomes Mediate Stromal Mobilization of Autocrine Wnt-PCP Signaling in Breast Cancer Cell Migration.” *Cell* 151 (7): 1542–56.
<https://doi.org/10.1016/j.cell.2012.11.024>.
- Ma, Liang, Ying Li, Junya Peng, Danni Wu, Xiaoxin Zhao, Yitong Cui, Lilian Chen, Xiaojun Yan, Yanan Du, and Li Yu. 2015. “Discovery of the Migrasome, an Organelle Mediating Release of Cytoplasmic Contents during Cell Migration.” *Cell Research* 25 (1): 24–38.
<https://doi.org/10.1038/cr.2014.135>.
- Maejima, Yasuhiro, Susumu Adachi, Hiroshi Ito, Kenzo Hirao, and Mitsuaki Isobe. 2008. “Induction of Premature Senescence in Cardiomyocytes by Doxorubicin as a Novel

- Mechanism of Myocardial Damage.” *Aging Cell* 7 (2): 125–36.
<https://doi.org/10.1111/j.1474-9726.2007.00358.x>.
- Magdalena Derbis, Marta Szajnik. 2012. “Exosomes in Plasma of Patients with Ovarian Carcinoma: Potential Biomarkers of Tumor Progression and Response to Therapy.” *Gynecology & Obstetrics* s4 (1): 1–7. <https://doi.org/10.4172/2161-0932.S4-003>.
- Maguire, Casey A., Leonora Balaj, Sarada Sivaraman, Matheus H.W. Crommentuijn, Maria Ericsson, Lucia Mincheva-Nilsson, Vladimir Baranov, et al. 2012. “Microvesicle-Associated AAV Vector as a Novel Gene Delivery System.” *Molecular Therapy* 20 (5): 960–71. <https://doi.org/10.1038/mt.2011.303>.
- Maguire, Ciaran M., Katherine Sillence, Matthias Roesslein, Claire Hannell, Guillaume Suarez, Jean Jacques Sauvain, Sonja Capracotta, et al. 2017. “Benchmark of Nanoparticle Tracking Analysis on Measuring Nanoparticle Sizing and Concentration.” *Journal of Micro and Nano-Manufacturing* 5 (4). <https://doi.org/10.1115/1.4037124>.
- Mallegol, Julia, Guillaume Van Niel, Corinne Lebreton, Yves Lepelletier, Céline Candalh, Christophe Dugave, Joan K. Heath, Graça Raposo, Nadine Cerf-Bensussan, and Martine Heyman. 2007. “T84-Intestinal Epithelial Exosomes Bear MHC Class II/Peptide Complexes Potentiating Antigen Presentation by Dendritic Cells.” *Gastroenterology* 132 (5): 1866–76. <https://doi.org/10.1053/j.gastro.2007.02.043>.
- Mathivanan, Suresh, Cassie J. Fahner, Gavin E. Reid, and Richard J. Simpson. 2012. “ExoCarta 2012: Database of Exosomal Proteins, RNA and Lipids.” *Nucleic Acids Research* 40 (D1): 1241–44. <https://doi.org/10.1093/nar/gkr828>.
- Mathivanan, Suresh, Hong Ji, and Richard J. Simpson. 2010. “Exosomes: Extracellular Organelles Important in Intercellular Communication.” *Journal of Proteomics* 73 (10): 1907–20. <https://doi.org/10.1016/j.jprot.2010.06.006>.
- Mathivanan, Suresh, and Richard J. Simpson. 2009. “ExoCarta: A Compendium of Exosomal Proteins and RNA.” *Proteomics* 9 (21): 4997–5000.
<https://doi.org/10.1002/pmic.200900351>.
- Mattila, Pieta K., Christoph Feest, David Depoil, Bebhinn Treanor, Beatriz Montaner, Kevin L. Otipoby, Robert Carter, Louis B. Justement, Andreas Bruckbauer, and Facundo D. Batista. 2013. “The Actin and Tetraspanin Networks Organize Receptor Nanoclusters to Regulate B

- Cell Receptor-Mediated Signaling.” *Immunity* 38 (3): 461–74.
<https://doi.org/10.1016/j.immuni.2012.11.019>.
- McNamara, Ryan P., Carolina P. Caro-Vegas, Lindsey M. Costantini, Justin T. Landis, Jack D. Griffith, Blossom A. Damania, and Dirk P. Dittmer. 2018. “Large-Scale, Cross-Flow Based Isolation of Highly Pure and Endocytosis-Competent Extracellular Vesicles.” *Journal of Extracellular Vesicles* 7 (1). <https://doi.org/10.1080/20013078.2018.1541396>.
- Meliani, Amine, Florence Boisgerault, Zachary Fitzpatrick, Solenne Marmier, Christian Leborgne, Fanny Collaud, Marcelo Simon Sola, et al. 2017. “Enhanced Liver Gene Transfer and Evasion of Preexisting Humoral Immunity with Exosome-Enveloped AAV Vectors.” *Blood Advances* 1 (23): 2019–31. <https://doi.org/10.1182/bloodadvances.2017010181>.
- Melo, Sonia A., Linda B. Luecke, Christoph Kahlert, Agustin F. Fernandez, Seth T. Gammon, Judith Kaye, Valerie S. LeBleu, et al. 2015. “Glypican-1 Identifies Cancer Exosomes and Detects Early Pancreatic Cancer.” *Nature* 523 (7559): 177–82.
<https://doi.org/10.1038/nature14581>.
- Mendt, Mayela, Sushrut Kamerkar, Hikaru Sugimoto, Kathleen M. McAndrews, Chia Chin Wu, Mihai Gagea, Sujuan Yang, et al. 2018. “Generation and Testing of Clinical-Grade Exosomes for Pancreatic Cancer.” *JCI Insight* 3 (8).
<https://doi.org/10.1172/jci.insight.99263>.
- Merchant, Michael L., David W. Powell, Daniel W. Wilkey, Timothy D. Cummins, Jeroen K. Deegens, Ilse M. Rood, K. Jill McAfee, Cornelia Fleischer, Elias Klein, and Jon B. Klein. 2010. “Microfiltration Isolation of Human Urinary Exosomes for Characterization by MS.” *Proteomics - Clinical Applications* 4 (1): 84–96. <https://doi.org/10.1002/prca.200800093>.
- Micco, Raffaella Di, Marzia Fumagalli, Angelo Cicalese, Sara Piccinin, Patrizia Gasparini, Chiara Luise, Catherine Schurra, et al. 2006. “Oncogene-Induced Senescence Is a DNA Damage Response Triggered by DNA Hyper-Replication.” *Nature* 444 (7119): 638–42.
<https://doi.org/10.1038/nature05327>.
- Mittelbrunn, María, Cristina Gutiérrez-Vázquez, Carolina Villarroya-Beltri, Susana González, Fátima Sánchez-Cabo, Manuel Ángel González, Antonio Bernad, and Francisco Sánchez-Madrid. 2011. “Unidirectional Transfer of MicroRNA-Loaded Exosomes from T Cells to Antigen-Presenting Cells.” *Nature Communications* 2 (1).

<https://doi.org/10.1038/ncomms1285>.

- Miyanishi, Masanori, Kazutoshi Tada, Masato Koike, Yasuo Uchiyama, Toshio Kitamura, and Shigekazu Nagata. 2007. "Identification of Tim4 as a Phosphatidylserine Receptor." *Nature* 450 (7168): 435–39. <https://doi.org/10.1038/nature06307>.
- Mizrak, Arda, Mehmet Fatih Bolukbasi, Gokhan Baris Ozdener, Gary J. Brenner, Sibylle Madlener, Erdogan Pekcan Erkan, Thomas Ströbel, Xandra O. Breakefield, and Okay Saydam. 2013. "Genetically Engineered Microvesicles Carrying Suicide mRNA/Protein Inhibit Schwannoma Tumor Growth." *Molecular Therapy* 21 (1): 101–8. <https://doi.org/10.1038/mt.2012.161>.
- Morelli, Adrian E., Adriana T. Larregina, William J. Shufesky, Mara L.G. Sullivan, Donna Beer Stolz, Glenn D. Papworth, Alan F. Zahorchak, et al. 2004. "Endocytosis, Intracellular Sorting, and Processing of Exosomes by Dendritic Cells." *Blood* 104 (10): 3257–66. <https://doi.org/10.1182/blood-2004-03-0824>.
- Morse, Michael A., Jennifer Garst, Takuya Osada, Shubi Khan, Amy Hobeika, Timothy M. Clay, Nancy Valente, et al. 2005. "A Phase I Study of Dexosome Immunotherapy in Patients with Advanced Non-Small Cell Lung Cancer." *Journal of Translational Medicine* 3: 1–8. <https://doi.org/10.1186/1479-5876-3-9>.
- Muñoz- Espín, Daniel, Miguel Rovira, Irene Galiana, Cristina Giménez, Beatriz Lozano-Torres, Marta Paez- Ribes, Susana Llanos, et al. 2018. "A Versatile Drug Delivery System Targeting Senescent Cells." *EMBO Molecular Medicine* 10 (9): 1–18. <https://doi.org/10.15252/emmm.201809355>.
- Muralidharan-Chari, Vandhana, James Clancy, Carolyn Plou, Maryse Romao, Philippe Chavrier, Graca Raposo, and Crislyn D'Souza-Schorey. 2009. "ARF6-Regulated Shedding of Tumor Cell-Derived Plasma Membrane Microvesicles." *Current Biology* 19 (22): 1875–85. <https://doi.org/10.1016/j.cub.2009.09.059>.
- Nabhan, Joseph F., Ruoxi Hu, Raymond S. Oh, Stanley N. Cohen, and Quan Lu. 2012. "Formation and Release of Arrestin Domain-Containing Protein 1-Mediated Microvesicles (ARMMs) at Plasma Membrane by Recruitment of TSG101 Protein." *Proceedings of the National Academy of Sciences of the United States of America* 109 (11): 4146–51. <https://doi.org/10.1073/pnas.1200448109>.

- Nakai, Wataru, Takeshi Yoshida, Diego Diez, Yuji Miyatake, Takahiro Nishibu, Naoko Imawaka, Ken Naruse, Yoshifusa Sadamura, and Rikinari Hanayama. 2016. "A Novel Affinity-Based Method for the Isolation of Highly Purified Extracellular Vesicles." *Scientific Reports* 6 (June): 1–11. <https://doi.org/10.1038/srep33935>.
- Nanbo, A., E. Kawanishi, R. Yoshida, and H. Yoshiyama. 2013. "Exosomes Derived from Epstein-Barr Virus-Infected Cells Are Internalized via Caveola-Dependent Endocytosis and Promote Phenotypic Modulation in Target Cells." *Journal of Virology* 87 (18): 10334–47. <https://doi.org/10.1128/jvi.01310-13>.
- Nanou, Afroditi, Mateus Crespo, Penny Flohr, Johann S. De Bono, and Leon W.M.M. Terstappen. 2018. "Scanning Electron Microscopy of Circulating Tumor Cells and Tumor-Derived Extracellular Vesicles." *Cancers* 10 (11): 1–17. <https://doi.org/10.3390/cancers10110416>.
- Nassar, Wael, Mervat El-Ansary, Dina Sabry, Mostafa A. Mostafa, Tarek Fayad, Esam Kotb, Mahmoud Temraz, Abdel Naser Saad, Wael Essa, and Heba Adel. 2016. "Umbilical Cord Mesenchymal Stem Cells Derived Extracellular Vesicles Can Safely Ameliorate the Progression of Chronic Kidney Diseases." *Biomaterials Research* 20 (1): 1–11. <https://doi.org/10.1186/s40824-016-0068-0>.
- Nazarenko, Irina, Sanyukta Rana, Alexandra Baumann, Jessica McAlear, Andrea Hellwig, Michael Trendelenburg, Günter Lochnit, Klaus T. Preissner, and Margot Zöller. 2010. "Cell Surface Tetraspanin Tspan8 Contributes to Molecular Pathways of Exosome-Induced Endothelial Cell Activation." *Cancer Research* 70 (4): 1668–78. <https://doi.org/10.1158/0008-5472.CAN-09-2470>.
- Németh, Andrea, Norbert Orgovan, Barbara W. Sódar, Xabier Osteikoetxea, Krisztina Pálóczi, Katalin Szabó-Taylor, Krisztina V. Vukman, et al. 2017. "Antibiotic-Induced Release of Small Extracellular Vesicles (Exosomes) with Surface-Associated DNA." *Scientific Reports* 7 (1): 1–16. <https://doi.org/10.1038/s41598-017-08392-1>.
- Niel, Guillaume van, Stéphanie Charrin, Sabrina Simoes, Maryse Romao, Leila Rochin, Paul Saftig, Michael S. Marks, Eric Rubinstein, and Graça Raposo. 2011. "The Tetraspanin CD63 Regulates ESCRT-Independent and -Dependent Endosomal Sorting during Melanogenesis." *Developmental Cell* 21 (4): 708–21.

- <https://doi.org/10.1016/j.devcel.2011.08.019>.
- Nolan, John P., and Jennifer C. Jones. 2017. "Detection of Platelet Vesicles by Flow Cytometry." *Platelets* 28 (3): 256–62. <https://doi.org/10.1080/09537104.2017.1280602>.
- Nolte T Hoen, Esther N.M., Henk P.J. Buermans, Maaïke Waasdorp, Willem Stoorvogel, Marca H.M. Wauben, and Peter A.C. 'T Hoen. 2012. "Deep Sequencing of RNA from Immune Cell-Derived Vesicles Uncovers the Selective Incorporation of Small Non-Coding RNA Biotypes with Potential Regulatory Functions." *Nucleic Acids Research* 40 (18): 9272–85. <https://doi.org/10.1093/nar/gks658>.
- Nordin, Joel Z., Yi Lee, Pieter Vader, Imre Mäger, Henrik J. Johansson, Wolf Heusermann, Oscar P.B. Wiklander, et al. 2015. "Ultrafiltration with Size-Exclusion Liquid Chromatography for High Yield Isolation of Extracellular Vesicles Preserving Intact Biophysical and Functional Properties." *Nanomedicine: Nanotechnology, Biology, and Medicine* 11 (4): 879–83. <https://doi.org/10.1016/j.nano.2015.01.003>.
- Ohno, Shin Ichiro, Masakatsu Takanashi, Katsuko Sudo, Shinobu Ueda, Akio Ishikawa, Nagahisa Matsuyama, Koji Fujita, et al. 2013. "Systemically Injected Exosomes Targeted to EGFR Deliver Antitumor Microrna to Breast Cancer Cells." *Molecular Therapy* 21 (1): 185–91. <https://doi.org/10.1038/mt.2012.180>.
- Ong, Sang-Ging, and Joseph C Wu. 2015. "Exosomes as Potential Alternatives to Stem Cell Therapy in Mediating Cardiac Regeneration." *Circulation Research* 117 (1): 7–9. <https://doi.org/10.1161/CIRCRESAHA.115.306593>.
- Ostrowski, Matias, Nuno B. Carmo, Sophie Krumeich, Isabelle Fanget, Graça Raposo, Ariel Savina, Catarina F. Moita, et al. 2010. "Rab27a and Rab27b Control Different Steps of the Exosome Secretion Pathway." *Nature Cell Biology* 12 (1): 19–30. <https://doi.org/10.1038/ncb2000>.
- Palmieri, Valentina, Donatella Lucchetti, Ilaria Gatto, Alessandro Maiorana, Margherita Marcantoni, Giuseppe Maulucci, Massimiliano Papi, Roberto Pola, Marco De Spirito, and Alessandro Sgambato. 2014. "Dynamic Light Scattering for the Characterization and Counting of Extracellular Vesicles: A Powerful Noninvasive Tool." *Journal of Nanoparticle Research* 16 (9). <https://doi.org/10.1007/s11051-014-2583-z>.
- Palmisano, Giuseppe, Søren Skov Jensen, Marie Catherine Le Bihan, Jeanne Lainé, James N.

- McGuire, Flemming Pociot, and Martin Røssel Larsen. 2012. "Characterization of Membrane-Shed Microvesicles from Cytokine-Stimulated β -Cells Using Proteomics Strategies." *Molecular and Cellular Proteomics* 11 (8): 230–43.
<https://doi.org/10.1074/mcp.M111.012732>.
- Park, Yong Hyun, Hyun Woo Shin, Ae Ryang Jung, Oh Sung Kwon, Yeong Jin Choi, Jaesung Park, and Ji Youl Lee. 2016. "Prostate-Specific Extracellular Vesicles as a Novel Biomarker in Human Prostate Cancer." *Scientific Reports* 6: 1–9.
<https://doi.org/10.1038/srep30386>.
- Patel, Girijesh Kumar, Mohammad Aslam Khan, Haseeb Zubair, Sanjeev Kumar Srivastava, Moh'd Khushman, Seema Singh, and Ajay Pratap Singh. 2019. "Comparative Analysis of Exosome Isolation Methods Using Culture Supernatant for Optimum Yield, Purity and Downstream Applications." *Scientific Reports* 9 (1): 1–10. <https://doi.org/10.1038/s41598-019-41800-2>.
- Pecq, Jean Bernard Le. 2005. "Dexosomes as a Therapeutic Cancer Vaccine: From Bench to Bedside." *Blood Cells, Molecules, and Diseases* 35 (2): 129–35.
<https://doi.org/10.1016/j.bcmed.2005.06.003>.
- Peinado, Héctor, Maša Alečković, Simon Lavotshkin, Irina Matei, Bruno Costa-Silva, Gema Moreno-Bueno, Marta Hergueta-Redondo, et al. 2012a. "Melanoma Exosomes Educate Bone Marrow Progenitor Cells toward a Pro-Metastatic Phenotype through MET." *Nature Medicine* 18 (6): 883–91. <https://doi.org/10.1038/nm.2753>.
- . 2012b. "Melanoma Exosomes Educate Bone Marrow Progenitor Cells toward a Pro-Metastatic Phenotype through MET." *Nature Medicine* 18 (6): 883–91.
<https://doi.org/10.1038/nm.2753>.
- Petersen, Kevin E., Eliana Manangon, Joshua L. Hood, Samuel A. Wickline, Diego P. Fernandez, William P. Johnson, and Bruce K. Gale. 2014. "A Review of Exosome Separation Techniques and Characterization of B16-F10 Mouse Melanoma Exosomes with AF4-UV-MALS-DLS-TEM." *Analytical and Bioanalytical Chemistry* 406 (30): 7855–66.
<https://doi.org/10.1007/s00216-014-8040-0>.
- Piper, Robert C, and David J Katzmann. 2010. "Biogenesis and Function of MVBs." *Annual Review of Cell and Developmental Biology* 23: 519–47.

- <https://doi.org/10.1146/annurev.cellbio.23.090506.123319>.Biogenesis.
- Pol, E. Van Der, M. J.C. Van Gemert, A. Sturk, R. Nieuwland, and T. G. Van Leeuwen. 2012. “Single vs. Swarm Detection of Microparticles and Exosomes by Flow Cytometry.” *Journal of Thrombosis and Haemostasis* 10 (5): 919–30. <https://doi.org/10.1111/j.1538-7836.2012.04683.x>.
- Pol, E. Van Der, A. G. Hoekstra, A. Sturk, C. Otto, T. G. Van Leeuwen, and R. Nieuwland. 2010. “Optical and Non-Optical Methods for Detection and Characterization of Microparticles and Exosomes.” *Journal of Thrombosis and Haemostasis* 8 (12): 2596–2607. <https://doi.org/10.1111/j.1538-7836.2010.04074.x>.
- Pryor, Paul R., and J. Paul Luzio. 2009. “Delivery of Endocytosed Membrane Proteins to the Lysosome.” *Biochimica et Biophysica Acta - Molecular Cell Research* 1793 (4): 615–24. <https://doi.org/10.1016/j.bbamcr.2008.12.022>.
- Purushothaman, Anurag, Shyam Kumar Bandari, Jian Liu, James A. Mobley, Elizabeth A. Brown, and Ralph D. Sanderson. 2016. “Fibronectin on the Surface of Myeloma Cell-Derived Exosomes Mediates Exosome-Cell Interactions.” *Journal of Biological Chemistry* 291 (4): 1652–63. <https://doi.org/10.1074/jbc.M115.686295>.
- Rajesh, Sundaresan, Pooja Sridhar, Birke Andrea Tews, Lucie Fénéant, Laurence Cocquerel, Douglas G. Ward, Fedor Berditchevski, and Michael Overduin. 2012. “Structural Basis of Ligand Interactions of the Large Extracellular Domain of Tetraspanin CD81.” *Journal of Virology* 86 (18): 9606–16. <https://doi.org/10.1128/jvi.00559-12>.
- Rak, Janusz, and Abhijit Guha. 2012. “Extracellular Vesicles - Vehicles That Spread Cancer Genes.” *BioEssays* 34 (6): 489–97. <https://doi.org/10.1002/bies.201100169>.
- Rana, Sanyukta, Christoph Claas, Cosima C. Kretz, Irina Nazarenko, and Margot Zoeller. 2011. “Activation-Induced Internalization Differs for the Tetraspanins CD9 and Tspan8: Impact on Tumor Cell Motility.” *International Journal of Biochemistry and Cell Biology* 43 (1): 106–19. <https://doi.org/10.1016/j.biocel.2010.10.002>.
- Rana, Sanyukta, Shijing Yue, Daniela Stadel, and Margot Zöller. 2012. “Toward Tailored Exosomes: The Exosomal Tetraspanin Web Contributes to Target Cell Selection.” *International Journal of Biochemistry and Cell Biology* 44 (9): 1574–84. <https://doi.org/10.1016/j.biocel.2012.06.018>.

- Rani, Sweta, Aideen E. Ryan, Matthew D. Griffin, and Thomas Ritter. 2015. "Mesenchymal Stem Cell-Derived Extracellular Vesicles: Toward Cell-Free Therapeutic Applications." *Molecular Therapy* 23 (5): 812–23. <https://doi.org/10.1038/mt.2015.44>.
- Rao, Swathi K., Chau Huynh, Veronique Proux-Gillardeaux, Thierry Galli, and Norma W. Andrews. 2004. "Identification of SNAREs Involved in Synaptotagmin VII-Regulated Lysosomal Exocytosis." *Journal of Biological Chemistry* 279 (19): 20471–79. <https://doi.org/10.1074/jbc.M400798200>.
- Raposo, G, H W Nijman, W Stoorvogel, R Liejendekker, C V Harding, C J Melief, and H J Geuze. 1996. "B Lymphocytes Secrete Antigen-Presenting Vesicles." *The Journal of Experimental Medicine* 183 (3): 1161–72. <https://doi.org/10.1084/jem.183.3.1161>.
- Ratajczak, J, K Miekus, M Kucia, J Zhang, R Reza, P Dvorak, and M Z Ratajczak. 2006. "Embryonic Stem Cell-Derived Microvesicles Reprogram Hematopoietic Progenitors : Evidence for Horizontal Transfer of mRNA and Protein Delivery," 847–56. <https://doi.org/10.1038/sj.leu.2404132>.
- Ridder, Kirsten, Alexandra Sevko, Janina Heide, Maria Dams, Anne Kathleen Rupp, Jadranka Macas, Julia Starmann, et al. 2015. "Extracellular Vesicle-Mediated Transfer of Functional RNA in the Tumor Microenvironment." *OncoImmunology* 4 (6): 1–8. <https://doi.org/10.1080/2162402X.2015.1008371>.
- Rocha-Perugini, V., M. Zamai, J. M. Gonzalez-Granado, O. Barreiro, E. Tejera, M. Yanez-Mo, V. R. Caiolfa, and F. Sanchez-Madrid. 2013. "CD81 Controls Sustained T Cell Activation Signaling and Defines the Maturation Stages of Cognate Immunological Synapses." *Molecular and Cellular Biology* 33 (18): 3644–58. <https://doi.org/10.1128/mcb.00302-13>.
- Rodrigues, Meryl, Jia Fan, Christopher Lyon, Meihua Wan, and Ye Hu. 2018. "Role of Extracellular Vesicles in Viral and Bacterial Infections: Pathogenesis, Diagnostics, and Therapeutics." *Theranostics* 8 (10): 2709–21. <https://doi.org/10.7150/thno.20576>.
- Santangelo, Laura, Giorgio Giurato, Carla Cicchini, Claudia Montaldo, Carmine Mancone, Roberta Tarallo, Cecilia Battistelli, Tonino Alonzi, Alessandro Weisz, and Marco Tripodi. 2016. "The RNA-Binding Protein SYNCRIP Is a Component of the Hepatocyte Exosomal Machinery Controlling MicroRNA Sorting." *Cell Reports* 17 (3): 799–808. <https://doi.org/10.1016/j.celrep.2016.09.031>.

- Saunderson, Sarah C., Amy C. Dunn, Paul R. Crocker, and Alexander D. McLellan. 2014. "CD169 Mediates the Capture of Exosomes in Spleen and Lymph Node." *Blood* 123 (2): 208–16. <https://doi.org/10.1182/blood-2013-03-489732>.
- Savina, Ariel, Claudio M. Fader, María T. Damiani, and María Isabel Colombo. 2005. "Rab11 Promotes Docking and Fusion of Multivesicular Bodies in a Calcium-Dependent Manner." *Traffic* 6 (2): 131–43. <https://doi.org/10.1111/j.1600-0854.2004.00257.x>.
- Savina, Ariel, Marcelo Furlán, Michel Vidal, and Maria I. Colombo. 2003. "Exosome Release Is Regulated by a Calcium-Dependent Mechanism in K562 Cells." *Journal of Biological Chemistry* 278 (22): 20083–90. <https://doi.org/10.1074/jbc.M301642200>.
- Schroder, J., R. Lullmann-Rauch, N. Himmerkus, I. Pleines, B. Nieswandt, Z. Orinska, F. Koch-Nolte, B. Schroder, M. Bleich, and P. Saftig. 2009. "Deficiency of the Tetraspanin CD63 Associated with Kidney Pathology but Normal Lysosomal Function." *Molecular and Cellular Biology* 29 (4): 1083–94. <https://doi.org/10.1128/mcb.01163-08>.
- Schultz, Carsten, and Maja Köhn. 2008. "Simultaneous Protein Tagging in Two Colors." *Chemistry and Biology* 15 (2): 91–92. <https://doi.org/10.1016/j.chembiol.2008.02.004>.
- Sebaihi, N., B. De Boeck, Y. Yuana, R. Nieuwland, and J. Pétry. 2017. "Dimensional Characterization of Extracellular Vesicles Using Atomic Force Microscopy." *Measurement Science and Technology* 28 (3). <https://doi.org/10.1088/1361-6501/28/3/034006>.
- Sedgwick, Alanna E., James W. Clancy, M. Olivia Balmert, and Crislyn D'Souza-Schorey. 2015. "Extracellular Microvesicles and Invadopodia Mediate Non-Overlapping Modes of Tumor Cell Invasion." *Scientific Reports* 5 (October): 1–14. <https://doi.org/10.1038/srep14748>.
- Segura, Elodie, Coralie Guérin, Nancy Hogg, Sebastian Amigorena, and Clotilde Théry. 2007. "CD8 + Dendritic Cells Use LFA-1 to Capture MHC-Peptide Complexes from Exosomes *In vivo* ." *The Journal of Immunology* 179 (3): 1489–96. <https://doi.org/10.4049/jimmunol.179.3.1489>.
- Serrano, Manuel, Athena W. Lin, Mila E. McCurrach, David Beach, and Scott W. Lowe. 1997. "Oncogenic Ras Provokes Premature Cell Senescence Associated with Accumulation of P53 and P16(INK4a)." *Cell* 88 (5): 593–602. [https://doi.org/10.1016/S0092-8674\(00\)81902-9](https://doi.org/10.1016/S0092-8674(00)81902-9).

- Sharma, Shivani, Haider I Rasool, Viswanathan Palanisamy, Cliff Mathisen, K Michael Schmidt, David T Wong, and James K Gimzewski. 2010. "Structural-Mechanical Characterization" 4 (4): 1921–26.
- Shelke, Ganesh Vilas, Cecilia Lässer, Yong Song Gho, and Jan Lötvall. 2014. "Importance of Exosome Depletion Protocols to Eliminate Functional and RNA-Containing Extracellular Vesicles from Fetal Bovine Serum." *Journal of Extracellular Vesicles* 3 (1). <https://doi.org/10.3402/jev.v3.24783>.
- Shields, S. Brookhart, Andrea J. Oestreich, Stanley Winistorfer, Doris Nguyen, Johanna A. Payne, David J. Katzmann, and Robert Piper. 2009. "ESCRT Ubiquitin-Binding Domains Function Cooperatively during MVB Cargo Sorting." *Journal of Cell Biology* 185 (2): 213–24. <https://doi.org/10.1083/jcb.200811130>.
- Sidhu, Sukhvinder S., Aklilu T. Mengistab, Andrew N. Tauscher, Jennifer LaVail, and Carol Basbaum. 2004. "The Microvesicle as a Vehicle for EMMPRin in Tumor-Stromal Interactions." *Oncogene* 23 (4): 956–63. <https://doi.org/10.1038/sj.onc.1207070>.
- Silva, Amanda K.A., Jelena Kolosnjaj-Tabi, Stephanie Bonneau, Iris Marangon, Nicole Boggetto, Kelly Aubertin, Olivier Clément, et al. 2013. "Magnetic and Photoresponsive Theranosomes: Translating Cell-Released Vesicles into Smart Nanovectors for Cancer Therapy." *ACS Nano* 7 (6): 4954–66. <https://doi.org/10.1021/nn400269x>.
- Simpson, Richard J., Hina Kalra, and Suresh Mathivanan. 2012. "Exocarta as a Resource for Exosomal Research." *Journal of Extracellular Vesicles* 1 (1). <https://doi.org/10.3402/jev.v1i0.18374>.
- Sitar, Simona, Anja Kejžar, David Pahovnik, Ksenija Kogej, Magda Tušek-Žnidarič, Metka Lenassi, and Ema Žagar. 2015. "Size Characterization and Quantification of Exosomes by Asymmetrical-Flow Field-Flow Fractionation." *Analytical Chemistry* 87 (18): 9225–33. <https://doi.org/10.1021/acs.analchem.5b01636>.
- Skardelly, Marco, Khaled Gaber, Swen Burdack, Franziska Scheidt, Heidegard Hilbig, Johannes Boltze, Annette Förschler, et al. 2011. "Long-Term Benefit of Human Fetal Neuronal Progenitor Cell Transplantation in a Clinically Adapted Model after Traumatic Brain Injury." *Journal of Neurotrauma* 28 (3): 401–14. <https://doi.org/10.1089/neu.2010.1526>.
- Skog, Johan, Tom Würdinger, Sjoerd van Rijn, Dimphna H. Meijer, Laura Gainche, William T.

- Curry, Bob S. Carter, Anna M. Krichevsky, and Xandra O. Breakefield. 2008. “Glioblastoma Microvesicles Transport RNA and Proteins That Promote Tumour Growth and Provide Diagnostic Biomarkers.” *Nature Cell Biology* 10 (12): 1470–76.
<https://doi.org/10.1038/ncb1800>.
- Sódar, Barbara W., Ágnes Kittel, Krisztina Pálóczi, Krisztina V. Vukman, Xabier Osteikoetxea, Katalin Szabó-Taylor, Andrea Németh, et al. 2016. “Low-Density Lipoprotein Mimics Blood Plasma-Derived Exosomes and Microvesicles during Isolation and Detection.” *Scientific Reports* 6 (April): 1–12. <https://doi.org/10.1038/srep24316>.
- Sokolova, Viktoriya, Anna Kristin Ludwig, Sandra Hornung, Olga Rotan, Peter A. Horn, Matthias Epple, and Bernd Giebel. 2011. “Characterisation of Exosomes Derived from Human Cells by Nanoparticle Tracking Analysis and Scanning Electron Microscopy.” *Colloids and Surfaces B: Biointerfaces* 87 (1): 146–50.
<https://doi.org/10.1016/j.colsurfb.2011.05.013>.
- Statello, Luisa, Marco Maugeri, Elena Garre, Muhammad Nawaz, Jessica Wahlgren, Alexandros Papadimitriou, Christina Lundqvist, et al. 2018. “Identification of RNA-Binding Proteins in Exosomes Capable of Interacting with Different Types of RNA: RBP-Facilitated Transport of RNAs into Exosomes.” *PLoS ONE* 13 (4): 1–30.
<https://doi.org/10.1371/journal.pone.0195969>.
- Steenbeek, Sander C, Thang V Pham, Joep Ligt, Anoek Zomer, Jaco C Knol, Sander R Piersma, Tim Schelfhorst, et al. 2018. “Cancer Cells Copy Migratory Behavior and Exchange Signaling Networks via Extracellular Vesicles.” *The EMBO Journal* 37 (15): 1–20.
<https://doi.org/10.15252/emj.201798357>.
- Stegmayr, B., and G. Ronquist. 1982. “Promotive Effect on Human Sperm Progressive Motility by Prostatosomes.” *Urological Research* 10 (5): 253–57.
<https://doi.org/10.1007/BF00255932>.
- Stuffers, Susanne, Catherine Sem Wegner, Harald Stenmark, and Andreas Brech. 2009. “Multivesicular Endosome Biogenesis in the Absence of ESCRTs.” *Traffic* 10 (7): 925–37.
<https://doi.org/10.1111/j.1600-0854.2009.00920.x>.
- Sugahara, Kazuki N., Tambet Teesalu, Priya Prakash Karmali, Venkata Ramana Kotamraju, Lilach Agemy, Olivier M. Girard, Douglas Hanahan, Robert F. Mattrey, and Erkki

- Ruoslahti. 2009. "Tissue-Penetrating Delivery of Compounds and Nanoparticles into Tumors." *Cancer Cell* 16 (6): 510–20. <https://doi.org/10.1016/j.ccr.2009.10.013>.
- Sung, Bong Hwan, Tatiana Ketova, Daisuke Hoshino, Andries Zijlstra, and Alissa M. Weaver. 2015. "Directional Cell Movement through Tissues Is Controlled by Exosome Secretion." *Nature Communications* 6 (May). <https://doi.org/10.1038/ncomms8164>.
- Svensson, Katrin J., Helena C. Christianson, Anders Wittrup, Erika Bourseau-Guilmain, Eva Lindqvist, Lena M. Svensson, Matthias Mörgelin, and Mattias Belting. 2013. "Exosome Uptake Depends on ERK1/2-Heat Shock Protein 27 Signaling and Lipid Raft-Mediated Endocytosis Negatively Regulated by Caveolin-1." *Journal of Biological Chemistry* 288 (24): 17713–24. <https://doi.org/10.1074/jbc.M112.445403>.
- Svensson, Katrin J., Paulina Kucharzewska, Helena C. Christianson, Stefan Sköld, Tobias Löfstedt, Maria C. Johansson, Matthias Mörgelin, Johan Bengzon, Wolfram Ruf, and Mattias Belting. 2011. "Hypoxia Triggers a Proangiogenic Pathway Involving Cancer Cell Microvesicles and PAR-2-Mediated Heparin-Binding EGF Signaling in Endothelial Cells." *Proceedings of the National Academy of Sciences of the United States of America* 108 (32): 13147–52. <https://doi.org/10.1073/pnas.1104261108>.
- Takahashi, Akiko, Ryo Okada, Koji Nagao, Yuka Kawamata, Aki Hanyu, Shin Yoshimoto, Masaki Takasugi, et al. 2017. "Exosomes Maintain Cellular Homeostasis by Excreting Harmful DNA from Cells." *Nature Communications* 8 (May): 1–14. <https://doi.org/10.1038/ncomms15287>.
- Takahashi, Kazutoshi, and Shinya Yamanaka. 2006. "Induction of Pluripotent Stem Cells from Mouse Embryonic and Adult Fibroblast Cultures by Defined Factors." *Cell* 126 (4): 663–76. <https://doi.org/10.1016/j.cell.2006.07.024>.
- Takasugi, Masaki, Ryo Okada, Akiko Takahashi, David Virya Chen, Sugiko Watanabe, and Eiji Hara. 2017. "Small Extracellular Vesicles Secreted from Senescent Cells Promote Cancer Cell Proliferation through EphA2." *Nature Communications* 8: 1–11. <https://doi.org/10.1038/ncomms15728>.
- Tamai, Keiichi, Nobuyuki Tanaka, Takashi Nakano, Eiji Kakazu, Yasuteru Kondo, Jun Inoue, Masaaki Shiina, et al. 2010. "Exosome Secretion of Dendritic Cells Is Regulated by Hrs, an ESCRT-0 Protein." *Biochemical and Biophysical Research Communications* 399 (3): 384–

90. <https://doi.org/10.1016/j.bbrc.2010.07.083>.
- Tamura, Ryo, Shinji Uemoto, and Yasuhiko Tabata. 2016. “Immunosuppressive Effect of Mesenchymal Stem Cell-Derived Exosomes on a Concanavalin A-Induced Liver Injury Model.” *Inflammation and Regeneration* 36 (1): 1–11. <https://doi.org/10.1186/s41232-016-0030-5>.
- Tauro, Bow J., David W. Greening, Rommel A. Mathias, Suresh Mathivanan, Hong Ji, and Richard J. Simpson. 2013. “Two Distinct Populations of Exosomes Are Released from LIM1863 Colon Carcinoma Cell-Derived Organoids.” *Molecular and Cellular Proteomics* 12 (3): 587–98. <https://doi.org/10.1074/mcp.M112.021303>.
- Teare, Gary F., Paul K. Horan, Susan E. Slezak, Cheryl Smith, and John B. Hay. 1991. “Long-Term Tracking of Lymphocytes *in vivo*: The Migration of PKH-Labeled Lymphocytes.” *Cellular Immunology* 134 (1): 157–70. [https://doi.org/10.1016/0008-8749\(91\)90339-D](https://doi.org/10.1016/0008-8749(91)90339-D).
- Terlecki-Zaniewicz, Lucia, Ingo Lämmermann, Julie Latreille, Madhusudhan Reddy Bobbili, Vera Pils, Markus Schosserer, Regina Weinmüllner, et al. 2018. “Small Extracellular Vesicles and Their MiRNA Cargo Are Anti-Apoptotic Members of the Senescence-Associated Secretory Phenotype.” *Aging* 10 (5): 1103–32. <https://doi.org/10.18632/aging.101452>.
- Terlecki-Zaniewicz, Lucia, Vera Pils, Madhusudhan Reddy Bobbili, Ingo Lämmermann, Ida Perrotta, Tonja Grillenberger, Jennifer Schwestka, et al. 2019. “Extracellular Vesicles in Human Skin: Cross-Talk from Senescent Fibroblasts to Keratinocytes by MiRNAs.” *Journal of Investigative Dermatology*. <https://doi.org/10.1016/j.jid.2019.05.015>.
- Thakur, Basant Kumar, Haiying Zhang, Annette Becker, Irina Matei, Yujie Huang, Bruno Costa-Silva, Yan Zheng, et al. 2014. “Double-Stranded DNA in Exosomes: A Novel Biomarker in Cancer Detection.” *Cell Research* 24 (6): 766–69. <https://doi.org/10.1038/cr.2014.44>.
- Theos, Alexander C., Steven T. Truschel, Daniele Tenza, Ilse Hurbain, Dawn C. Harper, Joanne F. Berson, Penelope C. Thomas, Graça Raposo, and Michael S. Marks. 2006. “A Luminal Domain-Dependent Pathway for Sorting to Intraluminal Vesicles of Multivesicular Endosomes Involved in Organelle Morphogenesis.” *Developmental Cell* 10 (3): 343–54. <https://doi.org/10.1016/j.devcel.2006.01.012>.
- Théry, Clotilde, Sebastian Amigorena, Graça Raposo, and Aled Clayton. 2006. “Isolation and

- Characterization of Exosomes from Cell Culture Supernatants and Biological Fluids.” *Current Protocols in Cell Biology* 30 (1): 3.22.1-3.22.29.
<https://doi.org/10.1002/0471143030.cb0322s30>.
- Théry, Clotilde, Muriel Boussac, Philippe Véron, Paola Ricciardi-Castagnoli, Graça Raposo, Jérôme Garin, and Sebastian Amigorena. 2001. “Proteomic Analysis of Dendritic Cell-Derived Exosomes: A Secreted Subcellular Compartment Distinct from Apoptotic Vesicles.” *The Journal of Immunology* 166 (12): 7309–18.
<https://doi.org/10.4049/jimmunol.166.12.7309>.
- Théry, Clotilde, Matias Ostrowski, and Elodie Segura. 2009. “Membrane Vesicles as Conveyors of Immune Responses.” *Nature Reviews Immunology* 9 (8): 581–93.
<https://doi.org/10.1038/nri2567>.
- Théry, Clotilde, Kenneth W. Witwer, Elena Aikawa, Maria Jose Alcaraz, Johnathon D. Anderson, Ramarosan Andriantsitohaina, Anna Antoniou, et al. 2018. “Minimal Information for Studies of Extracellular Vesicles 2018 (MISEV2018): A Position Statement of the International Society for Extracellular Vesicles and Update of the MISEV2014 Guidelines.” *Journal of Extracellular Vesicles* 7 (1).
<https://doi.org/10.1080/20013078.2018.1535750>.
- Tian, Yanhua, Suping Li, Jian Song, Tianjiao Ji, Motao Zhu, Gregory J. Anderson, Jingyan Wei, and Guangjun Nie. 2014. “A Doxorubicin Delivery Platform Using Engineered Natural Membrane Vesicle Exosomes for Targeted Tumor Therapy.” *Biomaterials* 35 (7): 2383–90.
<https://doi.org/10.1016/j.biomaterials.2013.11.083>.
- Tian, Ye, Ling Ma, Manfei Gong, Guoqiang Su, Shaobin Zhu, Wenqiang Zhang, Shuo Wang, et al. 2018. “Protein Profiling and Sizing of Extracellular Vesicles from Colorectal Cancer Patients via Flow Cytometry.” *ACS Nano* 12 (1): 671–80.
<https://doi.org/10.1021/acsnano.7b07782>.
- Todi, Sokol V., K. Matthew Scaglione, Jessica R. Blount, Venkatesha Basrur, Kevin P. Conlon, Annalisa Pastore, Kojo Elenitoba-Johnson, and Henry L. Paulson. 2010. “Activity and Cellular Functions of the Deubiquitinating Enzyme and Polyglutamine Disease Protein Ataxin-3 Are Regulated by Ubiquitination at Lysine 117.” *Journal of Biological Chemistry* 285 (50): 39303–13. <https://doi.org/10.1074/jbc.M110.181610>.

- Tokuyasu, K. T. 1973. "A Technique for Ultracryotomy of Cell Suspensions and Tissues." *Journal of Cell Biology* 57 (2): 551–65. <https://doi.org/10.1083/jcb.57.2.551>.
- Tompkins, Bryon A., Darcy L. Difede, Aisha Khan, Ana Marie Landin, Ivonne Hernandez Schulman, Marietsy V. Pujol, Alan W. Heldman, et al. 2017. "Allogeneic Mesenchymal Stem Cells Ameliorate Aging Frailty: A Phase II Randomized, Double-Blind, Placebo-Controlled Clinical Trial." *Journals of Gerontology - Series A Biological Sciences and Medical Sciences* 72 (11): 1513–21. <https://doi.org/10.1093/gerona/glx137>.
- Trajkovic, Katarina, Chieh Hsu, Salvatore Chiantia, Lawrence Rajendran, Dirk Wenzel, Felix Wieland, Petra Schwille, Britta Brügger, and Mikael Simons. 2008. "Ceramide Triggers Budding of Exosome Vesicles into Multivesicular Endosomes." *Science* 319 (5867): 1244–47. <https://doi.org/10.1126/science.1153124>.
- Trams, E G, C J Lauter, N Salem, and U Heine. 1981. "Exfoliation of Membrane Ecto-Enzymes in the Form of Micro-Vesicles." *Biochimica et Biophysica Acta* 645 (1): 63–70. [https://doi.org/10.1016/0005-2736\(81\)90512-5](https://doi.org/10.1016/0005-2736(81)90512-5).
- Trounson, Alan, and Courtney McDonald. 2015. "Stem Cell Therapies in Clinical Trials: Progress and Challenges." *Cell Stem Cell* 17 (1): 11–22. <https://doi.org/10.1016/j.stem.2015.06.007>.
- Ullal, Anirudh J., David S. Pisetsky, and Charles F. Reich. 2010. "Use of SYTO 13, a Fluorescent Dye Binding Nucleic Acids, for the Detection of Microparticles in in Vitro Systems." *Cytometry Part A* 77 (3): 294–301. <https://doi.org/10.1002/cyto.a.20833>.
- Valadi, Hadi, Karin Ekström, Apostolos Bossios, Margareta Sjöstrand, James J Lee, and Jan O Lötvall. 2007. "Exosome-Mediated Transfer of MRNAs and MicroRNAs Is a Novel Mechanism of Genetic Exchange between Cells" 9 (6). <https://doi.org/10.1038/ncb1596>.
- Varga, Zoltán, Yuana Yuana, Anita E. Grootemaat, Edwin van der Pol, Christian Gollwitzer, Michael Krumrey, and Rienk Nieuwland. 2014. "Towards Traceable Size Determination of Extracellular Vesicles." *Journal of Extracellular Vesicles* 3 (1): 1–10. <https://doi.org/10.3402/jev.v3.23298>.
- Verhage, Matthijs, and Jakob B. Sørensen. 2008. "Vesicle Docking in Regulated Exocytosis." *Traffic* 9 (9): 1414–24. <https://doi.org/10.1111/j.1600-0854.2008.00759.x>.
- Verweij, Frederik J., Monique A.J. Van Eijndhoven, Erik S. Hopmans, Tineke Vendrig, Tom

- Wurdinger, Ellen Cahir-Mcfarland, Elliott Kieff, et al. 2011. “LMP1 Association with CD63 in Endosomes and Secretion via Exosomes Limits Constitutive NF-KB Activation.” *EMBO Journal* 30 (11): 2115–29. <https://doi.org/10.1038/emboj.2011.123>.
- Vestad, Beate, Alicia Llorente, Axl Neurauter, Santosh Phuyal, Bente Kierulf, Peter Kierulf, Tore Skotland, Kirsten Sandvig, Kari Bente F. Haug, and Reidun Øvstebø. 2017. “Size and Concentration Analyses of Extracellular Vesicles by Nanoparticle Tracking Analysis: A Variation Study.” *Journal of Extracellular Vesicles* 6 (1). <https://doi.org/10.1080/20013078.2017.1344087>.
- Villarroya-Beltri, Carolina, Cristina Gutiérrez-Vázquez, Fátima Sánchez-Cabo, Daniel Pérez-Hernández, Jesús Vázquez, Noa Martín-Cofreces, Dannys Jorge Martínez-Herrera, Alberto Pascual-Montano, María Mittelbrunn, and Francisco Sánchez-Madrid. 2013. “Sumoylated HnRNPA2B1 Controls the Sorting of MiRNAs into Exosomes through Binding to Specific Motifs.” *Nature Communications* 4: 1–10. <https://doi.org/10.1038/ncomms3980>.
- Vojtech, Lucia, Sangsoon Woo, Sean Hughes, Claire Levy, Lamar Ballweber, Renan P. Sauteraud, Johanna Strobl, et al. 2014. “Exosomes in Human Semen Carry a Distinctive Repertoire of Small Non-Coding RNAs with Potential Regulatory Functions.” *Nucleic Acids Research* 42 (11): 7290–7304. <https://doi.org/10.1093/nar/gku347>.
- Vorselen, Daan, Susan M. van Dommelen, Raya Sorkin, Melissa C. Piontek, Jürgen Schiller, Sander T. Döpp, Sander A.A. Kooijmans, et al. 2018. “The Fluid Membrane Determines Mechanics of Erythrocyte Extracellular Vesicles and Is Softened in Hereditary Spherocytosis.” *Nature Communications* 9 (1). <https://doi.org/10.1038/s41467-018-07445-x>.
- Vorselen, Daan, Margherita Marchetti, Carmen López-Iglesias, Peter J. Peters, Wouter H. Roos, and Gijs J.L. Wuite. 2018. “Multilamellar Nanovesicles Show Distinct Mechanical Properties Depending on Their Degree of Lamellarity.” *Nanoscale* 10 (11): 5318–24. <https://doi.org/10.1039/c7nr09224e>.
- Vos, Kristan E. Van Der, Erik R. Abels, Xuan Zhang, Charles Lai, Esteban Carrizosa, Derek Oakley, Shilpa Prabhakar, et al. 2016. “Directly Visualized Glioblastoma-Derived Extracellular Vesicles Transfer RNA to Microglia/Macrophages in the Brain.” *Neuro-Oncology* 18 (1): 58–69. <https://doi.org/10.1093/neuonc/nov244>.

- Waldo, Geoffrey S., Blake M. Standish, Joel Berendzen, and Thomas C. Terwilliger. 1999. "Rapid Protein-Folding Assay Using Green Fluorescent Protein." *Nature Biotechnology* 17 (7): 691–95. <https://doi.org/10.1038/10904>.
- Wang, Qiyu, Jiujiu Yu, Tatenda Kadungure, Joseph Beyene, Hong Zhang, and Quan Lu. 2018. "ARMMs as a Versatile Platform for Intracellular Delivery of Macromolecules." *Nature Communications* 9 (1): 1–7. <https://doi.org/10.1038/s41467-018-03390-x>.
- Wang, Ting, Daniele M. Gilkes, Naoharu Takano, Lisha Xiang, Weibo Luo, Corey J. Bishop, Pallavi Chaturvedi, Jordan J. Green, and Gregg L. Semenza. 2014. "Hypoxia-Inducible Factors and RAB22A Mediate Formation of Microvesicles That Stimulate Breast Cancer Invasion and Metastasis." *Proceedings of the National Academy of Sciences of the United States of America* 111 (31). <https://doi.org/10.1073/pnas.1410041111>.
- Wang, Wei, Junfeng Wu, Zongyu Zhang, and Tanjun Tong. 2001. "Characterization of Regulatory Elements on the Promoter Region of P16 INK4a That Contribute to Overexpression of P16 in Senescent Fibroblasts." *Journal of Biological Chemistry* 276 (52): 48655–61. <https://doi.org/10.1074/jbc.M108278200>.
- Wäster, Petra, Ida Eriksson, Linda Vainikka, Inger Rosdahl, and Karin Öllinger. 2016. "Extracellular Vesicles Are Transferred from Melanocytes to Keratinocytes after UVA Irradiation." *Scientific Reports* 6 (June): 1–13. <https://doi.org/10.1038/srep27890>.
- Webley, K., J. A. Bond, C. J. Jones, J. P. Blaydes, A. Craig, T. Hupp, and D. Wynford-Thomas. 2000. "Posttranslational Modifications of P53 in Replicative Senescence Overlapping but Distinct from Those Induced by DNA Damage." *Molecular and Cellular Biology* 20 (8): 2803–8. <https://doi.org/10.1128/mcb.20.8.2803-2808.2000>.
- Weilner, Sylvia, Verena Keider, Melanie Winter, Eva Harreither, Benjamin Salzer, Florian Weiss, Elisabeth Schraml, et al. 2016. "Vesicular Galectin-3 Levels Decrease with Donor Age and Contribute to the Reduced Osteo-Inductive Potential of Human Plasma Derived Extracellular Vesicles." *Aging* 8 (1): 16–33. <https://doi.org/10.18632/aging.100917>.
- Weilner, Sylvia, Elisabeth Schraml, Matthias Wieser, Paul Messner, Karl Schneider, Klemens Wassermann, Lucia Micutkova, et al. 2016. "Secreted Microvesicular MiR-31 Inhibits Osteogenic Differentiation of Mesenchymal Stem Cells." *Aging Cell* 15 (4): 744–54. <https://doi.org/10.1111/acel.12484>.

- Welton, Joanne Louise, Jason Paul Webber, Laur Alexandru Botos, Michael Jones, and Aled Clayton. 2015. "Ready-Made Chromatography Columns for Extracellular Vesicle Isolation from Plasma." *Journal of Extracellular Vesicles* 4 (2015): 1–9.
<https://doi.org/10.3402/jev.v4.27269>.
- Wiklander, Oscar P.B., R. Beklem Bostancioglu, Joshua A. Welsh, Antje M. Zickler, Florian Murke, Giulia Corso, Ulrika Felldin, et al. 2018. "Systematic Methodological Evaluation of a Multiplex Bead-Based Flow Cytometry Assay for Detection of Extracellular Vesicle Surface Signatures." *Frontiers in Immunology* 9 (JUN).
<https://doi.org/10.3389/fimmu.2018.01326>.
- Wiklander, Oscar P.B., Joel Z. Nordin, Aisling O’Loughlin, Ylva Gustafsson, Giulia Corso, Imre Mäger, Pieter Vader, et al. 2015a. "Extracellular Vesicle *in vivo* Biodistribution Is Determined by Cell Source, Route of Administration and Targeting." *Journal of Extracellular Vesicles* 4 (2015): 1–13. <https://doi.org/10.3402/jev.v4.26316>.
- . 2015b. "Extracellular Vesicle *in vivo* Biodistribution Is Determined by Cell Source, Route of Administration and Targeting." *Journal of Extracellular Vesicles* 4 (2015): 1–13. <https://doi.org/10.3402/jev.v4.26316>.
- Willms, Eduard, Henrik J. Johansson, Imre Mäger, Yi Lee, K. Emelie M. Blomberg, Mariam Sadik, Amr Alaarg, et al. 2016. "Cells Release Subpopulations of Exosomes with Distinct Molecular and Biological Properties." *Scientific Reports* 6 (February): 1–12.
<https://doi.org/10.1038/srep22519>.
- Wisgrill, Lukas, Christian Lamm, Julia Hartmann, Falk Preißing, Klaus Dragosits, Annica Bee, Lena Hell, et al. 2016. "Peripheral Blood Microvesicles Secretion Is Influenced by Storage Time, Temperature, and Anticoagulants." *Cytometry Part A* 89 (7): 663–72.
<https://doi.org/10.1002/cyto.a.22892>.
- Witwer, Kenneth W., Carolina Soekmadji, Andrew F. Hill, Marca H. Wauben, Edit I. Buzás, Dolores Di Vizio, Juan M. Falcon-Perez, et al. 2017. "Updating the MISEV Minimal Requirements for Extracellular Vesicle Studies: Building Bridges to Reproducibility." *Journal of Extracellular Vesicles* 6 (1). <https://doi.org/10.1080/20013078.2017.1396823>.
- Wolf, P. 1967. "The Nature and Significance of Platelet Products in Human Plasma." *British Journal of Haematology* 13 (3): 269–88. <https://doi.org/10.1111/j.1365->

2141.1967.tb08741.x.

- Wubbolts, Richard, Rachel S. Leckie, Peter T.M. Veenhuizen, Guenter Schwarzmann, Wiebke Möbius, Joerg Hoernschemeyer, Jan Willem Slot, Hans J. Geuze, and Willem Stoorvogel. 2003. "Proteomic and Biochemical Analyses of Human B Cell-Derived Exosomes: Potential Implications for Their Function and Multivesicular Body Formation." *Journal of Biological Chemistry* 278 (13): 10963–72. <https://doi.org/10.1074/jbc.M207550200>.
- Xie, Hui, Zhenxing Wang, Liming Zhang, Qian Lei, Aiqi Zhao, Hongxiang Wang, Qiubai Li, Yilin Cao, Wen Jie Zhang, and Zhichao Chen. 2017. "Extracellular Vesicle-Functionalized Decalcified Bone Matrix Scaffolds with Enhanced Pro-Angiogenic and Pro-Bone Regeneration Activities." *Scientific Reports* 7 (June 2016): 1–13. <https://doi.org/10.1038/srep45622>.
- Yáñez-Mó, María, Olga Barreiro, Mónica Gordon-Alonso, Mónica Sala-Valdés, and Francisco Sánchez-Madrid. 2009. "Tetraspanin-Enriched Microdomains: A Functional Unit in Cell Plasma Membranes." *Trends in Cell Biology* 19 (9): 434–46. <https://doi.org/10.1016/j.tcb.2009.06.004>.
- Yang, Jialei, Xiufen Zhang, Xiangjie Chen, Lei Wang, and Guodong Yang. 2017. "Exosome Mediated Delivery of MiR-124 Promotes Neurogenesis after Ischemia." *Molecular Therapy - Nucleic Acids* 7 (June): 278–87. <https://doi.org/10.1016/j.omtn.2017.04.010>.
- Yosef, Reut, Noam Pilpel, Ronit Tokarsky-Amiel, Anat Biran, Yossi Ovadya, Snir Cohen, Ezra Vadai, et al. 2016. "Directed Elimination of Senescent Cells by Inhibition of BCL-W and BCL-XL." *Nature Communications* 7. <https://doi.org/10.1038/ncomms11190>.
- Yuana, Y., T. H. Oosterkamp, S. Bahatyrova, B. Ashcroft, P. Garcia Rodriguez, R. M. Bertina, and S. Osanto. 2010. "Atomic Force Microscopy: A Novel Approach to the Detection of Nanosized Blood Microparticles." *Journal of Thrombosis and Haemostasis* 8 (2): 315–23. <https://doi.org/10.1111/j.1538-7836.2009.03654.x>.
- Yuana, Yuana, Roman I. Koning, Maxim E. Kuil, Patrick C. N. Rensen, Abraham J. Koster, Rogier M Bertina, and Susanne Osanto. 2013. "Cryo-Electron Microscopy of Extracellular Vesicles in Fresh Plasma." *Journal of Extracellular Vesicles* 2 (1): 21494. <https://doi.org/10.3402/jev.v2i0.21494>.
- Yuana, Yuana, Johannes Levels, Anita Grootemaat, Auguste Sturk, and Rienk Nieuwland. 2014.

- “Co-Isolation of Extracellular Vesicles and High-Density Lipoproteins Using Density Gradient Ultracentrifugation.” *Journal of Extracellular Vesicles* 3 (1).
<https://doi.org/10.3402/jev.v3.23262>.
- Zelm, Menno C. Van, Julie Smet, Brigitte Adams, Françoise Mascart, Liliane Schandené, Françoise Janssen, Alina Ferster, et al. 2010. “CD81 Gene Defect in Humans Disrupts CD19 Complex Formation and Leads to Antibody Deficiency.” *Journal of Clinical Investigation* 120 (4): 1265–74. <https://doi.org/10.1172/JCI39748>.
- Zhang, Haiying, Daniela Freitas, Han Sang Kim, Kristina Fabijanic, Zhong Li, Haiyan Chen, Milica Tesic Mark, et al. 2018. “Identification of Distinct Nanoparticles and Subsets of Extracellular Vesicles by Asymmetric Flow Field-Flow Fractionation.” *Nature Cell Biology* 20 (3): 332–43. <https://doi.org/10.1038/s41556-018-0040-4>.
- Zhang, Haiying, and David Lyden. 2019. “Asymmetric-Flow Field-Flow Fractionation Technology for Exomere and Small Extracellular Vesicle Separation and Characterization.” *Nature Protocols* 14 (4): 1027–53. <https://doi.org/10.1038/s41596-019-0126-x>.
- Zhang, Jieyuan, Junjie Guan, Xin Niu, Guowen Hu, Shangchun Guo, Qing Li, Zongping Xie, Changqing Zhang, and Yang Wang. 2015. “Exosomes Released from Human Induced Pluripotent Stem Cells-Derived MSCs Facilitate Cutaneous Wound Healing by Promoting Collagen Synthesis and Angiogenesis.” *Journal of Translational Medicine* 13 (1): 1–14. <https://doi.org/10.1186/s12967-015-0417-0>.
- Zhao, Zheng, Yang Yang, Yong Zeng, and Mei He. 2016. “A Microfluidic ExoSearch Chip for Multiplexed Exosome Detection towards Blood-Based Ovarian Cancer Diagnosis.” *Lab on a Chip* 16 (3): 489–96. <https://doi.org/10.1039/c5lc01117e>.
- Zhu, Yi, Jacqueline L. Armstrong, Tamara Tchkonina, and James L. Kirkland. 2014. “Cellular Senescence and the Senescent Secretory Phenotype in Age-Related Chronic Diseases.” *Current Opinion in Clinical Nutrition and Metabolic Care* 17 (4): 324–28. <https://doi.org/10.1097/MCO.0000000000000065>.
- Zhuang, Xiaoying, Xiaoyu Xiang, William Grizzle, Dongmei Sun, Shuangqin Zhang, Robert C. Axtell, Songwen Ju, et al. 2011. “Treatment of Brain Inflammatory Diseases by Delivering Exosome Encapsulated Anti-Inflammatory Drugs from the Nasal Region to the Brain.” *Molecular Therapy* 19 (10): 1769–79. <https://doi.org/10.1038/mt.2011.164>.

- Zimmerman, Brandon, Brendan Kelly, Brian J. McMillan, Tom C.M. Seegar, Ron O. Dror, Andrew C. Kruse, and Stephen C. Blacklow. 2016. "Crystal Structure of a Full-Length Human Tetraspanin Reveals a Cholesterol-Binding Pocket." *Cell* 167 (4): 1041-1051.e11. <https://doi.org/10.1016/j.cell.2016.09.056>.
- Zitvogel, L, A Regnault, A Lozier, J Wolfers, C Flament, D Tenza, P Ricciardi-Castagnoli, G Raposo, and S Amigorena. 1998. "Eradication of Established Murine Tumors Using a Novel Cell-Free Vaccine: Dendritic Cell-Derived Exosomes." *Nature Medicine* 4 (5): 594–600. <https://doi.org/10.1038/nm0598-594>.
- Zomer, Anoek, Carrie Maynard, Frederik Johannes Verweij, Alwin Kamermans, Ronny Schäfer, Evelyne Beerling, Raymond Michel Schiffelers, et al. 2015. "In vivo Imaging Reveals Extracellular Vesicle-Mediated Phenocopying of Metastatic Behavior." *Cell* 161 (5): 1046–57. <https://doi.org/10.1016/j.cell.2015.04.042>.
- Zomer, Anoek, Sander Christiaan Steenbeek, Carrie Maynard, and Jacco Van Rheenen. 2016. "Studying Extracellular Vesicle Transfer by a Cre-LoxP Method." *Nature Protocols* 11 (1): 87–101. <https://doi.org/10.1038/nprot.2015.138>.

8. APPENDIX I

8.1. List of figures

FIGURE 1: SCHEMATIC VIEW OF DIFFERENT EV SUBPOPULATIONS.....	11
FIGURE 2: BIOGENESIS OF EXTRACELLULAR VESICLES.....	16
FIGURE 3: MAIN FEATURES OF EXTRACELLULAR VESICLES:.....	21
FIGURE 4: FATE OF EXTRACELLULAR VESICLES IN RECIPIENT CELLS.....	29
FIGURE 5: APPROACHES USED TO ANALYZE EV- MEDIATED TRANSFER <i>IN VIVO</i>	31
FIGURE 6: SCHEMATIC REPRESENTATION OF DIFFERENTIAL ULTRACENTRIFUGATION PROCEDURE.	34
FIGURE 7: SCHEMATIC ILLUSTRATING OF TFF.	37
FIGURE 8: EV ENGINEERING AND LOADING STRATEGIES.....	53
FIGURE 9: THE HALLMARKS OF AGING.....	56
FIGURE 10: SCHEMATIC REPRESENTATION OF DIFFERENT SNORKEL-TAGS (A), AND SNORKEL-TAGS FUSED TO CD81 FULL LENGTH OR TRUNCATED VERSIONS (B).	62
FIGURE 11: WESTERN BLOT FOR SNORKEL-TAG EPITOPE (HA-TAG) FROM HeLa CELL LYSATES EXPRESSING ALL VARIANTS OF CD81-SNORKEL-TAG.....	63
FIGURE 12: CONFIRMATION OF PRESCISSON PROTEASE CLEAVAGE SITE ACCESSIBILITY ON SNORKEL-TAG BOUND TO ANTI-HA AFFINITY MATRIX.	64
FIGURE 13: SCHEMATIC REPRESENTATION OF SNORKEL-TAG WITH G4S LINKER ON EITHER SIDE OF PRESCISSON PROTEASE AND RIGID LINKER BETWEEN TRANSMEMBRANE DOMAIN (TMD) AND FLAG-TAG (A), AND SNORKEL-TAG FUSED TO C-TERMINAL OF CD81 FULL LENGTH (B).....	65
FIGURE 14: EVALUATION OF CD81-SNORKEL-TAG IN STABLY EXPRESSING HeLa CELL.....	66
FIGURE 15: CD81-SNORKEL-TAG EXPRESSING HeLa CELLS DISPLAY SNORKEL-TAG ON THE SURFACE OF THE CELL MEMBRANE.....	67
FIGURE 16: SPECIFICITY OF PRESCISSON PROTEASE ACTIVITY.....	68
FIGURE 17: ISOLATION OF EVs USING TFF AND CHARACTERIZATION.	69
FIGURE 18: CHARACTERIZATION OF EVs FOR PURITY, SIZE AND MORPHOLOGY.	71

FIGURE 19: MULTIPLEX BEAD-BASED FLOW CYTOMETRY ASSAY FOR DETECTION OF EV SURFACE PROTEIN SIGNATURE.	73
FIGURE 20: MULTIPLEX BEAD-BASED FLOW CYTOMETRY ASSAY FOR DETECTION OF EV SURFACE PROTEIN SIGNATURE FOR EVS DERIVED FROM DIFFERENT CELL LINES.	76
FIGURE 21: CHARACTERIZATION OF EVS CARRYING SNORKEL-TAG.	77
FIGURE 22: MULTIPLEX BEAD-BASED FLOW CYTOMETRY BY INDIRECT LABELING.	78
FIGURE 23: QUANTIFICATION OF EVS ISOLATED BY ULTRAFILTRATION.	80
FIGURE 24: ISOLATION OF EVS USING SNORKEL-TAG BASED EV AFFINITY CHROMATOGRAPHY (StEVAC).	82
FIGURE 25: CHARACTERIZATION OF EVS PURIFIED BY THE StEVAC METHOD.	85
FIGURE 26: MULTIPLEX BEAD-BASED FLOW CYTOMETRY ASSAY TO EVALUATE THE StEVAC METHOD.	87
FIGURE 27: CONFIRMING StEVAC TO PURIFY EVS CARRYING SNORKEL-TAG FROM MIXED POPULATION OF EVS.	88
FIGURE 28: CONFIRMING PURITY OF EVS FROM MIXED POPULATIONS AFTER StEVAC USING THE MULTIPLEX BEAD-BASED FLOW CYTOMETRY ASSAY.	91
FIGURE 29: CRE-LOXP METHOD TO STUDY THE FUNCTIONAL TRANSFER OF EVS.	93
FIGURE 30: StEVAC PURIFIED EV UPTAKE IN HUH7 CELLS.	95
FIGURE 31: EVS ARE PART OF THE SENESCENT- ASSOCIATED SECRETORY PHENOTYPE (SASP).	97
FIGURE 32: EVIDENCE OF EV-LIKE STRUCTURES IN SKIN SECTIONS.	98
FIGURE 33: CHARACTERIZATION OF EVS PURIFIED FROM TISSUE BIOPSIES.	100
FIGURE 34: CHARACTERIZATIONS OF EVS DERIVED FROM HDF5 CELLS.	102
FIGURE 35: WESTERN BLOT ANALYSIS OF 17 MONOCLONAL ANTIBODIES AGAINST HDF AND HELA CELL LYSATES.	104
FIGURE 36: FLOW CYTOMETRY ANALYSIS FOR MONOCLONAL ANTIBODIES USING DIFFERENT CELL LINES.	106
FIGURE 37: NTA MEASUREMENTS FOR EVS DERIVED FROM HDF164-hTERT CELLS EXPRESSING CD63-GFP.	107
FIGURE 38: TITRATION OF EV AND 53F2-D6 CLONE ANTIBODY CONCENTRATIONS FOR EV UPTAKE ANALYSIS BY FLOW CYTOMETRY.	108

FIGURE 39: TITRATION OF MONOCLONAL ANTIBODY CONCENTRATIONS FOR EV UPTAKE ANALYSIS BY FLOW CYTOMETRY..... 110

FIGURE 40: 52F8-G6 AND 53F2-D6 MONOCLONAL ANTIBODIES FOR EV UPTAKE ANALYSIS BY FLOW CYTOMETRY..... 111

8.2. List of tables

TABLE 1: MONOCLONAL ANTIBODY CLONES WITH RESPECTIVE CONCENTRATIONS..... 102

8.3. Abbreviations

A

AAVs	Adeno-associated vectors
ADAM10	ADAM metallopeptidase domain 10
AF4	Asymmetric flow filed-flow fractionation
AFM	Atomic force microscopy
AGO2	Argonaute RISC catalytic component 2
ALIX	AGL-2-interacting protein
APC	Allophycocyanin
APP	Amyloid beta precursor protein
ARRDC1	Arrestin domain–containing protein 1
ARF6	ADP ribosylation factor 6
ASCs	Adipose-derived stem cells
ATM	ATM serine/threonine kinase
ATTAC	Apoptosis through targeted activation of caspase

B

BACE1	Beta-secretase 1
BBB	Blood-brain barrier

BCA	Bicinchoninic acid
BCCs	Breast cancer cells
BCL-2	BCL2 apoptosis regulator
BCL-W	BCL2 like 2
BCL-XL	BCL2 like 1
BSA	Bovine serum albumin
BubR1	BUB1 mitotic checkpoint serine/threonine kinase B
C	
Ca ²⁺	Calcium
CD	Protein-cytosine deaminase
CD1c	CD1c molecule
CD3	CD3g molecule
CD4	CD4 molecule
CD8	CD8 molecule
CD9	CD9 molecule
CD11c	Integrin subunit alpha X/ CD11c antigen
CD14	CD14 molecule
CD19	CD19 molecule
CD20	Membrane spanning 4-domains A1/ CD20 antigen
CD24	CD24 molecule
CD25	Interleukin 2 receptor subunit alpha/ CD25 antigen
CD29	Integrin subunit beta 1/ CD29 antigen
CD31	Platelet and endothelial cell adhesion molecule 1/ EndoCAM/ CD31 antigen
CD37	CD37 molecule
CD40	CD40 molecule
CD41b	Integrin subunit alpha 2b/ CD41b antigen
CD42a	Glycoprotein IX platelet
CD44	CD44 molecule
CD45	Protein tyrosine phosphatase receptor type C/ CD45 antigen
CD47	CD47 molecule

CD49e	Integrin subunit alpha 5/ CD49e antigen
CD53	CD53 molecule
CD56	Neural cell adhesion molecule/ CD56 antigen
CD62P	Selectin P/ CD62P antigen
CD63	CD63 molecule
CD69	CD69 molecule
CD81	CD81 molecule
CD82	CD82 molecule
CD86	CD86 molecule
CD105	Endoglin/ CD105 antigen
CD133	Prominin 1/ CD133 antigen
CD142	Coagulation factor III, tissue factor/ CD142 antigen
CD146	Melanoma cell adhesion molecule
CD169	Sialic acid binding Ig like lectin 1
CD209	CD209 molecule
CD326	Epithelial cell adhesion molecule
CDK4	Cyclin dependent kinase 4
CDK6	Cyclin dependent kinase 6
CHMP4A	Charged Multivesicular Body Protein 4A
CKD	Chronic kidney disease
CM	Conditioned media
CNS	Central nervous system
CRISPR	Clustered regularly interspaced short palindromic repeats
CXCR4	C-X-C Motif Chemokine Receptor 4

D

DCs	Dendritic cells
DDR	DNA damage response
Dex	DC-derived exosomes
Dil	1,1'-dioctadecyl-3,3,3',3'-tetramethylindocarbocyanine perchlorate
DiR	1,1'-dioctadecyl-3,3,3,3'-tetramethylindotricarbocyanine iodide

DLS	Dynamic light scattering
DNA	Deoxyribonucleic acid
E	
EC	Extracellular loop
eGFP	Enhanced Green Fluorescent Protein
EGFR	Epidermal growth factor receptor
EHD4	EH Domain Containing 4
EM	Electron microscopy
EpCAM	Epithelial cell adhesion molecule
ER	Endoplasmic reticulum
ERK	Extracellular Signal-Regulated Kinase
ESCRT	Endosomal sorting complex required for transport
esRNA	exosomal shuttle RNA
EVs	Extracellular vesicles
Exo-S	Small-exosomes
Exo-L	Large-exosomes
F	
FasL	Fas Ligand
FBS	fetal bovine serum
FC	Flow cytometry
FCS	Fetal calf serum
FKBP-Casp8	FK506-binding-protein-caspase 8
FOXO4	Forkhead box O4
G	
GAPDH	Glyceraldehyde-3-Phosphate Dehydrogenase
GFP	Green Fluorescent Protein
GM3	monosialodihexosylganglioside 3
GP130	Membrane glycoprotein 130
GPC1	Glypican-1
GPCRs	G-protein coupled receptors

GPI	Glycosylphosphatidylinositol- anchored proteins
gRNA	Guide RNA
GvHD	Graft-versus-host disease
H	
HA	Hemagglutinin
HD-Exo	High density exosomes
HDLs	High density lipoproteins
HDFs	Human dermal fibroblasts
HEK293	Human embryonic kidney 293 cells
HLA-ABC	Major histocompatibility complex, class I, A, B, C
HLA-DP	Major histocompatibility complex, class II, DP beta 1
HLA-DQ	Major histocompatibility complex, class II, DQ beta 1
HLA-DR	Major histocompatibility complex, class II, DR beta 1
HMC-1	Human mast cell line
hnRBP A2/B1	heterogenous RNA-binding protein A2/B1
HSP70	Heat Shock 70kD Protein 4
HSP72	Heat shock protein 72
HSP90B1	Heat Shock Protein 90 beta Family Member 1
HRS	Hepatocyte growth factor-regulated tyrosine kinase substrate
I	
ICAM	Intercellular Adhesion Molecule
ICAM-1	Intercellular adhesion molecule 1
iDSF	Dermal interstitial fluid
iExosomes	inhibitor exosomes
IFC	Imaging flow cytometry
IgG1	Immunoglobulin G1
ILVs	Intraluminal vesicles
ISEV	International society for extracellular vesicles
ITG α 6 β 1	Integrin α 6 β 1
ITG α 6 β 4	Integrin α 6 β 4

ITG α v β 5 Integrin α v β 5

K

kDa Kilo Dalton

Kras KRAS proto-oncogene, GTPase

L

LAFs Lipid- anchored fluorophores

LAMP1 Lysosomal Associated Membrane Protein 1

LAMP2b Lysosomal associated membrane protein 2

LD-Exo Low density exosomes

M

MC/9 mouse mast cell line

MCF7 cells Michigan Cancer Foundation-7 cells

MCSP Melanoma chondroitin sulfate proteoglycan

MET MET proto-oncogene, receptor tyrosine kinase

MHC I Major Histocompatibility complex, Class I

MHC II Major Histocompatibility complex, Class II

miRNA micro RNA

MISEV Minimal information for studies of extracellular vesicles

MLCK myosin light chain kinase

MMPs Matrix metalloproteinases

MP-IVM Multiphoton intravital microscopy

mPES Modified polyethersulfone

MSCs Mesenchymal stem cells

mRNA messenger RNA

mtRNA mitochondrial RNA

MVBs Multivesicular bodies

MVE multivesicular endosome

MVs Microvesicles

MWCO Molecular weight cut-off

N

NanoFCM	Nano flow cytometry
Nluc	Nano-luciferase
nm	Nanometer
nSMase	neutral sphingomyelinase
NSUN2	tRNA (Cytosine(34)-C(5))-methyltransferase
NTA	Nanoparticle tracking analysis

O

OFM	open flow perfusion
-----	---------------------

P

P21	Cyclin dependent kinase inhibitor 1A
P53	Tumor protein 53
PBS	Phosphate buffer saline
PCR	Polymerase chain reaction
PDCD6IP	Programmed cell death 6 interacting protein
PDGF	platelet-derived growth factor
PEG	Polyethylene glycol
PI3- kinase	Phosphatidylinositol 3- kinase
PIP3	Phosphatidylinositol 3-phosphate
PKH26	Paul karl horan 26
PKH67	Paul karl horan 67
PLD2	phospholipase D2
PLP	proteolipid protein
PM	Plasma membrane
PrP	Prion Protein
PS	Phosphatidyl serine

Q

Q	Quiescent cell
---	----------------

R

RAB	Member RAS oncogene family
RB	Retinoblastoma
Rluc	Renilla luciferase
RNA	ribonucleic acid
RNAi	RNA-mediated interference
ROCK	Rho Associated coiled-coil containing protein kinase
ROR1	Receptor tyrosine kinase like orphan receptor 1
RPL12	Ribosomal protein L12
RPS18	Ribosomal protein S18
rRNA	ribosomal RNA
RT-PCR	Quantitative reverse transcription PCR
S	
SA- β -gal	Senescence-associated beta-galactosidase
SASP	Senescent associated secretory phenotype
SDS-PAGE	Sodium dodecyl sulfate polyacrylamide gel electrophoresis
SEC	Size exclusion chromatography
SEM	Scanning electron microscopy
sEVs	small Extracellular vesicles
shRNA	Small hairpin RNA
SILAC	Stable isotope labeling by/with amino acids in cell culture
siRNA	Small inhibitory RNA
SIPS	Stress- induced premature senescent cells
SKD1	ATPase suppressor-of-potassium-transport-growth-defect-1 protein
SNAP23	Synaptosome Associated Protein 23
SNAP	soluble N-ethylmaleimide-sensitive fusion attachment protein
SNAREs	soluble N-ethylmaleimide-sensitive fusion attachment protein (SNAP) receptors
SSEA-4	stage-specific embryonic antigen 4
STAM	Signal transducing adaptor molecule
StEVAC	Snorkel-tag based extracellular vesicle affinity chromatography
SYNCRIP	synaptotagmin-binding cytoplasmic RNA-interacting protein

T

T1DM	Type 1 diabetes mellitus
TCR	T- cell receptor
TDP43	TAR DNA-Binding Protein
TEM	Transmission electron microscopy
TERMs	Tetraspanin-enriched microdomains
TFF	Tangential flow filtration
TfR	Transferrin receptor
TIM4	T-cell immunoglobulin mucin receptor 4
TMD	Transmembrane domain
tRNA	transfer RNA
t-SNARE	target- SNARE
TSG101	Tumor susceptibility 101
TSPAN6	Tetraspanin 6
TSPAN8	Tetraspanin 8

U

UC	Ultracentrifugation
UPRT	Uracil phosphoribosyltransferase

V

VAMP7	Vesicle Associated Membrane Protein 7
VEGF	Vascular endothelial growth factor
VPS4	Vacuolar Protein Sorting 4 Homolog A
v-SNARE	vesicle- SNARE
VT-RNA	vault RNA

W

Wnt11	Wnt Family Member 11
WT	Wild type

Y

Y-B1	Y-box binding protein
------	-----------------------

9. APPENDIX II

9.1. Publications

1. Terlecki-Zaniewicz L, Pils V, **Bobbili MR**, Lämmermann I, Perrotta I, Grillenberger T, Schwestka J, Weiß K, Pum D, Arcalis E, Schwingenschuh S, Birngruber T, Brandstetter M, Heuser T, Schosserer M, Morizot F, Mildner M, Stöger E, Tschachler E, Weinmüllner R, Gruber F, Grillari J. **Extracellular Vesicles in Human Skin: Cross-Talk from Senescent Fibroblasts to Keratinocytes by miRNAs.** *J Invest Dermatol.* 2019 Jun 18.
2. Terlecki-Zaniewicz L, Lämmermann I, Latreille J, **Bobbili MR**, Pils V, Schosserer M, Weinmüllner R, Dellago H, Skalicky S, Pum D, Almaraz JCH, Scheideler M, Morizot F, Hackl M, Gruber F, Grillari J. **Small extracellular vesicles and their miRNA cargo are anti-apoptotic members of the senescence-associated secretory phenotype.** *Aging (Albany NY).* 2018 May 19;10(5):1103-1132.
3. **Bobbili MR**, Mader RM, Grillari J, Dellago H. **OncomiR-17-5p: alarm signal in cancer?.** *Oncotarget.* 2017 Jul 18;8(41):71206-71222.
4. Dellago H*, **Bobbili MR***, Grillari J. **MicroRNA-17-5p: At the Crossroads of Cancer and Aging - A Mini-Review.** *Gerontology.* 2017;63(1):20-28.

**Extracellular Vesicles in Human Skin: Cross-Talk
from Senescent Fibroblasts to Keratinocytes by
miRNAs**

Extracellular Vesicles in Human Skin: Cross-Talk from Senescent Fibroblasts to Keratinocytes by miRNAs

Lucia Terlecki-Zaniewicz^{1,2}, Vera Pils^{1,2}, Madhusudhan Reddy Bobbili², Ingo Lämmermann^{1,2}, Ida Perrotta³, Tonja Grillenberger^{1,2}, Jennifer Schweska^{1,2}, Katrin Weiß^{1,2}, Dietmar Pum⁴, Elsa Arcalis⁵, Simon Schwingenschuh⁶, Thomas Birngruber⁶, Marlene Brandstetter⁷, Thomas Heuser^{7,8}, Markus Schosserer², Frederique Morizot⁹, Michael Mildner¹⁰, Eva Stöger⁵, Erwin Tschachler¹⁰, Regina Weinmüllner^{1,2}, Florian Gruber^{1,10} and Johannes Grillari^{1,2,8,11}

Extracellular vesicles (EVs) and their miRNA cargo are intercellular communicators transmitting their pleiotropic messages between different cell types, tissues, and body fluids. Recently, they have been reported to contribute to skin homeostasis and were identified as members of the senescence-associated secretory phenotype of human dermal fibroblasts. However, the role of EV-miRNAs in paracrine signaling during skin aging is yet unclear. Here we provide evidence for the existence of small EVs in the human skin and dermal interstitial fluid using dermal open flow microperfusion and show that EVs and miRNAs are transferred from dermal fibroblasts to epidermal keratinocytes in 2D cell culture and in human skin equivalents. We further show that the transient presence of senescent fibroblast derived small EVs accelerates scratch closure of epidermal keratinocytes, whereas long-term incubation impairs keratinocyte differentiation in vitro. Finally, we identify vesicular miR-23a-3p, highly secreted by senescent fibroblasts, as one contributor of the EV-mediated effect on keratinocytes in in vitro wound healing assays. To summarize, our findings support the current view that EVs and their miRNA cargo are members of the senescence-associated secretory phenotype and, thus, regulators of human skin homeostasis during aging.

Journal of Investigative Dermatology (2019) ■, ■-■; doi:10.1016/j.jid.2019.05.015

INTRODUCTION

Extracellular vesicles (EVs) are versatile and ubiquitously present membranous particles that participate in intercellular communication by shuttling their functional cargo, such as proteins, RNA, or DNA, to recipient cells (Iraci et al., 2016). In the context of the skin, they have been found in ex vivo

sections of the human papillary dermis (Cretoiu et al., 2015), at sites of age-related cutaneous disorders (Nakamura et al., 2016), at wounds (Huang et al., 2015), and in the stroma of human skin tumors (Jang et al., 2017). In addition, in vitro vesicular cross-talk has been observed between several types of skin cells, including keratinocytes, melanocytes, human dermal fibroblasts (HDF), dermal papilla cells, outer root sheath cells of the hair follicle, and microvascular endothelial cells (Lo Cicero et al., 2015; Huang et al., 2015; Merjaneh et al., 2017; Wäster et al., 2016; Zhou et al., 2018). However, nothing is known about EV-mediated cross-talk between skin fibroblasts and keratinocytes during cellular aging.

In the elderly, senescent cells have been observed in the dermis and in the epidermis (Ressler et al., 2006). Their accumulation with age and at sites of age-associated diseases contributes to cellular, molecular, and structural changes of the dermal and epidermal compartments, where they impair skin homeostasis, causing increased susceptibility for dermatological disorders (Velarde and Demaria, 2016; Waaijer et al., 2016).

Senescent cells are irreversibly growth arrested, partially de- or trans-differentiated, and the acquisition of the senescence-associated secretory phenotype (SASP) is discussed as the most potent contributor of senescent cells to organismal aging. The SASP consists of growth factors, cytokines, chemokines, matrix remodeling enzymes (Coppé et al., 2010), as well as lipids (Ni et al., 2016), and thereby creates a chronically inflamed and pro-tumorigenic

¹Christian Doppler Laboratory for Biotechnology of Skin Aging, Vienna, Austria; ²Department of Biotechnology, University of Natural Resources and Life Sciences, Vienna, Austria; ³Department of Biology, Ecology and Earth Sciences, University of Calabria, Cosenza, Italy; ⁴Department of Nanobiotechnology, University of Natural Resources and Life Sciences, Vienna, Austria; ⁵Department of Applied Genetics and Cell Biology, University of Natural Resources and Life Sciences, Vienna, Austria; ⁶HEALTH – Institut für Biomedizin und Gesundheitswissenschaften, Joanneum Research, Graz, Austria; ⁷Vienna BioCenter Core Facilities GmbH, Vienna, Austria; ⁸Austrian Cluster for Tissue Regeneration, Vienna, Austria; ⁹Department of Biology & Women's Beauty, Chanel, Pantin, France; ¹⁰Department of Dermatology, Medical University of Vienna, Vienna, Austria; and ¹¹Ludwig Boltzmann Institute for Experimental and Clinical Traumatology, Vienna, Austria

Correspondence: Johannes Grillari, Department of Biotechnology, BOKU - University of Natural Resources and Life Sciences, Muthgasse 18, A-1190 Vienna, Austria. E-mail: johannes.grillari@boku.ac.at

Abbreviations: dISF, dermal interstitial fluid; EV, extracellular vesicle; HDF, human dermal fibroblast; PBS, phosphate buffered saline; SASP, senescence-associated secretory phenotype; SEC, size exclusion chromatography; sEV, small extracellular vesicle; SIPS, stress-induced premature senescence/senescent; TEM, transmission electron microscopy

Received 23 April 2018; revised 9 May 2019; accepted 24 May 2019; accepted manuscript published online 18 June 2019; corrected proof published online XXX

microenvironment (Schosserer et al., 2017). The selective removal of senescent cells improves tissue homeostasis and repopulation of the hair bulge niche (Yosef et al., 2016), postpones the onset and severity of age-associated diseases, and thereby extends life- and health span of mice (Baker et al., 2016). However, their elimination in acute wounds delays the healing process, leading to fibrosis and impaired granulation tissue formation (Demaria et al., 2014; Jun and Lau, 2010).

Recently, EVs and their miRNA cargo emerged as communicators of the SASP of human dermal fibroblasts (EV-SASP; Terlecki-Zaniewicz et al., 2018; Urbanelli et al., 2016). In the skin, the presence of specific miRNAs within different layers and cell types regulates the balanced mRNA to miRNA ratio to maintain functional homeostasis (Botchkareva, 2012). Therefore, it is not surprising that the fine tuning of overlapping wound healing phases and skin aging-associated changes are regulated by the transient or constitutive presence of specific miRNAs (Sonkoly et al., 2010).

Here we shed light on the existence of EVs in human skin *ex vivo* and investigate an EV-miRNA cross-talk from fibroblasts to keratinocytes in monolayers and in 3D skin models. Finally, we evaluate how small EVs (sEVs) derived from senescent fibroblasts influence keratinocyte differentiation and their scratch closure capacity *in vitro*.

RESULTS

Extracellular vesicles are present in the human skin

To address if EVs are present in human skin *in vivo*, skin sections were studied by transmission electron microscopy (TEM) and images confirmed the presence of EV-like structures within dermal cells, adjacent to dermal cells in extracellular collagen structures (Figure 1a and b), and within intracellular multivesicular bodies (Figure 1c). These structures also stained positive for the EV marker CD63 by immunogold labeling of resin-free ultrathin cryo-cut skin sections (Figure 1d).

In order to isolate sEVs from human skin, tissue biopsies from two independent donors were disintegrated using dispase, and sEVs contained in accessible material were purified (see scheme in Supplementary Figure S1a). Particles from this crude extract were enriched by using tangential flow filtration with a cut-off of 300 kDa (Supplementary Figure S1b). Median size was approximately 110 nm as determined by nanoparticle tracking analysis (Figure 1e). These particles were positive for EV-markers TSG101 and syntenin, as shown by western blot analysis. However, calnexin, which is expected to be absent in sEVs, was also detectable (Figure 1f and Supplementary Figure S1c and d). Therefore, we further purified the EV enriched, skin derived preparations using size exclusion chromatography (SEC). Thereby, the majority of particles was eluted in the first six fractions and pools of fractions 1 to 3 and 4 to 6 (SEC 1–3, SEC 4–6) were prepared, and particle number was analyzed by nanoparticle tracking analysis, showing enrichment of particles in SEC 1–3, whereas lower numbers were recovered in fractions SEC 4–6 (Figure 1g); however, particle size of the fractions did not differ significantly (Figure 1h). These were then analyzed by western blotting analysis (Figure 1h). The SEC 4–6 fraction, however, showed strong enrichment of syntenin, whereas calnexin staining was close to the detection

limit in western blot analysis (Figure 1i). TEM analysis showed particles below 200 nm, which portrayed a cup-shape characteristic for EVs (Figure 1j). This indicates that with the sequence of purification methods used we were able to isolate sEVs from human skin.

As an additional approach to test the existence of EVs in human skin, dermal interstitial fluid (dISF) was collected by dermal open flow microperfusion (Bodenlenz et al., 2013) and EVs were enriched by two approaches (Supplementary Figure S1e). After removal of cell debris by centrifugation at 500g and 14,000g, respectively, irregularly shaped, double lipid membrane containing, cup-shaped EVs were visible, similar to those isolated from human skin biopsies (Figure 1k). Nanoparticle tracking analysis of these fractions confirmed a particle median size of around 100 nm (Figure 1l). To increase the purity of the EVs isolated from dISF, we performed SEC and analyzed isolated fractions by TEM. As particle counts were very low in the pooled SEC fractions (Supplementary Figure S1f), we were not able to perform western blot analysis or to capture EVs in fractions 4 to 6. However, in pooled SEC fractions 1 to 3, under omission of the 0.22 μm filtration step, cup-shaped particles with sizes between 50–500 nm were detected, albeit too dilute to capture multiple EVs on single frames because of limited dISF sample material (Figure 1m and Supplementary Figure S1g and h). Still, using immunogold labeling, we confirmed the presence of EV marker protein CD81 on the vesicular membrane of these skin derived EVs (Figure 1m, right image, and Supplementary Figure S1h).

Taken together these data strongly suggest the existence of EVs in the interstitium of the skin, which we were able to visualize and enrich for by using independent sample materials and enrichment strategies.

sEV packaged miRNAs are transferred from fibroblasts to keratinocytes in monolayers and 3D cultures

To confirm an EV-mediated miRNA transfer from HDF to primary normal human epidermal keratinocytes, HDF were transfected with *Caenorhabditis elegans*-specific cel-miR-39, which is packaged into EVs (Hergenreider et al., 2012). The sEVs were isolated from fibroblast supernatants and supplemented to keratinocyte culture media (Figure 2a). Cel-miR-39 was detected in fibroblasts (Figure 2b) and in 2D cultured keratinocytes exposed to the purified sEVs after 48 hours (Figure 2c).

In addition, to further test the transfer of miRNAs from fibroblasts to keratinocytes resembling the epidermis of 3D human skin equivalents, cel-miR-39 transfected fibroblasts were embedded into a collagen matrix (“dermis”; Figure 2a). After full maturation over 10 days, dermis and epidermis were separated, RNA isolated, and cel-miR-39 was confirmed to be still present in the dermis (Figure 2d) and in the epidermis (Figure 2e).

These findings suggest that miRNA cross-talk between fibroblasts and keratinocytes in skin equivalents is not limited by the collagen matrix.

sEVs derived from senescent fibroblasts modulate keratinocyte behavior *in vitro*

Since we recently identified sEVs and their miRNA cargo as, to our knowledge, previously unreported members of the

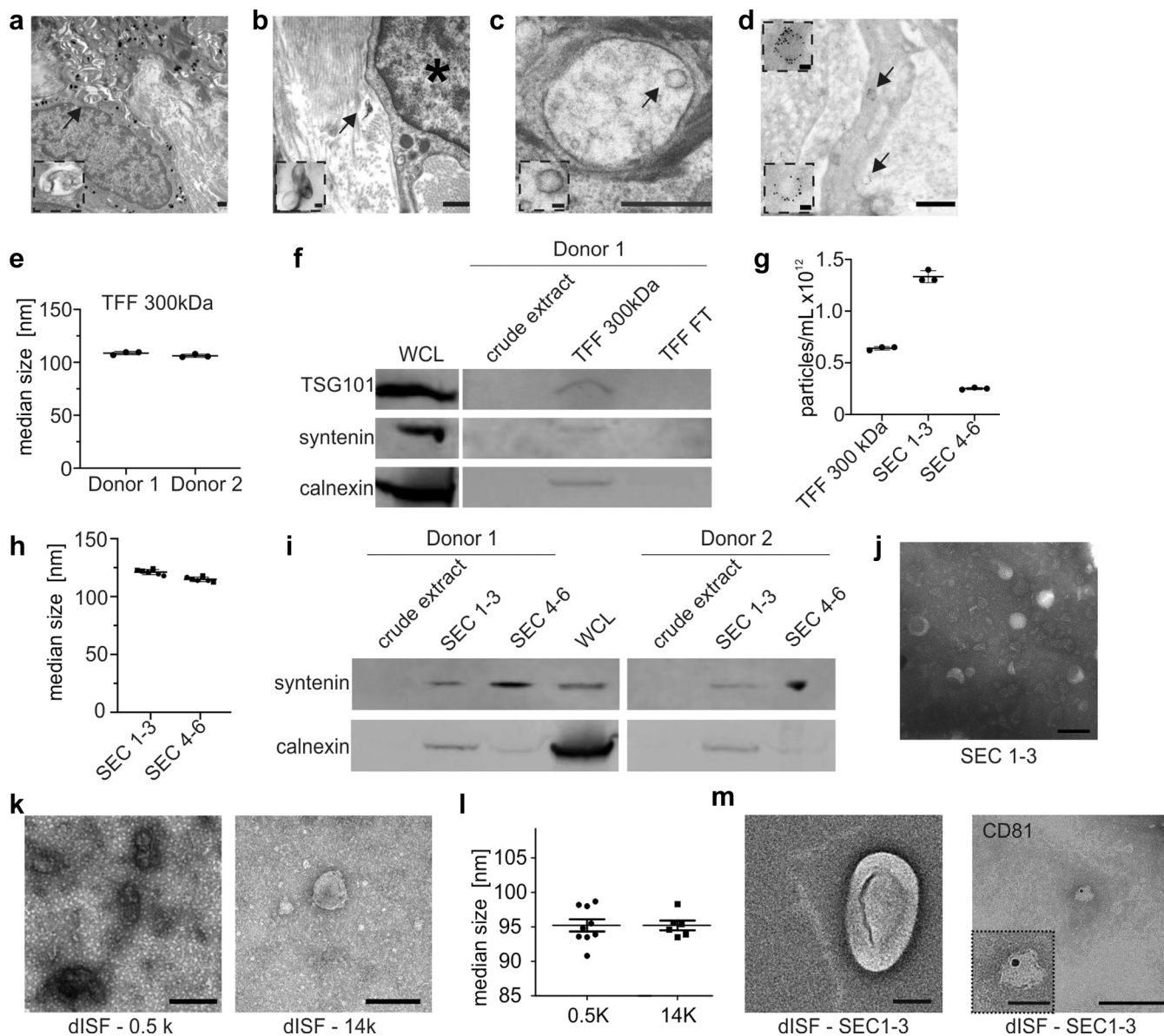


Figure 1. EVs are present in human skin. (a–d) Skin sections derived from 4 donors were used to detect EV-like structures in human skin by TEM. Scale bar = 500 nm (large image) and 50 nm (region of interest). In (b) a fibroblast cell is marked by *. (a) MVBs and EVs within fibroblasts that are secreted or taken up into/from the extracellular space. Arrow indicates one example MVB. (b) Individual EVs in the collagen matrix (arrow). (c) MVB containing intraluminal vesicles (arrow) in cells of the basal layer. (d) Immunogold labeled ultra-thin cryo-cut skin sections show positive staining for EV-specific protein CD63 on EVs (arrow). (e) NTA of sEVs from human skin sections of 2 donors measured in triplicates. sEVs enriched from the crude extract by TFF with a cut-off of 300 kDa show a median size of approximately 100 nm. (f) Western blots for expression of EV-specific protein TSG101 and syntenin, as well as non-EV protein calnexin. sEVs were enriched after TFF (cut-off of 300 kDa) of crude extract of human skin sections. Whole cell lysate (WCL) of fibroblasts served as positive control, the TFF flow through as negative control. (g) Enriched sEVs from f were further purified using SEC. The first 6 fractions were pooled into 2 samples (SEC 1–3 and SEC 4–6) and subsequently concentrated by spin-filters. NTA measurements reveal high particle count in the first 6 eluted fractions after SEC. (h) NTA of sEVs from g reveals a median size of approximately 121 nm in pooled fractions 1–3 and 114 nm in pooled fractions 4–6. Each donor (●, ■) was measured in triplicates. (i) Western blot for expression of EV-specific protein syntenin and non-EV protein calnexin in crude extracts and pooled SEC fractions from g reveals enrichment of EVs in section 4–6. WCL of fibroblasts served as a positive control. (j) TEM image of purified sEVs from g (1:10 dilution of fractions 1–3) reveals particles below 200 nm with a cup-shaped morphology, indicative of sEVs. Scale bar = 200 nm. (k) dISF from 2 donors collected at two positions was centrifuged at 500g (0.5K) and subsequently at 14,000g (14K). TEM images of both fractions show cup-shaped EVs with a double lipid membrane and sizes between 50 to 150 nm. Scale bar = 200 nm. (l) NTA of the 0.5K and 14K EV fraction from k reveals a median size of 95 nm. 0.5K fractions were measured in technical triplicates. 14K fractions were measured in duplicates. (m) After two centrifugations steps (700g and 2,000g) EVs from dISF of 2 different donors were further purified by SEC and spin-filters. TEM of pooled fractions 1–3 without (left image) or with (right image) immunogold labeling against tetraspanin CD81. Scale bar = 200 nm (large images) and 50 nm (region of interest). dISF, dermal interstitial fluid; EV, extracellular vesicle; MVB, multivesicular bodies; NTA, nanoparticle tracking analysis; SEC, size exclusion chromatography; sEV, small extracellular vesicle; TEM, transmission electron microscopy; TFF, tangential flow filtration; WCL, whole cell lysate.

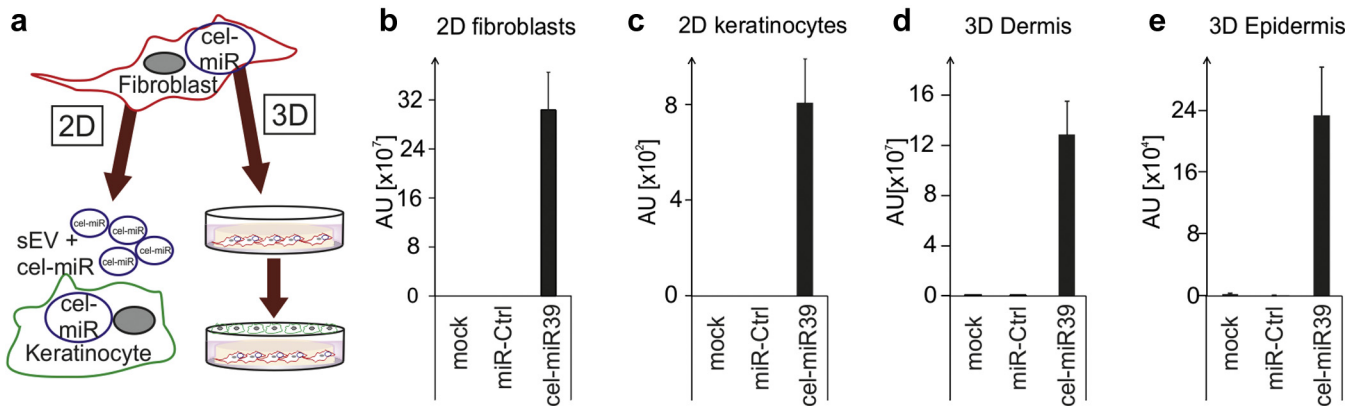


Figure 2. Extracellular vesicles and their miRNA cargo cross-talk between dermal and epidermal cells in monolayers and in 3D full thickness HSE. (a) Experimental design. Cel-miR-39 and a non-targeting control miRNA (miR-Ctrl) were overexpressed in HDF. 24 hours post transfection sEVs were harvested and added to NHEK medium for testing miRNA uptake (2D; left arm). Alternatively (3D; right arm), HDF were embedded into a collagen matrix to build 3D HSE. NHEK were seeded on top and functional HSE were formed in submerge followed by air-liquid interface cultivation. After 10 days, dermis and epidermis were harvested separately, RNA was isolated, and QPCR was performed. (b) 24 hours post transfection cel-miR-39 expression in HDF was evaluated by QPCR. (c) 48 hours post sEV-incubation, transfer of cel-miR-39 by fibroblast derived sEVs to keratinocytes was evaluated by QPCR. (d) 10 days post transfection cel-miR-39 expression was quantified in the dermis of HSE. (e) 10 days post transfection cel-miR-39 expression was quantified in the epidermis of HSE. Experiments were performed with fibroblasts and keratinocytes from three different donors. Data are shown as mean \pm SEM. For QPCR quantification, raw Ct values were transformed to arbitrary units (AU) by assuming a Ct value of 40 to be 10 AU. HDF, human dermal fibroblast; HSE, human skin equivalent; NHEK, normal human epidermal keratinocytes; QPCR, quantitative reverse transcriptase in real time; SEM, standard error of the mean; sEV, small extracellular vesicle.

senescence-associated secretory phenotype (EV-SASP) of fibroblasts (Terlecki-Zaniewicz et al., 2018), we aimed to test how these sEVs might alter the normal homeostasis of primary keratinocytes. Therefore, HDF were driven into stress-induced premature senescence (SIPS) by repetitive exposure to H₂O₂ (Lämmermann et al., 2018; Terlecki-Zaniewicz et al., 2018). Induction of SIPS was confirmed by increased p21 levels (Supplementary Figure S2a), irreversible growth arrest (not shown), by a flattened and enlarged morphology (Supplementary Figure S2b), and by an increase in SA- β -Gal activity (Supplementary Figure S2c and d). sEVs of senescent (SIPS) and quiescent control HDF were purified from conditioned media using differential centrifugation and analyzed by TEM (Figure 3a), nanoparticle tracking analysis (Figure 3b), and immunoblotting (Figure 3c). Membranous particles of around 110 nm in size were revealed, which stained positive for the EV-specific marker syntenin and TSG101, but negative for non-EV marker calnexin in western blots.

To monitor how the transient presence of senescent fibroblast derived sEVs modulates wound closure of keratinocytes in vitro, we used a 2D culture model to follow the dynamics of wound closure in terms of repopulation of the cell-free area (gap), as well as using scratch assays after a single addition of sEVs. Keratinocytes of three different donors were exposed for 48 hours to sEVs from quiescent or senescent fibroblasts. Exposure to the senescent cell derived sEVs doubled the number of cells in the cell-free area (Figure 3d and e, and Supplementary Figure S3a) and accelerated the closure dynamics in both assay setups compared with cells exposed to sEVs from quiescent fibroblasts (Figure 3f and Supplementary Figure S3b). Although we cannot differentiate between cell migration and proliferation in our experimental setup, appearance of filopodia and lamellipodia-like protrusions (Figure 3d and Supplementary Figure S3a) and an increase in vimentin expression upon exposure to senescent cell derived sEVs (Figure 3g) point toward an at least partial

contribution by migration, for which a more mesenchymal-like phenotype is a prerequisite (Yan et al., 2010).

In order to test the impact of chronic presence of the EV-SASP on keratinocyte differentiation in vitro, we exposed keratinocytes to sEVs from quiescent or senescent fibroblasts for one week. The presence of senescent cell derived sEVs changed the morphology of the confluent keratinocyte layer (Figure 3h) and reduced the expression levels of the late differentiation marker involucrin (Figure 3i), which is reported to be a main initiator of the cornification process in vivo (Robinson et al., 1996; Watt and Green, 1981).

To summarize, we observed an enhanced scratch/gap (wound) closure with a concomitant rise in vimentin expression after the short term presence of senescent derived sEVs, whereas their chronic presence affected terminal differentiation of keratinocytes in vitro.

miR-23a-3p contributes to the sEV-SASP mediated acceleration of wound closure

In order to test if imbalanced keratinocyte homeostasis might be attributable to specific miRNAs, we selected miR-23a-3p as a prominent candidate because it was highly secreted in sEVs of senescent fibroblasts (Terlecki-Zaniewicz et al., 2018) and repeatedly connected with cellular senescence and skin aging (Röck et al., 2015). Indeed, we confirmed secreted miR-23a-3p to be more abundantly secreted by senescent cells (Supplementary Figure S3c). RNase digestion in the absence of Triton X-100 was then used to determine miR-23a-3p levels presumably protected by lipid membrane structures (Figure 4a). The fraction of miR-23a-3p that is not accessible to RNase is still elevated in the sEV preparation of senescent cell supernatants, whereas almost all miR-23a-3p is digested by RNase treatment in the presence of Triton X-100. This suggests that the vast majority of miR-23a-3p is either freely accessible to RNase or protected by lipid membranes. The remaining small fraction, which is below

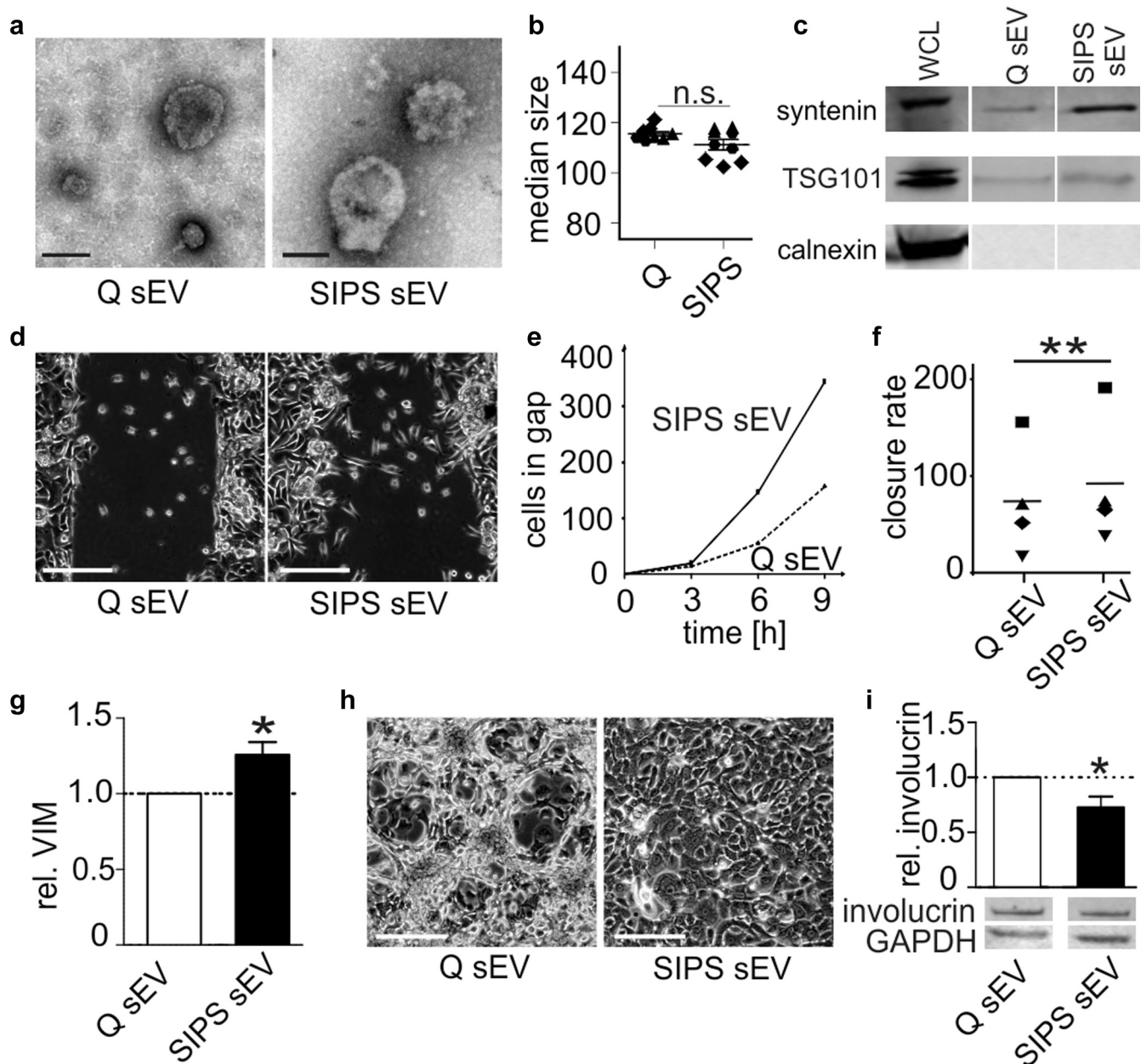


Figure 3. sEVs derived from senescent HDF modulate gap/scratch “wound” closure and differentiation of recipient keratinocytes in vitro. (a) Representative transmission electron microscopy image of sEVs purified by differential centrifugation from Q and SIPS HDF. Scale bar = 100 nm. (b) Median diameter ($\times 50$, [nm]) of sEVs isolated by differential centrifugation. Values ($\times 50$) from peak analysis are indicated as mean \pm SEM. Samples were measured in technical triplicates from three biological replicates. $P > 0.05$; unpaired Student t test. (c) Qualitative western blots for expression of EV-specific proteins TSG101 (44 kDa), syntenin (32 kDa), and non-EV specific protein calnexin (75 kDa) of sEV lysates isolated from conditioned media of quiescent (Q sEV) and senescent (SIPS sEV) fibroblasts by differential centrifugation. Total cell lysate (WCL) of fibroblasts (TSG101) or HeLa cells (syntenin, calnexin) served as a control. (d) Representative images of keratinocytes growing into cell-free area of 2D culture dishes 9 hours post removal of the inserts. Cells were either exposed to sEVs derived from SIPS or Q HDF for 48 hours. Scale bar = 400 μ m. (e) Number of keratinocytes within the gap of 2D culture dishes after transient (48 hours) exposure to Q or SIPS derived sEVs at various timepoints. One representative experiment is shown. (f) Closure rate of keratinocytes after transient (48 hours) exposure to Q or SIPS derived sEVs was calculated from first and last timepoint as assessed in 2D culture dishes. Dot plot shows single replicates and means from four independent experiments. sEV are derived from three different fibroblast strains (SIPS and Q) and were incubated with keratinocytes of two different donors. $**P < 0.01$; paired Student t test. (g) Relative VIM expression after transient (48 hours) exposure to SIPS or Q derived sEVs from HDF. FC \pm relative SEM from six independent experiments were calculated after normalization to B2M. $*P < 0.05$; one sample t test. (h) Representative images show morphological changes of keratinocytes after chronic exposure (1 week) to SIPS and Q derived sEVs from HDF. Scale bar = 400 μ m. (i) Representative western blot images of GAPDH and involucrin protein levels. Densitometric analysis of relative involucrin levels normalized to cells exposed to Q sEVs are shown. Averages \pm relative SEM from eight independent experiments from three different fibroblast strains and keratinocytes are shown. $*P < 0.05$; Wilcoxon signed rank test. EV, extracellular vesicle; FC, fold change; GAPDH, glyceraldehyde-3-phosphate dehydrogenase; HDF, human dermal fibroblast; n.s., not significant; Q, quiescent; SEM, standard error of the mean; sEV, small extracellular vesicle; SIPS, stress-induced premature senescence/senescent; VIM, vimentin.

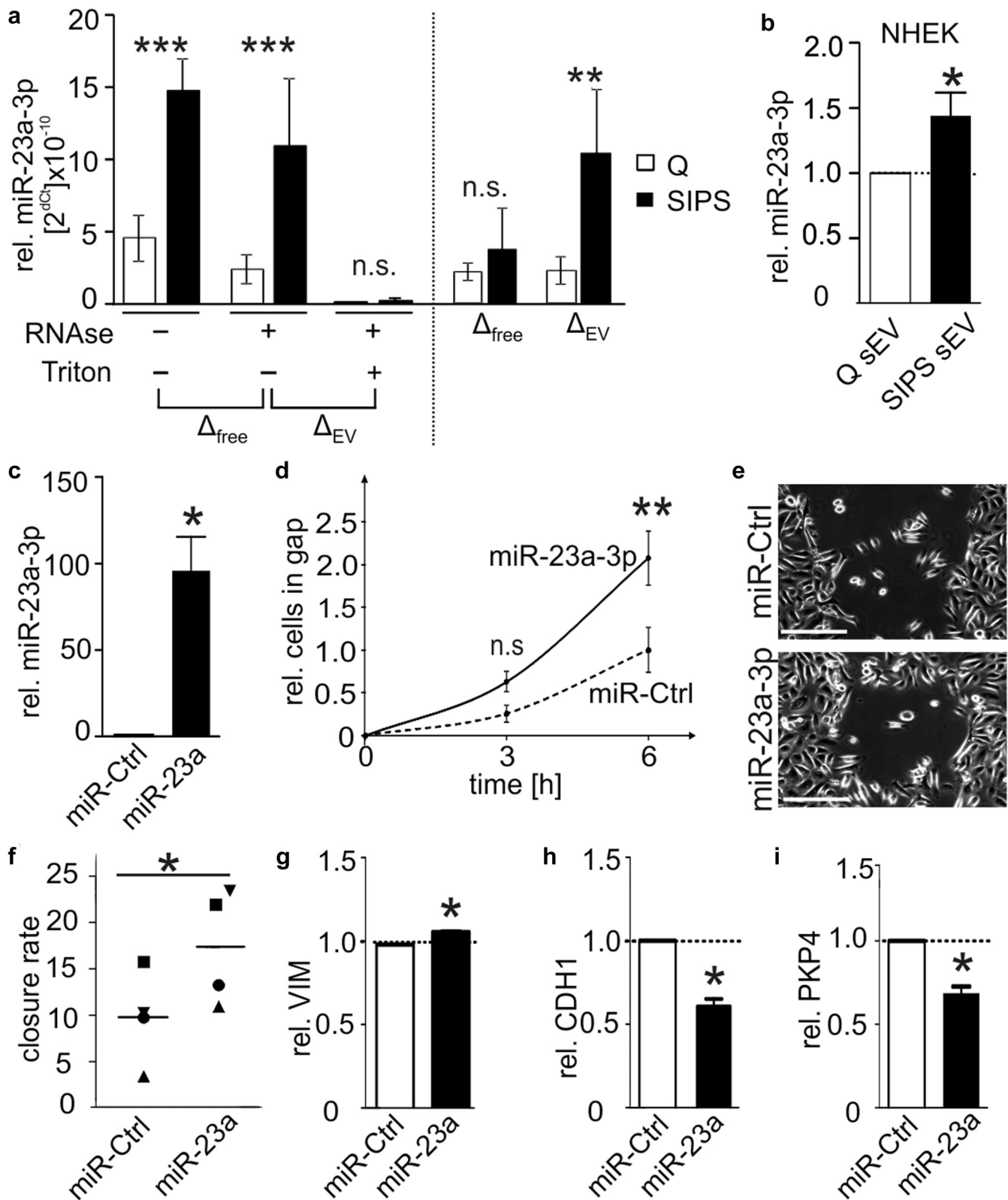


Figure 4. miR-23a-3p phenocopies the effect of senescent cell derived sEVs on wound closure. (a) After differential centrifugation, each sample was split into three equal parts, which were treated either with RNase and Triton X-100 (+/+), RNase only (+/-), or with HEPES only (-/-). MiR-23a-3p levels were measured by QPCR and normalized to spike-in control and cell count. The amount of free miR-23a-3p (Δ_{free}) is calculated by subtraction of (+/-) signal from (-/-) signal; vesicular miR-23a-3p (Δ_{EV}) by subtraction of (+/+) from (+/-). Data from three independent experiments are shown. Statistical analysis was performed using two-way randomized ANOVA tested for the factor "treatment" ($P < 0.001$) and "SIPS versus Q" ($P < 0.001$), or " Δ_{free} versus Δ_{EV} " ($P = 0.06$) and "SIPS versus Q" ($P = 0.014$). Bonferroni post hoc test was performed to compare individual samples. * $P > 0.05$, ** $P < 0.01$, *** $P > 0.001$. (b) miR-23a-3p expression in keratinocytes exposed to senescent or quiescent derived sEVs was normalized to U6 as a housekeeper. FC relative to cells exposed to Q derived sEVs were calculated. Mean \pm SEM values derived from 11 independent experiments using three different keratinocyte and fibroblast donors. * $P < 0.05$;

7% of the total quantitative reverse transcriptase in real time signal, might be protected by other structures, such as proteinaceous particles.

In order to visualize the influence of senescence on freely accessible (Δ_{free}) versus lipid membrane protected miR-23a-3p (Δ_{EV}), we calculated the respective differences (Figure 4a). Indeed, Δ_{EV} increases significantly in senescent versus control cells, while Δ_{free} miR-23a-3p does not. This indicates that the increase of total miR-23a-3p in the sEV preparations of senescent cells is indeed because of an increased EV-based secretion of this miRNA.

Then, keratinocytes were exposed to sEVs derived from senescent HDF for 48 hours, which resulted in a significant increase of intracellular miR-23a-3p levels (Figure 4b). This, in combination with the transfer of cel-miR-39 from fibroblasts to keratinocytes shown above, suggests an uptake of this miRNA via sEVs by keratinocytes in vitro. However, we have not excluded whether miR-23a-3p might be induced endogenously after sEV exposure within keratinocytes.

To investigate if miR-23a-3p might contribute to the accelerated scratch and gap (wound) closure seen by senescent cell derived sEVs, we transfected keratinocytes with pre-miR-23a-3p and a non-targeting control miRNA. Overexpression was confirmed (Figure 4c) and enhanced gap closure, in terms of cells present in the cell-free area (Figure 4d and e, and Supplementary Figure S3d), as well as closure dynamics (Figure 4f) were observed. In addition, miR-23a-3p transfected cells showed mesenchymal cell-like protrusions (Figure 4e and Supplementary Figure S3d), as it was similarly seen after exposure to senescent cell derived sEVs. In addition, a slight increase in vimentin expression (Figure 4g) and a concomitant decrease of miR-23a-3p's direct target E-cadherin (Cao et al., 2012) were observed (Figure 4h), suggesting again an at least partial epithelial-to-mesenchymal transition. Plakophilin 4 (PKP4/p0071) is a predicted putative target of miR-23a-3p in keratinocytes (Agarwal et al., 2015), which was significantly reduced by miR-23a-3p (Figure 4i). Plakophilin 4A interacts with the desmosomal plaques and the adherens junctions to regulate mechanical strength of keratinocyte monolayers (Calkins et al., 2003). However, miR-23a-3p did not modulate keratinocyte differentiation as assessed by involucrin levels one week after transfection (data not shown).

DISCUSSION

Cross-talk of fibroblasts to keratinocytes by soluble factors affect skin homeostasis, as knockout of AP-1 components in fibroblasts has been shown to impair epidermal

differentiation (Szabowski et al., 2000) and wound healing in mouse models in vivo (Florin et al., 2006). However, little is known as to whether EVs and their miRNA cargo exist in different layers of the human skin and if they are involved in the regulation of skin homeostasis during aging. Here we report the presence of multivesicular bodies as one source of secreted sEVs in fibroblasts. This presence of EVs in vivo is supported by indications of EVs at sides of wounds from human skin biopsies (Huang et al., 2015) and their visualization adjacent to interstitial dermal cells by 3D electron microscopy (Cretoiu et al., 2015).

In the context of fibroblast aging, little is known about EVs (Lehmann et al., 2008; Terlecki-Zaniewicz et al., 2018). Cellular senescence is a key driver of the aging process, and the SASP has been shown to promote tumorigenesis of epidermal cells (Krtolica et al., 2001) and to increase the number of senescent keratinocytes re-entering the cell cycle, concomitantly with a partial epithelial-to-mesenchymal transition of these escape-keratinocytes (Malaquin et al., 2013). Senescent cell derived EVs have been reported to confer part of this pro-tumorigenic activity (Takasugi et al., 2017), which might be partly attributable to increased secretion of senescent fibroblasts derived EVs (Lehmann et al., 2008) and/or to changes in their miRNA composition (Terlecki-Zaniewicz et al., 2018).

Intriguingly, our data suggest that senescent cell derived sEVs accelerate the scratch/gap closure of keratinocytes in vitro. This is in line with in vivo data showing enhanced wound healing (Demaria et al., 2014) and tissue regeneration (Ritschka et al., 2017) as a beneficial and elementary characteristic of the transient presence of senescent cells and the SASP. However, impaired removal of senescent cells because of decreased immunosurveillance and a constrained T-cell mobility through the extracellular matrix (Moreau et al., 2017) or because of accumulation of senescence by intrinsic or extrinsic stressors leads to chronic accumulation of senescent cells in the skin (Herbig et al., 2006; Lewis et al., 2011). This chronic presence of senescent cells and the SASP might impair tissue homeostasis leading to a gradual loss of barrier function and juvenile appearance, skin malignancies, and to an impaired fibroblasts contraction in wounds (Ballas and Davidson, 2001).

This is in accordance with a restrained epidermal differentiation, which was observed after chronic exposure to sEVs from senescent fibroblasts, substantiating the double-edged role of the SASP and its members, the sEVs. Considering the fine tuning capacity of EV-miRNAs during normal skin homeostasis (Lo Cicero et al., 2015) and their differential

← one sample *t* test. (c) miR-23a-3p expression in keratinocytes after 48 hours post transfection was normalized to U6 as a housekeeper and FC relative to miR-Ctrl transfected keratinocytes were calculated. Mean \pm SEM values derived from three independent experiments are shown. **P* < 0.05; one sample *t* test. (d) Number of keratinocytes within the gap of 2D culture dishes were counted after 3 and 6 hours post removal of the culture insert. Data is normalized to cell number of miR-Ctrl at the last timepoint. Mean \pm relative SEM values derived from four independent experiments are shown. Statistical analysis was performed using two-way randomized ANOVA tested for the factor "transfection" (*P* = 0.0009) and "time" (*P* = 0.069). Bonferroni post test was performed to compare individual samples. ***P* < 0.01. (e) Representative images of keratinocytes growing into cell-free area after miR-23a-3p overexpression. Scale bar = 400 μ m. (f) Closure rate was calculated from first and last timepoint as assessed in 2D culture dishes. Dot plot shows single replicates and calculated means from four independent experiments. **P* < 0.05; paired Student *t* test. (g–i) Vimentin (g), E-cadherin (h), and plakophilin 4 (i) expression 48 hours post transfection in NHEK was normalized to B2M as a housekeeper. FC \pm relative SEM from three independent experiments were calculated relative to miR-Ctrl transfected keratinocytes. **P* < 0.05; one sample *t* test. ANOVA, analysis of variance; FC, fold change; NHEK, normal human epidermal keratinocytes; n.s., not significant; Q, quiescent; qPCR, quantitative reverse transcriptase in real time; SEM, standard error of the mean; sEV, small extracellular vesicle.

secretion during senescence, we speculate that SASP-miRNAs of fibroblasts (Terlecki-Zaniewicz et al., 2018) affect normal keratinocyte homeostasis, as it was similarly shown for endothelial senescence-associated EV-miR-31 in the context of osteogenic differentiation (Weilner et al., 2016). Indeed, we identified miR-23a-3p, highly secreted from senescent fibroblasts, as a crucial mediator of the wound healing mediated effect induced by the EV-SASP.

miR-23a-3p is well connected to transforming growth factor β -induced epithelial-to-mesenchymal transition (Cao et al., 2012), cellular senescence (Guo et al., 2013; Markopoulos et al., 2017), and skin aging (Dreesen et al., 2013), showing an age dependent increase in skin sections of old mice and in fibroblasts derived from elderly donors (Röck et al., 2015). Known targets of miR-23a-3p include hyaluronan synthase 2 and E-cadherin, linking it to extracellular matrix production, cardiac development, and tumor progression (Bernert et al., 2011; Camenisch et al., 2001; Cao et al., 2012; Ma et al., 2017). In addition, the predicted target PKP4/p0071 was significantly reduced in keratinocytes upon miR-23a-3p overexpression. It directly interacts with E-cadherin reducing its activity (Keil et al., 2013) and mediates the fine tuning between desmosomal plaques and adherens junctions, in order to regulate mechanical strength versus cell migration (Calkins et al., 2003). Our data support this idea, since increased levels of E-cadherin confer an inhibitory effect on wound healing of epithelial cells (Setzer et al., 2004).

To conclude, we here unraveled the ubiquitous presence of EVs in human skin and their ability to deliver their miRNA cargo from fibroblasts through the collagen matrix into the epidermal layer of 3D human skin equivalents. Finally, we identified fibroblast derived vesicular miR-23a-3p as a crucial “miR-diator” of the EV-SASP induced acceleration of scratch/gap closure in keratinocytes in vitro.

Thus, we are confident that the presence of EVs and their miRNA cargo contributes to the development and recurrence of cutaneous lesions during age-associated diseases and emphasize the necessity to further investigate their functional role.

MATERIAL AND METHODS

Human skin samples

All cells and tissues are derived post liposuction from healthy adult female subjects in the age range of 30 to 40 years. The study was approved by the ethics committee of the Medical University of Vienna and was conducted in accordance with the principles of the Declaration of Helsinki. Written informed consent was obtained (vote no. 1149/2011).

Dermal open flow microperfusion

Human skin samples were used to collect dISF by dermal open flow microperfusion (Bodenlenz et al., 2013). The skin samples were obtained during plastic surgery and were provided by Biobank Graz, Austria, after approval of the ethics committee of the Medical University of Graz (vote no, 28-151 ex 15/16).

Three dermal probes were inserted into each skin sample at different locations immediately after excision. The probes were continuously perfused with physiological saline solution at a flow rate of 1 μ l/min in a push-pull manner using a OFM pump (Joanneum Research, Austria). dISF samples were collected at room

temperature in one-hour intervals. After each interval, the dISF samples were stored at 4 °C until the isolation of EVs and further TEM measurements and nanoparticle tracking analysis.

Cell culture

All cells were regularly tested for mycoplasma. They were cultivated at 95% air humidity, 7% CO₂, and at 37 °C.

Primary HDF from adult human skin of three healthy donors were acquired from Evercyte GmbH (Vienna, Austria). Cells were cultivated in DMEM/Ham's F-12 (1:1 mixture; Biochrom, Berlin, Germany) supplemented with 10% fetal calf serum and 4 mM L-Glutamine (Sigma-Aldrich GmbH, St Louis, MO, USA). Cells were passaged twice a week at a split ratio of 1:2.

Normal human epidermal keratinocytes from adult human skin of three health donors were acquired from Evercyte GmbH. Cells were grown in Dermalife K media supplemented with Dermalife K Life-Factors kit (LifeLine Cell Technology, Frederick, MD). Cells were regularly thawed in passage 2/PD2.5, passaged once in a split ratio of 1:4, and used upon confluence for subsequent experiments.

Stress-induced premature senescence

For induction of SIPS, HDF derived from three different donors were seeded at 3500 cells/cm² 24 hours before stress treatment. Cells were treated with nine doses of 80 μ M H₂O₂ for 1 hour per day followed by a media change (4 days stress, 2 days recovery, 5 days stress). Control cells were mock-treated and reached quiescence by contact inhibition. Induction of SIPS was confirmed earlier (Terlecki-Zaniewicz et al., 2018) by SA- β -Gal staining, CDKN1A (p21) expression, and by prominent morphological changes.

Full thickness human skin equivalents

Human skin equivalents were generated as published earlier (Mildner et al., 2006). A detailed protocol can be found in the supplementary material.

Culture insert for gap (wound) closure and scratch assay

Culture inserts to monitor gap closure. Keratinocytes were seeded with 3×10^4 cells/cm² into μ -Dish 35 wound healing chambers containing culture inserts (IBIDI, Martinsried, Germany). Twenty-four hours after seeding, sEVs were added, and upon confluence (24–48 hours incubation), the silicone insert was removed leaving behind a cell-free area (gap = wound). Fresh culture media was added, and cells were incubated at 37 °C at 7% CO₂.

Scratch assay. Keratinocytes were seeded into 12-well plates. Upon confluence, the monolayer was scratched using a 200 μ l pipette tip. Gap closure was monitored by capturing non-overlapping images along the entirety of the gap/scratch every 3 hours. For the culture inserts, number of cells within the cell-free area were counted manually in a blinded fashion. Scratch assays were quantified using the freehand line tool measuring the entire scratch area. For both assays, the wound closure rate (“slope”) per hour was calculated as shown below.

$$(\text{area or cells } t_{n+1} - \text{area or cells } t_0) \div (t_{n+1} - t_0)$$

Isolation of small extracellular vesicles

EV purification was performed according to standards recommended from the international society for extracellular vesicles (Hill et al., 2013).

From conditioned media of HDF. Fetal calf serum containing media was depleted from EVs by ultracentrifugation at 100,000g overnight and filtrated using 0.22 μm filter cups (Millipore, Darmstadt, Germany). Cells were allowed to secrete for 48 hours. Differential centrifugation was performed at 4 °C. Conditioned media was centrifuged at 500g (5804R; Eppendorf, Hamburg, Germany) for 15 minutes to exclude cellular debris, followed by centrifugation at 14,000g (Avanti JXN-26; Beckmann Coulter, Brea, CA) for 15 minutes. Large EVs were removed by filtration using 0.22 μm filter cups and supernatant was filled into Quick-Seal, Polyallomer, 39 ml, 25 \times 89 mm tubes (Beckmann Coulter) to enrich sEVs at 100,000g for 90 minutes using a 70Ti Rotor (Beckmann Coulter). For subsequent analysis, the pellet was resuspended in filtered phosphate buffered saline (PBS) or keratinocyte media. For functional assays and TEM, freezing and thawing were avoided. The amount of vesicles used for keratinocyte exposure was quantified by the number of secreting fibroblasts to the number of receiving keratinocytes. For functional studies, sEVs in a ratio of 5:1 (fibroblasts:keratinocytes) were used.

From skin sections. Adipose tissue of two skin sections was removed and tissue sections consisting of dermis and epidermis were disintegrated using 1.5 U dispase at 4 °C overnight with continuous agitation followed by incubation at 37 °C for 3 hours. Accessible soluble material was collected and pooled with filtered PBS that was used to wash skin sections twice (crude extract). Subsequently, the crude extract was used for sEV isolation by differential centrifugation followed by filtration using 0.45 μm and 0.22 μm syringe filters. Finally, sEVs were enriched by tangential flow filtration with a cut-off of 300 kDa (mPES MicroKros Filter Modules 300 kD, C02-E300-05-N; Spectrum Labs, Rancho Dominguez, CA) to 1 ml. During this process, flow through was collected. The retentate was then diafiltered twice using the same system with 15 ml 0.22 μm -filtered PBS. The retentate was then either analyzed as it was or further purified by SEC (see below).

From dermal interstitial fluid. The dISF samples of the first 2 hours were pooled and filled up to 200 μL with 10 mM HEPES buffer and centrifuged at 500g for 15 minutes (0.5k fraction). Supernatant was collected and further centrifuged at 14,000g for 15 minutes (14k fraction). Both fractions were used for TEM and nanoparticle tracking analysis. To achieve a greater purity, in a different setup dISF samples from 1-, 2-, and 3-hour timepoints of open flow microperfusion from two donors were pooled and filled up to 500 μL with 0.22 μm -filtered PBS. Samples were centrifuged at 500g for 5 minutes, supernatants collected and centrifuged again at 2,000g for 10 minutes. Supernatants were then applied to SEC columns (see below).

Size exclusion chromatography. SEC was used to achieve greater purity of EVs isolated from skin sections and dISF. We used qEV original columns (70 nm; IZON Science, Christchurch, New Zealand) according to the manufacturer's instructions. Briefly, approximately 500 μL of sample were applied on the column and after 3 ml of void volume, 22 fractions of approximately 0.5 ml each were collected. As according to the manufacturer, the first six fractions contain the bulk of EVs, we pooled fractions 1 to 3 and 4 to 6, and further concentrated them using Amicon spin-filters (10 kDa) until 1.5 ml sample were concentrated to \sim 30–50 μL . These were then used for subsequent analysis.

RNase and Triton X-100 treatment of isolated sEVs

sEVs were isolated from conditioned media of either quiescent or SIPS HDF according to the aforementioned protocol (see above). Each sample was split into three equal parts and treated either with the following: (i) 38 $\mu\text{g}/\text{ml}$ RNase (+/–, EN0531; Thermo Fisher Scientific, Waltham, MA); (ii) 38 $\mu\text{g}/\text{ml}$ RNase + 1% Triton X-100 (+/+); or (iii) equivalent amounts of 10 mM HEPES (–/–). After incubation at 37 °C for 30 minutes, samples were mixed with five times the original volume in QIAzol Lysis Reagent (79306; QIAGEN, Hilden, Germany) and 1 μL spike-in mix containing UniSp2, UniSp4, and UniSp5 (203203; Exiqon, Vedbaek, Denmark). MiR23a-3p Ct values were normalized to spike-in control (UniSp2) and cell count. Free miR-23a-3p levels were calculated by subtraction of (+/–) signals from (–/–) signals. Subtraction of (+/+) levels from (+/–) levels yielded the amount of vesicular miR-23a-3p.

Transmission electron microscopy

For TEM measurements two different protocols were used.

In one protocol (Figure 1k, left picture, and Figure 3a), solutions used for the staining procedure were prefiltered using 0.22 μm filter units. Athene Old 300 mesh copper grids (Agar Scientific, Stansted, Essex, United Kingdom) were used to adhere sEVs isolated from conditioned media or dISF. The sample was fixed with 1% glutaraldehyde, washed 3 times with nuclease free water, and sEVs were stained for 5 minutes with 2% phosphotungstic acid hydrate (Carl Roth, Karlsruhe, Germany). The grids were left to dry and the specimens were visualized using TEM (FEI Tecnai T20, FEI Eindhoven, Netherlands) operated at 160 kV.

In the second protocol (all other TEM images: Figure 1a–c, j, m), 5 μL of sample were added to glow-discharged Formvar-carbon type B coated electron microscopy grids for 3 minutes, after which the sample was removed by using wet Whatman filter paper. Grids were either prepared for immunogold labeling (see below) or carefully washed twice with filtered PBS before 5 μL of filtered 2% uranyl acetate were added for 10–30 seconds. Then, uranyl acetate was removed using wet Whatman filter paper, and grids were air dried for 2 minutes and imaged.

For immunogold labeling, grids were blocked after the initial binding step of the sample using filtered 2% BSA (in PBS) for 10 minutes. After blocking, grids were placed on 15 μL primary antibody solution (anti-CD81 1:50 in 0.2% BSA) for 60 minutes. Post incubation, grids were washed with 0.2% BSA six times and afterwards placed on a goat anti-mouse secondary antibody solution containing 10 nm gold particles (dilution 1:50) for 60 minutes. Post incubation, grids were washed six times with PBS followed by six washing steps with ddH₂O. Finally, grids were placed on 0.2% uranyl acetate for 10 to 30 seconds. Uranyl acetate was removed using a wet Whatman filter paper, and grids were air dried for 2 minutes and imaged.

TEM of resin embedded skin sections. All specimens were fixed in a buffered 3% glutaraldehyde solution, postfixed in osmium tetroxide (3%) for 2 hours, dehydrated through a graded acetone series, and embedded in Araldite (Fluka, Buchs, Switzerland). Ultrathin sections (60–90 nm thickness) were prepared using a diamond knife, collected on copper grids (G 300 Cu), and examined with a Jeol JEM-1400 Plus electron microscope.

Immunolabeling of resin-free ultrathin cryo-cut sections. Human skin biopsies were fixed in 2% paraformaldehyde and 0.2%

glutaraldehyde (both from EMS, Hatfield, USA) in 0.1 M PHEM buffer pH 6.9 for 2 hours at room temperature, then over night at 4 °C. Samples were cut into 1 mm³ blocks that were immersed in 2.3 M sucrose for 1 week at 4 °C. These blocks were mounted onto Leica specimen carrier (Leica Microsystems, Vienna, Austria) and frozen in liquid nitrogen. With a Leica UCT/fetal calf serum cryo-ultramicrotome (Leica Microsystems, Vienna, Austria) the frozen blocks were cut into ultrathin sections at a nominal thickness of 60 nm at -120 °C. A mixture of 2% methylcellulose and 2.3 M sucrose in a ratio of 1:1 was used as a pickup solution. Sections were picked up onto 200 mesh Ni grids (Gilder Grids, Lincolnshire, United Kingdom) with a carbon coated Formvar film (Fixation, embedding, and cryo-sectioning as described by Tokuyasu, 1973).

Before immunolabeling, grids were placed on plates with solidified 2% gelatin and warmed up to 37 °C for 20 minutes to remove the pickup solution. After quenching of free aldehyde-groups with glycine (0.1% for 15 minutes), a blocking step with 1% BSA (fraction V) in 0.1M Sörensen phosphate buffer pH 7.4 was performed for 30 minutes. The grids were incubated in primary antibody, mouse anti-CD63 (ab8219; Abcam, Cambridge, United Kingdom), diluted 1:1000 in 0.1 M Sörensen phosphate buffer containing 0.1% BSA (Fraction V) overnight at 4 °C, followed by a 2-hour incubation in the secondary antibody, a goat-anti-mouse antibody coupled with 6 nm gold (GAR 6 nm, Aurion, Wageningen, The Netherlands), diluted 1:20 in 0.1 M Sörensen phosphate buffer containing 0.1% BSA (Fraction V), performed at room temperature. The sections were stained with 4% uranyl acetate (Merck, Darmstadt, Germany) and 2% methylcellulose in a ratio of 1:9 (on ice). All labeling steps were done in a wet chamber. The sections were inspected in a FEI Morgagni 268D TEM (FEI, Eindhoven, The Netherlands) operated at 80 kV. Electron micrographs were acquired using an 11 megapixel Morada CCD camera from Olympus-SIS (Münster, Germany).

Statistical analysis

Routine statistics were either calculated with Excel or Graph Pad Prism, version 5.03, and respective tests are indicated in figure legends. Averages from at least three independent experiments with different cell strains are presented as mean ± standard error of the mean or standard deviation. Two-tailed *t* tests were performed using an error probability of 0.05.

Data was tested for Gaussian distribution using the Shapiro-Wilk test. If normal distributed, two groups were compared using unpaired or paired Student *t* test using raw values. One sample Student *t* test or Wilcoxon signed rank test was used to compare ratios to a hypothetical value of 1 after normalization. Comparison of more than two groups was performed using one-way analysis of variance after Tukey's multiple comparison tests. To analyze the impact of two independent factors a two-way repeated measure analysis of variance was performed followed by Bonferroni post test.

Additional information on the material and methods are available in the supplementary text.

Data availability statement

Datasets related to this article are available from the corresponding author upon reasonable request.

ORCID

Lucia, Terlecki-Zaniewicz: <https://orcid.org/0000-0003-2243-9869>

Vera, Pils: <https://orcid.org/0000-0002-3794-0376>

Madhusudhan Reddy, Bobbili: <https://orcid.org/0000-0001-9955-0675>

Ingo, Lämmermann: <https://orcid.org/0000-0001-6675-0734>

Ida, Perrotta: <https://orcid.org/0000-0002-9061-9776>

Tonja, Grillenberger: <https://orcid.org/0000-0002-4140-041X>

Jennifer, Schwestka: <https://orcid.org/0000-0001-8824-2159>

Katrin, Weiß: <https://orcid.org/0000-0002-0189-9885>

Dietmar, Pum: <https://orcid.org/0000-0002-1895-4940>

Elsa, Arcalis: <https://orcid.org/0000-0001-9883-465X>

Simon, Schwingenschuh: <https://orcid.org/0000-0001-9549-1065>

Thomas, Birngruber: <https://orcid.org/0000-0001-8827-4660>

Marlene, Brandstetter: <https://orcid.org/0000-0002-8134-4985>

Thomas, Heuser: <https://orcid.org/0000-0001-7385-0178>

Markus, Schosserer: <https://orcid.org/0000-0003-2025-0739>

Frédérique, Morizot: <https://orcid.org/0000-0003-0601-7885>

Michael, Mildner: <https://orcid.org/0000-0002-6892-925X>

Eva, Stoeger: <https://orcid.org/0000-0002-7651-7992>

Erwin, Tschachler: <https://orcid.org/0000-0002-0248-1798>

Regina, Weinmüller: <https://orcid.org/0000-0002-3971-4348>

Florian, Gruber: <https://orcid.org/0000-0003-1094-5641>

Johannes, Grillari: <https://orcid.org/0000-0001-5474-6332>

CONFLICT OF INTEREST

JG is cofounder of TAmiRNA GmbH and Evercyte GmbH. FM is employee of Chanel Research technology.

ACKNOWLEDGMENTS

This work was funded by the Christian Doppler Society and financially supported by the Austrian Federal Ministry of Economy, Family and Youth; the National Foundation for Research, Technology and Development; the Austrian Science Fund (FWF: I2514 to JG); and the Austrian Science Fund PhD Program BioToP—Biomolecular Technology of Proteins (W1224). We additionally acknowledge the FP7 EU project Frailomic.

We thank Barbara Schapfl and Petra Cazzanelli for technical assistance. The EM Facility of the Vienna BioCenter Core Facilities GmbH (VBCF) acknowledges funding from the Austrian Federal Ministry of Education, Science and Research and the City of Vienna.

AUTHOR CONTRIBUTIONS

Conceptualization: LTZ, JG, FG, FM; Data Curation: LTZ, VP, JG, FG, IL, MRB, DP, EA, ES, MB, TH, IP, MS; Formal Analysis: LTZ, VP, DP, EA, ES, IP, MB, TH, MRB, IL; Funding Acquisition: JG, FG; Investigation: LTZ, VP, TG, IP, JS, RW, IL, MRB, MS, KW, SS, TB, MB, EA, DP, TH, MM; Methodology: LTZ, MRB, IL, VP, RW, TB, SS; Project Administration: FG, JG; Resources: TB, SS, MM, ET; Supervision: JG, FG, ET, FM; Validation: MB, TH, EA, DP; Visualization: LTZ, RW, VP, IL, MS, JG; Writing - Original Draft Preparation: LTZ, JG, RW, VP, IL, MRB, MS, FG; Writing - Review and Editing: LTZ, VP, MRB, IL, IP, TG, JS, KW, DP, EA, SS, TB, MB, TH, MS, FM, MM, ES, ET, RW, FG, JG.

SUPPLEMENTARY MATERIAL

Supplementary material is linked to the online version of the paper at www.jidonline.org, and at <https://doi.org/10.1016/j.jid.2019.05.015>.

REFERENCES

- Agarwal V, Bell GW, Nam JW, Bartel DP. Predicting effective microRNA target sites in mammalian mRNAs. *Elife* 2015;4:e05005.
- Baker DJ, Childs BG, Durik M, Wijers ME, Sieben CJ, Zhong J, et al. Naturally occurring p16 Ink4a-positive cells shorten healthy lifespan. *Nature* 2016;530:184–9.
- Ballas CB, Davidson JM. Delayed wound healing in aged rats is associated with increased collagen gel remodeling and contraction by skin fibroblasts, not with differences in apoptotic or myofibroblast cell populations. *Wound Repair Regen* 2001;9:223–37.
- Bernert B, Porsch H, Heldin P. Hyaluronan synthase 2 (HAS2) promotes breast cancer cell invasion by suppression of tissue metalloproteinase inhibitor 1 (TIMP-1). *J Biol Chem* 2011;286:42349–59.
- Bodenlenz M, Aigner B, Dragatin C, Liebenberger L, Zahiragic S, Höfferer C, et al. Clinical applicability of dOFM devices for dermal sampling. *Skin Res Technol* 2013;19:474–83.
- Botchkareva NV. MicroRNA/mRNA regulatory networks in the control of skin development and regeneration. *Cell Cycle* 2012;11:468–74.
- Calkins CC, Hoepner BL, Law CM, Novak MR, Setzer SV, Hatzfeld M, et al. The armadillo family protein p0071 is a VE-cadherin- and desmoplakin-binding protein. *J Biol Chem* 2003;278:1774–83.

- Camenisch TD, Biesterfeldt J, Brehm-Gibson T, Bradley J, McDonald JA. Regulation of cardiac cushion development by hyaluronan. *Exp Clin Cardiol* 2001;6:4–10.
- Cao M, Seike M, Soeno C, Mizutani H, Kitamura K, Minegishi Y, et al. MiR-23a regulates TGF- β -induced epithelial-mesenchymal transition by targeting E-cadherin in lung cancer cells. *Int J Oncol* 2012;41:869–75.
- Coppé JP, Desprez PY, Krtolica A, Campisi J. The senescence-associated secretory phenotype: the dark side of tumor suppression. *Annu Rev Pathol* 2010;5:99–118.
- Cretoiu D, Gherghiceanu M, Hummel E, Zimmermann H, Simionescu O, Popescu LM. FIB-SEM tomography of human skin telocytes and their extracellular vesicles. *J Cell Mol Med* 2015;19:714–22.
- Demaria M, Ohtani N, Youssef SA, Rodier F, Toussaint W, Mitchell JR, et al. An essential role for senescent cells in optimal wound healing through secretion of PDGF-AA. *Dev Cell* 2014;31:722–33.
- Dreesen O, Ong PF, Chojnowski A, Colman A. The contrasting roles of lamin B1 in cellular aging and human disease. *Nucleus* 2013;4:283–90.
- Florin L, Knebel J, Zigrino P, Vonderstrass B, Mauch C, Schorpp-Kistner M, et al. Delayed wound healing and epidermal hyperproliferation in mice lacking JunB in the skin. *J Invest Dermatol* 2006;126:902–11.
- Guo Z, Zhou B, Liu W, Xu Y, Wu D, Yin Z, et al. MiR-23a regulates DNA damage repair and apoptosis in UVB-irradiated HaCaT cells. *J Dermatol Sci* 2013;69:68–76.
- Herbig U, Ferreira M, Condel L, Carey D, Sedivy JM. Cellular senescence in aging primates. *Science* 2006;311:1257.
- Hergenreider E, Heydt S, Tréguer K, Boettger T, Horrevoets AJG, Zeiher AM, et al. Atheroprotective communication between endothelial cells and smooth muscle cells through miRNAs. *Nat Cell Biol* 2012;14:249–56.
- Hill AF, Pegtel DM, Lambert U, Leonardi T, Driscoll LO, Pluchino S, et al. ISEV position paper: extracellular vesicle RNA analysis and bioinformatics. *J Extracell Vesicles* 2013;2.
- Huang P, Bi J, Owen GR, Chen W, Rokka A, Koivisto L, et al. Keratinocyte microvesicles regulate the expression of multiple genes in dermal fibroblasts. *J Invest Dermatol* 2015;135:3051–9.
- Iraci N, Leonardi T, Gessler F, Vega B, Pluchino S. Focus on extracellular vesicles: physiological role and signalling properties of extracellular membrane vesicles. *Int J Mol Sci* 2016;17:171.
- Jang SC, Crescitelli R, Cvjetkovic A, Belgrano V, Bagge RO, Hoog JL, et al. A subgroup of mitochondrial extracellular vesicles discovered in human melanoma tissues are detectable in patient blood [preprint]. *bioRxiv* 2017. (accessed 27 June 2019).
- Jun JII, Lau LF. Cellular senescence controls fibrosis in wound healing. *Aging (Albany NY)* 2010;2:627–31.
- Keil R, Schulz J, Hatzfeld M. P0071/PKP4, a multifunctional protein coordinating cell adhesion with cytoskeletal organization. *Biol Chem* 2013;394:1005–17.
- Krtolica A, Parrinello S, Lockett S, Desprez PY, Campisi J. Senescent fibroblasts promote epithelial cell growth and tumorigenesis: a link between cancer and aging. *Proc Natl Acad Sci U S A* 2001;98:12072–7.
- Lämmermann I, Terlecki-Zaniewicz L, Weinmüller R, Schosserer M, Dellago H, de Matos Branco AD, et al. Blocking negative effects of senescence in human skin fibroblasts with a plant extract. *NPJ Aging Mech Dis* 2018;4:4.
- Lehmann BD, Paine MS, Brooks AM, McCubrey JA, Renegar RH, Wang R, et al. Senescence-associated exosome release from human prostate cancer cells. *Cancer Res* 2008;68:7864–71.
- Lewis DA, Travers JB, Machado C, Somani AK, Spandau DF. Reversing the aging stromal phenotype prevents carcinoma initiation. *Aging (Albany NY)* 2011;3:407–16.
- Lo Cicero A, Delevoeye C, Gilles-Marsens F, Loew D, Dingli F, Guéré C, et al. Exosomes released by keratinocytes modulate melanocyte pigmentation. *Nat Commun* 2015;6:7506.
- Ma F, Li W, Liu C, Li W, Yu H, Lei B, et al. MiR-23a promotes TGF- β 1-induced EMT and tumor metastasis in breast cancer cells by directly targeting CDH1 and activating Wnt/ β -catenin signaling. *Oncotarget* 2017;8:69538–50.
- Malaquin N, Vercamer C, Bouali F, Martien S, Deruy E, Wernert N, et al. Senescent fibroblasts enhance early skin carcinogenic events via a paracrine MMP-PAR-1 axis. *PLoS ONE* 2013;8.
- Markopoulos GS, Roupakia E, Tokamani M, Vartholomatos G, Tzavaras T, Hatzia Apostolou M, et al. Senescence-associated microRNAs target cell cycle regulatory genes in normal human lung fibroblasts. *Exp Gerontol* 2017;96:110–22.
- Merjaneh M, Langlois A, Larochelle S, Cloutier CB, Ricard-Blum S, Moulin VJ. Pro-angiogenic capacities of microvesicles produced by skin wound myofibroblasts. *Angiogenesis* 2017;20:385–98.
- Mildner M, Ballaun C, Stichenwirth M, Bauer R, Gmeiner R, Buchberger M, et al. Gene silencing in a human organotypic skin model. *Biochem Biophys Res Commun* 2006;348:76–82.
- Moreau J-F, Pradeu T, GRignolio A, Nardini C, Castiglione F, Tieri P, et al. The emerging role of ECM crosslinking in T cell mobility as a hallmark of immunosenescence in humans. *Ageing Res Rev* 2017;35:322–35.
- Nakamura K, Jinnin M, Harada M, Kudo H, Nakayama W, Inoue K, et al. Altered expression of CD63 and exosomes in scleroderma dermal fibroblasts. *J Dermatol Sci* 2016;84:30–9.
- Ni C, Narzt MS, Nagelreiter IM, Zhang CF, Larue L, Rossiter H, et al. Autophagy deficient melanocytes display a senescence associated secretory phenotype that includes oxidized lipid mediators. *Int J Biochem Cell Biol* 2016;81:375–82.
- Ressler S, Bartkova J, Niederegger H, Bartek J, Scharfetter-Kochanek K, Jansen-Dürr P, et al. p16INK4A is a robust in vivo biomarker of cellular aging in human skin. *Aging Cell* 2006;5:379–89.
- Ritschka B, Storer M, Mas A, Heinzmann F, Ortells MC, Morton JP, et al. The senescence-associated secretory phenotype induces cellular plasticity and tissue regeneration. *Genes Dev* 2017;31.
- Robinson NA, LaCelle PT, Eckert RL. Involucrin is a covalently crosslinked constituent of highly purified epidermal corneocytes: evidence for a common pattern of involucrin crosslinking in vivo and in vitro. *J Invest Dermatol* 1996;107:101–7.
- Röck K, Tigges J, Sass S, Schütze A, Florea AM, Fender AC, et al. miR-23a–3p causes cellular senescence by targeting hyaluronan synthase 2: possible implication for skin aging. *J Invest Dermatol* 2015;135:369–77.
- Schosserer M, Grillari J, Breitenbach M. The dual role of cellular senescence in developing tumors and their response to cancer therapy. *Front Oncol* 2017;7:278.
- Setzer SV, Calkins CC, Garner J, Summers S, Green KJ, Kowalczyk AP. Comparative analysis of armadillo family proteins in the regulation of A431 epithelial cell junction assembly, adhesion and migration. *J Invest Dermatol* 2004;123:426–33.
- Sonkoly E, Wei T, Pavez L, Loric EP, Suzuki H, Kato M, Törmä H, et al. Protein kinase C-dependent upregulation of miR-203 induces the differentiation of human keratinocytes. *J Invest Dermatol* 2010;130:124–34.
- Szabowski A, Maas-Szabowski N, Andrecht S, Kolbus A, Schorpp-Kistner M, Fusenig NE, et al. C-Jun and JunB antagonistically control cytokine-regulated mesenchymal-epidermal interaction in skin. *Cell* 2000;103:745–55.
- Takasugi M, Okada R, Takahashi A, Virya Chen D, Watanabe S, Hara E. Small extracellular vesicles secreted from senescent cells promote cancer cell proliferation through EphA2. *Nat Commun* 2017;8:15729.
- Terlecki-Zaniewicz L, Lämmermann I, Latreille J, Bobbili MR, Pils V, Schosserer M, et al. Small extracellular vesicles and their miRNA cargo are anti-apoptotic members of the senescence-associated secretory phenotype. *Albany NY: Aging*; 2018.
- Tokuyasu KT. A technique for ultracryotomy of cell suspensions and tissues. *J Cell Biol* 1973;57:551–65.
- Urbanelli L, Buratta S, Sagini K, Tancini B, Emiliani C. Extracellular vesicles as new players in cellular senescence. *Int J Mol Sci* 2016;17.
- Velarde MC, Demaria M. Targeting senescent cells: possible implications for delaying skin aging: A mini-review. *Gerontology* 2016;62:513–8.
- Waaaijer MEC, Gunn DA, Adams PD, Pawlikowski JS, Griffiths CEM, van Heemst D, et al. P16INK4a positive cells in human skin are indicative of

L Terlecki-Zaniewicz et al.

EV-miRNA Cross-Talk of Skin Cells in Aging

- local elastic fiber morphology, facial wrinkling, and perceived age. *J Gerontol A. Biol Sci Med Sci* 2016;71:1022–8.
- Wäster P, Eriksson I, Vainikka L, Rosdahl I, Öllinger K. Extracellular vesicles are transferred from melanocytes to keratinocytes after UVA irradiation. *Sci Rep* 2016;6:27890.
- Watt FM, Green H. Involucrin synthesis is correlated with cell size in human epidermal cultures. *J Cell Biol* 1981;90:738–42.
- Weilner S, Schraml E, Wieser M, Messner P, Schneider K, Wassermann K, et al. Secreted microvesicular miR-31 inhibits osteogenic differentiation of mesenchymal stem cells. *Aging Cell* 2016;15:744–54.
- Yan C, Grimm WA, Garner WL, Qin L, Travis T, Tan N, et al. Epithelial to mesenchymal transition in human skin wound healing is induced by tumor necrosis factor-alpha through bone morphogenic protein-2. *Am J Pathol* 2010;176:2247–58.
- Yosef R, Pilpel N, Tokarsky-Amiel R, Biran A, Ovadya Y, Cohen S, et al. Directed elimination of senescent cells by inhibition of BCL-W and BCL-XL. *Nat Commun* 2016;7:11190.
- Zhou L, Wang H, Jing J, Yu L, Wu X, Lu Z. Regulation of hair follicle development by exosomes derived from dermal papilla cells. *Biochem Biophys Res Commun* 2018;500:325–32.

SUPPLEMENTARY MATERIALS AND METHODS

Full thickness human skin equivalents

A total of 2.5×10^5 human dermal fibroblasts were seeded in a collagen gel consisting of eight parts collagen G (Biochrom, Berlin, Germany), one part $10 \times$ HBSS (Thermo Fisher Scientific, Waltham, MA), and one part fetal calf serum (Sigma-Aldrich, St. Louis, MO) to form the dermis of human skin equivalents. The gel was equilibrated overnight with KGM-2 supplemented with KGM-2 Bullet Kit (Lonza, Basel, Switzerland) followed by a keratinocyte overlay of 1.5×10^6 cells on day 2. On day 3 they were lifted to the air-liquid interface to start differentiation using differentiation media (KGM, Lonza) supplemented with 1.15mM CaCl_2 (Sigma-Aldrich), 50 $\mu\text{g/ml}$ L-ascorbic acid (Sigma-Aldrich), 0.1% BSA (Sigma-Aldrich), 10 $\mu\text{g/ml}$ transferrin (Sigma-Aldrich), and the KGM BulletKit (Lonza) except bovine pituitary extract. The media was refreshed every other day throughout the whole differentiation process. On day 10, dermis (fibroblasts) and epidermis (keratinocytes) were harvested for RNA extraction.

Senescence-associated β -Gal staining

Senescent fibroblasts and corresponding subconfluent non-stressed fibroblast at the middle of their replicative lifespan were stained according to the standard protocol described. Quantification was performed in a blinded and randomized fashion. Senescence-associated β -Gal positive and negative cells from 15 images per well were counted.

miRNA transfection

Keratinocytes in passage 3/PD4.5 were reverse transfected with pre-miR-23a-3p (AM17100; Ambion, Foster City, CA) and scrambled control pre-miR-Ctrl#2 (AM 17111; Thermo Scientific) using siPORT NeoFX transfection agent (AM4511; Thermo Scientific). Per six well 2×10^4 to 3×10^4 cells/cm² (donor dependent) were transfected using 5 μl lipids and 30 nM final concentration of respective pre-miRNAs. Twenty-four hours post transfection, cells received a media change.

Similarly, fibroblasts in PD < 25 were transfected with *C. elegans*-specific cel-miR-39 and scrambled control pre-miR-Ctrl#2 (AM 17111; Thermo Scientific) using siPORT NeoFX transfection agent (AM4511; Thermo Scientific). Twenty-four hours post transfection, either fetal calf serum depleted media was added or the cells were harvested for embedding into skin equivalents.

RNA Isolation

Cells and small extracellular vesicles. Cells and small extracellular vesicles fractions from conditioned media were lysed in TRI Reagent (Sigma) and RNA was isolated according to the manufacturer's protocol. RNA concentration and quality was controlled using Nanodrop spectrometer (ND-1000). To monitor isolation efficiency of small extracellular vesicles-RNA, spike-ins (203203, UniSp2, UniSp4, UniSp5; Exiqon, Vedbaek, Denmark) were added before RNA isolation and RNA was extracted using the miRNeasy Mini kit (217004; Qiagen, Hilden, Germany) according to the manufacturer's instructions.

From dermis and epidermis of human skin equivalents.. Dermal and epidermal layers of human skin equivalents were separated and resuspended in 500 μl TRIzol reagent. Samples were homogenized for 30 seconds using pellet pestles (Z359947; Sigma) on ice, followed by sonication for 30 cycles (30 seconds sonication and 30 seconds hold). Subsequent RNA isolation was performed according to the standard protocol used for routine RNA isolation.

cDNA synthesis

For miRNA quantification. Equal volumes of vesicular-RNA and 10 ng of total RNA were used for cDNA synthesis using Universal cDNA Synthesis Kit II (Exiqon). UniSp6 control was included in small extracellular vesicle samples (Exiqon) to control for enzyme activity. cDNA was synthesized at 42 °C for 60 minutes, followed by 5 minutes at 95 °C.

For mRNA quantification. cDNA was synthesized from 500 ng of total RNA with the High-Capacity cDNA Reverse Transcription Kit including RNase inhibitor (Applied Biosystems, Foster City, CA) for 10 minutes at 25 °C, 120 minutes at 37 °C, 5 minutes at 85 °C.

Quantitative reverse transcriptase in real time (QPCR)

miRNA QPCR analyses were performed using ExiLent SYBR Green master mix and LNA-enhanced miRNA primer (Exiqon). QPCR for mRNA was performed with 5x HOT FIREPol EvaGreen QPCR Mix Plus with ROX (Medibena, Austria). All experiments were performed on a Rotor-GeneQcycler.

Intracellular miRNA expression was quantified using the ddCt method using U6 as a housekeeper.

Because of the absence of a robust vesicular housekeeping miRNA, we decided to use standardized secretion times and equal working volumes for all subsequent steps and normalized raw Ct values to total viable cell number of each sample. For better visualization, Ct values were further transformed to arbitrary units by assuming a Ct value of 40 to be 10 arbitrary units. Arbitrary units are presented as absolute values.

QPCR for mRNA expression levels was performed with 5x HOT FIREPol EvaGreen QPCR Mix Plus with ROX (Medibena) using a Rotor-GeneQcycler. Copy number was determined according to standard curves in duplicates. Samples were pipetted in quadruplicates and normalized to respective housekeeper genes to calculate fold changes. As reference genes we selected glyceraldehyde-3-phosphate dehydrogenase (GAPDH) for fibroblasts and B2M for keratinocytes. All negative controls tested were below detection limit of QPCR (>40).

Primers used for QPCR are the following: B2M sense: GAGATGTCTCGCTCCGTGG, B2M as: TACATGTCTC GATCCCACTTAAC; GAPDH sense: CGACCACTTTGT CAAGCTCA, GAPDH as: TGTGAGGAGGGGAGATTGAG; E-cadherin sense: CCCACCACGTACAAGGGTC, E-cadherin as: CTGGGGTATTGGGGGCATC; Plakophilin4/p0071 sense: AGGCTTGAGCAGAAATCACC, Plakophilin4/p0071 as: CCCTCACTTTCATGGAGAGATGT; VIM sense: GGAGTC CACTGAGTACCGGA, VIM as: GCTTCAACGGCAAAGTTCTC.

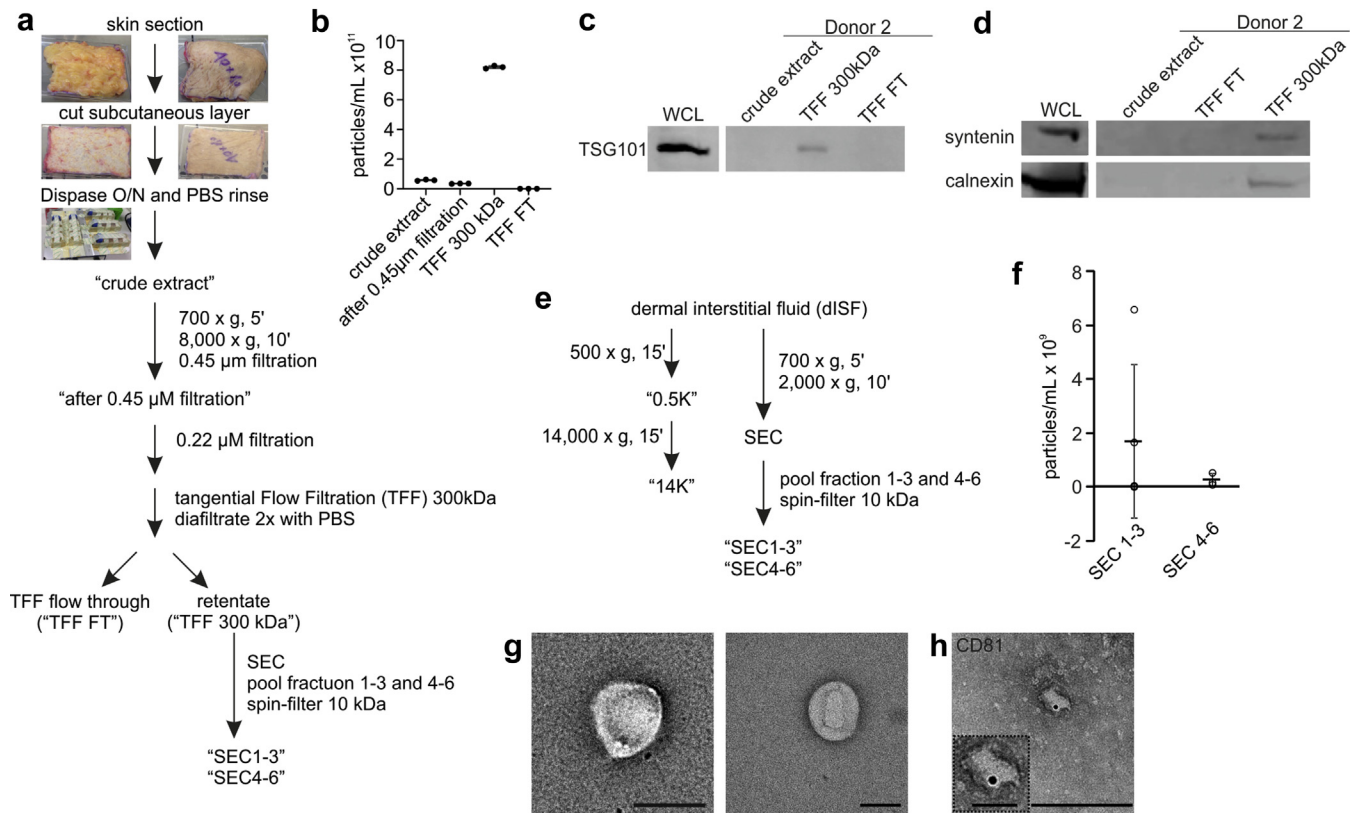
Protein quantification, western blot, and antibodies

Crude skin section extracts or extracellular vesicles enriched from skin sections by tangential flow filtration with a 300 kDa cut-off or size exclusion chromatography, as well as tangential flow filtration flow through, were directly combined with 4 × SDS loading dye (240 mM Tris/HCl, pH 6.8, 8% SDS, 40% glycerol, 0.05% bromophenolblue, 5% β-Mercaptoethanol) after Pierce BCA Protein Assay Kit (23227; Thermo Scientific) or nanoparticle tracking analysis, heated to 95 °C for 10 minutes and subsequently sonicated. Cell pellets of human dermal fibroblasts were lysed in 1 × TNE buffer (2 × TNE: 100 mM Tris/HCl, pH 8.0, 300 mM NaCl, 1 mM EDTA, 2% Triton X-100) or RIPA buffer (150 mM NaCl, 1% NP-40 substitute, 0.5% deoxycholic acid, 0.1% SDS, 20% SDS, 50 mM Tris, pH 8.0) and protein concentration was quantified using the Pierce BCA Protein Assay Kit (23227; Thermo Scientific) according to manufacturer's recommendations. For SDS-PAGE and subsequent western blotting, samples were resuspended in SDS loading dye, heated to 95 °C, and sonicated. Samples were separated either on a NuPAGE 4–12% Bis/Tris polyacrylamide gel (10472322; Invitrogen/Thermo Scientific) or on a 15% Mini-PROTEAN TBE Gel (4565054; Biorad, Hercules, CA) at 200 V and proteins were transferred to a PVDF membrane (170–4156; Biorad) in a Biorad SemiDry Blotting System at 1.3A, 25 V for 7 minutes. After blocking with either 3% milk or 2.5% BSA in 1 × PBS with 0.1% Tween-20 (P2287; Sigma-Aldrich GmbH) for 1 hour, membranes were incubated with primary antibodies in blocking buffer (see below). Proteins were detected using secondary antibodies

for IRDye 800CW donkey anti-rabbit IgG, 0.5 mg (926-32213; LI-COR Biosciences, Lincoln, NE), and IRDye 680RD donkey anti-mouse IgG, 0.5 mg (926-68072; LI-COR Biosciences), with a 1:10000 dilution using the Odysee (LI-COR Biosciences) infrared image system. In 2.5% BSA: TSG101 1:2000 (ab125011; Abcam), syntenin 1:1000 (TA504796; Origene, Rockville, MD), calnexin 1:1000 (ab22595; Abcam). In 3% milk: GAPDH 1:1000 (sc-25778; Santa Cruz, Dallas, TX) and involucrin 1:1000 (MA5-11803; Thermo Fisher).

Nanoparticle tracking analysis

The Zetaview system (Particle Metrix, Meerbusch, Germany) was used for determination of size and concentration of extracellular vesicles. The system was calibrated using 110 nm polystyrene standard beads (Particle Metrix, Meerbusch, Germany). Camera sensitivity was adjusted to fit the highest and lowest concentrated sample and all samples were measured with the same dilution and settings. Settings were the following: Gain 904, 98; Offset 0; 30 frames per seconds. Measurements were taken at 11 different camera positions and analysis was performed with software version 8.04.02.SP1. In case of pooled and concentrated size exclusion chromatography fractions from dISF samples, we used the Nanosight NS300 (Malvern Panalytical, Malvern, United Kingdom) under the following conditions: Temperature, 25 °C; Syringe Pump Speed/Arbitrary units, 50; Camera type, sCMOS; Laser Type, Blue488; number of videos, as stated in figure legend; video duration, 60 seconds; samples were minimally diluted.



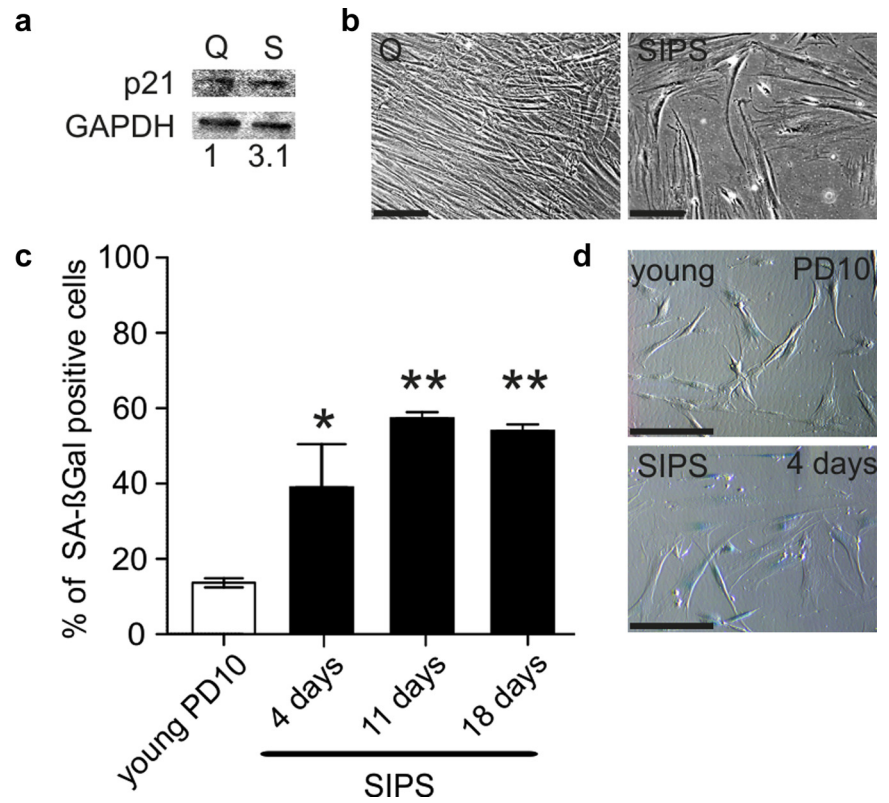
Supplementary Figure S1. Extracellular vesicles are present in the human skin. (a) Scheme of sEV purification from skin sections. Subcutaneous fat layer was removed. Skin sections were cut into small pieces, digested with dispase overnight (O/N), and rinsed with PBS. Solvents were collected making up the crude extract. After differential centrifugation, the crude extract was filtered through various pore sizes (0.45 μ m and 0.22 μ m) and subjected to tangential flow filtration with a cut-off of 300 kDa. The retentate was further purified using SEC. Fractions 1–3 and 4–6 were pooled and concentrated with 10 kDa spin-filters. (b) Particles in crude extract from skin sections are enriched by subsequent 0.45 μ m filtration and TFF (300 kDa) as determined by NTA. Each sample was measured in technical triplicates. (c) Western blot analysis of crude extract and enriched sEVs by TFF (TFF 300 kDa) from human skin sections for EV-specific protein TSG101. Whole cell lysate from human dermal fibroblasts was used as a positive control, TFF flow through as a negative control. (d) Western blot analysis of crude extract and enriched sEVs by TFF (TFF 300 kDa) from human skin sections for EV-specific protein syntenin and non-EV marker calnexin. Whole cell lysate from human dermal fibroblasts was used as a positive control, TFF flow through as a negative control. (e) Scheme of EV purification from dISF. Samples were either subjected to two centrifugation steps at 0.5K and 14Kg and supernatants analyzed or EVs were purified by SEC after two short centrifugation steps. SEC fractions 1 to 3 and 4 to 6 were pooled and concentrated by 10 kDa spin-filters. (f) EVs isolated from dISF by differential centrifugation and subsequent SEC were analyzed by NTA, revealing a very low particle count (concentration warning in all videos). SEC fractions 1–3 and 4–6 were pooled and concentrated using 10 kDa spin-filters. SEC 1–3 was measured in five videos and SEC 4–6 in three videos. (g) TEM images of EVs purified from dISF samples by differential centrifugation and subsequent SEC. Images show EVs in pooled SEC fractions 1–3, which were concentrated by 10 kDa spin-filters. Scale bar = 100 nm. (h) TEM images of EVs purified from dISF samples by differential centrifugation and subsequent SEC. Images show EVs positive for EV marker CD81 by immunogold labeling in pooled SEC fractions 1–3, which were concentrated by 10 kDa spin-filters. Scale bar = 200 nm and 50 nm (region of interest). dISF, dermal interstitial fluid; EV, extracellular vesicle; NTA, nanoparticle tracking analysis; PBS, phosphate buffered saline; SEC, size exclusion chromatography; sEV, small extracellular vesicle; TEM, transmission electron microscopy; TFF, tangential flow filtration.

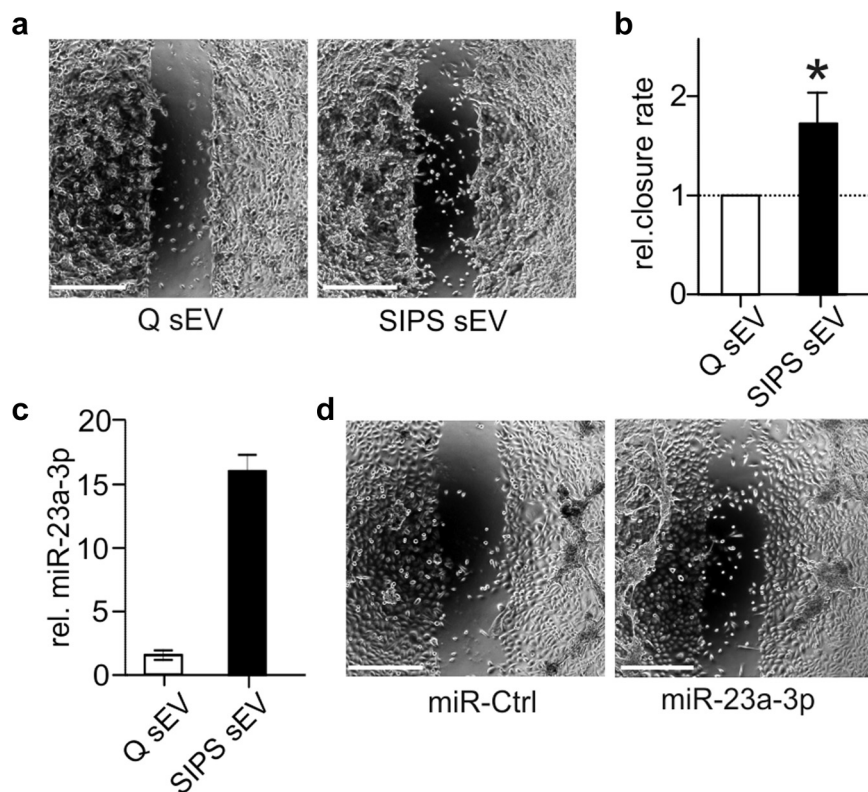
Supplementary

Figure S2. Characterization of stress-induced premature senescence. (a)

Representative western blot shows expression of the cell cycle inhibitor p21 in non-treated Q and SIPS cells. p21 levels were normalized to GAPDH as a housekeeper. (b)

Representative morphology of Q and SIPS cells after 2 weeks recovery post last stress treatment. Scale bar = 200 μ m. (c) Significant increase of SA- β -Galactosidase (SA- β -Gal) in SIPS cells after 4, 11, and 18 days post last stress treatment compared with young (PD10) proliferating cells. A total of 15 pictures were taken randomly at a magnification of $\times 10$ and counting was performed in blinded fashion. Percentages of SA- β -Gal positive cells from all images were calculated. Averages from one donor in triplicates are shown \pm SEM from raw values. * P < 0.05, ** P < 0.01; tested against young PD10. Statistical analysis was performed using one-way ANOVA following Tukey's multiple comparison test. (d) Representative image of SA- β -Galactosidase staining of proliferating (young PD10) and senescent (SIPS) fibroblasts 4 days post last stress treatment. Scale bar = 200 μ m. ANOVA, analysis of variance; GAPDH, glyceraldehyde-3-phosphate dehydrogenase; Q, quiescent; SA, senescence-associated; SEM, standard error of the mean; SIPS, stress-induced premature senescent.





Supplementary Figure S3. sEVs from senescent HDFs and miR-23a-3p overexpression enhance wound/gap closure of keratinocytes.

(a) Representative images of culture inserts show keratinocytes growing into the gap of the cell monolayer after exposure to senescent or quiescent control derived sEVs. Scale bar = 400 μm . (b) Relative closure rate determined in scratch assays of keratinocytes exposed to SIPS or Q derived sEVs. Closure rate was calculated using first and last timepoint and was normalized to Q control. Bar chart shows mean \pm SEM values from six independent experiments, with sEVs from three different fibroblast donors and three different donors of recipient keratinocytes. $*P < 0.05$; Wilcoxon signed rank test. (c) miR-23a-3p levels in sEVs of senescent and quiescent fibroblasts after 3 weeks post stress treatment. Raw Ct values of miR-23a-3p were normalized to the number of cells used for sEV purification, and arbitrary units were calculated from Ct values by assuming a Ct value of 40 to be 10 AU. Data of three biological replicates \pm SEM are presented. (d) Representative images of 2D culture dishes show keratinocytes transfected with miR-23a-3p or respective miR-Ctrl growing into the gap. Scale bar = 400 μm . AU, arbitrary units; HDF, human dermal fibroblast; Q, quiescent; SEM, standard error of the mean; sEV, small extracellular vesicle; SIPS, stress-induced premature senescent.

**Small extracellular vesicles and their miRNA cargo
are anti-apoptotic members of the senescence-
associated secretory phenotype**

Small extracellular vesicles and their miRNA cargo are anti-apoptotic members of the senescence-associated secretory phenotype

Lucia Terlecki-Zaniewicz^{1,2}, Ingo Lämmermann^{1,2}, Julie Latreille³, Madhusudhan Reddy Bobbili², Vera Pils^{1,2}, Markus Schosserer², Regina Weinmüller^{1,2}, Hanna Dellago⁹, Susanna Skalicky⁹, Dietmar Pum¹⁰, Juan Carlos Higareda Almaraz^{5,6,7,8}, Marcel Scheideler^{5,6,7,8}, Frédérique Morizot³, Matthias Hackl⁹, Florian Gruber^{1,4}, Johannes Grillari^{1,2}

¹Christian Doppler Laboratory for Biotechnology of Skin Aging, Vienna, Austria

²Department of Biotechnology, University of Natural Resources and Life Sciences, Vienna, Austria

³Department of Biology and Women Beauty, Chanel R&T, Pantin, France

⁴Division for Biology and Pathobiology of the Skin, Department of Dermatology, Medical University of Vienna, Vienna, Austria

⁵Institute for Diabetes and Cancer (IDC), Helmholtz Zentrum München, German Research Center for Environmental Health, Neuherberg, Germany

⁶Joint Heidelberg-IDC Translational Diabetes Program, Heidelberg University Hospital, Heidelberg, Germany

⁷Molecular Metabolic Control, Medical Faculty, Technical University Munich, Germany

⁸German Center for Diabetes Research (DZD), Neuherberg, Germany

⁹TAmiRNA GmbH, Vienna, Austria

¹⁰Department of Nanobiotechnology, University of Natural Resources and Life Sciences, Vienna, Austria

Correspondence to: Johannes Grillari; **email:** johannes.grillari@boku.ac.at

Keywords: senescence-associated secretory phenotype (SASP), cellular senescence, small extracellular vesicle (sEV), exosomes, microRNA (miRNA)

Received: February 16, 2018

Accepted: May 10, 2018

Published: May 19, 2018

Copyright: Terlecki-Zaniewicz et al. This is an open-access article distributed under the terms of the Creative Commons Attribution License (CC BY 3.0), which permits unrestricted use, distribution, and reproduction in any medium, provided the original author and source are credited.

ABSTRACT

Loss of functionality during aging of cells and organisms is caused and accompanied by altered cell-to-cell communication and signalling. One factor thereby is the chronic accumulation of senescent cells and the concomitant senescence-associated secretory phenotype (SASP) that contributes to microenvironment remodelling and a pro-inflammatory status. While protein based SASP factors have been well characterized, little is known about small extracellular vesicles (sEVs) and their miRNA cargo. Therefore, we analysed secretion of sEVs from senescent human dermal fibroblasts and catalogued the therein contained miRNAs. We observed a four-fold increase of sEVs, with a concomitant increase of >80% of all cargo miRNAs. The most abundantly secreted miRNAs were predicted to collectively target mRNAs of pro-apoptotic proteins, and indeed, senescent cell derived sEVs exerted anti-apoptotic activity. In addition, we identified senescence-specific differences in miRNA composition of sEVs, with an increase of miR-23a-5p and miR-137 and a decrease of miR-625-3p, miR-766-3p, miR-199b-5p, miR-381-3p, miR-17-3p. By correlating intracellular and sEV-miRNAs, we identified miRNAs selectively retained in senescent cells (miR-21-3p and miR-17-3p) or packaged specifically into senescent cell derived sEVs (miR-15b-5p and miR-30a-3p). Therefore, we suggest sEVs and their miRNA cargo to be novel, members of the SASP that are selectively secreted or retained in cellular senescence.

INTRODUCTION

Accumulation of senescent cells with age and at sites of age-associated diseases has been observed in the context of cardiovascular diseases, neurodegenerative disease, skin conditions and others [1]. Importantly, their removal in transgenic mice [2–4] or by senolytics [5,6] leads to later onset of several age-associated diseases [2,7–9].

Cellular senescence is triggered by various stimuli such as progressive telomere-shortening, hyperoncogenic signaling, accumulation of DNA damage, oxidative stress or mitochondrial dysfunctions, leading to an irreversible growth arrest mediated by the key cell cycle inhibitors CDKN1A and/or CDKN2A [10]. Most cell types activate pro-survival pathways and resist apoptosis when senescent [11]. They lose their cell type specific functionality and replicative potential required for tissue regeneration and acquire a senescence-associated secretory phenotype (SASP) [12].

The SASP is characterized by the secretion of growth factors, pro-inflammatory cytokines and chemokines, as well as extracellular matrix (ECM) remodeling enzymes [12]. These SASP factors are considered to over-proportionally exert negative effects on tissue homeostasis and regeneration *in vivo* if chronically present by acting in a paracrine manner on the neighboring cells and ECM. Attenuation of the negative effects of the SASP have been shown to restore the formation of functional human skin equivalents [13] and has been suggested as a putative target in preventing age-associated diseases and frailty [8,14].

Recently, extracellular vesicles (EVs) and their cargo have been reported to act in a similar manner as hormones or cytokines during intercellular communication [15]. They are secreted by many, if not all cells, and by encapsulation of their cargo, they transport proteins, mRNAs, lipids and non-coding RNAs, specifically miRNAs, over short or long distances [16]. When taken up by recipient cells, the cargo is considered to be still active and to regulate the behavior of recipient cells [17,18].

MiRNAs clearly modulate cellular senescence and organismal aging *in vitro and vivo* [19,20] and are in addition packaged into EVs [21], where they are able to influence osteogenic differentiation as one major age-associated disease [22]. Thus, although many protein based SASP factors have been identified, miRNAs [23,24] and EVs [25] are under suspicion to be part of the SASP [26,27]. However, a systematic catalogue of SASP-miRNAs has not yet been established and their

selective secretion during senescence has not been studied so far.

Here, we confirm that EVs and their miRNA cargo are indeed part of the SASP (EV-SASP) and identified a set of selectively retained and secreted miRNAs after the onset of senescence. In addition, senescent cell derived EVs might contribute to an anti-apoptotic environment in tissues where senescent cells have accumulated.

RESULTS

sEVs are members of the senescent-associated secretory phenotype (EV-SASP)

In order to test whether EVs and their enclosed miRNAs are members of the SASP, primary human dermal fibroblasts (HDF) of three different donors were driven into premature senescence by exposing them repeatedly to hydrogen peroxide (H₂O₂) [28]. Analysis were then performed one (D7) and 3 weeks (D21) after the last H₂O₂ treatment (Fig. S1A).

Onset and persistence of cellular senescence was confirmed in detail day 7 and (Table 1A and B), by senescence-associated (SA)-β-Gal staining (Fig. 1A), expression of CDKN1A/p21 (Fig. 1B), induction of an irreversible growth arrest (Fig. 1C), as well as by the acquiring of a fibroblast-specific flattened and enlarged senescent phenotype (Fig. 1D). In order to exclude contamination of EV preparations by apoptotic bodies, basal apoptosis rates of quiescent (Q) and senescent cells (SIPS) were analysed, whereby no significant difference was detected (Fig. 1E) at time points of EV purification as outlined in the scheme of Fig. S1A.

We here focused on small EVs (sEVs), therefore supernatants of SIPS and Q control cells were filtrated using 0.22 μm filters and subsequently ultracentrifugated. Size distribution as assessed by nanoparticle tracking analysis (NTA) revealed sEVs between 15 to 135 nm (Fig. 2A) with a median diameter of 65 to 80 nm, with no difference between senescent and quiescent cells at both time points, 7 and 21 days, after the last stress treatment (Fig. 2B). Transmission electron microscopy showed typical morphology and presence of lipid bilayers (Fig. 2C), and Western blotting confirmed the presence of TSG101, a known marker for exosome-like vesicles (Fig. 2D).

Finally, we compared the number of sEVs per cell by NTA and observed a 4-fold increased secretion of senescent fibroblasts derived sEVs of all three donors after both time points of cellular senescence (D7 and D21) (Fig. 2E).

Table 1A. Detailed characteristics of major hallmarks of cellular senescence of the individual donors HDF161, HDF76 and HDF85 each senescent and quiescent control after 7 (D7) days post last H₂O₂ application.

1 week recovery (D7)													
Donor	Total apoptotic cells (Annexin + PI positive) [%]			BrdU positive cells [%]			Sub-G1 peak (PI staining) [%]		CDKN1A mRNA expression norm.FC			SA-βGal positive cells [%]	
	Q	S	+	Q	S	Y	Q	S	Q	S	Y	Y	S
HDF161	1.7	4.3	49	15	5	55	2.5	3.9	0.6	1.1	0.9	16.1	50
HDF85	1.1	4.1	12	14	2.8	35	0.7	4.8	1.3	1.7	1.0	13	74
HDF76	1.5	4.7	40	15	8	48	1.2	3.3	1.2	1.9	0.8	13.8	49

Abbreviations: Q = quiescent control, S = stress induced premature senescent, + = positive control – Staurosporin 300nM overnight, Y = proliferating control.

Table 2B. Detailed characteristics of major hallmarks of cellular senescence of the individual donors HDF161, HDF76 and HDF85 each senescent and quiescent control after 21 days (D21) post last H₂O₂ application.

3 week recovery (D21)													
Donor	Total apoptotic cells (Annexin + PI positive) [%]			BrdU positive cells [%]			Sub-G1 peak (PI staining) [%]		CDKN1A mRNA expression norm.FC			SA-βGal positive cells [%]	
	Q	S	+	Q	S	Y	Q	S	Q	S	Y	S	
HDF161	1.1	2.8	40	4.5	1.5	35	0.8	3.3	1.2	1.3	13	70	
HDF85	0.7	5.4	26	3.8	0.4	16	1.2	3.2	1.1	1.5	14	69	
HDF76	0.6	5.6	43	3.5	1.1	54	1.3	6.8	0.8	1.4	19	54	

Abbreviations: Q = quiescent control, S = stress induced premature senescent, + = positive control – Staurosporin 300nM overnight, Y = proliferating control.

Considering the phenomenon of increased senescence-associated secretion of proteins summarized under the term SASP, our data strongly support the idea that sEVs are members of the SASP, for which we propose the term 'EV-SASP'.

sEV-miRNAs as part of the SASP are identified in a preliminary and final qPCR screening

In order to determine which miRNAs are detectable in

sEVs from quiescent control and senescent cells, a preliminary screening using a qPCR-panel of 752 miRNAs was performed and analysed in detail (Fig. 3A-B). From these, we designed a customized (final) qPCR panel with 375 miRNAs and spike in-controls (Supplementary List S1). Within that, 369 miRNAs were detected at Ct-values ≤ 38 (Fig. 3C) and 285 miRNAs were found in all three HDF cell strains under both conditions and at both time points (Fig. 3D).

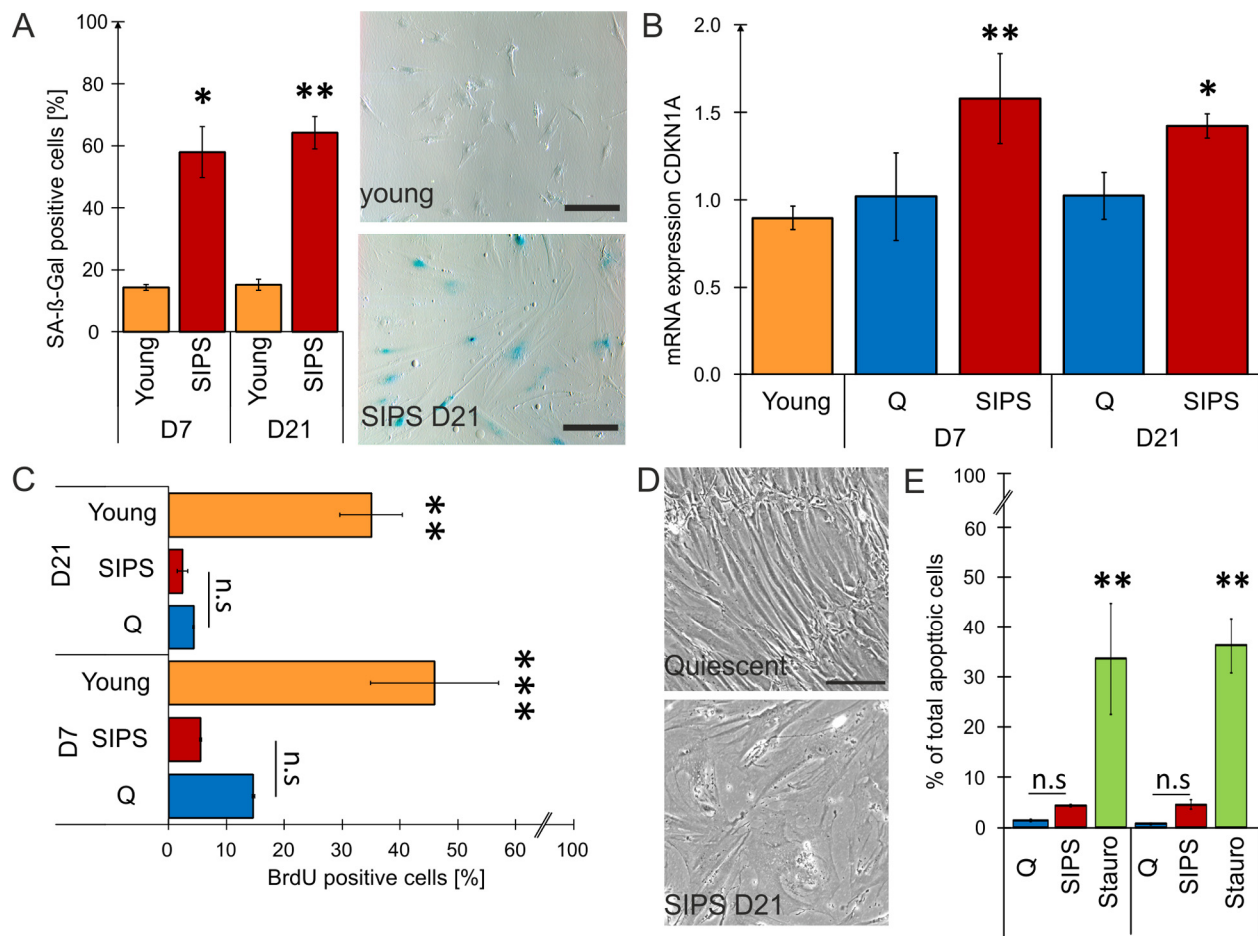


Figure 1. Stress-induced premature senescent (SIPS) fibroblasts mirror hallmarks of cellular senescence. (A) Quantification of SA-β-Gal staining shows a significant increase of β-Gal in SIPS HDF compared to young proliferating cells at both time points post stress treatment. Representative pictures show SA-β-Gal staining of donor HDF161 in SIPS on D21 (bottom) compared to young proliferating control (top - HDF161 in population doublings PD15). 15 pictures were taken randomly at a magnification of 100 X and counting was performed in a blinded fashion. Scale bar = 200 μm. Percentages of SA-β-Gal positive cells from all pictures were calculated. (B) Expression of CDKN1A confirms senescence of SIPS HDF at both time points. mRNA expression levels of CDKN1A (p21) were detected by qPCR. After normalization to GAPDH, fold changes of SIPS HDF relative to quiescent (Q) control cells from D7 were calculated. (C) SIPS treatment induces permanent cell cycle arrest. Incubation with the nucleoside derivate BrdU for 24 hours followed by FITC immunolabelling for flow cytometry shows no significant incorporation of BrdU into the DNA of Q and SIPS samples compared to young dividing HDF at both time points. (D) SIPS cells show flattened and enlarged morphology. Representative pictures from donor HDF161 Q and SIPS on D21 post H₂O₂ treatment. Scale bar = 200 μm. (E) Repeated H₂O₂ treatment does not induce apoptosis. SIPS and Q control cells do not show a substantial increase in percentage (%) of total apoptotic cells at both time points compared to a positive-control (+), treated with 300 nM staurosporin for 24 hours. (A-E) Stress-induced premature senescence (SIPS) of primary human dermal fibroblasts (HDF) derived from three different donors was triggered by chronic H₂O₂ treatment on nine consecutive days. Hallmarks of cellular senescence were confirmed after seven (D7) and 21 days (D21) post last stress treatment. Averages from three biological triplicates are shown +/- SEM from raw values (n = 3). Statistical analysis was performed using 2-way RM ANOVA tested for condition and day following Bonferroni post test. n.s. ≥ 0.05 ; *p < 0.05; **p < 0.01.

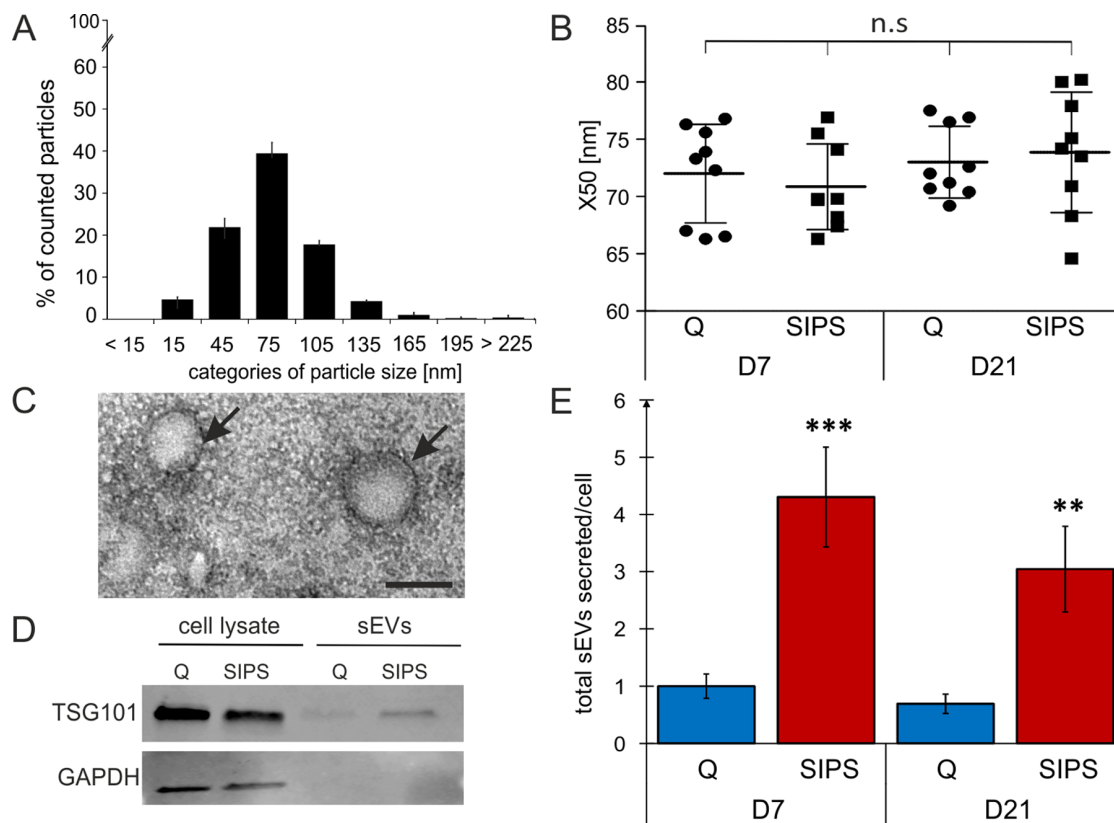


Figure 2. sEVs are members of the senescent-associated secretory phenotype (EV-SASP). (A) NTA reveals a vesicle population below 220 nm. Size distribution of vesicles determined by NTA shows percentage (%) of total counted particles against size presented in categories. (B) Media values (X50) from sEVs range from 65 to 80 nm. X50 values from peak analysis of NTA are indicated +/- SEM. circle: Q, squares: SIPS. Statistical analysis using one-way ANOVA was performed: not significant (n.s) $p > 0.05$. (C) Representative transmission electron microscopy image of sEVs isolated from HDF. Vesicles are around 100 nm in size and are surrounded by a double lipid membrane (arrows). Scale bar = 100 nm. A representative image of sEVs purified from HDF85 at D7 after the stress treatment is shown. (D) Representative Western blot shows expression of TSG101 (top) and GAPDH (below). Representative Western blot of total cell lysates (left) and sEVs (right lanes) from Q and SIPS HDF of donor HDF85 are shown. Total protein content of total cell lysates and purified sEV was analyzed by BCA assay and equal amounts of protein were loaded onto the gel (20 μ g). (E) Senescent cells secrete more sEVs per cell than quiescent controls. Total concentration of tracked particles was normalized to the total cell number used for secretion into conditioned media. Fold changes of total particles secreted per cell, relative to Q control cells from D7, +/- relative SEM, are shown. Statistical analysis was performed using 2-way RM ANOVA tested for condition ($p < 0.0001$) and day ($p = 0.28$) following Bonferroni post test. ** $p < 0.01$; *** $p < 0.01$. (A-B and E) Averages from three biological triplicates ($n = 3$) and two different time points each SIPS and Q, were measured in technical triplicates ($n = 18$) +/- relative SEM.

As quality control, interplate variation and PCR efficiency was monitored using five synthetic spike-ins (Unisp2, Unisp4, Unisp5, Unisp6, cel-miR39) controlling for RNA extraction, cDNA synthesis, and qPCR efficiency, resulting in Δ Ct_t-values (range of highest and lowest Ct-value from all samples each) below 1. Additionally, each plate included two interplate calibrators (IPC) and a negative control, showing Δ Ct_t-values below 0.44 suggesting robust signals (Fig. S2A) and thus allowing to exclude inter-assay variations.

Due to the absence of a robust extracellular house-keeping miRNA, we used standardized secretion times

and volumes for vesicle preparations and subsequent RNA isolation and normalized the data to the total viable cell number of each sample (Table 2).

Multivariate statistics on the 369 sEV-miRNAs clearly distinguished senescent from quiescent control cells as depicted by principal component analysis (Fig. 3E) and hierarchical clustering (Fig. 3F), showing an increase of almost all sEV-miRNAs. Due to 4-fold more sEVs per cell it is of no surprise, that almost all miRNAs are upregulated in the supernatants of senescent cells as indicated by the heatmap (Fig. 3F). Indeed, statistical evaluation confirmed 221 miRNAs (59%) with sig-

nificantly higher secretion levels on D7 (Fig. S2B), whereby miR-200c-3p and miR-196b-3p were identified to be the most differentially secreted miRNAs per cell. 3 weeks after induction of senescence (D21), 321 (85%) miRNAs were confirmed to be differentially secreted and miR-23a-5p reached the highest level (Fig. S2C), while none were downregulated significantly at both time points (Supplementary List S2). Thus, our findings indicate that sEVs and their miRNA cargo are *bona fide* members of the SASP.

Senescent cell derived sEVs confer anti-apoptotic activity

In order to get insight into a potential function of the EV-SASP, the top 20 most abundant sEV-miRNAs were identified (Fig. 4A) and screened for validated miRNA/mRNA target pairs. Thereby, we found in total 11,588 interactions comprising 5,437 target genes (Supplementary List S3). To evaluate potential regulated pathways, enrichment analysis of all annotated interactions between miRNAs and genes, discovered 125 GO terms with an adjusted p-value below 0.0001, among those, 54 comprise more than 50% of all associated genes (Fig. S3A).

Interestingly, the top 20 highly secreted miRNAs (Fig. 4A) were predicted to regulate a dynamic crosstalk of

three prominent meta-pathways by targeting five common transcription factors (PTEN, P53, APAF-1, CDKN1B and MYC) (Fig. S3B) that are also well known pro-apoptotic mediators [11,29–33].

Therefore, acutely stressed recipient fibroblasts were exposed to the entirety of senescent or quiescent cell derived sEVs and Annexin-V-PI staining for assessing apoptosis rates was performed (Scheme Fig. 4B). Indeed, the presence of senescent cell derived sEVs reduced the amount of apoptotic cells by approximately 27% (Fig. 4C-D), suggesting an anti-apoptotic activity of the EV-SASP. Whether and which miRNAs exert this effect will be subject of further studies.

Changes in miRNA composition of senescent cell derived sEVs

While in total almost all sEV-miRNAs are increasingly secreted when compared to cell numbers, we were interested, if also the miRNA composition of sEVs would change during senescence. Therefore, we performed global mean normalization [34] of all miRNAs assuming that the total amount of miRNAs is unchanged within sEVs irrespective of the condition, since vesicle size (Fig. 2B) and global means of total miRNA content from both time points, each SIPS and Q were similar (Fig. S4A).

Table 2. Summary and evaluation of secreted miRNAs by qPCR panels.

conditions	Preliminary screening		Final screening	
	Q	SIPS	Q	SIPS
biological replicates (HDF)	N = 1	N = 1	N = 3	N = 3
Time points (days post treatment)	D21	D21	D7; D21	D7; D21
number of cells used for sEV-RNA (average)	1.27E+07	9.13E+05	1,50E+07 ± 33%	1,65E+06 ± 30%
screened miRNAs (Exiqon)	752		375	
detected miRNAs in 2 conditions (average)	386		371	
detected miRNAs in 1 condition (average)	156		0	
not detected (average)	210		4	
raw Ct-values normalized to number of cells used for sEV-RNA				
detected miRNAs $Ct_{(Average)} \leq 31$	101	187	112	220
detected miRNAs $Ct_{(Average)} 31 - 35$	197	142	138	132
detected miRNAs $Ct_{(Average)} 35 - 38$	459	313	121	19
detected miRNAs $Ct_{(Average)} > 38$	366	235	0	0
Dataset of miRNAs for statistic quantification ($Ct_{(Average)} < 38$)			353	
miRNAs with complete dataset for 3 Donor D7/D21			280/290	
miRNAs with complete dataset for 2 Donor D7/D21			36/38	
miRNAs with complete dataset for 1 Donor D7/D21			36/24	

Preliminary screening of secreted miRNAs to determine detectable miRNAs in small EVs derived from HDFs, was performed using one HDF strain in both conditions, stress-induced premature senescent (SIPS) and quiescent control (Q), from one time point (D21). 375 miRNAs out of 752 screened were selected for the final screening with three different HDF cell strains (n = 3), in 2 conditions (SIPS and Q) and from two time points at 7 (D7) and 21 days (D21) after treatment.

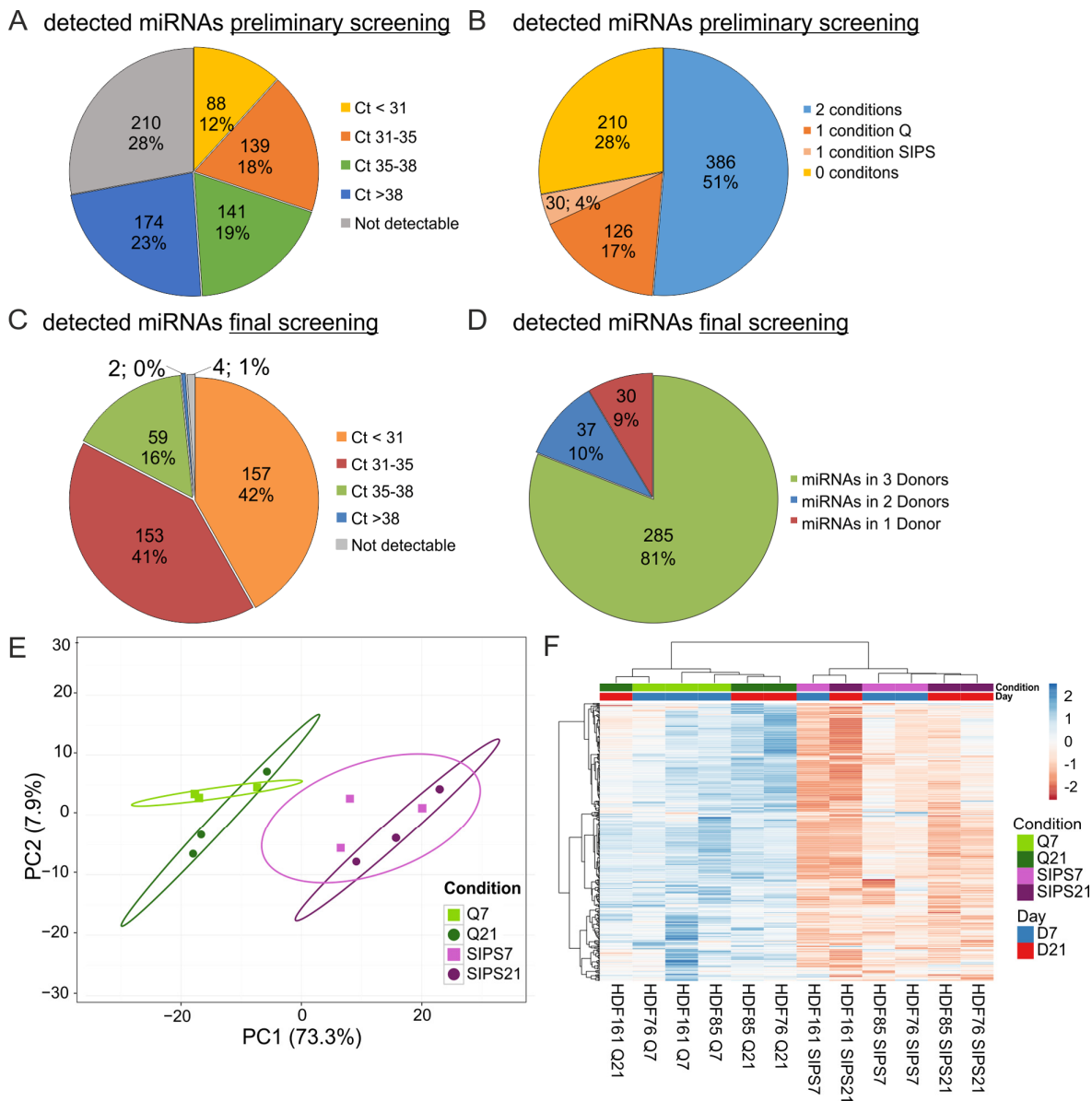


Figure 3. sEV-miRNAs as part of the SASP were identified in a preliminary and final qPCR screening. (A) miRNA profiling of the preliminary screening detects in total 542 (72%) secreted miRNAs. Categorization of Ct-values shows 368 miRNAs with an average signal < 38 in one or both conditions (Q, SIPS) tested. (B) The preliminary screening detects in total 386 miRNAs in both conditions tested. (C) The final qPCR screening detects 369 miRNAs with Ct-values below 38. 375 miRNAs were tested in all conditions and time points. % and number of total miRNAs detected in the screening experiment are shown. Categorization according to Ct-values. MiRNAs with an average Ct-value < 31, between 31 and 35, between 35 and 38, > 38 and not detectable are displayed. (D) The final qPCR screening detects 81% of all screened miRNAs in three donors. Averages from D7 and D21 are presented. 81% (285) of miRNAs were detected in all three donors SIPS and Q. 10% (37) of miRNAs were detected in at least two donors and 9% (30) of miRNAs were detected in one donor. (E) Principal Component analysis of sEV-miRNAs from SIPS and Q control cells from day 7 (D7) and day 21 (D21) after the treatment. The expression matrix shows the clustering of 12 samples and 369 miRNAs. Ellipses indicate a confidence level of 95% that a new observation will fall into it. Illustrated 2D-biplot explains a variance of 73.3% in principal component 1 and 7.9% in principal component 2, respectively. Exploratory analysis was done with ClustVis. Green: Q; Purple: SIPS; light colors and rectangular D7; dark colors and circle D21. (F) sEV-miRNAs are higher secreted from SIPS cells compared to Q controls. Heatmap and hierarchical clustering of 369 sEV-miRNAs after D7 and D21 (n = 12). Unit variance scaling was applied and rows are centered. MiRNAs were clustered according to correlation distance and Ward linkage method. Samples in columns are clustered using Euclidean distance and Ward linkage method. Green: Q; Purple: SIPS; light colors and blue D7; dark colors and red D21. Colors in matrix: red = upregulated, blue = downregulated. (A-B) Magnitude of secreted sEV-miRNAs was assessed in a preliminary screening using Q control and SIPS HDF of one cell strain (HDF76) and from one time point (D21). 752 miRNAs were screened using the qPCR ready to use panels supplied by Exiqon. (C-F) Final screening was performed with customized qPCR panels using three different HDF cell strains (n = 3) each Q and SIPS from two different time points (D7 and D21).

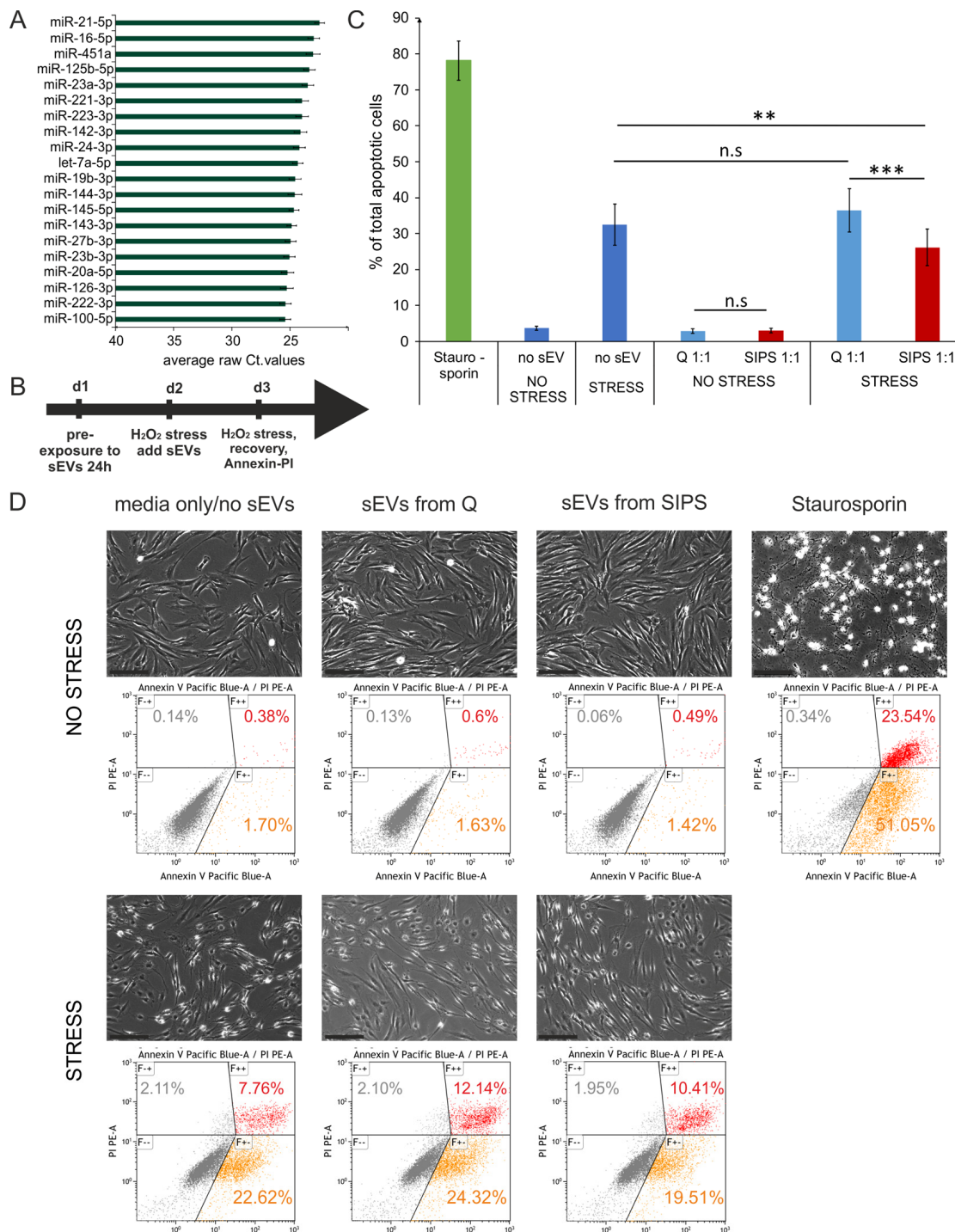


Figure 4. Senescent cell derived sEVs confer anti-apoptotic activity. (A) Bar chart of the top 20 most highly secreted sEV-miRNAs. To cell count normalized Ct-values from Q and SIPS from two time points were averaged and are plotted +/- SEM derived from all 12 samples. (B) Experimental setup to test the biological effect of the EV-SASP. Recipient fibroblasts were pre-exposed to sEVs for 24 hours followed by an acute stress treatment for 2 hours with 200 μ M H₂O₂ and fresh sEVs were added. On the next day a second stress treatment with 400 μ M for 2 hours was performed followed by a recovery time of 3 hours. Annexin-V-PI staining and flow cytometric measurement was used to determine % total number of apoptotic cells. (C) The EV-SASP reduces the amount of apoptotic cells of oxidatively stressed recipient cells. sEVs of SIPS and Q control cells of three different donors between 2 to 4 weeks of recovery post SIPS treatment were freshly harvested and applied before and after acute stress treatments. Human primary dermal (n = 3) and foreskin fibroblasts (n = 3) were used as recipient cells. Averages from 6 independent experiments +/- SEM are shown. Statistical analysis (n = 6) using 2-way RM ANOVA identified the factor 'EV/no EV' as a significant subject (p = 0.014) and the factor 'no stress/stress' as a significant factor (p = 0.00014). Groups were compared by Bonferroni post test, n.s \geq 0.05; **p < 0.01, ***p < 0.01. (D) Representative pictures of recipient fibroblasts of all conditions tested prior Annexin-V-PI staining. Representative flow cytometric data are shown. Scale bar = 200 μ m.

Indeed, statistical analysis identified 31 miRNAs differentially present per sEV at day 7 after induction of cellular senescence (Fig. 5A), and 32 miRNAs at day 21 (Fig. 5B).

Surprisingly, out of these, only two miRNAs (miR-23a-5p, miR-137) were more abundant in sEVs at both time points (Fig. 5C), while five miRNAs (miR-17-3p, miR-625-3p, miR-766-3p, miR-199b-5p, miR-381-3p) were less abundant in sEVs of senescent cells (Fig. 5D).

Taken together, these results indicate that senescent cells do not only secrete more miRNA containing sEVs

as part of the SASP, but that in addition the miRNA composition of single sEVs changes with senescence.

Intracellular miRNA analysis by next generation sequencing (NGS) identifies early and deep senescence specific miRNAs

Since differential secretion of sEV-miRNAs might be caused either by differential transcription, processing or packaging into sEVs, we decided to quantify also the intracellular miRNA composition of all three fibroblast cell strains at both time points (D7 and D21) by small RNA-NGS.

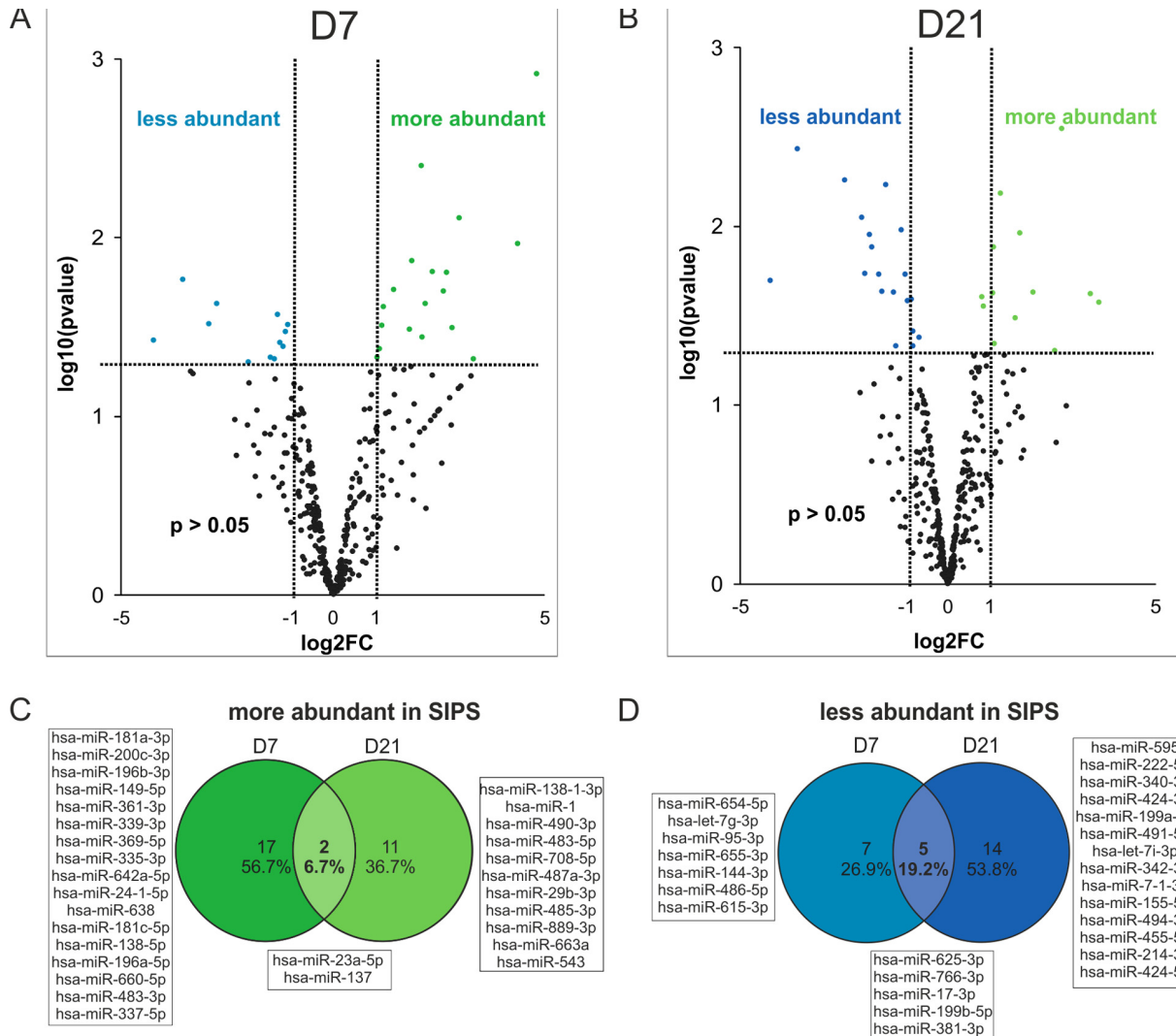


Figure 5. Changes in miRNA composition of senescent cell derived sEVs. (A) Volcano plot shows 31 significantly differently present senescence-associated (SA) sEV-miRNAs after normalization to the global means at D7 and (B) 32 SA sEV-miRNAs at D21 after the last H₂O₂ treatment. (C) Venn diagram shows miRNAs more abundantly present in sEVs of SIPS cells. (D) Venn diagram shows miRNAs less abundant in sEVs of SIPS cells. (A-B) Raw Ct-values from each sample were normalized to the respective global mean. Log₂FC of SIPS relative to Q control cells were calculated. Values from D7 (panel A) and D21 (panel B) recovery are plotted on x-axis against their individual -log₁₀(p-value) on y-axis. Horizontal dotted lines indicate a separation between miRNAs passing a p-value higher or lower than 0.05. Vertical dotted lines separate secreted miRNAs with log₂FC > 1 or log₂FC < 1. MiRNAs reaching a p-value < 0.05 are illustrated with green and blue dots and miRNAs with a p-value > 0.05 are shown in black. None reached the 0.05 cut-off value for the FDR of an adjusted p-values. Analysis was performed using three different HDF cell strains (n = 3) each Q and SIPS from two different time points (D7 and D21). (C-D) Log₂FC was calculated and significantly regulated (p-value < 0.05) miRNAs from D7 and D21 were compared in a Venn diagram.

Table 3. Summary of miRNA next generation sequencing (NGS) and data quality control.

Experimental Design	
Instrument	NextSeq 500
Average number of reads (1 flowcell)	4.00E+08
Number of sequencing cycles	50 bp single-end read
Annotation reference	miRBase 20
Quality control	
Base call accuracy (Q-Score)	>30
Averaged Total reads	1.26E+07 ± 29.38%
miRNAs (44.2%)	5.64E+06 ± 38.39%
smallRNA (7.8%)	9.78E+05 ± 30.48
Genome-mapped (11.2%)	1.42E+06 ± 35.37%
outmapped (28.5%)	3.56E+06 ± 29.01%
unaligned reads (8.1%)	1.02E+06 ± 28.93%
Grouping Quantity (Number of Identified RNAs)	
< 10 rawcounts on average	2124
10 - 50 rawcounts on average	146
> 50 rawcounts on average	308
Number of analyzed miRNAs	
5 - 500 TPM	158
> 500 TPM	274

Quality control and results of cDNA library preparation and NGS were assessed (Fig. S5A-F). On average 17.6 million reads per sample were obtained (Fig. S5G) and miRNAs were identified according to miRBase 20.0. The dataset was evaluated (Table 3), normalized to the total number of reads and 432 miRNAs that reached at least five tags per million (TPM) in at least one donor were included into the analysis.

Principal component analysis clearly separates senescent versus quiescent control cells independently from the time points (Fig. 6A), which was further confirmed by unsupervised hierarchical clustering (Fig. 6B).

Differentially transcribed miRNAs were identified (Supplementary List S5) and visualized by Volcano plot (Fig. 6C-D). Comparison of up- (Fig. 6E) and down-regulated miRNAs (Fig. 6F) from early (D7) and deep senescent (D21) fibroblasts revealed senescence-associated miRNAs identified earlier, either in senescent fibroblast [35,36] or in the dermis of elderly [37], and thus point to a very robust miRNA signature of senescent fibroblasts. Surprisingly, a higher percentage of intracellular miRNAs (46% up and 36% down) are both regulated in early as well as in deep senescence (Fig. 6E-F), while in contrast to secreted ones per vesicle, only 2% and 5% are jointly increased or decreased (compare to Fig. 5C-D). That means that senescence-associated changes over time are more pronounced in secretory miRNAs (21 sEV-miRNAs of

senescent cells change composition, Fig. S4B) as compared to intracellular ones (3 miRNAs differentially transcribed in senescent cells, Fig. S4C), so that these secreted miRNAs might be indicators of deep senescence.

We concluded that once senescence-signaling induces a specific intracellular miRNA pattern, it does not change significantly over time (Fig. S4C). Surprisingly however, the miRNA composition of secreted vesicles does change markedly with deepening of senescence (Fig. S4B), which might be attributable to the dynamic characteristics of the SASP [38–40].

Correlation of intracellular and sEV-miRNAs identifies specifically secreted versus retained miRNAs in cellular senescence

Next, we addressed whether all miRNAs with high intracellular abundance are also highly abundant in sEVs and if this depends on senescence. Thus, after restrictive cut-off criteria (see Material and Methods for details), all miRNAs detected intracellularly and in vesicles (228 miRNAs) were ranked according to their abundance to build the intersection of the top 20 miRNAs each by Venn diagrams (Fig. S6A-B, Supplementary List S6). Thereby, we identified 26.5% matching miRNAs and it became clear that particular miRNAs must be selectively secreted or retained in the two conditions (Fig. S6C).

In order to identify those miRNAs that are differentially packaged or retained in cells, we calculated the differences of ranks of the intracellular and the sEV contained miRNAs ($\Delta\text{rank} = \text{rank}_{\text{intra}} - \text{rank}_{\text{extra}}$) for quiescent and senescent cells separately (Supplementary

List S6, S7 Fig. 7A-B). Then the $\Delta\Delta\text{rank}(\Delta\text{rank}_{\text{SIPS}} - \Delta\text{rank}_{\text{Q}})$ were calculated, as a measure to indicate, if a miRNA would change its rank in dependence of the cell condition. That means, the higher the $\Delta\Delta\text{rank}$ -value is, the higher is also the selective secretion, and vice versa,

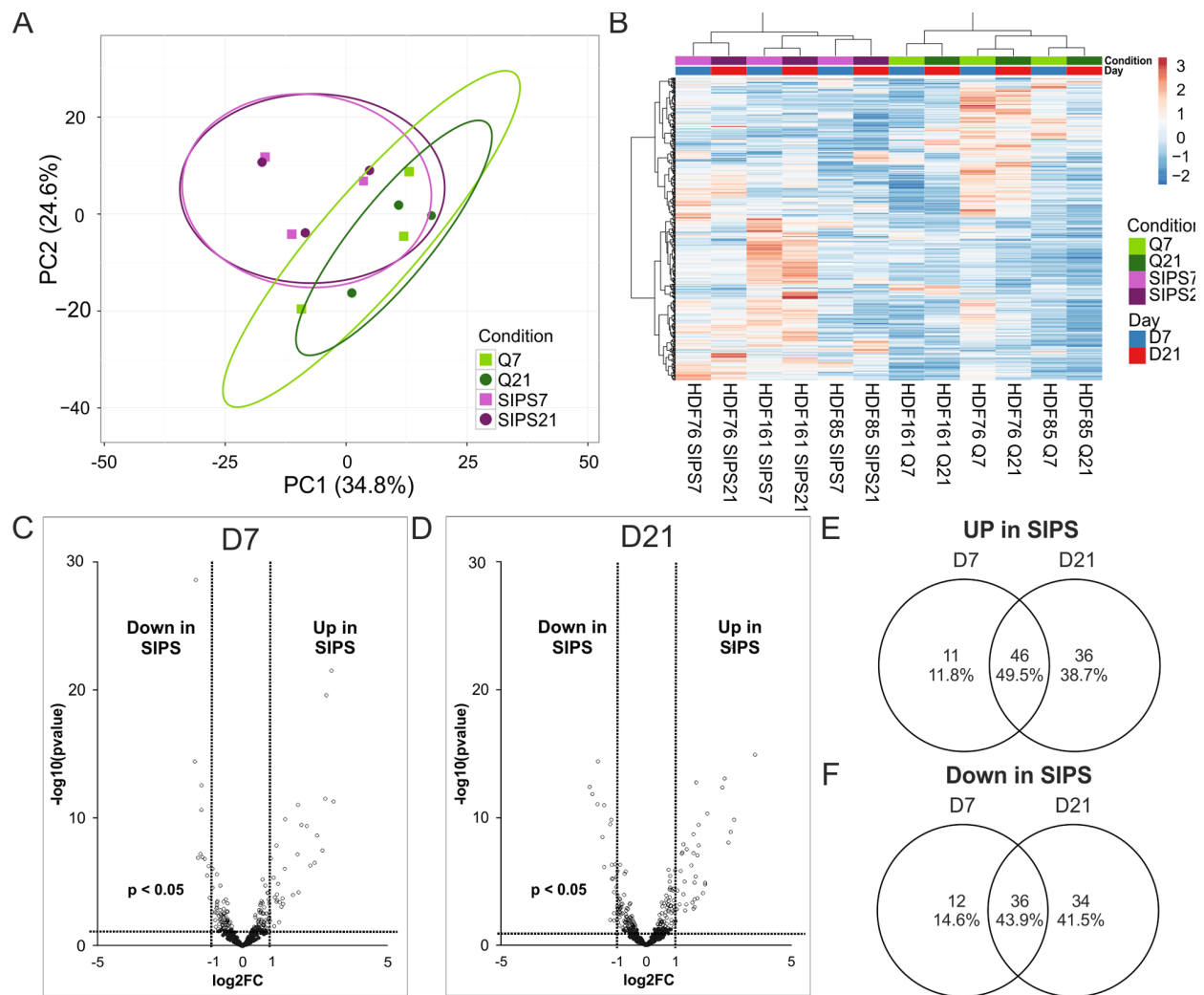


Figure 6. Intracellular miRNA analysis by NGS identifies early and deep senescence specific miRNAs. (A) Principal component analysis of SIPS versus Q HDF. Principal components were calculated using singular value decomposition (SVD) for imputation. Rows were scaled by applying unit variance scaling. Confidence level of 95% is indicated by ellipses assuming that a new observation from the same group will fall into it. Expression matrix of principal component 1 shows a variance of 34.8% and 24.6% in principal component 2. (B) Heatmap and hierarchical clustering of samples and miRNAs of SIPS versus Q human dermal fibroblasts. Clustering was done according to Euclidian distance and Ward linkage method. Samples in columns were clustered using correlation distance and Ward linkage method. (colors in matrix: red = highly transcribed = upregulated, blue = low transcribed = downregulated). (C) Volcano plot of differentially transcribed miRNAs in SIPS cells after seven (left D7) and (D) 21 days (right D21) post stress treatment. Log₂FC are plotted on x-axis against their individual -log₁₀ (p-value) on y-axis. Horizontal dotted lines indicate a separation between miRNA differences of a p-value higher or lower than 0.05. Vertical dotted lines separate transcribed miRNAs with log₂FC > 1 or log₂FC < -1. MiRNAs reaching a p-value < 0.05 are illustrated with white dots and miRNAs with a p-value > 0.05 are shown in black. (E) Venn diagram shows upregulated miRNAs of senescent cells on D7 and on D21. 46 miRNAs are commonly upregulated at both time points of senescence. (F) Venn diagram shows downregulated miRNAs of senescent cells on D7 and on D21. 36 miRNAs are commonly downregulated at both time points of senescence. (A-D) Analysis was performed using three different HDF cell strains (n = 3) each Q and SIPS from two different time points (D7 and D21). Differential expression analysis and statistics, calculated with Edge, was done with 432 miRNAs with normalized TPM signals > 5 in all conditions in at least 1 donor. (A-B) Each color and symbol represents another annotation defined by data input file. Green: Q; Purple: SIPS; light colors and rectangular D7; dark colors and circle D21.

the lower the value, the higher the specific retention within the cell (Supplementary List S6, Fig. S6D). Thereby, we identified specifically secreted senescence-

associated sEV-miRNAs, such as miR-15b-5p (Fig. 7A), while miR-30a-3p was found to be retained during quiescence (Fig. 7B).

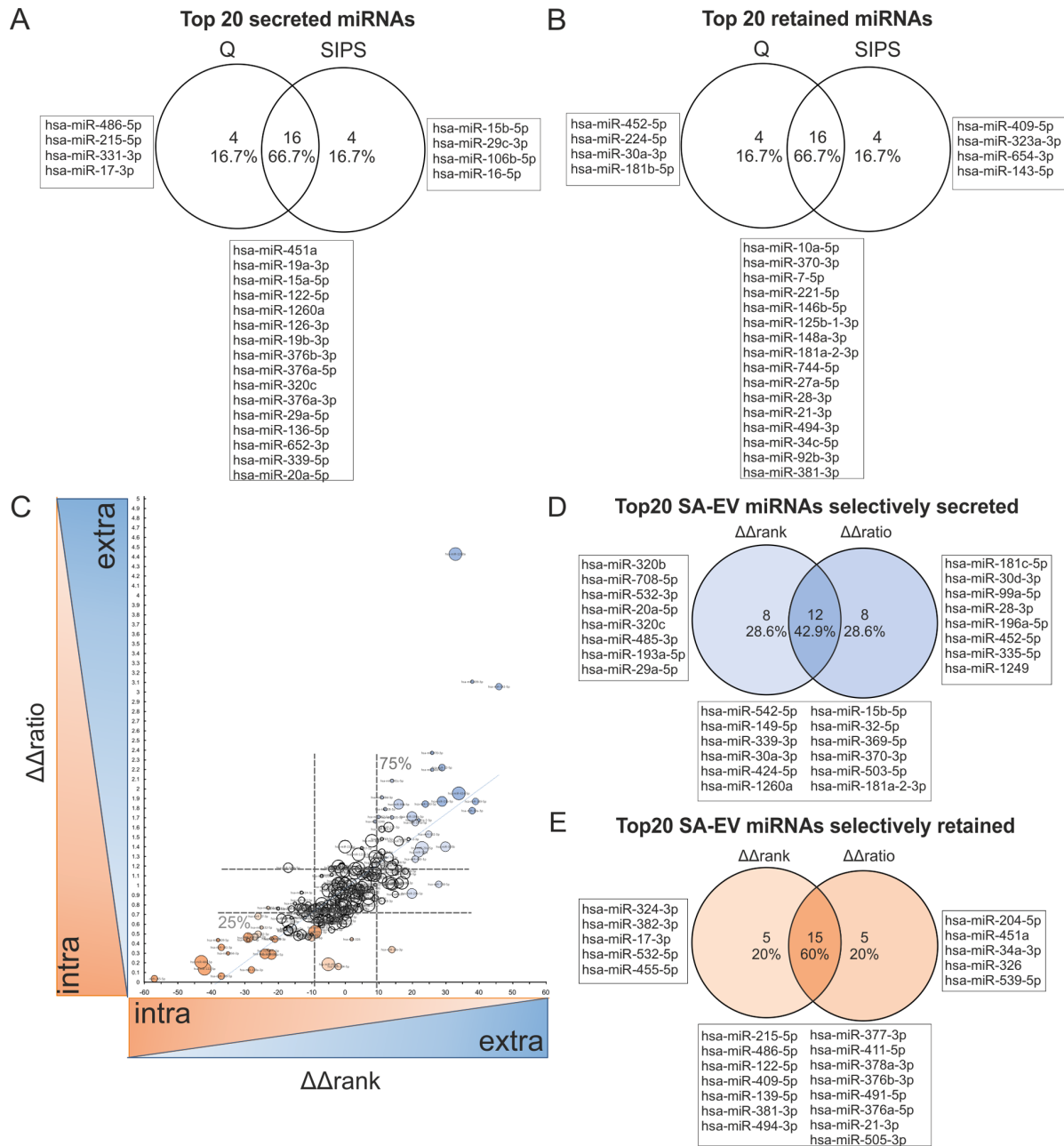


Figure 7. Correlation of intracellular and sEV-miRNAs identifies specifically secreted versus retained miRNAs in cellular senescence. (A) Venn diagram of top 20 secreted miRNAs (positive values) from HDF, calculated by $\Delta rank = rank_{intra} - rank_{extra}$ from Q and SIPS separately. (B) Venn diagram of top 20 retained (negative values) miRNAs in HDF, calculated by $\Delta rank = rank_{intra} - rank_{extra}$ from Q and SIPS separately. (C) Selectively senescence-associated secreted (high values) or retained (low values) miRNAs are identified. $\Delta \Delta rank$ and $\Delta \Delta ratio$ were correlated and specifically secreted (high values of $\Delta \Delta rank$ and $\Delta \Delta ratio$) or retained (low values of $\Delta \Delta rank$ and $\Delta \Delta ratio$) senescence-associated miRNAs were identified. Spearman correlation $R = 0.81$ with a 95% confidence interval 0.76 to 0.85 P value (two-tailed) < 0.0001 . Bubble size corresponds to quartiles calculated from transformed average Ct-values, whereby the larger the bubble size, the higher the expression value. Dotted lines represent the 25% and 75% percentiles, which define the specifically secreted and retained miRNAs in senescence. $\Delta \Delta rank$: 25%: 8.0; Median: -0.5; 75%: 9.0; $\Delta \Delta ratio$: 25%: 0.7099; Median: 0.927; 75%: 1.186. (D) Venn diagram of the top 20 specifically secreted senescence-associated sEV-miRNAs. MiRNAs are identified by comparing the top 20 of $\Delta \Delta rank$ and $\Delta \Delta ratio$ method. (E) Venn diagram of top 20 specifically retained senescence-associated miRNAs. MiRNAs are identified by comparing the top 20 of $\Delta \Delta rank$ and $\Delta \Delta ratio$ method. (F) (A-E) Correlation was performed with 228 miRNAs identified intracellularly (small RNA-NGS) as well as in sEVs (qPCR panels) in samples derived from three different HDF cell strains ($n = 3$) each Q and SIPS from two different time points (D7 and D21).

In order to confirm the $\Delta\Delta$ rank correlation by a different method to assess specific secretion, we additionally used the quantitative content of our intracellular and vesicular miRNA data. Therefore, we calculated ratios between vesicular and intracellular miRNA levels, and used these values to calculate ratios from quiescent ($\Delta ratio_Q$) and senescent cells ($\Delta ratio_{SIPS}$). Therefore, we transformed Ct-values to arbitrary units (AU), by defining a Ct-value of 40 to 10 AU. We then calculated $\Delta\Delta ratios$ ($\Delta ratio_{SIPS}/\Delta ratio_Q$) and normalized obtained values to the global means, resulting again in a list of specifically secreted or retained miRNAs (Supplementary List S6, S7 Fig. S6E).

To compare these two methods ('rank vs. ratio'), the results were plotted in an xy-diagram revealing ~80% of correlation as determined by Spearman correlation (Fig. 7C) and comparison of the top 20 selectively secreted and retained miRNAs each confirmed a similar set of the top 20 selectively secreted (Fig. 7D) or retained miRNAs after entry into cellular senescence (Fig. 7E), while some miRNAs were only detected with one of the two methods. Thereby, miR-15b-5p was again identified to be selectively secreted from senescent cells. Finally, by defining a cut-off of the 25% and 75% percentiles from both approaches, we identified ~24% of all analyzed miRNAs to be selectively secreted (blue) or retained (orange) in response to senescence, while the remaining ones seem to be evenly distributed between cells and sEVs (white). Interestingly, although miR-21-5p is the top abundant miRNA intracellularly as well as in vesicles, independent of the conditions, and therefore equally distributed between inside and outside (Supplementary List S6, S7 and Fig.S6A-B), its 3p-isoform was catalogued as a selectively retained miRNA during senescence.

To sum up, the 'ratio-' and 'rank-' approaches allow the correlation of vesicular versus intracellular miRNA abundance, independently from each other and identified a set of specific senescence-associated miRNAs selected for secretion (blue) or retention (orange) in response to senescence.

DISCUSSION

Accumulation of senescent cells is considered to drive several age-associated diseases. One of the characteristic of senescent cells that is considered to contribute to this phenomenon, is the cumulative secretion of several proteins involved in inflammation, growth promoting signaling and extracellular matrix remodeling, which is generally summarized under the term SASP [12]. With increasing numbers of reports on secretory miRNAs describing their almost 'hormonal'

action on recipient cells [15] and their potential as biomarkers or therapeutic targets for age-associated diseases [20], the question arises whether secreted miRNAs, especially those enclosed in EVs, might also be part of the SASP.

Indeed, we found a 4-fold higher secretion of sEVs from senescent as compared to quiescent human dermal fibroblasts with a concomitant increase of > 80% of all miRNAs per cell, whereby the stress-responsive miR-200c-3p [41,42] was found to be among the top differentially secreted miRNAs at an early time point of senescence. An increase of EVs in replicative senescence, as well as in irradiation-induced senescent prostate cancer cells [43] has already been observed. Even in human age-associated diseases, as in human atherosclerotic aortas [44], or in cerebrospinal fluid of Alzheimer's disease patients [45] where senescent cells have been found to accumulate *in vivo*, such an increase of EVs was evident. However, decreasing amounts of EVs with age have also been observed in the plasma of matched individuals [46]. It will thus be exciting to see, where and if EVs are differentially distributed between lesional sites of age-associated diseases versus the aged systemic environment.

As a consequence of elevated sEV and miRNA secretion per senescent cell, we performed pathway analysis of the most highly secreted miRNAs enclosed in the sEVs. Surprisingly, they were predicted to collectively silence five well known pro-apoptotic factors [11,29–33] at the crossroad of longevity, cancer and signalling pathways. Indeed sEVs from senescent fibroblasts reduced the amount of apoptotic cells in acutely stressed recipient fibroblasts. Even though the single factors of the sEVs are yet not identified, we postulate that the secretion of anti-apoptotic sEVs into the microenvironment of senescent cells might counteract the apoptotic removal of damaged neighbouring cells, thereby potentially contributing to a pro-tumorigenic microenvironment as known to be conferred by senescent cells and their EVs [47,48]. EVs per se have already been suggested to exert anti-apoptotic functions on the surrounding tissue and cells [49], however, this is to our knowledge the first report that experimentally proves that the SASP, and specifically the EV-SASP exerts anti-apoptotic activity. This is in line with a bioinformatic driven study of the protein factors comprising the SASP that postulates a potential anti-apoptotic activity of SASP proteins [50]. However, it is still to be determined, which miRNAs or if the entire cocktail of secreted miRNAs are indeed conferring this activity.

In addition, we identified differences in miRNA composition per single vesicle from senescent versus

control cells. In accordance to being upregulated intracellularly in senescent fibroblasts [51,52] we found miR-23a-5p and miR-137 to be more abundant per vesicle. Among the less abundantly present miRNAs in senescent sEV we found miR-17-3p and miR-199b-5p, both were already published to be downregulated intracellularly in skin of elderly [53] and in senescence of mesenchymal stem cells [54].

Similarly, intracellular miRNA transcription of senescent versus quiescent fibroblasts, revealed similar miRNAs that have been previously reported in fibroblasts [55–58], as well as miRNAs differentially found in the dermis of elderly [37], where estimates suggest 60% of fibroblasts to be senescent [59]. In addition, several miRNAs were identified so far not yet described in fibroblast senescence, such as miR-1197 and miR-450-2-3p.

With intracellular and extracellular miRNA quantitative data in hand, we next tested, if (i) specific miRNAs are selectively packaged into sEVs or retained within fibroblasts as it has been reported for other cell types [60] and (ii) if this is dependent on senescence, which has so far never been tested. Therefore, we ranked the abundance of miRNAs in- and outside of the cells and compared the resulting ranks. Most of the miRNAs, such as miR-21-5p are similar in rank, suggesting that most of the sEV cargo is mirroring the cytoplasmic content of the respective cell, while some miRNAs are indeed overrepresented intracellularly or in the sEVs. However, these specifically retained or secreted miRNAs were only partially overlapping when comparing the senescent and quiescent cells, suggesting that upon induction of senescence, also specific packaging or retaining does change, which was indeed the case for ~24% of all analyzed miRNAs.

It is still a matter of debate, if packaging of selected miRNAs into EVs is an active process for conveying messages or a passive form of garbage disposal [discussed in 42] e.g for the secretion of damaged RNA fragments [62] or for the release of tumor-suppressive miRNAs to maintain tumor progression [63]. However, our findings, together with the few reports that show specific retaining or packaging in response to external stimuli [64] and changes in EV-miRNA composition of PBMCs [65] would suggest controlled and active packaging, in line with several reports showing an active mechanism of miRNA packaging into exosomes [60,66]. Finally, as miRNAs in EVs have been widely shown to alter recipient cell behavior [17,18] a mere garbage disposal seems unlikely, while it could be envisaged that ‘garbage’ gotten rid of by one cell might be an alarm - or any other type of signal for recipient cells.

Which miRNAs are now selectively secreted by senescent cells and what effect on the microenvironment might such specifically packaged miRNAs have?

One of these is miR-15b-5p, which we found to be selectively secreted and downregulated in senescence as it was reported before in senescent fibroblasts as well as in photoaged skin biopsies [67]. The fact that it is preferentially packaged and secreted in senescence might be an additional mechanism to keep miR-15b-5p levels low in senescence cells. Interestingly, it is also low abundant in the dermis of elderly, while it appears highly enriched in the epidermis [67]. Thus, it is tempting to speculate that EV mediated cross talk between fibroblasts and keratinocytes contributes to low dermal levels versus high epidermal levels. Functionally, low intracellular miR-15-5p levels might be involved in de-repressing SIRT4, which has a regulatory role in stress-induced senescence-associated mitochondrial dysfunction [67] and in driving a NF-κB mediated induction of the SASP [68]. On the other hand, it might exert pro-proliferative activity on recipient keratinocytes as it does on several epithelial cell types [69], a function that in situation of transient appearance of senescent cells during wound healing might be favorable [70], while in situations of chronic accumulation of senescent cells, as in the skin of elderly, it might be detrimental.

Interestingly, several miRNAs mainly selectively retained in senescence including miR-122-5p [71], miR-21-3p [72] and miR-17-3p [73] are implicated with keratinocyte differentiation and/or proliferation, suggesting that senescent fibroblasts might impact on epidermal differentiation and function.

Taken together, we conclude that miRNAs are specifically secreted depending on cellular conditions and/or external stimuli. The specific molecular mechanism of selective release and retention of senescence-associated sEV-miRNAs and the EV-SASP cross-talk between different cell types and its consequences in the context of aging and age-associated diseases, however, remains to be elucidated. Still, the here presented detailed catalogue based on human dermal fibroblast strains derived from three different donors builds the basis for such studies. Finally, we introduce sEVs and sEV-miRNAs as novel, *bona fide* members of the SASP to be crucially involved to maintain the anti-apoptotic activity of senescent cells and suggest to use the term ‘EV-SASP’.

METHODS

Detailed experimental procedures are provided in the supplementary information.

Cell culture

Human dermal fibroblasts (HDF) from adult skin of three healthy donors and human foreskin fibroblasts of one healthy donor were provided by Evercyte GmbH. Cells were grown in DMEM/Ham's F-12 (1:1 mixture) (BIOCHROME, Germany) supplemented with 10 % fetal calf serum (FCS) and 4 mM L-Glutamine (Sigma Aldrich GmbH St Louis, MO, USA) at 95% air humidity, 7% CO₂ and 37°C.

Stress-induced premature senescence (SIPS)

For induction of SIPS, the Hayflick limit of each of the here used donors was assessed and cells in the middle of their replicate life span were used. Two donors (HDF161 and HDF85) reached the end of their replicative lifespan very early. HDF161 at a PD of ~ 37, HDF85 at a PD ~ 28, while HDF76 entered replicative senescence at a PD ~ 53. Therefore, HDF161 and HDF85 in PD ~ 12 – 15 and HDF76 in PD ~ 24 – 26 were seeded with 3500 cells/cm² one day (d) prior stress treatment using 9 (4 d stress – 2 d recovery – 5 d stress) consecutive doses of 100 µM H₂O₂ for one hour per day followed by a media change. Non-stressed control cells reached quiescence (Q) by contact inhibition.

SIPS was confirmed with bromodeoxyuridine (BrdU) incorporation, senescence-associated (SA)-β-Gal staining, CDKN1A (p21) expression and Annexin-V-PI staining after 7 (D7) and 21 days (D21) post stress treatment. See supplementary Information for detailed experimental procedures.

Isolation of small extracellular vesicles (sEVs)

Small EV Isolation was performed according to standards recommended from the international society for extracellular vesicles (ISEV) [74]. DMEM/Ham's + FCS was depleted of EVs by ultracentrifugation at 100,000 x g overnight and filtrated using 0.22 µm filter cups (MILLIPORE, Germany). Conditioned media (after 48 hours secretion) was centrifuged for 15 min at 500 x g (Eppendorf, 5804R) to remove cellular debris at 14,000 x g (Beckmann, Coulter, Brea, CA, USA, Avanti JXN-26) for 15 min, large EVs were excluded by filtration using 0.22 µm filter cups. On average 92 ml supernatant from SIPS and 75 ml supernatant from Q cells were filled into Quick-Seal, Polyallomer, 39 ml, 25x89 mm tubes (BECKMANN, Brea, CA, USA). sEVs were enriched using a 70Ti Rotor Beckman coulter at 100,000 x g for 90 min (BECKMANN, Brea, CA, USA) and pellets in different tubes but from the same samples were pooled. Dependent on the subsequent analysis, the pellet was either resuspended in QIAzol reagent (Qiagen) or in filtered 1 x PBS. For

TEM freezing and thawing was avoided. sEVs were isolated on D7 and D21.

Biological assay – exposure to sEVs and stress treatment

To test the biological effect of the EV-SASP, we selected early passage human dermal and foreskin fibroblasts as recipient cells. After 48 hours secretion into EV depleted media, the sEVs from SIPS and Q donor cells were freshly harvested from all three different fibroblast cell strains between two to four weeks of cellular senescence. The experiment was performed as followed (Fig. 4B):

D -1 EV depleted media was added to donor cells of SIPS and Q fibroblasts for 48 hours before sEV harvesting.

D 0 recipient dermal or foreskin fibroblasts were seeded into 6 well plates with 70,000 cells/well.

D 1 sEVs of SIPS and Q donor cells were harvested and recipient fibroblasts were pre-treated with sEVs in a ratio of 1:1 (meaning same amount of secreting cells to receiving cells).

D 2 sEVs were removed and recipient cells were treated with 200 µM H₂O₂ for 2 hours. Afterwards fresh sEVs were added again.

D 3 sEVs were removed and recipient cells were treated with 400 µM H₂O₂ for 2 hours followed by a recovery of 3 hours. Finally, the cells were stained for Annexin-V and with PI and were measured by flow cytometry (Gallios Beckman coulter, Brea, CA, USA). As a positive control, fibroblasts were treated with 300 nM Staurosporin for 24 hours. Total amount of apoptotic cells correspond to: Annexin positive + double positive (Annexin-V-PI) + PI positive cells and were quantified using Kaluza software (Beckman Coulter, Brea, CA, USA, Version 1.2).

RNA Isolation

Cell pellets and sEVs were lysed in QIAzol Reagent (QIAGEN) and RNA was automatically extracted by miRNeasy Mini kit (QIAGEN) based on QIAcube technology. To monitor isolation efficiency of sEV-RNA, a spike-in mix containing UniSp2, UniSp4, UniSp5 (EXIQON, Denmark,) was added before RNA isolation. As total sEV-RNA amounts were too low for quantification by Bioanalyzer (Agilent) or with comparable, more sensitive techniques such as Ribogreen assay, we normalized the data (i) to total viable cell number and (ii) to the global means of each, which is an

accepted method, not only in EV-research [34,74]. No significant differences in the global means of different samples were observed (Fig. S4A).

Intracellular total RNA concentration and quality was controlled using Nanodrop spectrometer (ND-1000) and 2100 Bioanalyzer (Agilent) using the RNA-6000 Nano Kit. Average RNA concentration as determined by Nanodrop and Bioanalyzer revealed average concentrations as followed: For Q = 955 ng/μl and for SIPS = 234 ng/μl purified in a volume of 20 μl NFW. RIN of intracellular RNAs was determined by 2100 Bioanalyzer, revealing for Q = 7.3 and for SIPS = 7.5. For cDNA library preparation 1 μg of total RNA was used.

cDNA synthesis

Equal volumes of sEV-RNA were used for cDNA synthesis using Universal cDNA Synthesis Kit II (EXIQON, Denmark). UniSp6 and cel-miR-39 (EXIQON, Denmark) were used to control for enzyme activity. cDNA was synthesized by 42°C for 60 min followed by heat inactivation for 5 min at 95°C.

For mRNA quantification, cDNA was synthesized from 500 ng of total RNA with the High-Capacity cDNA Reverse Transcription Kit including RNase inhibitor, (APPLIED BIOSYSTEMS, USA) for 10 min at 25°C - 120 min 37°C - 5 min 85°C.

Quantitative Real Time PCR (qPCR)

MiRNA qPCR analyses were performed using ExiLent SYBR® Green master mix and LNA-enhanced miRNA primer (EXIQON, Denmark) on a LC 480 Real Time PCR system (ROCHE, Germany). Activation: Cycles 1, Analysis Mode: None, 95°C, 10min, Ramp 4.4°C/s. Cycles: Cycles 45, Analysis Mode: Quantification 95°C, 10s, Ramp 4.4°C/s, 60°C, 60s, Acquisition Mode: Single, Ramp 1.6°C/s. Melting Curve: Cycles 1, Analysis Mode: Melting Curves, 95°C, 10s, Ramp 4.4°C/s; 55°C, 60s, Ramp 2.2°C/s; 99°C, Acquisition Mode: Continuous, Ramp 0.11°C/s, Acquisition per °C: 5. Cooling: Cycles 1, Analysis Mode: None. The second derivative method was used to calculate the cycle of quantification values (Ct-values).

The microRNA, Ready-to-Use PCR, Human panel I+II, V3.R, EXIQON, Denmark, were used for a preliminary screening. Based on that, a customized qPCR panel was designed comprising 375 miRNAs and internal and negative controls.

QPCR for mRNA was performed with 5x HOT FIREPol® EvaGreen® qPCR Mix Plus with ROX (MEDIBENA, Austria) using a Rotor-GeneQcycler. Determination of CDKN1A and GAPDH was quantified using Standard curves for determination of copy numbers in duplicates. Average expression values from quadruplicates were normalized to GAPDH as a reference gene and fold changes were calculated.

Negative controls tested as NFW only, and no template control derived from cDNA synthesis, were below detection limit of qPCR (> 40). Primer used for qPCR is presented in Table 4.

All analyses were performed in biological triplicates in two conditions (Q and SIPS) and two time points (D7 and D21). In total, 12 qPCR panels were set up on three consecutive days. MiRNA analysis was performed according to the ddCT method.

qPCR panel, analysis of sEVs-miRNAs

Spike-ins were detected in all 384-well plates to monitor purification efficiency of RNA Isolation (UniSp2, UniSp4, UniSp5), the presence of enzyme inhibitors during cDNA synthesis (Unisp6 and cel-miR-39–3p) and equal processing of RT-qPCR amplification (interplate calibrator IPC - UniSp3). NFW was used to determine background levels of each miRNA. Constant expression of all spike-ins was evaluated with a range calculated by the difference of the highest and lowest value of all samples/plates. ΔC_t values below 1 define the experiment to be robust and thus allow the exclusion of inter-assay variations (for details, see manual from EXIQON, QC PCR panel #203887-203892, September 2014).

Illumina small RNA library preparation

Intracellular small RNA cDNA library for Illumina Sequencing was synthesized according to the manual

Table 4. Primer used for qPCR.

Gene name	Sense primer	Anti-sense primer
GAPDH	CGACCACTTTGTCAAGCTCA	TGTGAGGAGGGGAGATTCAG
CDKN1A (p21)	GGCGGCAGACCAGCATGACAGATT	GCAGGGGGCGCCAGGGTAT

provided by NEBNext® Small RNA Library Prep Set for Illumina® (Multiplex Compatible) (NEB, E7330S). From initially 1 µg of total RNA, small RNA fragments from approximately 18 – 36 nucleotides were gel purified on a 10% TBE Gel (Invitrogen/ Thermo Scientific, EC62752), quantified by 2100 Bioanalyzer (Agilent, Santa Clara, CA, USA) and equimolar amounts were pooled and sent to Exiqon (Denmark) for Illumina RNA-Seq.

RNA isolation and cDNA library preparation were quality controlled prior to NGS (Fig. S5A-C). After adapter trimming and mapping, on average 17.6 million reads per sample were obtained (Fig. S5G-H). The entire dataset was evaluated (Table 3 and Fig. S5D-F), normalized to the number of total reads and 432 miRNAs that reached at least five tags per million (TPM) in one donor were included into the analysis.

Illumina, miRNA next generation sequencing (NGS)

The cDNA library pool was used to generate the clusters on the surface of a flowcell and NGS was performed using NextSeq 500 (EXIQON, Denmark). The collected reads were quality controlled, aligned and identified miRNAs were annotated to miRBase20 by Exiqon.

Differential expression analysis of NGS data

Differential expression analysis was done using the R (version 3.2.2)/Bioconductor software package DESeq [75]. Low expressed miRNAs were first excluded from the analysis (TPM < 5 for all the samples). Then, the raw read counts were normalized using the DESeq normalization and a model based on negative binomial distribution and local regression was fitted for each miRNA. In the model, ‘fibroblast cell strains (n = 3)’, were defined as a block ‘effect’ and ‘day’ and ‘condition’ as factor of 2 levels. The Benjamini and Hochberg (BH) procedure [76] was applied to adjust the raw p-values into false discovery rate (FDR). A FDR < 0.05 was chosen as the cut-off value.

Differential expression analysis of qPCR panels of sEV-miRNAs

Ct-values were either normalized to total number of cells used for secretion or by the mean-centering restricted (MCR) normalization [34,77], also known as the global mean normalization. Thereby, the mean Ct-value across all detected miRNAs of a single sample was subtracted from each individual miRNA. Differences in global means are presented in Fig. S4A.

Both datasets were subjected to differential expression analysis with the R (version 3.2.2)/Bioconductor software package Limma [78]. A linear model was applied for each miRNA and moderated t-tests were computed. In the model, ‘fibroblast cell strains (n = 3)’, were defined as a ‘block effect’ and ‘day’ and ‘condition’ as factor of 2 levels. The raw p-values were corrected using BH method to control FDR.

Statistical analysis

Routine statistics

Were either calculated with Excel or Graph Pad Prism, and respective tests are indicated below figures in result sections. Averages +/- standard error (SEM) or deviation (STDEV) were derived from at least 3 independent experiments. Two tailed tests were performed using an error probability of 0.05.

Data were tested for Gaussian distribution if possible. If normally distributed, two groups were compared using unpaired or paired student T-test using the raw values. One sample students T-test was used to compare ratios to a hypothetical value of 1, respectively. In order to analyze the impact of two independent factors (for example ‘treatment’ and ‘day’) a two-way repeated measures (RM) ANOVA was performed followed by Bonferroni post test if asked.

Descriptive statistics

ClustVis a web tool for the preparation of principal component 2D-biplots and heatmap analysis based on multivariate datasets using different R packages was used [79]. For all exploratory analyses, normalized Ct-values and TPM values were used. Principal component analysis (PCA) of 371 extracellular miRNAs (out of 375) was calculated by iteration of missing values with Nipals PCA and unit variance scaling was applied to rows. Heatmap preparation and unsupervised hierarchical clustering of secreted miRNAs was performed by applying correlation distance and Ward linkage. Samples in columns are clustered using Euclidean distance and Ward linkage method.

PCA for intracellular miRNAs was done for 432 miRNAs with TPM > 5 in at least one donor. We used Singular Value Decomposition (SVD) for imputation and unit variance scaling was applied on TPM values. Expression matrix and unsupervised hierarchical clustering of 432 intracellularly transcribed miRNAs was done by applying unit variance scaling and rows were clustered using Euclidean distance and Ward linkage. Columns are clustered using correlation distance and Ward linkage.

Correlation of intracellular and vesicular miRNAs

Only miRNAs, included in the customized qPCR panels for determination of vesicular miRNA abundance (375) and corresponding intracellular miRNA expression obtained by NGS were selected. Prior correlation of intracellular and vesicular miRNAs restrictive cut-off criteria were applied.

Quartiles from Ct-values and TPM values were calculated and miRNAs being low expressed (quartile 1 corresponds to the lowest 25% of data) in NGS and qPCR were excluded from analysis (330 miRNAs). Then miRNAs giving no signal in NGS experiment (TPM = 0) were excluded (291 miRNAs), and finally all miRNAs not present in all three donors and conditions were excluded. Therefore, correlation was done on 228 miRNAs.

In order to reduce sequence specific bias obtained with NGS and qPCR, we calculated the differences in retaining versus specific secretion by 2 different approaches; (i) by ranking the miRNAs and calculating the change in rank within the NGS and the qPCR datasets; (ii) by calculating the abundances via ratios. The overlap of both methods is presented as result and considered to be a strict way of analysis which rather takes the risk to miss some miRNAs than to provide false positives.

In detail: ranks from averages were calculated from SIPS and Q separately. Rank order was done according to intracellular TPM values to identify most abundant miRNAs transcribed intracellularly, or according to vesicular Ct-values, to discover most abundantly present miRNAs in sEVs. By calculating Δrank ($\text{rank}_{\text{intra}} - \text{rank}_{\text{extra}}$) from Q and SIPS separately, retained (negative value of Δrank) and secreted miRNAs (positive value of Δrank) were identified. By further calculating $\Delta\Delta\text{rank}$ ($\Delta\text{rank}_{\text{SIPS}} - \Delta\text{rank}_{\text{Q}}$) and the 25% and 75% percentiles, selectively higher secreted (high value of $\Delta\Delta\text{rank}$) or retained (low value of $\Delta\Delta\text{rank}$) miRNAs in SIPS were discovered.

Next, we analyzed the same dataset with a different method to review our data, using the 'ratio-approach'. For a better visualization, Ct-values were transformed to arbitrary units, defining a Ct-value of 40 to '10' arbitrary units – assuming around 10 miRNA copies. Δratios were calculated from values $\text{intra}_{\text{SIPS}}/\text{extra}_{\text{SIPS}}$ and $\text{intra}_{\text{Q}}/\text{extra}_{\text{Q}}$ separately. Then $\Delta\Delta\text{ratios}$ from $\Delta\text{ratio}_{\text{SIPS}}/\Delta\text{ratio}_{\text{Q}}$ were calculated and normalized to the global mean of those ratios. Again, the 25% and 75% percentiles were calculated, and selectively higher secreted (high value of $\Delta\Delta\text{ratio}$) or retained (low value of

$\Delta\Delta\text{ratio}$) miRNAs in SIPS were discovered. For Fig. S6D miRNAs were sorted according to $\Delta\Delta\text{rank}$ values from smallest to largest values and they were plotted on y-axis, $\Delta\Delta\text{ratio}$ values were then plotted in another diagram (Fig. S6E) in the same order as it was sorted before.

Pathway analysis of secretory miRNAs

MiRWalk 'microRNA- gene target' tool [80] was used to find all validated targets for each of the 20 most highly secreted miRNAs. To evaluate the putative network on pathway level, enrichment analysis of pathway-based sets of the common regulated genes (targets) was performed using ConsensusPathDB [81], with the overrepresentation analysis tool. As input, HGNC symbol identifiers of our dataset were used and search was done against pathways with a minimal overlap of a p-value cutoff of 0.0001. Cytoscape [82] and the BisoGenet plug-in [83] was then used to generate a potential miRNA-regulated network using the list of validated targets and the modules obtained in the previous step. Crosstalk maps were created, linking curated pathways to metapathways [84–86] where several pathways modules share a common set of genes.

Accession Number

miRNA NGS data from differentially transcribed miRNAs in stress-induced premature senescence (SIPS) have been deposited to the GEO repository under the accession number GSE95354 <https://www.ncbi.nlm.nih.gov/geo/query/acc.cgi?token=ytojsgmknqbtix&acc=GSE95354>.

Abbreviations

BH: Benjamini and Hochberg (BH) procedure; BrdU: bromodeoxyuridine; CDKN2A: cyclin-dependent inhibitor 2A, p21CIP1; D7/21: day 7/21 after stress treatment/recovery; (s)EV: (small) extracellular vesicle; EV-miRNAs: miRNAs enclosed in extracellular vesicle; FC: fold change; FCS: fetal calf serum; FDR: false discovery rate; GAPDH: glyceraldehyde-3-phosphate dehydrogenase; HDF: human dermal fibroblast; ISEV: international society for extracellular vesicles; MCR: mean-centering restricted normalization; NTA: nanoparticle tracking analysis, RM: repeated measurements; SA sEV-miRNA: Senescence-associated miRNAs enclosed in small extracellular vesicles; SASP: Senescence-associated secretory phenotype; SA- β -gal: Senescence-associated β -galactosidase; SIPS: stress induced premature senescence; SVD: singular value decomposition; TPM: tags per million; TSG10: tumour-susceptibility protein.

AUTHOR CONTRIBUTIONS

TZ, JG, FG, FM: planned the study; LTZ, JG, IL and FG: designed experiments, interpreted the results. LTZ, JG: prepared and wrote the manuscript, designed the Figures. LTZ, JL: performed bioinformatics and statistics. LTZ, MRB, VP, RW performed experiments. MScho: contributed to planning of experiments and interpreted the data. SK, MH: contributed to cDNA library preparation and qPCR analysis. JCHA, MSche: performed pathway analysis and prepared the Figures. DP: performed electron microscopy. JG and MScho supervised the writing of the manuscript. All authors read, edited and approved the final manuscript.

ACKNOWLEDGEMENTS

We wish to thank Sylvia Weilner, Severin Mühleder and Jacqueline Friedmann for technical support and helpful advices, Selma Osmanagic-Myers for reading the manuscript critically, as well as Jennifer Schwestka, Matthias Mattanovich and Michaela Hauser for experimental support.

CONFLICTS OF INTEREST

MH and JG, are co-founders of TAmiRNA GmbH. JG is co-founder of Evercyte GmbH. FM and JL are employees of Chanel Research and Technology.

FUNDING

This work was funded by the Christian Doppler Society. The financial support by the Austrian Federal Ministry of Economy, Family and Youth; the National Foundation for Research, Technology and Development is also gratefully acknowledged, as is funding by the Austrian Science Fund by the PhD program “BioTop” (Grant W1224) and FWF I2514. In addition, we gratefully acknowledge the FP7 EU projects Frailomics and Sybil.

REFERENCES

1. Muñoz-Espín D, Serrano M. Cellular senescence: from physiology to pathology. *Nat Rev Mol Cell Biol.* 2014; 15:482–96. <https://doi.org/10.1038/nrm3823>
2. Baker DJ, Childs BG, Durik M, Wijers ME, Sieben CJ, Zhong J, Saltness R a, Jeganathan KB, Casaclang Verzosa G, Pezeshki A, Khazaie K, Miller JD, Van Deursen JM. Naturally occurring p16 Ink4a -positive cells shorten healthy lifespan. *Nature.* 2016; 530:184–49. <https://doi.org/10.1038/nature16932>
3. Jeon OH, Kim C, Laberge RM, Demaria M, Rathod S, Vasserot AP, Chung JW, Kim DH, Poon Y, David N, Baker DJ, van Deursen JM, Campisi J, Elisseeff JH. Local clearance of senescent cells attenuates the development of post-traumatic osteoarthritis and creates a pro-regenerative environment. *Nat Med.* 2017; 23:775–81. <https://doi.org/10.1038/nm.4324>
4. Childs BG, Baker DJ, Wijshake T, Conover CA, Campisi J, van Deursen JM. Senescent intimal foam cells are deleterious at all stages of atherosclerosis. *Science.* 2016; 354:472–77. <https://doi.org/10.1126/science.aaf6659>
5. Zhu Y, Tchkonja T, Fuhrmann-Stroissnigg H, Dai HM, Ling YY, Stout MB, Pirtskhalava T, Giorgadze N, Johnson KO, Giles CB, Wren JD, Niedernhofer LJ, Robbins PD, Kirkland JL. Identification of a novel senolytic agent, navitoclax, targeting the Bcl-2 family of anti-apoptotic factors. *Aging Cell.* 2016; 15:428–35. <https://doi.org/10.1111/ace1.12445>
6. Zhu Y, Dornnebal EJ, Pirtskhalava T, Giorgadze N, Wentworth M, Fuhrmann-Stroissnigg H, Niedernhofer LJ, Robbins PD, Tchkonja T, Kirkland JL. New agents that target senescent cells: the flavone, fisetin, and the BCL-X inhibitors, A1331852 and A1155463. *Aging (Albany NY).* 2017; 9:1–9. <https://doi.org/10.18632/aging.101202>
7. Farr JN, Xu M, Weivoda MM, Monroe DG, Fraser DG, Onken JL, Negley BA, Sfeir JG, Ogrodnik MB, Hachfeld CM, LeBrasseur NK, Drake MT, Pignolo RJ, et al. Targeting cellular senescence prevents age-related bone loss in mice. *Nat Med.* 2017; 23:1072–79. <https://doi.org/10.1038/nm.4385>
8. Tchkonja T, Zhu Y, van Deursen J, Campisi J, Kirkland JL. Cellular senescence and the senescent secretory phenotype: therapeutic opportunities. *J Clin Invest.* 2013; 123:966–72. <https://doi.org/10.1172/JCI64098>
9. Baar MP, Brandt RM, Putavet DA, Klein JD, Derks KW, Bourgeois BR, Stryeck S, Rijksen Y, van Willigenburg H, Feijtel DA, van der Pluijm I, Essers J, van Cappellen WA, et al. Targeted Apoptosis of Senescent Cells Restores Tissue Homeostasis in Response to Chemotoxicity and Aging. *Cell.* 2017; 169:132–147.e16. <https://doi.org/10.1016/j.cell.2017.02.031>
10. Rodier F, Campisi J. Four faces of cellular senescence. *J Cell Biol.* 2011; 192:547–56. <https://doi.org/10.1083/jcb.201009094>
11. Childs BG, Baker DJ, Kirkland JL, Campisi J, van Deursen JM. Senescence and apoptosis: dueling or complementary cell fates? *EMBO Rep.* 2014; 15:1139–53. <https://doi.org/10.15252/embr.201439245>
12. Freund A, Orjalo AV, Desprez PY, Campisi J. Inflammatory networks during cellular senescence:

- causes and consequences. *Trends Mol Med.* 2010; 16:238–46.
<https://doi.org/10.1016/j.molmed.2010.03.003>
13. Lämmermann I, Terlecki-Zaniewicz L, Weinmüller R, Schosserer M, Dellago H, de Matos Branco AD, Autheried D, Sevcnikar B, Kleissl L, Berlin I, Morizot F, Lejeune F, Fuzzati N, et al. Blocking negative effects of senescence in human skin fibroblasts with a plant extract. *NPJ Aging Mech Dis.* 2018; 4:4.
<https://doi.org/10.1038/s41514-018-0023-5>
 14. Childs BG, Durik M, Baker DJ, van Deursen JM. Cellular senescence in aging and age-related disease: from mechanisms to therapy. *Nat Med.* 2015; 21:1424–35.
<https://doi.org/10.1038/nm.4000>
 15. Cortez MA, Bueso-Ramos C, Ferdin J, Lopez-Berestein G, Sood AK, Calin GA. MicroRNAs in body fluids—the mix of hormones and biomarkers. *Nat Rev Clin Oncol.* 2011; 8:467–77.
<https://doi.org/10.1038/nrclinonc.2011.76>
 16. Chen X, Liang H, Zhang J, Zen K, Zhang CY. Horizontal transfer of microRNAs: molecular mechanisms and clinical applications. *Protein Cell.* 2012; 3:28–37.
<https://doi.org/10.1007/s13238-012-2003-z>
 17. Weilner S, Keider V, Winter M, Harreither E, Salzer B, Weiss F, Schraml E, Messner P, Pietschmann P, Hildner F, Gabriel C, Redl H, Grillari-Voglauser R, Grillari J. Vesicular Galectin-3 levels decrease with donor age and contribute to the reduced osteo-inductive potential of human plasma derived extracellular vesicles. *Aging (Albany NY).* 2016; 8:16–33. <https://doi.org/10.18632/aging.100865>
 18. Weilner S, Schraml E, Wieser M, Messner P, Schneider K, Wassermann K, Micutkova L, Fortschegger K, Maier AB, Westendorp R, Resch H, Wolbank S, Redl H, et al. Secreted microvesicular miR-31 inhibits osteogenic differentiation of mesenchymal stem cells. *Aging Cell.* 2016; 15:744–54.
<https://doi.org/10.1111/accel.12484>
 19. Weilner S, Schraml E, Redl H, Grillari-Voglauser R, Grillari J. Secretion of microvesicular miRNAs in cellular and organismal aging. *Exp Gerontol.* 2013; 48:626–33.
<https://doi.org/10.1016/j.exger.2012.11.017>
 20. Hackl M, Heilmeyer U, Weilner S, Grillari J. Circulating microRNAs as novel biomarkers for bone diseases – Complex signatures for multifactorial diseases? *Mol Cell Endocrinol.* 2016; 432:83–95.
<https://doi.org/10.1016/j.mce.2015.10.015>
 21. Olivieri F, Bonafè M, Spazzafumo L, Gobbi M, Prattichizzo F, Recchioni R, Marcheselli F, La Sala L, Galeazzi R, Rippo MR, Fulgenzi G, Angelini S, Lazzarini R, et al. Age- and glycemia-related miR-126-3p levels in plasma and endothelial cells. *Aging (Albany NY).* 2014; 6:771–87.
<https://doi.org/10.18632/aging.100693>
 22. Weilner S, Schraml E, Wieser M, Messner P, Schneider K, Wassermann K, Micutkova L, Fortschegger K, Maier AB, Westendorp R, Resch H, Wolbank S, Redl H, et al. Secreted microvesicular miR-31 inhibits osteogenic differentiation of mesenchymal stem cells. *Aging Cell.* 2016; 15:744–54.
<https://doi.org/10.1111/accel.12484>
 23. Panda AC, Abdelmohsen K, Gorospe M. SASP regulation by noncoding RNA. *Mech Ageing Dev.* 2017; 168:37–43.
<https://doi.org/10.1016/j.mad.2017.05.004>
 24. Hackl M, Suh Y, Grillari J. Editorial: non-coding RNA in aging and age-associated diseases – from intracellular regulators to hormone like actions. *Mech Ageing Dev.* 2017; 168:1–2.
<https://doi.org/10.1016/j.mad.2017.11.014>
 25. Urbanelli L, Buratta S, Sagini K, Tancini B, Emiliani C. Extracellular vesicles as new players in cellular senescence. *Int J Mol Sci.* 2016; 17:17.
<https://doi.org/10.3390/ijms17091408>
 26. Robbins PD. Extracellular vesicles and aging. *Stem Cell Investig.* 2017; 4:98–98.
<https://doi.org/10.21037/sci.2017.12.03>
 27. Kadota T, Fujita Y, Yoshioka Y, Araya J, Kuwano K, Ochiya T. Emerging role of extracellular vesicles as a senescence-associated secretory phenotype: insights into the pathophysiology of lung diseases. *Mol Aspects Med.* 2018. 60:92-103.
<https://doi.org/10.1016/j.mam.2017.11.005>
 28. Toussaint O, Dumont P, Remacle J, Dierick JF, Pascal T, Fripiat C, Magalhaes JP, Zdanov S, Chainiaux F. Stress-induced premature senescence or stress-induced senescence-like phenotype: one *in vivo* reality, two possible definitions? *Sci World J.* 2002; 2:230–47. <https://doi.org/10.1100/tsw.2002.100>
 29. Zhao H, Dupont J, Yakar S, Karas M, LeRoith D. PTEN inhibits cell proliferation and induces apoptosis by downregulating cell surface IGF-IR expression in prostate cancer cells. *Oncogene.* 2004; 23:786–94.
<https://doi.org/10.1038/sj.onc.1207162>
 30. Bratton SB, Walker G, Srinivasula SM, Sun XM, Butterworth M, Alnemri ES, Cohen GM. Recruitment, activation and retention of caspases-9 and -3 by Apaf-1 apoptosome and associated XIAP complexes. *EMBO J.* 2001; 20:998–1009.
<https://doi.org/10.1093/emboj/20.5.998>
 31. Chaturvedi V, Qin JZ, Denning MF, Choubey D, Diaz MO, Nickoloff BJ. Apoptosis in proliferating,

- senescent, and immortalized keratinocytes. *J Biol Chem.* 1999; 274:23358–67.
<https://doi.org/10.1074/jbc.274.33.23358>
32. Fujieda S, Inuzuka M, Tanaka N, Sunaga H, Fan GK, Ito T, Sugimoto C, Tsuzuki H, Saito H. Expression of p27 is associated with Bax expression and spontaneous apoptosis in oral and oropharyngeal carcinoma. *Int J Cancer.* 1999; 84:315–20.
[https://doi.org/10.1002/\(SICI\)1097-0215\(19990621\)84:3<315::AID-IJC20>3.0.CO;2-U](https://doi.org/10.1002/(SICI)1097-0215(19990621)84:3<315::AID-IJC20>3.0.CO;2-U)
 33. Hoffman B, Liebermann DA. Apoptotic signaling by c-MYC. *Oncogene.* 2008; 27:6462–72.
<https://doi.org/10.1038/onc.2008.312>
 34. Mestdagh P, Van Vlierberghe P, De Weer A, Muth D, Westermann F, Speleman F, Vandesompele J. A novel and universal method for microRNA RT-qPCR data normalization. *Genome Biol.* 2009; 10:R64.
<https://doi.org/10.1186/gb-2009-10-6-r64>
 35. Greussing R, Hackl M, Charoentong P, Pauck A, Monteforte R, Cavinato M, Hofer E, Scheideler M, Neuhaus M, Micutkova L, Mueck C, Trajanoski Z, Grillari J, Jansen-Dürr P. Identification of microRNA-mRNA functional interactions in UVB-induced senescence of human diploid fibroblasts. *BMC Genomics.* 2013; 14:224. <https://doi.org/10.1186/1471-2164-14-224>
 36. Mancini M, Lena AM, Saintigny G, Mahé C, Di Daniele N, Melino G, Candi E. MicroRNAs in human skin ageing. *Ageing Res Rev.* 2014; 17:9–15.
<https://doi.org/10.1016/j.arr.2014.04.003>
 37. Li T, Yan X, Jiang M, Xiang L. The comparison of microRNA profile of the dermis between the young and elderly. *J Dermatol Sci.* 2016; 82:75–83.
<https://doi.org/10.1016/j.jdermsci.2016.01.005>
 38. Coppé JP, Patil CK, Rodier F, Sun Y, Muñoz DP, Goldstein J, Nelson PS, Desprez PY, Campisi J. Senescence-associated secretory phenotypes reveal cell-nonautonomous functions of oncogenic RAS and the p53 tumor suppressor. *PLoS Biol.* 2008; 6:2853–68. <https://doi.org/10.1371/journal.pbio.0060301>
 39. Meyer P, Maity P, Burkovski A, Schwab J, Müssel C, Singh K, Ferreira FF, Krug L, Maier HJ, Wlaschek M, Wirth T, Kestler HA, Scharffetter-Kochanek K. A model of the onset of the senescence associated secretory phenotype after DNA damage induced senescence. *PLOS Comput Biol.* 2017; 13:e1005741.
<https://doi.org/10.1371/journal.pcbi.1005741>
 40. Hudgins AD, Tazearslan C, Tare A, Zhu Y, Huffman D, Suh Y. Age- and Tissue-Specific Expression of Senescence Biomarkers in Mice. *Front Genet.* 2018; 9:59. <https://doi.org/10.3389/fgene.2018.00059>
 41. Magenta A, Cencioni C, Fasanaro P, Zaccagnini G, Greco S, Sarra-Ferraris G, Antonini A, Martelli F, Capogrossi MC. miR-200c is upregulated by oxidative stress and induces endothelial cell apoptosis and senescence via ZEB1 inhibition. *Cell Death Differ.* 2011; 18:1628–39.
<https://doi.org/10.1038/cdd.2011.42>
 42. Carlomosti F, D’Agostino M, Beji S, Torcinaro A, Rizzi R, Zaccagnini G, Maimone B, Di Stefano V, De Santa F, Cordisco S, Antonini A, Ciarapica R, Dellambra E, et al. Oxidative Stress-Induced miR-200c Disrupts the Regulatory Loop Among SIRT1, FOXO1, and eNOS. *Antioxid Redox Signal.* 2017; 27:328–44.
<https://doi.org/10.1089/ars.2016.6643>
 43. Lehmann BD, Paine MS, Brooks AM, McCubrey JA, Renegar RH, Wang R, Terrian DM. Senescence-associated exosome release from human prostate cancer cells. *Cancer Res.* 2008; 68:7864–71.
<https://doi.org/10.1158/0008-5472.CAN-07-6538>
 44. Perrotta I, Aquila S. Exosomes in human atherosclerosis: an ultrastructural analysis study. *Ultrastruct Pathol.* 2016; 40:101–06.
<https://doi.org/10.3109/01913123.2016.1154912>
 45. Agosta F, Dalla Libera D, Spinelli EG, Finardi A, Canu E, Bergami A, Bocchio Chiavetto L, Baronio M, Comi G, Martino G, Matteoli M, Magnani G, Verderio C, Furlan R. Myeloid microvesicles in cerebrospinal fluid are associated with myelin damage and neuronal loss in mild cognitive impairment and Alzheimer disease. *Ann Neurol.* 2014; 76:813–25.
<https://doi.org/10.1002/ana.24235>
 46. Eitan E, Green J, Bodogai M, Mode NA, Bæk R, Jørgensen MM, Freeman DW, Witwer KW, Zonderman AB, Biragyn A, Mattson MP, Noren Hooten N, Evans MK. Age-Related Changes in Plasma Extracellular Vesicle Characteristics and Internalization by Leukocytes. *Sci Rep.* 2017; 7:1342.
<https://doi.org/10.1038/s41598-017-01386-z>
 47. Krtolica A, Parrinello S, Lockett S, Desprez PY, Campisi J. Senescent fibroblasts promote epithelial cell growth and tumorigenesis: a link between cancer and aging. *Proc Natl Acad Sci USA.* 2001; 98:12072–77.
<https://doi.org/10.1073/pnas.211053698>
 48. Takasugi M, Okada R, Takahashi A, Virya Chen D, Watanabe S, Hara E. Small extracellular vesicles secreted from senescent cells promote cancer cell proliferation through EphA2. *Nat Commun.* 2017; 8:15729. <https://doi.org/10.1038/ncomms15728>
 49. Barile L, Lionetti V, Cervio E, Matteucci M, Gherghiceanu M, Popescu LM, Torre T, Siclari F, Moccetti T, Vassalli G. Extracellular vesicles from human cardiac progenitor cells inhibit cardiomyocyte apoptosis and improve cardiac function after

- myocardial infarction. *Cardiovasc Res.* 2014; 103:530–41. <https://doi.org/10.1093/cvr/cvu167>
50. Özcan S, Alessio N, Acar MB, Mert E, Omerli F, Peluso G, Galderisi U. Unbiased analysis of senescence associated secretory phenotype (SASP) to identify common components following different genotoxic stresses. *Aging (Albany NY)*. 2016; 8:1316–29. <https://doi.org/10.18632/aging.100971>
 51. Zhang JA, Zhou BR, Xu Y, Chen X, Liu J, Gozali M, Wu D, Yin ZQ, Luo D, Zhang J, Zhou B, Xu Y, Chen X, et al. MiR-23a-depressed autophagy is a participant in PUVA- and UVB-induced premature senescence. *Oncotarget*. 2016; 7:37420–35. <https://doi.org/10.18632/oncotarget.9357>
 52. Neault M, Mallette FA, Richard S. miR-137 Modulates a Tumor Suppressor Network-Inducing Senescence in Pancreatic Cancer Cells. *Cell Reports*. 2016; 14:1966–78. <https://doi.org/10.1016/j.celrep.2016.01.068>
 53. Hackl M, Brunner S, Fortschegger K, Schreiner C, Micutkova L, Mück C, Laschober GT, Lepperdinger G, Sampson N, Berger P, Herndler-Brandstetter D, Wieser M, Kühnel H, et al. miR-17, miR-19b, miR-20a, and miR-106a are down-regulated in human aging. *Aging Cell*. 2010; 9:291–96. <https://doi.org/10.1111/j.1474-9726.2010.00549.x>
 54. Yoo JK, Kim CH, Jung HY, Lee DR, Kim JK. Discovery and characterization of miRNA during cellular senescence in bone marrow-derived human mesenchymal stem cells. *Exp Gerontol*. 2014; 58:139–45. <https://doi.org/10.1016/j.exger.2014.07.020>
 55. Faraonio R, Salerno P, Passaro F, Sedia C, Iaccio A, Bellelli R, Nappi TC, Comegna M, Romano S, Salvatore G, Santoro M, Cimino F. A set of miRNAs participates in the cellular senescence program in human diploid fibroblasts. *Cell Death Differ*. 2012; 19:713–21. <https://doi.org/10.1038/cdd.2011.143>
 56. Marasa BS, Srikantan S, Martindale JL, Kim MM, Lee EK, Gorospe M, Abdelmohsen K. MicroRNA profiling in human diploid fibroblasts uncovers miR-519 role in replicative senescence. *Aging (Albany NY)*. 2010; 2:333–43. <https://doi.org/10.18632/aging.100159>
 57. Dhahbi JM, Atamna H, Boffelli D, Magis W, Spindler SR, Martin DI. Deep sequencing reveals novel microRNAs and regulation of microRNA expression during cell senescence. *PLoS One*. 2011; 6:e20509. <https://doi.org/10.1371/journal.pone.0020509>
 58. Martinez I, Cazalla D, Almstead LL, Steitz JA, DiMaio D. miR-29 and miR-30 regulate B-Myb expression during cellular senescence. *Proc Natl Acad Sci USA*. 2011; 108:522–27. <https://doi.org/10.1073/pnas.1017346108>
 59. Lewis DA, Travers JB, Somani AK, Spandau DF. The IGF-1/IGF-1R signaling axis in the skin: a new role for the dermis in aging-associated skin cancer. *Oncogene*. 2010; 29:1475–85. <https://doi.org/10.1038/onc.2009.440>
 60. Guduric-Fuchs J, O'Connor A, Camp B, O'Neill CL, Medina RJ, Simpson DA. Selective extracellular vesicle-mediated export of an overlapping set of microRNAs from multiple cell types. *BMC Genomics*. 2012; 13:357. <https://doi.org/10.1186/1471-2164-13-357>
 61. Turchinovich A, Tonevitsky AG, Burwinkel B. Extracellular miRNA: A Collision of Two Paradigms. *Trends Biochem Sci*. 2016; 41:883–92. <https://doi.org/10.1016/j.tibs.2016.08.004>
 62. van Balkom BW, Eisele AS, Pegtel DM, Bervoets S, Verhaar MC. Quantitative and qualitative analysis of small RNAs in human endothelial cells and exosomes provides insights into localized RNA processing, degradation and sorting. *J Extracell Vesicles*. 2015; 4:26760. <https://doi.org/10.3402/jev.v4.26760>
 63. Ostefeld MS, Jeppesen DK, Laurberg JR, Boysen AT, Bramsen JB, Primdal-Bengtson B, Hendrix A, Lamy P, Dagnaes-Hansen F, Rasmussen MH, Bui KH, Fristrup N, Christensen EI, et al. Cellular disposal of miR23b by RAB27-dependent exosome release is linked to acquisition of metastatic properties. *Cancer Res*. 2014; 74:5758–71. <https://doi.org/10.1158/0008-5472.CAN-13-3512>
 64. Cha DJ, Franklin JL, Dou Y, Liu Q, Higginbotham JN, Demory Beckler M, Weaver AM, Vickers K, Prasad N, Levy S, Zhang B, Coffey RJ, Patton JG. KRAS-dependent sorting of miRNA to exosomes. *eLife*. 2015; 4:e07197. <https://doi.org/10.7554/eLife.07197>
 65. Yentrapalli R, Merl-Pham J, Azimzadeh O, Mutschelknaus L, Peters C, Hauck SM, Atkinson MJ, Tapio S, Moertl S. Quantitative changes in the protein and miRNA cargo of plasma exosome-like vesicles after exposure to ionizing radiation. *Int J Radiat Biol*. 2017; 93:569–80. <https://doi.org/10.1080/09553002.2017.1294772>
 66. Pigati L, Yaddanapudi SC, Iyengar R, Kim DJ, Hearn SA, Danforth D, Hastings ML, Duelli DM. Selective release of microRNA species from normal and malignant mammary epithelial cells. *PLoS One*. 2010; 5:e13515. <https://doi.org/10.1371/journal.pone.0013515>
 67. Lang A, Grether-Beck S, Singh M, Kuck F, Jakob S, Kefalas A, Altinoluks-Hambüchen S, Graffmann N, Schneider M, Lindecke A, Brenden H, Felsner I, Ezzahoini H, et al. MicroRNA-15b regulates mitochondrial ROS production and the senescence-associated secretory phenotype through sirtuin

- 4/SIRT4. *Aging* (Albany NY). 2016; 8:484–505. <https://doi.org/10.18632/aging.100905>
68. Kang C, Xu Q, Martin TD, Li MZ, Demaria M, Aron L, Lu T, Yankner BA, Campisi J, Elledge SJ. The DNA damage response induces inflammation and senescence by inhibiting autophagy of GATA4. *Science*. 2015; 349:aaa5612. <https://doi.org/10.1126/science.aaa5612>
 69. Ofir M, Hacoheh D, Ginsberg D. MiR-15 and miR-16 are direct transcriptional targets of E2F1 that limit E2F-induced proliferation by targeting cyclin E. *Mol Cancer Res*. 2011; 9:440–47. <https://doi.org/10.1158/1541-7786.MCR-10-0344>
 70. Demaria M, Ohtani N, Youssef SA, Rodier F, Toussaint W, Mitchell JR, Laberge RM, Vijg J, Van Steeg H, Dollé ME, Hoeijmakers JH, de Bruin A, Hara E, Campisi J. An essential role for senescent cells in optimal wound healing through secretion of PDGF-AA. *Dev Cell*. 2014; 31:722–33. <https://doi.org/10.1016/j.devcel.2014.11.012>
 71. Jiang M, Ma W, Gao Y, Jia K, Zhang Y, Liu H, Sun Q. IL-22-induced miR-122-5p promotes keratinocyte proliferation by targeting Sprouty2. *Exp Dermatol*. 2017; 26:368–74. <https://doi.org/10.1111/exd.13270>
 72. Ahmed MI, Mardaryev AN, Lewis CJ, Sharov AA, Botchkareva NV. MicroRNA-21 is an important downstream component of BMP signalling in epidermal keratinocytes. *J Cell Sci*. 2011; 124:3399–404. <https://doi.org/10.1242/jcs.086710>
 73. Wu N, Sulpice E, Obeid P, Benzina S, Kermarrec F, Combe S, Gidrol X. The miR-17 family links p63 protein to MAPK signaling to promote the onset of human keratinocyte differentiation. *PLoS One*. 2012; 7:e45761. <https://doi.org/10.1371/journal.pone.0045761>
 74. Hill AF, Pegtel DM, Lambert U, Leonardi T, Driscoll LO, Pluchino S, Ter-ovanesyan D. Hoen ENMN-. ISEV position paper: extracellular vesicle RNA analysis and bioinformatics. *J Extracell Vesicles*. 2013; 1:1–8. <https://doi.org/10.3402/jev.v2i0.22859>
 75. Anders S, Huber W. Differential expression analysis for sequence count data. *Genome Biol*. 2010; 11:R106. <https://doi.org/10.1186/gb-2010-11-10-r106>
 76. Benjamini Y, Yekutieli D. The Control of the False Discovery Rate in Multiple Testing under Dependency. *Ann Stat*. 2001; 29:1165–88. <https://projecteuclid.org/euclid.aos/1013699998>
 77. Deo A, Carlsson Jessica, Lindlöf A. How to choose a normalization strategy for miRNA quantitative. *J Bioinform Comput Biol*. 2011; 9:795–812.
 78. Smyth GK. *Limma: linear models for microarray data* [Internet]. Gentleman R, Carey V, Dudoit S, R Irizarry WH, editors. New York: Springer; 2005. p. 397–420.
 79. Metsalu T, Vilo J. ClustVis: a web tool for visualizing clustering of multivariate data using Principal Component Analysis and heatmap. *Nucleic Acids Res*. 2015; 43:W566–70. <https://doi.org/10.1093/nar/gkv468>
 80. Dweep H, Gretz N. miRWalk2.0: a comprehensive atlas of microRNA-target interactions. *Nat Meth*. 2015; 12:697. <https://doi.org/10.1038/nmeth.3485>
 81. Kamburov A, Stelzl U, Lehrach H, Herwig R. The ConsensusPathDB interaction database: 2013 update. *Nucleic Acids Res*. 2013; 41:D793–800. <https://doi.org/10.1093/nar/gks1055>
 82. Smoot ME, Ono K, Ruscheinski J, Wang PL, Ideker T. Cytoscape 2.8: new features for data integration and network visualization. *Bioinformatics*. 2011; 27:431–32. <https://doi.org/10.1093/bioinformatics/btq675>
 83. Martin A, Ochagavia ME, Rabasa LC, Miranda J, Fernandez-de-Cossio J, Bringas R. BisoGenet: a new tool for gene network building, visualization and analysis. *BMC Bioinformatics*. 2010; 11:91. <https://doi.org/10.1186/1471-2105-11-91>
 84. Fertig EJ, Markovic A, Danilova LV, Gaykalova DA, Cope L, Chung CH, Ochs MF, Califano JA. Preferential activation of the hedgehog pathway by epigenetic modulations in HPV negative HNSCC identified with meta-pathway analysis. *PLoS One*. 2013; 8:e78127. <https://doi.org/10.1371/journal.pone.0078127>
 85. Higareda-Almaraz JC, Ruiz-Moreno JS, Klimentova J, Barbieri D, Salvador-Gallego R, Ly R, Valtierra-Gutierrez IA, Dinsart C, Rabinovich GA, Stulik J, Rösl F, Rincon-Orozco B. Systems-level effects of ectopic galectin-7 reconstitution in cervical cancer and its microenvironment. *BMC Cancer*. 2016; 16:680. <https://doi.org/10.1186/s12885-016-2700-8>
 86. Higareda-Almaraz JC, Valtierra-Gutiérrez IA, Hernandez-Ortiz M, Contreras S, Hernandez E, Encarnación-Guevara S. Analysis and prediction of pathways in HeLa cells by integrating biological levels of organization with systems-biology approaches. *PLoS One*. 2013; 8:e65433. <https://doi.org/10.1371/journal.pone.0065433>

SUPPLEMENTARY MATERIAL

Supplementary Figures

Figure S1. Scheme of experimental workflow. (A) SIPS was triggered in three donors of primary human dermal fibroblasts' (HDF) by chronic low doses of H₂O₂. Seven days (D7) and 21 days (D21) after the last H₂O₂ pulse, intracellular RNA was harvested and cDNA library for small RNA NGS was synthesized. Correspondingly, sncRNA from small extracellular vesicles (sEVs) was isolated from conditioned supernatants by differential centrifugation. SEV-RNA was prepared for qPCR panels to identify senescence-associated sEV-miRNAs.

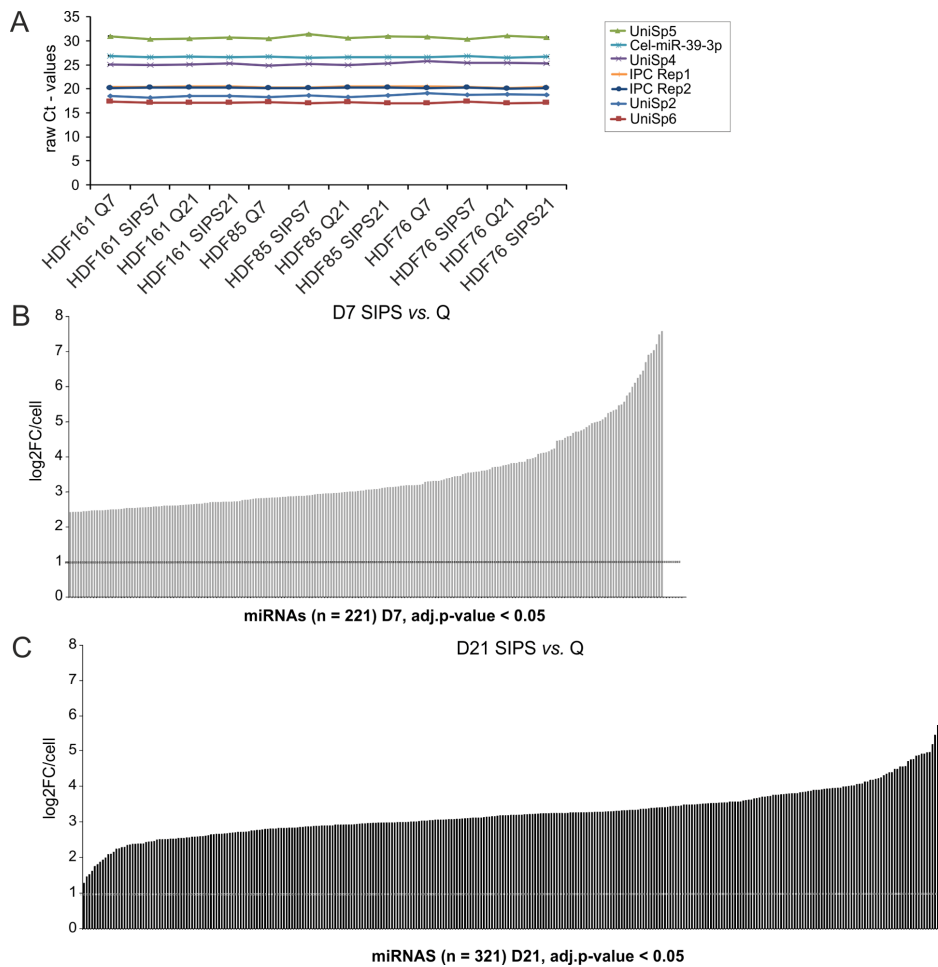
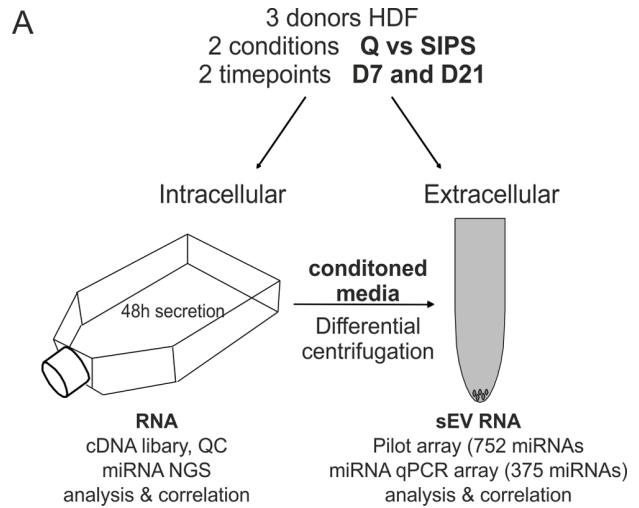


Figure S2. Data quality control and analysis of miRNAs enclosed in small extracellular vesicles. (A) Quality control using synthetic RNA-spike-in confirms technical coverage (ΔC_t , values below 1) of screening comprising 12 samples of vesicular RNA from three different donors and two different time points (D7 and D21). Each qPCR plate contained primer for synthetic spike in RNAs that were added during RNA isolation (Unisp2, Unisp4, Unisp5) and cDNA synthesis (Unisp6, cel-miR-39). Additionally, each panel included two interplate calibrator (IPC) and an empty negative control. (B) Bar chart of significantly higher secreted miRNAs of SIPS HDF on D7 after the treatment. Log₂FC values from three biological triplicates were calculated and plotted on y-axis. Bars plotted on y-axis show all miRNAs reaching an adjusted p-value < 0.05 after applying the BH method for FDR. On D7, 221 EV-miRNAs passed the adjusted p-value. Dotted lines represent log₂FC = 1. (C) Bar chart of significantly higher secreted sEV-miRNAs of SIPS HDF on D21 after the treatment. Log₂FC values from three biological triplicates were calculated and plotted on y-axis. Bars plotted on y-axis show all miRNAs reaching an adjusted p-value < 0.05 after applying the Benjamini Hochberg method for FDR. On D21, 321 EV-miRNAs passed the adjusted p-value. Dotted lines represent log₂FC = 1.

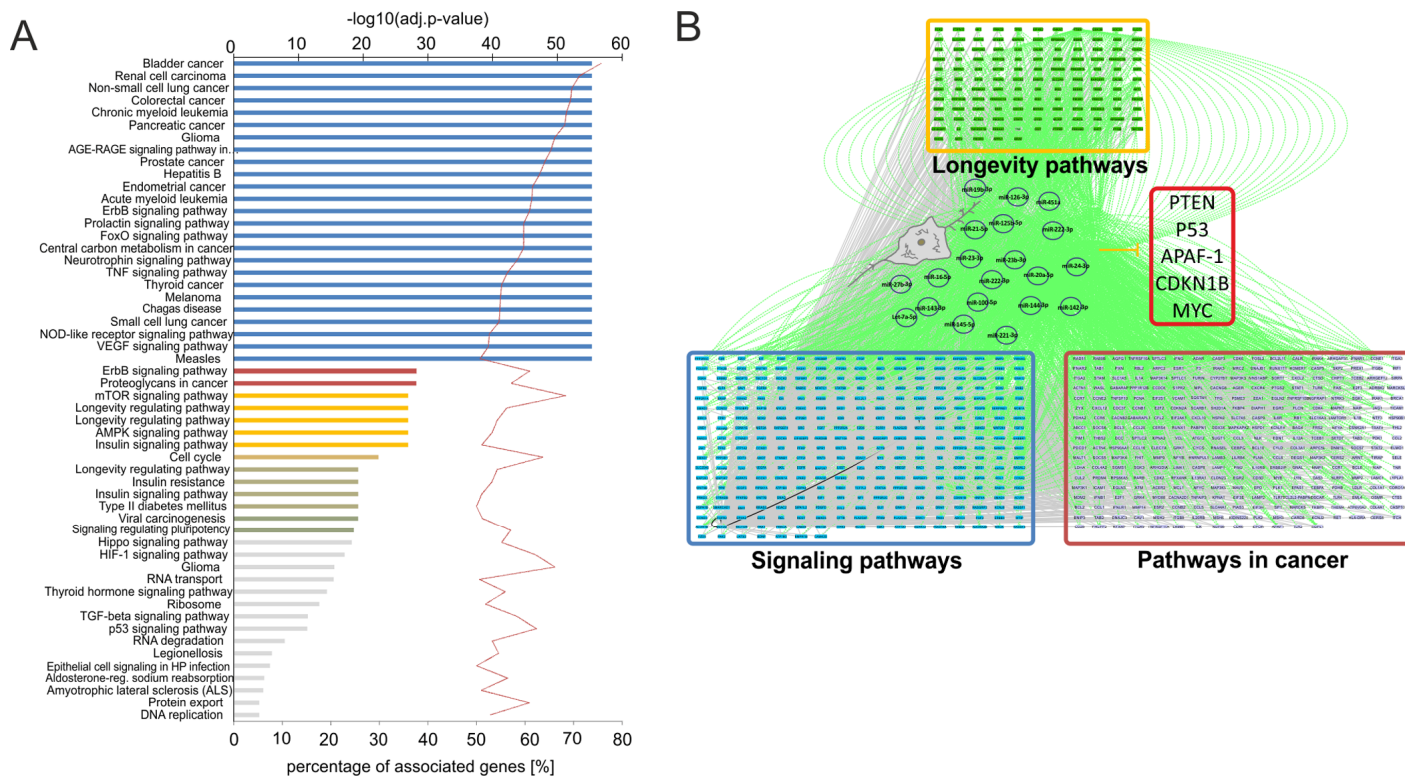


Figure S3. Pathway analysis of the EV-SASP. (A) Bar chart shows 54 network modules with more than 50% of all associated genes targeted by the 20 most abundantly secreted miRNAs with an adjusted p-value < 0.0001. GO terms are plotted against their -log₁₀(adj.p-value). Red line indicates the number of associated target genes identified within all interactions (5,437 validated targets were identified). Color of bar charts (blue, red, yellow, olive, avocado green, gold) correspond to one GO group that contain more GO-Terms. Grey bars correspond to different GO groups that contain only one GO term. Abbreviation HP: Helicobacter pylori infection. (B) Top20 secreted miRNAs regulate a dynamic crosstalk of three prominent metapathways and five common transcription factors (PTEN, P53, APAF-1, CDKN1B and MYC). Several gene modules were detected to participate repeatedly in several pathways, indicating a crosstalk of pleiotropic genes and various gene modules involved in series of cellular activities. Based on that finding, large metapathways identified a complex network that pinpoints towards an interplay between signaling, longevity and cancer pathways, which are supposed to be orchestrated by the secreted miRNAs and their target genes suggesting a potential anti-apoptotic activity of the EV-SASP on target cells. Longevity pathways, signaling pathways and pathways in cancer are shown. Green edges represent miRNA regulation over their targets across different pathways. Grey edges represent protein-protein interactions and transcriptional regulation. Graphic illustrates the top 20 highly secreted miRNAs commonly targeting five transcription factors.

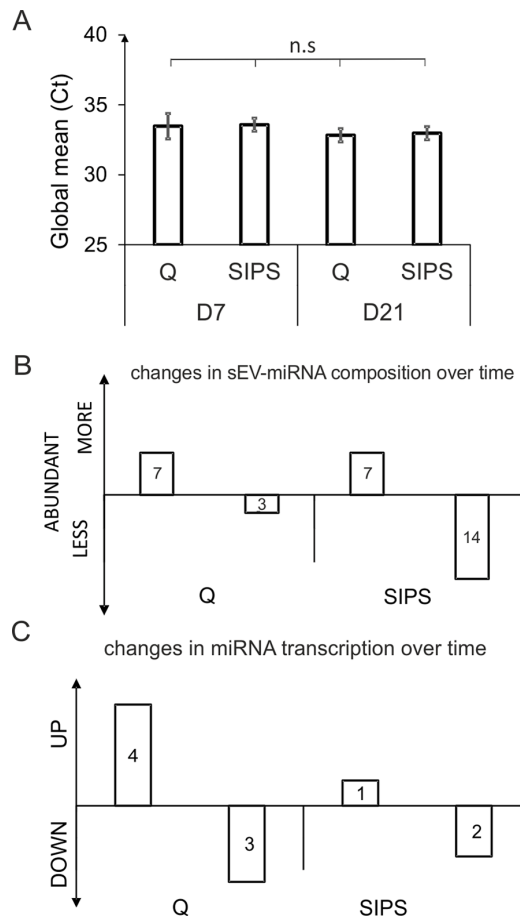


Figure S4. Calculation of Global means and changes in miRNA abundances over time in vesicles and intracellularly. (A) Global mean used for normalization. Averages of three different HDF strains +/- STDEV is shown. 2-way ANOVA was used to test for condition ($p = 0.73$) and day ($p = 0.11$); (n.s) $p > 0.05$. (B) 21 sEV-miRNAs of SIPS cells change their composition over time. Global mean-normalized Ct-values from biological triplicates were averaged and \log_2FC relative to day 7 recovery were calculated (p -value < 0.05). (C) 3 miRNAs are differentially transcribed in SIPS cells over time. Intracellular miRNA transcription relative to day 7 was calculated from NGS data. miRNAs with an adj. p -value < 0.05 were taken into account.

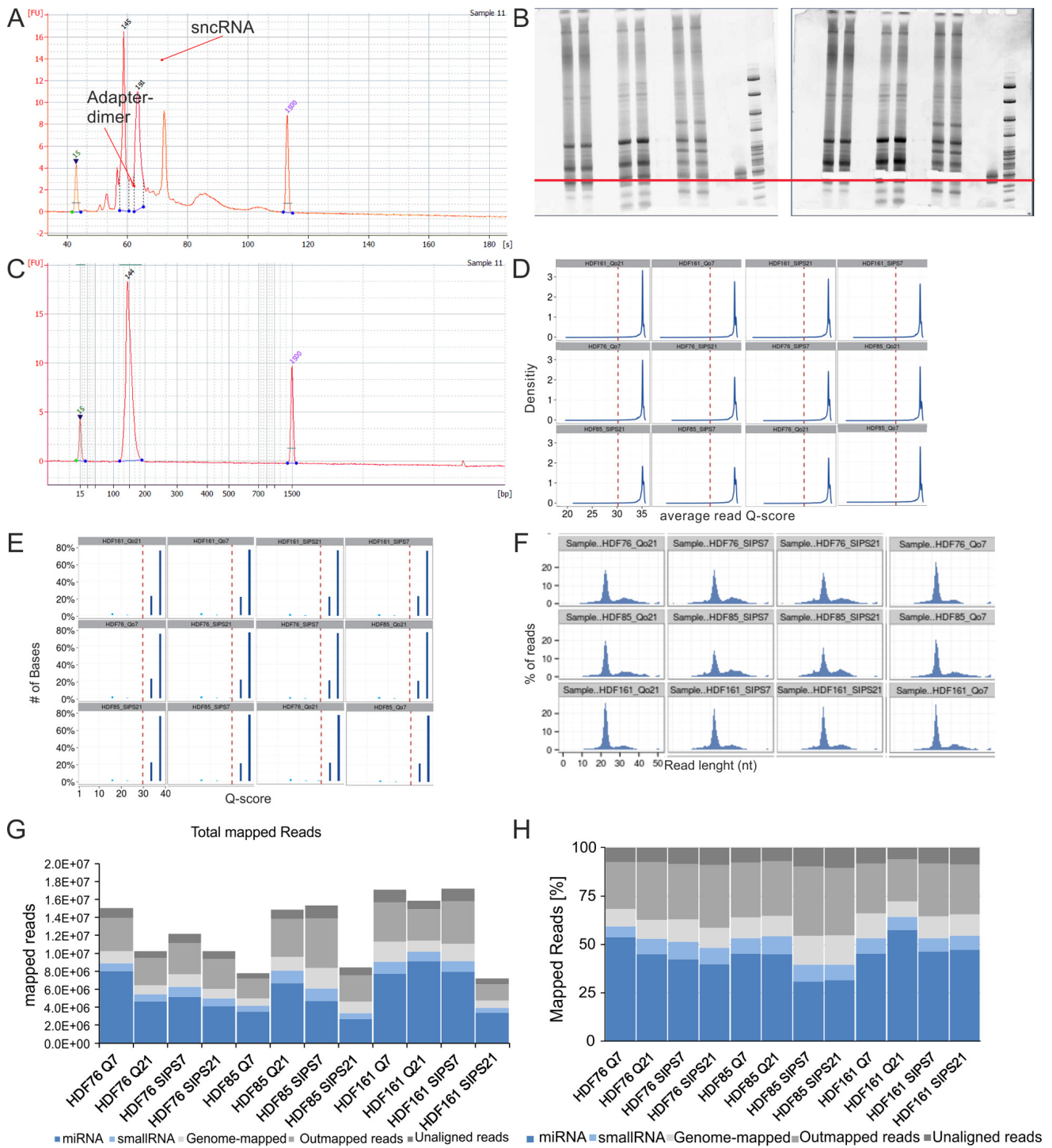


Figure S5. Data quality control of cDNA library preparation and NGS carried out by Exiqon. (A) Representative picture of cDNA library after adapter ligation and PCR amplification measured with Agilent Bioanalyzer2100. Bound and free adapter dimers are visible. Peak for sncRNAs is indicated. (B) Representative pictures of cDNA library separated on a 10% TBE Gel. Fragments corresponding to sncRNAs from approx. 18 to 36bp were cut (left: before cutting. Right: after cutting). (C) Representative picture of cDNA library after gel purification analyzed with Agilent Bioanalyzer2100 shows the sncRNA peak but no adapter fragments. (D) Representative pictures of average read Q-scores from data quality control after NGS. All data have a Q-score > 30 (red line), indicating more than 99.9% accuracy of base calling. (E) Blue bars show percentage of reads with the indicated score. (F) Read length distribution after adapter trimming reveals a prominent miRNA peak with 18-22 nt and few longer sequences of 30 – 50 nt belonging to other ncRNAs such as tRNAs, rRNAs, ect. (G) Total mapped reads of sequencing. Reads were annotated to miRBase20 and classified according to the following categories: ‘not aligned’, ‘outmapped’, ‘genome-mapped’, ‘smallRNA’ and ‘miRNA’. (H) % of total mapped reads. Reads were annotated to miRBase20 and classified according to the following categories: ‘not aligned’, ‘outmapped’, ‘genome-mapped’, ‘smallRNA’ and ‘miRNA’.

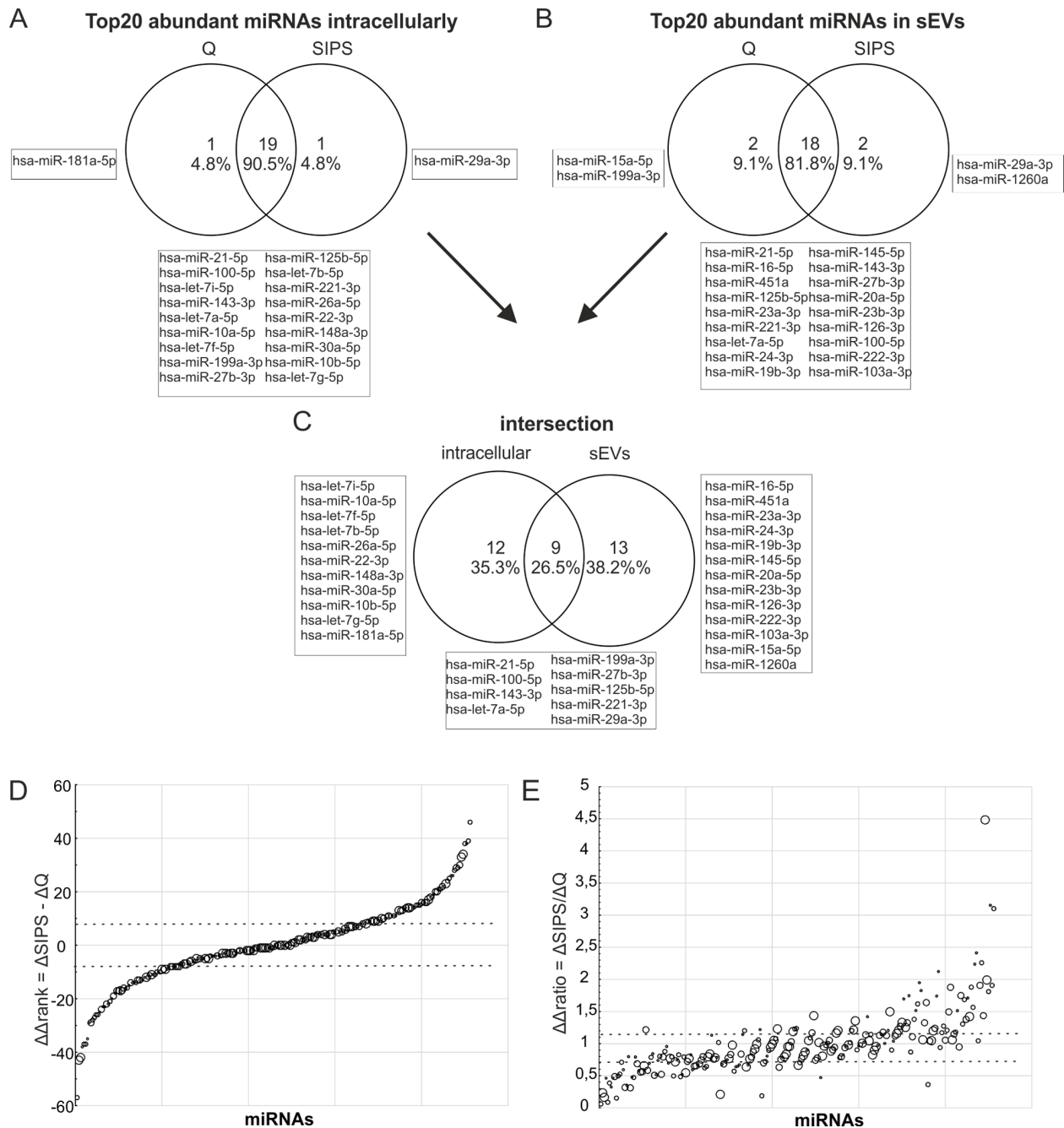


Figure S6. (A) Venn diagram of the top 20 abundantly transcribed miRNAs in cells from Q and SIPS cells, sorted by ranks, used to identify commonly transcribed miRNAs in HDF. (B) Venn diagram of the top 20 abundant sEV-miRNAs secreted from Q and SIPS cells, sorted by ranks, used to identify commonly secreted sEV-miRNAs of HDF. (C) Positively ('mirroring effect' of inside and outside) and negatively matching miRNAs are identified by building the intersection from A + B. 26.5% matching miRNAs were found. (D) Specifically senescence-associated secreted (high values) or retained (low values) miRNAs are identified by the rank method. Δrank values were calculate from Δrank values derived from Q and SIPS separately. High Δrank s indicate 'secreted' and low Δrank s indicate 'retained'. Bubble size corresponds to the average expression value from the transformed Ct-values. Dotted lines represent the 25% and 75% percentiles, which defines the cut-off for specifically secreted and retained miRNAs in SIPS. Δrank : 25%: 8.0; Median: -0.5; 75%: 9.0; (E) Specifically senescence-associated secreted (high value) or retained (low value) miRNAs are identified by the ratio method. Ratios between intracellular and vesicular values are calculated. By further calculating and normalizing Δratios , specifically senescence-associated secreted (high values) or retained (low values) miRNAs are identified. Due to differences in units, it is not possible to set the threshold to 1. Results are sorted from smallest to largest. They are plotted in the same manner as it resulted after sorting of Δratios and appear in a similar shape as in (D), indicating that we identified a similar set of miRNAs. High Δrank s indicate 'secreted', and low Δrank s indicate 'retained'. Bubble size corresponds to average expression value from transformed Ct-values. Dotted lines represent the 25% and 75% percentiles, which define the specifically secreted and retained miRNAs in SIPS. Δratio : 25%: 0.7099; Median: 0.927; 75%: 1.186.

Supplementary Methods

Annexin-V-PI staining

For staining of apoptotic cells, the Pacific Blue™ Annexin-V Kit (Biolegend, San Diego, CA, USA, 640918) was used. Cells and supernatants were harvested, pooled, centrifuged at 200 x g for 10 minutes (min) and pellets were washed twice with Annexin-V binding buffer (10 mM HEPES/NaOH pH 7.4, 140 mM NaCl, 5 mM CaCl₂). After centrifugation at 500 x g, the pellet was resuspended and incubated for 15 min in Annexin-V/PI staining solution (250 ng/mL propidium iodide PI, Sigma Aldrich GmbH, St Louis, MO, USA P4864, 200 ng/mL Pacific Blue, diluted in Annexin-V binding buffer). The analysis was performed on a Gallios flow cytometer (Beckman Coulter, Brea, CA, USA) using an excitation wavelength of 488 nm and a 600 nm emission filter for detection of PI (FL-3) and an excitation of 405 nm and a 450/50nm emission filter for Pacific-Blue-Annexin (FL-9). Cells treated with 300 nM Staurosporin for 24 hours were used as a positive control. Flow cytometry data were analyzed with Kaluza software (Beckman Coulter, Brea, CA, USA, Version 1.2).

BrdU incorporation

In order to verify growth arrest, cells were incubated for 24 hours with 10 μM BrdU (Sigma Aldrich GmbH, St Louis, MO, USA, B5002). The cells were harvested by trypsinization, centrifuged at 170 x g for 5 min and the pellet was fixed with ice cold 70% ethanol for at least one hour at 4°C. Cells were permeabilized for 30 min with 2 M HCl and 1% Triton X-100 (Sigma Aldrich GmbH, St Louis, MO, USA, X100), followed by neutralization with 0.1 M Na-Borat, pH 8.5. Pellets were resuspended in TBS (0.5% Tween20, 1% BSA in 1 x PBS) containing anti-BrdU antibody 1:50 (BD Biosciences, USA, 347580) and incubated for 30 min. After washing with TBS and counterstaining with anti-mouse FITC-conjugated antibody 1:100 (Sigma Aldrich GmbH, St Louis, MO, USA F8264) for 30 minutes, the pellet was washed with TBS and resuspended in 1 x PBS with 2.5 μg/ml PI (Sigma Aldrich GmbH, St Louis, MO, USA, P4864). For compensation, cells were stained with either PI or BrdU alone. The analysis was performed by flow cytometry (Gallios Beckman Coulter, Brea, CA, USA), using an excitation wavelength of 488 nm and a 600 nm emission filter for detection of PI (FL-3) and a 535 nm filter for BrdU-FITC (FL-1). Proliferating cells were used as positive controls. Flow cytometry data were analyzed with Kaluza software (Beckman Coulter, Brea, CA, USA, Version 1.2).

Senescence associated (SA) β-Gal staining

SIPS HDF and sub-confluent HDF at the middle of their replicative lifespan were stained according to the standard protocol described by Dimri et al. 1995 [1]. 15 pictures per well were taken at 100 x magnification and after randomization and blinding, SA-β-Gal positive and negative cells were counted.

Nanoparticle tracking analysis

Experiments related to sEV Isolation were performed according to standards recommended from the inter-national society for extracellular vesicles (ISEV) [2].

For determination of size and concentration of vesicles, the ZetaView® system (Particle Metrix, Meerbusch, Germany) was used. After calibrating the system with 110 nm polystyrene standard beads (Particle Metrix, Meerbusch, Germany), vesicles resuspended in 1000 μl after ultracentrifugation were diluted 1:200 in filtered 1 x PBS and 3 consecutive measurements were performed. Camera sensitivity was adjusted to fit the highest and lowest concentrated sample into the dynamic range and all samples were measured with the same dilution and settings. Settings: Gain 904, 98; Offset 0. Measurements were taken at two different camera positions and a total of ~1x10¹⁰ particles/cm² were tracked, which corresponds to 150 – 400 counted particles per measurement. Particles secreted per cell were calculated using the cell number measured with an automated cell counter, Vi-CELL XR (Beckman Coulter, Brea, CA, USA). Categories of particle size determination was defined by the device. Categories below 15 nm, 15 nm, 45 nm, 105 nm, 135 nm, 165 nm, 195 nm and bigger than 225 nm are shown.

Electron microscopy

SEVs for Transmission Electron microscopy (TEM) were freshly prepared. Solutions used for the staining procedure were pre-filtered using 0.22 μm filter units (Millipore, Germany, SCGPU05RE). SEVs were adhered on Athene Old 300 mesh copper grids (Agar Scientific, Stansted, Essex, UK) and fixed with 1% glutaraldehyde. After washing three times with nuclease free water, vesicles were stained for 5 min with 2% phosphotungstic acid hydrate (Carl Roth, Karlsruhe, Germany). The grids were left to dry and the specimens were visualized using TEM (FEI Tecnai T20, FEI Eindhoven, Netherlands) operated at 160 kV.

Protein quantification, western blot and antibodies

Vesicles and corresponding cells were lysed in 1 x TNE buffer (2 x TNE: 100 mM Tris/HCl, pH 8.0, 300 mM

NaCl, 1 mM EDTA, 2 % Triton X-100) to quantify membrane markers of sEVs. Protein content of lysates was quantified with the Pierce® BCA Protein Assay Kit (Thermo Scientific, USA, 23227) according to manufacturer's recommendations and equal amounts of protein were loaded onto the gel (20 µg). For SDS page and subsequent western blotting, samples were resuspended in SDS loading dye (4 x SDS loading dye: 240 mM Tris/HCl, pH 6.8, 8% SDS, 40% glycerol, 0.05% bromophenolblue, 5% β-Mercaptoethanol), sonicated and heated to 95°C. Then, samples were separated on a NuPAGE 4–12% Bis/Tris polyacrylamide gel (Invitrogen/Thermo Scientific, USA, 10472322) at 200V and proteins were transferred to a PVDF membrane (Biorad, Hercules, CA, USA, 170-4156) in a BioRad SemiDry Blotting System at 1.3A 25V for 7 minutes. Membranes were incubated with antibodies targeting TSG101 1:2000 (Abcam, ab125011) and GAPDH 1:1000 (Pierce, MA5-15738). Proteins were detected using secondary antibodies for IRDye® 800CW Donkey anti-Rabbit IgG, 0.5 mg (LI-COR Biosciences, USA, 926-32213) and IRDye® 680RD Donkey anti-Mouse IgG, 0.5 mg (LI-COR Biosciences, USA, 926-68072) with a 1:10000 dilution using the Odysee (LI-COR Biosciences, USA) infrared image system. All antibodies were diluted in 3% milk-powder dissolved in 1 x PBS with 0.1% Tween-20 (Sigma Aldrich GmbH, St Louis, MO, USA, P2287).

Supplementary References

1. Dimri GP, Lee XH, Basile G, Acosta M, Scott C, Roskelley C, Medrano EE, Linskens M, Rubelj I, Pereirasmith O, Peacocke M, Campisi J. A Biomarker That Identifies Senescent Human-Cells in Culture and in Aging Skin in-Vivo. *Proc Natl Acad Sci U S A*. 1995; 92: 9363–7.
2. Hill AF, Pegtel DM, Lambertz U, Leonardi T, Driscoll LO, Pluchino S, Ter-ovanesyan D, Hoen ENMN-. ISEV position paper: extracellular vesicle RNA analysis and bioinformatics. 2013; 1: 1–8.

Supplementary Data Set

Please browse Full Text version to find the data related to this manuscript.

Supplementary Lists in one Excel spreadsheet
2017_Terlecki_HDF_H2O2_SIPS_Supplementary_Lists.

S1 S1_customized_QPCR_panel S2_Secreted_per_cell
S3_pathway_miRNA_gene_interact
S4_EV_composition_GlobalMean S5_Intracellular
S6_Correlation_Top20 S7_details_correlation

OncomiR-17-5p: alarm signal in cancer?

OncomiR-17-5p: alarm signal in cancer?

Madhusudhan Reddy Bobbili¹, Robert M. Mader³, Johannes Grillari^{1,2,4} and Hanna Dellago^{2,5}

¹Department of Biotechnology, BOKU–University of Natural Resources and Life Sciences, Vienna, Austria

²Christian Doppler Laboratory on Biotechnology of Skin Aging, Department of Biotechnology, BOKU–University of Natural Resources and Life Sciences, Vienna, Austria

³Department of Medicine I, Comprehensive Cancer Center of the Medical University of Vienna, Vienna, Austria

⁴Evercyte GmbH, Vienna, Austria

⁵TAmiRNA GmbH, Vienna, Austria

Correspondence to: Johannes Grillari, **email:** johannes.grillari@boku.ac.at

Keywords: miRNA, miR-17-5p, biomarker, cancer

Received: March 23, 2017

Accepted: June 28, 2017

Published: July 18, 2017

Copyright: Bobbili et al. This is an open-access article distributed under the terms of the Creative Commons Attribution License 3.0 (CC BY 3.0), which permits unrestricted use, distribution, and reproduction in any medium, provided the original author and source are credited.

ABSTRACT

Soon after microRNAs entered the stage as novel regulators of gene expression, they were found to regulate -and to be regulated by- the development, progression and aggressiveness of virtually all human types of cancer. Therefore, miRNAs in general harbor a huge potential as diagnostic and prognostic markers as well as potential therapeutic targets in cancer.

The miR-17-92 cluster was found to be overexpressed in many human cancers and to promote unrestrained cell growth, and has therefore been termed onco-miR-1. In addition, its expression is often dysregulated in many other diseases. MiR-17-5p, its most prominent member, is an essential regulator of fundamental cellular processes like proliferation, autophagy and apoptosis, and its deficiency is neonatally lethal in the mouse. Many cancer types are associated with elevated miR-17-5p expression, and the degree of overexpression might correlate with cancer aggressiveness and responsiveness to chemotherapeutics – suggesting miR-17-5p to be an alarm signal. Liver, gastric or colorectal cancers are examples where miR-17-5p has been observed exclusively as an oncogene, while, in other cancer types, like breast, prostate and lung cancer, the role of miR-17-5p is not as clear-cut, and it might also act as tumor-suppressor.

However, in all cancer types studied so far, miR-17-5p has been found at elevated levels in the circulation. In this review, we therefore recapitulate the current state of knowledge about miR-17-5p in the context of cancer, and suggest that elevated miR-17-5p levels in the plasma might be a sensitive and early alarm signal for cancer ('alarmiR'), albeit not a specific alarm for a specific type of tumor.

INTRODUCTION

The role of miRNAs in human development, homeostasis and disease is by now well acknowledged. Especially in the context of cancer, a large set of studies has by now accumulated which shows the role of some miRNAs as bona fide oncomiRs. Among these, the miRNA-17-92 cluster seems of special interest as it has been the first oncomiR to be described, but one of the

cluster members, miR-17-5p, has also been found to decrease with aging and might even prolong the life span of mice upon overexpression. With this in mind, we set out to summarize the current knowledge of miR-17-5p in the context of cancer. We thereby surprisingly found that it is elevated in the serum or plasma of a large variety of solid and hematologic tumor types, which prompts us to here postulate a function of circulating miR-17-5p as an alarm signal that is sensitive for tumors in general, albeit

not specific for a defined tumor type. Such a biomarker, however, might be useful to prompt physicians to demand a thorough clinical check-up of individuals for early cancer detection.

Biogenesis and function of miRNAs

MiRNAs are a class of small non-coding silencing RNAs of approximately 22 nucleotides in length which have a significant role in regulating gene expression. miRNAs bind to complementary regions in the mRNAs of protein-coding genes and mediate translational silencing or decay of their targets. miRNAs are encoded by intergenic regions or by intronic or even exonic regions of other genes and transcribed as a long primary miRNA (pri-miRNA) and processed to precursor miRNA (pre-miRNA) in the nucleus by Drosha [1]. Then they are exported to the cytoplasm by Ran-GTP and Exportin-5 where they are processed to mature microRNA (miRNA) by the type III RNase Dicer [2, 3] (Figure 1). Members of a specific cluster can also be processed in a context-dependent manner, as explained by Cáceres JF *et al.*, where miR-18a stability is changed by hnRNP A1 (Heterogeneous Nuclear Ribonucleoprotein A1) in comparison to the other cluster members [4]. The first miRNA discovered was lin-4 in *Caenorhabditis elegans* [5] and was at first considered a nematode peculiarity. Only after discovery of let-7 and determination of its evolutionary conservation [6] was the door opened for the discovery of a whole new world of non-coding RNAs (ncRNAs) well beyond tRNAs, snRNAs or snoRNAs, comprising so far more than 2500 known mature miRNAs produced from nearly 2000 individual miRNA precursors in the human genome. Gradually, miRNAs turned out to form an entirely new layer of complexity that modulates and regulates virtually all aspects of cellular and organismal life.

miRNAs regulate gene expression of target genes post-transcriptionally by a ‘loose specificity binding’ manner. This binding depends on the “seed” region consisting of nucleotides 2–8 of the miRNA, and additional interactions with other regions of the miRNA stabilizes this interaction [7]. Thus, one miRNA is able to regulate up to 100 mRNA targets and therefore potentially orchestrates a large variety of cellular processes similar to transcription factors [8–10] and post-transcriptional operons [11]. There are two proposed models of how miRNAs target mRNAs, the standard model and the expanded model [12–15].

According to the “standard” model, miRNA and target mRNA form exact, that is, Watson–Crick base pairs absent of any bulges and wobbles in the seed region. The “expanded” model additionally allows wobble base pairing between U and G and creation of bulges either on the miRNA or the target mRNA side. Members of miR-17-92 cluster have at least two G/U bases in their seed region and therefore potentially bind to their targets according to the expanded model.

One of the best-studied set of miRNAs so far are the miR17-92 cluster members. This cluster contains 6 miRNAs with each of them having specific roles. Here in this review we focus on one of its member, miRNA-17-5p, and present current state of knowledge in the context of cancer, plasma or serum levels for specific type of tumors making it an ‘alarm signal’ for early detection of tumors.

Circulating miRNAs

Over the past decade, circulating miRNAs have emerged as promising biomarkers for a broad spectrum of age-associated diseases. In one cross-sectional study, circulating miRNA profiles were able to discriminate osteoporotic fracture patients from non-fractured individuals [16]. In the circulation miRNAs are rescued from RNase degradation either by extracellular vesicles (EVs), by RNA-binding proteins or by associating with apolipoproteins. EVs like exosomes (30–100 nm), or microvesicles (100–1000 nm) play an important role in cell-to-cell communication by carrying miRNA, proteins, metabolites etc., from the cell of origin to a target cell. EVs can be loaded with miRNA and released into circulation by mechanisms like the ceramide-dependent secretory machinery, the tetraspanin or ESCRT (endosomal sorting complexes required for transport) transport machineries. However, not all the circulatory miRNAs are loaded into EVs, as a large number of miRNAs in the circulation are associated with Ago2 (Argonaute 2) protein, one of the subunit of the RNA-induced silencing complex [17]. Alternatively, miRNAs can be associated with HDL (High-density Lipoprotein) molecules which not only transport, but also target miRNAs to their recipient [18] (Figure 1).

Transcriptional regulation and target mRNAs of miRNA-17-92 cluster and miR-17-5p

Transcriptional regulation of the miRNA-17-92 cluster

The locus of the miR-17-92 cluster is on chromosome 13 in the non-protein-coding gene MIR17HG (the miR-17-92 cluster host gene) within the open reading frame 25 (C13orf25). The miR-17-92 cluster transcript comprises six miRNAs - miR-17-5p, miR-18a, miR-19a, miR-20a, miR-19b-1 and miR-92a-1 - and is highly conserved among vertebrates [19, 20]. Expression of miR-17 as well as its seed region is strongly conserved in higher animals. In humans paralogous versions are present in the miR-106a-363 and miR-106b-25 clusters which have supposedly been formed by intra-genomic gene duplication as reviewed previously [21].

Several transcription factors are involved in miRNA-17-92 cluster transcriptional activation. One well known transcriptional factor which regulates miR-17-92 cluster is the transcription factor c-Myc, an important

proto-oncogene. C-myc is known to regulate 10–15% of genes in the human genome which are involved in a wide variety of functions like cell cycle, apoptosis, energy metabolism and macromolecular synthesis. In human cancer, c-myc mutations are most frequent [22, 23, 24]. C-myc not only activates the miR-17-92 cluster but

simultaneously also prevents the abundance of mRNA by a negative feedback loop targeting genes which are also known or predicted targets of the miR-17-92 cluster like RPS6KA5 (ribosomal protein S6 kinase, 90 kDa, polypeptide 5), BCL11B (B-cell CLL/lymphoma 11B), PTEN and HCFC2 (host cell factor C2) [25, 26].

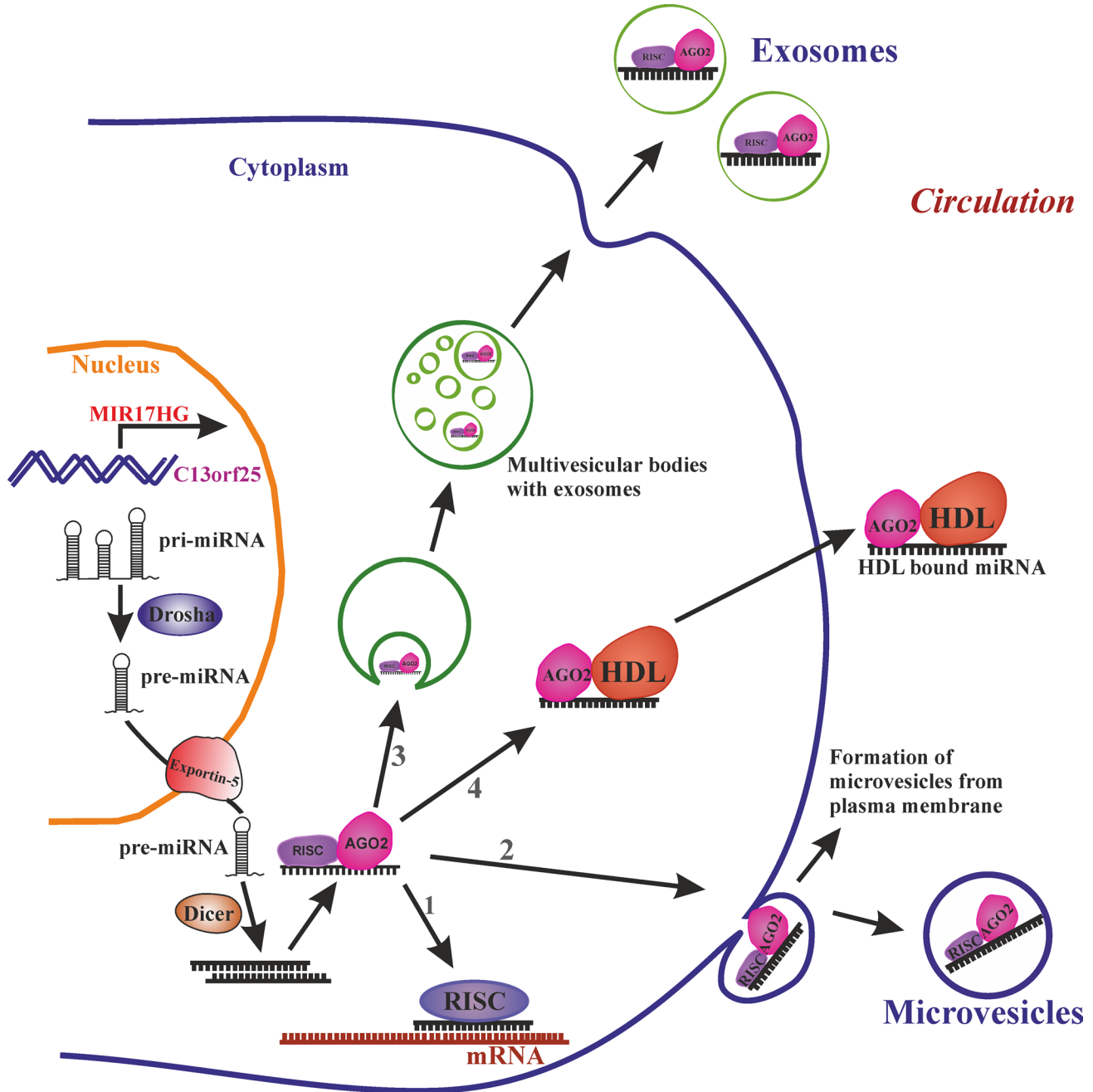


Figure 1: miRNA biogenesis and release into circulation. Transcribed primary miRNA (Pri-miRNA) processed to precursor miRNA (Pre-miRNA) in the nucleus is exported to cytoplasm by exportin-5. In the cytoplasm pre-miRNA is processed to mature miRNA by Dicer. The mature miRNA further (1) can target the mRNA in cytoplasm, or bind to RNA-binding protein Ago-2 and release to circulation via (2) loading the miRNA-Ago2 complex to microvesicles which are formed by budding of plasma membrane or (3) loaded in to smaller vesicles called exosomes which are formed by endosomal invagination, can form multivesicular bodies (MVB) and upon fusion of MVBs to plasma membrane exosomes are released into circulation or (4) miRNA-Ago2 complex can directly interact with high-density lipoproteins (HDL) and be released into circulation.

In addition, the E2F family of transcription factors like E2F1, E2F2 and E2F3 activates the genes that are involved in cell progression from G₁ to S phase and are reported to be direct targets of miR-17-92 cluster. In parallel, there is a tight regulatory loop where E2F1 and E2F3 in specific can induce the transcription of the miR-17-92 cluster. Aurora kinase A (AURKA), a serine/threonine kinase is overexpressed in many cancer types. AURKA is a known upstream regulator of E2F1 by inhibiting its proteosomal degradation, thus promoting expression of the miR-17-92 cluster [27]. miR-17-5p and miR-20a in turn negatively regulate E2F1 expression [28].

In contrast, p53 acts as negative regulator of miR-17-92 cluster transcription. Under hypoxic conditions p53 represses transcription of the miR-17-92 cluster promoting hypoxia induced apoptosis [29]. In addition, the ENCODE (Encyclopedia of DNA Elements) project revealed additional transcriptional factors like BCL3 (B-cell CLL/lymphoma 3), IRF1 (Interferon Regulatory Factor 1), SP1 (Sp1 transcription factor), TAL1 (T-cell acute lymphocytic leukemia 1) and ZBTB33 (zinc finger and BTB domain containing 33) regulating the miR-17-92 cluster [30] (also reviewed by Mogilyansky & Rigoutsos [31] and Dellago *et al.* [21]).

In terms of ubiquitous transcription of miR-17-5p, it was found to be expressed in all 40 different normal human tissues tested including brain, muscle, circulatory, respiratory, lymphoid, gastrointestinal, urinary, reproductive and endocrine systems [32]. High level of expression was observed in thymus and lowest in PBMCs (peripheral blood mononuclear cells). Expression of miR-17-3p is approximately half of the level of miR-17-5p except for PBMCs, where expression was below detection limits [32]. MicroRNA expression and sequence analysis database (mESAdb) [33], which integrates data from several databases like e.g. the one by Basekerville and Bartel [34] substantiates these findings and emphasize the importance of miR-17-5p in all tissues.

Targets of miR-17-92 cluster and miR-17-5p

Experimentally confirmed targets of the miR-17-92 cluster are PTEN and E2Fs in the context of cell cycle progression and apoptosis [35]. Various studies report a wide range of targets of the miR-17-92 cluster like members of the TGF β (transforming growth factor- β) signaling pathway [36], BCL2L11 (BCL2 Like 11), IRF1, JAK2 (Janus Kinase 2), PKD1 (Polycystin 1, Transient Receptor Potential Channel Interacting), PKD2 (Polycystin 2, Transient Receptor Potential Cation Channel), RBL1 (RB Transcriptional Corepressor Like 1), and STAT3 [37–40]. Heinrich Kovar *et al.* elucidated the targets of miR-17-92 cluster in Ewing sarcoma and found CTGF (Connective Tissue Growth Factor), FOSL2 (FOS Like 2, AP-1 Transcription Factor Subunit), GBP3 (Guanylate Binding Protein 3) and SERPINE1 (Serpin Family E

Member 1) are effectively targeted by cluster [41]. It was reported by Felsher *et al.* that miR-17-92 cluster can target specific chromatin regulatory genes, such as Sin3b (SIN3 transcription regulator family member B; a transcriptional repressor for MYC-responsive genes), Hbp1, Suv420h1 (suppressor of variegation 4–20 homolog 1; a histone methyltransferase, targeted to histone H3 by retinoblastoma proteins), and Btg1 (B-cell translocation gene 1, anti-proliferative; a regulator of cell growth and differentiation) [42], as well as the apoptosis regulator Bim (Bcl-2 interacting mediator of cell death; an activator of neuronal and lymphocyte apoptosis) [42–44]. miR-17-92 cluster seems to target the genes involved in maintenance of cell proliferation and survival. We summarize confirmed targets of miR-17-5p by luciferase reporter assay in Table 1.

miR-17-5p: a link between proliferation, cancer and aging

miR-17-5p plays a different role in cancer and aging. Aging is a well known risk factor for many types of cancer prognosis. Inhibition of mTOR (mammalian target of rapamycin) slows aging and postpones age-related diseases like diabetes, cancer and cardiovascular diseases and widely accepted aging model [45] by activating autophagy. Autophagy helps in clearance of unnecessary molecules or organelles and nutrient provision by degradation of intracellular pathogens where autophagic potential was lost in normal and premature aging [46]. During the process of aging, autophagy maintains cellular function by removing protein aggregates and allowing degradation of aged cellular components [45]. Two regulatory loops exist where mTOR is inhibited in autophagy. On the one hand, miR-17-5p inhibits mTOR by inducing MKP7 (Mitogen-Activated Protein Kinase Phosphatase 7) via targeting ADCY5 (Adenylate Cyclase 5): Upon dephosphorylation of mTOR by MKP7, mTOR dimerizes with PRAS40 (40-kDa proline-rich AKT substrate) and gets inhibited [21, 47]. On the other hand miR-17-5p targets IRS1 thus activating AMPK (AMP-activated protein kinase) which stops phosphorylation of ULK1 (Unc-51 like autophagy activating kinase 1) by mTOR and promotes formation of ULK1-ATG13-FIP200 (ATG13, autophagy related 13; FIP200, focal adhesion kinase family kinase-interacting protein of 200 kDa) complex required for the initiation of autophagy, a major complex involved in the formation of autophagosome [21].

In many types of cancer deregulation of mTOR is observed, which is a central regulator of cell proliferation. mTOR inhibitors like Rapamycin and its analogs are widely used as potential anti-tumour agents, some already approved for clinical use in cancer therapy. mTOR plays an important role in cell physiology and tissue maintenance, and use of its inhibitors like rapamycin leads to up-regulation of the miR-17-92 cluster and down-

Table 1: Validated gene targets of miR-17 and pathways affected by their regulation in cancers

Pathology	Process	Pathways affected	Targets of miR-17	References
Aging	Autophagy	MKP7/mTOR pathway	ADCY5	[47]
Organ aging	Autophagy	FoxO3a and LC3B pathways	IRS-1	[47]
	Heart failure	Matrix remodelling	TIMP1, TIMP2	[126]
	Cardiac aging	Par4/CEBPB/FAK signalling	Par-4	[127]
Prostate cancer	Tumor suppressor	antioxidant pathway in mitochondria	MnSOD, Gpx2, TrxR2	[118]
	Cell proliferation and invasion (Metastasis)	Matrix Metallopeptidase regulation	TIMP3	[117]
Hepatocellular carcinoma	Cell proliferation and migration (Metastasis)	PI3K pathway, glycosylation	PTEN, GalNT7, vimentin	[28, 63]
	Cell proliferation and migration (Metastasis)	p38-HSP27 signalling	E2F1	[63]
Breast cancer	Cell migration and invasion	Wnt/ β -catenin pathway	HBP1	[67]
	Tumor suppressor (growth arrest)	IGF-1/AIB1 pathway	AIB1, E2F1	[68]
	Tumor suppressor	Translation initiation	PDCD4	[70]
	Tumor suppressor	Cell cycle	CCND1	[71]
	Tumor suppressor	PI3K pathway	PTEN	[70]
Lung cancer	Apoptosis	Initiation of autophagy	Beclin-1	[80]
Gastric cancer	Inhibition of apoptosis	cell proliferation	TP53INP1, P21	[86]
	Cell proliferation and migration	TGF β	TGFBR2	[88]
	Cell proliferation	Cytokine mediated signalling	SOCS6	[87]
Colorectal cancer	Cell proliferation and invasion (Metastasis)	GABBR1 signalling	GABBR1	[98]
	Cell cycle progression	Cytoskeletal organization	RND3	[97]
Osteosarcoma	Cell proliferation and differentiation	Wnt/ β -catenin pathway	SMAD7	[105]
	Cell migration and invasion	Akt pathway	BRCC2	[106]
Leukaemia	Cell differentiation	Cytokine mediated signaling: JAK-STAT pathway	STAT3	[111]

Abbreviations: ADCY5, Adenylate Cyclase 5; AIB1, Amplified in breast cancer 1; BRCC2, Breast Cancer Cell Protein 2; CCND1, Cyclin D1; E2F1, E2F Transcription Factor 1; CEBPB, CCAAT/Enhancer Binding Protein Beta; FAK, Focal Adhesion Kinase; FOXO3a, Forkhead Box O3; GABBR1, Gamma-Aminobutyric Acid Type B Receptor Subunit 1; GalNT7, Polypeptide N-Acetylgalactosaminyltransferase 7; GPX2, Glutathione Peroxidase 2; HBP1, HMG-Box Transcription Factor 1; HSP27, Heat Shock 27kD Protein 1; IGF-1, Insulin Like Growth Factor 1; IRS1, Insulin Receptor Substrate 1; LC3B, Microtubule Associated Protein 1 Light Chain 3 Beta; MKP7, Mitogen-Activated Protein Kinase Phosphatase 7; MnSOD, Mitochondrial Superoxide Dismutase 2; mTOR, Mechanistic Target Of Rapamycin; PAR4, Prostate Apoptosis Response 4 Protein; PDCD4, Programmed Cell Death 4; PI3K, Phosphatidylinositol-4,5-Bisphosphate 3-Kinase; PTEN, Phosphatase And Tensin Homolog; RND3, Rho Family GTPase 3; SOCS6, Suppressor Of Cytokine Signaling 6; SMAD7, SMAD Family Member 7; STAT3, Signal Transducer And Activator Of Transcription 3; TGFBR2, Transforming growth factor- β receptor 2; TIMP1, TIMP Metallopeptidase Inhibitor 1; TIMP2, TIMP Metallopeptidase Inhibitor 2; TIMP3, TIMP Metallopeptidase Inhibitor 3; TP53INP1, Tumor Protein P53 Inducible Nuclear Protein 1; TXNRD2, Thioredoxin Reductase 2.

regulation of tumor suppressors [48]. Inhibitors of miR-17 could potentially serve as adjuvants in chemotherapy as oncogenic miRNAs like miR-17 are upregulated

in rapamycin-resistant cells and inhibition of miR-17 restored rapamycin sensitivity. For details on miR-17-5p's role in aging, please refer to a recent review [21].

miR-17-5p and its role in cancer

Evidence from many different tumors support the idea that miR-17-5p is an oncogene, even though its other cluster member, miR-18a is considered the most oncogenic [49]. Large-scale miRnome analysis on 540 samples including lung, breast, stomach, prostate, colon and pancreatic tumors identified miR-17-5p as upregulated in all solid tumors [50]. Its overexpression in hamster derived tumor cells also increases proliferation and protein production [51]. Due to the oncogenic properties of the miR-17-92 cluster, its members were also considered to be oncogenic. By now a more differentiated view has emerged, as miR-17-5p alone, by stimulating T cells can suppress cancer growth [52], while still able to drive hepatocellular carcinoma in a transgenic mouse model. In addition, it seems to have metastasis suppressor functions as well, at least by suppressing epithelial-to-mesenchymal-transition (EMT) and increasing tissue adherence and thus potentially inhibiting metastatic spreading of basal-like breast tumor cells [53]. On the other hand overexpression of miR-17 promotes the cancer cell migration by reducing cell adhesion and promoting cell detachment in immortalized rat prostate endothelial cells [54]. It was found that patients suffering from several different types of cancer have high circulating miR-17-5p levels in serum [55, 56], implying that increased serum levels of miR-17-5p could be an alarm signal for different types of cancers. Hence oncomiR-17-5p might be termed ‘alarmiR’.

The effect of miR-17-5p is highly dependent on many factors like type of cancer, model systems used and constructs used in model systems for knockdown or overexpression, as well as on the relative expression levels of miR-17-3p and miR-17-5p which was discussed in few cancer types where miR-17-3p did have synergistic or rescue effect. While we here focus on the role of the single miR-17-5p in formation and progression of distinct cancer types, Xiang and Wu [57] have reviewed the tumor-suppressive and tumorigenic properties of the miR-17-92 cluster as a whole.

Hepatocellular carcinoma

Emerging evidence indicates that the miR-17-92 cluster and specifically miR-17-5p play an important role in carcinogenesis in the liver.

A liver-specific miR-17-92 transgenic mouse showed significantly increased hepatocellular cancer development. These results were complemented by overexpression of the miR-17-92 cluster in cultured human hepatocellular cancer cells, which enhanced proliferation, colony formation and invasiveness *in vitro*, whereas inhibition of the miR-17-92 cluster had the opposite effect [58].

MiR-17 might be largely responsible for the effect of the cluster, since overexpression of pre-miR-17 in

a transgenic mouse model results in hepatocellular carcinoma (HCC). In addition, both miR-17-5p and miR-17-3p are abundantly processed from precursor miR-17 and have synergetic effects on developing HCC by binding different targets on different signaling pathways: miR-17-5p targets PTEN, one of the most frequently lost tumor suppressor in human cancers, while miR-17-3p represses expression of vimentin, an intermediate filament with the ability to modulate metabolism, and GalNT7, an enzyme that regulates metabolism of liver toxin galactosamine. These three proteins work in separate signaling pathways, but independently contribute to regulating proliferation and migration [59]. Thereby, miR-17-5p also targets the long non-coding RNA PTENP1, a pseudogene of PTEN. When overexpressed, PTENP1 sequesters miR-17, which would otherwise target PTEN and the negative Akt-regulator PHLPP (PH Domain And Leucine Rich Repeat Protein Phosphatase). Hence PTENP1 functions as miR-17 antagonist, representing an appealing approach for HCC treatment based on miR-17 function in tumorigenesis [60].

MiRNA-17-5p expression is highly elevated in patient-derived HCC tissues, especially in metastasis derived tissues when compared to controls [61]. This correlates with the observation that serum levels of circulating miR-17-5p were upregulated in a relapse group of patients and downregulated in the post-operative group. In addition, serum levels of miR-17-5p were associated with metastasis status and staging, suggesting that the miRNA in the serum indeed is tumor cell derived [62].

HCC cell lines overexpressing miR-17-5p injected either subcutaneously or into the livers of nude mice generating an orthotopic intrahepatic tumor model, miR-17-5p supported tumor growth and intrahepatic metastasis [63]. This was due to activating the p38 MAPK-HSP27 pathway by directly targeting the transcription factor E2F1, a transcriptional regulator of Wip1, which dephosphorylates and thus deactivates p38 (Figure 2). The p38 MAPK-HSP27 pathway mediates miR-17-5p's effect on migration, but, however, is not involved in its effect on proliferation.

Summarized, miR-17-5p possesses oncogenic activity in the context of hepatocellular carcinoma.

Breast cancer

Cumulative data clearly point to a role of miR-17-5p in the development and progression of breast cancer, and is currently being explored as biomarker for diagnosis, prognosis and therapeutic target.

qPCR-based miRNA expression profiling revealed that miR-17-5p, miR-18a-5p and miR-20a-5p exhibit enhanced expression in tissue samples derived from triple-negative as compared to luminal A breast tumors, which are less aggressive and have much better prognosis as well as lower recurrence rate [64]. In addition, Lehmann and co-workers studied miR-17 -among other miRNAs-

as potential molecular marker to evaluate grade, receptor status and molecular type in breast cancer. Six miRNAs and five mRNAs were analyzed pairwise and examined for a possible correlation with histological breast cancer groups. The miR17/miR27b pair best discriminated samples with different tumour grades, but others correlated better with lymph node status, tumor size and oestrogen/progesterone receptor status, so that multiple marker pairs are required to characterize a tumor sample [65].

For a comprehensive review on the use of miRNAs as biomarkers for prognosis, diagnosis, therapeutic

prediction and therapeutic tool in breast cancer, please refer to Bertoli *et al.* [66], who also discuss the potential of miR-17-5p as potential diagnostic biomarker.

Even though correlating miR-17-5p expression levels with various tumor properties might be very useful in the development of biomarkers, it does not give evidence about its tumorigenic or tumour-suppressive potential. After all, elevated miR-17-5p expression could either contribute to tumor formation and progression, or could represent a defense mechanism that is intended to limit carcinogenesis. So, far there exists evidence for both explanatory approaches.

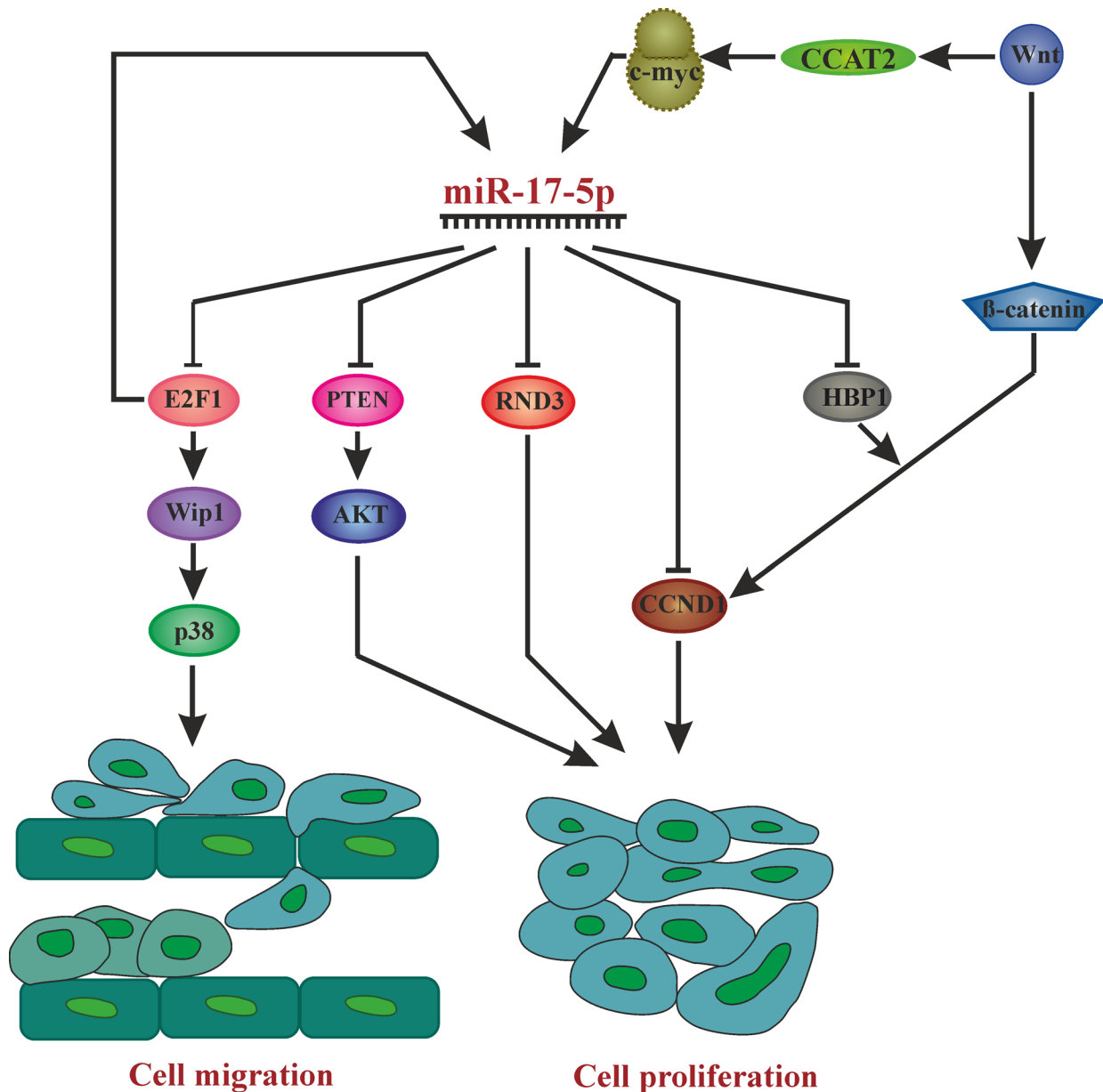


Figure 2: Overview of pathways affected by miR-17-5p in different cancer phenotypes leading to cell proliferation and migration. AKT: Proto-oncogene c-Akt, c-myc: V-Myc Avian Myelocytomatosis Viral Oncogene Homolog, CCAT2: Colon Cancer Associated Transcript 2, E2F1: E2F transcription factor 1, CCND1: Cyclin D1, HBP1: HMG-Box Transcription Factor 1, P38: Mitogen-Activated Protein Kinase 14, PTEN: Phosphatase And Tensin Homolog, RND3: Rho Family GTPase 3, Wnt: wingless-type MMTV integration site family, Wip1: Protein Phosphatase, Mg²⁺/Mn²⁺ Dependent 1D.

According to Li *et al.* [67], miR-17-5p promotes human breast cancer cell migration and invasion through suppression of HMG box-containing protein 1 (HBP1), which they confirmed as a direct target of miR-17-5p. HBP1 is a component of the Wnt/ β -catenin signaling pathway, which is frequently mutated in various cancer types (Figure 2). They found that miR-17-5p was highly expressed in strongly invasive, but not in weakly invasive BC cells, and that miR-17-5p overexpression enhanced migratory and invasive abilities of BC cells, while its downregulation had the opposite effect. Apart from promoting breast cancer cell migration and invasion by miR-17-5p, Liao XH *et al.* showed that miR-17-5p also promotes cell proliferation by down-regulating p21 which is a direct target of miR-17-5p in ER α (Estrogen receptor α)-positive breast cancer cells. ER α plays an important role in cell-cycle progression by promoting the expression of PCNA and Ki-67 along with miR-17-5p. Downregulation of p21 by miR-17-5p in turn promotes PCNA (proliferating cell nuclear antigen) activity, where p21 is a negative regulator of PCNA and thus ER α promotes breast cancer cell cycle progression and proliferation in p21/PCNA/E2F1-dependent pathway [68].

In contrast, miR-17-5p was described as tumor suppressor [69]. Downregulation of AIB1 (“Amplified in breast cancer 1”) by miR-17-5p decreased proliferation and abrogated insulin-like growth factor 1-mediated, anchorage-independent growth of breast cancer cells. A recent study from Liao XH *et al.* also established that miR-17-5p acts as a tumor suppressor by directly targeting STAT3 and inducing apoptosis in breast cancer cells by inhibiting STAT3/p53 pathway [70]. This shows how miR-17-5p tightly regulates the genes involved in cell proliferation and cell apoptosis.

Similarly, miR17-5p was identified as metastatic suppressor of basal-like breast cancer [53]. Out of 4000 genes linked to BC progression, miR-17-5p was confirmed *in vitro* and *in vivo* as regulator of multiple pro-metastatic genes, hence had an anti-metastatic effect, while miR-17-5p inhibition in BC cells enhanced expression of pro-metastatic genes and accelerated lung metastasis from orthotopic xenografts. Therefore, the authors suggest miR-17-5p as a potential therapeutic target for treatment of basal-like breast cancer.

The therapeutic potential of miR-17-5p inhibition in triple negative BC (TNBC), one of the most aggressive breast cancer forms, was also assessed as a therapeutic target [71]. Assuming that miR-17-5p inhibition would restore protein expression of tumor suppressive miR-17-5p targets Programmed cell death 4 (PDCD4) and Phosphatase and tensin homolog (PTEN), human TNBC cells were transfected with antisense oligonucleotides against miR-17-5p. The results showed that miR-17-3p seems to act as a back-up mechanism of miR-17-5p for these targets, and therefore, due to the high sequence homology between the antisense

molecules and miR-17-3p, as well as to excess binding sites for miR-17-3p on the 3'UTR of PDCD4 and PTEN mRNAs, the antisense oligo acted as a miR-17-3p mimic and reduced PDCD4 and PTEN expression instead of restoring it.

In support of miR-17-5p's tumor-suppressive role, recent bioinformatics and *in vitro* analysis revealed that levels of miR-17-5p are decreased in triple negative breast cancer cells resulting increase in CCND1 (cyclin D1) levels which is reason for uncontrolled proliferation. Expression of CCND1 was inhibited by overexpression of miR-17-5p [72]. Circulatory/serum miR-17-5p levels are deregulated which also reflects the differential biology of breast cancer subtypes [73]. Hence it even acts as a biomarker even to predict the stage of cancer.

Summarized, the tumorigenic or tumor-suppressive functions of miR-17-5p might depend on the cellular context, that is, on the model system used, cell type, cancer stage and many other factors, like for example “BRCAness”. De Summa *et al.* [74] show that overexpression of miR-17 in both mesenchymal-like BRCA1-proficient and in BRCA1- and BRCA2-mutated BC cell lines in addition to the significant overexpression of miR-17 in sporadic patients seems to suggest that downregulation of BRCA1, a presumed target of miR-17-5p mimics a ‘BRCAness’ phenotype, that is, a phenotype that some sporadic cancers share with BRCA1- or BRCA2-mutation carriers. Hence, miR17 might represent a biomarkers of ‘BRCAness’ phenotype, indicating which patients who could most benefit from PARP inhibitor therapies.

Lung cancer

Several studies have investigated the relationship between miR-17-5p and lung cancer, mainly in view to its potential clinical application of miRNA expression profiles as diagnostic and prognostic marker.

For example, elevated miR-17-5p expression levels are present in tumor tissue and serum of lung cancer patients—including adenocarcinoma, squamous cell and adenosquamous carcinoma- compared to healthy controls. In addition, serum miR-17-5p levels were inversely related to the survival of patients with lung cancer, that is, high levels correlated with shorter survival times [75].

This is in contrast to studies that found miR-17 (no distinction between 5p and 3p) downregulated in lung adenocarcinoma initiating cells [76] and in non-small cell lung cancer (NSCLC). It should be mentioned though, that although miR-17-5p expression levels allowed distinction between NSCLC and healthy control, it was not useful as diagnostic marker for discriminating between NSCLC and chronic obstructive pulmonary disease (COPD) [77].

Other studies concluded that miR-17-5p expression levels did not have sufficient informative values to serve as diagnostic tool, at least using sputum miRNA profiling [78]. This study confirms previous results of the same

group [79], where miR-17-5p was not found either over- or under-expressed in human lung cancer.

In addition to exploring its diagnostic potential, miR-17-5p might also serve as therapeutic target in lung cancer treatment. According to Matsubara *et al.* [80], inhibition of miR-17-5p and miR-20a with antisense oligonucleotides (ONs) can induce apoptosis selectively in lung cancer cells overexpressing miR-17-92, suggesting the possibility of targeting an 'oncomiR addiction' to expression of these miRNAs in a subset of lung cancers. In marked contrast, antisense oligonucleotides against miR-18a, miR-19a or miR-92-1 led to no or slight inhibition of cell growth, indicating that single miRNAs of the miR-17-92 cluster have distinct roles on cancer formation and progression.

On the other hand, downregulation of miR-17-5p upregulates its target, the autophagy regulator beclin-1, which leads to apoptosis resistance of cancer cells upon paclitaxel treatment [81]. This is in accordance with the notion that miR-17-5p overexpression reduces cytoprotective autophagy by targeting Beclin-1 in paclitaxel resistant lung cancer cells [82]. To justify miR-17-5p acts as tumor suppressor, a study shows that low expression levels of miR-17 results in cisplatin resistance of NSCLC by high expression of CDKN1A (cyclin-dependent kinase inhibitor 1A) and RAD21 (Rad21 homolog (*Schizosaccharomyces pombe*)) [83]. Hence miR-17-5p plays a tumor suppressor role in this setting.

Thus, miR-17-5p can either promote or curb apoptosis of lung cancer cells. Again, the final effect of miR-17-5p seems to be highly context-dependent.

Gastric cancer

Circulating miR-17-5p was found to be significantly elevated in the serum of patients with gastric cancer compared to healthy controls, and correlates with circulating tumor cells [84, 85]. However, a follow-up study failed to assign a prognostic value to miR-17-5p plasma levels, since there was a slight, but not significant difference in the survival rates of patient groups exhibiting low or high miR-17-5p plasma levels, although the trend might turn significant when based on larger sample size ($n = 31$ vs. 38) [86]. This assumption has been verified by Wang *et al.* [55], they not only found that concentrations of miR-17-5p/20a were significantly associated with the differentiation status and tumor progression, but also revealed that high expression levels of miR-17-5p/20a were significantly correlated with poor overall survival. In addition, therapeutic potential for antagomirs against miR-17-5p/20a was suggested, which was applied as chemotherapeutics in a mouse tumor model. Indeed, levels of serum miR-17-5p/20a were notably reduced in post-treated mice with tumor volume regression.

A follow-up study from the same group investigated the cellular mechanisms involving miR-17-5p in gastric

cancer and found that miR-17-5p/20a promote gastric cancer by directly targeting the tumor suppressors p21 and p53-induced nuclear protein 1 (TP53INP1), which results in unrestrained proliferation and apoptosis inhibition, respectively, and involve a positive regulatory circuit between miR-17-5p/20a and MDM2 (murine double minute 2). Their findings in gastric cancer cells were backed-up by administering antagomiRs against miR-17-5p/20a to reduce tumor formation in a xenograft mouse model [87].

Likewise, miR-17-5p increased the proliferation and growth of gastric cancer cells *in vitro* and *in vivo*, by targeting SOCS6, a cytokine-induced STAT inhibitor [88]. Another study shows that high levels of miR-17-5p decreased expression of its direct target TGFBR2 (transforming growth factor- β receptor 2), further promoting gastric cancer cell proliferation and migration [89]. Supporting the above studies, a clinical study states that serum levels of miR-17 from patients with gastric cancer are high compared to healthy individuals [90].

As mentioned in section 3.1, AURKA activates transcription of miR-17-92 by stabilizing the transcription factor E2F1. AURKA inhibitors are currently applied in clinical trials for treatment of gastrointestinal cancer [27], and since miR-17-92 represents one branch of AURKA-dependent oncogenic signaling, also direct inhibitors of miR-17-92 members might serve as potential targets in gastric and other types of cancer, but before that, more research on specific functions of single miR-17-92 members is required.

In summary, in the context of gastric cancer, miR-17-5p clearly acts as oncogene and targets the components of many pathways involved in cell proliferation and migration.

Colorectal cancer

Among all the miRNAs of the miR-17-92 cluster, miR-17-5p showed highest expression in epithelial colon cells and expression levels increased in the transitional zone from normal to adenoma to adenocarcinoma (N-A-AC), suggesting a role in sequential evolution of early colon cancer [91].

Several studies confirm miR-17-5p overexpression in CRC (colorectal cancer) tissue samples [92, 93, 94]. Elevated miR-17-5p expression is also observed in early embryonic colon epithelium, and is sustained only in the proliferative crypt progenitor compartment. Downregulation of E2F1 by miR-17-5p is of importance for proliferation both during embryonic colon development and colon carcinogenesis [95].

What causes miR-17-5p overexpression leading up to CRC pathogenesis and by what targets does it regulate proliferation? The long noncoding RNA CCAT2, a WNT downstream target, induces miR-17-5p and MYC through TCF7L2 (Transcription Factor 7 Like 2) -mediated

transcriptional regulation (Figure 2) [96]. Accordingly, miR-17-5p targets P130 (Retinoblastoma-Like 2, a presumed tumor suppressor, present in a complex that represses cell cycle-dependent genes) and subsequently activates the WNT/ β -catenin pathway [97]. Hence, there exists a positive WNT signaling feedback loop involving miR-17-5p.

In addition, miR-17-5p directly targets RND3, a Rho Family GTPase that acts as tumor suppressor by promoting adhesion [98]. MiR-17 along with miR-106a/b and miR-20a/b targets GABBR1 (gamma-amino-butyric acid type B receptor 1) thus promoting colorectal cancer cell proliferation and invasion [99].

What prognostic and therapeutic implications can be derived from miR-17-5p expression data? miR-17-5p expression levels might be used as predictive factor for chemotherapy response and a prognostic factor for overall survival in CRC, since patients with high miR-17-5p expression in tumor tissue have shorter overall survival rates [97, 100] and respond better to adjuvant chemotherapy than patients with low miRNA expression [97]. On the other hand, chemotherapy was found to further increase the expression levels of miR-17-5p in CRC cells *in vitro*, thereby repressing the pro-apoptotic factor PTEN and promoting chemoresistance [101]. A very similar observation was made in another tumor entity, pancreatic cancer, where an overexpressed nerve growth factor receptor (GFR α 2) led to PTEN inactivation mediated by induction of miR-17-5p [102]. Downregulation of miR-17-5p by curcumin and its synthetic analogs inhibits CRC cell proliferation and induces apoptosis, and could provide the basis for future therapeutic approaches [103]. Supporting *in vitro* and tissue level high expression of miR-17-5p, a clinical study proves serum levels of miR-17 along with miR-19a, miR-20a and miR-223 were significantly upregulated in CRC patients compared to controls [104].

Briefly, miR-17-5p plays a key role in colorectal cancer pathogenesis and progression. Henceforth miR-17-5p could be used as a diagnostic biomarker for colorectal cancer.

Osteosarcoma

Expression of miR-17-5p is also high in osteosarcoma, whereby PTEN seems to be an important target contributing to progression and metastasis [105]. This seems in keeping with its role in osteoblastogenesis [106]. In addition to PTEN, SMAD7 and thus Wnt signalling is a direct target for miR-17-5p in this context. By targeting SMAD7, miR-17-5p promotes nuclear translocation of β -catenin, enhances expression of COL1A1 (Collagen Type I Alpha 1 Chain) and finally facilitates the proliferation and differentiation of femoral head mesenchymal stem (HMS) cells promoting osteonecrosis [106].

A very recent article explores the effects of miR-17-5p in osteosarcoma tumorigenesis and development. MiR-17-5p expression levels were associated with clinical stage, positive distant metastasis and poor response to neo-adjuvant chemotherapy. The tumor suppressor BRCC2, which is thought to induce apoptosis in a caspase-dependent manner, is a direct target of miR-17-5p [107]. Hence, miR-17-5p may be used as diagnostic and prognostic marker, but also as a potential target for molecular therapy of osteosarcoma.

Thus, in the context of the bone, miR-17-5p seems to have tumorigenic activity.

Leukemia

Not only in solid tumors, but also in tumors of hematopoietic origin miR-17-5p is upregulated, like in both acute myeloid leukemia (AML) and chronic myeloid leukemia (CML). Expression profiling of acute myeloid leukemia (AML) identified a set of seven miRNAs comprising miR-17-5p that allows discrimination of three common AML-causing chromosomal translocations with a diagnostic accuracy of > 94%, and is significantly overexpressed in MLL (mixed lineage leukemia) rearrangements, which causes particularly aggressive leukemia with poor prognosis [108].

A study in multiple myeloma (MM) patients showed that high levels of miR-17-5p, miR-20a and miR-92-1 of miR-17-92 cluster are associated with shorter progression-free survival, suggesting poor prognosis [109]. Most interestingly, upon resistance to therapy of multiple myeloma with bortezomib, the exosomal transfer of several microRNAs seems to be altered, among them miR-17-5p, which was significantly reduced [110]. High levels of miR-17-5p, which further downregulate CDKN1A (Cyclin Dependent Kinase Inhibitor 1A), p21 and E2F1 tumor suppressor genes in imatinib sensitive and resistant chronic myeloid leukemia (CML) cells compared to peripheral blood mononuclear cells (PBMCs), have also been observed [111]. Hypoxia was suggested to induce differentiation of AML cells by mechanisms independent of transcription. Indeed, this was shown to happen via inhibition of miR-17-5p. HIF-1 α (Hypoxia Inducible Factor 1 Alpha Subunit) downregulates the expressions of miR-17-5p and miR-20a through a mechanism that is dependent of c-Myc but independent of its transcription partner HIF-1 β . As p21 and STAT 3 are direct targets of miR-17-5p and miR-20a, downregulation of miR-17-5p and miR-20a induces myeloid differentiation and growth arrest in AML cells *in vitro* and *in vivo* [112]. This further supports that upregulation of miR-17-5p is at least associated to myeloid leukemia.

In lymphocytic leukemia, the available data is more ambiguous. According to Zanette *et al.* [113], the miR-17-92 cluster was upregulated in acute lymphocytic leukemia (ALL), but no cluster member was among the most highly expressed miRNAs in chronic lymphocytic leukemia

(CLL). However, miR-17-5p was found downregulated in chronic lymphocytic leukemia both with normal p53 and with mutated/deleted p53, but downregulation was more pronounced in the latter patient group [114, 115]. Nonetheless, results derived from a SCID mouse model suggests the suitability of miR-17 as a therapeutic target for CLL treatment. This is due to results showing that antagomiR-17 strongly reduced tumor growth and increased survival when injected *in vivo* in tumors generated by MEC-1 cell injection into SCID mice [116]. How these contradictory findings could be reconciled is subject to further research. A comprehensive review discusses the roles of miRNAs in B-cell lymphoma with much emphasis on the miR-17-92 cluster [117].

Prostate cancer

Conflicting results on tumor suppressor versus promoter function exist for prostate cancer (PC): Both mature miR-17-5p and passenger strand miR-17-3p target TIMP3 which has synergetic effect on enhancing prostate tumor growth and invasion [118]. However, high levels of miR-17-3p have also been reported to suppress tumorigenicity of PC cells through inhibition of mitochondrial antioxidant enzymes [119]. This effect seems mediated by p300/CBP-associated factor (PCAF) as a target of miR-17-5p modulating the androgen receptor transcriptional activity [120]. Androgen receptor (AR) signaling is critical for most aspects of prostate growth and tumorigenesis [120]. A potential anti-prostate cancer drug, glucosinolate-derived phenethyl isothiocyanate (PEITC), results in miR-17-5p-mediated suppression of PCAF and again AR-regulated transcriptional activity and cell growth of prostate cancer cells, suggesting a new mechanism by which PEITC modulates prostate cancer cell growth [121].

Resveratrol and Pterostilbene decrease the levels of endogenous as well as exogenously expressed miR-17, miR-20a and miR-106b thereby upregulating their target PTEN [122] and eventually leading to reduced tumor growth *in vivo*. According to a recent report, circulating exosomes from prostate cancer cells carry long non-coding RNAs which are themselves enriched with miRNA seed regions that can bind to let-7 and miR-17 families like a miRNA sponge [123]. This indicates that they are part of tumorigenic pathways and might find use as a therapeutic target and biomarker also in the context of prostate cancer.

In cancers like glioblastomas, under stress conditions miR-17 plays a dual role depending on the conditions. It acts as a tumor suppressor in normal growth conditions by inhibiting PTEN through miR-17-5p and at unfavorable conditions miR-17-3p promotes tumor cell survival by inhibiting MDM2 [124]. These results state that miR-17-3p also plays an important role in different cancers either in synergetic way or as rescue for miR-17-5p. Further studies on miR-17-3p are required to establish a firm regulation between miR-17-5p and miR-17-3p.

CONCLUSIONS

The role of miR-17-5p as an oncomiR is supported by many studies, while also the opposite, a tumor suppressive role has been found in some studies. Therefore, its role seems to be cell type and tumor type dependent and more work in specific settings will be necessary to dissect all of its roles in oncology. In Figure 2, we summarize the pathways effected by miR-17-5p in different cancer types.

In the context of biomarkers, miRNAs are considered as promising emerging biomarkers in cancer, especially when considering circulating miRNAs as minimally invasive analytes within liquid biopsies [16]. We here have summarized studies that indicate that elevated levels of miR-17-5p might be an alarm signal for cancer, that might be sensitive, albeit not specific for a single type of cancer. Still, circulating miRNAs as biomarkers or alarmiRs still lack sufficient studies to be able to define the range of inter-individual variation in the general healthy population and consequently define thresholds for e.g. miR-17-5p in serum or plasma that would lead to the decision of careful follow up clinical testing for the presence of a tumor. Still, tissue based miRNA signatures have already reached the markets of diagnostics in cancer, e.g. Rosetta Genomics [125, 126] for determination of the primary tumor origin of metastasis, emphasizing that also circulating miRNAs might soon lead to biomarker signatures that can support clinical decisions.

ACKNOWLEDGMENTS AND FUNDING

This work was funded by the BioToP – ‘Biomolecular technology of proteins’ PhD Programme, Austrian Science Funds (FWF) Project W1224, and the Christian Doppler Society. The financial support by the Austrian Federal Ministry of Economy, Family and Youth, the National Foundation for Research, Technology and Development as well as the FP7 EU projects Frailomic and Sybil are also gratefully acknowledged.

CONFLICTS OF INTEREST

J.G. is a co-founder of Evercyte GmbH and TAmiRNA GmbH, HD is an employee of TAmiRNA GmbH.

REFERENCES

1. Lee Y, Ahn C, Han J, Choi H, Kim J, Yim J, Lee J, Provost P, Rådmark O, Kim S, Kim VN. The nuclear RNase III Drosha initiates microRNA processing. *Nature*. 2003; 425:415–9. <https://doi.org/10.1038/nature01957>.
2. Lund E, Güttinger S, Calado A, Dahlberg JE, Kutay U. Nuclear export of microRNA precursors. *Science*. 2004; 303:95–8. <https://doi.org/10.1126/science.1090599>.
3. Yi R, Qin Y, Macara IG, Cullen BR. Exportin-5 mediates the nuclear export of pre-microRNAs and short hairpin RNAs.

- Genes Dev. 2003; 17:3011–6. <https://doi.org/10.1101/gad.1158803>.
4. Guil S, Cáceres JF. The multifunctional RNA-binding protein hnRNP A1 is required for processing of miR-18a. *Nat Struct Mol Biol.* 2007; 14:591–6. <https://doi.org/10.1038/nsmb1250>.
 5. Ambros V, Horvitz HR. Heterochronic mutants of the nematode *Caenorhabditis elegans*. *Science.* 1984; 226:409–16.
 6. Reinhart BJ, Slack FJ, Basson M, Pasquinelli a E, Bettinger JC, Rougvie AE, Horvitz HR, Ruvkun G. The 21-nucleotide let-7 RNA regulates developmental timing in *Caenorhabditis elegans*. *Nature.* 2000; 403:901–6. <https://doi.org/10.1038/35002607>.
 7. Brennecke J, Stark A, Russell RB, Cohen SM. Principles of MicroRNA–Target Recognition. *PLoS Biol.* 2005; 3:e85. <https://doi.org/10.1371/journal.pbio.0030085>.
 8. Lim LP, Lau NC, Garrett-Engele P, Grimson A, Schelter JM, Castle J, Bartel DP, Linsley PS, Johnson JM. Microarray analysis shows that some microRNAs downregulate large numbers of target mRNAs. *Nature.* 2005; 433:769–73. <https://doi.org/10.1038/nature03315>.
 9. Stefani G, Slack FJ. Small non-coding RNAs in animal development. *Nat Rev Mol Cell Biol.* 2008; 9:219–30. <https://doi.org/10.1038/nrm2347>.
 10. Weilner S, Schraml E, Redl H, Grillari-Voglauer R, Grillari J. Secretion of microvesicular miRNAs in cellular and organismal aging. *Exp Gerontol.* 2013; 48:626–33. <https://doi.org/10.1016/j.exger.2012.11.017>.
 11. Stiefel F, Fischer S, Hackl M, Handrick RR, Hesse F, Grillari J, Borth N, Otte K, Grillari J. Noncoding RNAs, post-transcriptional RNA operons and Chinese hamster ovary cells. *Pharm Bioprocess.* 2015; 3:227–47. <https://doi.org/10.4155/pbp.14.65>.
 12. Brodersen P, Voinnet O. Revisiting the principles of microRNA target recognition and mode of action. *Nat Rev Mol Cell Biol.* 2009; 10:141–8. <https://doi.org/10.1038/nrm2619>.
 13. Lal A, Navarro F, Maher C, Maliszewski LE, Yan N, Day EO, Chowdhury D, Dykxhoorn DM, Tsai P, Becker KG, Gorospe M, Hide W, Lieberman J. miR-24 inhibits cell proliferation by suppressing expression of E2F2, MYC and other cell cycle regulatory genes by binding to “seedless” 3'UTR microRNA recognition elements. *Mol Cell.* 2009; 35:610–625. <https://doi.org/10.1016/j.molcel.2009.08.020>.
 14. Tay Y, Zhang J, Thomson AM, Lim B, Rigoutsos I. MicroRNAs to Nanog, Oct4 and Sox2 coding regions modulate embryonic stem cell differentiation. *Nature.* 2008; 455:1124–8. <https://doi.org/10.1038/nature07299>.
 15. Chi SW, Hannon GJ, Darnell RB. An alternative mode of microRNA target recognition. *Nat Struct Mol Bio.* 2012; 19:321–7. <https://doi.org/10.1038/nsmb.2230>.
 16. Kocijan R, Muschitz C, Geiger E, Skalicky S, Baiert A, Dormann R, Plachel F, Feichtinger X, Heimel P, Fahrleitner-pammer A, Grillari J, Redl H, Resch H, et al. Circulating microRNA Signatures in Patients With Idiopathic and Postmenopausal Osteoporosis and Fragility Fractures. *J Clin Endocrinol Metab.* 2016; 101:4125–4134. <https://doi.org/10.1210/jc.2016-2365>.
 17. Turchinovich A, Weiz L, Langheinz A, Burwinkel B. Characterization of extracellular circulating microRNA. *Nucleic Acids Res.* 2011; 39:7223–33. <https://doi.org/10.1093/nar/gkr254>.
 18. Vickers KC, Palmisano BT, Shoucri BM, Shamburek RD, Remaley AT. MicroRNAs are transported in plasma and delivered to recipient cells by high-density lipoproteins. *Nat Cell Biol.* 2011; 13:423–33. <https://doi.org/10.1038/ncb2210>.
 19. Concepcion CP, Bonetti C, Ventura A. The microRNA-17-92 family of microRNA clusters in development and disease. *Cancer J.* 2012; 18:262–7. <https://doi.org/10.1097/PPO.0b013e318258b60a>.
 20. Mendell JT. miRiad roles for the miR-17-92 cluster in development and disease. *Cell.* 2008; 133:217–22. <https://doi.org/10.1016/j.cell.2008.04.001>.
 21. Dellago H, Bobbili MR, Grillari J. MicroRNA-17-5p: At the Crossroads of Cancer and Aging - A Mini-Review. *Gerontology.* 2017; 63:20–28. <https://doi.org/10.1159/000447773>.
 22. Dang CV. c-Myc Target Genes Involved in Cell Growth, Apoptosis, and Metabolism. *Mol Cell Biol.* 1999; 19:1–11.
 23. Dang CV. MYC on the path to cancer. *Cell.* 2012; 149:22–35. <https://doi.org/10.1016/j.cell.2012.03.003>.
 24. Meyer N, Penn LZ. Reflecting on 25 years with MYC. *Nat Rev Cancer.* 2008; 8:976–90. <https://doi.org/10.1038/nrc2231>.
 25. Lewis BP, Shih I, Jones-Rhoades MW, Bartel DP, Burge CB. Prediction of mammalian microRNA targets. *Cell.* 2003; 115:787–98.
 26. Zeller KI, Jegga AG, Aronow BJ, O'Donnell KA, Dang C V. An integrated database of genes responsive to the Myc oncogenic transcription factor: identification of direct genomic targets. *Genome Biol.* 2003; 4:R69. <https://doi.org/10.1186/gb-2003-4-10-r69>.
 27. He S, Yang S, Deng G, Liu M, Zhu H, Zhang W, Yan S, Quan L, Bai J, Xu N. Aurora kinase A induces miR-17-92 cluster through regulation of E2F1 transcription factor. *Cell Mol Life Sci.* 2010; 67:2069–76. <https://doi.org/10.1007/s00018-010-0340-8>.
 28. O'Donnell KA, Wentzel EA, Zeller KI, Dang CV., Mendell JT. c-Myc-regulated microRNAs modulate E2F1 expression. *Nature.* 2005; 435:839–43. <https://doi.org/10.1038/nature03677>.
 29. Yan H, Xue G, Mei Q, Wang Y, Ding F, Liu MF, Lu MH, Tang Y, Yu H, Sun S. Repression of the miR-17-92 cluster by p53 has an important function in hypoxia-induced apoptosis. *EMBO J.* 2009; 28:2719–32. <https://doi.org/10.1038/emboj.2009.214>.
 30. Gerstein MB, Kundaje A, Hariharan M, Landt SG, Yan K-K, Cheng C, Mu XJ, Khurana E, Rozowsky J, Alexander R,

- Min R, Alves P, Abyzov A, et al. Architecture of the human regulatory network derived from ENCODE data. *Nature*. 2012; 489:91–100. <https://doi.org/10.1038/nature11245>.
31. Mogilyansky E, Rigoutsos I. The miR-17/92 cluster: a comprehensive update on its genomics, genetics, functions and increasingly important and numerous roles in health and disease. *Cell Death Differ*. 2013; 20:1603–14. <https://doi.org/10.1038/cdd.2013.125>.
 32. Liang Y, Ridzon D, Wong L, Chen C. Characterization of microRNA expression profiles in normal human tissues. *BMC Genomics*. 2007; 8:166. <https://doi.org/10.1186/1471-2164-8-166>.
 33. Kaya KD, Karakulah G, Yalciner CM, Acar AC, Konu O. mESAdb: microRNA expression and sequence analysis database. *Nucleic Acids Res*. 2011; 39:D170–80. <https://doi.org/10.1093/nar/gkq1256>.
 34. Baskerville S, Bartel DP. Microarray profiling of microRNAs reveals frequent coexpression with neighboring miRNAs and host genes. *RNA*. 2005; 11:241–7. <https://doi.org/10.1261/rna.7240905>.
 35. Trompeter HI, Abbad H, Iwaniuk KM, Hafner M, Renwick N, Tuschl T, Schira J, Müller HW, Wernet P. MicroRNAs MiR-17, MiR-20a, and MiR-106b act in concert to modulate E2F activity on cell cycle arrest during neuronal lineage differentiation of USSC. *PLoS One*. 2011; 6:e16138. <https://doi.org/10.1371/journal.pone.0016138>.
 36. Dews M, Fox JL, Hultine S, Sundaram P, Wang W, Liu YY, Furth E, Enders GH, El-Deiry W, Schelter JM, Cleary MA, Thomas-Tikhonenko A. The myc-miR-17~92 axis blunts TGF β signaling and production of multiple TGF β -dependent antiangiogenic factors. *Cancer Res*. 2010; 70:8233–46. <https://doi.org/10.1158/0008-5472.CAN-10-2412>.
 37. Carraro G, El-Hashash A, Guidolin D, Tiozzo C, Turcatel G, Young BM, De Langhe SP, Bellusci S, Shi W, Parnigotto PP, Warburton D. miR-17 family of microRNAs controls FGF10-mediated embryonic lung epithelial branching morphogenesis through MAPK14 and STAT3 regulation of E-Cadherin distribution. *Dev Biol*. 2009; 333:238–50. <https://doi.org/10.1016/j.ydbio.2009.06.020>.
 38. Cloonan N, Brown MK, Steptoe AL, Wani S, Chan WL, Forrest ARR, Kolle G, Gabrielli B, Grimmond SM. The miR-17-5p microRNA is a key regulator of the G1/S phase cell cycle transition. *Genome Biol*. 2008; 9:R127. <https://doi.org/10.1186/gb-2008-9-8-r127>.
 39. Petrocca F, Visone R, Onelli MR, Shah MH, Nicoloso MS, de Martino I, Iliopoulos D, Pillozzi E, Liu CG, Negrini M, Cavazzini L, Volinia S, Alder H, et al. E2F1-Regulated MicroRNAs Impair TGF β -Dependent Cell-Cycle Arrest and Apoptosis in Gastric Cancer. *Cancer Cell*. 2008; 13:272–86. <https://doi.org/10.1016/j.ccr.2008.02.013>.
 40. Wang Q, Li YC, Wang J, Kong J, Qi Y, Quigg RJ, Li X. miR-17-92 cluster accelerates adipocyte differentiation by negatively regulating tumor-suppressor Rb2/p130. *Proc Natl Acad Sci USA*. 2008; 105:2889–94. <https://doi.org/10.1073/pnas.0800178105>.
 41. Schwentner R, Herrero-Martin D, Kauer MO, Cornelia N, Kovar H. The role of miR-17-92 in the miRegulatory landscape of Ewing sarcoma. *Oncotarget*. 2017; 8:10980–10993. <https://doi.org/10.18632/oncotarget.14091>.
 42. Li Y, Choi PS, Casey SC, Dill DL, Felsher DW. MYC through miR-17-92 suppresses specific target genes to maintain survival, autonomous proliferation, and a neoplastic state. *Cancer Cell*. 2014; 26:262–72. <https://doi.org/10.1016/j.ccr.2014.06.014>.
 43. Li Y, Deutzmann A, Choi PS, Fan AC, Felsher DW. BIM mediates oncogene inactivation-induced apoptosis in multiple transgenic mouse models of acute lymphoblastic leukemia. *Oncotarget*. 2016; 7:26926–34. <https://doi.org/10.18632/oncotarget.8731>.
 44. Li Y, Choi PS, Felsher DW. Oncogene addiction: resetting the safety switch? *Oncotarget*. 2014; 5:7986–7. <https://doi.org/10.18632/oncotarget.2474>.
 45. Johnson SC, Rabinovitch PS, Kaerberlein M. mTOR is a key modulator of ageing and age-related disease. *Nature*. 2013; 493:338–45. <https://doi.org/10.1038/nature11861>.
 46. Rubinsztein DC, Mariño G, Kroemer G. Autophagy and aging. *Cell*. 2011; 146:682–95. <https://doi.org/10.1016/j.cell.2011.07.030>.
 47. Du WW, Yang W, Fang L, Xuan J, Li H, Khorshidi a, Gupta S, Li X, Yang BB. miR-17 extends mouse lifespan by inhibiting senescence signaling mediated by MKP7. *Cell Death Dis*. 2014; 5:e1355. <https://doi.org/10.1038/cddis.2014.305>.
 48. Totary-Jain H, Sanoudou D, Ben-Dov IZ, Dautriche CN, Guarnieri P, Marx SO, Tuschl T, Marks AR. Reprogramming of the microRNA transcriptome mediates resistance to rapamycin. *J Biol Chem*. 2013; 288:6034–44. <https://doi.org/10.1074/jbc.M112.416446>.
 49. Komatsu S, Ichikawa D, Takeshita H, Morimura R, Hirajima S, Tsujiura M, Kawaguchi T, Miyamae M, Nagata H, Konishi H, Shiozaki A, Otsuji E. Circulating miR-18a: A sensitive cancer screening biomarker in human cancer. *In Vivo* (Brooklyn). 2014; 28:293–7.
 50. Volinia S, Calin GA, Liu CG, Ambs S, Cimmino A, Petrocca F, Visone R, Iorio M, Roldo C, Ferracin M, Prueitt RL, Yanaihara N, Lanza G, et al. A microRNA expression signature of human solid tumors defines cancer gene targets. *Proc Natl Acad Sci USA*. 2006; 103:2257–61. <https://doi.org/10.1073/pnas.0510565103>.
 51. Jadhav V, Hackl M, Klanert G, Hernandez Bort J a, Kunert R, Grillari J, Borth N. Stable overexpression of miR-17 enhances recombinant protein production of CHO cells. *J Biotechnol*. 2014; 175:38–44. <https://doi.org/10.1016/j.jbiotec.2014.01.032>.
 52. Li H, Gupta S, Du WW, Yang BB. MicroRNA-17 inhibits tumor growth by stimulating T-cell mediated host immune response. *Oncoscience*. 2014; 1:531–9. <https://doi.org/10.18632/oncoscience.69>.
 53. Fan M, Sethuraman A, Brown M, Sun W, Pfeffer LM. Systematic analysis of metastasis-associated genes identifies

- miR-17-5p as a metastatic suppressor of basal-like breast cancer. *Breast Cancer Res Treat.* 2014; 146:487–502. <https://doi.org/10.1007/s10549-014-3040-5>.
54. Shan SW, Lee DY, Deng Z, Shatseva T, Jeyapalan Z, Du WW, Zhang Y, Xuan JW, Yee SP, Siragam V, Yang BB. MicroRNA MiR-17 retards tissue growth and represses fibronectin expression. *Nat Cell Biol.* 2009; 11:1031–8. <https://doi.org/10.1038/ncb1917>.
 55. Wang M, Gu H, Wang S, Qian H, Zhu W, Zhang L, Zhao C, Tao Y, Xu W. Circulating miR-17-5p and miR-20a: molecular markers for gastric cancer. *Mol Med Rep.* 2012; 5:1514–20. <https://doi.org/10.3892/mmr.2012.828>.
 56. Zeng X, Xiang J, Wu M, Xiong W, Tang H, Deng M, Li X, Liao Q, Su B, Luo Z, Zhou Y, Zhou M, Zeng Z, et al. Circulating miR-17, miR-20a, miR-29c, and miR-223 combined as non-invasive biomarkers in nasopharyngeal carcinoma. *PLoS One.* 2012; 7:e46367. <https://doi.org/10.1371/journal.pone.0046367>.
 57. Xiang J, Wu J. Feud or Friend? The Role of the miR-17-92 Cluster in Tumorigenesis. *Curr Genomics.* 2010; 11:129–35. <https://doi.org/10.2174/138920210790886853>.
 58. Zhu H, Han C, Wu T. MiR-17-92 cluster promotes hepatocarcinogenesis. *Carcinogenesis.* 2015; 36:1213–22. <https://doi.org/10.1093/carcin/bgv112>.
 59. Shan SW, Fang L, Shatseva T, Rutnam ZJ, Yang X, Du W, Lu WY, Xuan JW, Deng Z, Yang BB. Mature miR-17-5p and passenger miR-17-3p induce hepatocellular carcinoma by targeting PTEN, GalNT7 and vimentin in different signal pathways. *J Cell Sci.* 2013; 126:1517–30. <https://doi.org/10.1242/jcs.122895>.
 60. Chen CL, Tseng YW, Wu JC, Chen GY, Lin KC, Hwang SM, Hu YC. Suppression of hepatocellular carcinoma by baculovirus-mediated expression of long non-coding RNA PTENP1 and MicroRNA regulation. *Biomaterials.* 2015; 44:71–81. <https://doi.org/10.1016/j.biomaterials.2014.12.023>.
 61. Chen L, Jiang M, Yuan W, Tang H. miR-17-5p as a novel prognostic marker for hepatocellular carcinoma. *J Invest Surg.* 2012; 25:156–61. <https://doi.org/10.3109/08941939.2011.618523>.
 62. Zheng J, Dong P, Gao S, Wang N, Yu F. High expression of serum miR-17-5p associated with poor prognosis in patients with hepatocellular carcinoma. *Hepatogastroenterology.* 2013; 60:549–52. <https://doi.org/10.5754/hge12754>.
 63. Yang F, Yin Y, Wang F, Wang Y, Zhang L, Tang Y, Sun S. miR-17-5p Promotes migration of human hepatocellular carcinoma cells through the p38 mitogen-activated protein kinase-heat shock protein 27 pathway. *Hepatology.* 2010; 51:1614–23. <https://doi.org/10.1002/hep.23566>.
 64. Calvano Filho CMC, Calvano-Mendes DC, Carvalho KC, Maciel GA, Ricci MD, Torres AP, Filassi JR, Baracat EC. Triple-negative and luminal A breast tumors: differential expression of miR-18a-5p, miR-17-5p, and miR-20a-5p. *Tumour Biol.* 2014; 35:7733–41. <https://doi.org/10.1007/s13277-014-2025-7>.
 65. Lehmann TP, Korski K, Gryczka R, Ibbs M, Thieleman A, Grodecka-Gazdecka S, Jagodziński PP. Relative levels of let-7a, miR-17, miR-27b, miR-125a, miR-125b and miR-206 as potential molecular markers to evaluate grade, receptor status and molecular type in breast cancer. *Mol Med Rep.* 2015; 12:4692–702. <https://doi.org/10.3892/mmr.2015.4002>.
 66. Bertoli G, Cava C, Castiglioni I. MicroRNAs: New Biomarkers for Diagnosis, Prognosis, Therapy Prediction and Therapeutic Tools for Breast Cancer. *Theranostics.* 2015; 5:1122–43. <https://doi.org/10.7150/thno.11543>.
 67. Li H, Bian C, Liao L, Li J, Zhao RC. miR-17-5p promotes human breast cancer cell migration and invasion through suppression of HBP1. *Breast Cancer Res Treat.* 2011; 126:565–75. <https://doi.org/10.1007/s10549-010-0954-4>.
 68. Liao XH, Lu DL, Wang N, Liu LY, Wang Y, Li YQ. Estrogen receptor a mediates proliferation of breast cancer MCF – 7 cells via a p21 / PCNA / E2F1-dependent pathway. *FEBS J.* 2014; 281:927–42. <https://doi.org/10.1111/febs.12658>.
 69. Hossain A, Kuo MT, Saunders GF. Mir-17-5p regulates breast cancer cell proliferation by inhibiting translation of AIB1 mRNA. *Mol Cell Biol.* 2006; 26:8191–201. <https://doi.org/10.1128/MCB.00242-06>.
 70. Liao X, Xiang Y, Yu C, Li J, Li H, Nie Q. STAT3 is required for MiR-17-5p-mediated sensitization to chemotherapy-induced apoptosis in breast cancer cells. *Oncotarget.* 2017; 8:15763–15774. <https://doi.org/10.18632/oncotarget.15000>.
 71. Jin YY, Andrade J, Wickstrom E. Non-Specific Blocking of miR-17-5p Guide Strand in Triple Negative Breast Cancer Cells by Amplifying Passenger Strand Activity. *PLoS One.* 2015; 10:e0142574. <https://doi.org/10.1371/journal.pone.0142574>.
 72. Karami F, Mohammadi-Yeganeh S, Abedi N, Koochaki A, Kia V, Paryan M. Bioinformatics Prediction and in Vitro Analysis Revealed That miR-17 Targets Cyclin D1 mRNA in Triple Negative Breast Cancer Cells. *Chem Biol Drug Des.* 2016; 87:317–20. <https://doi.org/10.1111/cbdd.12671>.
 73. Eichelser C, Flesch-Janys D, Chang-Claude J, Pantel K, Schwarzenbach H. Deregulated serum concentrations of circulating cell-free microRNAs miR-17, miR-34a, miR-155, and miR-373 in human breast cancer development and progression. *Clin Chem.* 2013; 59:1489–96. <https://doi.org/10.1373/clinchem.2013.205161>.
 74. De Summa S, Pinto R, Pilato B, Sambiasi D, Porcelli L, Guida G, Mattioli E, Paradiso a, Merla G, Micale L, De Nittis P, Tommasi S. Expression of base excision repair key factors and miR17 in familial and sporadic breast cancer. *Cell Death Dis.* 2014; 5:e1076. <https://doi.org/10.1038/cddis.2014.30>.
 75. Chen Q, Si Q, Xiao S, Xie Q, Lin J, Wang C, Chen L, Chen Q, Wang L. Prognostic significance of serum miR-17-5p in lung cancer. *Med Oncol.* 2013; 30:353. <https://doi.org/10.1007/s12032-012-0353-2>.
 76. Lin S, Sun JG, Wu JB, Long HX, Zhu CH, Xiang T, Ma H, Zhao ZQ, Yao Q, Zhang AM, Zhu B, Chen ZT. Aberrant microRNAs expression in CD133+/CD326+ human lung

- adenocarcinoma initiating cells from A549. *Mol Cells*. 2012; 33:277–83. <https://doi.org/10.1007/s10059-012-2252-y>.
77. Leidinger P, Brefort T, Backes C, Krapp M, Galata V, Beier M, Kohlhaas J, Huwer H, Meese E, Keller A. High-throughput qRT-PCR validation of blood microRNAs in non-small cell lung cancer. *Oncotarget*. 2016; 7:4611–23. <https://doi.org/10.18632/oncotarget.6566>.
 78. Roa WH, Kim JO, Razzak R, Du H, Guo L, Singh R, Gazala S, Ghosh S, Wong E, Joy AA, Xing JZ, Bedard EL. Sputum microRNA profiling: a novel approach for the early detection of non-small cell lung cancer. *Clin Invest Med*. 2012; 35:E271.
 79. Roa W, Brunet B, Guo L, Amanie J, Fairchild A, Gabos Z, Nijjar T, Scrimger R, Yee D, Xing J. Identification of a new microRNA expression profile as a potential cancer screening tool. *Clin Invest Med*. 2010; 33:E124.
 80. Matsubara H, Takeuchi T, Nishikawa E, Yanagisawa K, Hayashita Y, Ebi H, Yamada H, Suzuki M, Nagino M, Nimura Y, Osada H, Takahashi T. Apoptosis induction by antisense oligonucleotides against miR-17-5p and miR-20a in lung cancers overexpressing miR-17-92. *Oncogene*. 2007; 26:6099–105. <https://doi.org/10.1038/sj.onc.1210425>.
 81. Chatterjee A, Chattopadhyay D, Chakrabarti G. miR-17-5p downregulation contributes to paclitaxel resistance of lung cancer cells through altering beclin1 expression. *PLoS One*. 2014; 9:e95716. <https://doi.org/10.1371/journal.pone.0095716>.
 82. Chatterjee A, Chattopadhyay D, Chakrabarti G. MiR-16 targets Bcl-2 in paclitaxel-resistant lung cancer cells and overexpression of miR-16 along with miR-17 causes unprecedented sensitivity by simultaneously modulating autophagy and apoptosis. *Cell Signal*. 2015; 27:189–203. <https://doi.org/10.1016/j.cellsig.2014.11.023>.
 83. Zhao J, Fu W, Liao H, Dai L, Jiang Z, Pan Y, Huang H, Mo Y, Li S, Yang G, Yin J. The regulatory and predictive functions of miR-17 and miR-92 families on cisplatin resistance of non-small cell lung cancer. *BMC Cancer*. 2015; 15:731. <https://doi.org/10.1186/s12885-015-1713-z>.
 84. Zhou H, Guo JM, Lou YR, Zhang XJ, Zhong FD, Jiang Z, Cheng J, Xiao BX. Detection of circulating tumor cells in peripheral blood from patients with gastric cancer using microRNA as a marker. *J Mol Med (Berl)*. 2010; 88:709–17. <https://doi.org/10.1007/s00109-010-0617-2>.
 85. Tsujiura M, Ichikawa D, Komatsu S, Shiozaki A, Takeshita H, Kosuga T, Konishi H, Morimura R, Deguchi K, Fujiwara H, Okamoto K, Otsuji E. Circulating microRNAs in plasma of patients with gastric cancers. *Br J Cancer*. 2010; 102:1174–9. <https://doi.org/10.1038/sj.bjc.6605608>.
 86. Komatsu S, Ichikawa D, Tsujiura M, Konishi H, Takeshita H, Nagata H, Kawaguchi T, Hirajima S, Arita T, Shiozaki A, Kubota T, Fujiwara H, Okamoto K, et al. Prognostic impact of circulating miR-21 in the plasma of patients with gastric carcinoma. *Anticancer Res*. 2013; 33:271–6.
 87. Wang M, Gu H, Qian H, Zhu W, Zhao C, Zhang X, Tao Y, Zhang L, Xu W. miR-17-5p/20a are important markers for gastric cancer and murine double minute 2 participates in their functional regulation. *Eur J Cancer*. 2013; 49:2010–21. <https://doi.org/10.1016/j.ejca.2012.12.017>.
 88. Wu Q, Luo G, Yang Z, Zhu F, An Y, Shi Y, Fan D. miR-17-5p promotes proliferation by targeting SOCS6 in gastric cancer cells. *FEBS Lett*. 2014; 588:2055–62. <https://doi.org/10.1016/j.febslet.2014.04.036>.
 89. Qu Y, Zhang H, Duan J, Liu R, Deng T, Bai M. MiR-17-5p regulates cell proliferation and migration by targeting transforming growth factor- β receptor 2 in gastric cancer. *Oncotarget*. 2016; 7:33286–96. <https://doi.org/10.18632/oncotarget.8946>.
 90. Zeng Q, Jin C, Chen W, Xia F, Wang Q, Fan F, Du J, Guo Y, Lin C, Yang K, Li J, Peng X, Li X, et al. Downregulation of serum miR-17 and miR-106b levels in gastric cancer and benign gastric diseases. *Chin J Cancer Res*. 2014; 26:711–6. <https://doi.org/10.3978/j.issn.1000-9604.2014.12.03>.
 91. Knudsen KN, Nielsen BS, Lindebjerg J, Hansen TF, Holst R, Sørensen FB. microRNA-17 Is the Most Up-Regulated Member of the miR-17-92 Cluster during Early Colon Cancer Evolution. *PLoS One*. 2015; 10:e0140503. <https://doi.org/10.1371/journal.pone.0140503>.
 92. Motoyama K, Inoue H, Takatsuno Y, Tanaka F, Mimori K, Uetake H, Sugihara K, Mori M. Over- and under-expressed microRNAs in human colorectal cancer. *Int J Oncol*. 2009; 34:1069–75.
 93. Chen XJ, Shi KQ, Wang YQ, Song M, Zhou W, Tu HX, Lin Z. Clinical value of integrated-signature miRNAs in colorectal cancer: miRNA expression profiling analysis and experimental validation. *Oncotarget*. 2015; 6:37544–56. <https://doi.org/10.18632/oncotarget.6065>.
 94. Kara M, Yumrutas O, Ozcan O, Celik OI, Bozgeyik E, Bozgeyik I, Tasdemir S. Differential expressions of cancer-associated genes and their regulatory miRNAs in colorectal carcinoma. *Gene*. 2015; 567:81–6. <https://doi.org/10.1016/j.gene.2015.04.065>.
 95. Monzo M, Navarro A, Bandres E, Artells R, Moreno I, Gel B, Ibeas R, Moreno J, Martínez F, Diaz T, Martínez A, Balagué O, Garcia-Foncillas J. Overlapping expression of microRNAs in human embryonic colon and colorectal cancer. *Cell Res*. 2008; 18:823–33. <https://doi.org/10.1038/cr.2008.81>.
 96. Ling H, Spizzo R, Atlasi Y, Nicoloso M, Shimizu M, Redis RS, Nishida N, Gafà R, Song J, Guo Z, Ivan C, Barbarotto E, De Vries I, et al. CCAT2, a novel noncoding RNA mapping to 8q24, underlies metastatic progression and chromosomal instability in colon cancer. *Genome Res*. 2013; 23:1446–61. <https://doi.org/10.1101/gr.152942.112>.
 97. Ma Y, Zhang P, Wang F, Zhang H, Yang Y, Shi C, Xia Y, Peng J, Liu W, Yang Z, Qin H. Elevated oncofetal miR-17-5p expression regulates colorectal cancer progression by repressing its target gene P130. *Nat Commun*. 2012; 3:1291. <https://doi.org/10.1038/ncomms2276>.
 98. Luo H, Zou J, Dong Z, Zeng Q, Wu D, Liu L. Up-regulated miR-17 promotes cell proliferation, tumour growth and cell

- cycle progression by targeting the RND3 tumour suppressor gene in colorectal carcinoma. *Biochem J.* 2012; 442:311–21. <https://doi.org/10.1042/BJ20111517>.
99. Longqiu Y, Pengcheng L, Xuejie F, Peng Z. A miRNAs panel promotes the proliferation and invasion of colorectal cancer cells by targeting GABBR1. *Cancer Medicine.* 2016; 5:2022–31. <https://doi.org/10.1002/cam4.760>.
 100. Díaz R, Silva J, García JM, Lorenzo Y, García V, Peña C, Rodríguez R, Muñoz C, García F, Bonilla F, Domínguez G. Deregulated expression of miR-106a predicts survival in human colon cancer patients. *Genes Chromosomes Cancer.* 2008; 47:794–802. <https://doi.org/10.1002/gcc.20580>.
 101. Fang L, Li H, Wang L, Hu J, Jin T, Wang J, Yang BB. MicroRNA-17-5p promotes chemotherapeutic drug resistance and tumour metastasis of colorectal cancer by repressing PTEN expression. *Oncotarget.* 2014; 5:2974–87. <https://doi.org/10.18632/oncotarget.1614>.
 102. Gu J, Wang D, Zhang J, Zhu Y, Li Y, Chen H, Shi M, Wang X, Shen B, Deng X, Zhan Q, Wei G, Peng C. GFR α 2 prompts cell growth and chemoresistance through down-regulating tumor suppressor gene PTEN via Mir-17-5p in pancreatic cancer. *Cancer Lett.* 2016; 380:434–41. <https://doi.org/10.1016/j.canlet.2016.06.016>.
 103. Gandhi SU, Kim K, Larsen L, Rosengren RJ, Safe S. Curcumin and synthetic analogs induce reactive oxygen species and decreases specificity protein (Sp) transcription factors by targeting microRNAs. *BMC Cancer.* 2012; 12:564. <https://doi.org/10.1186/1471-2407-12-564>.
 104. Zekri ARN, Youssef ASER, Lotfy MM, Gabr R, Ahmed OS, Nassar A, Hussein N, Omran D, Medhat E, Eid S, Hussein MM, Ismail MY, Alenzi FQ, Bahnassy AA. Circulating Serum miRNAs as Diagnostic Markers for Colorectal Cancer. *PLoS One.* 2016; 11:e0154130. <https://doi.org/10.1371/journal.pone.0154130>.
 105. Gao Y, Luo L, Li S, Yang C. miR-17 inhibitor suppressed osteosarcoma tumor growth and metastasis via increasing PTEN expression. *Biochem Biophys Res Commun.* 2014; 444:230–4. <https://doi.org/10.1016/j.bbrc.2014.01.061>.
 106. Jia J, Feng X, Xu W, Yang S, Zhang Q, Liu X, Feng Y. MiR-17-5p modulates osteoblastic differentiation and cell proliferation by targeting SMAD7 in non-traumatic osteonecrosis. *Exp Mol Med.* 2014; 46:e107–8. <https://doi.org/10.1038/emmm.2014.43>.
 107. Wang W, Zhang L, Zheng K, Zhang X. miR-17-5p promotes the growth of osteosarcoma in a BRCC2-dependent mechanism. *Oncol Rep.* 2016; 35:1473–82. <https://doi.org/10.3892/or.2016.4542>.
 108. Li Z, Lu J, Sun M, Mi S, Zhang H, Luo RT, Chen P, Wang Y, Yan M, Qian Z, Neilly MB, Jin J, Zhang Y, et al. Distinct microRNA expression profiles in acute myeloid leukemia with common translocations. *Proc Natl Acad Sci USA.* 2008; 105:15535–40. <https://doi.org/10.1073/pnas.0808266105>.
 109. Gao X, Zhang R, Qu X, Zhao M, Zhang S, Wu H, Jianyong L, Chen L. MiR-15a, miR-16-1 and miR-17-92 cluster expression are linked to poor prognosis in multiple myeloma. *Leuk Res.* 2012; 36:1505–9. <https://doi.org/10.1016/j.leukres.2012.08.021>.
 110. Zhang L, Pan L, Xiang B, Zhu H, Wu Y, Chen M, Guan P, Zou X, Valencia CA, Dong B, Li J, Xie L, Ma H, et al. Potential role of exosome-associated microRNA panels and *in vivo* environment to predict drug resistance for patients with multiple myeloma. *Oncotarget.* 2016; 7:30876–91. <https://doi.org/10.18632/oncotarget.9021>.
 111. Firatligil B, Biray Avcı C, Baran Y. miR-17 in imatinib resistance and response to tyrosine kinase inhibitors in chronic myeloid leukemia cells. *J BUON.* 2013; 18:437–41.
 112. He M, Wang QY, Yin QQ, Tang J, Lu Y, Zhou CX, Duan CW, Hong DL, Tanaka T, Chen GQ, Zhao Q. HIF-1 α downregulates miR-17/20a directly targeting p21 and STAT3: a role in myeloid leukemic cell differentiation. *Cell Death Differ.* 2013; 20:408–18. <https://doi.org/10.1038/cdd.2012.130>.
 113. Zanette DL, Rivadavia F, Molfetta GA, Barbuzano FG, Proto-Siqueira R, Silva-Jr WA, Falcão RP, Zago MA. miRNA expression profiles in chronic lymphocytic and acute lymphocytic leukemia. *Braz J Med Biol Res.* 2007; 40:1435–40.
 114. Mraz M, Pospisilova S, Malinova K, Slapak I, Mayer J. MicroRNAs in chronic lymphocytic leukemia pathogenesis and disease subtypes. *Leuk Lymphoma.* 2009; 50:506–9. <https://doi.org/10.1080/10428190902763517>.
 115. Mraz M, Malinova K, Kotaskova J, Pavlova S, Tichy B, Malcikova J, Stano Kozubik K, Smardova J, Brychtova Y, Doubek M, Trbusek M, Mayer J, Pospisilova S. miR-34a, miR-29c and miR-17-5p are downregulated in CLL patients with TP53 abnormalities. *Leukemia.* 2009; 23:1159–63. <https://doi.org/10.1038/leu.2008.377>.
 116. Dereani S, Macor P, D'Agaro T, Mezzaroba N, Dal-Bo M, Capolla S, Zucchetto A, Tissino E, Del Poeta G, Zorzet S, Gattei V, Bomben R. Potential therapeutic role of antagomiR17 for the treatment of chronic lymphocytic leukemia. *J Hematol Oncol.* 2014; 7:79. <https://doi.org/10.1186/s13045-014-0079-z>.
 117. Musilova K, Mraz M. MicroRNAs in B-cell lymphomas: how a complex biology gets more complex. *Leukemia.* 2015; 29:1004–17. <https://doi.org/10.1038/leu.2014.351>.
 118. Yang X, Du WW, Li H, Liu F, Khorshidi a., Rutnam ZJ, Yang BB. Both mature miR-17-5p and passenger strand miR-17-3p target TIMP3 and induce prostate tumor growth and invasion. *Nucleic Acids Res.* 2013; 41:9688–704. <https://doi.org/10.1093/nar/gkt680>.
 119. Xu Y, Fang F, Zhang J, Jossion S, St Clair WH, St Clair DK. miR-17* suppresses tumorigenicity of prostate cancer by inhibiting mitochondrial antioxidant enzymes. *PLoS One.* 2010; 5:e14356. <https://doi.org/10.1371/journal.pone.0014356>.
 120. Gong AY, Eischeid AN, Xiao J, Zhao J, Chen D, Wang ZY, Young CY, Chen XM. miR-17-5p targets the p300/

- CBP-associated factor and modulates androgen receptor transcriptional activity in cultured prostate cancer cells. *BMC Cancer*. 2012; 12:492. <https://doi.org/10.1186/1471-2407-12-492>.
121. Yu C, Gong AY, Chen D, Solelo Leon D, Young CY, Chen XM. Phenethyl isothiocyanate inhibits androgen receptor-regulated transcriptional activity in prostate cancer cells through suppressing PCAF. *Mol Nutr Food Res*. 2013; 57:1825–33. <https://doi.org/10.1002/mnfr.201200810>.
122. Dhar S, Kumar A, Rimando AM, Zhang X, Levenson AS. Resveratrol and pterostilbene epigenetically restore PTEN expression by targeting oncomiRs of the miR-17 family in prostate cancer. *Oncotarget*. 2015; 6:27214–26. <https://doi.org/10.18632/oncotarget.4877>.
123. Ahadi A, Brennan S, Kennedy PJ, Hutvagner G, Tran N. Long non-coding RNAs harboring miRNA seed regions are enriched in prostate cancer exosomes. *Sci Rep*. 2016; 6:24922. <https://doi.org/10.1038/srep24922>.
124. Li H, Yang BB. Stress Response of Glioblastoma Cells Mediated by miR-17-5p Targeting PTEN and the Passenger Strand miR-17-3p Targeting MDM2. *Oncotarget*. 2012; 3:1653–68. <https://doi.org/10.18632/oncotarget.810>.
125. Rosenfeld N, Aharonov R, Meiri E, Rosenwald S, Spector Y, Zepeniuk M, Benjamin H, Shabes N, Tabak S, Levy A, Lebanony D, Goren Y, Silberschein E, et al. MicroRNAs accurately identify cancer tissue origin. *Nat Biotechnol*. 2008; 26:462–9. <https://doi.org/10.1038/nbt1392>.
126. Pentheroudakis G, Pavlidis N, Fountzilias G, Krikelis D, Goussia A, Stoyianni A, Sanden M, Cyr BS, Yerushalmi N, Benjamin H, Meiri E, Chajut A. Novel microRNA-based assay demonstrates 92 % agreement with diagnosis based on clinicopathologic and management data in a cohort of patients with carcinoma of unknown primary. *Mol Cancer*. 2013; 12:57. <https://doi.org/10.1186/1476-4598-12-57>.
127. Du WW, Li X, Li T, Li H, Khorshidi A, Liu F, Yang BB. The microRNA miR-17-3p inhibits mouse cardiac fibroblast senescence by targeting Par4. *J Cell Sci*. 2015; 128:293–304. <https://doi.org/10.1242/jcs.158360>.

**MicroRNA-17-5p: At the Crossroads of Cancer and
Aging - A Mini-Review**

MicroRNA-17-5p: At the Crossroads of Cancer and Aging – A Mini-Review

Hanna Dellago Madhusudhan Reddy Bobbili Johannes Grillari

Christian Doppler Laboratory on Biotechnology of Skin Aging, Department of Biotechnology, BOKU – University of Natural Resources and Life Sciences Vienna, Vienna, Austria

Key Words

miRNA · miR-17-5p · Aging · Longevity · Biomarker · Cancer

Abstract

The miR-17-92 cluster, led by its most prominent member, miR-17-5p, has been identified as the first miRNA with oncogenic potential. Thus, the whole cluster containing miR-17-5p has been termed oncomiR-1. It is strongly expressed in embryonic stem cells and has essential roles in vital processes like cell cycle regulation, proliferation and apoptosis. The importance of miR-17-5p for fundamental biological processes is underscored by the fact that a miR17-deficient mouse is neonatally lethal. Recently, miR-17-5p was identified in the context of aging, since it is comprised in a common signature of miRNAs that is downregulated in several models of aging research. Recently, miR-17-5p turned out to be the first ‘longevimiR’ in an animal model, extending the lifespan of a transgenic miR-17-5p-overexpressing mouse. Here, we summarize the current status of research on miR-17-5p with emphasis on its role in cellular senescence, aging and cancer, which points to a pleiotropic function of miR-17-5p regulating multiple targets involved in autophagy, cell cycle regulation and apoptosis in a tissue-dependent fashion. In addition, its elevated presence in serum or plasma of a wide range of tumor patients suggests using it as an ‘alarm-

IR’, a general indicator of a potential tumor pathology. However, amounts of circulating miR-17-5p of healthy individuals as reference values are still missing, before any miRNA can be classified as such an ‘alarmiR’. In conclusion, miR-17-5p is at the crossroads of aging, longevity and cancer and might represent a promising biomarker or even therapeutic tool and target in this context.

© 2016 The Author(s)
Published by S. Karger AG, Basel

Introduction

The increasing mean lifespan of the population is a big success story of humanity, but also poses a challenge that industrialized countries are currently facing, since aging is associated with increased susceptibility to many diseases like cancer, type 2 diabetes, neurodegenerative disorders and steatohepatitis. Aging is considered to be caused by limitations in somatic maintenance as a trade-off to reproduction, resulting in an accumulation of molecular and consequently tissue and organ damage over time [1]. Multiple mechanisms that cause or promote damage to macromolecules, cells and tissues, kept at bay by an equal number of mechanisms counteracting, pre-

H.D. and M.R.B. contributed equally to this work.

venting and repairing damage, have to be elucidated to develop a complete understanding of the aging process.

One prominent mechanism strongly related with cellular aging is cellular senescence. Senescence represents a permanent growth arrest induced by telomere attrition, oncogenic or environmental stress that functions a tumor-suppressor mechanism. Besides, senescent cells are now increasingly appreciated for their role in embryonic development, wound healing and tissue repair [2]. However, as senescent cells accumulate during lifetime, they exert detrimental effects on tissue function, contribute to chronic inflammatory states, and thus contribute to tissue, organ and organismal aging [3], and removal of naturally occurring senescent cells in the mouse postpones the development of age-related pathologies and extends the lifespan [4].

However, precise molecular understanding is still scarce, especially concerning miRNAs, which have been established as an important layer of gene expression control and might represent an attractive target for interventions aiming at healthy aging. Biogenesis, function and mechanisms of action of miRNAs are reviewed in great detail (e.g. [5]). In brief, one miRNA is able to regulate up to hundred mRNA targets and therefore potentially orchestrates a large variety of cellular processes similar to transcription factors [6, 7], contributing even to a potential posttranscriptional operon concept [8].

The miR-17-92 cluster comprises some of the best-studied miRNAs so far. This cluster contains 6 miRNA members with overlapping and specific roles. Here, we focus on miRNA-17-5p and its role in aging, age-related diseases and cancer, emphasizing the emerging role of 'longevimiR'-17 in cellular and organismal aging.

Transcriptional Regulation and Target mRNAs

Conservation and Regulation of the miRNA-17-92 Cluster

The miR-17-92 cluster is located in the locus of the nonprotein-coding gene MIR17HG on chromosome 13. The miR-17-92 transcript spans 800 nucleotides within its host gene and comprises six miRNAs – miR-17-5p, miR-18a, miR-19a, miR-20a, miR-19b-1 and miR-92a-1. Its sequence is highly conserved among vertebrates [9], especially in the seed region (fig. 1a), as also shown by phylogenetic tree analysis (fig. 1b). No homologues are found in nonvertebrates so far according to miRbase [10].

In addition, paralogous versions of miR-17 have arisen by intragenomic gene duplication in the miR-106a-363

and miR-106b-25 clusters. While the seed regions are well conserved (fig. 1c), differences in the 3' and 5' regions suggest overlapping, but different sets of target mRNAs and thus functions. How is the miR-17-92 cluster regulated on a transcriptional level? So far, several regulators of miR-17-92 transcription have been described.

c-Myc, the cellular homolog of the retroviral v-myc oncogene, is a well-studied proto-oncogene. Besides regulating transcription of a plethora of protein-coding genes, c-myc activates the miR-17-92 cluster and represses a dozen of other miRNAs. Interestingly, a number of c-myc transcriptional targets (fig. 2), like RPS6KA5 (ribosomal protein S6 kinase, 90 kDa, polypeptide 5), BCL11B (B-cell CLL/lymphoma 11B), PTEN (phosphatase and tensin homolog), E2F1 (E2F transcription factor 1) and HCFC2 (host cell factor C2) are also predicted targets of the miR-17-92 cluster [11], which suggests a delicate regulatory mechanism by which c-myc simultaneously activates transcription and restricts abundance of respective mRNAs.

A similar mechanism is thought to be at work between Aurora Kinase A (AURKA), the miR-17-92 cluster and the transcription factor E2F1. AURKA is a serine/threonine kinase essential for regulation of mitosis and is overexpressed in many cancers. AURKA stabilizes the transcription factor E2F1 by inhibiting its proteasomal degradation (fig. 2), which again induces miR-17-92 transcription [12] and is at the same time its target.

p53 acts as negative transcriptional regulator of the miR-17-92 cluster. Under hypoxia, p53 represses miR-17-92 transcription and thereby sensitizes cells for hypoxia-induced apoptosis, while overexpression of the miR-17-92 cluster inhibits apoptosis under hypoxia [13].

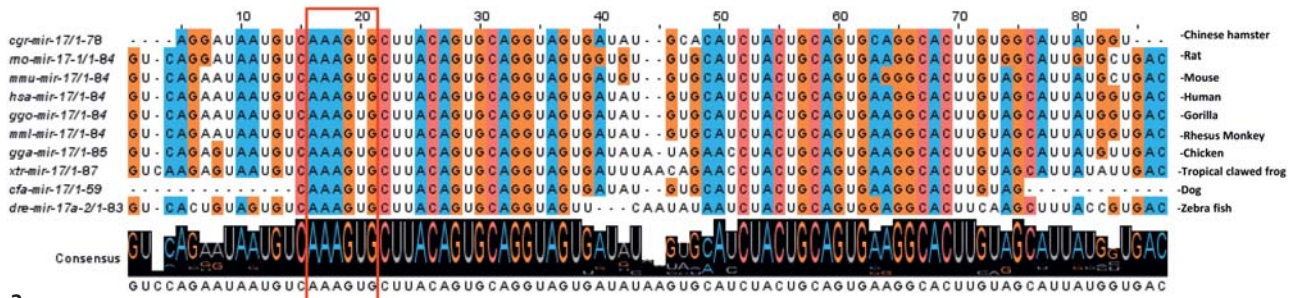
Results of the ENCODE (Encyclopedia of DNA Elements) project further revealed that along with these experimentally confirmed transcription factors, BCL3 (B-cell CLL/lymphoma 3), IRF1 (interferon regulatory factor 1), SP1 (Sp1 transcription factor), TAL1 (T-cell acute lymphocytic leukemia 1) and ZBTB33 (zinc finger and BTB domain containing 33) might regulate the miR-17-92 cluster (fig. 2) and are also targeted by individual miRNAs of the cluster [14].

On the posttranscriptional level, several studies find that the miR-17-92 cluster members are not expressed to equal degrees in cells and tissues as would be expected from their joint transcription as a primary miRNA. This might be due to factors that differentially protect or degrade the single miRNA members after the pre-miRNA status, as it has been published for miR-18 [15]. However, so far, no such reports exist on miR-17-5p. In terms of

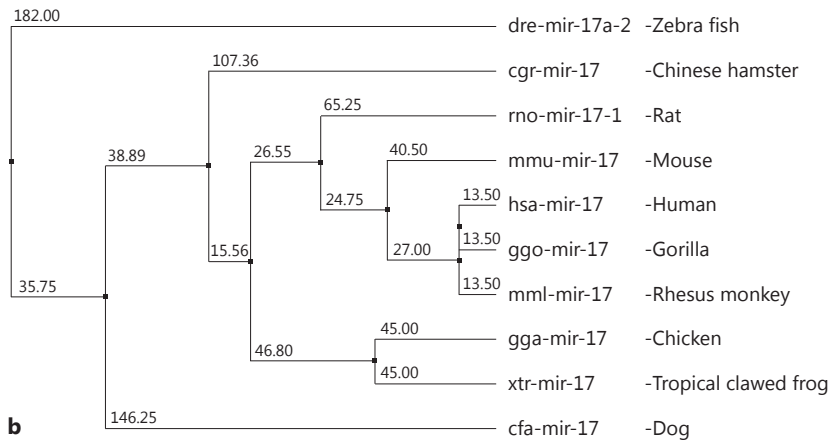
Multiple sequence alignment of miR-17-5p in different species

>hsa-miR-17-5p MI0000071

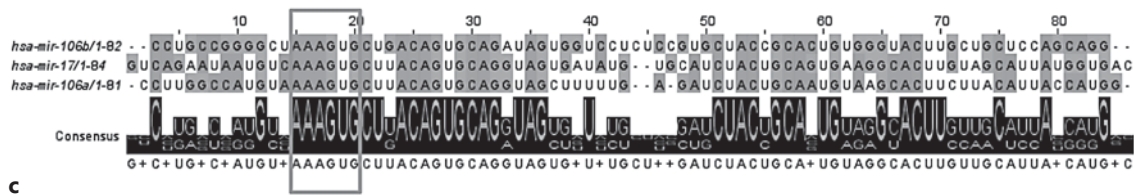
GUCAGAAUAAUGCAAAGUGCUUACAGUGCAGGUAGUGAUUUGUGCAUCUACUGCAGUGAAGGCACUUGUAGCAUUAUGGUGAC
 miR-17-5p miR-17-3p



a



b



c

Fig. 1. Sequence similarities of miR-17-5p. **a** Phylogenetic comparison of miR-17-5p shows almost 100% sequence identity in monkey and gorilla and a high degree of similarity down to Zebra fish. **b** miR-17-5p is conserved among vertebrates. The numbers in the phylogenetic tree indicate the evolutionary distance between

the organisms. **c** miR-17-5p has two homologous miRNAs encoded in the miR-106a-363 and miR-106b-25 clusters. The consensus sequence of these 3 seed family members, i.e. mature sequences with identical seed region, is shown.

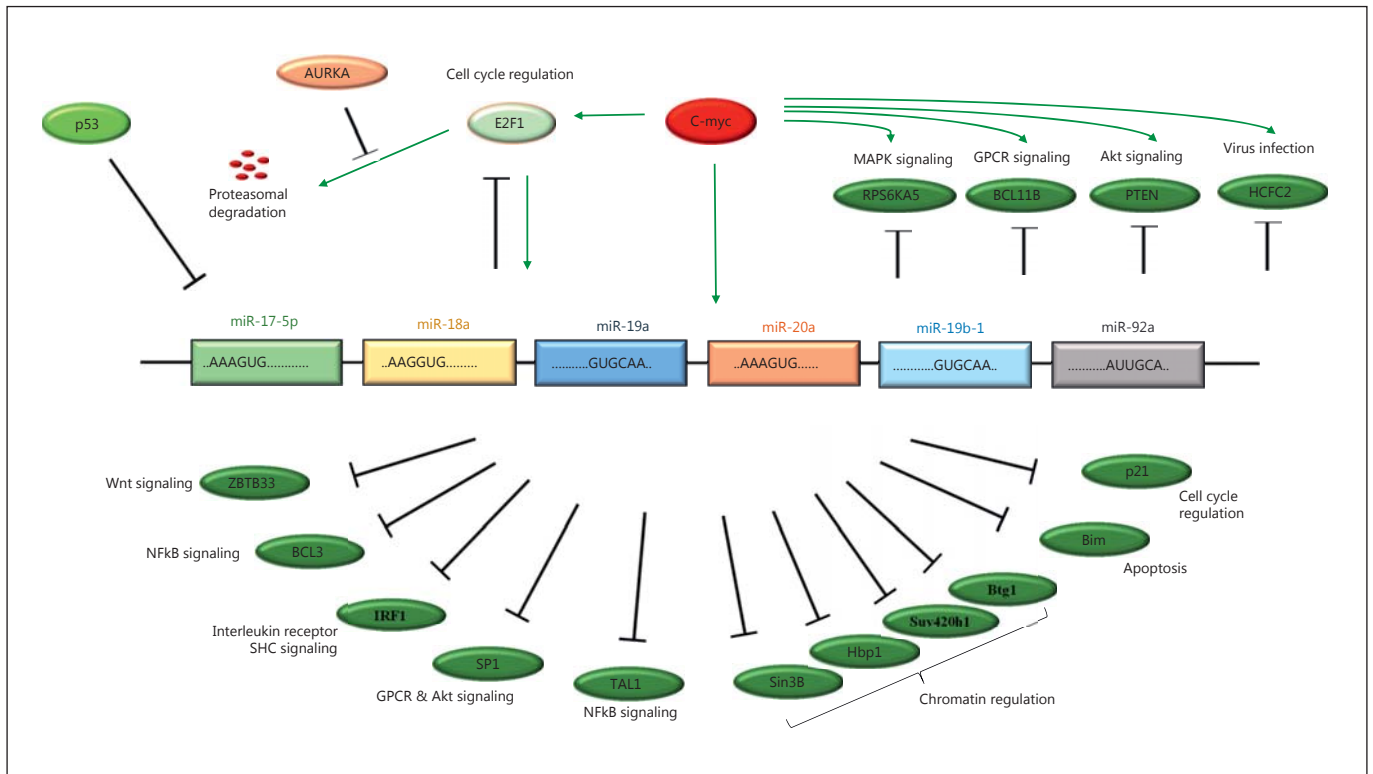


Fig. 2. The miR-17-92 regulatory network. Expression of the miR-17-92 cluster is controlled by multiple upstream regulators, some of which are in turn directly or indirectly targeted by miR-17-92 cluster members. miR-17-92 expression is induced by c-myc, and several c-myc transcriptional targets like RPS6KA5, BCL11B, PTEN, E2F1 and HCFC2 are targeted by miR-17-92, guaranteeing a delicate balance of miRNA and protein abundance. AURKA = Aurora kinase A; Akt = V-Akt murine thymoma viral oncogene homolog; BCL3 = B-cell CLL/lymphoma 3; BCL11B = B-cell CLL/lymphoma 11B; Bim = BCL2 like 11; Btg1 = B-cell translocation gene 1, antiproliferative; E2F1 = E2F transcription factor 1; Hbp1 = HMG-box transcription factor 1; GPCR = G protein-cou-

pled receptor; HCFC2 = host cell factor C2; IRF1 = interferon regulatory factor 1; MAPK = mitogen-activated protein kinase; myc = V-Myc avian myelocytomatosis viral oncogene homolog; NFkB = nuclear factor kappa B; p21 = cyclin-dependent kinase inhibitor 1A; p53 = tumor protein P53; PTEN = phosphatase and tensin homolog; RPS6KA5 = ribosomal protein S6 kinase, 90 kDa, polypeptide 5; SHC = Src homology 2 domain containing transforming protein 1; Sin3b = SIN3 transcription regulator family member B; SP1 = Sp1 transcription factor; Suv420h1 = suppressor of variegation 4-20 homolog 1; TAL1 = T-cell acute lymphocytic leukemia 1; Wnt = wingless-type MMTV integration site family; ZBTB33 = zinc finger and BTB domain containing 33.

tissue and cell type specificity, miR-17-5p is expressed ubiquitously and highly in all tissues tested so far [16], pointing to a generally high importance of this miRNA.

Target mRNAs of the miR-17-92 Cluster and miR-17-5p

PTEN and E2Fs were the first confirmed targets of the miR-17-92 cluster in the context of cell cycle progression and apoptosis [17]. By now, a multitude of targets of the miR-17-92 cluster have been reported including members of the TGFβ (transforming growth factor-β) signaling pathway [18]. In addition, it also targets specific chromatin regulatory genes, such as Sin3b (SIN3 transcription regulator family member B; a transcriptional repressor

for MYC-responsive genes), Hbp1 (HMG-box transcription factor 1; a transcriptional repressor that negatively regulates the Wnt-mediated beta catenin signaling pathway), Suv420h1 (suppressor of variegation 4–20 homolog 1; a histone methyltransferase, targeted to histone H3 by retinoblastoma proteins), and Btg1 (B-cell translocation gene 1, antiproliferative; a regulator of cell growth and differentiation), as well as the apoptosis regulator Bim (Bcl-2 interacting mediator of cell death; an activator of neuronal and lymphocyte apoptosis) [19] and the cell cycle inhibitor p21 (fig. 2) [20]. Hence, miR-17-92 seems to maintain cell proliferation and survival, which might result in a neoplastic or progenitor/regenerative state of cells [19].

A series of mouse strains with targeted deletions of individual miR-17-92 members and subsequent phenotypic and gene expression analysis have recently provided a detailed picture of how miR-17-92 affects gene expression in vivo [21].

In the following, we recapitulate data that point to a dual role of this cluster that might well result in an antagonistic pleiotropic function of miR-17-5p in young versus elderly individuals.

Ageing, the miR-17-92 Cluster, and miR-17-5p

Ageing- and Senescence-Dependent Regulation of miR-17-5p

In recent years, the important role of miRNAs in aging became increasingly evident [22]. In an effort to identify miRNAs commonly regulated during aging, microarray studies were performed comparing four human replicative cell-aging models – endothelial cells, skin fibroblasts, T-cells and renal proximal tubular epithelial cells – as well as three organismal aging models comprising skin, T-cells and mesenchymal stem cells. These very different model systems shared a set of commonly downregulated miRNAs, among them members of the miR-17-92 cluster including miR-17-5p, miR-19b, miR-20a and miR-106a [23]. Several studies using different model systems have confirmed the downregulation of the miR-17-92 cluster during aging [24], and its upregulation in centenarians who are considered successful agers [25, 26].

These expression changes are recapitulated by stress-induced senescence, as microarray data revealed that members of the miR-17-92 cluster, including miR-17-5p, are downregulated in stress-induced senescence of human diploid fibroblasts and human trabecular meshwork cells [27]. Figure 3a gives an overview over up- and down-regulation of miR-17-5p expression during aging and age-related diseases.

A Long-Lived Pre-miR-17-Overexpressing Mouse Model

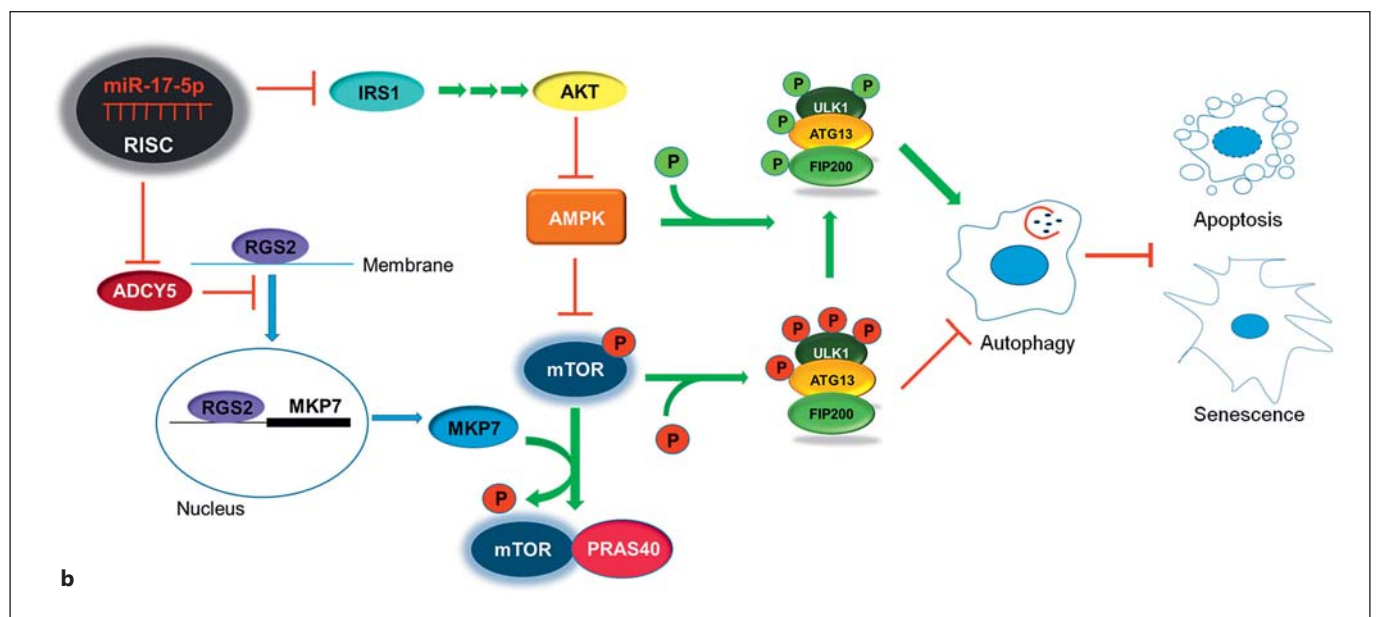
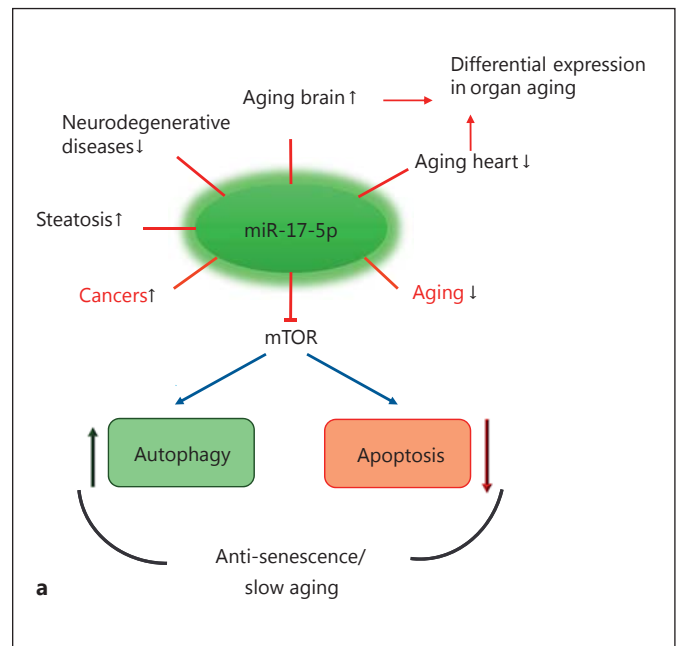
The interest in the role of miR-17-5p in aging research has peaked with the report that its overexpression in mouse extends the organismal lifespan by approximately 16% [28]. This finding was somewhat surprising after the same authors had previously observed that miR-17 represses fibronectin expression, leading to cellular defects, growth retardation, smaller organs and strongly reduced hematopoietic cell lineages in miR-17-overexpressing mice [29], results that do not seem well reconciled yet.

However, in favor of its life-prolonging role, miR-17-5p targets IRS1 (Insulin Receptor Substrate 1) and ADCY5 (Adenylate Cyclase 5), which modulate a complex signaling network, leading to upregulation of genes involved in autophagy and repressing senescence and apoptosis (fig. 3b) [28].

To be more precise, IRS1 on the one hand activates AKT, which suppresses the mTOR inhibitor AMPK. Therefore, miR-17-5p-dependent silencing of IRS1 abrogates AMPK suppression, enabling mTOR inhibition and thus activating autophagy. On the other hand, IRS1 promotes expression of FOXO3A (forkhead box O3) and LC3- β (microtubule-associated protein 1 light chain 3 beta), which also enhance autophagy. At the same time, repression of miR-17-5p's direct target ADCY5 leads to translocation of RGS2 (regulator of G-protein signaling 2) from the membrane into the nucleus, where it interacts with and activates transcription of MKP7 (mitogen-activated protein kinase phosphatase 7). The MKP7 protein dephosphorylates PRAS40 (40-kDa proline-rich AKT substrate) and mTOR (mechanistic target of rapamycin), which thereupon bind each other, resulting in a suppression of mTOR activity that in consequence leads to attenuation of protein synthesis and stimulation of autophagy, resulting in reduced senescence. In fact, miR-17 transgenic mice exhibited increased bone mass and decreased presence of senescent cells in the skin, intestine, lung and heart. In addition, MKP7 acts as a negative regulator of c-Jun amino-terminal kinase and extracellular signal-regulated kinase (ERK) pathways. ERKs function in the control of cell division, and inhibitors of these enzymes are potential anticancer agents, hence miR-17-5p might also extend the organismal life span by reducing cancer risk, but that is still subject to speculation, since – as stated above – miR-17 transgenic mice develop liver tumors [28]. The authors do not give any information about the causes of death in their miR-17 mice, and a potential confounder might be that both miR-17-5p and miR-17-3p are expressed from the pre-miR-17 construct to a comparable degree, and hence the relative effect of each specific miRNA to the observed organismal phenotype cannot be determined [28].

Only few other miRNAs have been described to postpone cellular or organismal aging, one of them being inhibition of miR-21 in endothelial cell senescence [30]. Since elongation of the life span is still considered the golden standard for proving an activity in the aging process, we suggest tagging such miRNAs with the label 'longevi-miR'.

Fig. 3. miR-17-5p in aging and age-related diseases. **a** Overview of miR-17-5p expression levels during aging and age-related pathologies. ↑ and ↓ designate up- and downregulation, respectively. **b** Relationship between miR-17-5p and mTOR, a central regulator of autophagy and apoptosis. miR-17-5p targets ACDY5, causing translocation of the GTPase activator RGS2 from the membrane to the nucleus, where it induces expression of MKP7. MKP7 dephosphorylates mTOR, which thereupon dimerizes with PRAS40 and is inactivated. Inhibitory phosphorylation of the ULK1-ATG13-FIP200 heterotrimer by mTOR is consequently abolished and activating phosphorylation catalyzed by AMPK. Consequently, the ULK1 complex activates autophagy, which in turn attenuates senescence and apoptosis. Simultaneously, miR-17-5p targets IRS1. IRS1 can activate AKT via PI3K, and AKT inhibits the autophagy activator AMPK. Therefore, IRS1 downregulation by miR-17-5p activates autophagy via two pathways. AKT = Proto-oncogene c-Akt; AMPK = AMP-activated protein kinase; ATG13 = autophagy related 13; FIP200 = focal adhesion kinase family kinase-interacting protein of 200 kDa; IRS1 = insulin receptor substrate 1; MKP7 = mitogen-activated protein kinase phosphatase 7; PRAS40 = 40-kDa proline-rich AKT substrate; RISC = RNA-induced silencing complex; ULK1 = Unc-51 like autophagy activating kinase 1.



Cardiac Function and miR-17-5p

In transgenic mice, miR-17-5p is upregulated in damaged heart regions after induced infarction. It directly targets two inhibitors of matrix metalloproteinases (MMPs), TIMP1 (tissue inhibitor of metalloproteinases 1) and TIMP2 (tissue inhibitor of metalloproteinases 2), leading to matrix remodeling after infarction [31]. In turn, miR-17 inhibition in a mouse model in vivo decreased MMP activity, enhanced cardiac function and

helped prevent heart failure after infarction. Similarly, miR-17-5p is protective in a kidney ischemia-reperfusion model [32].

In addition, overexpression of pre-miR-17 in mouse cardiac fibroblasts enhances cell survival upon oxidative stress, increases proliferation and reduces senescence-associated β -galactosidase staining [33], whereby the miR-17-3p component of the pre-miR-17 activates a transcriptional program that promotes epithelial-to-

mesenchymal transition and self-renewal while suppressing senescence, and might even act as a miR-17-5p antagomiR.

In summary, miR-17-5p and -3p play a role in cardiac aging in transgenic mice and cells in vitro. Again, both miR-17-5p and miR-17-3p are expressed from the same pre-miR-17, and therefore the relative contribution of each miRNA to the observed phenotype is not clear.

Aging, the Bone and miR-17-5p

The miR-17-92 cluster plays an important role in bone formation, as knockout in mice results in reduced bone mineral content and reduced bone strength [34]. Furthermore, miR-17-5p overexpression promotes osteogenic differentiation of MSCs (mesenchymal stem cells) [35]. However, during aging and in pro-inflammatory diseases, miR-17-5p expression was observed low in MSCs, concomitant with compromised osteogenic differentiation [36]. miR-17 overexpression partially rescued this defect by repressing Smurf1 (Smad ubiquitin regulatory factor one) [37] and SMAD7.

Since low miR-17-92 expression is a hallmark of aging and senescence [23], and senescent cells contribute to reduced osteogenesis [38, 39], it might be speculated that it is involved in loss of bone mineral density in the elderly. However, data on senescence and bone disease are still scarce, while one hint into this direction is that telomerase-deficient mice lose bone mass, most probably due to the SASP (senescence-associated secretory phenotype) [40].

miR-17-5p in the Aging Brain

Surprisingly, miR-17 expression is increased in the brains of old mice compared to young mice [41], while the relative abundance of the majority of miRNAs tested decreased in the mouse brain during aging. The informative value of this study is limited, though, by the fact that data are based on pooled cDNA libraries derived from only 2 individuals for each condition. Such an unexpected increase might be interpreted in the context of astrogliosis. Astrogliosis (or reactive astrogliosis) is an abnormal increase in the number of astrocytes due to the destruction of nearby neurons. It can be observed in age-related neurodegenerative diseases like Alzheimer's disease [42] or after spinal cord injury (SCI), where it leads to glial scar formation and inhibits axonal regeneration. miR-17-5p is upregulated after SCI and contributes to astrocyte proliferation [43] and hence potentially also to the astrogliosis phenotype observed in age-related neurodegenerative diseases.

miR-17-5p and mTOR – A Connection between Proliferation, Cancer and Aging

One focus in research on interventions that slow aging is on the mammalian target of rapamycin (mTOR). Inhibition of mTOR is one of the few accepted and universal interventions in model organisms that extends the lifespan and postpones age-related diseases like cardiovascular diseases, cancer and diabetes, and mTOR inhibitors are widely used to treat these diseases. Inhibition of mTOR activates many pathways that upregulate autophagy. Thereby, it fulfills multiple purposes – the clearance of dysfunctional or unnecessary molecules or organelles, the provision of nutrients and the degradation of intracellular pathogens. Both normal and premature aging are accompanied by a decline in autophagic potential, and a lack of functional autophagy leads to tissue degeneration similar to that observed in aged tissue [44]. In addition, mTOR is a central coordinator of cell proliferation whose function is deregulated in many cancers. Therefore, inhibitors of mTOR like rapamycin and its analogues are potential antitumor agents, some already approved for clinical use in cancer therapy.

Given its importance in cell physiology and tissue maintenance, it comes as no surprise that the mTOR pathway is subject to regulation by miRNAs, among them also the miR-17-92 cluster [45].

As shown in figure 3b, inhibition of mTOR by miR-17-5p upregulates autophagy and slows down the aging process in the mouse model presented by Du et al. [28], discussed in the section A Long-Lived Pre-miR-17 Overexpressing Mouse Model. Indeed, oncogenic miRNAs like miR-17 are upregulated in rapamycin-resistant cells and inhibition of miR-17 restored rapamycin sensitivity. Thus, inhibitors of miR-17 could potentially serve as adjuvants in chemotherapy. However, it becomes clear from these studies that miR-17-5p is at the crossroads between aging and cancer.

miR-17-5p and Its Role in Cancer

In general, miR-17-5p is considered as an oncogene, supported by a large body of evidence from many different tumors. However, it might also be 'guilty-by-association' with its oncogenic miR-17-92 cluster members [46], especially miR-19, which has been postulated as having the highest oncogenic potential [47]. By now, a more differentiated view has emerged in literature, where miR-17-5p alone possesses metastasis suppressor functions [48]. In addition, it seems to suppress cancer growth by stimu-

lating T cells [49]. Finally, high circulating levels of miR-17-5p have been found in serum of patients suffering of several different types of cancer [50, 51], suggesting that high levels of circulating miR-17-5p might serve as an alarm signal, or ‘alarmiR’.

In sum, the effect of miR-17-5p varies according to cancer type, model system, and probably also to the relative expression levels of miR-17-3p and miR-17-5p, depending on the constructs used for overexpression and knockdown. The tumor-suppressive and tumorigenic properties of the miR-17-92 cluster are summarized in more detail in other recent reviews, e.g. [52, 53].

Conclusion

In this review, we focused on the role of miR-17-5p in cellular senescence, aging and age-related diseases and opposed this role to cancer. miR-17-5p plays a major role in regulating many genes involved in autophagy, apoptosis and cell cycle regulation. Its overexpression in the mouse model extends the lifespan by promoting autophagy, and hence we suggest terming miR-17-5p the first ‘longevi-miRNA’. At the same time, circulating miR-17-5p levels turned out to be high in almost all cancers, atherosclerosis and obesity, and might act as a biomarker or alarming signal, meriting the designation ‘alarmiR-17’. While miR-17-5p is ubiquitously expressed, its biological

function seems very cell, tissue and disease specific, which accounts for the confusingly high number of reports suggesting it to have a dual role, as a tumor suppressor and as an oncogene. Not only miR-17-5p, but also miR-17-3p surprisingly plays a role as tumor suppressor and as oncogene, sometimes synergistically with miR-17-5p, sometimes independently. Therefore, more research is needed to understand the basic biology of miR-17-3p and miR-17-5p in order to establish them as prognostic, diagnostic and therapeutic targets for aging and age-related diseases as well as cancer.

Acknowledgements

This work was funded by the BioToP – ‘Biomolecular technology of proteins’ PhD Programme, Austrian Science Funds (FWF) Project W1224, and the Christian Doppler Society. The financial support by the Austrian Federal Ministry of Economy, Family and Youth, the National Foundation for Research, Technology and Development as well as the FP7 EU projects Frailomic and Sybil are also gratefully acknowledged.

We apologize to all the authors who contributed to today’s state of knowledge in the field and to whom we could not give credit due to the limited numbers of references.

Disclosure Statement

J.G. is a co-founder of Evercyte GmbH and TAmiRNA GmbH.

References

- 1 Kirkwood TB: Understanding the odd science of aging. *Cell* 2005;120:437–447.
- 2 Demaria M, Ohtani N, Youssef SA, Rodier F, Toussaint W, Mitchell JR, et al: An essential role for senescent cells in optimal wound healing through secretion of PDGF-AA. *Dev Cell* 2014;31:722–733.
- 3 Coppé J-P, Desprez P-Y, Krtolica A, Campisi J: The senescence-associated secretory phenotype: the dark side of tumor suppression. *Annu Rev Pathol* 2010;5:99–118.
- 4 Baker DJ, Childs BG, Durik M, Wijers ME, Sieben CJ, Zhong J, et al: Naturally occurring p16Ink4a-positive cells shorten healthy lifespan. *Nature* 2016;530:184–189.
- 5 Jonas S, Izaurralde E: Towards a molecular understanding of microRNA-mediated gene silencing. *Nat Rev Genet* 2015;16:421–433.
- 6 Stefani G, Slack FJ: Small non-coding RNAs in animal development. *Nat Rev Mol Cell Biol* 2008;9:219–230.
- 7 Weilner S, Schraml E, Redl H, Grillari-Voglauer R, Grillari J: Secretion of microvesicular miRNAs in cellular and organismal aging. *Exp Gerontol* 2013;48:626–633.
- 8 Fischer S, Mathias S, Schaz S, Emmerling VV, Buck T, Kleemann M, et al: Enhanced protein production by microRNA-30 family in CHO cells is mediated by the modulation of the ubiquitin pathway. *J Biotechnol* 2015;212:32–43.
- 9 Mendell JT: miRiad roles for the miR-17-92 cluster in development and disease. *Cell* 2008;133:217–222.
- 10 Kozomara A, Griffiths-Jones S: miRBase: annotating high confidence microRNAs using deep sequencing data. *Nucleic Acids Res* 2014;42:D68–D73.
- 11 Lewis BP, Shih I, Jones-Rhoades MW, Bartel DP, Burge CB: Prediction of mammalian microRNA targets. *Cell* 2003;115:787–798.
- 12 He S, Yang S, Deng G, Liu M, Zhu H, Zhang W, et al: Aurora kinase A induces miR-17-92 cluster through regulation of E2F1 transcription factor. *Cell Mol Life Sci* 2010;67:2069–2076.
- 13 Yan H, Xue G, Mei Q, Wang Y, Ding F, Liu M-F, et al: Repression of the miR-17-92 cluster by p53 has an important function in hypoxia-induced apoptosis. *EMBO J* 2009;28:2719–2732.
- 14 Gerstein MB, Kundaje A, Hariharan M, Landt SG, Yan K-K, Cheng C, et al: Architecture of the human regulatory network derived from ENCODE data. *Nature* 2012;489:91–100.
- 15 Guil S, Cáceres JF: The multifunctional RNA-binding protein hnRNP A1 is required for processing of miR-18a. *Nat Struct Mol Biol* 2007;14:591–596.
- 16 Kaya KD, Karakulah G, Yakicier CM, Acar AC, Konu O: mESAdb: microRNA expression and sequence analysis database. *Nucleic Acids Res* 2011;39:D170–D180.

- 17 Cloonan N, Brown MK, Steptoe AL, Wani S, Chan WL, Forrest ARR, et al: The miR-17-5p microRNA is a key regulator of the G1/S phase cell cycle transition. *Genome Biol* 2008; 9:R127.
- 18 Petrocca F, Vecchione A, Croce CM: Emerging role of miR-106b-25/miR-17-92 clusters in the control of transforming growth factor beta signaling. *Cancer Res* 2008;68:8191–8194.
- 19 Li Y, Choi PS, Casey SC, Dill DL, Felsher DW: MYC through miR-17-92 suppresses specific target genes to maintain survival, autonomous proliferation, and a neoplastic state. *Cancer Cell* 2014;26:262–272.
- 20 Fontana L, Fiori ME, Albin S, Cifaldi L, Giovannazzi S, Forloni M, et al: Antagomir-17-5p abolishes the growth of therapy-resistant neuroblastoma through p21 and BIM. *PLoS One* 2008;3:e2236.
- 21 Han Y, Vidigal JA, Mu P, Yao E, Singh I, González AJ, et al: An allelic series of miR-17~92 – mutant mice uncovers functional specialization and cooperation among members of a microRNA polycistron. *Nat Genet* 2015;47:766–775.
- 22 Grillari J, Grillari-Voglauer R: Novel modulators of senescence, aging, and longevity: Small non-coding RNAs enter the stage. *Exp Gerontol* 2010;45:302–311.
- 23 Hackl M, Brunner S, Fortschegger K, Schreiner C, Micutkova L, Mück C, et al: miR-17, miR-19b, miR-20a, and miR-106a are down-regulated in human aging. *Aging Cell* 2010;9: 291–296.
- 24 Dhahbi JM, Atamna H, Boffelli D, Magis W, Spindler SR, Martin DIK: Deep sequencing reveals novel MicroRNAs and regulation of MicroRNA expression during cell senescence. *PLoS One* 2011;6:e20509.
- 25 Serna E, Gambini J, Borrás C, Abdelaziz KM, Mohammed K, Belenguer A, et al: Centenarians, but not octogenarians, up-regulate the expression of microRNAs. *Sci Rep* 2012;2: 961.
- 26 Gombar S, Jung HJ, Dong F, Calder B, Atzmon G, Barzilai N, et al: Comprehensive microRNA profiling in B-cells of human centenarians by massively parallel sequencing. *BMC Genomics* 2012;13:353.
- 27 Li G, Luna C, Qiu J, Epstein DL, Gonzalez P: Alterations in microRNA expression in stress-induced cellular senescence. *Mech Ageing Dev* 2009;130:731–741.
- 28 Du WW, Yang W, Fang L, Xuan J, Li H, Khorshidi A, et al: miR-17 extends mouse lifespan by inhibiting senescence signaling mediated by MKP7. *Cell Death Dis* 2014;5:e1355.
- 29 Shan SW, Lee DY, Deng Z, Shatseva T, Jeyapalan Z, Du WW, et al: MicroRNA MiR-17 retards tissue growth and represses fibronectin expression. *Nat Cell Biol* 2009;11:1031–1038.
- 30 Dellago H, Preschitz-Kammerhofer B, Terlecki-Zaniewicz L, Schreiner C, Fortschegger K, Chang MW, et al: High levels of oncomiR-21 contribute to the senescence induced growth arrest in normal human cells and its knock-down increases the replicative life span. *Aging Cell* 2013;12:446–458.
- 31 Li S-H, Guo J, Wu J, Sun Z, Han M, Shan SW, et al: miR-17 targets tissue inhibitor of metalloproteinase 1 and 2 to modulate cardiac matrix remodeling. *FASEB J* 2013;27:4254–4265.
- 32 Kaucsár T1, Révész C, Godó M, Krenács T, Albert M, Szalay CI, Rosivall L, Benyó Z, Bátkai S, Thum T, Sznéási G, Hamar P: Activation of the miR-17 family and miR-21 during murine kidney ischemia-reperfusion injury. *Nucleic Acid Ther* 2013;23:344–354.
- 33 Du WW, Li X, Li T, Li H, Khorshidi A, Liu F, et al: The microRNA miR-17-3p inhibits mouse cardiac fibroblast senescence by targeting Par4. *J Cell Sci* 2015;128:293–304.
- 34 Mohan S, Wergedal JE, Das S, Kesavan C: Conditional disruption of miR17-92 cluster in collagen type I-producing osteoblasts results in reduced periosteal bone formation and bone anabolic response to exercise. *Physiol Genomics* 2015;47:33–43.
- 35 Jia J, Feng X, Xu W, Yang S, Zhang Q, Liu X, et al: MiR-17-5p modulates osteoblastic differentiation and cell proliferation by targeting SMAD7 in non-traumatic osteonecrosis 2014;46:e107–e108.
- 36 Liu W, Qi M, Konermann A, Zhang L, Jin F, Jin Y: The p53/miR-17/Smurf1 pathway mediates skeletal deformities in an age-related model via inhibiting the function of mesenchymal stem cells. *Aging (Albany NY)* 2015; 7:205–216.
- 37 Zhu H, Kavsak P, Abdollah S, Wrana JL, Thomsen GH: A SMAD ubiquitin ligase targets the BMP pathway and affects embryonic pattern formation. *Nature* 1999;400:687–693.
- 38 Weilner S, Grillari-Voglauer R, Redl H, Grillari J, Nau T: The role of microRNAs in cellular senescence and age-related conditions of cartilage and bone. *Acta Orthop* 2015;86:92–99.
- 39 Weilner S, Schraml E, Wieser M, Messner P, Schneider K, Wassermann K, et al: Secreted microvesicular miR-31 inhibits osteogenic differentiation of mesenchymal stem cells. *Aging Cell* 2016, Epub ahead of print.
- 40 Saeed H, Abdallah BM, Ditzel N, Catala-lehnen P, Qiu W, Amling M, et al: Telomerase-deficient mice exhibit bone loss owing to defects in osteoblasts and increased osteoclastogenesis by inflammatory microenvironment. *J Bone Miner Res* 2011;26:1494–1505.
- 41 Inukai S, de Lencastre A, Turner M, Slack F: Novel microRNAs differentially expressed during aging in the mouse brain. *PLoS One* 2012;7:e40028.
- 42 Rodríguez-Arellano JJ, Parpura V, Zorec R, Verkhratsky A: Astrocytes in physiological aging and Alzheimer's disease. *Neuroscience* 2016;323:170–182.
- 43 Hong P, Jiang M, Li H: Functional requirement of dicer1 and miR-17-5p in reactive astrocyte proliferation after spinal cord injury in the mouse. *Glia* 2014;62:2044–2060.
- 44 Rubinsztein DC, Mariño G, Kroemer G: Autophagy and aging. *Cell* 2011;146:682–695.
- 45 Totary-Jain H, Sanoudou D, Ben-Dov IZ, Dautriche CN, Guarnieri P, Marx SO, et al: Reprogramming of the microRNA transcriptome mediates resistance to rapamycin. *J Biol Chem* 2013;288:6034–6044.
- 46 Hayashita Y, Osada H, Tatematsu Y, Yamada H, Yanagisawa K, Tomida S, et al: A polycistronic microRNA cluster, miR-17-92, is over-expressed in human lung cancers and enhances cell proliferation. *Cancer Res* 2005;65: 9628–9632.
- 47 van Haaften G, Agami R: Tumorigenicity of the miR-17-92 cluster distilled. *Genes Dev* 2010;24:1–4.
- 48 Fan M, Sethuraman A, Brown M, Sun W, Pfeffer LM: Systematic analysis of metastasis-associated genes identifies miR-17-5p as a metastatic suppressor of basal-like breast cancer. *Breast Cancer Res Treat* 2014;146:487–502.
- 49 Li H, Gupta S, Du WW, Yang BB: MicroRNA-17 inhibits tumor growth by stimulating T-cell mediated host immune response. *Oncoscience* 2014;1:531–539.
- 50 Wang M, Gu H, Wang S, Qian H, Zhu W, Zhang L, et al: Circulating miR-17-5p and miR-20a: molecular markers for gastric cancer. *Mol Med Rep* 2012;5:1514–1520.
- 51 Zeng X, Xiang J, Wu M, Xiong W, Tang H, Deng M, et al: Circulating miR-17, miR-20a, miR-29c, and miR-223 combined as non-invasive biomarkers in nasopharyngeal carcinoma. *PLoS One* 2012;7:e46367.
- 52 Fuziwarra CS, Kimura ET: Insights into regulation of the miR-17-92 cluster of miRNAs in Cancer. *Front Med* 2015;2:64.
- 53 Mendell JT: miRiad roles for the miR-17-92 cluster in development and disease. *Cell* 2008; 133:217–222.

10. APPENDIX III

10.1. Curriculum Vitae

Curriculum Vitae



Madhusudhan Reddy Bobbili

Lazarettgasse 9/25,
1090 Wien, Österreich

Mobile: +436765126986
Madhusudhan.bobbili@boku.ac.at

Summary

PhD student with a focus on Engineering Extracellular Vesicles.

Good communicator and action-oriented.

Born in 28.10.1986 in Guntakal, India

LinkedIn: <https://www.linkedin.com/in/madhusudhan-reddy-bobbili-244b281b/>

Skills

- Extracellular vesicle related techniques
- Molecular and cellular biology
- Protein engineering
- Cell culture techniques

- Proficiency with flow cytometry practices and software
- Microscopic techniques
- Presentation/communication

Education

10/2015- Current

PhD Student (BioToP Doctoral School), Department of Biotechnology, University for Natural Resources and Life Sciences, Vienna, group of Dr. Johannes Grillari.

09/2007-06/2009

MSc. in Biochemistry, Bangalore University, Bangalore, India.

09/2004-06/2007

BSc. in Biotechnology, Bangalore University, Bangalore, India.

Experience

10/2015-Current

PhD Thesis on engineering extracellular vesicles (EVs) for isolation of tissue-specific vesicles.
Established the EV platform which includes isolation methods, characterization, engineering EVs for therapeutic purpose.
Responsible for three master students.

05/2018-11/2018

Research Intern, Group Dr. Samir EL Andaloussi, Department of Laboratory, Medicine, Karolinska Institute, Stockholm, Sweden.
Worked a great deal on EV isolation, characterization and uptake studies.

Curriculum Vitae

03/2014-06/2015 Research associate, NDDD, Lupin pharmaceuticals Ltd., India.

03/2010-03/2014 Research scientist, Connexios life sciences Pvt. Ltd., India.

Publications:

Terlecki-Zaniewicz L, Pils V, **Bobbili MR**, Lämmermann I, Perrotta I, Grillenberger T, Schwestka J, Weiß K, Pum D, Arcalis E, Schwingenschuh S, Birngruber T, Brandstetter M, Heuser T, Schosserer M, Morizot F, Mildner M, Stöger E, Tschachler E, Weinmüllner R, Gruber F, Grillari J. Extracellular Vesicles in Human Skin: Cross-Talk from Senescent Fibroblasts to Keratinocytes by miRNAs. *J Invest Dermatol.* 2019 Jun 18. pii: S0022-202X(19)31754-3. doi: 10.1016/j.jid.2019.05.015.

Terlecki-Zaniewicz, L., Lämmermann, I., Latreille, J., **Bobbili, M.R.**, Pils, V., Schosserer, M., Weinmüllner, R., Dellago, H., Skalicky, S., Pum, D., Higareda Almaraz, J.C., Scheideler, M., Morizot, F., Hackl, M., Gruber, F., Grillari, J., (2018) Extracellular vesicles and their miRNA cargo are anti-apoptotic members of the SASP. *Aging*10, 1103 – 1132, doi:10.18632/aging.101452

Bobbili, M.R., Mader, R.M., Grillari, J., Dellago, H. (2017) OncomiR-17-5p: alarm signal in cancer? *Oncotarget* 8, 71206-71222. doi: 10.18632/oncotarget.19331

Dellago, H*, **Bobbili, M.R.***, Grillari, J. (2017) MicroRNA-17-5p: At the Crossroads of Cancer and Aging - A Mini-Review. *Gerontology* 63, 20-28. doi: 10.1159/000447773

Sadasivuni MK*, **Reddy BM***, Singh J*, Anup MO, Sunil V, Lakshmi MN, et al. CNX-013-B2, a unique pan tissue acting rexinoid, modulates several nuclear receptors and controls multiple risk factors of the metabolic syndrome without risk of hypertriglyceridemia, hepatomegaly and body weight gain in animal models. *Diabetol Metab Syndr.* (2014) 6:83. doi: 10.1186/1758-5996-6-83

Oral presentations at conferences:

Bobbili, M.R., Vogt, S., Muehleder, S., Arcalis, E., Barbaria, S., Schosserer, M., Patrioli, C., Pum, D., Holnthoner, W., Terlecki-Zaniewicz, L., Grillari, J. (2018) Recombinal tetraspanins as a novel tool for studying extracellular vesicles (talk) [14th Asian Congress on Biotechnology (ACB), Taipei, Taiwan, 1-4 July 2019]

Bobbili, M.R., Vogt, S., Muehleder, S., Arcalis, E., Barbaria, S., Schosserer, M., Patrioli, C., Pum, D., Holnthoner, W., Terlecki-Zaniewicz, L., Grillari, J. (2018) Recombinal tetraspanins as a novel tool for studying extracellular vesicles (Talk), [Annual Conference of the International Society for Extracellular Vesicles – ISEV2019, Kyoto, Japan, April 24-28 2019].

Bobbili, M.R., Vogt, S., Muehleder, S., Arcalis, E., Patrioli, C., Barbaria, S., Schosserer, M., Pum, D., Holnthoner, W., Redl, H., Terlecki-Zaniewicz, Grillari, J. (2019) Recombinant extracellular vesicles (EVs):

Curriculum Vitae

From basic characterization to targeting tools(Talk) [Austrian Cluster for Tissue Regeneration Annual Meeting, Medical university of Vienna, 1090 Vienna, March 11-12, 2019].

Bobbili, M.R., Vogt, S., Muehleder, S., Arcalis, E., Patrioli, C., Barbaria, S., Schosserer, M., Pum, D., Holnthoner, W., Redl. H., Terlecki- Zaniewicz, Grillari, J. (2018) Strategies of EV targeting and in vivo tracking(Talk) [Austrian Society for Extracellular Vesicles Annual meeting, Donau-Universität Krems, November 21-22, 2018].

Bobbili, M.R., Vogt, S., Muehleder, S., Arcalis, E., Barbaria, S., Schosserer, M., Patrioli, C., Pum, D., Holnthoner, W., Terlecki-Zaniewicz, L., Grillari, J. (2018) Unraveling the distribution of extracellular vesicles in vivo using recombinant tetraspanins (Poster and Talk), [Annual Conference of the International Society for Extracellular Vesicles – ISEV2018, Barcelona, Spain, May 2-6 2018]

Bobbili, M.R., Vogt, S., Muehleder, S., Arcalis, E., Patrioli, C., Barbaria, S., Schosserer, M., Pum, D., Holnthoner, W., Redl. H., Terlecki- Zaniewicz, Grillari, J. (2018) Strategies of EV targeting and in vivo tracking(Talk) [Austrian Cluster for Tissue Regeneration Annual Meeting, FH Technikum Wien, Höchstädtplatz 5, 1200 Vienna, March 12-13, 2018].

Poster presentations at conferences:

Bobbili, M.R., Vogt, S., Muehleder, S., Arcalis, E., Patrioli, C., Barbaria, S., Schosserer, M., Pum, D., Holnthoner, W., Redl. H., Terlecki- Zaniewicz, L., Görgens. A., El, Andaloussi, S., Grillari, J. (2018) Recombinant tetraspanins to understand trafficking of the extracellular vesicles in vivo (Poster) [Gordon Research Conference- Extracellular vesicles, Sunday River, Newry, Maine, USA , August 19-24, 2018].

Bobbili, MR., Terlecki-Zaniewicz, L., Schosserer, M., Patrioli, C., Pum, D., Grillari, J. (2017) Transfer of extracellular between fibroblasts and keratinocytes in cellular senescence- Generate, Track & purify recombinant EVs (Poster) [ISEV2017-Annual Meeting, Toronto, Canada, May 18-21, 2017].

Bobbili, M.R., Terlecki-Zaniewicz, L., Schosserer, M., Patrioli, C., Pils, V., Pum, D., Grillari, J. (2017) In vitro Transfer of Extracellular Vesicles in Cellular Senescence -Tools to generate, purify & trace recombinant EVs (Poster) [9th International Conference On Recombinant Protein Production, Dubrovnik, Croatia, April 23 - 25 , 2017].

Bobbili, MR., Terlecki-Zaniewicz, L., Schosserer, M., Pum, D., Grillari, J. (2016) Characterization of extracellular vesicles in cellular senescence (Poster) [RNA Biochemistry Meeting, Bonn 2016: Extracellular RNA, Bonn, Germany, 06-09 October, 2016].